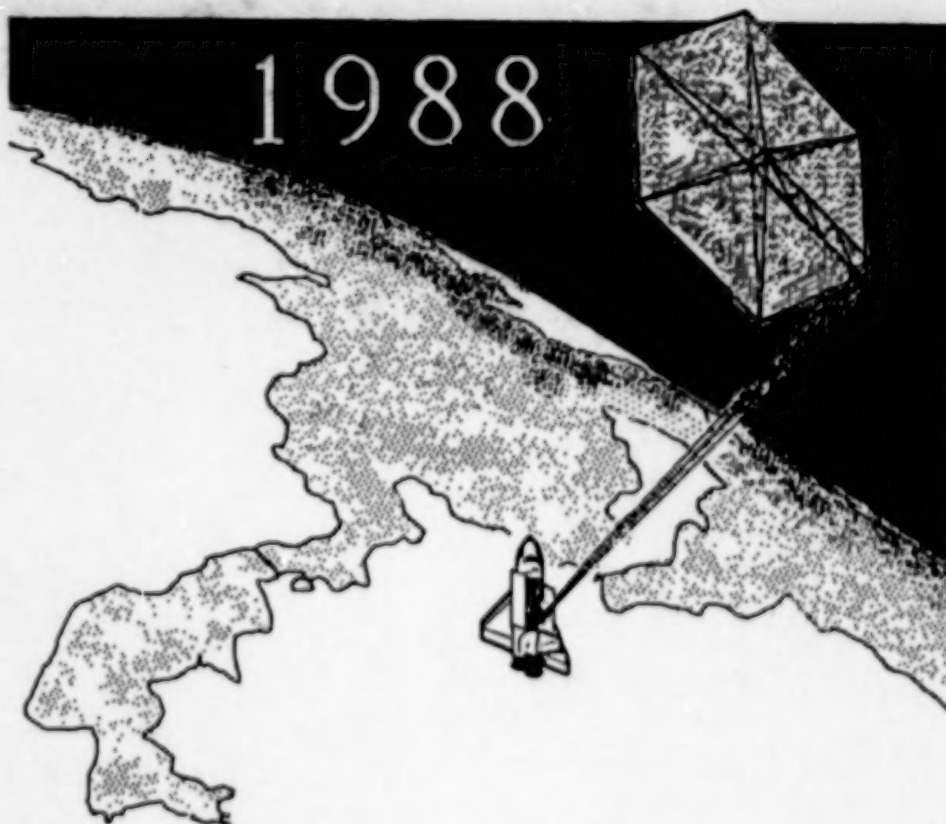


NASA Conference Publication 10057  
Part 1

# 5th Annual NASA Spacecraft Control Laboratory Experiment (SCOLE) Workshop



*Compiled by  
Lawrence W. Taylor, Jr.  
Langley Research Center  
Hampton, Virginia*

Proceedings of a workshop  
sponsored by the National  
Aeronautics and Space  
Administration and held  
at the Hilton Lodge  
Lake Arrowhead, California  
October 31, 1988

DECEMBER 1990

**NASA**

National Aeronautics and  
Space Administration

**Langley Research Center**  
Hampton, Virginia 23665-5225

(NASA-CP-10057-PT-1) THE 5TH ANNUAL NASA  
SPACECRAFT CONTROL LABORATORY EXPERIMENT  
(SCOLE) WORKSHOP, PART 1 (NASA) 383 p

CSC 228

N91-18186

Unclass  
0326328

H1/18

## Introduction

**SCOLE** stands for the "Spacecraft Control Laboratory Experiment". The objective of the SCOLE Program is to provide an example configuration and control objectives which enables direct comparison of different techniques in modeling, systems identification and control. The "SCOLE Design Challenge" was formulated in 1983 by L. W. Taylor and A. V. Balakrishnan. The details of this challenge are reprinted at the end of this document.

Annual SCOLE Workshops have been held for specialists to share and compare their research results. This proceedings is a compilation of the material presented at the 5th Workshop held at Hilton Lodge at Lake Arrowhead, California on October 31, 1988.



# Table of Contents - Part I

	Page
"Dynamic Analysis of the Joint Dominated Beam (Truss Beam)" .....	1
Elias G. Abu-Saba, Raymond C. Montgomery, William M. McGinley	
"Design of the SCOLE Boom Based on the Dynamic Analysis of the Joint Dominated Beam" .....	13
Elias G. Abu-Saba, Raymond C. Montgomery, William M. McGinley	
"Nonlinear Damping Model: Response to Random Excitation" .....	27
Weijian Zhang	
"Damping Operators in Continuum Models of Flexible Structures" .....	39
A. V. Balakrishnan	
"A Special Class of Nonlinear Damping Models in Flexible Space Structures" .....	65
Anren Hu, Lawrence W. Taylor, Jr. and Ramendra P. Singh	
"Hysteretic Damping Model for the Mini-MAST Truss" .....	99
Lawrence W. Taylor, Jr.	
"Efficiency and Capabilities of Multi-Body Simulations" .....	129
Richard J. Vandervoort	
"Automatic Generation of the Equations of Motion and Their Solution for Flexible Structures" .....	151
Ramendra P. Singh and Lawrence W. Taylor, Jr.	
"Control Design Challenges of Large Space Systems and Spacecraft Control Laboratory Experiment (SCOLE)" .....	177
Jiguan Gene Lin	
"Slew Maneuver Dynamics of Spacecraft Control Laboratory Experiment (SCOLE)" .....	247
Y. P. Kakad	

## Table of Contents, Continued

---

	Page
"Optimal Planar Slewing of the Flexible Orbiting SCOPE".....	291
Peter M. Bainum and Feiyue Li	
"Experimental Results in Modeling, Analysis, and Control of Flexible Multi-Body Systems".....	317
A. Galip Ulsoy	
"Minimum Attainable RMS Attitude Error Using Co-Located Rate Sensors".....	357
A. V. Balakrishnan	
"A Wave Equation Formulation for the SCOPE".....	369
Robert Araya	

---

## Table of Contents - Part II\*

---

"Quasi-Time Optimal Controllers Designed for the SCOPE Laboratory Model".....	379
Howard Kaufman	
"Model Reference Control of the Linearized SCOPE Model".....	407
A. Musalem and Howard Kaufman	
"Control and Identification Experiments for the NASA LaRC SCOPE Program".....	459
Stephen Yurkovich, Umit Ozguner and Kathleen Ossman	
"Parameter Identification for Vibration Control of SCOPE".....	547
Dean Sparks, Raymond Montgomery, Robin Elder, Danette Lenox	
"Identification and Control of Large Flexible Spacecraft".....	555
Sue Harris and Y. P. Kakad	

\*Published under separate cover.

## Table of Contents, Continued

---

	Page
"Description of the Spacecraft Control Laboratory Experiment (SCOLE) Facility".....	561
Jeffrey P. Williams and Rosemary A. Rallo	
"Analytical Redundancy Management for SCOLE".....	607
Raymond C. Montgomery	
"Spacecraft COntrols Laboratory Experiment (SCOLE) Software User's Manual".....	619
Danette Lenox	
"A Mathematical Problem and a Spacecraft Control Laboratory Experiment (SCOLE) Used to Evaluate Control Laws for Flexible Spacecraft....Reprint of the "NASA/IEEE Design Challenge".....	691
L. W. Taylor and A. V. Balakrishnan	
"Status and Future Plans of the SCOLE Experimental Facility".....	719
J. Shenhar	

**DYNAMIC ANALYSIS OF THE JOINT  
DOMINATED BEAM (TRUSS BEAM)**

**by**

**Elias G. Abu-Saba**

**Raymond C. Montgomery**

**William M. McGinley**

**(1)**

# **INTRODUCTION**

**Construction in Outer Space of:**

- Platforms for Space Stations**
- Antenna Systems for Space Explorations**
- Support Structures for Solar Panels**
- Housing for Space Workers**



# **ABSTRACT**

## **Method Presents**

- Theoretical Analysis of the Vibrational Modes of the Joint Dominated Beam**
- Cantilever Truss Beam is Used for the Analysis**
- Chord Members Contribute Most Deformations. Web Members are Ignored**
- Lumped Mass System is Used for Analysis**

- Algorithms are Developed to determine Flexibility of the System**
- System is Analysed With and Without Joint Contribution**
- A Set of Joint Flexibility is Used**
- Computer Programs are Developed to Obtain Numerical Results: Frequencies and Mode Shapes**
- Conclusions and Recommendations are Provided**

## DYNAMICS

### EQUATION OF MOTION OF SYSTEM

$$[B]\{Y\} = 0$$

$$[B] = [A] - \frac{1}{m \omega^2} [I]$$

$$A_{ii} = \frac{1}{24EI} (2i-1)^3, \quad i = 1, \dots, N$$

$$R_i = \frac{1}{24EI} 3(2i-1)^2, \quad i = 1, \dots, N$$

$$A_{ij} = A_{i,j-1} + R_i, \quad j = i+1, \dots, N$$

$$A_{ij} = A_{ji}$$

(5)

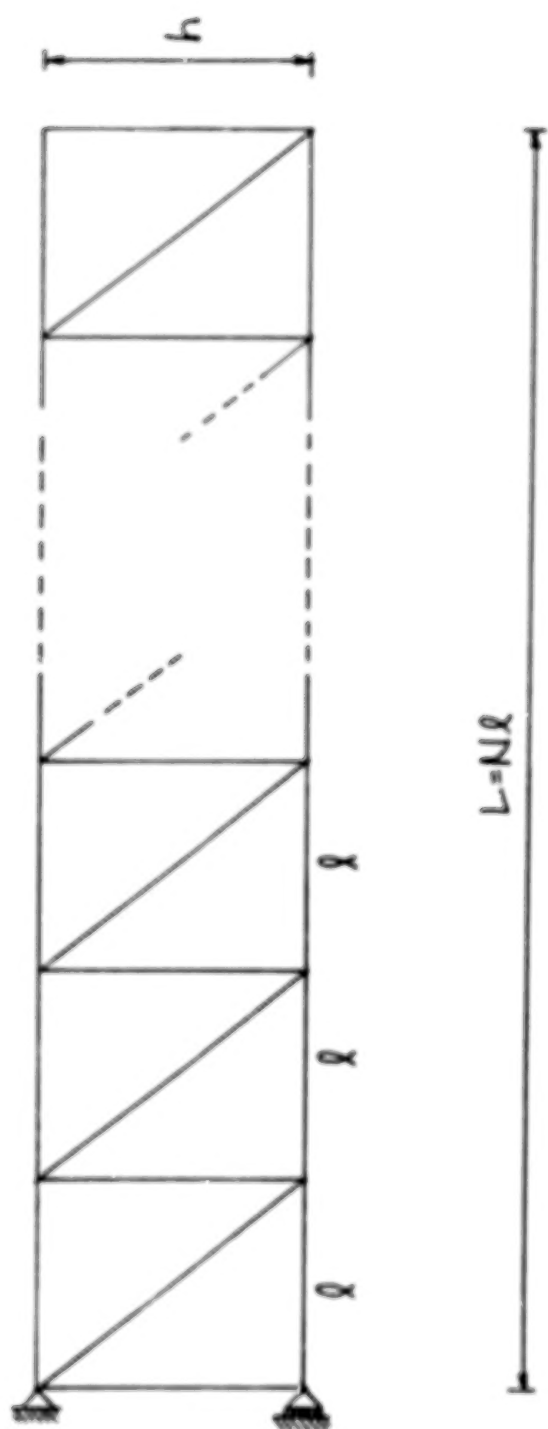


FIGURE • 1-TRUSS, BEAM

(5a)

# **JOINT PARTICIPATION**

## **Assumptions**

- Behavior of the Joint is Linear**
- Damping of the Joint is Not Included**
- Free Play is Not Considered**
- Forces in Members are Axial**



## MODIFIED FLEXIBILITY MATRIX

$$A^*_{ij} = A_{ij} + \frac{l^3}{24EI} s(i)^2 (2j-1)$$

$$i = 1, \dots, N$$

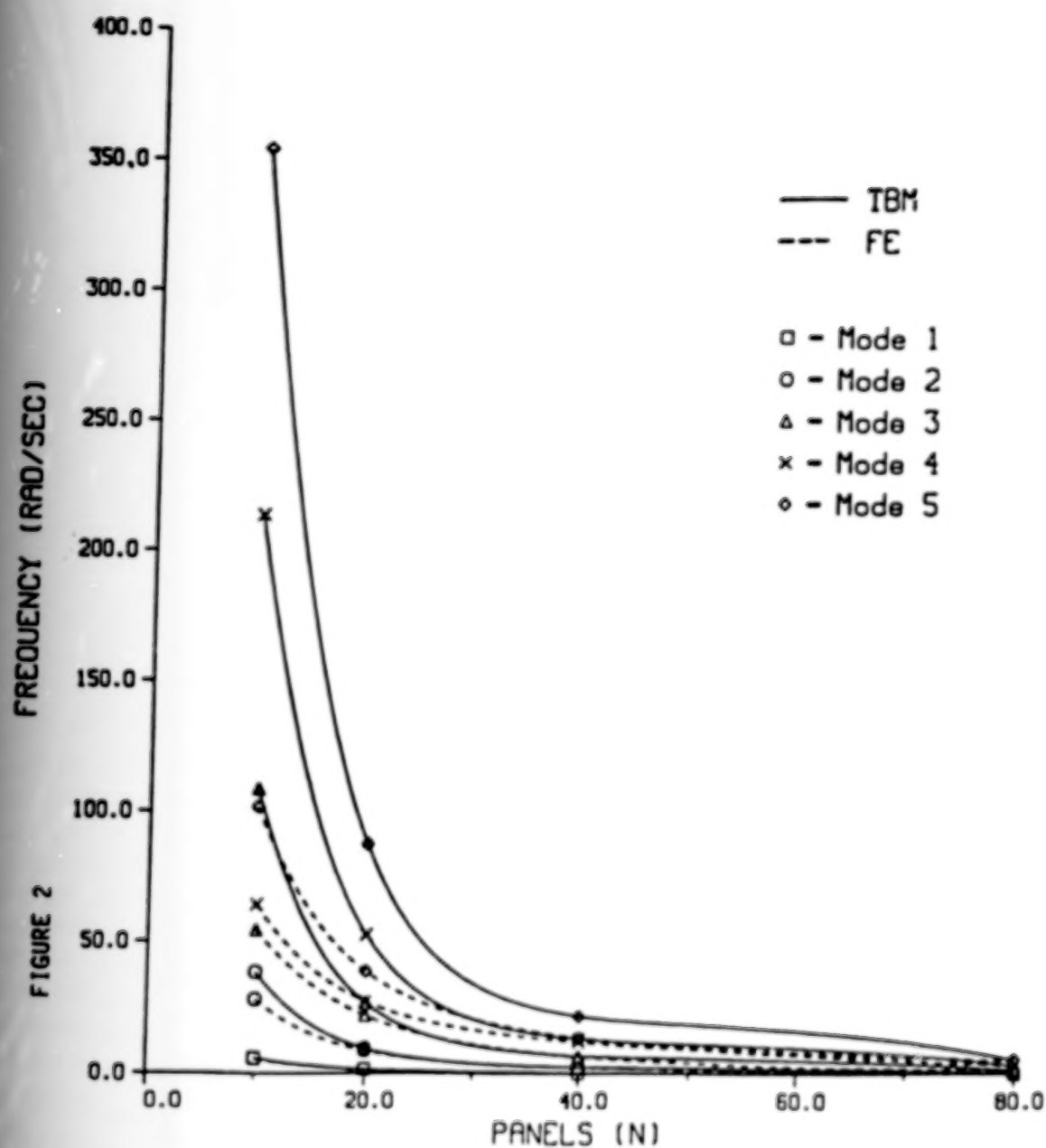
$$j = 1, \dots, N$$

$$s = \frac{12EI}{h^2} k_l$$

**k = Flexibility of the Joint**

(7)

## FREQUENCY CORRELATION



## **CONCLUSIONS**

- **A Practical and Simple Approach for Predicting Frequency Response of Structures**
- **Computational Cost, Time and Storage Requirements Provide a Clear Advantage over Finite Element Method**

# **EXPERIMENTAL PROGRAM**

## **STAGE 1 Static Loading**

- 1. Determine the flexibility of the joint assembly.**
- 2. Determine the combined flexibility of the truss and joint assembly for increasing numbers of truss panels.**
- 3. Under the action of static loading measure the stress distribution in the truss panels.**

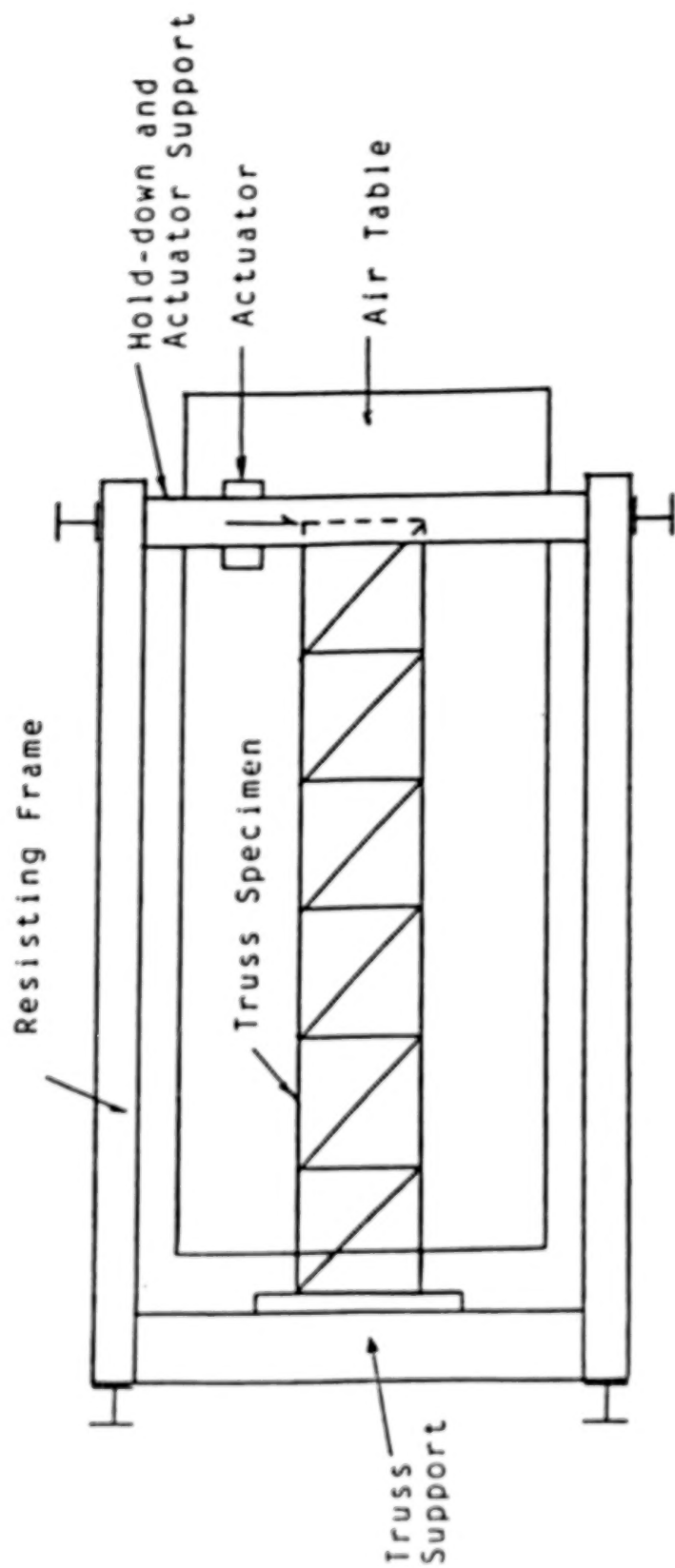
# **EXPERIMENTAL PROGRAM**

## **Stage 2 Dynamic Response**

- 1. Measure the deflection and the truss cord stress variations for a single truss panel and joint assembly.**
- 2. Measure the dynamic response (deflections and stresses) of an increasing number of truss panel and joint assemblies. Frequency response will be determined from these measurements.**



PLAN VIEW



Schematic of Testing Apparatus

Figure #3

DESIGN OF THE SCOPE BOOM  
BASED ON THE DYNAMIC ANALYSIS OF THE JOINT DOMINATED  
BEAM

Elias G. Abu-Saba  
North Carolina A&T State University

Raymond C. Montgomery  
NASA Langley Research Center

William M. McGinley  
North Carolina A&T State University

## ABSTRACT

Mathematical models have been developed to predict the dynamic response of the joint dominated beam. Various assumptions of the force interaction between the beam elements and the joints have been studied using these models. However, the validity of these models have not been adequately determined. In any dynamic analysis of assemblies, the effects of joint imperfections must be also included. To accomplish these tasks, a combined analytical and experimental investigation will be conducted to evaluate the significance of the various joint behaviours with respect to the overall stiffness of the beam. Results of the experimental analysis will be incorporated in the dynamic analysis of the beam.

Models of the truss-beam will be constructed at North Carolina A&T State University and tested to determine the validity of the analytical method. Test data will be obtained for a particular joint type with negligible free play. Using the measured material properties of the joints and truss model, the equation of motion will then be used to predict the dynamic behaviour of the truss-beam. A comparison of predicted and observed behaviour will be made

and the adequacy of the analytical methods evaluated. Modifications of the analytical procedures will be made as required by the comparison study. This approach of the dynamic study of the truss-beam system can be used in the dynamic analysis of the scale.

## INTRODUCTION

Manned space stations are on the drawing board, and structures to house astronauts and support personnel will be erected in outer space. These stations will be used for communication, power generation, docking, and launching space vehicles in the future. Since all structural components have to be fabricated and preassembled on earth and packaged for shipment via the space shuttle, weight and volume become a determining factor in the design. Light weight materials as epoxy graphites are used in the members, and interlocking joints are provided to facilitate deployment.

As the exploration of outer space is increased, the need for more reliable structures which perform various tasks in orbit becomes essential. Since these structures are deployable, large, and highly flexible, their dynamic analysis and control using established methods yields results that differ from those obtained on board testing. Hence further modifications of the mathematical model will be necessary to increase convergence between theoretical and experimental results.

## DYNAMIC EQUATION

The general equation of motion for a linear structural system is expressed as

$$\{ \ddot{Y} \} = - \omega^2 [A] [M] \{ Y \} \dots\dots (1)$$



where

- $\{ Y \}$  = Displacement vector
- $[ A ]$  = Flexibility matrix of the structure
- $[ M ]$  = Mass matrix of the structure
- $\omega$  = Natural frequency of the system  
rad/sec

The dynamic study of the truss-beam is seen to depend on its flexibility.

#### FLEXIBILITY OF THE TRUSS BEAM

Consider that the truss-beam behaves as a cantilever as shown in Figure (1). For a slender truss the transverse nodal displacements will be mainly attributed to the axial

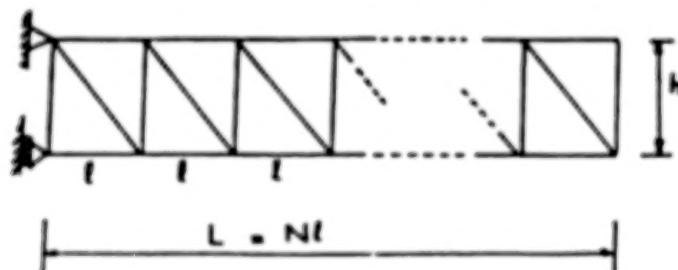


FIG. 1. TRUSS BEAM

strain in the chords. Thus the contribution from the web members can be neglected with very little error. If the joint response were to be excluded initially, the flexibility matrix  $[ A ]$  for the structure can be readily obtained from the following algorithms:

$$A_{ii} = \frac{l^3}{24EI} (2i - 1)^3, \quad i = 1, N$$

$$R_i = \frac{l^3}{24EI} 3(2i - 1)^2, \quad i = 1, N \quad (2)$$

$$A_{ij} = A_{ij-1} + R_i, \quad j = i + 1, N$$

$$A_{ij} = A_{ji}$$

When the bays are identical, the nodal masses will be equal throughout the structure. Letting  $m$  represent the mass of one bay, the mass matrix can be expressed by:

$$[M] = m [1] \quad (3)$$

Substituting Equation 3 into Equation 1 and simplifying the result yields

$$[B] \{Y\} = 0 \quad (4)$$

where

$$[B] = [A] - \lambda [1] \quad (5)$$

$$\lambda = \frac{24EI}{m \omega^2 l^3} \quad (6)$$

Given the material property E, the cross sectional area of the members of the truss-beam, the depth of the bay h, and the length l, the number of bays N and the density of the material used in the structure, a computer program has been written to provide the natural frequencies of the system.

#### FLEXIBILITY OF THE TRUSS BEAM WITH JOINT RESPONSE

To simplify the response of the joint, it is assumed that the joint displacements are caused by the strain in the chord members. Another assumption which is used in the study is that the displacement in the joint is due to axial forces in the chords acting on the connecting pin as a spring. The joint is thus replaced by a flexibility k. No other factors that contribute to joint imperfections are included at this stage.

Introducing the joint flexibility k, the modified flexibility matrix is given by

$$A_{ij}^* = A_{ij} + \frac{s l^3}{24EI} i^2 (2j - 1) \quad (7)$$

$$i = 1, N; \quad j = 1, N$$

where  $A_{ij}$  is given by Equation 2 and  $s$  is obtained from the following expression:

$$s = \frac{12 E I k}{h^3} \quad (8)$$

#### APPLICATION TO THE METHOD

An example is used with a typical panel of 20" in length and 20" in depth. The cross sectional area of the chord is 0.25 sq. in. The values of  $E$  and the density are  $3E+7$  psi and 0.282 pci, respectively. The finite element method is applied to the same example for comparison. Since the finite element method does not include joint imperfections, the value of  $k$  is taken as zero. The results of this comparison are shown in table 1 and Figure 2 for  $N$  varying from 3 to 80.

#### EXPERIMENTAL PROGRAM

To confirm the accuracy of the theoretical procedure, an experimental approach has been proposed to be performed at North Carolina Agricultural and Technical State University. The proposal has been submitted to NASA at Langley Research Center for funding.

Since the accuracy of the analysis is highly dependent on the mass and flexibility of the truss panels, in addition to the flexibility of the joint, these quantities must be accurately measured before a reliable evaluation of the analytical procedure can be made.

Table 1 - Natural Frequencies, Rad/sec

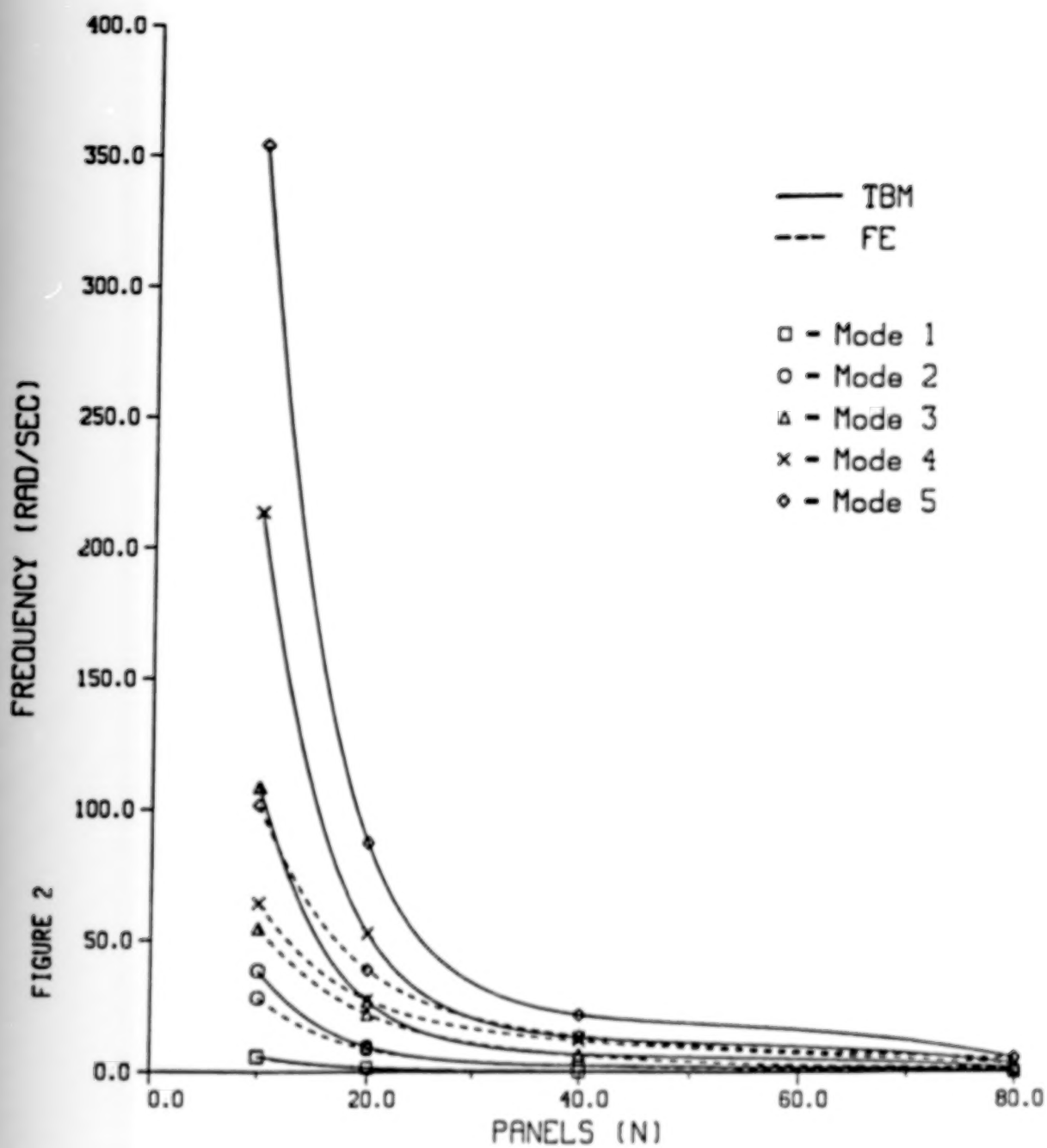
MODE	N=3		N=10		N=20		N=40		N=80	
	TB	FEM	TB	FEM	TB	FEM	TB	FEM	TB	FEM
1	69.57	43.16	6.11	5.66	1.53	1.49	0.38	0.30	0.095	0.095
2	466.2	131.9	38.55	28.22	9.58	8.66	2.39	2.32	0.6	0.59
3	1498.	183.6	108.5	54.56	26.85	21.99	6.7	6.31	1.67	1.65
4		230.5	213.5	64.21	52.7	27.28	13.13	11.85	3.28	3.19
5		309.5	354.0	101.6	87.22	38.73	21.71	13.64	5.42	5.19
6		475.3	528.2	137.4	130.43	56.94	32.44	18.72	8.10	6.81
7		504.4	730.1	162.5	182.33	76.0	45.33	26.53	11.31	7.63
8		515.7	942.2	171.6	242.88	81.76	60.37	35.01	15.07	10.44
9		539.8	1125.0	202.1	311.95	95.49	77.56	40.89	19.35	13.61
10		585.2	1540.0	226.5	389.34	114.1	96.9	44.11	24.17	17.07

FREQUENCY (RADS/SEC)

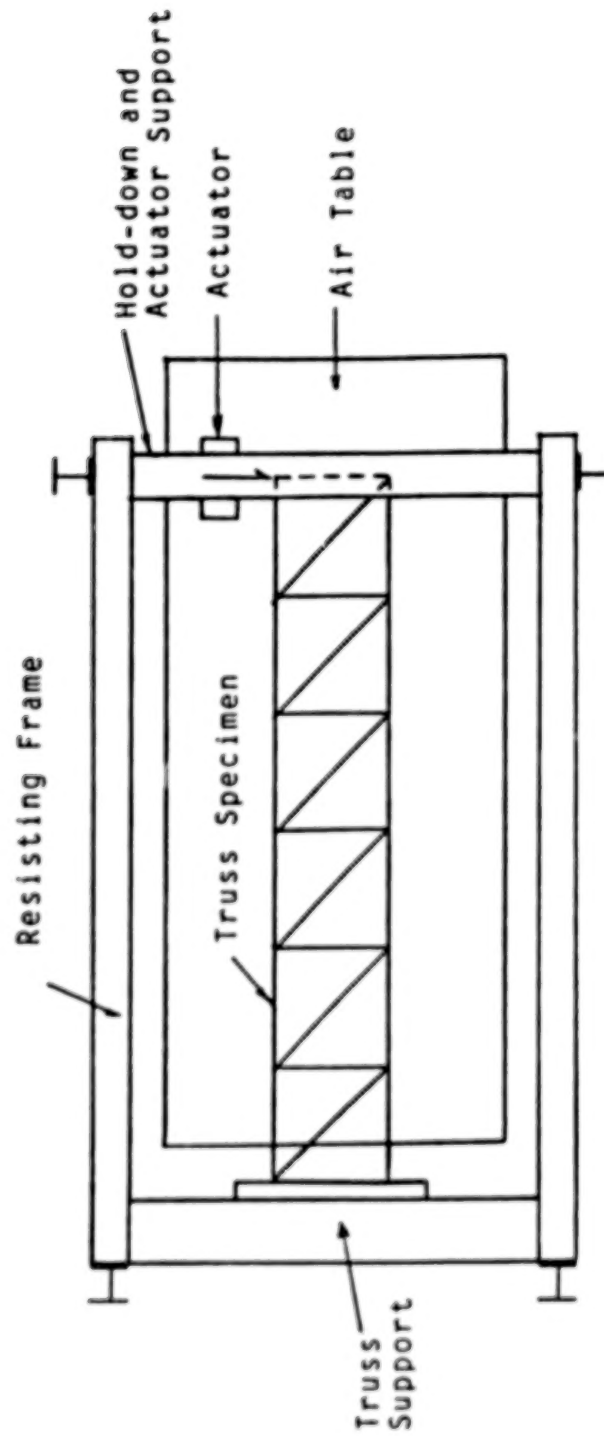
N = Number of panels

No joint imperfection i.e.  $k=0$

## FREQUENCY CORRELATION



PLAN VIEW



Schematic of Testing Apparatus

Figure 3

Only one type of joint will be evaluated during the experimental phase. Furthermore, the joints will be fabricated so that free play in the joint is negligible and can be ignored. Once the accuracy of the analytical procedure have been confirmed for this type of joint, subsequent investigations can determine the effects of varying joint flexibility and free play.

#### TESTING APPARATUS

Truss joint specimen will be tested using a Forney Material Testing machine located in the Structures Laboratory at the North Carolina Agricultural and Technical State University in Greensboro, North Carolina.

In an effort to reduce cost, the same apparatus will be used to test the truss panels and truss panel assemblies. A schematic of the proposed testing apparatus is shown in Figure 3. It consists of a truss support frame, air cushion table, actuator, and an adjustable actuator support and "hold-down". The apparatus will also include devices to measure the deformation and chord strains at various positions on the specimen, in conjunction with a high speed data acquisition system and a micro-computer.



## REMARKS AND CONCLUSIONS

The approximation of a large space truss by a beam model provides a practical approach for predicting the frequency response of the structure. The computational cost, time and storage requirements may render discrete finite element analysis impractical, particularly in the conceptual and design phases when parameter studies and alternate designs are being evaluated.

The proposed beam method offers a structural model with significantly fewer elements ( $N$ ) and degrees of freedom ( $N$ ), compared to a finite element model with  $(4N+1)$  degrees of freedom, where  $N$  is the number of panels in the actual structure. Frequencies for the first five modes obtained by the beam model are found in good agreement with those obtained by the finite element, especially as  $N$  gets large. The proposed algorithm saves significant programming effort as well as results in considerable economy of computational time, cost and storage.

# Nonlinear Damping Model: Response to Random Excitation

Weijian Zhang\*  
Electrical Engineering Department  
6731 Boelter Hall  
UCLA  
Los Angeles, CA 90024

November 10, 1988

## Abstract

The objective of this study is to investigate stationary Fokker-Planck equation corresponding to nonlinear random vibration problem. A method of energy approximation (MEA) is proposed to obtain a modified model as an approximation of the exact model. The closed form solution of the stationary Fokker-Planck equation corresponding to the modified model is obtained, and so are the various moments of the stationary response. Comparisons are made between MEA and MEL (method of equivalent linearization) to illustrate the advantage of MEA over MEL. The MEA also overcomes the shortcoming of non-Gaussian closure method in which the density might have negative value caused by truncation.

---

\*Research supported in part under AFOSR grant No. 83-0318. Presented at the 5th Annual NASA SCOLE Workshop, Lake Arrowhead, California. Nov., 1988.

## 1 Introduction

Experimental evidence in SCOLE [1] seems to support the need for nonlinear models-the decrement is much smaller than predicted by linear models. Nonlinear damping model under random excitation becomes a random vibration problem which has received significant attention in recent years in both civil and mechanical engineering. When the excitation is a white noise process, the response is Markovian. The transition probability density function, which together with an initial distribution completely describes the response, satisfies the Fokker-Planck equation which is a linear but degenerate parabolic type partial differential equation. A variety of approximate methods have been proposed to solve the Fokker-Planck equation corresponding to broad-band excitation of a nonlinear dynamic system. All of the methods investigated so far appear to involve prodigious amounts of labor.

In this paper, a *Method of Energy Approximation (MEA)* is proposed to find the approximate solution of the stationary Fokker-Planck equation corresponding to one-dimensional nonlinear damping model under white noise excitation.

## 2 Energy Approximation Model

Let us first consider a concrete model due to Balakrishnan and Taylor [2]:

$$\ddot{x} + 2\xi\omega_0\dot{x} + \gamma x^{2m}|x|^\alpha \dot{x}^{2n+1}|\dot{x}|^\beta + \omega_0^2 x = \sigma n(t) \quad (1)$$

where  $0 \leq \alpha, \beta \leq 1$ ,  $\xi, \gamma > 0$ , and  $m, n$  are nonnegative integers.  $n(t)$  is a Gaussian white noise process.

Notations:

$$\begin{aligned} E &= \frac{\omega_0^2 x^2 + y^2}{2} \\ y &= \dot{x} \\ q &= m + n + \frac{\alpha + \beta}{2} \end{aligned}$$

We observe the following:

$$\begin{aligned} &\gamma x^{2m} |x|^{\alpha} \dot{x}^{2n+1} |\dot{x}|^{\beta} \\ &= \gamma |x|^{2m+\alpha} |y|^{2n+\beta} y \\ &= \frac{\gamma}{\omega_0^{2m+\alpha}} (\omega_0^2 x^2)^{m+\frac{\alpha}{2}} (y^2)^{n+\frac{\beta}{2}} y \\ &= \frac{\gamma}{\omega_0^{2m+\alpha}} (2E - y^2)^{m+\frac{\alpha}{2}} (2E - \omega_0^2 x^2)^{n+\frac{\beta}{2}} y \end{aligned}$$

We consider the following replacement of the above:

$$\mu_0 \frac{\gamma}{\omega_0^{2m+\alpha}} (2E)^q y$$

Here  $\mu_0$  is chosen such that

$$\int_0^{2\pi} \left[ \left| \frac{\sqrt{2E}}{\omega_0} \sin \psi \right|^{2m+\alpha} \left| \sqrt{2E} \cos \psi \right|^{2n+\beta} \sqrt{2E} \cos \psi - \mu_0 (2E)^q \sqrt{2E} \cos \psi \right]^2 d\psi$$

is minimized.

In the above minimization, we consider  $E$  as a constant because in situations where the response has reached stationarity and where the damping is small, the energy dissipated through damping and the energy input through the excitation during one cycle, will, on average, be small fractions of the total energy level in that cycle.

Computation gives:

$$\begin{aligned}\mu_0 &= \frac{4}{\pi} \int_0^{\pi/2} \sin^{2m+\alpha} \psi \cos^{2n+2+\beta} \psi d\psi \\ &= \frac{2}{\pi} \frac{\Gamma(m + \frac{\alpha+1}{2}) \Gamma(n + 1 + \frac{\beta+1}{2})}{\Gamma(q+2)}\end{aligned}$$

Then, we obtained the following energy approximation model:

$$\ddot{x} + 2\xi\omega_0\dot{x} + \frac{\gamma\mu_0}{\omega_0^{2m+\alpha}}(\omega_0^2x^2 + \dot{x}^2)^q\dot{x} + \omega_0^2x = \sigma n(t) \quad (2)$$

When there is no random noise excitation, computer simulation shows the Krylov-Bogoliubov approximation of (1) is a very good approximation when  $\gamma$  is small. It happens that (1) and (2) have exactly the same Krylov-Bogoliubov approximation, which is an evidence to support the validity of the energy approximation model. Of course, this fact only refers to no noise models.

**Proposition 1** *Both the exact model (1) and the modified model (2) have the same Krylov-Bogoliubov approximation given by*

$$\begin{aligned}\frac{da(t)}{dt} &= -\xi\omega_0a(t) - \frac{\gamma\mu_0}{2}\omega_0^{2n+\beta}a^{2q+1}(t) \\ \frac{d\phi(t)}{dt} &= 0\end{aligned} \quad (3)$$

*Proof:* Straightforward computation based upon Krylov-Bogoliubov approximation [5]:

$$\begin{aligned}\frac{da(t)}{dt} &= -\frac{1}{2\pi\omega_0} \int_0^{2\pi} D(a \sin \psi, a\omega_0 \cos \psi) \cos \psi d\psi \\ \frac{d\phi(t)}{dt} &= \frac{1}{2\pi\omega_0a} \int_0^{2\pi} D(a \sin \psi, a\omega_0 \cos \psi) \sin \psi d\psi\end{aligned}$$

### 3 Stationary Fokker-Planck Equation

In this section, we solve the stationary Fokker-Planck equation corresponding to the energy approximation model. The technique is used in [3].

The stationary Fokker-Planck equation is

$$\begin{aligned} 0 &= -\frac{\partial}{\partial x}(yp) + \frac{\partial}{\partial y}(\omega_0^2 xp) \\ &\quad + \frac{\partial}{\partial y}[(2\xi\omega_0 y + \frac{\gamma\mu_0}{\omega_0^{2m+a}}(2E)^q y)p] + \frac{\sigma^2}{2} \frac{\partial^2 p}{\partial y^2} \\ 0 &= -\frac{\partial}{\partial x}(\frac{\partial E}{\partial y} p) + \frac{\partial}{\partial y}(\frac{\partial E}{\partial x} p) \\ &\quad + \frac{\partial}{\partial y}[(2\xi\omega_0 y + \frac{\gamma\mu_0}{\omega_0^{2m+a}}(2E)^q y)p] + \frac{\sigma^2}{2} \frac{\partial p}{\partial y} \\ 0 &= y[(2\xi\omega_0 + \frac{\gamma\mu_0}{\omega_0^{2m+a}}(2E)^q)p + \frac{\sigma^2}{2} \frac{\partial p}{\partial E}] \end{aligned}$$

In the above, we used the following fact

$$p(x, y) = p(E) \implies \begin{cases} -\frac{\partial}{\partial x}(\frac{\partial E}{\partial y} p) + \frac{\partial}{\partial y}(\frac{\partial E}{\partial x} p) = 0 \\ \frac{\partial p}{\partial y} = y \frac{\partial p}{\partial E} \end{cases}$$

Therefore, the stationary density is given by

$$\begin{aligned} p(x, y) &= C_0 \exp[-\frac{2\xi\omega_0}{\sigma^2}(2E) - \gamma_1(2E)^{q+1}] \\ &= C_0 \exp[-\frac{2\xi\omega_0}{\sigma^2}(\omega_0^2 x^2 + y^2) - \gamma_1(\omega_0^2 x^2 + y^2)^{q+1}] \end{aligned}$$

where

$$\begin{aligned} \gamma_1 &= \frac{\gamma\mu_0}{\sigma^2 \omega_0^{2m+a}(q+1)} \\ \frac{1}{C_0} &= \frac{\pi}{\omega_0} \int_0^\infty e^{-\frac{2\xi\omega_0}{\sigma^2}\rho - \gamma_1 \rho^{q+1}} d\rho \\ &= \frac{\pi}{\omega_0 \gamma_1^{\frac{1}{q+1}}} F(s_0) \end{aligned}$$

$$F(s) = \int_0^{\infty} e^{-st} e^{-t^{q+1}} dt$$

$$s_0 = \frac{2\xi\omega_0}{\sigma^2\gamma_1^{\frac{1}{q+1}}}$$

## 4 Moments of Stationary Response

$E x^k y^l = 0$  if either  $k$  or  $l$  is odd. If both  $k$  and  $l$  are even, then

$$\begin{aligned} E x^k y^l &= \frac{1}{\omega_0^k} E (\omega_0 x)^k y^l \\ &= \frac{C_0 \Gamma(\frac{k+1}{2}) \Gamma(\frac{l+1}{2})}{\omega_0^{\frac{k+1}{2}} (\frac{k+l}{2})!} \\ &\quad \times \int_0^{\infty} \rho^{\frac{k+l}{2}} \exp[-\frac{2\xi\omega_0}{\sigma^2} \rho - \gamma_1 \rho^{q+1}] d\rho \\ &= \frac{\Gamma(\frac{k+1}{2}) \Gamma(\frac{l+1}{2})}{\pi \omega_0^k (\frac{k+l}{2})!} \frac{(-1)^{\frac{k+l}{2}} F(\frac{k+l}{2})(s_0)}{\gamma_1^{\frac{k+l}{2q+2}} F(s_0)} \end{aligned}$$

## 5 Comparison with MEL (Method of Equivalent Linearization)

Consider  $\xi < 0$  case of (1). The Krylov-Bogoliubov approximation of (1) is given by (3), which can be solved as

$$a(t) = \frac{a(0) e^{|\xi| \omega_0 t}}{|1 + a^{2q}(0) \frac{\gamma \mu_0 \omega_0^{2q+\beta-1}}{2|\xi|} (e^{2|\xi| \omega_0 t} - 1)|^{\frac{1}{2q}}} \quad (4)$$

We have

$$\lim_{t \rightarrow \infty} a(t) = \left| \frac{2|\xi|}{\gamma \mu_0 \omega_0^{2q+\beta-1}} \right|^{\frac{1}{2q}} \triangleq \bar{a}$$

for any  $a(0) \neq 0$ . This fact implies that the exact model (1) has a stable limit cycle with radius between  $\bar{a}$  and  $\omega_0 \bar{a}$  (approximately).

Actually, the modified model (2) does have a limit cycle

$$\begin{cases} x^0(t) = a \sin \omega_0 t \\ y^0(t) = \omega_0 a \cos \omega_0 t \end{cases} \quad (5)$$

or, on phase plane  $(\frac{x}{a})^2 + (\frac{y}{\omega_0 a})^2 = 1$ .

**Proposition 2** *The limit cycle (5) of the energy approximation model (2) is asymptotically stable.*

*Proof:* To prove the asymptotic stability of the limit cycle (5), we consider the corresponding linear variational equation

$$\begin{cases} \frac{dx}{dt} = y \\ \frac{dy}{dt} = \frac{\partial Y}{\partial x}(x^0(t), y^0(t))x + \frac{\partial Y}{\partial y}(x^0(t), y^0(t))y \end{cases} \quad (6)$$

where

$$Y(x, y) = -2\xi\omega_0 y - \frac{\gamma\mu_0}{\omega_0^{2n+a}}(\omega_0^2 x^2 + y^2)^q y - \omega_0^2 x$$

The linear system (6) with periodic coefficients always has a non-trivial  $\frac{2\pi}{\omega_0}$ -periodic solution which is given by  $(x^0(t), y^0(t))$ . Therefore  $\rho_1 = 1$  is a characteristic multiplier. By Theorem 2.1 of [4, page 217], it is sufficient to show the other characteristic multiplier  $\rho_2 < 1$ .

Since

$$\rho_2 = \rho_1 \cdot \rho_2 = \exp\left[\int_0^{\frac{2\pi}{\omega_0}} \frac{\partial Y}{\partial y}(x^0(t), y^0(t)) dt\right]$$

it is sufficient to show

$$\int_0^{\frac{2\pi}{\omega_0}} \frac{\partial Y}{\partial y}(x^0(t), y^0(t)) dt < 0$$

In fact, by noticing the definition of  $a$  we have

$$\begin{aligned} \frac{\partial Y}{\partial y}(x^0(t), y^0(t)) &= -2\xi\omega_0 - \gamma\mu_0\omega_0^{2n+\beta}a^{2q}(1 + 2q\cos^2\omega_0 t) \\ &= -2\xi\omega_0 - 2|\xi|\omega_0(1 + 2q\cos^2\omega_0 t) \\ &= -4q|\xi|\omega_0\cos^2\omega_0 t \end{aligned}$$



and hence

$$\int_0^{\frac{2\pi}{\omega_0}} -4q|\xi|\omega_0 \cos^2 \omega_0 t dt = -4\pi q|\xi| < 0$$

which establishes the asymptotic stability of (5).  $\square$

What is more interesting is that the stationary solution of the corresponding Fokker-Planck equation given by

$$p(x, y) = C_0 \exp \left[ \frac{2|\xi|\omega_0}{\sigma^2} (\omega_0^2 x^2 + y^2) - \gamma_1 (\omega_0^2 x^2 + y^2)^{q+1} \right] \quad (7)$$

achieves maximum on the ellipse (limit cycle).

$$\left(\frac{x}{a}\right)^2 + \left(\frac{y}{\omega_0 a}\right)^2 = 1$$

and achieves local minimum at the origin.

The following Van-der-Pol self-excited oscillator

$$\ddot{x} + (\gamma x^2 - \eta)\dot{x} + x = \sigma n(t) \quad (8)$$

is a particular case of the above discussion with  $\xi = -\eta/2$  ( $\eta > 0$ ),  $m = 1$ ,  $n = \alpha = \beta = 0$ ,  $\omega_0 = 1$ .

One can easily find  $\mu_0 = 1/4$ ,  $a = 2\sqrt{\eta/\gamma}$  and the energy approximation model is given by

$$\ddot{x} + [\gamma/4(x^2 + \dot{x}^2) - \eta]\dot{x} + x = \sigma n(t)$$

with the corresponding stationary density

$$p(x, y) = C_0 \exp \left[ \frac{\eta}{\sigma^2} (x^2 + y^2) - \frac{\gamma}{8\sigma^2} (x^2 + y^2)^2 \right]$$

where

$$\frac{1}{C_0} = \sqrt{2/\gamma} \pi^{3/2} \sigma e^{2\eta^3/\sigma^2\gamma} [1 + \Phi(\frac{2\eta}{\sigma\sqrt{\gamma}})]$$

$$\Phi(x) \stackrel{\text{def}}{=} \sqrt{2/\pi} \int_0^x e^{-t^2/2} dt$$

## 6 Generalization

The MEA described above can be easily generalized to nonlinear random vibration problem in the following general form

$$\ddot{x} + D(x, \dot{x}) + \omega_0^2 x = \sigma n(t) \quad (9)$$

Our conclusion is that the exact model (9) can be approximated by the following modified model

$$\ddot{x} + \mu \left( \frac{\omega_0^2 x^2 + \dot{x}^2}{2} \right) \dot{x} + \omega_0^2 x = \sigma n(t) \quad (10)$$

where  $\mu(E)$  minimizes

$$\int_0^{2\pi} \left| D\left(\frac{\sqrt{2E}}{\omega_0} \sin \psi, \sqrt{2E} \cos \psi\right) - \mu(E) \sqrt{2E} \cos \psi \right|^2 d\psi$$

and is given by

$$\mu(E) = \frac{4}{\pi \sqrt{2E}} \int_0^{\frac{\pi}{2}} D\left(\frac{\sqrt{2E}}{\omega_0} \sin \psi, \sqrt{2E} \cos \psi\right) \cos \psi d\psi \quad (11)$$

**Proposition 3** *If  $D(x, y)$  is even with respect  $x$  and odd with respect to  $y$ , then both the exact model (9) and the modified model (10) have the same Krylov-Bogoliubov approximation.*

*Proof:* For the exact model (9),

$$\frac{da(t)}{dt} = -\frac{1}{2\pi\omega_0} \int_0^{2\pi} D(a \sin \psi, a\omega_0 \cos \psi) \cos \psi d\psi \quad (12)$$

By the assumption on  $D(x, y)$ ,

$$\begin{aligned} \frac{d\phi(t)}{dt} &= \frac{1}{2\pi\omega_0 a} \int_0^{2\pi} D(a \sin \psi, a\omega_0 \cos \psi) \sin \psi d\psi \\ &= -\frac{1}{\pi\omega_0 a} \int_{-\frac{\pi}{2}}^{\frac{\pi}{2}} D(a \cos \psi, a\omega_0 \sin \psi) \cos \psi d\psi \\ &= 0 \end{aligned}$$

For the modified model (10), the Krylov-Bogoliubov approximation is given by

$$\begin{aligned}\frac{da(t)}{dt} &= -\frac{1}{2\pi\omega_0} \int_0^{2\pi} \mu\left(\frac{\omega_0^2 a^2}{2}\right) \omega_0 a \cos^2 \psi d\psi \\ &= -\frac{a}{2} \mu\left(\frac{\omega_0^2 a^2}{2}\right) \\ &= -\frac{1}{2\pi\omega_0} \int_0^{2\pi} D(a \sin \psi, \omega_0 a \cos \psi) \cos \psi d\psi \\ \frac{d\phi(t)}{dt} &= \frac{1}{2\pi\omega_0 a} \int_0^{2\pi} \mu\left(\frac{\omega_0^2 a^2}{2}\right) \omega_0 a \cos \psi \sin \psi d\psi \\ &= 0\end{aligned}$$

Therefore, (9) and (10) have the same Krylov-Bogoliubov approximation.  $\square$

The solution of the stationary Fokker-Planck equation corresponding to (10) is given by

$$p(x, y) = C \exp\left[-\frac{2}{\sigma^2} \int_0^{\frac{-\frac{1}{2}x^2 + y^2}{1}} \mu(z) dz\right] \quad (13)$$

where

$$\frac{1}{C} = \frac{2\pi}{\omega_0} \int_0^\infty \exp\left[-\frac{2}{\sigma^2} \int_0^\rho \mu(z) dz\right] d\rho \quad (14)$$

*Example:* Consider the following saturation type active damping model

$$\ddot{x} + 2\xi\omega_0\dot{x} + \lambda \tan^{-1}(b\dot{x}) + \omega_0^2 x = \sigma n(t) \quad (15)$$

By the identity

$$\int_0^{x/2} \tan^{-1}(b \cos x) \cos x dx = \frac{\pi}{2} \frac{\sqrt{1+b^2} - 1}{b} \quad b \in \mathbb{R}^1$$

one can compute

$$\begin{aligned}\mu(E) &= \frac{4}{\pi\sqrt{2E}} \int_0^{\frac{\pi}{2}} [2\xi\omega_0\sqrt{2E} \cos \psi + \lambda \tan^{-1}(b\sqrt{2E} \cos \psi)] \cos \psi d\psi \\ &= 2\xi\omega_0 + \lambda \frac{\sqrt{1+2b^2E} - 1}{bE}\end{aligned} \quad (16)$$

And consequently, one has

$$\begin{aligned} & -\frac{2}{\sigma^2} \int_0^E \mu(z) dz \\ &= -\frac{2\xi\omega_0}{\sigma^2} (2E) - \frac{4\lambda}{\sigma^2 b} \sqrt{1+2b^2 E} \\ & \quad + \frac{4\lambda}{\sigma^2 b} \ln[1 + \sqrt{1+2b^2 E}] + \text{const.} \end{aligned}$$

The solution of the stationary Fokker-Planck equation:

$$\begin{aligned} p(x, y) &= C [1 + \sqrt{1 + b^2(\omega_0^2 x^2 + y^2)}]^{\frac{4\lambda}{\sigma^2 b}} \\ & \times \exp\left[-\frac{2\xi\omega_0}{\sigma^2} (\omega_0^2 x^2 + y^2) - \frac{4\lambda}{\sigma^2 b} \sqrt{1 + b^2(\omega_0^2 x^2 + y^2)}\right] \end{aligned}$$

where

$$\begin{aligned} \frac{1}{C} &= \frac{\pi}{\omega_0 b^2} \exp\left(\frac{2\xi\omega_0}{\sigma^2 b^2}\right) \\ & \times \int_1^\infty (1 + \sqrt{x})^{\frac{4\lambda}{\sigma^2 b}} \exp\left[-\frac{2\xi\omega_0}{\sigma^2 b^2} x - \frac{4\lambda}{\sigma^2 b} \sqrt{x}\right] dx \end{aligned}$$

It is easy to realize that  $p(x, y)$  achieves maximum at the origin.

## 7 Concluding Remarks

A Method of Energy Approximation(MEA) is proposed for the investigation of nonlinear damping problem under random excitation. Closed form steady state density is obtained for the energy approximation model. It is shown through an example that MEA gives better accuracy than MEL and MEA reflects the nonlinear nature in the damping. This problem is pending further research. Problems such as spectral density of the nonlinear damping model, the absolute difference between the exact steady state density and the density obtained by MEA are under investigation by the author.

## References

- [1] *Proceedings of the 3rd NASA SCOLE Workshop*, Nov., 1986. Edited by L. W. Taylor.
- [2] A. V. Balakrishnan. Some nonlinear damping models in flexible structures. *Proceedings of the 4th NASA SCOLE Workshop*, Nov., 1987. Edited by L. W. Taylor.
- [3] A. T. Fuller. Analysis of nonlinear stochastic systems by means of the Fokker-Planck equation. *Int. J. Control*. Vol. 9, No. 6, 1969. 603-655
- [4] J. K. Hale. *Ordinary Differential Equations*. Wiley-Interscience, 1969.
- [5] N. Krylov and N. Bogoliubov. *Introduction to Non-linear Mechanics*. Princeton: Princeton University Press, 1949.

# **DAMPING OPERATORS IN CONTINUUM MODELS OF FLEXIBLE STRUCTURES**

**A. V. Balakrishnan<sup>†</sup>**

**UCLA**

<sup>†</sup> Research supported in part under Grant No. 88-0252, AFOSR, USAF.

To be published in the Proceedings of the "Workshop on Stabilization of Flexible Structures,"  
January 1989, Montpellier, France.

### Abstract

A new, explicit representation of damping operators for strictly proportional damping for the torsion mode of a finite beam with end mass is presented. The damping operator is the square root of the stiffness operator (enhanced to include the boundary) and is calculated using the Balakrishnan formula. It is nonlocal, and turns out to be a finite-limit version of the Hilbert transform for the clamped-clamped case. If strict proportionality is required, the operator is more general and involves boundary terms which, however, tend to zero as mode frequency increases.

## 1. Introduction

In the design of active controllers for stability augmentation of flexible structures it is naturally important to have a model for the inherent passive damping already present. Often it is assumed that the damping in each mode is strictly proportional to the mode frequency. If, as in [1], we formulate the problem in the abstract wave equation form as:

$$M\ddot{x}(t) + Ax(t) + 2\zeta D\dot{x}(t) + Bu_c(t) = 0,$$

for strictly proportional damping we will need to have

$$D = \sqrt{M} \sqrt{T} \sqrt{M}$$

where

$$T = \sqrt{M^{-1}} A \sqrt{M^{-1}}.$$

Usually  $M$  commutes with  $A$  so that

$$D = \sqrt{M} \sqrt{A}.$$

In any event we are left with the problem of calculating  $\sqrt{A}$ . In this, the first part of a two-part paper we calculate the square root for the case of a beam torsion model — or the familiar "string" equation. When the controls are on the boundary — as in current large space structure control design [2] — the square root introduces terms on the boundary. This should certainly be considered much more unnatural than the fact that the damping operators are nonlocal (*not* differential operators). Asymptotically however the modes do approach those of the clamped-clamped (or fixed-ends for the string case) beam. In particular for the clamped case the square root has the form of a "finite-limit" Hilbert transform. Our point of departure is the fractional-power formulas due to the author [3].



## 2. Beam Torsion Model

We begin with the torsional mode of vibration of a uniform Bernoulli beam of finite length, with one end fixed and the other end with control force. Thus we have:

$$\left. \begin{aligned} \rho a \frac{\partial^2 u(t, s)}{\partial t^2} - G I_{\Psi} \frac{\partial^2 u(t, s)}{\partial s^2} &= 0, \quad 0 < t; -\ell < s < \ell \\ u(t, -\ell) &= 0, \quad 0 \leq t \\ G I_{\Psi} u'(t, \ell) + I_4 \ddot{u}(t, \ell) + u_c(t) &= 0 \end{aligned} \right\} \quad (2.1)$$

where for our purposes we need only note that  $\rho a$ ,  $G I_{\Psi}$  and  $I_4$  are given positive constants.

The primes denote derivative with respect to  $s$ , and the superdots derivative with respect to  $t$ .

The abstract formulation is obtained by taking

$$\mathcal{H} = L_2[-\ell, \ell] \times R^1.$$

Let us use the following notation for elements in  $\mathcal{H}$ :

$$w \in \mathcal{H}; \quad w = \begin{bmatrix} u(\cdot) \\ b \end{bmatrix}, \quad u(\cdot) \in L_2[-\ell, \ell], \quad b \in R^1.$$

We shall shorten  $L_2[-\ell, \ell]$  to  $L_2$  in the sequel. Define the operator  $A$  with the domain in  $\mathcal{H}$  given by:

$$\mathcal{D}(A) = \left[ w = \begin{bmatrix} u(\cdot) \\ u(\ell) \end{bmatrix}, \quad u''(\cdot) \in L_2, \quad u(-\ell) = 0 \right]$$

(where primes denote derivatives with respect to the space variable), and

$$Aw = \begin{bmatrix} -u''(\cdot) \\ u'(\ell) \end{bmatrix}$$

mapping  $\mathcal{D}(A)$  into  $\mathcal{H}$ .

Then it is readily verified that  $A$  is closed, self-adjoint and,  $[\cdot, \cdot]$  denoting inner-product in  $\mathcal{H}$ :

$$[Aw, w] = \int_{-\ell}^{\ell} -u''(s) u(s) ds + u(\ell) u'(\ell) = \int_{-\ell}^{\ell} u'(s)^2 ds.$$

Hence  $A$  is nonnegative definite. Also  $A$  has a compact (Hilbert-Schmidt) resolvent and zero is in the resolvent set. As in [1] we may reformulate (2.1) as an abstract wave-equation in  $\mathcal{H}$ :

$$M\ddot{x}(t) + Ax(t) + Bu_c(t) = 0 \quad (2.2)$$

where  $B$  maps  $R^1$  into  $\mathcal{H}$  by

$$Bu = w = \begin{bmatrix} 0 \\ u/GI_\Psi \end{bmatrix}; \quad Mw = \begin{bmatrix} (\rho a^2/GI_\Psi)u(\cdot) \\ (I_4/GI_\Psi)b \end{bmatrix}. \quad (2.3)$$

Our first objective is to calculate the (positive) square root of  $A$  denoted  $\sqrt{A}$ . For this purpose it is helpful to use the notation

$$R(\lambda, -A) = (\lambda I + A)^{-1}$$

so that we can write the Balakrishnan formula [3] for the square root:

$$\sqrt{A}w = \frac{1}{\pi} \int_0^\infty \lambda^{-1/2} (\lambda I + A)^{-1} A w \, d\lambda, \quad \text{for } w \text{ in } \mathcal{D}(A). \quad (2.4)$$

It is convenient now to introduce the operator  $\alpha_0$  with domain in  $L_2$  with

$$\mathcal{D}(\alpha_0) = [u(\cdot) \mid u''(\cdot) \in L_2, u(-\ell) = 0 = u(\ell)]$$

and

$$\alpha_0 u = -u''.$$

Then  $\alpha_0$  is closed, self-adjoint and nonnegative definite and hence we may proceed to define  $\sqrt{\alpha_0}$ , by

$$\sqrt{\alpha_0} u = \frac{1}{\pi} \int_0^\infty \lambda^{-1/2} (\lambda I + \alpha_0)^{-1} \alpha_0 u \, d\lambda \quad (2.5)$$

Our first result is:

*Theorem 2.1.*

$$\mathcal{D}(\sqrt{\alpha_0}) = [u(\cdot) \mid u'(\cdot) \in L_2; u(-\ell) = 0 \text{ and } u(\ell) = 0] \quad (2.6)$$

and

$$\sqrt{\alpha_0} u = v$$

has the representation

$$v(s) = \frac{1}{2\ell} \int_{-\ell}^{\ell} \frac{\cos(\pi s/2\ell)}{\sin(\pi s/2\ell) - \sin(\pi \sigma/2\ell)} u'(\sigma) d\sigma, \quad \text{a.e. } -\ell < s < \ell. \quad (2.7)$$

*Proof.* We use (2.5). Let  $u \in \mathcal{D}(\alpha_0)$  and let:

$$\mu_0(\lambda) = (\lambda J + \alpha_0)^{-1} \alpha_0 u.$$

Then  $\mu_0(\lambda)$  is the unique solution of

$$\left. \begin{aligned} \lambda \mu_0(\lambda, s) - \mu_0''(\lambda, s) &= -u''(s) \\ \mu_0(\lambda, -\ell) &= \mu_0(\lambda, \ell) = 0 \end{aligned} \right\}$$

and is given by:

$$\begin{aligned} \mu_0(\lambda, s) &= \int_{-\ell}^s \frac{\sinh \sqrt{\lambda}(\ell-s) \sinh \sqrt{\lambda}(\ell+\sigma)}{\sqrt{\lambda} \sinh 2\sqrt{\lambda} \ell} (-u''(\sigma)) d\sigma \\ &\quad + \int_s^{\ell} \frac{\sinh \sqrt{\lambda}(\ell+s) \sinh \sqrt{\lambda}(\ell-\sigma)}{\sqrt{\lambda} \sinh 2\sqrt{\lambda} \ell} (-u''(\sigma)) d\sigma. \end{aligned}$$

Integration by parts yields

$$\begin{aligned} \mu_0(\lambda, s) &= \int_{-\ell}^s \frac{\sinh \sqrt{\lambda}(\ell-s) \cosh \sqrt{\lambda}(\ell+\sigma)}{\sinh 2\sqrt{\lambda} \ell} (u'(\sigma)) d\sigma \\ &\quad - \int_s^{\ell} \frac{\sinh \sqrt{\lambda}(\ell+s) \cosh \sqrt{\lambda}(\ell-\sigma)}{\sinh 2\sqrt{\lambda} \ell} (u'(\sigma)) d\sigma. \end{aligned} \quad (2.8)$$

Using the known formula: [6, p. 344]

$$\int_0^{\infty} \frac{\sinh ax \cosh bx}{\sinh cx} dx = \frac{\pi}{2c} \frac{\sin(a\pi/c)}{\cos(a\pi/c) + \cos(b\pi/c)}, \quad c > a+b,$$

we can see that for  $\sigma < s$

$$\begin{aligned} \frac{1}{\pi} \int_0^{\infty} \lambda^{-1/2} \frac{\sinh \sqrt{\lambda}(\ell-s) \cosh \sqrt{\lambda}(\ell+\sigma)}{\sinh 2\sqrt{\lambda} \ell} d\lambda \\ = \frac{2}{\pi} \int_0^{\infty} \frac{\sinh x(\ell-s) \cosh x(\ell+\sigma)}{\sinh 2x\ell} dx \\ = \frac{1}{2\ell} \frac{\cos(\pi s/2\ell)}{\sin(\pi s/2\ell) - \sin(\pi \sigma/2\ell)} \end{aligned} \quad (2.9)$$

and for  $s < \sigma$

$$\begin{aligned} -\frac{1}{\pi} \int_0^{\infty} \lambda^{-1/2} \frac{\sinh \sqrt{\lambda}(\ell+s) \cosh \sqrt{\lambda}(\ell-\sigma)}{\sinh 2\sqrt{\lambda} \ell} d\lambda \\ = -\frac{2}{\pi} \int_0^{\infty} \frac{\sinh x(\ell+s) \cosh x(\ell-\sigma)}{\sinh 2x\ell} dx \\ = \frac{1}{2\ell} \frac{\cos(\pi s/2\ell)}{\sin(\pi s/2\ell) - \sin(\pi \sigma/2\ell)}. \end{aligned}$$

Hence for a.e. in  $(-\ell, \ell)$

$$\frac{1}{\pi} \int_0^{\infty} \lambda^{-1/2} u(\lambda, s) d\lambda = \frac{1}{2\ell} \int_{-\ell}^{\ell} \frac{\cos(\pi s/2\ell)}{\sin(\pi s/2\ell) - \sin(\pi \sigma/2\ell)} u'(\sigma) d\sigma \quad (2.10)$$

providing of course that we can justify the change in order of integration. Let

$$H_F(s, \sigma) = \frac{1}{2\ell} \left( \frac{\cos \pi s/2\ell}{\sin \pi s/2\ell - \sin \pi \sigma/2\ell} \right) \quad -\ell < s, \sigma < \ell. \quad (2.11)$$

and let

$$v_F(s) = \int_{-\ell}^{\ell} H_F(s, \sigma) u'(\sigma) d\sigma$$

where  $u(\cdot) \in \mathcal{I}(\alpha_0)$ . We can decompose  $H_F(s, \sigma)$  as

$$H_F(s, \sigma) = \frac{1}{4\ell} \cot \frac{\pi(s - \sigma)}{4\ell} - \frac{1}{4\ell} \tan \frac{\pi(s + \sigma)}{4\ell}.$$

For any  $u(\cdot)$  in  $L_2$ ,

$$v_1(s) = \frac{1}{4\ell} \int_{-\ell}^{\ell} \left( \cot \frac{\pi(s - \sigma)}{4\ell} \right) u(\sigma) d\sigma, \quad -\ell < s < \ell$$

the integral taken in the Cauchy sense at  $s = \sigma$ , is defined wherever the Hilbert transform

$$\frac{1}{\pi} \int_{-\ell}^{\ell} \frac{u(\sigma)}{(s - \sigma)} d\sigma$$

is defined, and hence we note that  $v_1(\cdot)$  is actually also in  $L_2(-\ell, \ell)$ . Hence

$$v_2(s) = \frac{1}{4\ell} \int_{-\ell}^{\ell} \tan \frac{\pi(s + \sigma)}{4\ell} u'(\sigma) d\sigma$$

which is defined in the open interval  $-\ell < s < \ell$ , must be in  $L_2$ , if  $v_1(\cdot) + v_2(\cdot)$  is.

Next, for a finite  $L$ , we can clearly change the order of integration, and hence let:

$$v_L(s) = \frac{1}{\pi} \int_0^L u_0(\lambda, s) \lambda^{-1/2} d\lambda = \int_{-\ell}^{\ell} H(L, s, \sigma) u'(\sigma) d\sigma.$$

Let

$$\begin{aligned} R(L, s, \sigma) &= \frac{2}{\pi} \int_L^{\infty} \frac{\sinh x(\ell - s) \cosh x(\ell + \sigma)}{\sinh 2x\ell} dx, \quad -\ell < \sigma < s < \ell \\ &= -\frac{2}{\pi} \int_L^{\infty} \frac{\sinh x(\ell + s) \cosh x(\ell - \sigma)}{\sinh 2x\ell} dx, \quad -\ell < s < \sigma < \ell \end{aligned}$$

so that

$$v_F(s) - v_L(s) = \int_{-\ell}^{\ell} R(L, s, \sigma) u'(\sigma) d\sigma.$$

Now for  $x > L$  and  $L$  sufficiently large,

$$\frac{\sinh x(\ell - s) \cosh x(\ell + \sigma)}{\sinh 2x\ell} \sim e^{-x(s - \sigma)}, \quad s > \sigma$$

$$\frac{\sinh x(\ell+s) \cosh x(\ell-\sigma)}{\sinh 2x\ell} \sim e^{-x(\sigma-s)}, \quad \sigma > s.$$

Hence

$$R(L, s, \sigma) \sim \frac{2}{\pi} \frac{e^{-L(s-\sigma)}}{(s-\sigma)}, \quad s > \sigma$$

$$\sim -\frac{2}{\pi} \frac{e^{-L(\sigma-s)}}{(\sigma-s)}, \quad \sigma > s$$

and hence

$$\int_{-\ell}^{\ell} R(L, s, \sigma) u'(\sigma) d\sigma = \int_{|s-\sigma|>\ell} R(L, s, \sigma) u'(\sigma) d\sigma + \int_{|s-\sigma|\leq\ell} R(L, s, \sigma) u'(\sigma) d\sigma.$$

The first term goes to zero as  $L \rightarrow \infty$ , for any  $\ell > 0$ . The second term can be written

$$\frac{2}{\pi} \int_0^{\ell} \frac{u'(s+\tau) - u'(s-\tau)}{\tau} e^{-L\tau} d\tau$$

and since  $u(\cdot) \in \mathcal{I}(\alpha_0)$ ,

$$u'(s+\tau) - u'(s-\tau) = \int_{-\tau}^{\tau} u''(s+\sigma) d\sigma$$

goes to zero with  $\sqrt{\tau}$ . Hence  $v_L(s)$  converges to  $v_F(s)$ , a.e. in  $(-\ell, \ell)$ . But  $v_L(\cdot)$  converges to  $\sqrt{\alpha_0} u$  in  $L_2$  and hence

$$v_F(\cdot) = \sqrt{\alpha_0} u,$$

or we have justified changing the order of integration. Of course, we have also proved that  $v_F(\cdot)$  defined by (2.12) is actually in  $L_2$ , for  $u$  in  $\mathcal{I}(\alpha_0)$ .

Let us next establish (2.6). The orthonormalized eigenfunctions of  $\alpha_0$  are

$$\phi_k(s) = \frac{1}{\sqrt{\ell}} \sin \frac{k\pi(s+\ell)}{2\ell}, \quad -\ell < s < \ell$$

and

$$\sqrt{\alpha_0} \phi_k = \frac{k\pi}{2\ell} \phi_k.$$

Hence for  $\lambda > 0$ ,

$$(\sqrt{\alpha_0} + \lambda J)g = f$$

has the solution

$$g = \sum_1^{\infty} \frac{[f, \phi_k]}{\lambda + \frac{k\pi}{2\ell}} \phi_k$$

where the series is absolutely convergent. Hence

$$g(\ell) = 0.$$

Also term-wise differentiation is valid, showing that  $g'(\cdot) \in L_2$ .

Since the domain of  $\sqrt{\alpha_0}$  is precisely the range of the resolvent  $(\lambda + \sqrt{\alpha_0})^{-1}$ , it follows that for  $g$  in the domain of  $\sqrt{\alpha_0}$  we must have that

$$g(\ell) = 0; \quad g'(\cdot) \in L_2.$$

Conversely for any  $g$  in  $L_2$  with these properties we can find a sequence  $u_n$  in  $\mathcal{D}(\alpha_0)$  such that  $u_n'$  converges to  $g'(\cdot)$  in  $L_2$ , and  $u_n$  converges to  $g$ . We have only to take, for example

$$u_n = n(n + \alpha_0)^{-1} g = \sum_1^{\infty} \frac{n}{n + \left(\frac{k\pi}{2\ell}\right)^2} [g, \phi_k] \phi_k.$$

Then

$$\|\sqrt{\alpha_0}(u_n - u_{n+p})\|^2 = \|u_n' - u_{n+p}'\|^2.$$

Hence  $\sqrt{\alpha_0} u_n$  converges. Hence it follows that  $g \in \mathcal{D}(\sqrt{\alpha_0})$ , or (2.6) is proved. Also

$$\sqrt{\alpha_0} u_n = v_n$$

where

$$\begin{aligned} v_n(s) &= \int_{-t}^t H_F(s, \sigma) u_n'(\sigma) d\sigma \\ &= \frac{1}{4\ell} \int_{-t}^t \cot \frac{\pi(s - \sigma)}{4\ell} u_n'(\sigma) d\sigma - \frac{1}{4\ell} \int_{-t}^t \tan \frac{\pi(s + \sigma)}{4\ell} u_n'(\sigma) d\sigma \end{aligned}$$

where the first term converges in  $L_2$  and the second term for each  $|s| < \ell$ . Hence it follows

that if

$$v = \lim_n v_n,$$

$$v(s) = \int_{-\ell}^{\ell} H_F(s, \sigma) g'(\sigma) d\sigma, \quad \text{a.e., } -\ell < s < \ell.$$

Hence for every  $g$  in  $\mathfrak{L}(\sqrt{\alpha_0})$  we have the representation above.

Let us note in conclusion that

$$v(s) = \int_{-\ell}^{\ell} H_F(s, \sigma) u(\sigma) d\sigma$$

is defined a.e. in  $(-\ell, \ell)$  for every  $u(\cdot)$  in  $L_2$ , but  $v_F(\cdot)$  is in  $L_2$  if (and in fact only if)

$$\int_{-\ell}^{\ell} u(\sigma) d\sigma = 0.$$

Finally, for  $\ell = +\infty$ , it is known (see [4, 5] for example) that  $\sqrt{\alpha_0} u$  is  $Hu'$  where  $H$  is the Hilbert transform. Hence (2.12) may be viewed as the Finite-limit Hilbert transform, new with this paper.

We can now get back to  $\sqrt{A}$ .

*Theorem 2.2.*

$$\mathfrak{L}(\sqrt{A}) = \left[ w: \begin{vmatrix} u(\cdot) \\ u(\ell) \end{vmatrix}, u(\cdot) \in L_2, u(-\ell) = 0 \right]$$

and we have the representation:

$$\sqrt{A} w = \sqrt{A} \begin{vmatrix} u(\cdot) \\ u(\ell) \end{vmatrix} = D_0 w + \mathcal{T} w \quad (2.12)$$

where  $\mathcal{T}$  is a compact linear bounded operator on  $\mathfrak{H}$  into  $\mathfrak{H}$ , and  $D_0$  has the same domain as  $\sqrt{A}$  and is closed thereon, and has the form:

$$D_0 w = \begin{vmatrix} Lu'(\cdot) + u(\ell)\phi \\ [h, u'] \end{vmatrix}$$

where  $L$  is linear-bounded on  $L_2$  into  $L_2$ , and  $h(\cdot) \in L_2$ ,  $\phi(\cdot) \in L_2$



*Proof.* We use (2.5). Let  $w \in \mathfrak{L}(A)$ ; and

$$w = \begin{vmatrix} u(\cdot) \\ u(\ell) \end{vmatrix}.$$

Let

$$w(\lambda) = (\lambda I + A)^{-1} A w, \quad \lambda > 0.$$

Then

$$w(\lambda) = \begin{vmatrix} u(\lambda, \cdot) \\ u(\lambda, \ell) \end{vmatrix}$$

is the unique solution of

$$\lambda u(\lambda, s) - u''(\lambda, s) = -u''(s), \quad -\ell < s < \ell$$

$$\lambda u(\lambda, \ell) + u'(\lambda, \ell) = u'(\ell)$$

$$u(\lambda, -\ell) = 0.$$

Let, as in the proof of Theorem 2.1,

$$u_0(\lambda, \cdot) = (\lambda + \alpha_0)^{-1} \alpha_0 u(\cdot),$$

and let

$$z(\lambda, s) = u(\lambda, s) - u_0(\lambda, s).$$

Then  $z(\lambda, \cdot)$  is the unique solution of

$$\lambda z(\lambda, s) - z''(\lambda, s) = 0$$

$$z(\lambda, -\ell) = 0$$

$$\lambda z(\lambda, \ell) + z'(\lambda, \ell) = u'(\ell) - u_0'(\lambda, \ell).$$

Hence

$$z(\lambda, s) = a(\lambda) \sinh \sqrt{\lambda} (\ell + s) \tag{2.13}$$

$$a(\lambda)(\lambda \sinh 2\sqrt{\lambda} \ell + \sqrt{\lambda} \cosh 2\sqrt{\lambda} \ell) = u'(\ell) - u_0'(\lambda, \ell).$$

But

$$u_0'(\lambda, s) = u'(s) - \int_{-l}^s \sqrt{\lambda} \frac{\cosh \sqrt{\lambda}(\ell-s) \cosh \sqrt{\lambda}(\ell+\sigma)}{\sinh 2\sqrt{\lambda} \ell} u'(\sigma) d\sigma \\ - \int_s^{\ell} \sqrt{\lambda} \frac{\cosh \sqrt{\lambda}(\ell+s) \cosh \sqrt{\lambda}(\ell-\sigma)}{\sinh 2\sqrt{\lambda} \ell} u'(\sigma) d\sigma.$$

Hence

$$a(\lambda) = \int_{-l}^{\ell} \frac{\cosh \sqrt{\lambda}(\ell+\sigma)}{(\sinh 2\sqrt{\lambda} \ell)(\sqrt{\lambda} \sinh 2\sqrt{\lambda} \ell + \cosh 2\sqrt{\lambda} \ell)} u'(\sigma) d\sigma. \quad (2.14)$$

Hence

$$\frac{1}{\pi} \int_0^{\infty} \lambda^{-1/2} z(\lambda, s) d\lambda \\ = \frac{1}{\pi} \int_0^{\infty} \lambda^{-1/2} d\lambda \int_{-l}^{\ell} \frac{\sinh \sqrt{\lambda}(\ell+s) \cosh \sqrt{\lambda}(\ell+\sigma)}{(\sinh 2\sqrt{\lambda} \ell)(\sqrt{\lambda} \sinh 2\sqrt{\lambda} \ell + \cosh 2\sqrt{\lambda} \ell)} u'(\sigma) d\sigma \quad (2.15)$$

$$= \frac{2}{\pi} \int_0^{\infty} \frac{dx}{(\sinh 2x\ell)(x \sinh 2x\ell + \cosh 2x\ell)} \left( \int_{-l}^{\ell} \sinh x(\ell+s) (\cosh x(\ell+\sigma)) u'(\sigma) d\sigma \right) \quad (2.16)$$

and the second integral in parenthesis can be expressed

$$\frac{1}{2} \int_{-l}^{\ell} (\sinh x(2\ell+s+\sigma)) u'(\sigma) d\sigma + \frac{1}{2} \int_{-l}^{\ell} (\sinh x(s-\sigma)) u'(\sigma) d\sigma. \quad (2.17)$$

The second integral in (2.17) can be integrated by parts to yield

$$= \frac{1}{2} (\sinh x(s-l)) u(l) + \frac{1}{2} \int_{-l}^{\ell} x (\cosh x(s-\sigma)) u(\sigma) d\sigma.$$

Hence (2.15) can be expressed

$$\frac{1}{\pi} \int_0^{\infty} \frac{dx}{(\sinh 2x\ell)(x \sinh 2x\ell + \cosh 2x\ell)} \int_{-l}^{\ell} (\sinh x(2\ell+s+\sigma)) u'(\sigma) d\sigma \\ + \int_{-l}^{\ell} M(s, \sigma) u(\sigma) d\sigma + \phi(s) u(l) \quad (2.18)$$

where

$$\phi(s) = \frac{1}{\pi} \int_0^{\infty} \frac{\sinh x(s-\ell)}{\sinh 2x\ell} \frac{1}{(x \sinh 2x\ell + \cosh 2x\ell)} dx, \quad -\ell \leq s \leq \ell \quad (2.19)$$

and is an absolutely continuous function which goes to zero as  $\ell \rightarrow \infty$ , and the kernel  $M(\cdot, \cdot)$  is given by

$$M(s, \sigma) = \frac{1}{\pi} \int_0^{\infty} \frac{x \cosh x(s-\sigma)}{(\sinh 2x\ell)(x \sinh 2x\ell + \cosh 2x\ell)} dx \quad (2.20)$$

and is absolutely continuous in  $-\ell \leq s, \sigma \leq \ell$ , (and also goes to zero as  $\ell \rightarrow \infty$ ). Hence

$$\begin{aligned} & \frac{1}{\pi} \int_0^{\infty} \lambda^{-1/2} u(\lambda, s) d\lambda \\ &= \phi(s)u(\ell) + \int_{-\ell}^{\ell} M(s, \sigma)u(\sigma) d\sigma \\ &+ \frac{1}{\pi} \int_0^{\infty} \frac{dx}{(\sinh 2x\ell)(x \sinh 2x\ell + \cosh 2x\ell)} \int_{-\ell}^{\ell} \sinh x(2\ell + s + \sigma)u'(\sigma) d\sigma \\ &+ \frac{2}{\pi} \int_0^{\infty} dx \frac{\sinh x(\ell - s)}{\sinh 2x\ell} \int_{-\ell}^s \cosh x(\ell + \sigma)u'(\sigma) d\sigma \\ &- \frac{2}{\pi} \int_0^{\infty} dx \frac{\sinh x(\ell + s)}{\sinh 2x\ell} \int_s^{\ell} \cosh x(\ell - \sigma)u'(\sigma) d\sigma. \end{aligned}$$

We now combine the last three terms and then justify interchanging the order of integration. The sum of the last three terms can be expressed as:

$$\begin{aligned} &= \frac{1}{\pi} \int_0^{\infty} \frac{dx}{(\sinh 2x\ell)(x \sinh 2x\ell + \cosh 2x\ell)} \int_{-\ell}^{\ell} \sinh x(2\ell + s + \sigma)u'(\sigma) d\sigma \\ &- \frac{1}{\pi} \int_0^{\infty} \frac{dx}{\sinh 2x\ell} \int_{-\ell}^{\ell} \sinh x(s + \sigma)u'(\sigma) d\sigma \\ &+ \frac{1}{\pi} \int_0^{\infty} \frac{dx}{\sinh 2x\ell} \int_{-\ell}^s \sinh x(2\ell + \sigma - s)u'(\sigma) d\sigma \\ &- \frac{1}{\pi} \int_0^{\infty} \frac{dx}{\sinh 2x\ell} \int_s^{\ell} \sinh x(2\ell + s - \sigma)u'(\sigma) d\sigma. \end{aligned}$$

The sum of the first two terms

$$v_3(s) = \frac{1}{\pi} \int_0^{\infty} \frac{dx}{(x \sinh 2x\ell + \cosh 2x\ell)} \int_{-\ell}^{\ell} (\cosh x(s+\sigma) - x \sinh x(s+\sigma)) u'(\sigma) d\sigma \quad (2.21)$$

For  $w(\cdot)$  in  $\mathcal{D}(A)$ ,  $u''(\cdot)$  is in  $L_2$ , and hence we can change the order of integration in the last two terms and express their sum as:

$$v_4(s) = \frac{1}{4\ell} \int_{-\ell}^{\ell} u'(\sigma) \cot \frac{\pi(s-\sigma)}{4\ell} d\sigma, \quad -\ell < s < \ell. \quad (2.22)$$

Defined wherever the Hilbert transform is,

$$v(s) = \frac{1}{4\ell} \int_{-\ell}^{\ell} u(\sigma) \cot \frac{\pi(s-\sigma)}{4\ell} d\sigma, \quad -\ell < s < \ell \quad (2.23)$$

yields a bounded linear transformation mapping  $L_2$  into  $L_2$ . It follows in particular that  $v_3(\cdot)$  is in  $L_2$ . Let

$$K(L, s, \sigma) = \int_0^L \left( \frac{\cosh x(s+\sigma) - x \sinh x(s+\sigma)}{x \sinh 2x\ell + \cosh 2x\ell} \right) dx$$

and

$$K(t) = \frac{1}{\pi} \int_0^{\infty} \left( \frac{\cosh tx - x \sinh tx}{x \sinh 2x\ell + \cosh 2x\ell} \right) dx, \quad -2\ell < t < 2\ell. \quad (2.24)$$

Then

$$\int_{-\ell}^{\ell} K(L, s, \sigma) u'(\sigma) d\sigma, \quad -\ell < s < \ell$$

converges in  $L_2$  to  $v_3(\cdot)$  as  $L \rightarrow \infty$ . Now

$$|K(s+\sigma)| = O\left(\frac{2}{2\ell - s - \sigma}\right), \quad (s+\sigma) < 2\ell$$

and hence the integral

$$\int_{-\ell}^{\ell} K(s+\sigma) u'(\sigma) d\sigma$$

is defined for each  $s$ ,  $s \neq \ell$ . Also for some  $M < \infty$ ,

$$\begin{aligned} \int_{-\ell}^{\ell} |K(s+\sigma) - K(L, s, \sigma)| |u'(\sigma)| d\sigma &\leq M \int_{-\ell}^{\ell} \frac{e^{-L(2\ell-s-\sigma)}}{2\ell-s-\sigma} |u'(\sigma)| d\sigma \\ &\leq \frac{e^{-L(2\ell-s)}}{2\ell-s} M \int_{-\ell}^{\ell} |u'(\sigma)| d\sigma \end{aligned}$$

and hence

$$v_3(s) = \int_{-\ell}^{\ell} K(s+\sigma) u'(\sigma) d\sigma, \quad -\ell < s < \ell. \quad (2.25)$$

Hence finally, we have, for  $w$  in  $\mathcal{D}(A)$ :

$$\sqrt{A} w = \sqrt{A} \begin{pmatrix} u(\cdot) \\ u(\ell) \end{pmatrix} = \begin{pmatrix} v(\cdot) \\ v(\ell) \end{pmatrix}$$

where

$$v(s) = v_1(s) + v_2(s) + v_3(s)$$

where

$$v_1(s) = \phi(s) u(\ell) + \int_{-\ell}^{\ell} M(s, \sigma) u(\sigma) d\sigma$$

$$v_2(s) = \frac{1}{4\ell} \int_{-\ell}^{\ell} u'(\sigma) \cot \frac{\pi(s-\sigma)}{4\ell} d\sigma$$

$$v_3(s) = \int_{-\ell}^{\ell} K(s+\sigma) u'(\sigma) d\sigma.$$

Next let us calculate

$$\begin{aligned} \int_0^{\infty} \lambda^{-1/2} u(\lambda, \ell) d\lambda &= \int_0^{\infty} \lambda^{-1/2} z(\lambda, \ell) d\lambda, \quad (\text{since } u_0(\lambda, \ell) = 0) \\ &= \frac{2}{\pi} \int_0^{\infty} dx \int_{-\ell}^{\ell} \frac{\cosh x(\ell+\sigma)}{x \sinh 2x\ell + \cosh 2x\ell} u'(\sigma) d\sigma. \end{aligned} \quad (2.26)$$

Now

$$\left| \int_{-\ell}^{\ell} \cosh x(\ell + \sigma) u'(\sigma) d\sigma \right| \leq \int_{-\ell}^{\ell} \cosh x(\ell + \sigma) |u'(\sigma)| d\sigma$$

$$\leq \|u'(\cdot)\| \sqrt{\int_{-\ell}^{\ell} \cosh^2 x(\ell + \sigma) d\sigma}$$

and

$$\int_{-\ell}^{\ell} \cosh^2 x(\ell + \sigma) d\sigma = \frac{\sinh 4x\ell}{2x} \left( 1 + \frac{2x\ell}{\sinh 4x\ell} \right).$$

Hence (2.26) is smaller in absolute value than

$$\|u'(\cdot)\| \int_0^{\infty} \frac{\sqrt{\sinh 4x\ell} \sqrt{1 + \frac{2x\ell}{\sinh 4x\ell}}}{\sqrt{2x} (x \sinh 2x\ell + \cosh 2x\ell)} dx$$

and because of the presence now of  $\sqrt{x}$  in the denominator, the integral is readily verified to be finite. Hence we can change the order of integration in (2.26) and express it as

$$\int_{-\ell}^{\ell} h(s) u'(s) ds \quad (2.27)$$

where  $h(\cdot)$  is defined for  $-\ell \leq s < \ell$  by

$$h(s) = \int_0^{\infty} \frac{\cosh x(\ell + s)}{x \sinh 2x\ell + \cosh 2x\ell} dx \quad (2.28)$$

and is positive for every  $s$ . Moreover since

$$\left( \int_{-\ell}^{\ell} h(s) |u'(s)| ds \right) \leq \|u'(\cdot)\| \cdot \text{const.}$$

it is clear that

$$\int_{-\ell}^{\ell} h(s) u(s) ds$$

defines a continuous linear functional on  $L_2$  and in particular

$$\int_{-\ell}^{\ell} h(s)^2 ds < \infty.$$

Define the operators on  $L_2$  into  $L_2$ :

$$v = Tu; \quad v(s) = \phi(s)u(\ell) + \int_{-\ell}^{\ell} M(s, \sigma)u(\sigma) d\sigma. \quad (2.29)$$

and

$$v = Hu; \quad v(s) = \int_{-\ell}^{\ell} u(\sigma) \cot \frac{\pi(s - \sigma)}{4\ell} d\sigma, \quad \text{a.e. } -\ell < s < \ell, \quad (2.30)$$

where the integral is defined in the Cauchy sense at  $s = \sigma$ . Then for  $w$  in  $\mathcal{D}(A)$ :

$$\sqrt{A} w = \begin{vmatrix} v(\cdot) \\ \int_{-\ell}^{\ell} h(s)u'(s) ds \end{vmatrix}$$

where

$$v(s) = v_1(s) + v_2(s) + v_3(s), \quad \text{a.e.},$$

where

$$\begin{aligned} v_1 &= Tu \\ v_2 &= Hu' \\ v_3(s) &= \int_{-\ell}^{\ell} K(s + \sigma)u'(\sigma) d\sigma \end{aligned} \quad (2.31)$$

Next we let  $w \in \mathcal{D}(\sqrt{A})$ . Then we can find  $w_n \in \mathcal{D}(A)$  such that

$$w_n \rightarrow w$$

and

$$\sqrt{A} w_n \rightarrow \sqrt{A} w.$$

Let

$$w_n = \begin{vmatrix} u_n(\cdot) \\ u_n(\ell) \end{vmatrix}$$

$$\|\sqrt{A} w_n - \sqrt{A} w_m\|^2 = \|u_n' - u_m'\|^2$$

and hence  $u_n'(\cdot)$  converges in  $L_2$  to  $u'$ , where

$$w = \begin{vmatrix} u(\cdot) \\ u(\ell) \end{vmatrix}, \quad \text{and } u' \in L_2.$$

$$Tu_n + Hu_n' \rightarrow Tu + Hu'.$$

Hence

$$v_{3,n}(s) = \int_{-\ell}^{\ell} K(s + \sigma) u_n'(\sigma) d\sigma, \quad -\ell \leq s < \ell$$

is such that

$$v_{3,n}(\cdot)$$

converges in  $L_2$ . But for each  $s$ ,  $s < \ell$ , we do have that

$$\int_{-\ell}^{\ell} K(s + \sigma) u_n'(\sigma) d\sigma \rightarrow \int_{-\ell}^{\ell} K(s + \sigma) u'(\sigma) d\sigma.$$

Hence

$$\int_{-\ell}^{\ell} K(s + \sigma) u'(\sigma) d\sigma, \quad \text{a.e. } -\ell < s < \ell$$

is in  $L_2$ . Now given any  $z(\cdot)$  in  $L_2$ , we can define

$$u(s) = \int_{-\ell}^s z(\sigma) d\sigma$$

and

$$\int_{-\ell}^{\ell} K(s + \sigma) z(\sigma) d\sigma = \int_{-\ell}^{\ell} K(s + \sigma) u'(\sigma) d\sigma.$$

Hence it follows that



$$Ku = v; \quad v(s) = \int_{-\ell}^{\ell} K(s+\sigma)u(\sigma) d\sigma \quad (2.32)$$

actually defines a linear bounded operator on  $L_2$  into  $L_2$ .

Next let us consider the sequence

$$\int_{-\ell}^{\ell} h(s)u_n'(s) ds.$$

This sequence converges to

$$[h, u']$$

since  $u_n'$  converges to  $u'$ .

Let us next show that any  $w$  in  $\mathcal{H}$  of the form

$$w = \begin{vmatrix} u(\cdot) \\ u(\ell) \end{vmatrix}, \quad u(-\ell) = 0,$$

where  $u(\cdot) \in L_2$  belongs to  $\mathcal{I}(\sqrt{A})$ . Then we can find  $u_n$  in  $L_2$  such that

$$u_n(-\ell) = 0$$

$$u_n'(\cdot) \in L_2$$

and such that  $u_n'(\cdot)$  converges to  $u'(\cdot)$  in  $L_2$ . Let

$$w_n = \begin{vmatrix} u_n(\cdot) \\ u_n(\ell) \end{vmatrix}.$$

Then  $w_n \in \mathcal{I}(A)$  and

$$w_n \rightarrow w.$$

Also

$$\|\sqrt{A} w_n - \sqrt{A} w_m\|^2 = \int_{-\ell}^{\ell} |u_n'(s) - u_m'(s)|^2 ds$$

and hence

$$\sqrt{A} w_n \text{ converges.}$$

Hence  $w \in \mathfrak{I}(\sqrt{A})$ .

Thus finally for any  $w$  in  $\mathfrak{I}(\sqrt{A})$  we have the representation

$$w = \begin{vmatrix} u(\cdot) \\ u(\ell) \end{vmatrix}$$

$$\sqrt{A} w = \begin{vmatrix} v(\cdot) \\ [h, u'] \end{vmatrix}$$

where

$$v = Hu' + Ku' + Tu.$$

We can decompose  $\sqrt{A} w$  in various ways. For instance let  $L = H + K$ , and

$$D_0 w = \begin{vmatrix} Lu' + u(\ell)\phi \\ [h, u'] \end{vmatrix}$$

on  $\mathfrak{I}(\sqrt{A})$ . Then  $D_0$  is closed thereon. Let

$$\mathcal{T}w = \begin{vmatrix} Mu \\ 0 \end{vmatrix},$$

where

$$Mu = v; \quad v(s) = \int_{-\ell}^{\ell} M(s, \sigma) u(\sigma) d\sigma.$$

and  $M(\cdot, \cdot)$  is given by (2.20). Then  $\mathcal{T}$  is compact and we have representation (2.12).

### 3. Strictly Proportional Damping

It is known [1] that to obtain a "strictly proportional" damping model where the damping is strictly proportional to the mode frequency, the abstract wave-equation (2.2) must have an additional damping operator and be reformulated as:

$$M\ddot{x}(t) + Ax(t) + D\dot{x}(t) + Bu_c(t) = 0 \quad (3.1)$$

where, as in our case,  $M$  commutes with  $A$ , we must have

$$D = 2\zeta\sqrt{M}\sqrt{A} \quad (3.2)$$

where  $\zeta$  is the damping constant,  $0 < \zeta < 1$ . The eigenvectors  $\phi_k$  of  $A$ , defined by

$$A\phi_k = \omega_k^2 M\phi_k$$

and

$$\phi_k(s) = a_k \sin \omega_k \sqrt{\rho a / GI_\Psi} (\ell + s), \quad -\ell \leq s \leq \ell$$

where  $\omega_k$  satisfies

$$\phi_k'(\ell) = \omega_k^2 \left( \frac{I_A}{GI_\Psi} \right) \phi_k(\ell)$$

and as a result

$$\left| \omega_k - \frac{k\pi}{2\ell} \sqrt{\frac{GI_\Psi}{\rho a}} \right| < \frac{\pi}{4\ell} \sqrt{\frac{GI_\Psi}{\rho a}} \quad (3.3)$$

Rewriting (3.1) as:

$$\dot{Y}(t) = AY(t) + Bu_c(t) \quad (3.4)$$

where

$$A = \begin{bmatrix} 0 & I \\ -M^{-1}A & -M^{-1}D \end{bmatrix}$$

$$Bu_c = \begin{bmatrix} 0 \\ -M^{-1}Bu_c \end{bmatrix}$$

where

$$Y = \begin{bmatrix} x_1 \\ x_2 \end{bmatrix}, \quad \begin{array}{l} x_1 \in \mathfrak{I}(\sqrt{A}) \\ x_2 \in \mathfrak{K} \end{array}$$

and we introduce the energy inner product on  $\mathfrak{I}(\sqrt{A}) \times \mathfrak{K}$  by

$$\|Y\|^2 = [\sqrt{A} x_1, \sqrt{A} x_2] + [M x_2, x_2]$$

the eigenvectors of  $A$  are given by

$$\Psi_k^1 = \begin{bmatrix} \phi_k \\ \gamma \omega_k \phi_k \end{bmatrix}; \quad \Psi_k^2 = \overline{\Psi_k^1}$$

and the eigenvalues are

$$\lambda_k = -\zeta \omega_k \pm i \omega_k \sqrt{1 - \zeta^2}$$

where

$$\gamma = -\zeta + i \sqrt{1 - \zeta^2}.$$

We have thus strictly proportional damping in the sense that

$$\left| \frac{\operatorname{Re} \lambda_k}{\operatorname{Im} \lambda_k} \right| = \text{constant} = \frac{\zeta}{\sqrt{1 - \zeta^2}}.$$

The concrete version of (3.1) is

$$\rho a \frac{\partial^2 u(t, s)}{\alpha + 2} - G I_{\Psi} \frac{\partial^2 u(t, s)}{\alpha s^2} + 2 \zeta (\sqrt{\rho a G I_{\Psi}}) \left( \phi(s) \frac{d}{dt} u(t, \ell) \right. \quad (3.5)$$

$$\left. + \int_{-\ell}^{\ell} R(s, \sigma) \frac{\partial^2 u(t, \sigma)}{\partial t \partial \sigma} d\sigma + \int_{-\ell}^{\ell} M(s, \sigma) \frac{\partial}{\partial t} u(t, \sigma) d\sigma \right) = 0$$

$$G I_{\Psi} u'(t, \ell) + I_4 \ddot{u}(t, \ell) + 2 \zeta \sqrt{I_4 G I_{\Psi}} \int_{-\ell}^{\ell} h(s) \frac{\partial^2}{\partial t \partial s} u(t, s) ds + u_c(t) = 0 \quad (3.6)$$

where

$$R(s, \sigma) = \frac{1}{4\ell} \cot \frac{\pi(s - \sigma)}{4\ell} + K(s + \sigma).$$

The main unnatural feature of this operator is the presence of the new terms in the boundary equation (3.6). Unfortunately, this is essential for strictly proportional damping. It would be interesting to search for an operator without this feature that yet retains asymptotically proportional damping:

$$\lim_k \left| \frac{\operatorname{Re} \lambda_k}{\operatorname{Im} \lambda_k} \right| = \frac{\zeta}{\sqrt{1 - \zeta^2}}.$$

In particular this would also retain the main feature of (3.4) in that  $\mathcal{A}$  generates an analytic semigroup [1]. Of course the eigenfunctions  $\phi_k(\cdot)$  approach those of  $\alpha_0$  as  $k \rightarrow \infty$ , because of (3.3) —  $\phi_k(\ell)$  goes to zero as  $k \rightarrow \infty$ .

## References

- [1] A. V. Balakrishnan. "Control of Flexible Flight Structures." In *Mathematique et Applications*. Paris: Gauthier-Villars, 1988. Pp. 23-34.
- [2] L. W. Taylor and A. V. Balakrishnan. "A Mathematical Problem and a Spacecraft Control Laboratory Experiment (SCOLE) Used to Evaluate Control Laws for Flexible Spacecraft, NASA/IEEE Design Challenge." In *Proceedings of the NASA SCOLE Workshop*. NASA Langley Research Center, December 1984.
- [3] A. V. Balakrishnan. "Fractional Powers of Closed Operators and the Semigroups Generated by Them." *Pacific Journal of Mathematics*, 1960, pp. 417-437.
- [4] E. Hille and R. S. Phillips. *Functional Analysis and Semigroups*. Amer. Math. Soc. Colloquium Publications, Vol. 31. Providence, Rhode Island: 1957.
- [5] H. Fattorini. *Cauchy Problem*. New York: Addison-Wesley Publishing Company, 1983.
- [6] I. S. Gradshteyn and I. M. Ryzhik. *Table of Integrals, Series and Products*. New York: Academic Press, 1980.

## A Special Class of Nonlinear Damping Models in Flexible Space Structures

Anten Hu<sup>1</sup>, Dynacs Engineering Corporation

Clearwater Florida

Lawrence W. Taylor<sup>2</sup>, NASA Langley Research Center

Hampton Virginia

Ramendra P. Singh<sup>3</sup>, Dynacs Engineering Corporation

Clearwater Florida

<sup>1</sup>Research Engineer, Member AIAA

<sup>2</sup>Chief Scientist, Associate Fellow of AIAA

<sup>3</sup>President, Associate Fellow of AIAA

### Abstract

A special class of nonlinear damping models is investigated in which the damping force is proportional to the product of positive integer or the fractional power of the absolute values of displacement and velocity. For a one degree of freedom system, the classical Krylov-Bogoliubov "averaging" method is used, whereas for a distributed system, both an ad hoc perturbation technique and the finite difference method are employed to study the effects of nonlinear damping. The results are compared with linear viscous damping models. The amplitude decrement of free vibration for a single mode system with nonlinear models depends not only on the damping ratio, but also on the initial amplitude, the time to measure the response, the frequency of the system, and the powers of displacement and velocity. For the distributed system, the action of nonlinear damping is found to reduce the energy of the system and to pass energy to lower modes.

### 1.0 Introduction

One of the major challenges remaining in the development of large space structures is to determine a damping mechanism in order to stabilize flexible flight structures such as solar arrays, antennas and platforms. As the size and flexibility of space structures increase, the need to characterize energy dissipation in a more appropriate and accurate manner also increases. Under the assumption of linear viscous damping, the amplitude decrement of free vibration depends only on the damping ratio, regardless of what the frequency or initial condi-



tions might be. Numerous experimental results, such as those in the Spacecraft Control Laboratory Experiment (SCOLE)<sup>[1,2]</sup>, indicate that this is far from sufficient and that there is a great need for understanding the damping mechanism which may be inherently nonlinear.

Various nonlinear models, such as linear dampers with clearance, Coulomb friction dampers, velocity- $n$ th power damping, etc., have been investigated in the past <sup>[3-5]</sup>. In many cases, these models can be represented by a damping force that is proportional to the product of integer or fractional powers of the absolute values of displacement and velocity. Balakrishnan introduced this nonlinear model in <sup>[6]</sup> and obtained approximate solutions using the Krylov-Bogoliubov "averaging" method <sup>[7]</sup>. He also showed that these results can be quite useful to study the response of flexible structures to nonlinear boundary feedback control. In this paper we further study this special class of nonlinear damping models. We use the Krylov-Bogoliubov "averaging" technique for a one degree of freedom system and employ both an ad hoc perturbation method and a finite difference technique for a distributed system.

This paper is organized as follows. In Section 2, the approximate equations of amplitude are derived for a single degree of freedom system with nonlinear damping. In Section 3, the transient response of free vibration of a single mode nonlinear system is compared to that of a system with linear viscous damping. In Section 4, the perturbation solution is derived for the vibration of a pinned-pinned beam with nonlinear damping. In Section 5, the vibration of the

pinned-pinned beam with nonlinear damping is simulated via finite-difference methods and the results are compared with those obtained using the perturbation solution discussed in Section 4.

## 2.0 Single Degree of Freedom System

The classical Krylov-Bogoliubov "averaging" method, introduced in 1947, is basically a method of variation of parameters. Over the decades, this averaging technique has been employed to study nonlinear mechanics and solutions can be found in the literature [8] for special cases of nonlinear differential equations. Balakrishnan applied this averaging method to a particular class of nonlinear damping models [6] which will be discussed in detail in this section. Since this damping model is representative of a variety of nonlinear damping mechanisms, we further study the effects of the model on vibrating structures of the special class of nonlinear damping represented as

$$m\ddot{x} + c|x|^a|\dot{x}|^b\dot{x} + kx = 0 \quad (1a)$$

or

$$\ddot{x} + \gamma|x|^a|\dot{x}|^b\dot{x} + \omega^2x = 0 \quad (1b)$$

$$x(0) = A_0, \text{ and } \dot{x}(0) = 0 \quad (1c)$$

where  $\gamma = \frac{c}{m}$  and  $\omega^2 = \frac{k}{m}$ ,  $c$  is damping constant, and " $a, b$ "  $> 0$

Note that the term  $\gamma|x|^a|\dot{x}|^b\dot{x}$  represents the dissipating effect of a nonlinear damper with " $a$ " and " $b$ " both being positive integers or fractions.

When  $\gamma \ll 1$  ( $c$  small relative to  $m$ ) we may apply the averaging method of Krylov-Bogoliubov [7] to obtain an approximate equation

$$x(t) = A(t) \sin(\omega t + \phi(t))$$

where the amplitude  $A(t)$  and phase angle  $\phi(t)$  satisfy the following equations

$$\frac{dA(t)}{dt} = -\frac{\gamma}{\omega} K_0(t) \quad (2a)$$

and

$$\frac{d\phi(t)}{dt} = \frac{\gamma}{\omega A} P_0(t) \quad (2b)$$

The functions  $K_0(t)$  and  $P_0(t)$  in equations (2a) and (2b) are defined as

$$K_0(t) = \frac{1}{2\pi} \int_0^{2\pi} D(A \sin \phi, A\omega \cos \phi) \cos \phi d\phi \quad (3a)$$

$$P_0(t) = \frac{1}{2\pi} \int_0^{2\pi} D(A \sin \phi, A\omega \cos \phi) \sin \phi d\phi \quad (3b)$$

where  $D(x, \dot{x})$  is equal to  $|x|^a |\dot{x}|^b$  for the choice of nonlinear damper in equations (1a-1b), that is,  $D(x, \dot{x}) \triangleq D(A \sin \phi, A\omega \cos \phi)$ . Substituting  $D(x, \dot{x})$  into equations (3a) and (3b) we obtain

$$K_0(A) = \omega^{b+1} A^{a+b+1} \mu \quad (4a)$$

$$P_0(A) = 0 \quad (4b)$$

where

$$\mu = \frac{1}{2\pi} \int_0^{2\pi} |\sin \phi|^a |\cos \phi|^{b+2} d\phi \quad (4c)$$

Equation (4b) implies that for the choice of a nonlinear damper represented by  $\gamma|x|^a |\dot{x}|^b \dot{x}$ , the phase angle  $\phi(t)$  does not, on the average, change over time.

The positive number  $\mu$  in equation (4c) is called the nonlinear damping factor. By changing variables in equation (4c), it can be shown that

$$\mu = \frac{2}{\pi} \int_0^{\pi/2} |\sin \phi|^a |\cos \phi|^{b+2} d\phi \quad (4d)$$

The above expression for  $\mu$  is very similar to that for the so-called "damping force amplitude ratio  $\gamma_n$ " proposed by Jacobsen [9] when studying equivalent viscous damping. By employing the properties of the Gamma function, it is found that

$$\mu = \frac{\Gamma[\frac{a+1}{2}] \Gamma[\frac{b+3}{2}]}{\pi \Gamma[\frac{a+1}{2} + 2]} \quad (4e)$$

where  $\Gamma(\cdot)$  represents the Gamma function. Furthermore, when "a" is an odd number, it can be shown that

$$\mu = \frac{2(n+1)n!}{(b+3)(b+5) \cdots (b+3+2n)} \quad \text{for any } b > 0$$

With the above information we are in a position to derive equations for the amplitude  $A(t)$  and displacement  $x(t)$  for a system with nonlinear damping.

For the nonlinear damping system, (" $a + b$ "  $> 0$ ), we substitute equation (4a) into equation (2a) to obtain a differential equation for the amplitude  $A(t)$

$$\frac{dA(t)}{dt} = -\gamma \mu \omega^b A(t)^{a+b+1}$$

It can be shown that

$$A(t) = \left( \frac{m}{c\mu(a+b)\omega^b(t+t_c)} \right)^{\frac{1}{(a+b)}} \quad (5a)$$

where

$$t_c = \frac{m}{c\mu\omega^b(a+b)A_0^{a+b}} \quad (5b)$$

and

$$x(t) = \left( \frac{m}{c\mu(a+b)\omega^b(t+t_c)} \right)^{\frac{1}{(a+b)}} \cos \omega t \quad (5c)$$

Recall that for linear damping viscous damping ("a + b" = 0) [10]

$$x(t) = A_0 e^{-\zeta \omega t} \cos \omega t$$

In equation (5c), the quantity  $t_c$  is associated with the initial conditions but is not the initial time. The constant  $t_c$  has units of time and is never equal to zero.

Defining  $t + t_c \triangleq n \frac{2\pi}{\omega}$  and replacing  $A(n \frac{2\pi}{\omega} - t_c)$  by  $A(n)$  in equation (5a), we obtain an expression for the amplitude in terms of the number of cycles of nonlinear vibration

$$A(n) = \left( \frac{m^{\frac{(b+1)}{2}}}{c\mu(a+b)t^{\frac{(b-1)}{2}}(2\pi n)} \right)^{\frac{1}{(a+b)}} \quad (5d)$$

where n is the number of cycles of oscillation.

### 3.0 Transient Response of Nonlinear Damping

Using the solution for the nonlinear damping system in equations (1a) - (1c), it can be shown that the logarithmic decrement,  $\delta$ , which is the ratio of two

successive amplitudes, is given by

$$\delta = \frac{1}{a+b} \ln \left( 1 + \frac{T}{t_1 + t_c} \right) \quad (6a)$$

In equation (6a),  $t_1$  is the time when the response is first measured to compute the amplitude ratio,  $\delta$ , and  $T$  is the period of oscillation. Assuming  $t_1 = 0$  and using equation (5b) for  $t_c$ , we obtain

$$\delta = \frac{1}{a+b} \ln \left( 1 + \frac{2\pi\mu c(a+b)\omega^{k-1}A_0^{a+b}}{m} \right) \quad (6b)$$

For linear viscous damping it is well known that the logarithmic decrement is [10] given by

$$\delta = \ln \left( \frac{t_1}{x(t_1 + T)} \right) = 2\pi\zeta \quad (6c)$$

Comparing equation (6b) with (6c) one may conclude that while the rate of amplitude decay depends only upon the damping ratio,  $\zeta$ , for the linear damping model, the amplitude associated with the nonlinear damping system decreases more rapidly as:

- a) the initial amplitude  $A_0$  increases
- b) the frequency increases
- c) " $a + b$ ", especially " $b$ ", increases
- d) damping ratio  $\zeta$  increases

### Numerical Examples

Some numerical results are summarized in Figures 1 through 4, which contain the time histories for the nonlinear and linear damping models ( $a = b = 0$ ) and for the single degree of freedom system with mass  $m = 1$ , stiffness  $k = 4$ , and damping coefficient  $c = 0.01$ .

For the nonlinear damping cases, " $a + b$ "  $= 1$  in both Figures 1 and 2, but " $a + b$ "  $= 2$  in Figure 3. The initial amplitude  $A_0$  is 25 in Figures 1 and 3, and 50 in Figure 2. It can be seen that while the amplitude decrement remains constant for all of the linear damping cases in Figures 1 through 3, it decreases more rapidly for the nonlinear damping model. This condition is more evident: (a) at the initial time than at a later time, (b) as the initial amplitude increases and (c) as " $a + b$ ", especially " $b$ " increases. This is in agreement with observations made in practical engineering problems.

Figure 4 compares the logarithmic amplitude decay in terms of the number of cycles of vibration represented by equation (5d) for a system with the same parameters as in Figures 1 through 3. The sum of " $a + b$ " remains constant (" $a + b$ "  $= 3$ ) as " $a$ " and " $b$ " vary individually. It is found that the rate of amplitude decrease is greater as the value of " $b$ " increases, even though the sum of " $a$ " and " $b$ " remains constant.

#### 4.0 Perturbation Solutions of Nonlinear Damping for Distributed Systems

Consider the vibration of a pinned-pinned beam with non-linear damping

$$\rho \ddot{u} + C_{ab} |u''|^\alpha |\dot{u}''|^{\beta} \dot{u}'' + EI u^{(4)} = 0 \quad (7a)$$

$$u(0, t) = u(L, t) = u''(0, t) = u''(L, t) = 0 \quad (7b)$$

$$u(x, 0) = A \sin \frac{m\pi x}{L} \quad (7c)$$

where  $\rho$  is the mass per unit length,  $L$  is the length of the beam, and  $C_{ab}$  is the nonlinear damping constant.

In [6], Balakrishnan applied the Krylov-Bogoliubov method to a multi-dimensional system and obtained expressions similar to those in the single mode case. A common approach to treat an elastic system, such as the pinned-pinned beam discussed here, is to use a modal expansion method to convert a partial differential equation into a series of ordinary differential equations; however, great difficulties were encountered in the modal expansion due to the presence of the absolute value function in equation (7a). For this reason, both an ad hoc perturbation technique and the finite difference method presented in Sections 4 and 5 were utilized to study the effects of nonlinear damping for a pinned-pinned beam.

For small values of nonlinear damping coefficient,  $C_{ab}$ , the system will oscillate at the frequency



$$\omega_m = \left(\frac{m\pi}{L}\right)^2 \sqrt{\frac{EI}{\rho}} \quad (7d)$$

and period

$$p_m = 2\pi/\omega_m \quad (7e)$$

Let the perturbation solution after one period be

$$u(x, p_m) = u^o(x, p_m) + \Delta u(x, p_m)$$

where  $u^o(x, t)$  is the unperturbed solution of equations (7a-7c) with  $C_{ab} = 0$ , and  $\Delta u(x, t)$  the perturbed solution. In other words

$$u^o(x, p_m) = A \sin \frac{m\pi x}{L} \quad (8a)$$

and

$$\Delta u(x, p_m) = \sum_{k=1}^{\infty} A_k \sin \frac{k\pi x}{L} \quad (8b)$$

The values of the coefficients  $A_k$  in equation (8b) indicate the degree to which the initial mode is damped out and the other modes are excited. The perturbed solution in equation (8b) is given approximately by

$$\Delta \ddot{u} = \frac{C_{ab}}{\rho} |u^o|^a |\dot{u}^o|^b \ddot{u}^o \quad (9a)$$

with  $u(x, t)$  on the right hand side of equation (9a) being further approximated by  $u^o(x, t)$ , that is,

$$u(x, t) = u^o(x, t) = A \sin \frac{m\pi x}{L} \cos \omega_m t \quad (9b)$$

hence

$$u''(x, t) = -A \left( \frac{m\pi}{L} \right)^2 \sin \frac{m\pi x}{L} \cos \omega_m t \quad (9c)$$

Substitution of equations (9b-9c) into equation (9a) gives

$$\Delta \ddot{u} = \beta_m \left| \sin \frac{m\pi x}{L} \right|^{a+b} \sin \frac{m\pi x}{L} |\cos \omega_m t|^a \cdot |\sin \omega_m t|^b \sin \omega_m t \quad (9d)$$

where  $\beta_m$  is a constant that depends on many of the system parameters, such as the nonlinear damping coefficient,  $C_{ab}$ , the amplitude  $A$ , and the mode number  $m$ , etc., that is,

$$\beta_m \triangleq \beta_m(a, b) = \frac{C_{ab}}{\rho} A^{a+b+1} \omega_m^{b+1} \left( \frac{m\pi}{L} \right)^{2f}$$

where  $f \triangleq a + b + 1$

The coefficient  $\beta_m$  is proportional to  $2(a + b + 1)$  powers of the mode number  $m$ , hence,  $\Delta \ddot{u}$  in equation (9d) may become quite large for higher modes. This suggests that the perturbation solution may apply only to low frequency modes and not to higher frequency modes.

Because we are mainly interested in the maximum perturbation of the amplitude decay due to nonlinear damping after half a period, we integrate equation (9d) twice from 0 to  $t(t \leq p_m/2)$  to obtain

$$\Delta u(x, \frac{p_m}{2}) = \beta_m c_T \left| \sin \frac{m\pi x}{L} \right|^{a+b} \sin \frac{m\pi x}{L} \quad (9e)$$

where

$$c_T \triangleq \int_0^{p_m/2} dt \int_0^L |\cos \omega_m t|^a |\sin \omega_m t|^b \sin \omega_m \tau d\tau$$

The quantity  $c_T$  is a constant that depends on the half period  $p_m$  as well as "a" and "b", but does not depend on  $x$ . In order to examine the interaction between different modes in  $\Delta u(x, \frac{p_m}{2})$  in equation (9e), we expand  $\Delta u(x, \frac{p_m}{2})$  into a sine Fourier series in terms of the multiples of the initial mode  $\sin \frac{m\pi x}{L}$ , that is

$$\Delta u(x, \frac{p_m}{2}) = \sum_{n=1}^{\infty} A_{nm} \sin \frac{n\pi x}{L} \quad (9f)$$

It can be shown that if the pinned-pinned beam in equation (7) is excited only by a single mode  $A \sin \frac{m\pi x}{L}$ , then for any positive numbers "a" and "b", all of the even multiples of the initial mode will not be excited; only the odd multiples of the initial mode get excited. In other words

$$\begin{cases} A_{nm} = 0, & \text{for } n = 2j \\ A_{nm} = \frac{2\beta_m c_T}{L} \int_0^L \left| \sin \frac{m\pi x}{L} \right|^{a+b} \sin \frac{m\pi x}{L} \sin \frac{n\pi x}{L} dx \\ & \text{for } n = 2j - 1 \end{cases}$$

Now expand  $\Delta u(x, \frac{p_m}{2})$  into a sine Fourier series to obtain the Fourier coefficients  $A_{nm}$ , as represented in equation (9f).

It can be shown that for  $a = 0$ ,  $b = 1$

$$\begin{cases} A_{nm} = 0, & \text{for } n = 2j \\ A_{nm} = \frac{2C_{22} \pi^2 m^2 A^2}{[(2j-2)(2j-1)(2j+1)]\rho L^4}, & \text{for } n = 2j-1 \end{cases} \quad (10)$$

Similar expressions can be derived for any positive integers "a" and "b". Equation (10) relates the initial mode  $A \sin \frac{m\pi x}{L}$  to the distributed nonlinear damping coefficient  $A_{nm}$ . Because the perturbation solution contains components of other modes, they too will be excited. The degree of excitation is illustrated by the values of  $A_{nm}$ . It is obvious that the even-multiples of initial modes are not excited while all of the odd-multiples are. It will be shown later that for a beam excited by fundamental modes, equation (10) provides an estimate for the amplitude decay after a half period due to nonlinear damping.

### 5.0 Finite Difference Simulation for Nonlinear Damping

In this section, the transversal vibration of a pinned-pinned beam excited by a single mode is simulated via the finite-difference method. We will present a finite difference scheme for solving the partial differential equation, derive the stability conditions and then discuss numerical results. Specifically, we will compute amplitude decay after half a period and compare the results with both linear and nonlinear damping. We treat only the case of  $a = 0$ ,  $b = 1$  for nonlinear damping. Finally, we compare the amplitude decrement using the finite difference method with the amplitude decrement obtained using the perturbation method presented in Section 4.

### Finite Difference Formulations

When modeling the nonlinear differential equation (7a) with the finite difference method, we represent beam displacement as  $u(x_i, t_j) \hat{=} u_{ij}$ , where  $x_i$  is defined as  $x_i \hat{=} i\Delta x$ , and  $t_j$  is defined as  $t_j \hat{=} j\Delta t$ . Both grids  $\Delta x$  and  $\Delta t$  are defined as  $\Delta x \hat{=} \frac{L}{m}$ , and  $\Delta t \hat{=} \frac{T}{n}$ , where  $m$  and  $n$  are the numbers of grids used for  $L$  and  $T$ .  $L$  is the beam length and  $T$  represents the half period for the initial mode. With the above definition, the nonlinear finite difference equation (corresponding to equation (7a)) for the displacement at  $x_i, t_{j+1}$  is given by

$$\begin{aligned} u_{i,j+1} = & \gamma(u_{i+2,j} - 4u_{i+1,j} + 6u_{i,j} - 4u_{i-1,j} + u_{i-2,j}) + (2u_{i,j} - u_{i,j-1}) \\ & + \beta[(u_{i+1,j} - u_{i+1,j-1}) - 2(u_{i,j} - u_{i,j-1}) + (u_{i-1,j} - u_{i-1,j-1})] \\ & - \alpha[(u_{i+1,j} - u_{i+1,j-1}) - 2(u_{i,j} - u_{i,j-1}) + (u_{i-1,j} - u_{i-1,j-1})] \end{aligned} \quad (11a)$$

If linear damping is assumed ( $\alpha = \beta = 0$ ), then equation (7a) becomes

$$\rho \ddot{u} + c \dot{u} + EI u^{(4)} = 0 \quad (11b)$$

and the corresponding finite difference equation is

$$\begin{aligned} u_{i,j+1} = & \gamma(u_{i+2,j} - 4u_{i+1,j} + 6u_{i,j} - 4u_{i-1,j} + u_{i-2,j}) + (2u_{i,j} - u_{i,j-1}) \\ & + \alpha[(u_{i+1,j} - u_{i+1,j-1}) - 2(u_{i,j} - u_{i,j-1}) + (u_{i-1,j} - u_{i-1,j-1})] \end{aligned} \quad (11c)$$

Finally, if no damping is present, equation (11c) is further simplified as

$$u_{i,j+1} = \gamma(u_{i+2,j} - 4u_{i+1,j} + 6u_{i,j} - 4u_{i-1,j} + u_{i-2,j}) + (2u_{i,j} - u_{i,j-1}) \quad (11d)$$

where

$$\gamma = -\frac{EI\Delta t^2}{\rho\Delta x^4}, \beta = -\frac{C_{st}}{\rho\Delta x^4}, \text{ and } \alpha = -\frac{c\Delta t}{\Delta x^2} \quad (11e)$$

Formulas for central differences have been used to approximate both  $u''$  and  $\ddot{u}$ . Forward differences for  $t$  and central differences for  $x$  are used to obtain the mixed derivative  $\dot{u}''$  in equations (11a), (11c), and (11d). Two fictitious boundary conditions have been created such that the zero moment conditions are satisfied at both ends for the pinned-pinned beam. They are

$$u_{m+1,j} = -u_{m-1,j} \text{ and } u_{-1,j} = -u_{1,j}$$

$$j = 0, 1, 2, \dots, n$$

### Stability Conditions

It should be noted that equations (11a), (11c), and (11d) belong to the explicit forms of finite difference formulation, for which there always exists a stability problem for the specific finite difference scheme [11]. In other words, when the finite difference scheme is stable, there exists an upper limit to the

extent to which any error arising during the simulation can be amplified. This implies that the numerical solution will not diverge. Clearly, stability alone does not necessarily guarantee that the deviation between the true solution to a certain partial differential equation and its finite difference approximation will be small in any sense. Stability only implies the boundedness of the finite difference solution, at a given time, as  $\Delta t$  approaches zero.

In the case of a beam without damping, the equation of motion is

$$\rho \ddot{u} + EI u^{(4)} = 0 \quad (12a)$$

Assuming harmonic motion, that is,

$$u(x, t) = e^{j\lambda x} T(t) \quad (12b)$$

Using the finite difference method, equation (12a) can be replaced by

$$\begin{aligned} T(t + \Delta t) - 2T(t) + T(t - \Delta t) + \gamma[(e^{2j\Delta x} + e^{-2j\Delta x}) \\ - 4(e^{j\Delta x} + e^{-j\Delta x}) + 6]T(t) = 0 \end{aligned} \quad (12c)$$

Since  $[e^{2j\Delta x} + e^{-2j\Delta x} - 4(e^{j\Delta x} + e^{-j\Delta x}) + 6] = 16 \cos^4(\frac{\Delta x}{2})$ , equation (12c) is simplified to obtain

$$T(t + \Delta t) - [2 - 16\gamma \cos^4(\frac{\Delta x}{2})]T(t) + T(t - \Delta t) = 0 \quad (12d)$$

Substituting  $\gamma$  in equation (11c) into equation (12d) and utilizing the stability criteria for the eigenvalues of a difference equation, we find the stability

condition for the finite difference equation (11d) to be

$$\frac{EI\Delta t^2}{\rho\Delta x^4} \cos^4\left(\frac{\Delta x}{2}\right) \leq \frac{1}{4} \quad (12e)$$

or

$$\frac{EI\Delta t^2}{\rho\Delta x^4} \leq \frac{1}{4} \quad (12f)$$

For a beam vibrating with linear damping, represented by equation (11b), the difference equation for the stability condition is

$$\begin{aligned} T(t + \Delta t) - [2 - 16\gamma \cos^4\left(\frac{\Delta x}{2}\right) - 4\alpha \sin^2\left(\frac{\Delta x}{2}\right)]T(t) \\ + [1 - 4\alpha \sin^2\left(\frac{\Delta x}{2}\right)]T(t - \Delta t) = 0 \end{aligned} \quad (13a)$$

This can be further simplified to

$$\frac{4EI\Delta t^2}{\rho\Delta x^4} \cos^4\left(\frac{\Delta x}{2}\right) + \frac{2\zeta\sqrt{ET\rho}\Delta t}{\rho\Delta x^2} \sin^2\left(\frac{\Delta x}{2}\right) \leq 1$$

or

$$\frac{EI\Delta t^2}{\rho\Delta x^4} + \frac{\zeta\sqrt{ET\rho}\Delta t}{2\rho\Delta x^2} \leq \frac{1}{4} \quad (13b)$$

which is similar to equation (12f).

Notice that the stability condition similar to equations (12f) and (13b) is not available for the nonlinear difference equation. This is mainly because of the difficulties encountered due to the presence of the absolute value function in equation (11a).



### Numerical Examples

The numerical example used for the simulation is a pinned-pinned beam which resembles the SCOLE project mast [1] with  $L = 130$  ft,  $EI = 4E07$  lb.ft<sup>2</sup>,  $\rho = 0.09556$  slug/ft. The beam is initially at rest and is excited by a single mode  $A \sin \frac{i\pi x}{L}$  with  $A = 1.3$  ft and  $i = 1, 2, 3, 4$ . The first frequency is 11.95 rad/sec and its corresponding period is 0.5258 second. We proceed to evaluate the displacement of the beam for the first half period  $T$ .

Because the stability condition (12f) implies that  $\Delta x$  can not be arbitrarily small, we first chose  $m = i0$  ( $\Delta x = L/m = 13ft$ ) when verifying the stability condition. It was found that if  $n > 64$ ,  $\Delta t = T/n < 0.0041$ ,  $|\gamma| = 0.2473 < 0.25$ , then the numerical scheme was always stable. On the other hand, if  $n = 63$ ,  $|\gamma| = 0.2552 > 0.25$ , the numerical scheme was found to be unstable, which confirms our stability criteria represented by equation (12f).

Before we compare the amplitude decrement using the perturbation and the finite difference methods, it is necessary to verify the finite difference scheme used in the simulation. We compare the finite difference displacement results with those obtained using an analytical solution after a half period for a beam vibrating without damping (corresponding to equation (12a)). We also compare the finite difference results with that for the logarithmic decrements of the amplitude for a beam vibrating with linear viscous damping (corresponding to equation (11b)). We believe that as long as the finite-difference scheme converges reasonably well for both equations (12a) and (11b), the scheme should

work for equation (11a) with nonlinear damping.

The relative errors were computed for the displacement of a beam vibrating without damping after half a period when 20 intervals in  $L$  and 1100 intervals in  $T$  were used. The relative errors are defined as the difference between the displacement using finite difference method and that using an analytical method. The difference is then normalized by the analytical values. The relative errors are quite uniform for each mode over all locations of the beam with their maximum values being 0.0025%, 0.037%, 0.23%, and 0.54% for modes 1, 2, 3, and 4 respectively. This implies that the finite difference method provides quite accurate results for beam vibrations without damping. Notice that the errors can be greatly reduced if more intervals are used for  $L$  and  $T$ , subject to the stability condition of equation (12f).

For free vibration of a pinned-pinned beam with linear viscous damping, represented by equation (11b), it can be shown that by assuming harmonic motion (as in equation (12b)), the damping ratio,  $\zeta$ , for each mode depends only on damping constant  $c$ , beam properties  $\rho$  and  $EI$ , but not on the mode number  $i$ , that is,

$$\zeta = \frac{c}{2\sqrt{\rho EI}} \quad (14a)$$

According to classical vibration theory [10], it is well known that the amplitude decay after half a period for single degree of freedom system is

$$\delta \triangleq \frac{\Delta A}{A} = \pi\zeta \quad (14b)$$

which also does not depend on the mode number  $i$ . Specifically, if  $\zeta = 0.003$ , then theoretically  $\delta$  should equal to 0.0094 after half a period for any single DOF system. Using the same numbers of grid points for L and T as before, the amplitude decay,  $\delta$ , after half a period for modes 1 and 2 at a variety of locations on a beam with linear damping ( $\zeta = 0.003$ ) were computed. For both mode 1 and 2, the amplitude decay,  $\delta$ , remains almost identical at all locations of the beam, as if each point on the beam vibrated as a single DOF system. It is interesting to note that the amplitude decay,  $\delta$ , is about 0.0094 for mode 1, and 0.0096 - 0.0097 for mode 2, both of which are close to 0.0094 ( $= \pi\zeta$ ). These results are in good agreement with equations (14a-14b) and further confirm that the finite-difference algorithm used is quite reliable.

Figures 5 and 6 compare the values of the amplitude decay for modes 1-3 after half a period  $T$  for the same beam with: (1) linear damping using finite-difference method, (2) nonlinear damping using finite-difference method, and (3) the perturbation method discussed in Section 4. The abscissas are a dimensionless quantity damping ratio  $\zeta$ . Linear damping coefficient  $c$  is equal to  $2\zeta\sqrt{\rho ET}$ , and the nonlinear damping coefficient  $C_{nl}$  is equal to  $4c$ . These values are used for both finite-difference and perturbation methods. For the case of linear damping, the amplitude decay takes almost the same value for modes 1-3 (e.g.,  $\delta = 0.0064$  for modes 1-3 when  $\zeta = 0.02$ ), which is consistent

with equation (14a).

From Figures 5 and 6 we observed that: (1) the effect of linear damping exceeds that of nonlinear damping for mode 1, (2) the effect of linear damping is about the same as that of nonlinear damping for mode 2, and (3) the effect of nonlinear damping outweighs that of linear damping for mode 3. These results imply that in the case of nonlinear damping the amplitude of higher modes will be damped out faster than the lower modes, whereas in the case of linear damping, the modes are all equally damped. This is consistent with the results of Section 3 for a single degree of freedom system, as well as with common engineering judgement.

Finally, when comparing the results in Figures 5 and 6 for nonlinear damping using either finite-difference or perturbation methods, it is observed that for fundamental modes the perturbation method provides a very conservative upper bound of amplitude decrement after half a period. This result might be useful in preliminary assessment of the impact of nonlinear damping effect, since in many occasions, we are mainly concerned with the system's fundamental frequencies.

### Conclusions

A space systems dynamics and controls analyst is often confronted with the problem of gaining a better understanding of the damping mechanism which is inherently nonlinear. Fortunately, some of the difficulty in handling nonlinearities is offset by the fact that damping is still small. This makes it possible to

obtain approximate solutions using the classical Krylov-Bogoliubov "averaging" technique to study a class of nonlinear damping models.

In this paper, the damping force is assumed to be proportional to the product of positive integer or fractional powers of the absolute values of displacement and velocity. As is expected that for a typical nonlinear system, the amplitude decrement of free vibration with nonlinear models depends not only on damping ratio, but also on the initial amplitude, the time to measure the response, the frequency of the system, and the powers of displacement and velocity. For a pinned-pinned beam, both an ad hoc perturbation method and a finite difference technique are used to study the vibration of a beam with nonlinear damping. The action of nonlinear damping is found to reduce the energy of the system as well as to pass energy to lower modes. As a result, the amplitude of higher modes will be damped out faster than the lower modes. All of these results are very useful to study the response of a flexible structure to the action of a nonlinear boundary feedback control.

#### References

- [1] "Proceedings of 3rd Annual NASA SCOLE Workshop", November 1986. NASA Technical Memorandum 89075, Edited by Taylor, L.W., 1986.
- [2] Taylor, L.W. and Latimer, K. "Nonlinearities in Spacecraft Structural Dynamics", 4th Annual SCOLE Workshop, Colorado Springs, CO,

Nov. 1987, 67-102.

[3] Snowdon, J.C. "Vibration and shock in Damped Mechanical Systems", John Wiley & Sons, New York, 1968, pp. 423-450.

[4] Ruzicka, J.E. and Derby, T. F. "Influence of Damping in Vibration Isolation", The Shock and Vibration information Center. United States Department of Defense, 1971, pp. 8-9.

[5] Nashif, A.D., Jones, D.I.G and Henderson, J.P. "Vibration Damping", John Wiley & Sons, New York, 1985, pp. 51-61.

[6] Balakrishnan, A.V. "Some Nonlinear Damping Models in Flexible Structures", 4th Annual NASA SCOLE Workshop, Colorado Springs, CO, Nov 1987, pp. 54-66.

[7] Krylov, N. and Bogoliubov, N. "Introduction to Nonlinear Mechanics", Princeton University Press, 1947, pp. 8-26.

[8] Ross, S.L. "Differential Equations", Second Edition, John Wiley & Sons, New York, 1974, pp. 617-625.

[9] Jacobsen, L.S. and Ayre, R.S. "Engineering Vibrations", McGraw-Hill, New York, 1958, pp. 226-232.

[10] Thomson, W.T. "Theory of Vibration with Applications", Prentice-Hall, New Jersey, 1981, pp. 31-32.

[11] Carnahan, B., Luther, H and Wilkes, J. "Applied Numerical Methods", John Wiley & Sons, New York, 1969, pp. 362-364.

**Figure 1** Time History for Linear and Nonlinear Damping:  $a+b=1$

$A_0 = 25$ , Mass = 1, Stiffness = 4, Damping Coef. = 0.01

**Figure 2** Time History for Linear and Nonlinear Damping:  $a+b=1$

$A_0 = 50$ , Mass = 1, Stiffness = 4, Damping Coef. = 0.01

**Figure 3** Time History for Linear and Nonlinear Damping:  $a+b=2$

$A_0 = 25$ , Mass = 1, Stiffness = 4, Damping Coef. = 0.01

**Figure 4** Amplitude vs. Number of Cycles for Linear and

Nonlinear Damping

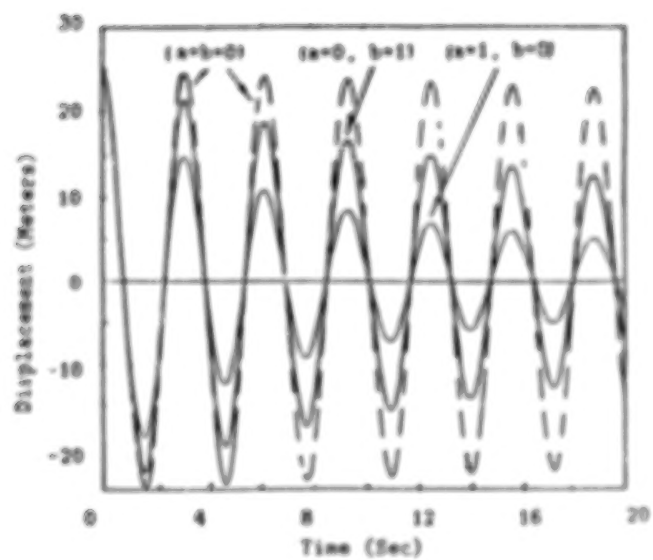
**Figure 5** Amplitude Decay vs. Damping Ratio after Half Period

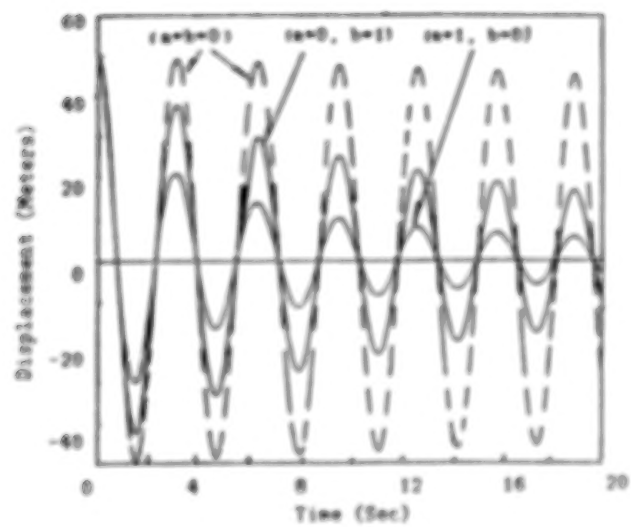
FDS: Finite Difference Simulation

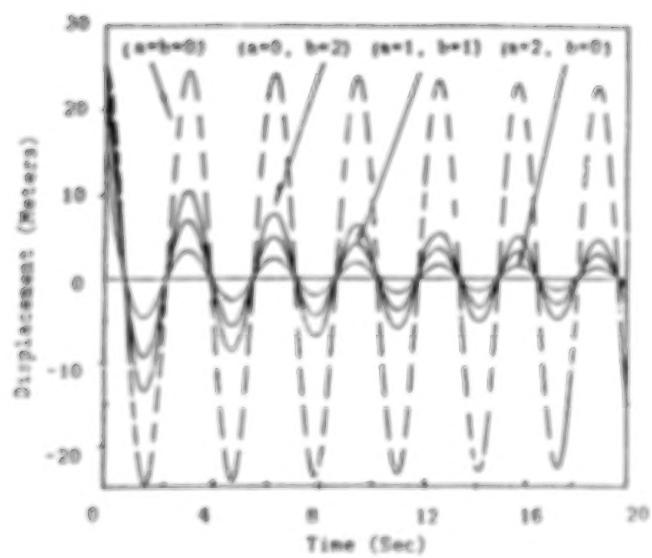
**Figure 6** Amplitude Decay vs. Damping Ratio after Half Period

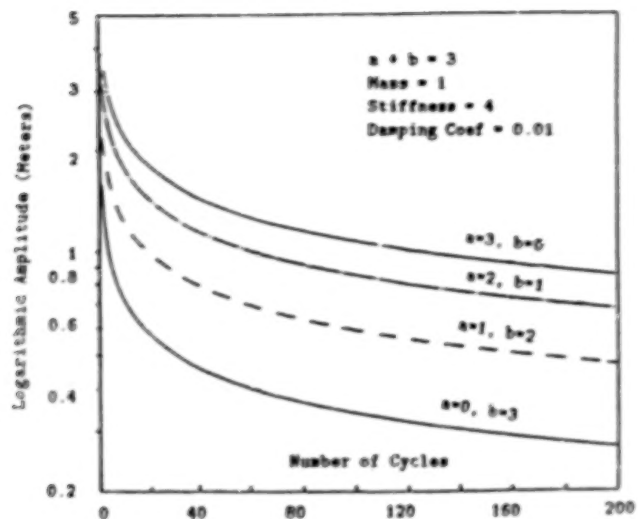
FDS: Finite Difference Simulation

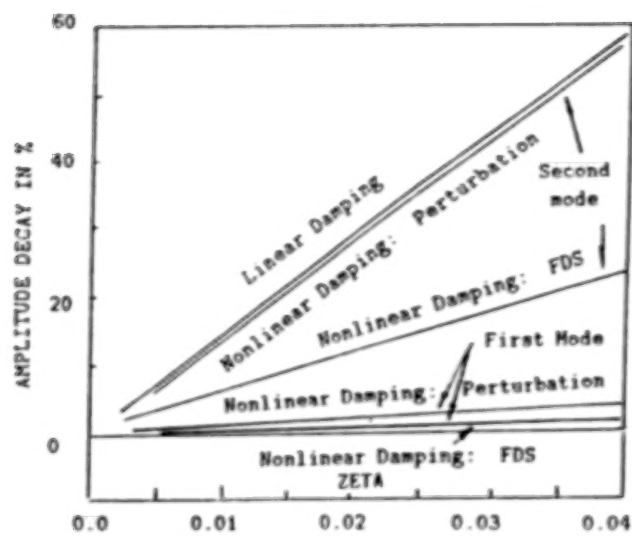


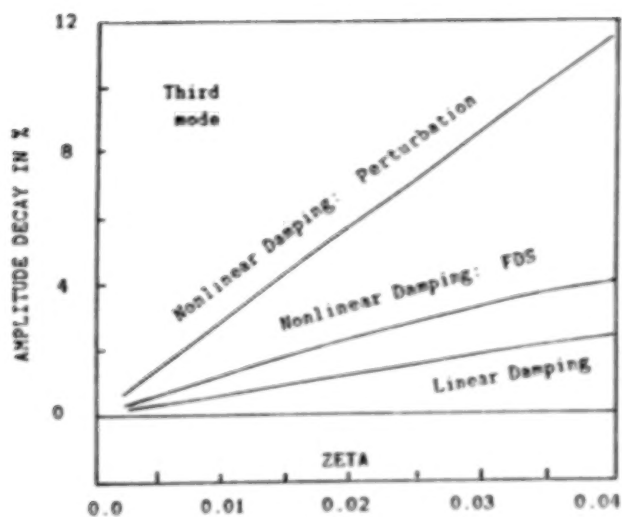


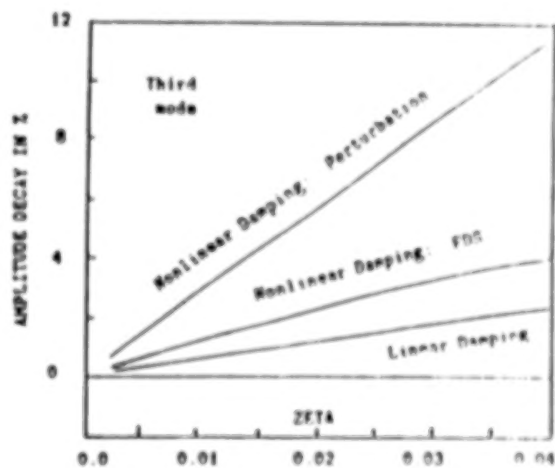
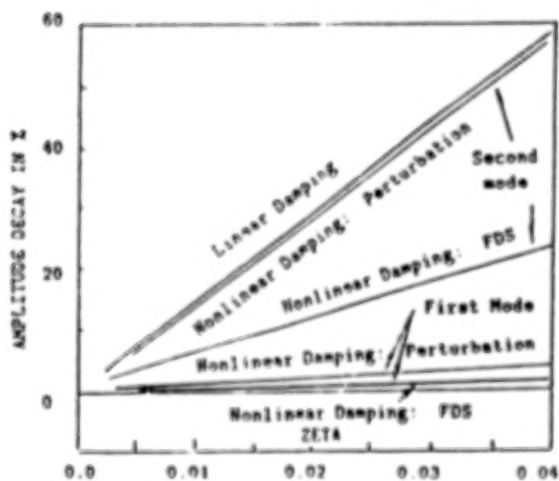
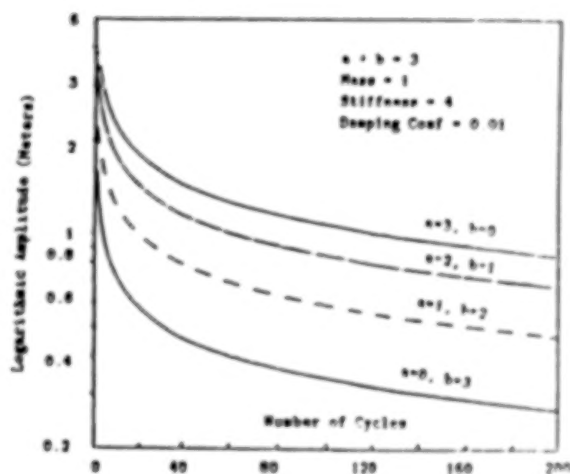
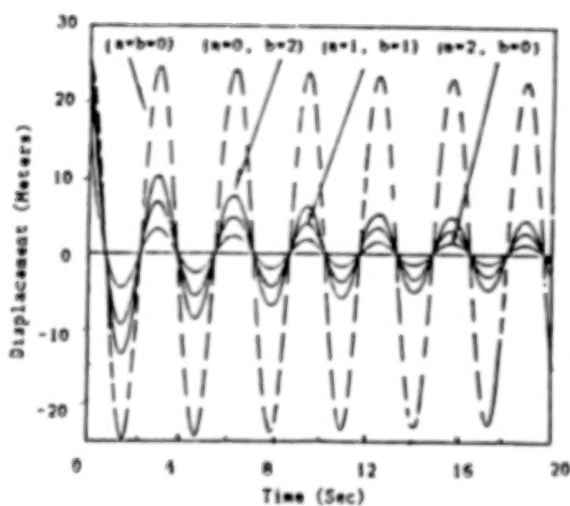
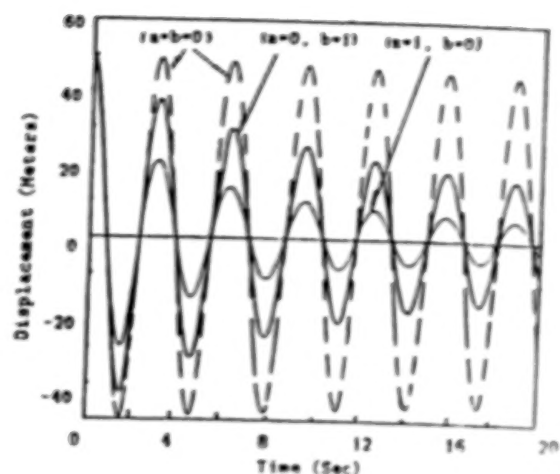
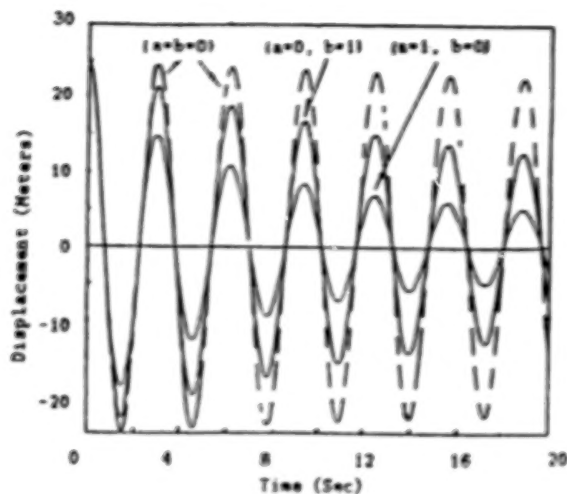


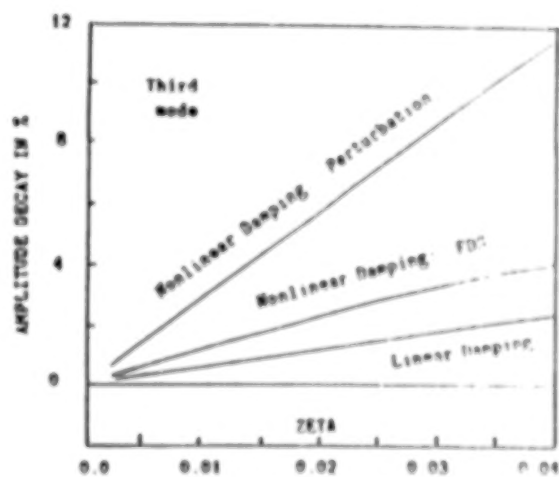
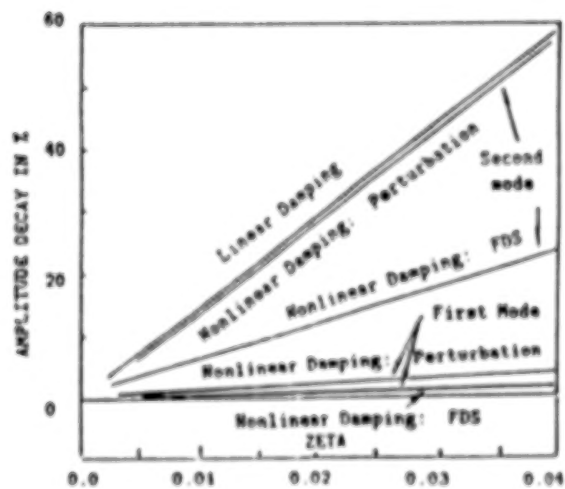
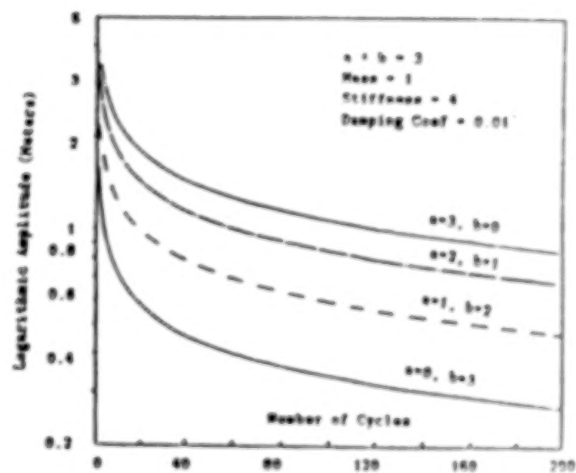
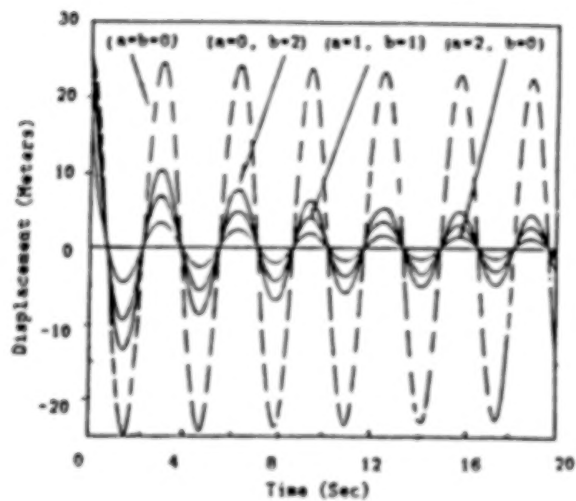
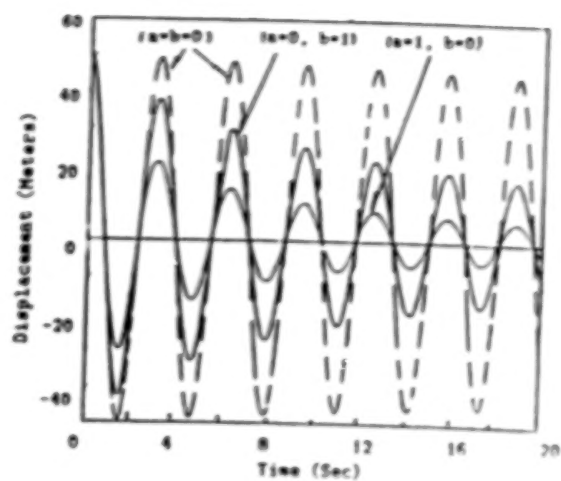
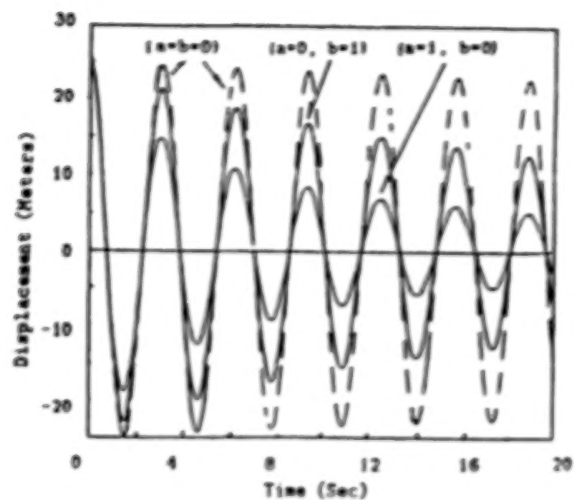








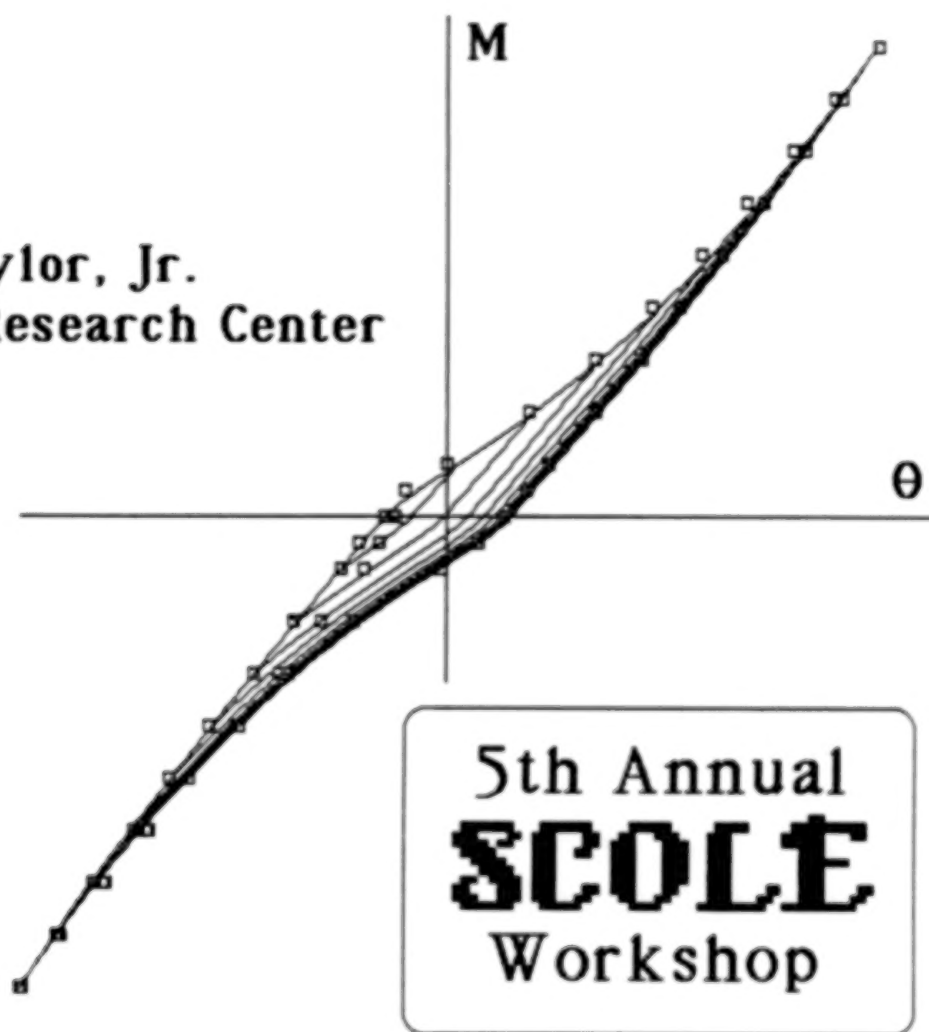






# Hysteretic Damping Model for the Mini-MAST Truss

Lawrence W. Taylor, Jr.  
NASA Langley Research Center



## **Nonlinear and Distributed Parameter Models of the Mini-MAST Truss**

**Lawrence W. Taylor, Jr.  
NASA Langley Research Center  
Hampton, Virginia**

### **ABSTRACT**

Large spacecraft such as Space Station Freedom employ large trusses in their construction. The structural dynamics of such trusses often exhibit nonlinear behavior and little damping which can impact significantly the performance of control systems. The mini-MAST truss was constructed to research such structural dynamics and control systems. The mini-MAST truss is an object of study for the Guest Investigator Program as part of NASA's Controls-Structures Interaction Program. The Mini-MAST truss is deployable and about 65 feet long. Although the bending characteristics of the Mini-MAST truss are essentially linear, the angular deflection under torsional loading has exhibited significant hysteresis and nonlinear stiffness. It is the purpose of this study to develop nonlinear and distributed parameter models of the truss and to compare the model dynamics with actual measurements. Distributed parameter models have the advantage of requiring fewer model parameters. A tangent function is used to describe the nonlinear stiffness in torsion, partly because of the convenience of its easily expressed inverse. Hysteretic slip elements are introduced and extended to a continuum to account for the observed hysteresis in torsion. The contribution of slipping to the structural damping is analyzed and found to be strongly dependent on the applied loads. Because of the many factors which affect the damping and stiffness in a truss, it is risky to assume linearity.

### **INTRODUCTION**

Future missions in space require spacecraft which are considerably larger and more flexible than current spacecraft. Large spacecraft such as Space Station Freedom employ large, complex trusses in their construction. The structural dynamics of such trusses often exhibit nonlinear behavior and low structural damping which can impact significantly the performance of control systems. For example, in reference 1, Lallman studies the effect

of damping on the performance of the attitude control system of the Space Station Freedom. The mini-MAST truss was constructed to research the interaction of such structural dynamics and control systems and is an object of study for the Guest Investigator Program as part of NASA's Controls-Structures Interaction Program.

The Mini-MAST truss was designed to be deployable to a length of 66.14 feet when fully extended. The bending characteristics of the Mini-MAST truss are essentially linear. The angular deflection under torsional loading, however, has exhibited significant hysteresis and nonlinear stiffness during laboratory tests.

The complexity of such structures create a burden to optimal design and to systems identification for upgrading dynamic model parameters by analyzing experimental test data. The large number of model parameters which results if each structural mode is assumed to be independent can be greatly reduced if distributed parameter models are used.

It is the purpose of this study to develop distributed parameter models of the Mini-MAST truss and to compare the model dynamics with the actual dynamic characteristics. A second purpose is to model the nonlinear stiffness and damping properties of this joint-dominated truss. It is hoped that the study results will be useful in designing control systems for large spacecraft such as Space Station Freedom which employ similar trusses.

## DISCUSSION

Because the Mini-MAST truss is representative of structures that will be used for large spacecraft such as the Space Station Freedom, the study of its structural dynamics is valuable in assuring the dependability and high performance of spacecraft control systems. Figure 1a. pictures the Mini-MAST truss being deployed. The reduction in volume is striking when compared to the deployed truss shown in figure 1b. Reference 2 describes in detail the design of the Mini-MAST. Because of the complexity of the truss it is important to study simplifying models of its dynamics. Figure 2 shows how many modes are required to depict accurately the static deflection of a cantilevered beam. The problem is compounded if the modal parameters are considered to be independent. Because of the resulting complexity there is considerable advantage in using distributed parameter models. Due to the greatly reduced numbers of parameters required for such models as shown in figure 3, the ability to employ systems

identification (Reference 3) and optimal design techniques is greatly facilitated. Because of these advantages it is valuable to determine the accuracy with which distributed parameter models can represent the Mini-MAST truss. For example, can such simple models predict accurately the peaks of the frequency response shown in figure 4? If distributed parameter models represent accurately the dynamics of the Mini-MAST truss, then the model equations can be used to upgrade the model parameters using systems identification. Also the models will be useful in integrated control-structures design because their form provides easy access to global variables such as the modulus of elasticity.

The Mini-MAST truss, being deployable, requires a large number of joints. The compliance and possible slippage of the joints may affect the overall stiffness of the truss when viewed as an equivalent beam. The action of the joints may also affect the damping of the truss as well. It is important to know accurately the damping of a spacecraft in order to assure reliable and high performance control. It is also important to understand and to model any nonlinear behavior caused by the numerous joints.

### Distributed Parameter Bending Model

The Mini-MAST truss is modeled as a cantilevered beam with an added tip mass as depicted in the schematic in figure 5. The partial differential equations (Euler beam equation) and boundary condition equations (Cantilevered and tip mass) are solved thereby determining the modal characteristics. First, the calculated static deformation resulting from a constant 15 pound force applied to the tip is compared to actual test results in figure 6. The value of the stiffness parameter,  $EI$ , for an equivalent Euler beam derived from this test is  $27.6 \times 10^6$  pound feet squared. The comparison suggests that the model deformation matches the actual deformation within the measurement error. The resulting modal frequencies in bending are then compared with experimental results and those for a finite element model (Reference 4) in figure 7. The frequencies for the first few bending modes of the distributed parameter model accurately match the actual bending frequencies of the truss. At higher mode numbers, however, the actual modal frequencies are lower than the theoretical values for the Euler beam model. Belvin, in reference 5, showed that the shear deformation of a similar truss cannot be ignored as is done in the Euler beam model. Belvin used the techniques of reference 6 in his study. The Timoshenko beam, in contrast, accounts for the shear

deformation and more accurately models the frequencies in bending as shown in figure 7.

Figure 7 also shows the accuracy with which the frequencies of a finite element model match the actual frequencies of the truss. The finite element model is reasonably accurate even at high mode numbers. The parameter,  $EI$ , used in the finite element model equals  $29.8 \times 10^6$  pound feet squared. In figure 8 the bending mode shapes generated by the same finite element model exhibit shapes similar to Euler beams with one exception. Examination of the third mode reveals that the shear deformation is significant enough to give a change in slope almost at the bottom of the truss. The general contour of the mode shapes in figure 8 compare well with those of the Timoshenko beam (not shown) but the irregularities which show significant local deformation will be missing from the distributed parameter models. It is possible that overlooking such local deformations could cause control system instability.

The effect on the first bending mode frequency of changing the mass at the tip of the equivalent beam is shown in figure 9. The frequency response measurements of figure 4 had a tip mass which weighs 70.125 pounds (mass ratio = .31). The Mini-MAST truss excluding its tip mass weighs 229 pounds. The Euler beam model depicts accurately the change in frequency when the tip mass is removed. The assembly for the active control of the Mini-MAST is expected to weigh in excess of 300 pounds. The frequencies for higher mode numbers will not change as much as that for the first mode because as mode number increases the motion of the tip mass diminishes, thereby approaching a pinned end condition.

### Distributed Parameter Torsion Model

Similar to the bending case, the truss is modeled in torsion as an uniform shaft which is fixed at one end and has a tip body attached to the other end. Based on the angular deformation due to an applied moment the torsional parameter  $GI_{\text{polar}}$  equals  $2.16 \times 10^6$  pound feet squared per radian. The partial differential equations and end conditions are solved and in figure 10 the model's torsional frequencies are compared with experimental results and the finite element model of reference 4. The close comparison indicates that the modal frequencies for both the distributed parameter model and the finite element model compare closely with the actual frequencies.



## Nonlinear Torsional Stiffness

Because the Mini-MAST truss exhibits significant nonlinear stiffness and hysteretic behavior in torsion, it is necessary to model these characteristics. The nonlinear stiffness model will be discussed first. The hysteretic model will be treated in the next section.

Although the form of the nonlinear stiffness is approximately cubic, a tangent function is used because (1) its form gives the nearly linear plus cubic relationship that is needed, and (2) the tangent has a conveniently express inverse. Figure 11 depicts the tangent model of the nonlinear stiffness in torsion and introduces the parameters,  $K$ , and,  $B$ , which govern the linear and the cubic contribution, respectively. The parameter,  $K$ , then is the usual torsional stiffness.

In figure 12 it is evident that the tangent relationship compares well with the experimental results. The data shown is believed to not involve any slipping as it represents the relaxation from a load having been applied. As the load is increased slipping does take place and will next be considered.

## Torsional Slip Model

The torsional hysteretic model is comprised of an infinite number of slip elements. An individual slip element is assumed to slip instantaneously upon reaching a particular moment threshold. A reverse slip is assumed to take place at a moment of equal level but opposite sign as depicted in figure 13. A slip distribution function is introduced which describes the probability density function of the values of moment threshold. The second order exponential form of the function, shown in figure 14, was chosen to fit the experimental data. Effort is underway to link this distribution function to the vertical loading of the joints. The total deflection amplitude consists of (1) the deflection due to compliance without slipping plus (2) the deflection due to an accumulation of slips due to the applied moment. The expected value of the accumulation of slips is given by the integral of the slip distribution function between the last moment reversal or zero and the current applied moment. The deflection equation is depicted in figure 15.

The total hysteretic model which contains both the nonlinear stiffness and the hysteretic slipping is compared with actual test results in figure 16. The close comparison of the model results and the actual hysteretic behavior gives validity to the model for torsional deflection due to applied moment.

The hysteretic behavior is expected to be dependent on the vertical loading. When the 300 pound plus active control assembly is attached to the top of the Mini-MAST the total angular deflections are not expected to change significantly, but an increase in the moment threshold is expected. Because of the effect of gravity it is difficult to determine the hysteretic behavior in an unloaded condition as in space.

### Structural Damping

The damping for the first bending mode is affected by the mass of the tip body as shown in figure 17. The damping ratio which was measured for the truss without tip mass was about 3.3%. This value was about three times the value expected based on the assumption that the dimensional damping of the truss would not change. The damping ratio would be expected to double from the value of about .45% for the 70 pound tip mass. This discrepancy is probably due to slipping being affected by vertical loading, as is the case for torsion.

In torsion it is possible to link slipping to damping by accounting for the loss of energy due to slipping. Figure 18 shows that the expected contribution to damping from slipping for oscillations about the unloaded condition reflect the shape of the slip distribution function. The damping contribution for oscillations in torsion about a loaded condition may be as low as zero because of the complete lack of slipping.

The statically determinant truss to be used on the Space Station Freedom can be expected to involve internal loading. As a result the damping of the truss for small amplitudes is not expected to involve slipping and will consequently exhibit very low damping.

Laboratory tests have revealed a damping ratio for bending modes for the cantilevered truss to be about .0045. The damping ratio will decrease when large bodies are added to the truss. In the absence of air, the damping can be expected to be even smaller, perhaps approaching .002.

Past practices of using a constant damping ratio of .005 for space station studies does not represent the worst case. Lower values of damping should be used which reflect mass loading and internal loading effects.

## CONCLUDING REMARKS

The Mini-MAST truss has been tested and analyzed for the purpose of understanding the dynamic characteristics, nonlinear stiffness and hysteretic damping of large spacecraft.

It was necessary to use a Timoshenko beam model for bending to account for the shear deformation of the Mini-MAST truss. The modal frequencies of the Euler beam model were higher than the actual values.

A tangent function model of the nonlinear torsional stiffness was developed and its parameters estimated to match experimental results.

A hysteretic slip model for torsion was developed using the experimental test data. The slip distribution function used has a second order, exponential form. The hysteretic behavior is expected to be affected by changes in the vertical loading due to gravity.

The damping contribution in torsion of the hysteretic behavior was deduced by analyzing the torsional slip model. The damping due to slipping was determined to be quite dependent on loading conditions. A steady load, for example, might eliminate slipping and consequently any damping contribution due to slipping.

Future studies of control system performance should use lower values of structural damping than the .005 used in the past, and should consider the nonlinear effects.



## REFERENCES

1. Young, John W. and Frederick J. Lallman: Control/Structures Interaction Study of Two 300 KW Dual-Keel Space Station Concepts. NASA Technical Memorandum 87679. May, 1986.
2. Adams, Louis R.: Design, Development and Fabrication of a Deployable/Retractable Truss Beam Model for Large Space Structures Application. NASA Contractor Report 178287. June, 1987.
3. Taylor, Lawrence W., Jr.: On-Orbit Systems Identification of Flexible Spacecraft. 7th IFAC Symposium on Identification and System Parameter Estimation. York, England. July 2-8, 1985.
4. Bailey, James: Finite Element Model of the Mini-MAST Truss. Not yet published.
5. Belvin, W. Keith: Simplified Analysis of NASA's COFSI MAST-Beam. Not yet published.
6. Noor, A. K., Anderson, M. S. Anderson and W. H. Greene: Continuum Models for Beam- and Platelike lattice Structures. AIAA J., v. 16, no.12, December, 1978.

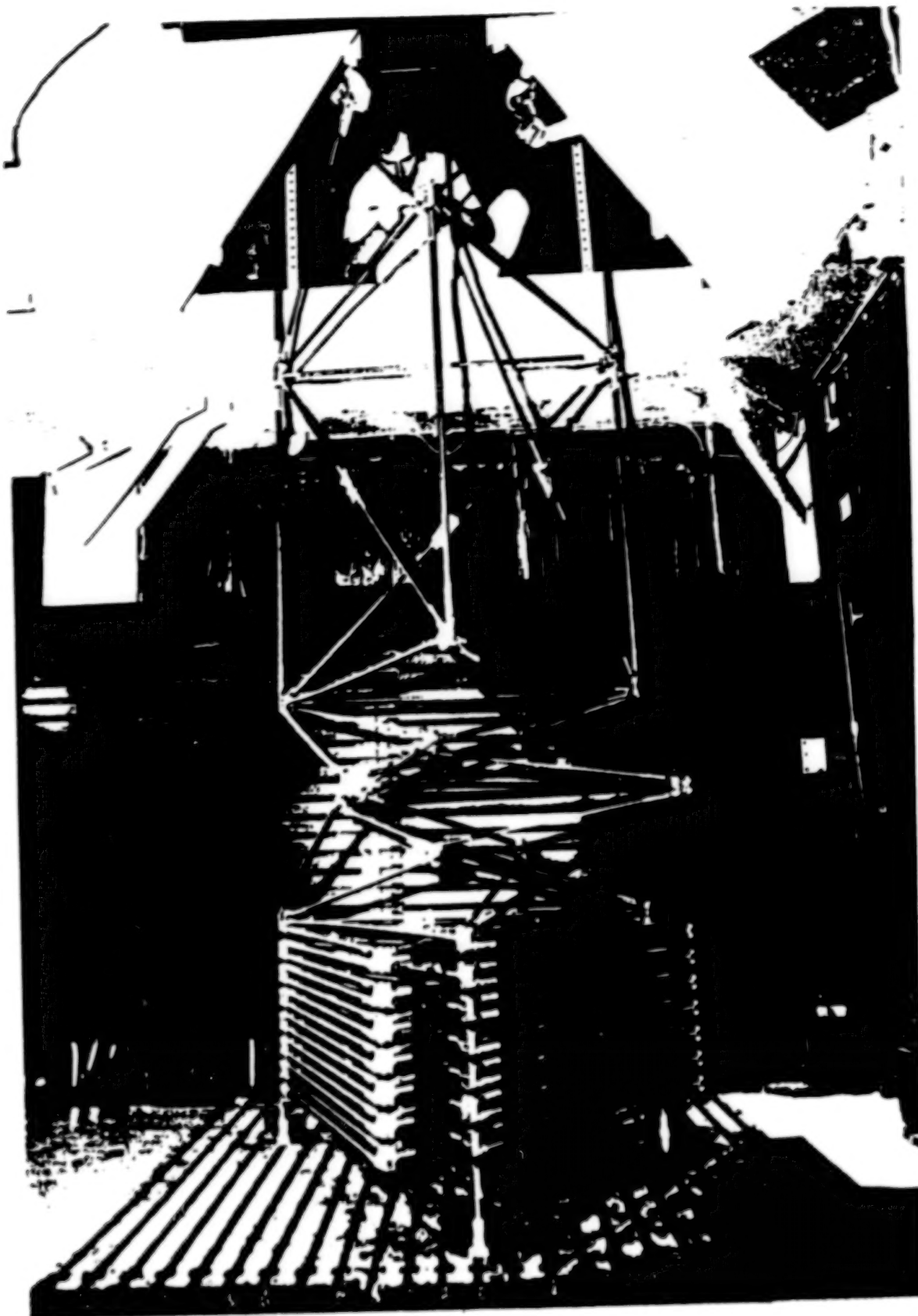


Figure 1 The Mini-MAST Truss Being Deployed.

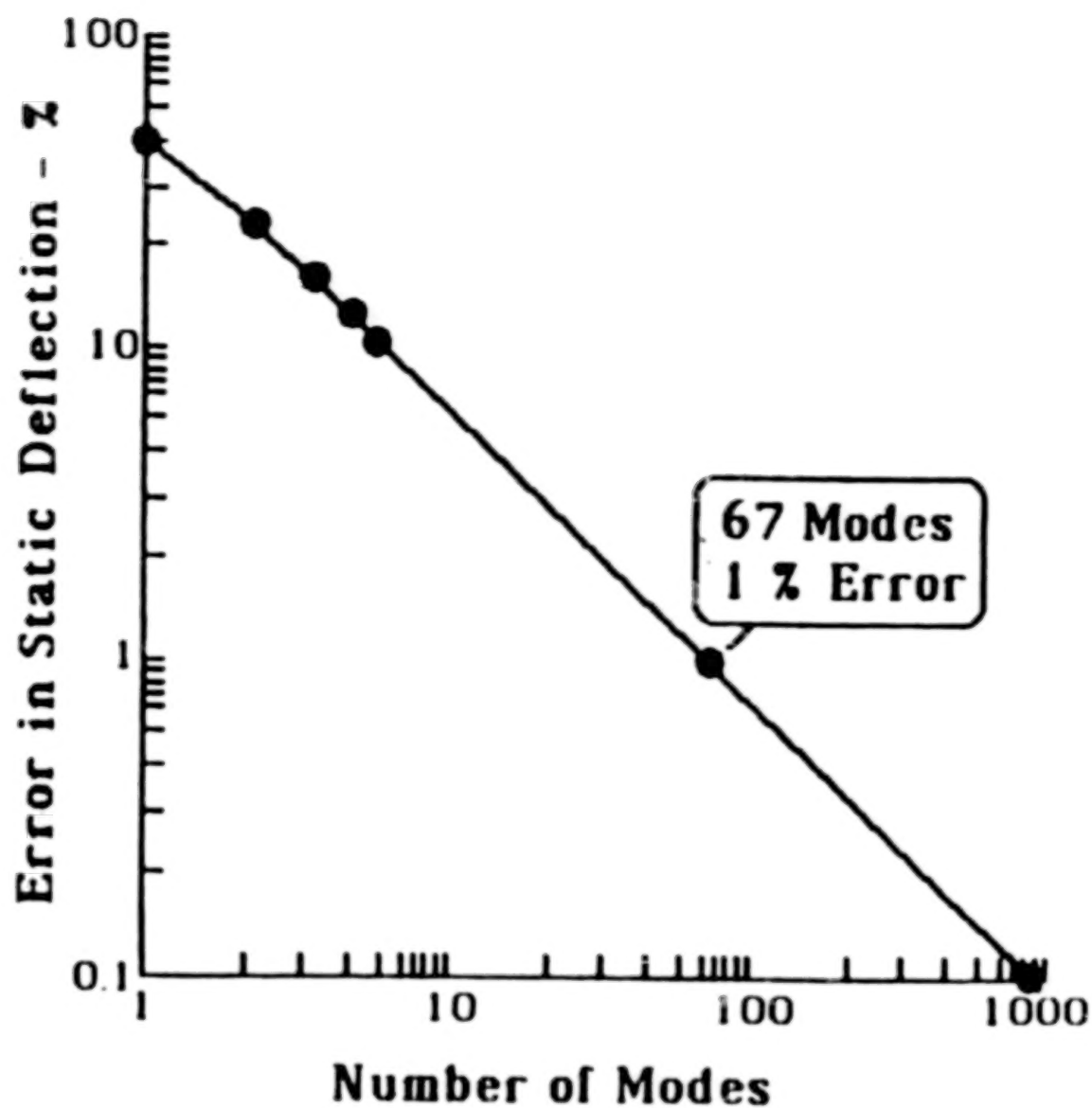


Figure 2. The Number of Modes Required for a Modal Model to Accurately Represent the Static Deflection of a Cantilevered Euler Beam.

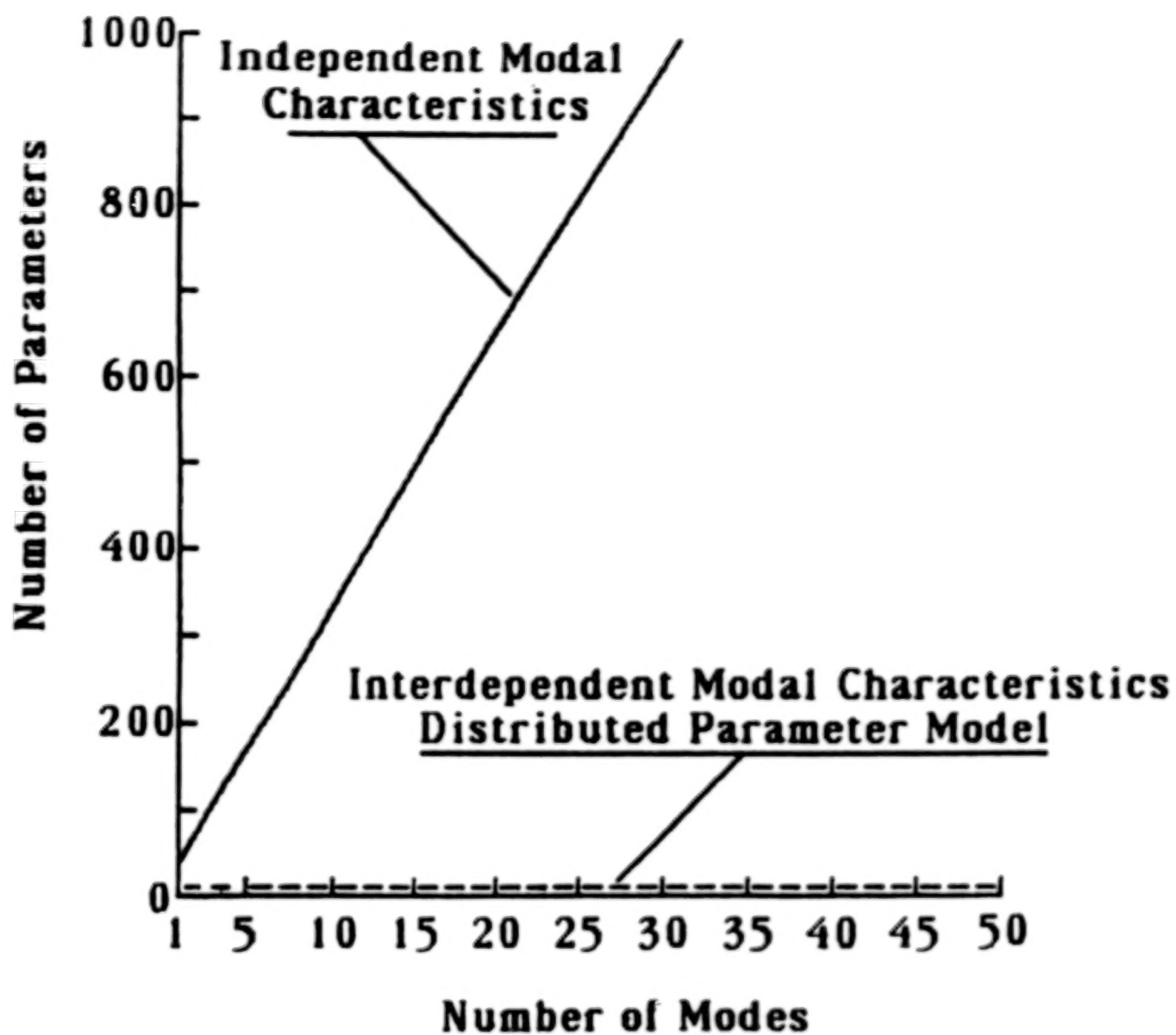


Figure 3. Comparison of the Number of Model Parameters for Modal Models and Distributed Parameter Models.

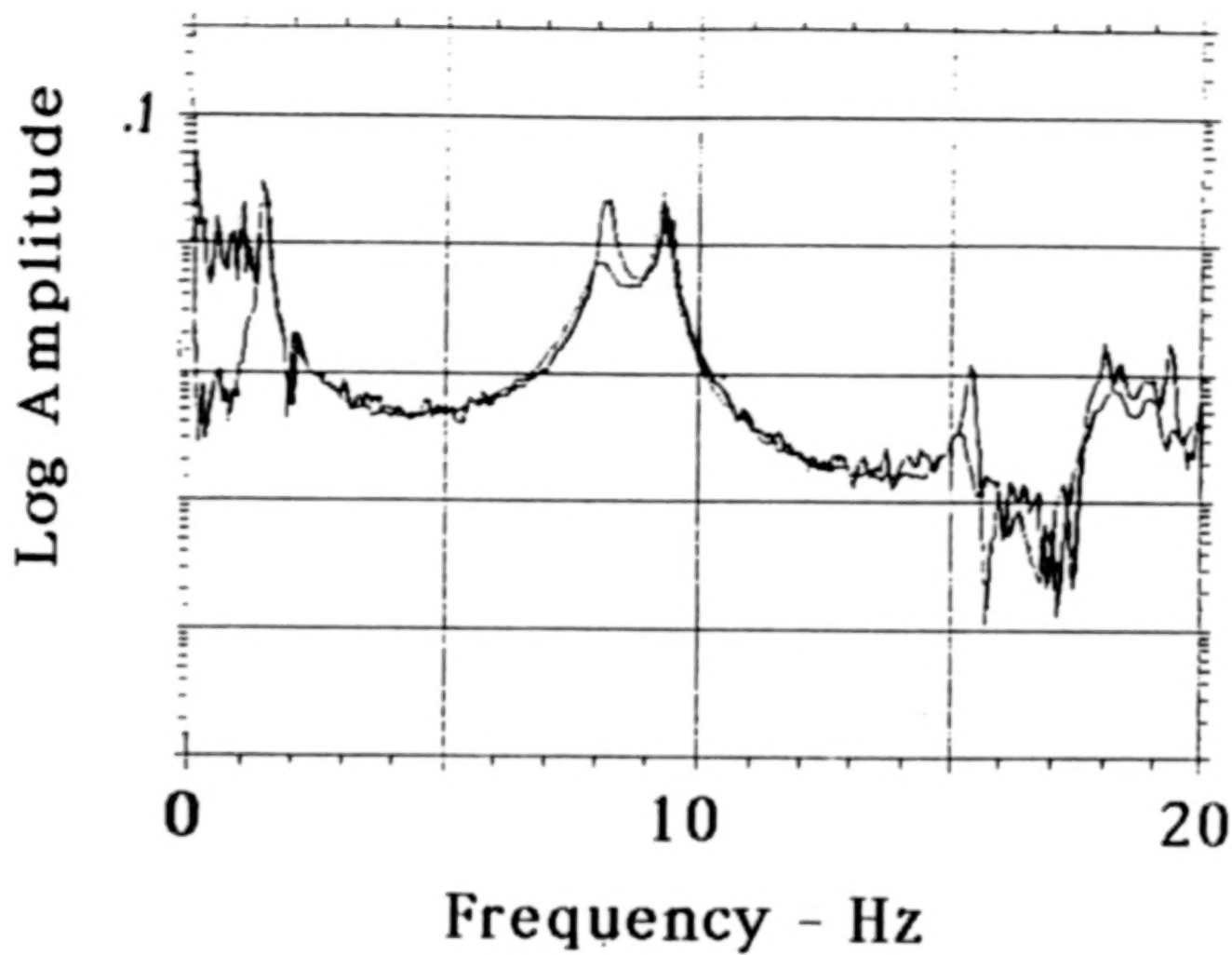


Figure 4a. Frequency Response of the Mini-MAST Truss in Term of Inches of Response per Pound of Input. Frequency from 0 to 20 Hz.

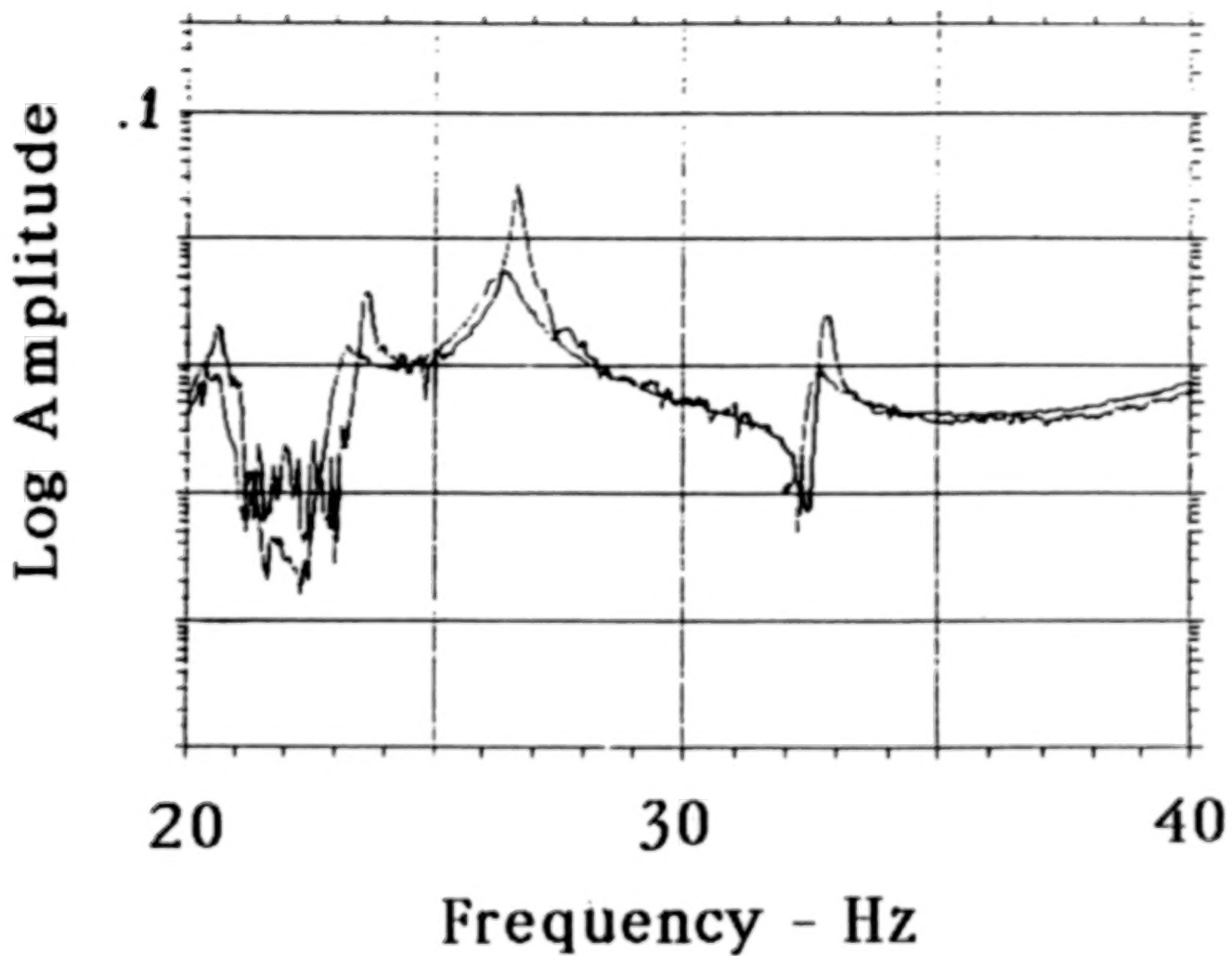


Figure 4b. Frequency Response of the Mini-MAST Truss in Term of Inches of Response per Pound of Input. Frequency from 20 to 40 Hz.

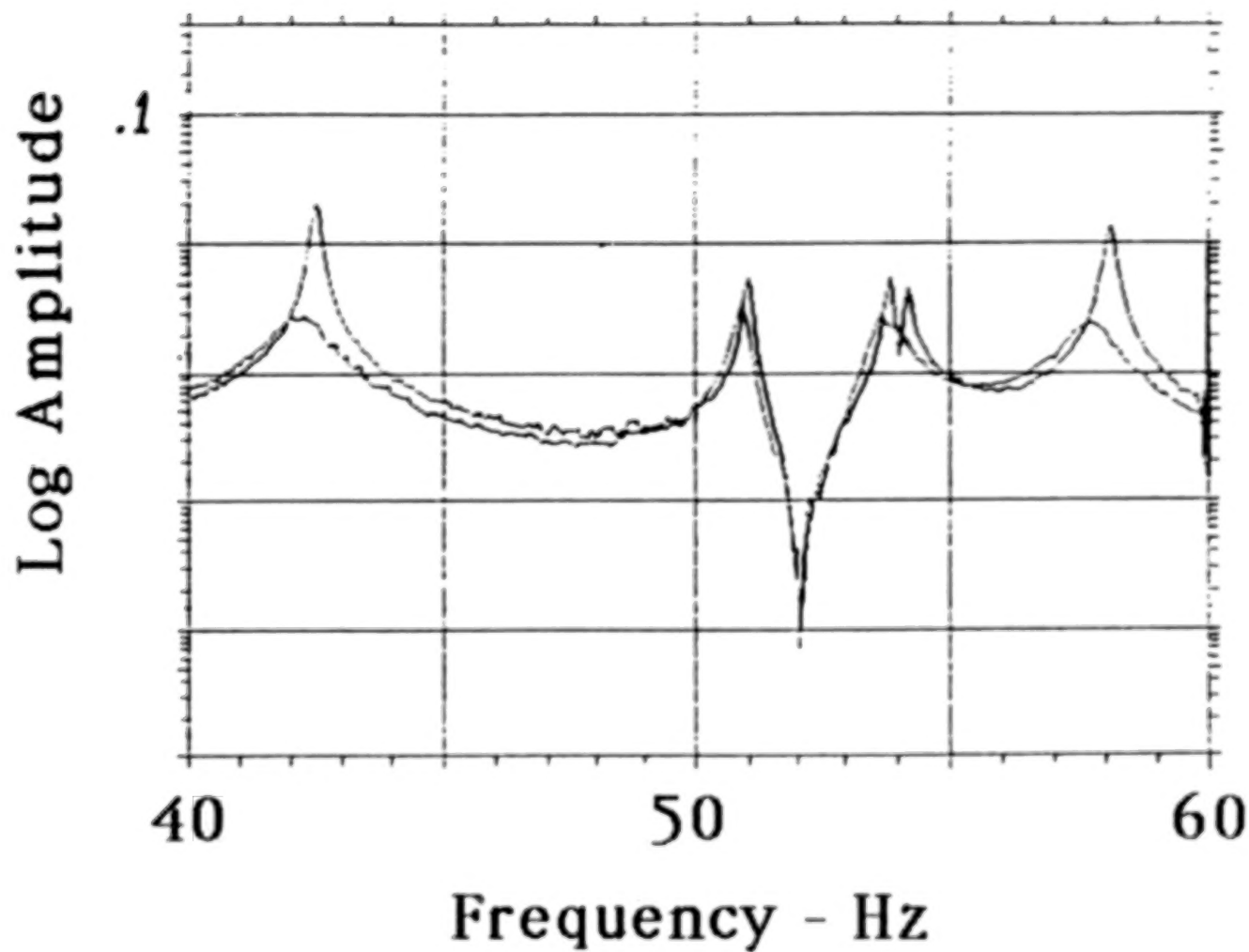


Figure 4c. Frequency Response of the Mini-MAST Truss in Term of Inches of Response per Pound of Input. Frequency from 40 to 60 Hz.

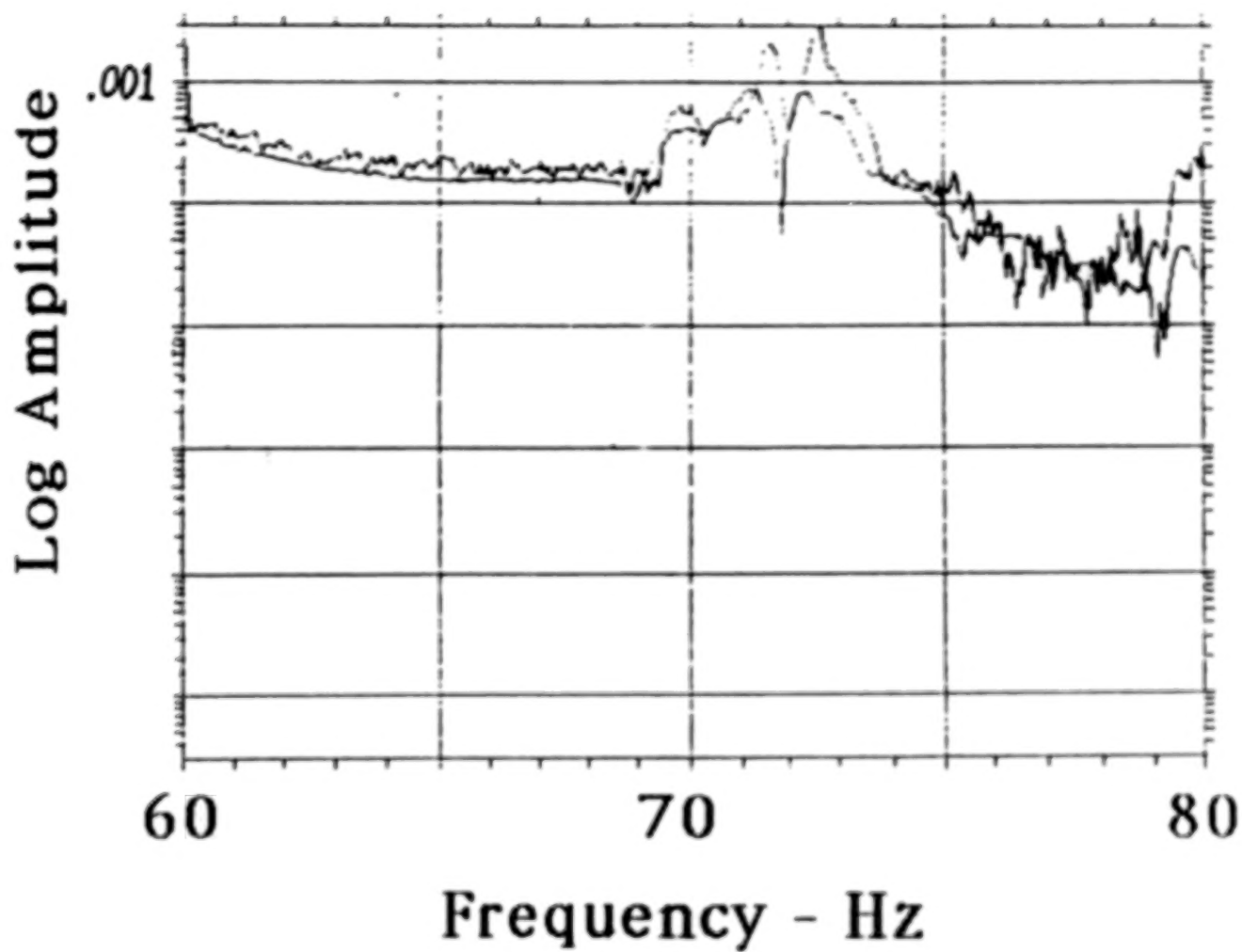


Figure 4d. Frequency Response of the Mini-MAST Truss in Term of Inches of Response per Pound of Input. Frequency from 60 to 80 Hz.



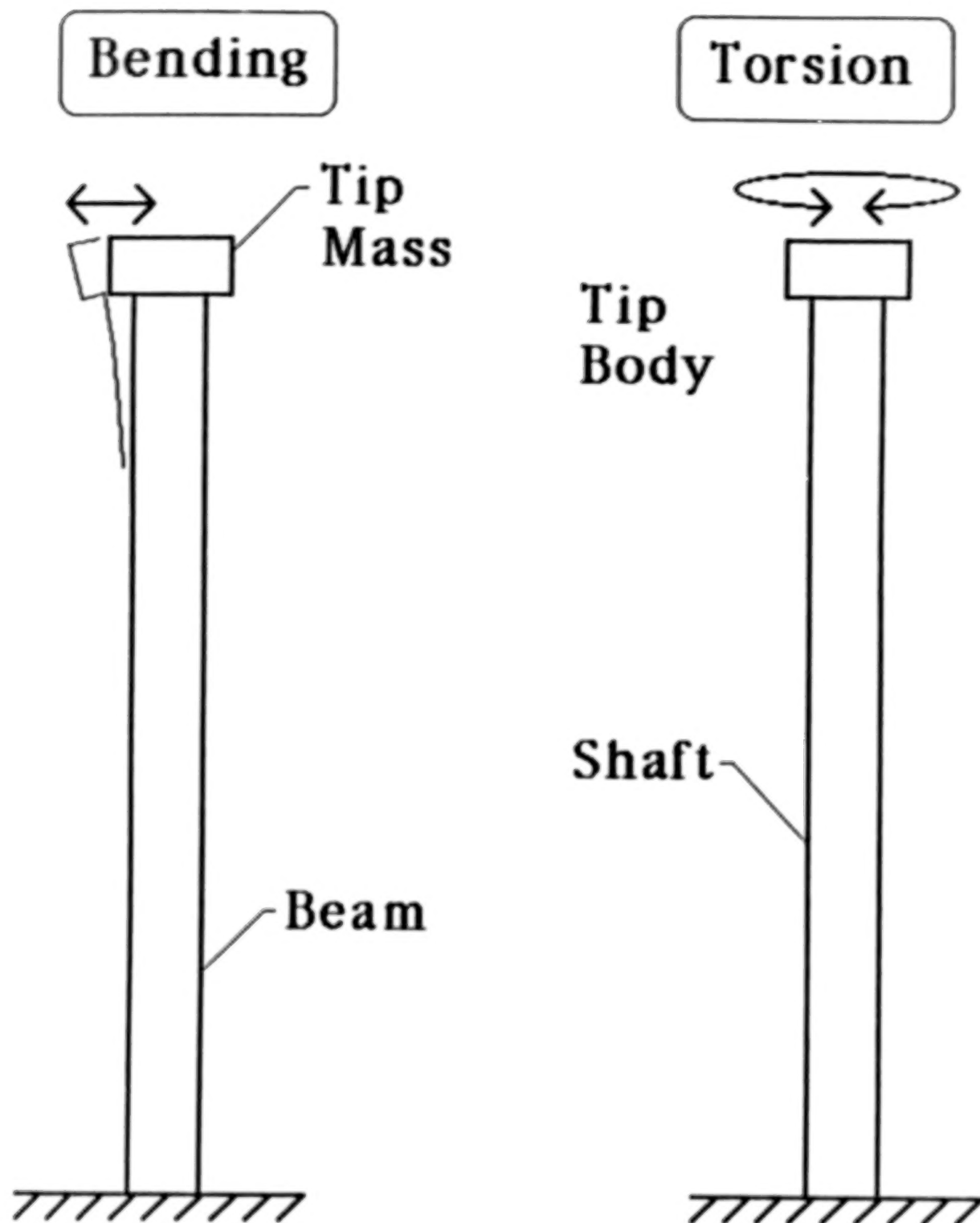


Figure 5. Schematics of Distributed Parameter Models for Bending and Torsion.

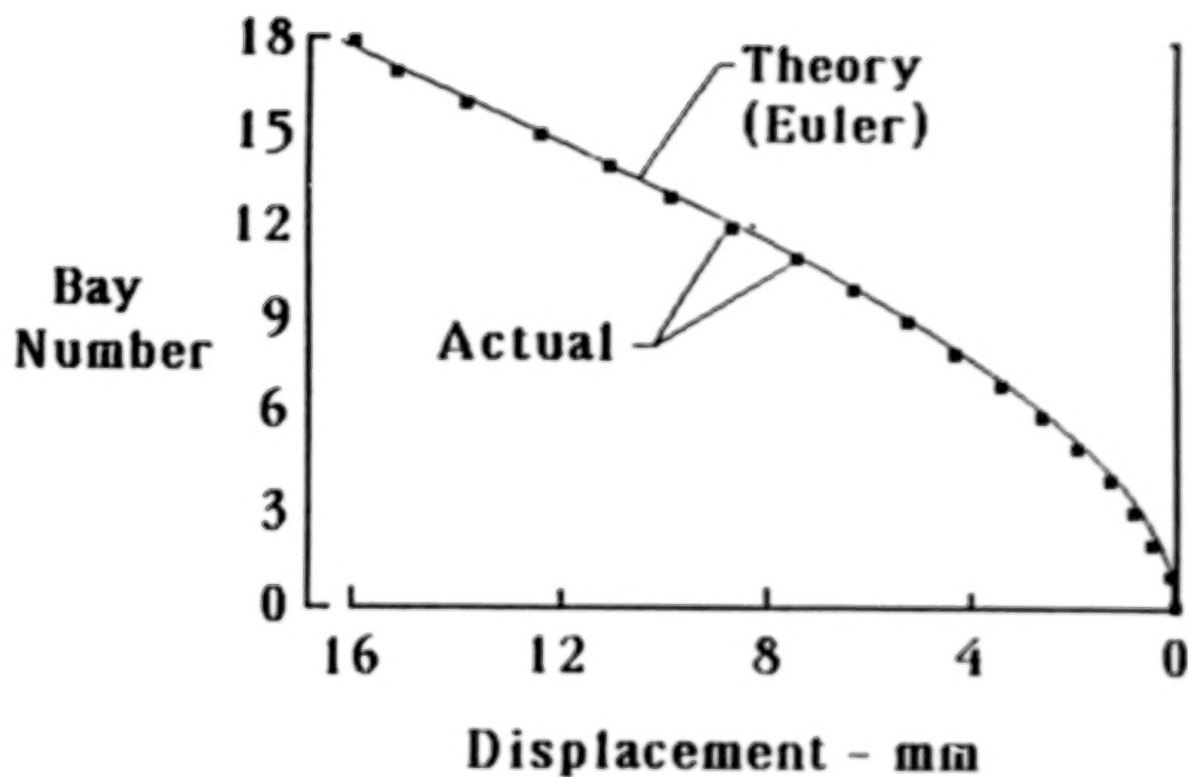


Figure 6. Comparison of the Model and Actual Static Deflection in Bending of the Mini-MAST Truss Subjected to a 15 Pound Force at the Top.

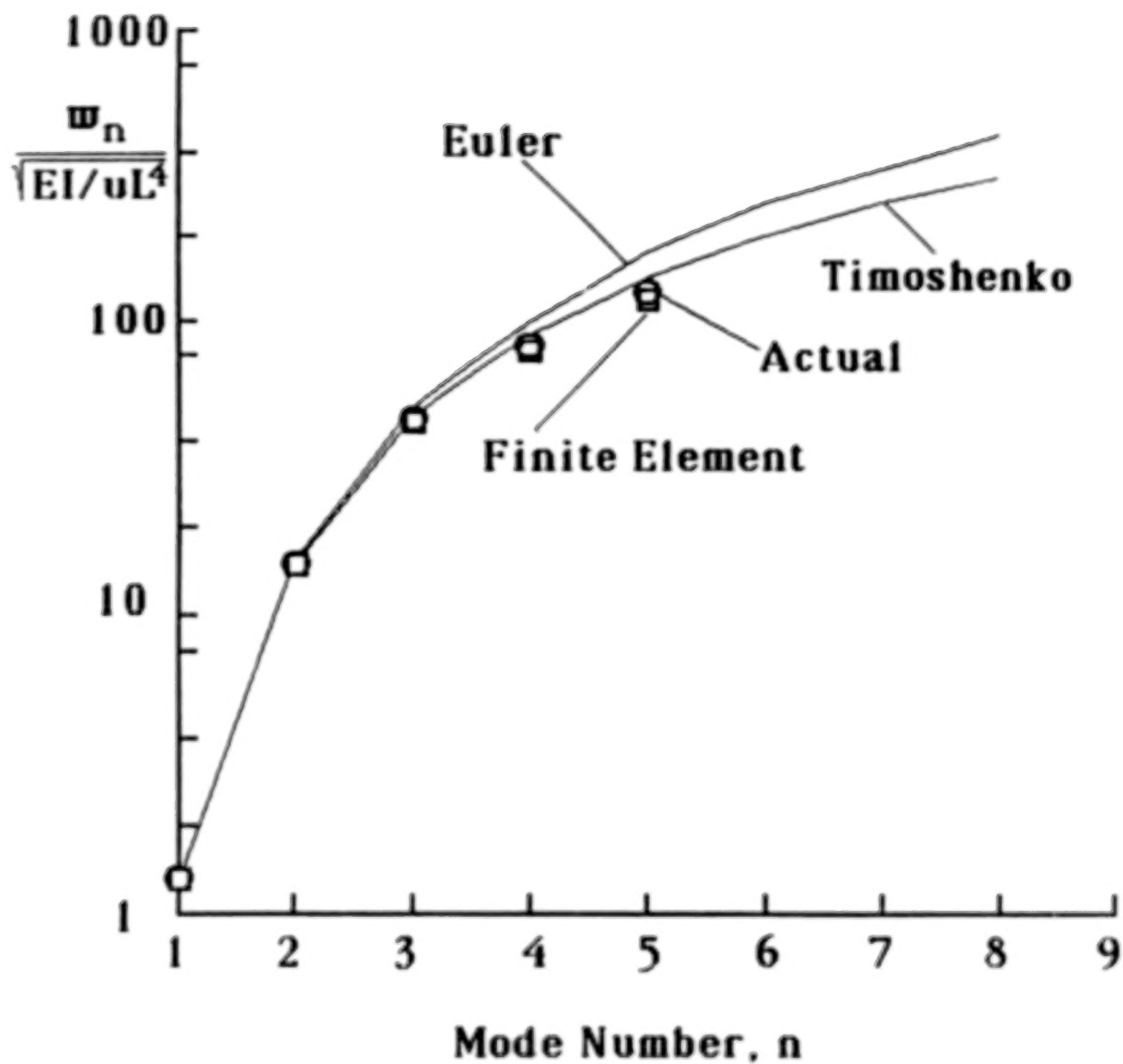


Figure 7. Comparison of Distributed Parameter Model, Finite Element Model and Actual Normalized Bending Frequencies.

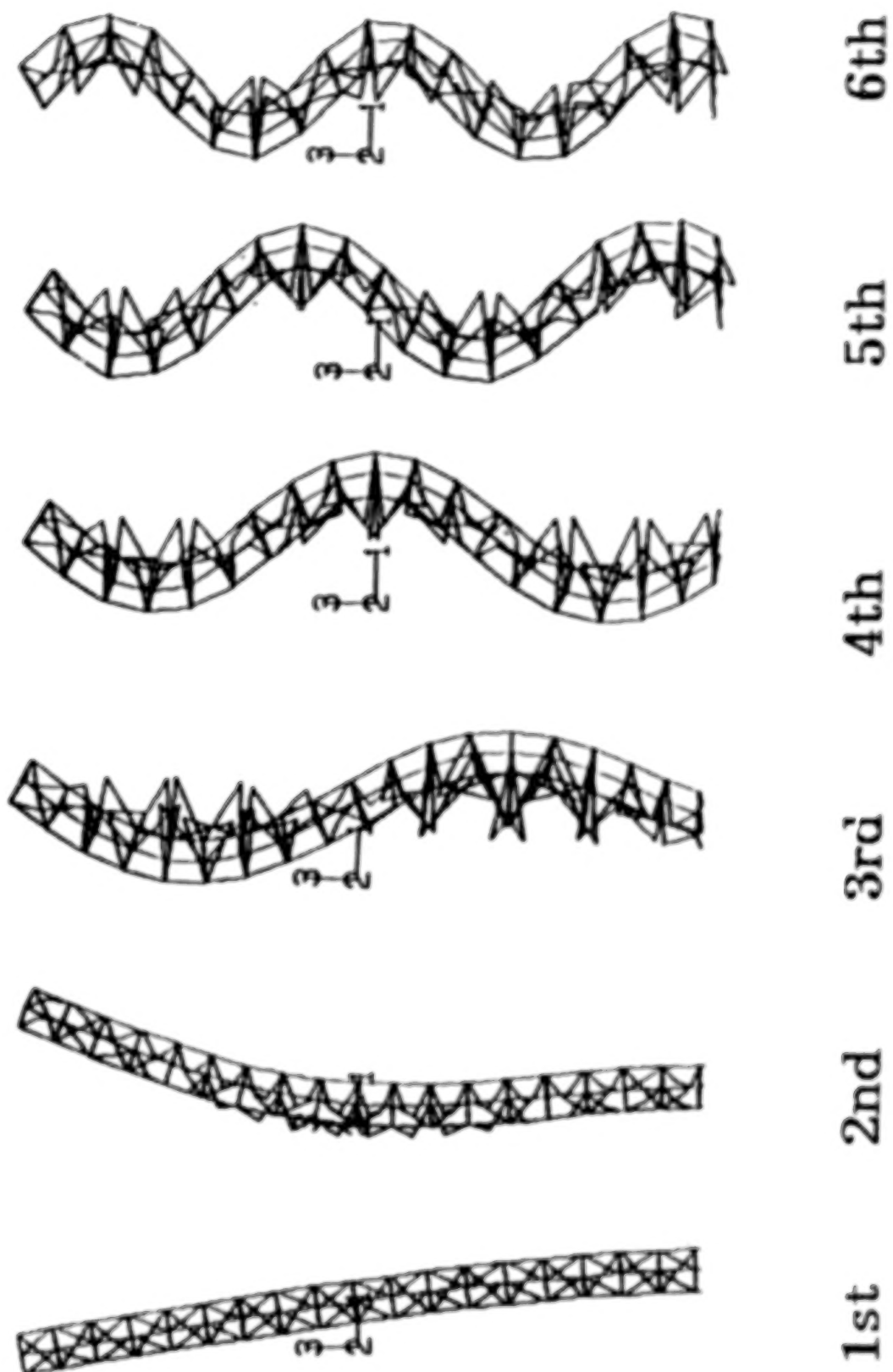


Figure 8. Finite Element Model Mode Shapes for Bending.

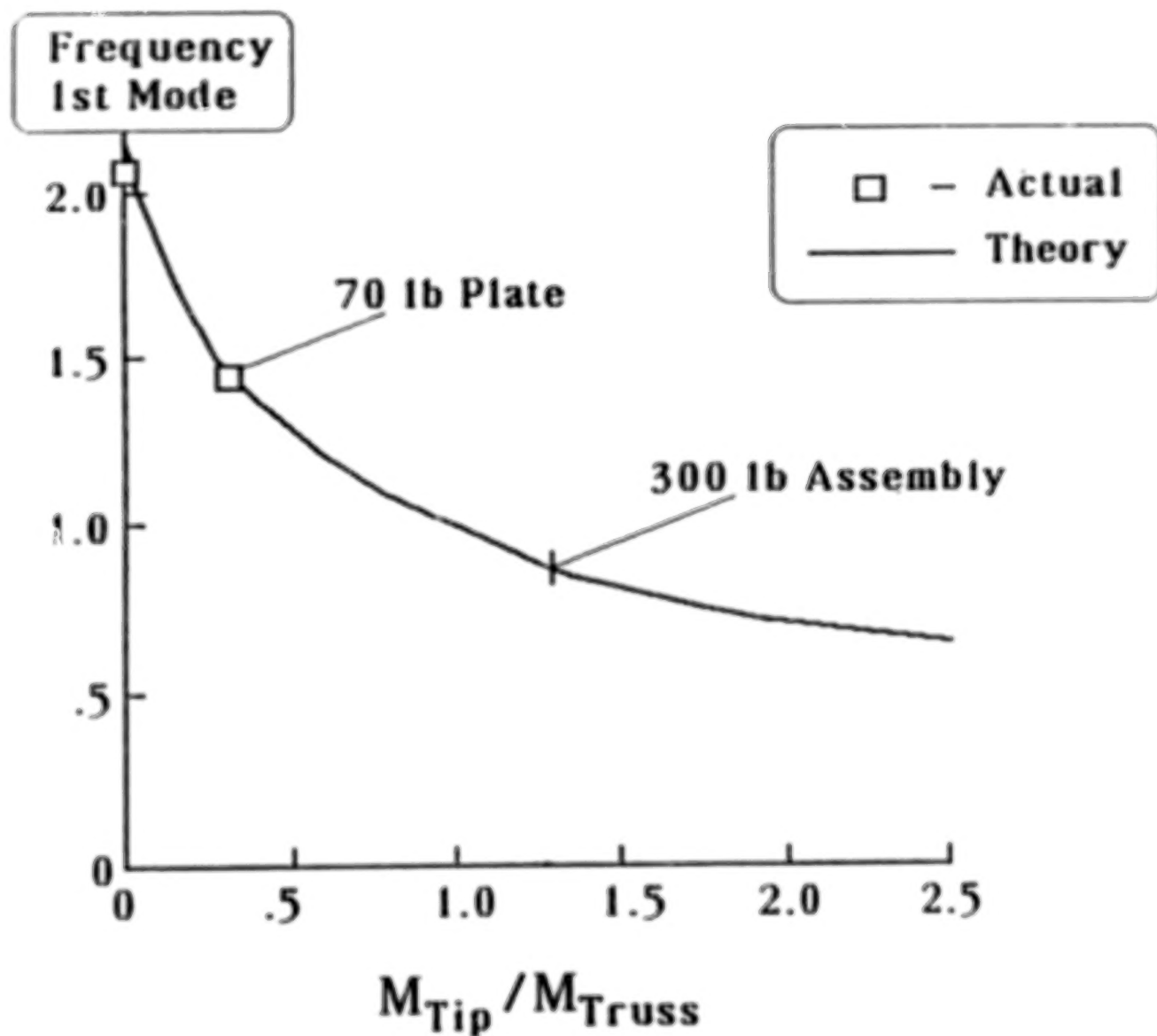


Figure 9. Comparison of the Model and Actual First Mode Bending Frequencies as a Function of Tip Mass to Truss Mass Ratio.

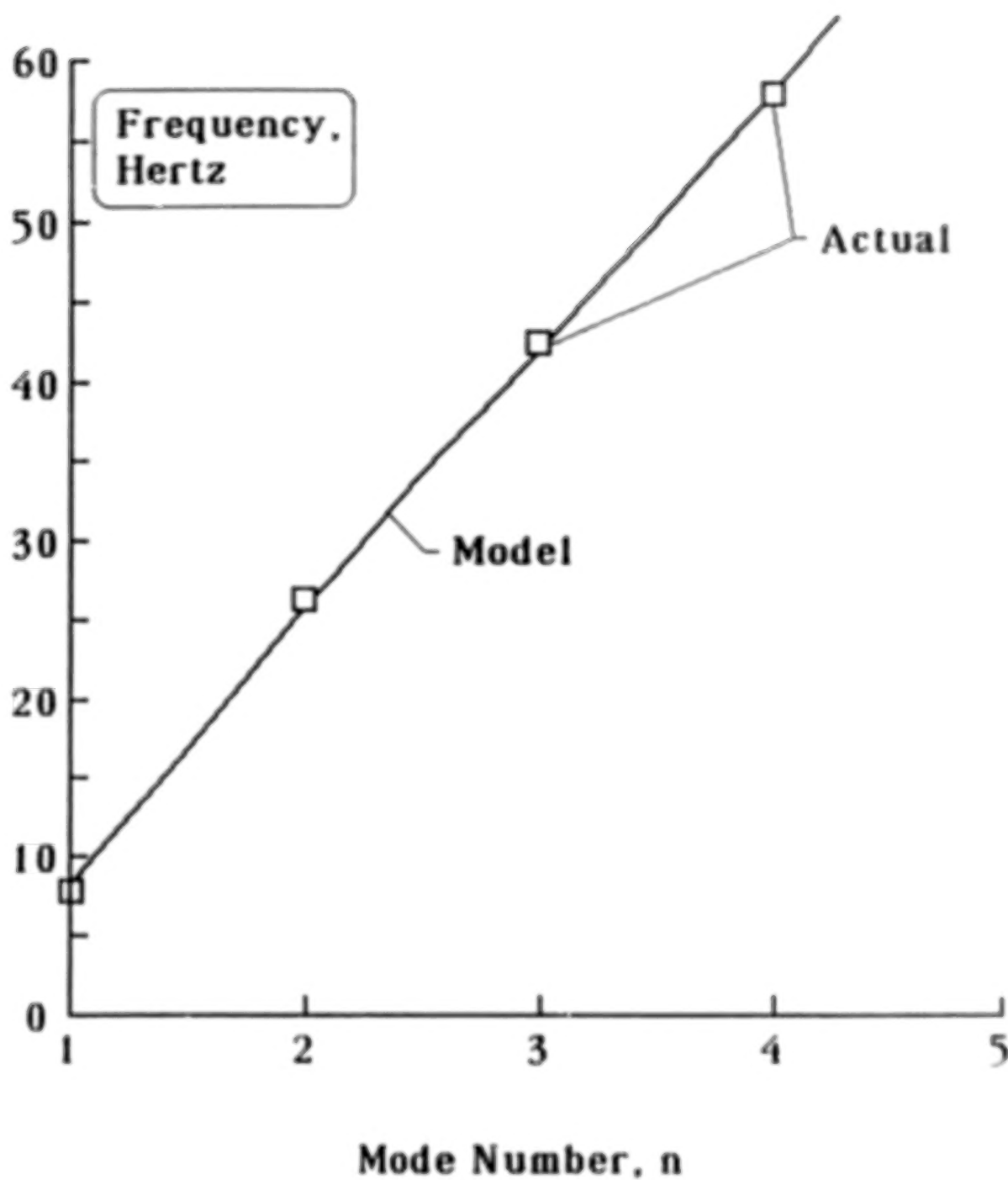
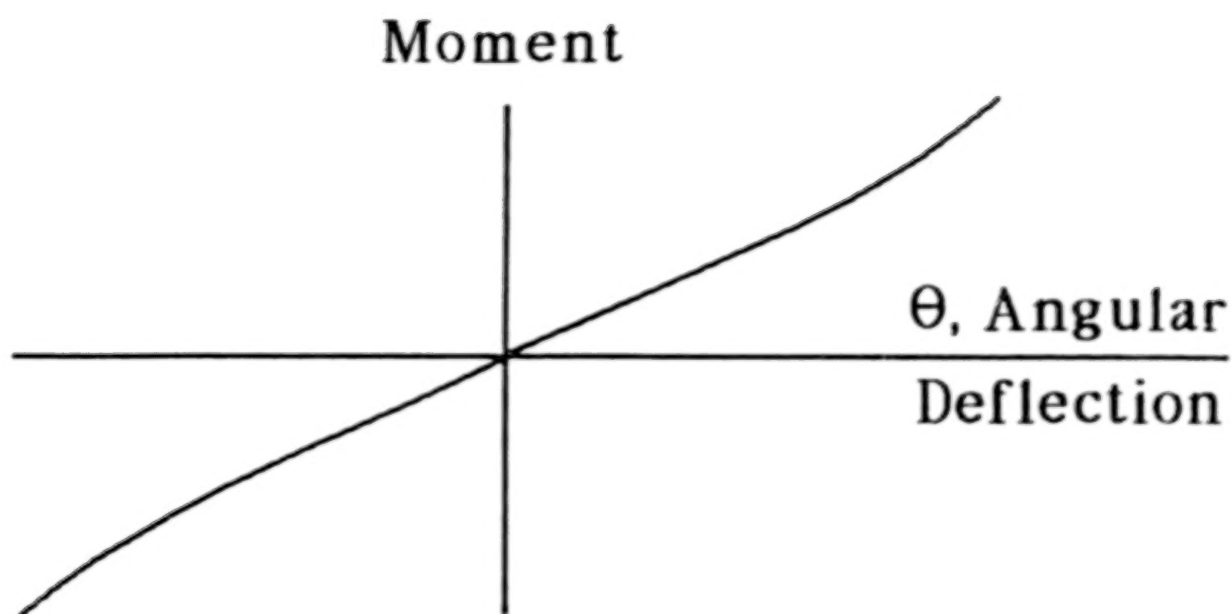


Figure 10. Comparison of Model and Actual Torsion Mode Frequencies.



$$M = \frac{K}{B} \tan(B\theta) \quad \text{or} \quad \theta = \frac{1}{B} \arctan\left(\frac{MB}{K}\right)$$

$$\left. \frac{d\theta}{dM} \right|_{M=0} = \frac{1}{K}$$



Linear

$$\left. \frac{d^3\theta}{dM^3} \right|_{M=0} = \frac{2B^2}{K^3}$$



Cubic

Figure 11. Nonlinear Stiffness Formulation Used for the Torsion Model.

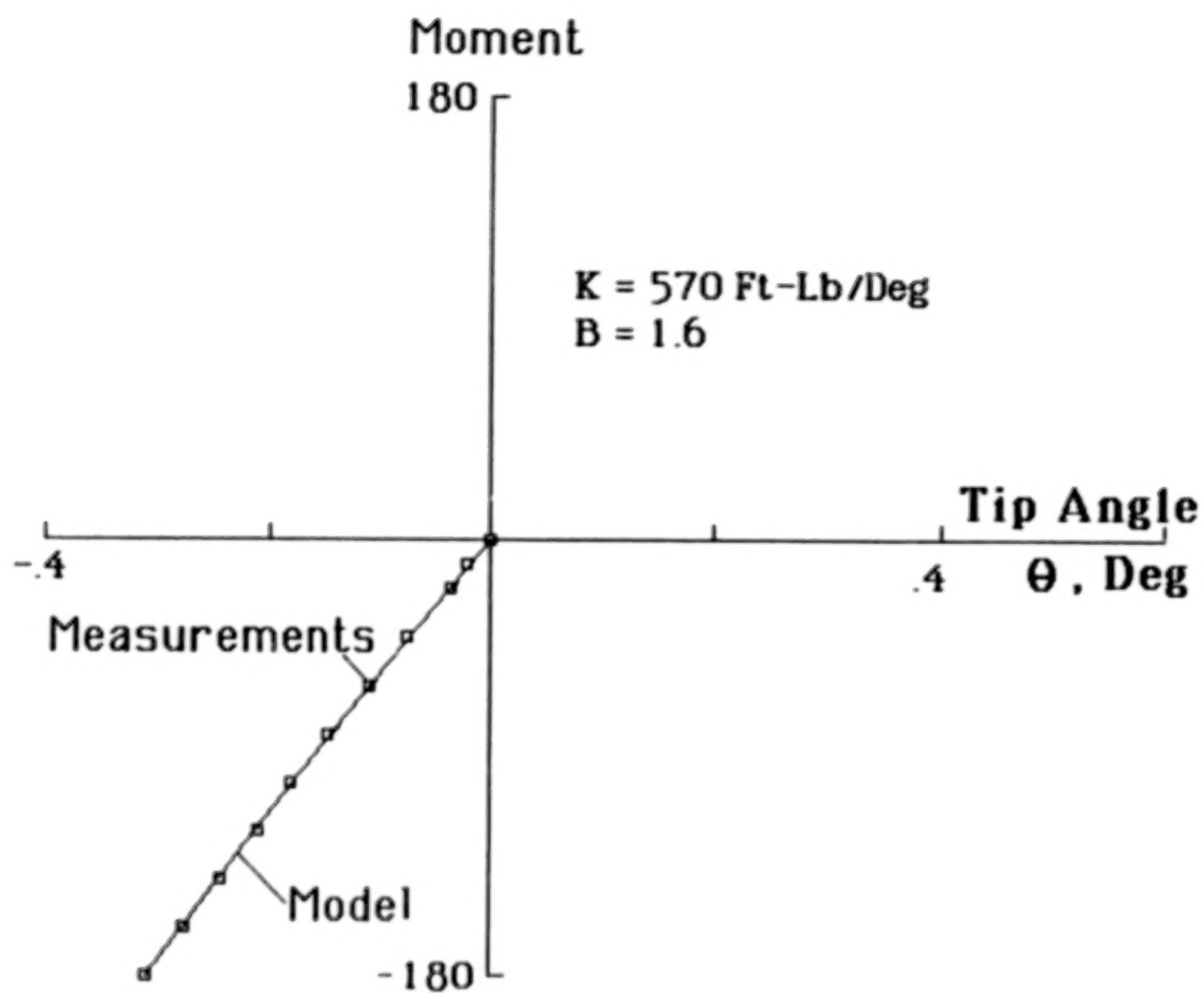


Figure 12. Comparison of Model and Actual Static Deflection in Torsion.



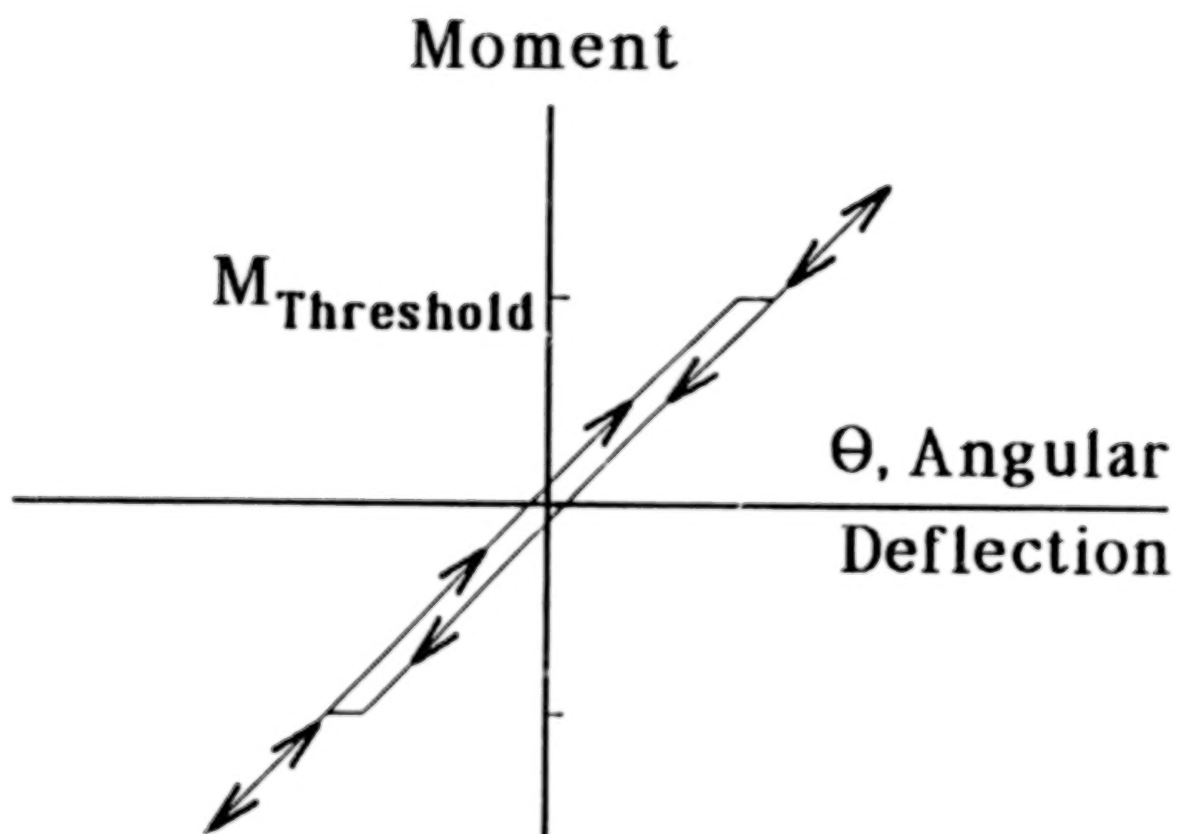
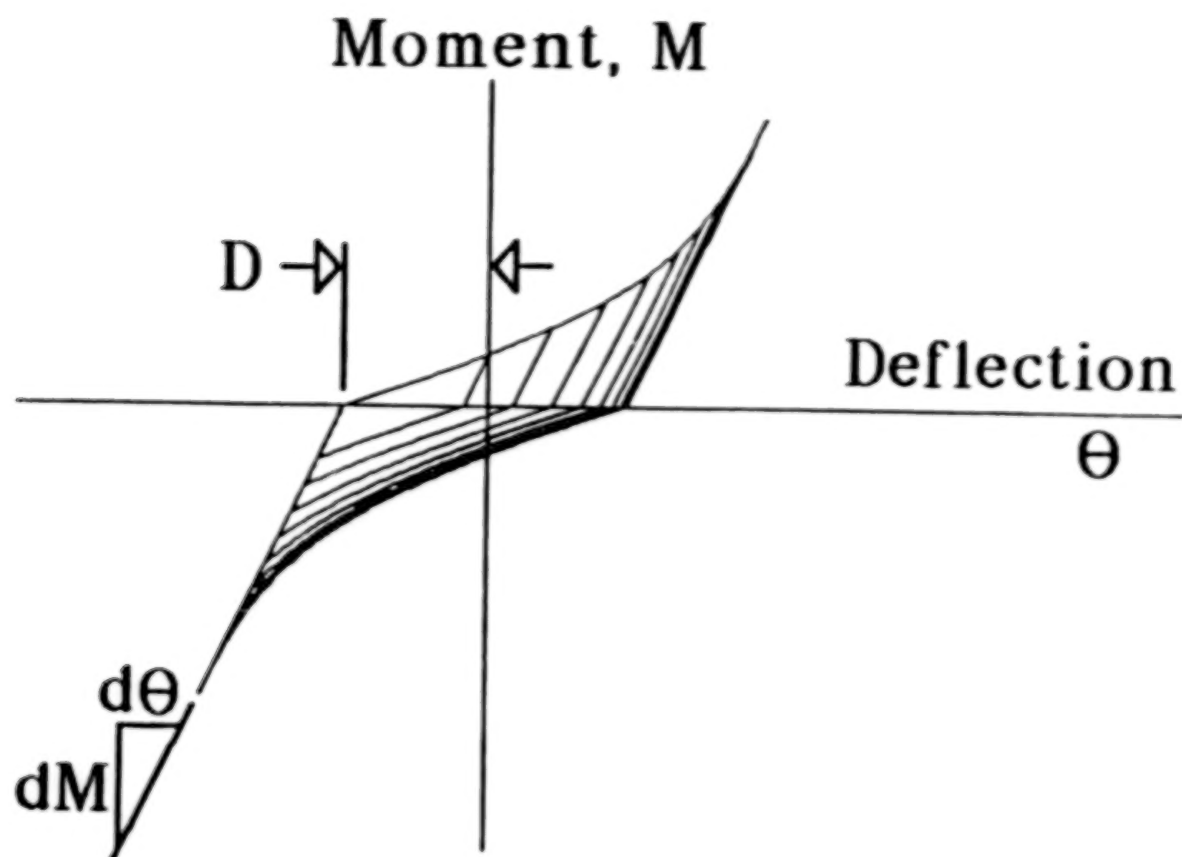


Figure 13. An Individual Nonlinear Slip Element for the Torsion Model.



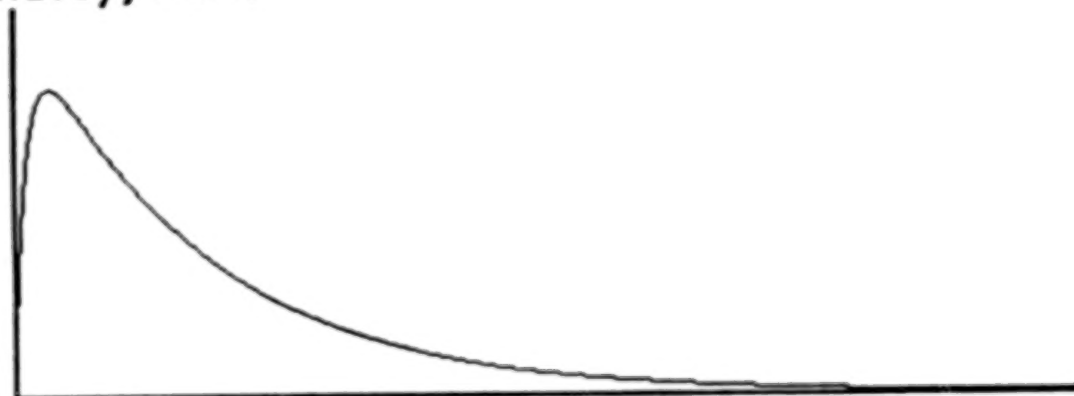
$$\theta = M/K + D \int_A^M P'(M) dM$$

$$A = M_{\text{reversal}} \quad \text{if} \quad M_{\text{reversal}} > 0$$

$$= 0 \quad \text{if} \quad M_{\text{reversal}} < 0$$

Figure 14. Nonlinear Hysteretic Model for Torsion.

Probability  
Density,  $P'(M)$



Slip Threshold Moment,  $M$

$$P'(M) = -\frac{e^{-M/X_1}}{X_2 - X_1} + \frac{e^{-M/X_2}}{X_2 - X_1}$$

Figure 15. The Slip Distribution Function.

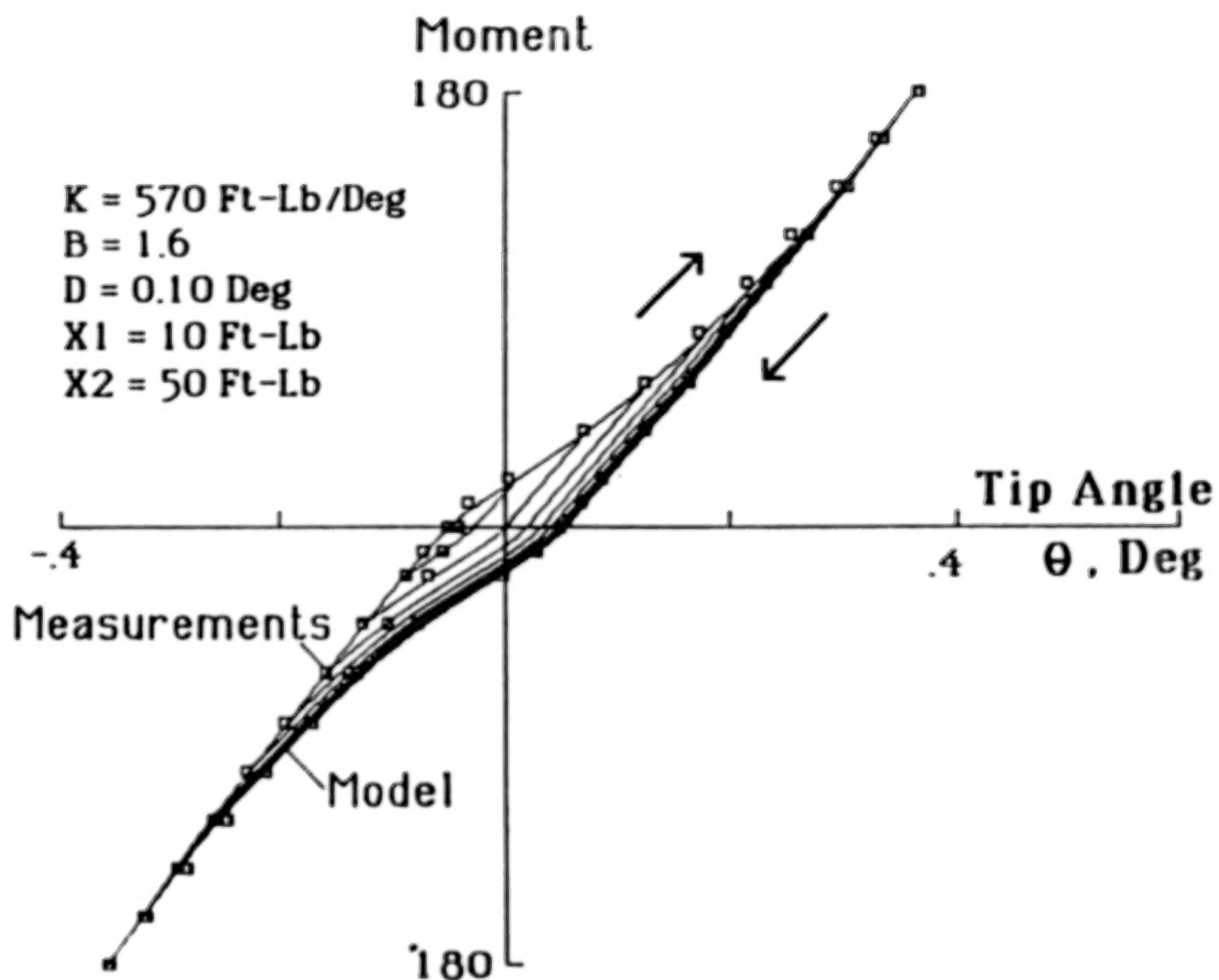


Figure 16. Comparison of Hysteretic Model and Actual Static Deflection in Torsion.

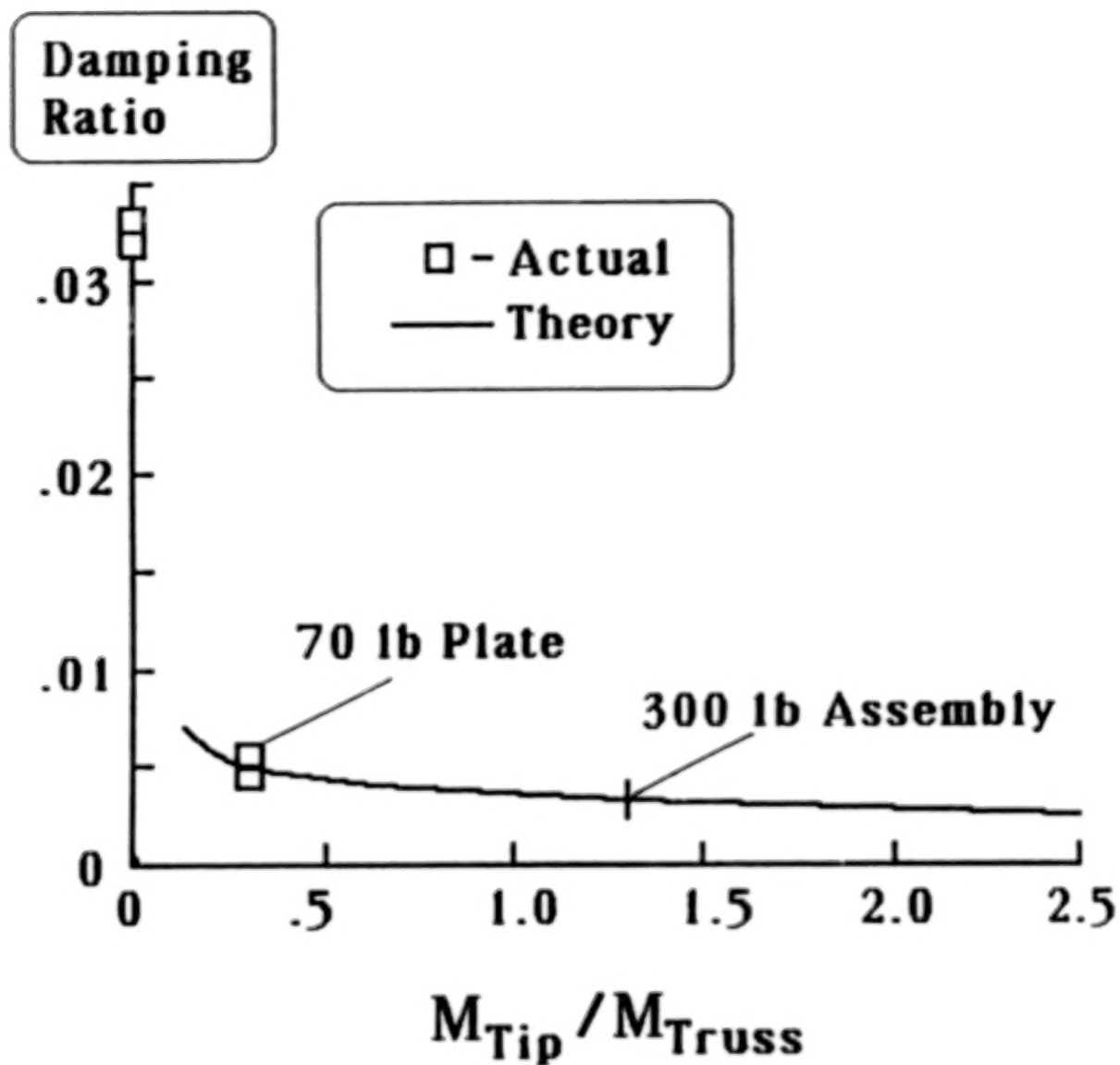


Figure 17. Comparison of Model and Actual Damping Ratios in Bending as a Function of Tip Mass to Truss Mass Ratio.

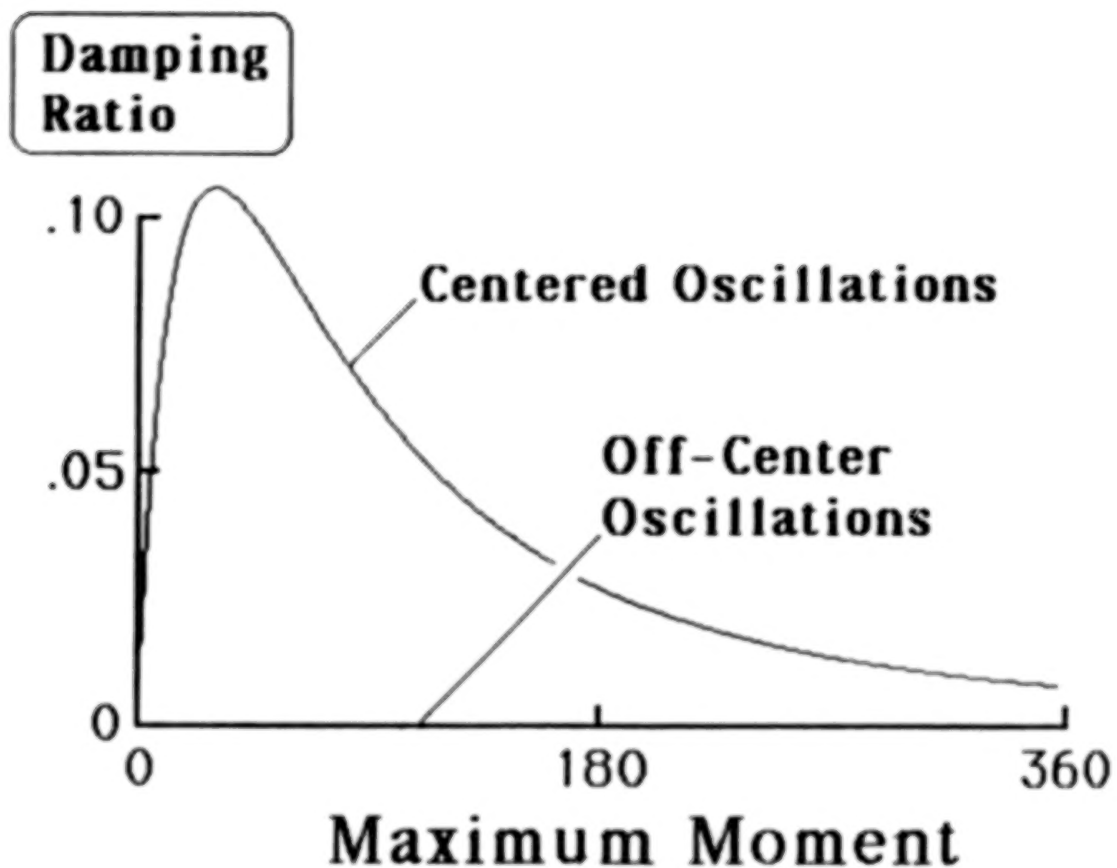


Figure 18. Effect of the Hysteretic Behavior on Damping in Torsion.

## EFFICIENCY AND CAPABILITIES OF MULTI-BODY SIMULATIONS

R.J. VanderVoort  
DYNACS Engineering Co., Inc.  
Clearwater, Fl

### ABSTRACT

Simulation efficiency and capability go hand in hand. The more capability you have the lower the efficiency will be. Section 1 of this paper discusses efficiency and section 2 deals with capabilities. The lesson we have learned about generic simulation is: Don't rule out any capabilities at the beginning but keep each one on a switch so it can be bypassed when warranted by a specific application.

### 1. EFFICIENCY

Efficiency means different things to different people. For the person running simulations interactively on a terminal quick turn around time is efficiency. For the person making 10,000 Monte-Carlo runs low cost is efficiency. For the person running real time simulations minimum CPU time is efficiency.

Three aspects of a simulation should be considered when dealing with efficiency; hardware, software and modeling.

Hardware A fast processor will reduce CPU time for a given simulation but this doesn't necessarily equate to improved efficiency. For example, the Monte-Carlo simulation may take 10 minutes on a super computer and 2 weeks on a PC but if time is free on the PC then that may be an efficient solution. We will not discuss hardware related issues except for two points. 1.) Fast hardware is of primary importance to the real time simulation because it means higher fidelity models can be incorporated 2.) Vector processors and parallel processors should use custom algorithms that take full advantage of the special machine architecture.

Software A fast algorithm will also reduce CPU time but again this doesn't necessarily equate to improved efficiency. For example, it is generally accepted that an ad-hoc simulation is much faster than a generic simulation. The cost of developing and testing the ad-hoc simulation may exceed the run time saving thereby reducing overall efficiency.

Recent work in the area of symbolic programming has shown that significant savings can be achieved by symbolically forming the equation of motion and numerically solving them. Other algorithms have been proposed that promise similar savings. There is one point that software developers should keep in mind. With generic simulations the user must have complete flexibility in retaining or deleting different parts of his model. This is because generic simulations are often used for model development and validation. In that environment an analyst will add or delete certain features to determine the effect on performance and whether or not the feature should be retained in the model.

More on this subject in section 2.

Modeling This is the domain of the simulation user and the area in which many improvements in efficiency can be made. For example, deleting a high order mode in a flexible body model has a compound effect. It reduces the model complexity and at the same time allows a bigger integration step size both of which reduce run time. Often times the reduced fidelity is justified by the savings in run time.

The point to be made is that the analyst is the end authority on the "correct" model for a given application. The more flexibility he has in changing his model the easier it is for him to select the best model for the job.

## 2. CAPABILITIES

Capability in our context is synonymous with flexibility and not with complexity. A simulation may be very detailed and complex but if it can't be changed then it's only useful in a narrow range of applications and has limited capability.

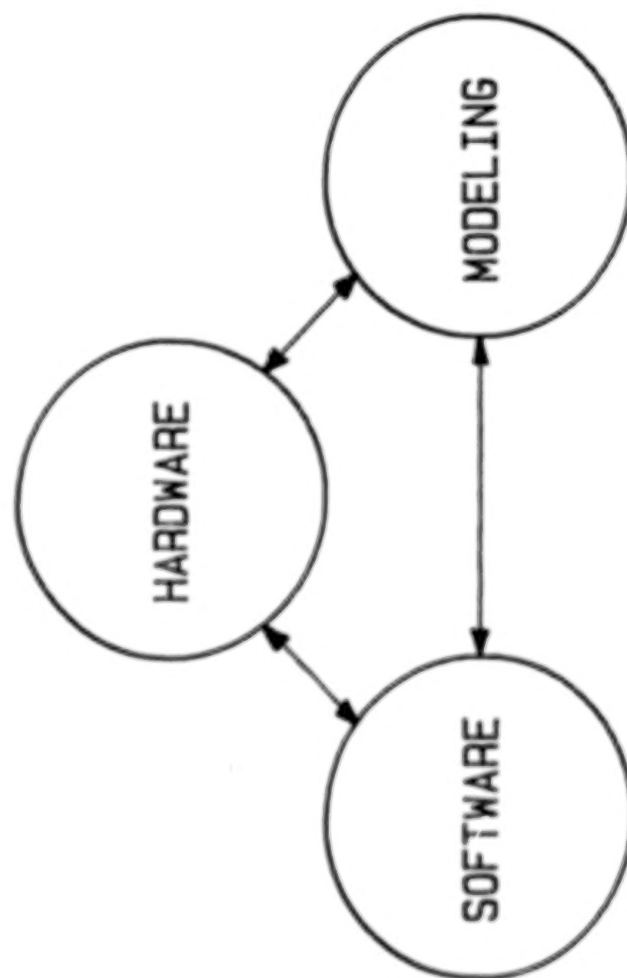
In our experience with TREETOPS and DCAP we have found that it is much easier to generate a model and obtain a response than it is to predict the correct response. In other words, when we don't get the expected response the simulation is usually correct and our expectation is wrong. This is not entirely unexpected because it is very difficult, even for an expert, to solve the equations of anything but the simplest dynamical systems. The solution to this dilemma is flexibility. Start with simple models that have known analytic solutions. Then add complexity one step at a time while gaining confidence in your model and insight into the behavior of your system.



For multibody systems with flexible bodies the same arguments apply but the complexity of the model increases more rapidly than for rigid bodies. The person doing software development makes assumptions that simplify the resulting equations of motion. If this is done carelessly then terms are dropped that may prove essential in specific applications. On the other hand, if simplifications are not made then the computation burden becomes too great.

The lesson we learned is that you must retain as many terms as possible in the kinematics but they must have associated switches so you can easily add or delete them from a specific application. This is done for two reasons. 1.) to give you insight into the effect of various model elements on system response and 2.) to allow the selection of the most efficient model for a given application.

# SIMULATION EFFICIENCY



- |                         |                                |
|-------------------------|--------------------------------|
| • BYPASS TERMS          | • BYPASS TERMS                 |
| • MULTI-RATE ALGORITHMS | • INTEGRATION TYPE & STEP SIZE |
| • SYMBOLIC PROGRAMMING  | • REDUCED ORDER                |
| • ADHOC SIMULATION      | •                              |
| •                       | •                              |

# SPEED-UP OPTIONS

COORDINATE TRANSFORMATIONS	MASS MATRIX FORMULATION (M)	NON-LINEAR TERMS $(\dot{\omega} \times I \cdot \dot{\omega})$	CONSTRAINT FORMULATION (A)
PERFORM ALL COMPUTATIONS			
COMPUTE ONLY ON FIRST PASS OF R-K INTEGRATION			
COMPUTE ONLY ON FIRST PASS OF NTH R-K STEP			
BYPASS COMPUTATIONS			



# TREETOPS SOFTWARE IMPROVEMENTS

	<u>EQUATION FORMULATION</u>	<u>EQUATION SOLUTION</u>	<u>PROCESSING HARDWARE</u>
CURRENT STATUS	NUMERIC	NUMERIC	SERIAL
FIRST STEP	NUMERIC SYMBOLIC	NUMERIC	SERIAL PARALLEL
SECOND STEP	SYMBOLIC	NUMERIC	

$$M\ddot{q} = f + A^T \lambda$$

$$A\dot{q} = B$$

# SIMULATION CAPABILITY-MENUS

<u>BODIES</u>	<u>SENSORS</u>	<u>ACTUATORS</u>	<u>CONSTRAINTS</u>	<u>DEVICES</u>	<u>CONTROLLERS</u>
1. RIGID	1. RATE GYRO	1. REACTION JET	1. CLOSED LOOP	1. SPRINGS	1. CONTINUOUS
2. FLEXIBLE	2. RESOLVER	2. HYDRAULIC	2. VELOCITY-TIME	2. DAMPERS	2. DISCRETE
	3. ANGULAR	3. REACTION	3. VELOCITY	3. COULOMB	3. BLOCK DIAGRAM
	ACCELEROMETER	WHEEL	-DIRECTION	DAMPER	(FREQUENCY
	4. VELOCITY	4. TORQUE	4. RATE-TIME	4. QUADRATIC	DOMAIN)
	5. POSITION	5. MOTOR	5. RATE-DIRECTION	5. SPRING/DAMPER	4. MATRIX
	6. ACCELEROMETER	6. MOMENT	6. CUT JPINT	5. SOLID DAMPER	(STATE SPACE)
	7. TACHOMETER	7. LOCK		6. HARDSTOP	5. USER
	8. INTEGRATING	8. SINGLE GIMBAL		7. CONTACT	
	RATE GYRO	CMG		SPRINGS	
	9. SUN SENSOR				
	10. STAR SENSOR				
	11. IMU	9. DOUBLE GIMBAL			
	12. POSITION VECTOR	CMG			
	13. VELOCITY VECTOR	10. MAGNETIC			

SWITCHES FOR MODAL DATA

● HIGH LEVEL

— LUMPED MASS SWITCH

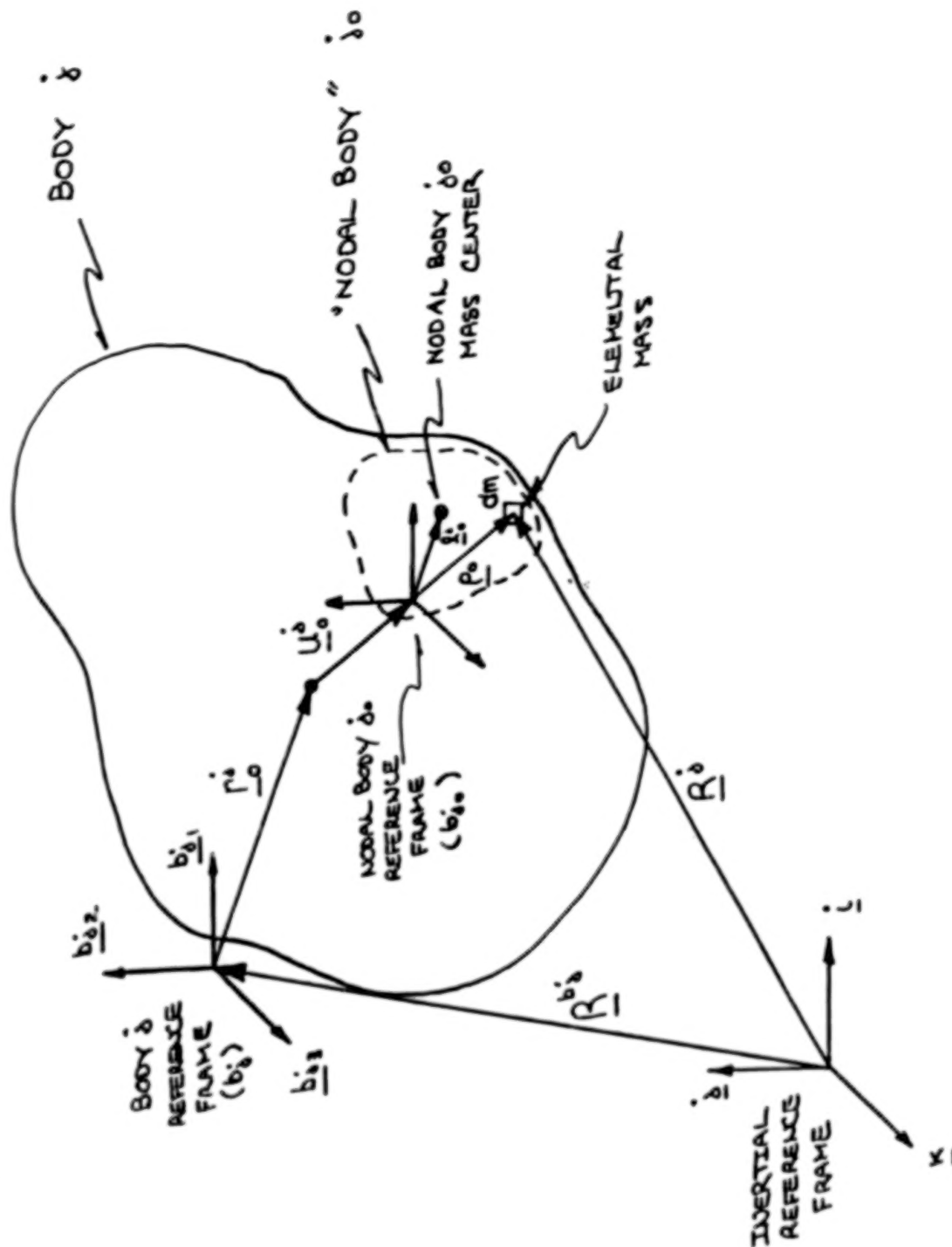
● MID LEVEL

- FIRST ORDER SWITCH
- SECOND ORDER SWITCH
- THIRD ORDER SWITCH

● LOW LEVEL

— ONE SWITCH FOR EACH TERM

# FLEXIBLE BODY DISPLACEMENT FIELD



$$\underline{\dot{f}}_K + \underline{\dot{f}}_K^* = 0 ; K = 1, \dots, N$$

$$\begin{aligned} \underline{\dot{f}}_K &= \sum_{i=0}^{N-1} \left\{ \underline{\dot{V}}_K^i \cdot \underline{\dot{d}}_i^i \right\} \\ -\underline{\dot{f}}_K^* &= \sum_{i=0}^{N-1} \left\{ \sum_{j=0}^{N-1} \underline{\dot{V}}_K^i \cdot \underline{\dot{R}}_j^i \underline{\dot{d}}_m \right\} \end{aligned}$$

FROM NEWTON'S LAW

$$\int_{b_i} \underline{\dot{d}}_i^i - \underline{\dot{R}}_i^i \underline{\dot{d}}_m = 0$$

NOTE: OPEN DOT  
DENOTES LOCAL TIME  
DERIVATIVE, SOLID DOT  
DENOTES INERTIAL TIME  
DERIVATIVE.

$$\underline{\dot{V}}_K^i = \underline{\dot{V}}_K^i + \underline{\dot{U}}_K^i \times (\underline{\dot{r}}_0^i + \underline{\dot{u}}_0^i + \underline{\dot{p}}_0^i) + \underline{\dot{V}}_K^i$$

$$\underline{\dot{R}}_i^i = \underline{\dot{R}}_i^i + \underline{\dot{U}}_i^i \times (\underline{\dot{r}}_0^i + \underline{\dot{u}}_0^i + \underline{\dot{p}}_0^i) + \underline{\dot{U}}_i^i + \underline{\dot{U}}_0^i \times \underline{\dot{p}}_0^i + 2 \underline{\dot{U}}_i^i \times \underline{\dot{U}}_0^i$$

$$+ (\underline{\dot{U}}_i^i \times \underline{\dot{U}}_0^i) \times \underline{\dot{p}}_0^i + \underline{\dot{U}}_i^i \times (\underline{\dot{r}}_0^i + \underline{\dot{u}}_0^i + \underline{\dot{p}}_0^i)$$

$$+ \underline{\dot{U}}_i^i \times (\underline{\dot{U}}_0^i \times \underline{\dot{p}}_0^i) + \underline{\dot{U}}_i^i \times (\underline{\dot{U}}_0^i \times \underline{\dot{p}}_0^i)$$



## COEFFICIENTS OF GENERALIZED SPEEDS

### TRANSLATIONAL D.O.F.

LET  $K$  CORRESPOND TO THE  $i$ -TH TRANSLATIONAL D.O.F. OF THE  $q$ -TH HINGE.

$$\underline{V}_K^{\dot{b}_i} = \begin{cases} \underline{g}_i^q ; & \dot{b}_i \in E(q) \\ \underline{0} ; & \text{OTHERWISE} \end{cases}$$

$$\underline{\omega}_K^{\dot{b}_i} = \underline{0}$$

$$\underline{\ddot{V}}_K^{\dot{b}_i} = \underline{0}$$

### ROTATIONAL D.O.F.

LET  $K$  CORRESPOND TO THE  $i$ -TH ROTATIONAL D.O.F. OF THE  $q$ -TH HINGE.

$$\underline{V}_K^{\dot{b}_i} = \begin{cases} \underline{g}_i^q(\theta_i^q) \times (\underline{g}_i^q \underline{z}_i^q - (\underline{r}_{iq} + \underline{u}_{iq})) ; & \dot{b}_i \in E(q) \\ \underline{0} ; & \text{OTHERWISE} \end{cases}$$

$$\underline{\omega}_K^{\dot{b}_i} = \begin{cases} \underline{g}_i^q(\theta_i^q) ; & \dot{b}_i \in E(q) \\ \underline{0} ; & \text{OTHERWISE} \end{cases}$$

$$\underline{\ddot{V}}_K^{\dot{b}_i} = \underline{0}$$

### MODAL D.O.F.

LET  $K$  CORRESPOND TO THE  $i$ -TH MODAL D.O.F. OF THE  $q$ -TH BODY.

$$\underline{V}_K^{\dot{b}_i} = \begin{cases} -\underline{g}_i^q(\underline{r}_{iq}) \times \underline{z}_i^q + \underline{g}_i^q(\underline{r}_{iq}) \times \underline{z}_i^q (1 - \delta_{iq}) \\ \underline{0} ; & \text{OTHERWISE} \end{cases}$$

$$+ \underline{g}_i^q(\underline{r}_{iq}) \times (1 - \delta_{iq}) - \underline{g}_i^q(\underline{r}_{iq}) ; \quad \dot{b}_i \in E(q)$$

$$\underline{\omega}_K^{\dot{b}_i} = \begin{cases} -\underline{g}_i^q(\underline{r}_{iq}) + \underline{g}_i^q(\underline{r}_{iq}) \times (1 - \delta_{iq}) ; & \dot{b}_i \in E(q) \\ \underline{0} ; & \text{OTHERWISE} \end{cases}$$

$$\underline{\ddot{V}}_K^{\dot{b}_i} = \begin{cases} \underline{g}_i^q(\underline{r}_i^q) + \underline{g}_i^q(\underline{r}_i^q) \times \underline{p}_0 ; & \dot{b}_i = q \\ \underline{0} ; & \text{OTHERWISE} \end{cases}$$

$\underline{q}_i^j \equiv i$ -TH TRANSLATION AXIS OF THE  $q$ -TH HINGE, FIXED IN  $L(q)$ , BODY INBOARD OF THE  $q$ -TH BODY

$\underline{l}_i^j(\theta_i^j) \equiv i$ -TH ROTATION AXIS (EULER AXIS) OF THE  $q$ -TH HINGE

${}^i\chi_i^j \equiv$  VECTOR LOCATING BODY  $j$  REFERENCE WRT BODY  $q$  REFERENCE

$\underline{r}_{iq} =$  VECTOR LOCATING UNDEFORMED HINGE ATTACH POINT ON BODY  $q$  WRT BODY  $q$  REFERENCE.

$\underline{u}_{iq} \equiv$  DEFORMATION AT  $\underline{r}_{iq}$  ON BODY  $q$  ( $\underline{u}_{iq} = \sum_{i=1}^{NM(q)} \underline{\phi}_i^j(\underline{r}_{iq}) \eta_i^j$ )

${}^{iq}\underline{z}^{b_i} \equiv$  VECTOR LOCATING BODY  $j$  REFERENCE WRT BODY  $q$  HINGE ATTACH POINT ON BODY  $q$ .

${}^{iq}\underline{s}^{b_i} \equiv$  VECTOR FROM POINT  $P(q)$  ON BODY  $q$  (LEADING TO BODY  $j$ ) TO BODY  $j$  REFERENCE. (IF  $j=q$ ,  ${}^{iq}\underline{s}^{b_i} = \underline{0}$ )

$E(q) \equiv$  SET OF ALL BODIES OUTBOARD OF THE  $q$ -TH BODY INCLUDING BODY  $q$

"GENERALIZED INERTIAL FORCE"  
(EXPRESSION FOR  $-f_k^*$ )

$$-f_k^* = \sum_{i=1}^{NB} \left\{ m_i (\ddot{\underline{R}}_i + \ddot{\underline{L}}_i) \cdot \underline{V}_k + (\ddot{\underline{H}}_i + m_i \underline{L}_i \times \ddot{\underline{R}}_i) \cdot \underline{\omega}_k + \sum_{o=1}^{MM_i} \int_{V_{i0}} \underline{V}_k \cdot \ddot{\underline{R}}_o dm \right\}$$

MODAL TERMS

K CORRESPONDING TO THE  $i$ -TH MODAL D.O.F. OF THE  $i$ -TH BODY

$$(I.) \quad m_i \underline{\alpha}_i \cdot \ddot{\underline{R}}_i$$

$$(II.) \quad (\underline{h}_i + \sum_{m=1}^{MM_i} \underline{Y}_{ki}^m \underline{\eta}_k^m + \sum_{m=1}^{MM_i} \sum_{n=1}^{MM_i} \underline{Z}_{mki}^n \underline{\eta}_m^n) \cdot \underline{\omega}_i$$

$$(III.) \quad 2 \underline{\omega}_i \cdot \left( \sum_{m=1}^{MM_i} \underline{Y}_{ki}^m \underline{\eta}_k^m + \sum_{m=1}^{MM_i} \sum_{n=1}^{MM_i} \underline{Y}_{mki}^n \underline{\eta}_m^n \right)$$

(IV.) MODAL MASS (ASSUMED BODY BASIS)

— SCALAR REPRESENTATION FOR "LUMPED APPROACH"

$$\left\{ \sum_{i=1}^{NN_i} \left( \{ \dot{\phi}_{i0} \}^T \{ \dot{\phi}_{i0} \} \right) \left( m_{i0} \tilde{l}_0 \right) \right\} \left( \begin{array}{c} \{ m_{i0} \tilde{l}_0 \} \\ \{ \dot{\gamma}_0 + \ddot{\gamma}_0 - \ddot{\gamma}_0 \tilde{\gamma}_0 - \ddot{\gamma}_0 \tilde{\gamma}_0 \} \end{array} \right) \left( \begin{array}{c} \{ \dot{\phi}_{i0} \} \\ \{ \dot{\gamma}_0 \} \end{array} \right)$$

$$\begin{aligned} \text{(V.) } \underline{\dot{y}} \cdot \left( \underline{\dot{W}} + \sum_{k=1}^{NN_k} \underline{\dot{W}}_{ki} \dot{\eta}_k + \sum_{k=1}^{NN_k} \underline{\dot{W}}_{ki} \dot{\eta}_k \right) \cdot \underline{\dot{y}} \\ \sum_{i=1}^{NN_i} (\underline{\dot{y}} + \underline{\dot{y}}_0) \cdot \left( \underline{\dot{T}} + \sum_{k=1}^{NN_k} \underline{\dot{T}}_{ki} \dot{\eta}_k + \sum_{k=1}^{NN_k} \underline{\dot{T}}_{ki} \dot{\eta}_k \right) \cdot (\underline{\dot{y}} + \underline{\dot{y}}_0) \end{aligned}$$

$$(VI.) \quad \dot{z}_i \cdot \left( \sum_{k=1}^{m_k} \dot{w}_{ki} \dot{\eta}_k + \sum_{k=1}^{m_k} \dot{w}_{mki} \dot{\eta}_m \right)$$

$$(VII.) \quad \sum_{\alpha=1}^{m_{\alpha}} (\dot{w}_{\alpha} \times \dot{u}_{\alpha}) \cdot \left( \dot{D}_{\alpha} + \sum_{k=1}^{m_k} \dot{D}_{ki} \dot{\eta}_k + \sum_{k=1}^{m_k} \dot{D}_{mki} \dot{\eta}_m \right)$$

RATE OF CHANGE OF BODY'S ANGULAR MOMENTUM  
(CONSOLIDATED EXPRESSION FOR  $\dot{H}_i^0$ )

$$\dot{H}_i^0 = \underline{I}_i^0 \cdot \underline{\omega}_i^0 + \sum_{j=1}^{NN_j} \left( \underline{h}_i^0 + \sum_{k=1}^{NN_k} \underline{Y}_{ki}^0 \eta_k^0 + \sum_{m=1}^{NN_m} \sum_{n=1}^{NN_n} \underline{z}_{mki}^0 \eta_m^0 \eta_n^0 \right) \eta_i^0 + \underline{\omega}_i^0 \times \underline{I}_i^0 \cdot \underline{\omega}_i^0 \\ + \left( 2 \sum_{j=1}^{NN_j} \{ \underline{M}_{ji}^0 + \sum_{k=1}^{NN_k} \underline{P}_{ki}^0 \eta_k^0 \} \eta_i^0 + \underline{K}_i^0 \right) \cdot \underline{\omega}_i^0 + \underline{R}_i^0$$

WHERE :

$$\underline{I}_i^0 = \underline{I}_{R_i}^0 + \sum_{j=1}^{NN_j} \{ \underline{M}_{ji}^0 + \underline{N}_{ji}^0 \} \eta_j^0 + \sum_{m=1}^{NN_m} \sum_{k=1}^{NN_k} \underline{P}_{mki}^0 \eta_m^0 \eta_k^0$$



# DEFINITION OF VECTORS AND DYADICS

DEFINE:  $\underline{\dot{b}} = \begin{bmatrix} \underline{\dot{b}}_{11} \\ \underline{\dot{b}}_{12} \\ \underline{\dot{b}}_{13} \end{bmatrix}$ ;  $\underline{\dot{b}}^T = (\underline{\dot{b}}_{11} \quad \underline{\dot{b}}_{12} \quad \underline{\dot{b}}_{13})$ , BODY  $\dot{}$  REFERENCE BASIS

VARIABLE	ORDER	D.O.F. ASSOCIATION	DEFINITION
$\underline{\dot{\alpha}}_i$	0	MODAL	$\frac{1}{m_i} \left\{ \sum_{j=1}^{n_{m_i}} m_{ij} \underline{\dot{\phi}}_j - m_{ij} \underline{\dot{L}}_i \times \underline{\dot{\phi}}_j - \sum_{j=1}^{n_{m_i}} m_{ij} (\underline{\dot{\phi}}_j \times \underline{\dot{L}}_i) \times \underline{\dot{\phi}}_j \right\}$
$\underline{\dot{U}}_{i0}$	0, 1, 2	ROTATIONAL / MODAL	$\underline{\dot{b}}^T \{ \underline{\dot{J}}_{i0} + \underline{\dot{U}}_{i0} \underline{\dot{J}}_{i0} - \underline{\dot{J}}_{i0} \underline{\dot{U}}_{i0} - \underline{\dot{U}}_{i0} \underline{\dot{J}}_{i0} \} \underline{\dot{U}}_{i0}$ <div> <math>\underline{\dot{J}}_{i0}</math> IS INERTIA MATRIX (3x3) OF NODAL BODY <math>\dot{}</math> WRT NODAL BODY <math>\dot{}</math> REFERENCE FRAME, <math>\dot{}</math> </div>
$\underline{\dot{h}}_i$	0	ROTATIONAL / MODAL	$\underline{\dot{b}}^T \left\{ \sum_{j=1}^{n_{m_i}} \left( m_{ij} \underline{\dot{L}}_i \{ \underline{\dot{\phi}}_j \} - \underline{\dot{L}}_i m_{ij} \underline{\dot{L}}_i \{ \underline{\dot{\phi}}_j \} \right. \right.$ $\left. \left. + m_{ij} \underline{\dot{L}}_i \{ \underline{\dot{\phi}}_j \} + \underline{\dot{J}}_{i0} \{ \underline{\dot{\phi}}_j \} \right\} \right\}$ <div> <math>\{x\}</math> DENOTES COLUMN MATRIX         </div>

VARIABLE	ORDER	D.O.F. ASSOCIATION	DEFINITION
$\underline{Y}_i^j$		NOTATIONAL/ MODAL	$\underline{b}^T \left\{ \sum_{o=1}^{n_{oi}} \left[ \tilde{m}_o \tilde{\theta}_{ok}^j \{ \theta_{ok}^j \} + \tilde{r}_o (m_o \tilde{L}_o \{ \theta_{ok}^j \}) \{ \theta_{ok}^j \} \right. \right. \\ \left. \left. - \tilde{\theta}_{ok}^j m_o \tilde{L}_o \{ \theta_{ok}^j \} \right] - m_o (\tilde{L}_o \{ \theta_{ok}^j \}) \{ \theta_{ok}^j \} \right. \\ \left. + (\tilde{\theta}_{ok}^j \mathcal{J}_{ok}^o - \mathcal{J}_{ok}^o \tilde{\theta}_{ok}^j) \{ \theta_{ok}^j \} \right\}$
$\underline{Z}_{nki}^j$		ROTATIONAL/ MODAL	$\underline{b}^T \left\{ \sum_{o=1}^{n_{oi}} \left[ \tilde{\theta}_{ok}^j (m_o \tilde{L}_o \{ \theta_{ok}^j \}) \{ \theta_{ok}^j \} - \tilde{\theta}_{ok}^j \mathcal{J}_{ok}^o \tilde{\theta}_{ok}^j \{ \theta_{ok}^j \} \right] \right\}$
$\underline{Y}_{nki}^j$		MODAL	$\underline{b}^T \left\{ \sum_{o=1}^{n_{oi}} \left[ m_o \tilde{\theta}_{ok}^j \{ \theta_{ok}^j \} - \tilde{\theta}_{ok}^j m_o \tilde{L}_o \{ \theta_{ok}^j \} \right] \right\}$
$\underline{Y}_{nki}^j$		MODAL	$\underline{b}^T \left\{ \sum_{o=1}^{n_{oi}} \left[ \tilde{\theta}_{ok}^j (m_o \tilde{L}_o \{ \theta_{ok}^j \}) \{ \theta_{ok}^j \} \right] \right\}$
$\underline{W}_i^j$		MODAL	$\underline{b}^T \left\{ \sum_{o=1}^{n_{oi}} \left[ m_o \tilde{\theta}_{ok}^j \tilde{r}_o - (m_o \tilde{L}_o \{ \theta_{ok}^j \}) \tilde{r}_o \right] \right\} \underline{b}$
$\underline{W}_{ki}^j$		MODAL	$\underline{b}^T \left\{ \sum_{o=1}^{n_{oi}} \left[ (m_o \tilde{L}_o \{ \theta_{ok}^j \}) \{ \theta_{ok}^j \} \tilde{r}_o + m_o \tilde{\theta}_{ok}^j \tilde{\theta}_{ok}^j \right. \right. \\ \left. \left. - (m_o \tilde{L}_o \{ \theta_{ok}^j \}) \tilde{\theta}_{ok}^j \right] \right\} \underline{b}$



VARIABLE	ORDER	D.O.F. ASSOCIATION	DEFINITION
$\underline{W}_{nki}^i$		MODAL	$\underline{b}^T \{ \underline{\tilde{T}}_{n1}^i [ (m_i \underline{\tilde{I}}_0 \{ \theta_{n1}^i \} \tilde{\theta}_{n1}^i ) \} \} \underline{b}$
$\underline{T}_{n1}^i$		MODAL	$\underline{b}^T \{ \tilde{\theta}_{n1}^i m_i \underline{\tilde{I}}_0 + \underline{J}^i \tilde{\theta}_{n1}^i \} \underline{b}$
$\underline{T}_{n2}^i$		MODAL	$\underline{b}^T \{ -\tilde{\theta}_{n1}^i (m_i \underline{\tilde{I}}_0 \{ \theta_{n1}^i \}) + \tilde{\theta}_{n1}^i \underline{J}^i \tilde{\theta}_{n1}^i - \underline{J}^i \tilde{\theta}_{n2}^i \} \underline{b}$
$\underline{T}_{n3}^i$		MODAL	$\underline{b}^T \{ -\tilde{\theta}_{n1}^i \underline{J}^i \tilde{\theta}_{n1}^i \tilde{\theta}_{n2}^i \} \underline{b}$
$\underline{W}_{n1}^i$		MODAL	$\underline{b}^T \{ \underline{\tilde{T}}_{n1}^i [ \tilde{\theta}_{n1}^i m_i \underline{\tilde{I}}_0 \{ \theta_{n1}^i \} ] \} \}$
$\underline{W}_{n2}^i$		MODAL	$\underline{b}^T \{ \underline{\tilde{T}}_{n1}^i [ -\tilde{\theta}_{n1}^i (m_i \underline{\tilde{I}}_0 \{ \theta_{n1}^i \}) \tilde{\theta}_{n2}^i ] \} \}$
$\underline{D}_{n1}^i$		MODAL	$\underline{b}^T \{ \underline{J}^i \tilde{\theta}_{n1}^i \} \}$
$\underline{D}_{n2}^i$		MODAL	$\underline{b}^T \{ \tilde{\theta}_{n1}^i \underline{J}^i \{ \theta_{n1}^i \} - \underline{J}^i \tilde{\theta}_{n1}^i \{ \theta_{n2}^i \} \} \}$
$\underline{D}_{n3}^i$		MODAL	$\underline{b}^T \{ -\tilde{\theta}_{n1}^i \underline{J}^i \tilde{\theta}_{n1}^i \{ \theta_{n2}^i \} \} \}$

VARIABLE	ORDER	D.O.F. ASSOCIATION	DEFINITION
$\underline{\underline{I}}_A^i$	0	ROTATIONAL	$\underline{\underline{I}}^T \left\{ \sum_{i=1}^{NM} \left( J_{i0}^{i0} + m_i \tilde{r}_i^0 \tilde{r}_i^0 - \tilde{r}_i^0 m_i \tilde{r}_i^0 - m_i \tilde{r}_i^0 \tilde{r}_i^0 \right) \right\} \underline{\underline{I}}$
$\underline{\underline{M}}_i^i$	1	ROTATIONAL	$\underline{\underline{I}}^T \left\{ \sum_{i=1}^{NM} \left( -m_i \tilde{r}_i^0 \tilde{\theta}_i^0 + \tilde{r}_i^0 (m_i \tilde{r}_i^0 \{ \tilde{\theta}_i^0 \}) - m_i \tilde{r}_i^0 \tilde{\theta}_i^0 - J_{i0}^{i0} \tilde{\theta}_i^0 \right) \right\} \underline{\underline{I}}$
$\underline{\underline{N}}_i^i$	1	ROTATIONAL	$\underline{\underline{I}}^T \left\{ \sum_{i=1}^{NM} \left( -m_i \tilde{\theta}_i^0 \tilde{r}_i^0 - \tilde{\theta}_i^0 m_i \tilde{r}_i^0 + (m_i \tilde{r}_i^0 \{ \tilde{\theta}_i^0 \}) \tilde{r}_i^0 + \tilde{\theta}_i^0 J_{i0}^{i0} \right) \right\} \underline{\underline{I}}$
$\underline{\underline{P}}_{K_i}^i$	2	ROTATIONAL	$\underline{\underline{I}}^T \left\{ \sum_{i=1}^{NM} \left( -m_i \tilde{\theta}_i^0 \tilde{\theta}_i^0 + \tilde{\theta}_i^0 (m_i \tilde{r}_i^0 \{ \tilde{\theta}_i^0 \}) + (m_i \tilde{r}_i^0 \{ \tilde{\theta}_i^0 \}) \tilde{\theta}_i^0 - \tilde{\theta}_i^0 J_{i0}^{i0} \tilde{\theta}_i^0 \right) \right\} \underline{\underline{I}}$
$\underline{\underline{K}}_i^i$	MULTIPLE	ROTATIONAL	$\underline{\underline{K}}^i = \sum_{i=1}^{NM} \underline{\underline{K}}_{i,i}^i + \sum_{i=1}^{NM} \sum_{k=1}^{NM} \underline{\underline{K}}_{i,k}^i \eta_i^i \eta_k^i + \sum_{i=1}^{NM} \sum_{k=1}^{NM} \sum_{m=1}^{NM} \underline{\underline{K}}_{i,k,m}^i \eta_i^i \eta_k^i \eta_m^i$

VARIABLE	ORDER	D.O.F. ASSOCIATION	DEFINITION
$\underline{\underline{K}}_i^i$		ROTATIONAL	$\underline{\underline{b}}^T \left\{ \sum_{\alpha=1}^{n_{\alpha}} \left[ \underline{\underline{J}}_{\alpha}^i \underline{\underline{\phi}}_{\alpha}^i + \underline{\underline{\phi}}_{\alpha}^i \underline{\underline{J}}_{\alpha}^{i0} \right] \right\} \underline{\underline{b}}$
$\underline{\underline{K}}_{ki}^i$		ROTATIONAL	$\underline{\underline{b}}^T \left\{ \sum_{\alpha=1}^{n_{\alpha}} \left[ \underline{\underline{\phi}}_{\alpha}^i \underline{\underline{J}}_{\alpha}^k \underline{\underline{\phi}}_{\alpha}^i + \underline{\underline{J}}_{\alpha}^k \underline{\underline{\phi}}_{\alpha}^i \underline{\underline{\phi}}_{\alpha}^i + \underline{\underline{\phi}}_{\alpha}^i \underline{\underline{\phi}}_{\alpha}^k \underline{\underline{J}}_{\alpha}^{i0} \right. \right. \\ \left. \left. - \underline{\underline{\phi}}_{\alpha}^i \underline{\underline{J}}_{\alpha}^{i0} \underline{\underline{\phi}}_{\alpha}^k + 2 \underline{\underline{r}}_{\alpha}^i \left( \underline{\underline{\phi}}_{\alpha}^i \left( \underline{\underline{m}}_{\alpha}^i \underline{\underline{r}}_{\alpha}^i \left\{ \underline{\underline{\phi}}_{\alpha}^i \right\} \right) \right) \right] \right\} \underline{\underline{b}}$
$\underline{\underline{K}}_{mki}^i$		ROTATIONAL	$\underline{\underline{b}}^T \left\{ \sum_{\alpha=1}^{n_{\alpha}} \left[ 2 \underline{\underline{\phi}}_{\alpha}^i \left( \underline{\underline{\phi}}_{\alpha}^i \left( \underline{\underline{m}}_{\alpha}^i \underline{\underline{r}}_{\alpha}^i \left\{ \underline{\underline{\phi}}_{\alpha}^i \right\} \right) \right) + \underline{\underline{\phi}}_{\alpha}^i \underline{\underline{J}}_{\alpha}^k \underline{\underline{\phi}}_{\alpha}^i \underline{\underline{\phi}}_{\alpha}^i \right. \right. \\ \left. \left. - \underline{\underline{\phi}}_{\alpha}^i \underline{\underline{\phi}}_{\alpha}^k \underline{\underline{J}}_{\alpha}^{i0} \underline{\underline{\phi}}_{\alpha}^i \right] \right\} \underline{\underline{b}}$
$\underline{\underline{R}}_i$	MULTIPLE	ROTATIONAL	$\sum_{\alpha=1}^{n_{\alpha}} \left\{ \underline{\underline{y}}_{\alpha}^i \times \underline{\underline{I}}_{\alpha}^{i0} \cdot \underline{\underline{y}}_{\alpha}^i + \underline{\underline{y}}_{\alpha}^i \times \underline{\underline{I}}_{\alpha}^{i0} \cdot \underline{\underline{y}}_{\alpha}^i \right. \\ \left. + (\underline{\underline{r}}_{\alpha}^i + \underline{\underline{y}}_{\alpha}^i) \times (\underline{\underline{y}}_{\alpha}^i \times (\underline{\underline{y}}_{\alpha}^i \times (\underline{\underline{m}}_{\alpha}^i \underline{\underline{r}}_{\alpha}^i + \underline{\underline{y}}_{\alpha}^i \times \underline{\underline{m}}_{\alpha}^i \underline{\underline{r}}_{\alpha}^i))) \right\}$

AUTOMATIC GENERATION OF THE  
EQUATIONS OF MOTION AND THEIR  
SOLUTION FOR FLEXIBLE STRUCTURES

Ramen P. Singh and Larry Taylor.

**151**

PRECEDING PAGE BLANK NOT FILMED

1963 FLETCHER, RONGUED & YU



3 RIGID BODIES

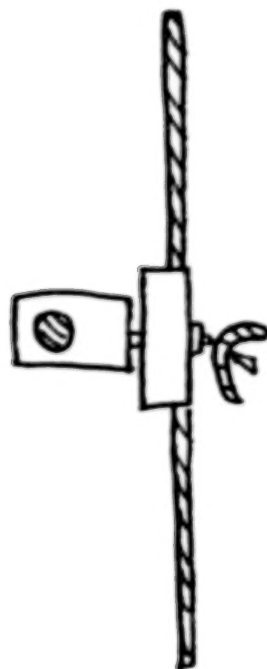
1965-75 (KANE & WANG)  
HOOKER & MARGULIES  
ROBERSON & WITTENBURG  
VELMAN  
RUSSELL  
HOOKER, ROBERSON  
.



N POINT-CONNECTED  
RIGID BODIES IN A  
TOPOLOGICAL TREE

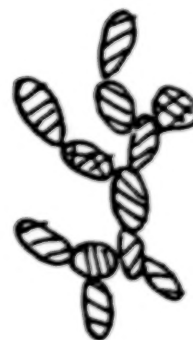
LIKINS

1964-75 BUCKENS  
MEIROVITCH  
LIKINS  
FLEISCHER  
HUGHES  
WILLEMS  
GROTE, McMUNN & GLUCK  
NESS & FORRENKOPF  
LAURENSEN



SYSTEMS OF RIGID  
BODIES WITH FLEXIBLE  
APPENDAGES

1972-83 BODLEY & PARK  
BOLAND, SAMIN & WILLEMS  
HO  
JERKOVSKY  
HUGHES  
HUSTON



N POINT-CONNECTED  
FLEXIBLE BODIES IN A  
TOPOLOGICAL TREE

## APPROACHES

- 1. Lagrange's method
- 2. Lagrange's for of D'Alembert's principle
- 3. Order 'n' algorithms

## General purpose software

DISCOS, TREETOPS . . . .

## COMMON FEATURES OF THE PROGRAMS

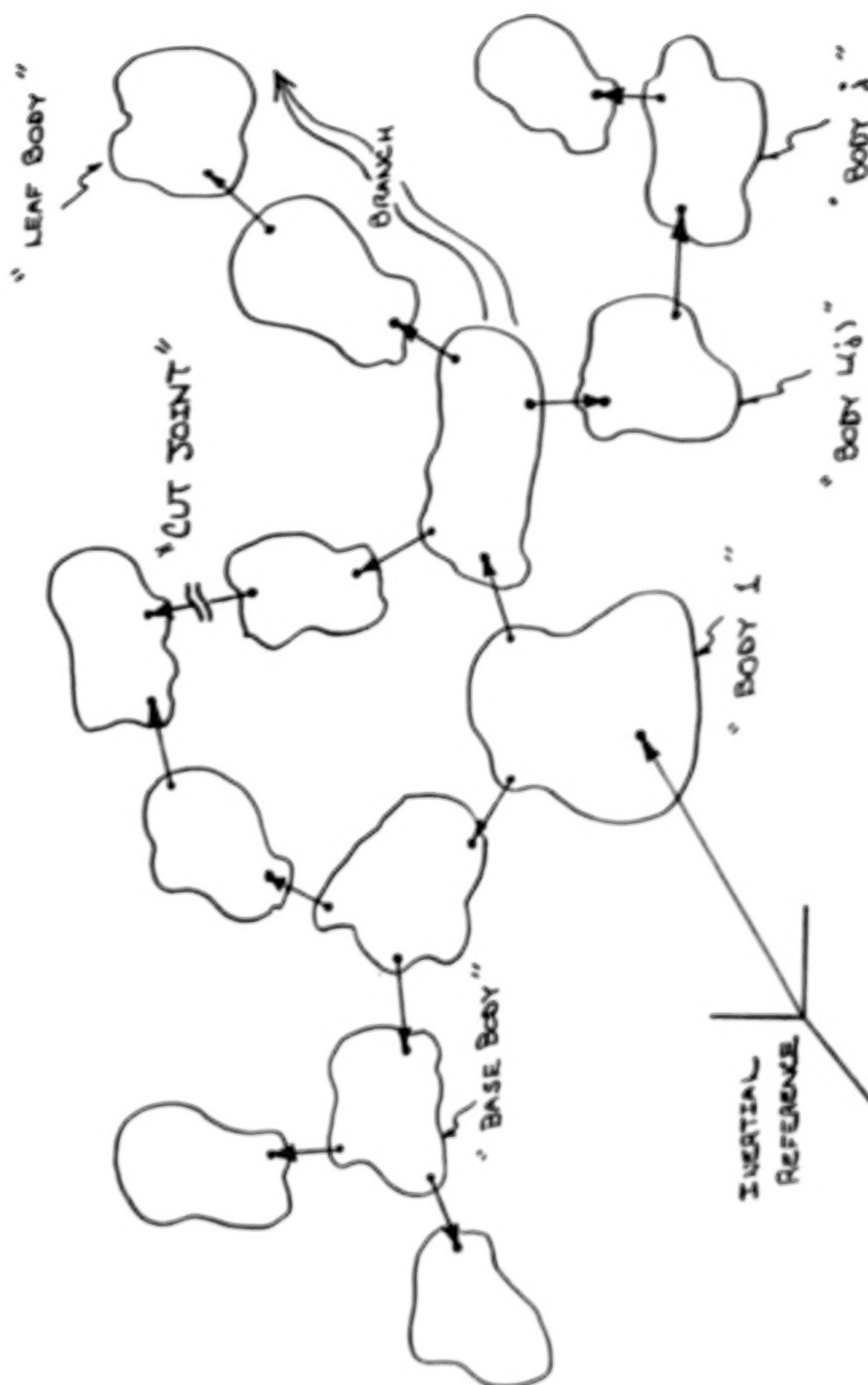
- 1. Concept of a "joint".
- 2. System of interconnected bodies.
- 3. Small elastic deformations.
- 4. Large relative motion

## LIMITATIONS

- 1. Large computational burden for the evaluation of Lagrange multipliers.
- 2. Order ' $n^3$ ' type behavior with minimum dimension approach.
- Real-time simulations hard to achieve.



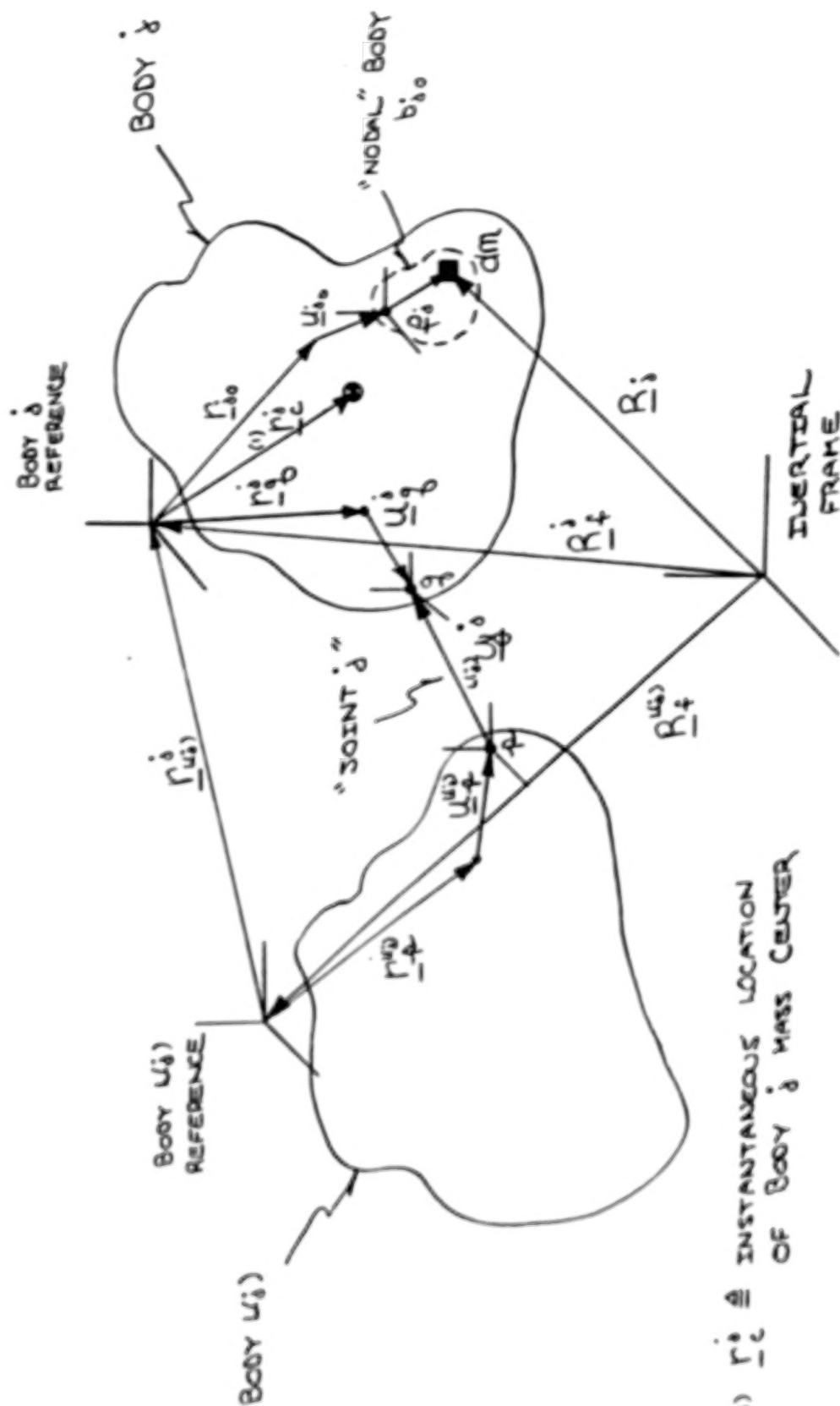
SYSTEM TOPOLOGY



## SYSTEM TOPOLOGY

- DEFINED IN TERMS OF : LEVELS, BASE BODIES, BRANCHES, LEAF BODIES, ETC.
  - A LEAF BODY IS ONE WHICH HAS NO BODIES DIRECTLY OUTBOARD
  - BRANCHES ARE DEFINED AS A SET OF BODIES IN A CHAIN TOPOLOGY
  - BASE BODIES ARE BODIES WHICH CONTAIN MORE THAN ONE BODY DIRECTLY OUTBOARD
  - LEVELS ARE USED TO ESTABLISH SETS OF BASE BODIES
- THESE SYSTEM TOPOLOGY VARIABLES ARE COMPLETELY DEFINED VIA THE DEFINITIONS OF BODY  $i$  AND  $L(j)$ , i.e., FOR ANY BODY  $j$ ,  $L(j)$  IS THE BODY DIRECTLY INBOARD.
- RELATIVE MOTION BETWEEN BODY PAIRS PROVIDED VIA THE DEFINITION OF JOINTS THE ALGORITHM ALLOWS FOR ZERO TO SIX DEGREE OF FREEDOM JOINTS.
- THE JOINT IS THE PHYSICAL LINK BETWEEN MATERIAL POINTS FIXED IN BODY  $j$  AND  $L(j)$  PAIRS.
- BODIES CAN BE RIGID OR FLEXIBLE WHERE FOR FLEXIBLE WHERE FOR FLEXIBLE BODIES THE ALGORITHM ALLOWS FOR UNRESTRICTED BOUNDARY CONDITIONS (i.e. NOT LIMITED TO "FREE-FREE" OR "FIXED-FREE"), AS WELL AS PROVIDES FOR ECCENTRICITY EFFECTS.

### • BASED ON BODY $j$ , $L(j)$ PAIRS



(1)  $\underline{r}_{i0}^i \triangleq$  INSTANTANEOUS LOCATION OF BODY  $j$  MASS CENTER

- MOTION OF BODY  $i$  WRITTEN IN TERMS OF MOTION OF BODY  $L(i)$  RELATIVE JOINT DEGREES OF FREEDOM, AND BODY  $j$  DEFORMATION
- LOCATION OF BODY  $j$  MASS ELEMENT  $dm$  IN INERTIAL

$$\underline{R}_i = \underline{R}_i^0 + \underline{r}_{i0} + \underline{u}_{i0} + \underline{p}_i$$

WHERE :

$$\underline{R}_i^0 = \underline{R}_i^{(0)} + (\underline{r}_{ip}^{(0)} + \underline{u}_{ip}^{(0)}) + \omega_i \underline{y}_i^0 - (\underline{r}_q^0 + \underline{u}_q^0)$$

$\underline{R}_i^{(0)} \triangleq$  LOCATION OF BODY  $L(i)$  REFERENCE WRT INERTIAL

$\underline{r}_{ip}^{(0)} \triangleq$  UNDEFORMED LOCATION OF MATERIAL POINT  $p$  OF BODY  $L(i)$  WRT BODY  $L(j)$  REFERENCE

$\underline{u}_{ip}^{(0)} \triangleq$  DEFORMATION OF POINT  $p$  IN BODY  $L(j)$

$\omega_i \underline{y}_i^0 \triangleq$  RELATIVE TRANSLATION ACROSS THE JOINT

$\underline{r}_q^0 \triangleq$  UNDEFORMED LOCATION OF MATERIAL POINT  $q$  OF BODY  $j$  WRT BODY  $j$  REFERENCE

$\underline{u}_q^0 \triangleq$  DEFORMATION OF POINT  $q$  IN BODY  $j$

- CHOICE OF KINEMATIC VARIABLES (GENERALIZED COORDINATES)
- JOINT TRANSLATION

$$\omega_i \underline{y}_i^0 \triangleq \sum_{i=1}^{NT} \underline{g}_i^0 \dot{y}_i^0 ; \omega_i \underline{y}_i^0 \triangleq \sum_{i=1}^{NT} \underline{g}_i^0 \dot{y}_i^0$$

- JOINT ROTATION

$$\omega \underline{\dot{\omega}} \triangleq \sum_{i=1}^{NR} \underline{l}_i^{\dot{}}(\theta^{\dot{}}) \dot{\theta}_i^{\dot{}}$$

- DEFORMATION

$$\underline{\dot{u}} \triangleq \sum_{i=1}^{NR} \underline{\phi}_i^{\dot{}}(\underline{r}_i^{\dot{}}) \eta_i^{\dot{}} ; \quad \underline{\dot{u}} \triangleq \sum_{i=1}^{NR} \underline{\phi}_i^{\dot{}}(\underline{r}_i^{\dot{}}) \eta_i^{\dot{}}$$

$$\{ \dot{\mathbf{q}}^{\dot{}} \}^T = \{ \dot{y}_1^{\dot{}} \dots \dot{y}_{NR}^{\dot{}} \mid \dot{\theta}_1^{\dot{}} \dots \dot{\theta}_{NR}^{\dot{}} \mid \dot{\eta}_1^{\dot{}} \dots \dot{\eta}_{NR}^{\dot{}} \}$$



• BODY j INERTIAL FORCES

- TRANSLATION

$$\underline{f}_{T_o}^* \triangleq m_o (\ddot{\underline{R}}_t^o + \ddot{\underline{r}}_c^o)$$

- ROTATION

$$\underline{f}_{R_o}^* \triangleq \underline{H}_t^o + m_o (\underline{r}_c^o \times \ddot{\underline{R}}_t^o)$$

CAST IN MATRIX - DYADIC FORM

$$\begin{bmatrix} \underline{f}_{T_o}^* \\ \underline{f}_{R_o}^* \end{bmatrix} = \begin{bmatrix} m_o \underline{E} & -m_o (\underline{r}_c^o) \underline{E} \\ (\underline{r}_c^o) \underline{E} & \underline{0} \end{bmatrix} \cdot \begin{bmatrix} \ddot{\underline{R}}_{to}^o \\ \dot{\underline{\omega}}_{to}^o \end{bmatrix} +$$

FUNCTIONS  
OF BODY j  
ACCELERATIONS  
DEGREES OF FREEDOM

$$(\underline{B}_o^T \underline{B}_o)^T \begin{bmatrix} (m_{to}^i) (m_{to}^i) \\ (m_{to}^i) (m_{to}^i) \\ (m_{to}^i) (m_{to}^i) \end{bmatrix} \begin{bmatrix} \ddot{y}^i \\ \ddot{\theta}^i \\ \ddot{\eta}^i \end{bmatrix} + \begin{bmatrix} \underline{Q}_R^i \\ \underline{\alpha}_R^i \end{bmatrix}$$

BODY j  
DEGREES OF FREEDOM

REMAINDER TERMS  
e.g., CORIOLIS

- BODY j MODAL, FLEX INERTIAL FORCES
- FROM WORK - ENERGY PRINCIPLES,

$$f_{i,j}^* \triangleq \int_{V_i} \dot{V}_i^* \cdot \ddot{R}_i \, dm \quad ; \text{ FOR } i = 1, \dots, NM_i \text{ (* OF FLEX MODES)}$$

- FROM KINEMATICS

$$\dot{V}_i^* = \frac{\partial \dot{R}_i}{\partial \dot{\eta}_i} = \frac{\partial \dot{R}_i}{\partial \dot{\eta}_i} + \frac{\partial \dot{\omega}_i}{\partial \dot{\eta}_i} \times (\underline{r}_{i0} + \underline{u}_{i0} + \underline{\rho}_i) + \frac{\partial \dot{u}_{i0}}{\partial \dot{\eta}_i} + \frac{\partial \dot{u}_{i0}}{\partial \dot{\eta}_i} \times \underline{\rho}_i$$

162

- AFTER SUBSTITUTION AND EVALUATION OF THE INTEGRALS FOR WE RESULT WITH THE FOLLOWING.

$$\{f_{i,j}^*\} = \left[ \{M_{i1}^*\} \{M_{i2}^*\} \left[ \frac{\ddot{R}_{i0}}{\ddot{u}_{i0}} \right] \left[ \frac{\ddot{u}_{i0}}{\ddot{\omega}_{i0}} \right] \right] + \{M_{i3}^*\} \{ \ddot{u}_{i0}^* \} + \{M_{i4}^*\} \{ \ddot{\eta}_{i0}^* \} + \{f_{i,j}^*\}_R$$

REMAINDER  
TERMS

SQUARE  
SYMMETRIC  
MODAL MATRIX

• ACTIVE FORCES

- TRANSLATION

$$\underline{\dot{F}}^a = \int_{b_a} d\underline{f}$$

RESULTANT OF ALL EXTERNAL FORCES  
ACTING ON BODY  $j$  INCLUDING BODY  
 $j$ ,  $L(j)$  UNKNOWN CONTACT MOMENTS

- ROTATION

$$\underline{\dot{M}}^a = \int_{b_a} \underline{r} \times d\underline{f} + \int_{b_a} d\underline{\tau}$$

RESULTANT MOMENT ACTING ON  
BODY  $j$  INCLUDING BODY  $j$ ,  $L(j)$   
UNKNOWN CONTACT MOMENTS

- MODAL, FLEX ACTIVE FORCES, FOR  $i = 1, \dots, NM_j$

$$\underline{f}_{\eta i} = \int_{b_a} \underline{V}_i^a \cdot d\underline{f} + \text{"MODAL DAMPING"} + \text{"MODAL STIFFNESS"}$$

OR,

$$\{ \underline{f}_{\eta i} \} = \begin{Bmatrix} \underline{f}_{\eta i_1} \\ \vdots \\ \underline{f}_{\eta i_{NM_j}} \end{Bmatrix}$$



SOLUTION ALGORITHM DEVELOPMENT

\* ELIMINATION OF EXPRESSIONS INVOLVING BODY  $j$  DEGREES OF FREEDOM

(1) ELIMINATE BODY  $j$  FLEXURE DEGREES OF FREEDOM FROM,

$$\{f_{q_j}^*\} = \{f_{q_j}\}$$

$$\{\ddot{\eta}_0\} = [M_{qq}^0]^{-1} (\{f_{q_j}\} - [M_{q\eta_1}^0 \ M_{q\eta_2}^0] \begin{bmatrix} \ddot{\eta}_1 \\ \ddot{\eta}_2 \end{bmatrix} \cdot \begin{bmatrix} R_{\eta_1}^0 \\ R_{\eta_2}^0 \end{bmatrix})$$

$$- ([M_{\eta_1\eta}^0 \ M_{\eta_2\eta}^0] \begin{bmatrix} \ddot{\eta}_1 \\ \ddot{\eta}_2 \end{bmatrix} - \{f_{\eta_j}^*\}_R)$$

(2) THE EXPRESSION FOR  $\{\ddot{\eta}_0\}$  IS SUBSTITUTED INTO THE TRANSLATION AND ROTATION INERTIAL FORCE EXPRESSIONS;  $\{f_{T_0}^*\}, \{f_{R_0}^*\}$

THE RESULTING EXPRESSIONS FOR BODY  $j$  TRANSLATIONAL AND ROTATIONAL INERTIAL FORCES CAN BE WRITTEN AS FOLLOWS.

$$\begin{bmatrix} \underline{f}_{Tj}^* \\ \underline{f}_{Rj}^* \end{bmatrix} = \begin{bmatrix} (M_{11}^{(j)})E \\ (M_{21}^{(j)})E \end{bmatrix} \begin{bmatrix} \underline{\ddot{y}}_j \\ \underline{\dot{\omega}}_j \end{bmatrix} + \begin{bmatrix} (B_j^T B_j)^T \\ (M_{12}^{(j)}) \\ (M_{22}^{(j)}) \end{bmatrix} \begin{bmatrix} \underline{\ddot{y}}_j \\ \underline{\ddot{\theta}}_j \end{bmatrix} + \begin{bmatrix} \underline{A}_{QR}^* \\ \underline{A}_{\phi R}^* \end{bmatrix}$$

(3) ELIMINATION OF  $\{\ddot{y}_j\}, \{\ddot{\theta}_j\}$  FROM,

$$\underline{V}_K^* \cdot \underline{f}_{-j}^* = \underline{V}_K^* \cdot \underline{f}_{-j}^* ; \text{ FOR } K \text{ CORRESPONDING TO TRANSLATION AND ROTATION DEGREES OF FREEDOM}$$

WHERE :

- FOR TRANSLATION,

$$\underline{V}_K^* = \frac{\partial \underline{R}_j^*}{\partial \underline{y}_K^*} ; K=1, \dots, N_T^j$$

- FOR ROTATION,

$$\underline{V}_K^* = \frac{\partial \underline{R}_j^*}{\partial \underline{\theta}_K^*} ; K=1, \dots, N_R^j$$

NOTE : DOTTING  $\underline{f}_j^*$  WITH  $\underline{V}_K^*$  ELIMINATES NON-WORKING CONSTRAINT OR CONTACT FORCES AND MOMENTS

THE RESULTING EQUATIONS FOR ELIMINATION OF  $\{\ddot{y}_\delta\}$ ,  $\{\ddot{\theta}_\delta\}$  ARE WRITTEN AS FOLLOWS.

$$\begin{bmatrix} [M_\delta] & -m_\delta(\tilde{L}_\delta)' \\ m_\delta(\tilde{L}_\delta)' & [I_\delta] \end{bmatrix} \begin{bmatrix} \{\ddot{y}_\delta\} \\ \{\ddot{\theta}_\delta\} \end{bmatrix} = \begin{bmatrix} \{f_{T_\delta}\}_R \\ \{f_{R_\delta}\}_R \end{bmatrix} - \begin{bmatrix} [M_{\delta u_1}]' \\ [M_{\delta u_2}]' \end{bmatrix} \begin{bmatrix} [b_\delta] \\ [b_\delta] \end{bmatrix} \cdot \begin{bmatrix} [\ddot{R}_{u_1}] \\ [\ddot{\omega}_{u_2}] \end{bmatrix}$$

SQUARE - SYMMETRIC  
POSITIVE DEFINITE  
MATRIX

SOLVING THESE EQUATIONS FOR  $\{\ddot{y}_\delta\}$ ,  $\{\ddot{\theta}_\delta\}$  AND THEN SUBSTITUTING BACK INTO THE TRANSLATIONAL AND ROTATIONAL INERTIAL FORCE EXPRESSIONS YIELDS THE FOLLOWING.

$$\begin{bmatrix} f_{T_\delta}^* \\ f_{R_\delta}^* \end{bmatrix} = \begin{bmatrix} \ddot{y}_{(u_1)} \\ \ddot{\omega}_{(u_2)} \end{bmatrix} \cdot \begin{bmatrix} [\ddot{R}_{u_1}] \\ [\ddot{\omega}_{u_2}] \end{bmatrix} + \begin{bmatrix} \frac{A_{\delta R_{u_2}}}{A_{\delta R_{u_2}}} \\ \frac{A_{\delta R_{u_2}}}{A_{\delta R_{u_2}}} \end{bmatrix}$$

SOLUTION ALGORITHM DEVELOPMENT

\* "SHIFTING" OF BODY  $j$  INERTIAL AND ACTIVE FORCES TO BODY  $L(j)$  VIA KINEMATIC OPERATOR APPROACH

(1) FROM KINEMATICS,

$$\begin{bmatrix} \ddot{\underline{R}}_{u_3} \\ \dot{\underline{\omega}}_{u_3} \end{bmatrix} = \begin{bmatrix} \underline{E} & -(\tilde{\underline{r}}_{u_3}^i) \underline{E} \\ \underline{O} & \underline{E} \end{bmatrix} \cdot \begin{bmatrix} \ddot{\underline{R}}_+^{u_3} \\ \dot{\underline{\omega}}_+^{u_3} \end{bmatrix} + \begin{bmatrix} (\underline{b}_{u_3}^T, \underline{b}_{u_3})^T \{(\underline{\varphi}_{u_3}^{u_3}) - (\tilde{\underline{r}}_{u_3}^{u_3})(\underline{\varphi}_{u_3}^{u_3})\} \{ \ddot{\eta}_{u_3} \} \} \\ \{(\underline{\varphi}_{u_3}^{u_3})\} \end{bmatrix}$$

(2) NOW DEFINE,

$$(\underline{T}_{u_3}^i) = \begin{bmatrix} (\underline{I}) & -(\tilde{\underline{r}}_{u_3}^i) \{(\underline{\varphi}_{u_3}^{u_3}) - (\tilde{\underline{r}}_{u_3}^{u_3})(\underline{\varphi}_{u_3}^{u_3})\} \\ (\underline{O}) & (\underline{I}) \{(\underline{\varphi}_{u_3}^{u_3})\} \end{bmatrix}$$

(3) USING  $\{(\underline{T}_{u_3}^i)\}$  WE SHIFT BODY  $j$  INERTIAL FORCE EQUATIONS TO BODY  $L(j)$  AS FOLLOWS.

(4) PARTITION  $\{(\underline{T}_{u_3}^i)\}$  INTO THE FOLLOWING FORM

$$(\underline{T}_{u_3}^i) = [(\underline{A}_{u_3}^i) | (\underline{B}_{u_3}^i)] ; (\underline{A}_{u_3}^i) \equiv (6 \times 6), (\underline{B}_{u_3}^i) \equiv (6 \times 6 \times 6)$$

(5) NOW DEFINE

$$\{M_{u_3}^{1,1}\} = \{A_{u_3}^{1,1}\}^T \{I^1\} \{A_{u_3}^{1,1}\} ; (6 \times 6)$$

$$\{M_{u_3}^{1,2}\} = \{A_{u_3}^{1,1}\}^T \{I^1\} \{B_{u_3}^{1,2}\} ; (6 \times NM_{u_3})$$

$$\{M_{u_3}^{1,3}\} = \{M_{u_3}^{1,2}\}^T ; (NM_{u_3} \times 6)$$

$$\{M_{u_3}^{1,4}\} = \{B_{u_3}^{1,2}\}^T \{I^1\} \{B_{u_3}^{1,2}\} ; (NM_{u_3} \times NM_{u_3})$$

$$\left[ \begin{array}{c} \underline{A_{dRas u_3}^{1,1}} \\ \underline{A_{dRas u_3}^{1,2}} \end{array} \right] = \left[ \begin{array}{c} [B_{u_3}^T] [A_{u_3}^{1,1}]^T [B_{u_3}] \cdot \left[ \frac{\underline{A_{dRas}^{1,1}}}{\underline{A_{dRas}^{1,2}}} \right] \end{array} \right]$$

ALSO FOR BODY L(j) MODAL FLEX EQUATIONS

$$\{A_{Rq}^{1,1}\}_{u_3} = \{B_{u_3}^{1,2}\}^T \{B_{u_3}^{1,2}\} \cdot \left[ \frac{\underline{A_{dRas}^{1,1}}}{\underline{A_{dRas}^{1,2}}} \right]$$

FROM :

$$\left( \begin{array}{c} T_{u_3}^{1,1} \\ T_{u_3}^{1,2} \end{array} \right) \cdot \left( \begin{array}{c} f_{R_3}^{1,1} \\ f_{R_3}^{1,2} \end{array} \right)$$

(6) RECORD BODY  $L(j)$  INERTIAL FORCE EXPRESSIONS INCLUDING AUGMENTATION FORM BODY  $j$

- TRANSLATION AND ROTATION INERTIAL FORCES

$$\begin{pmatrix} f_{T(u_i)}^* \\ f_{R(u_i)}^* \end{pmatrix} = \begin{pmatrix} \left[ \frac{m_{u_i} E}{m_{u_i}(\tilde{r}_c)E} \right] \left[ \frac{-m_{u_i}(\tilde{r}_c)E}{\tilde{r}_c} \right] + \left[ \frac{M_{u_i}^1}{M_{u_i}^2} \right] \left[ \frac{\ddot{r}_{u_i}}{\ddot{r}_{u_i}} \right] \cdot \left[ \frac{\ddot{r}_{u_i}}{\ddot{r}_{u_i}} \right] + \left[ \frac{(\underline{B}_{u_i}^T \underline{B}_{u_i})}{\{ (M_{u_i}^1) + (M_{u_i}^2) \}} \right] \left[ \{ (M_{u_i}^1) + (M_{u_i}^2) \} \right] \end{pmatrix}$$

$$\begin{pmatrix} \{ (M_{u_i}^1) + (M_{u_i}^2) \} \left[ \frac{\ddot{u}_i}{\ddot{u}_i} \right] + \left[ \frac{A_{u_i}^1}{A_{u_i}^2} \right] \left[ \frac{\ddot{u}_i}{\ddot{u}_i} \right] + \left[ \frac{Q_R}{Q_R} \right] \left[ \frac{\ddot{u}_i}{\ddot{u}_i} \right] \\ \{ (M_{u_i}^1) + (M_{u_i}^2) \} \left[ \frac{\ddot{\theta}_i}{\ddot{\theta}_i} \right] + \left[ \frac{A_{u_i}^1}{A_{u_i}^2} \right] \left[ \frac{\ddot{\theta}_i}{\ddot{\theta}_i} \right] + \left[ \frac{Q_R}{Q_R} \right] \left[ \frac{\ddot{\theta}_i}{\ddot{\theta}_i} \right] \end{pmatrix}$$

- BODY  $L(j)$  MODAL, FLEX INERTIAL FORCES

$$\{ f_{u_i}^* \} = \left[ \left[ \{ M_{u_i}^1 \} \right] \left[ \{ M_{u_i}^2 \} \right] + \left[ \{ M_{u_i}^1 \} \right] \left[ \{ M_{u_i}^2 \} \right] + \left[ \{ M_{u_i}^1 \} + \{ M_{u_i}^2 \} \right] \left[ \{ M_{u_i}^1 \} + \{ M_{u_i}^2 \} \right] \right] \left[ \{ \ddot{u}_i \} \right]$$

$$+ \left[ \{ M_{u_i}^1 \} + \{ M_{u_i}^2 \} \right] \left[ \{ \ddot{\theta}_i \} \right] + \left[ \{ A_{u_i}^1 \} \right] \left[ \{ \ddot{u}_i \} \right] + \left[ \{ f_{u_i}^* \} \right]$$

WE HAVE IN ESSENCE AUGMENTED BODY  $L(j)$  INERTIAL FORCE EXPRESSION WITH THE "SHIFTED" INERTIAL FORCES OF BODY  $j$ .

- (7) USING  $\{T_L(j)\}$  WE PERFORM THE SIMILAR "SHIFT" ON BODY  $j$  ACTIVE FORCE EXPRESSIONS, SO THAT FOR BODY  $L(j)$ ,

$$\begin{bmatrix} \underline{F}_{TOTAL}^{(u_j)} \\ \underline{M}_{TOTAL}^{(u_j)} \end{bmatrix} = \begin{bmatrix} \underline{F}^{(u_j)} \\ \underline{M}^{(u_j)} \end{bmatrix} + \begin{bmatrix} \underline{B}_{u_j}^T \underline{B}_{u_j} \end{bmatrix} \begin{bmatrix} \underline{A}^{(u_j)} \\ \underline{B}_{u_j} \end{bmatrix} \begin{bmatrix} \underline{F}^{(j)} \\ \underline{M}^{(j)} \end{bmatrix}$$

AND,  $\{f_{q_{u_j}TOTAL}\} = \{f_{q_{u_j}}\} + \{B_{u_j}^{(j)}\}^T \begin{bmatrix} \underline{B}_{u_j} \\ \underline{B}_{u_j} \end{bmatrix} \begin{bmatrix} \underline{F}^{(j)} \\ \underline{M}^{(j)} \end{bmatrix}$

- (8) BODY  $j$  INERTIAL AND ACTIVE FORCES ARE NOW COMPLETELY RETAINED INCLUDED IN BODY  $L(j)$  EQUATIONS OF MOTION WHERE WE HAVE ELIMINATED EXPLICIT EXPRESSIONS INVOLVING BODY  $j$  DEGREES OF FREEDOM. THE PROCESS IS NOW REPEATED FOR BODY  $L(j)$  TO BODY  $L(L(j))$ .
- (9) THE PROCESS DESCRIBED IS REFERRED TO AS THE "FRONTAL" PART OF THE SOLUTION ALGORITHM.
- (10) IN THE END RESULT, ONCE BODY  $L(j)$  KINEMATIC ACCELERATIONS ARE KNOWN WE CAN SUBSTITUTE TO SOLVE FOR BODY  $j$  BACK ACCELERATIONS. THIS PROCESS IS REFERRED TO AS "BACK SUBSTITUTION".

## SOLUTION ALGORITHM OVERVIEW

- BASED ON THE DEVELOPMENT PROVIDED THE SOLUTION ALGORITHM IS SUMMARIZED AS FOLLOWS.

- (1) PERFORM INITIALIZATION PROCESSING AND COMPUTATIONS
  - SYSTEM TOPOLOGY PARAMETER IDENTIFICATION
  - COMPUTATION OF FLEXURE TIME-INVARIANT MATRICES AND VECTORS

- (2) GIVEN THE TOPOLOGY DEFINITION FROM (1), PERFORM THE "FRONTAL" ALGORITHM COMPUTATIONS AS FOLLOWS.

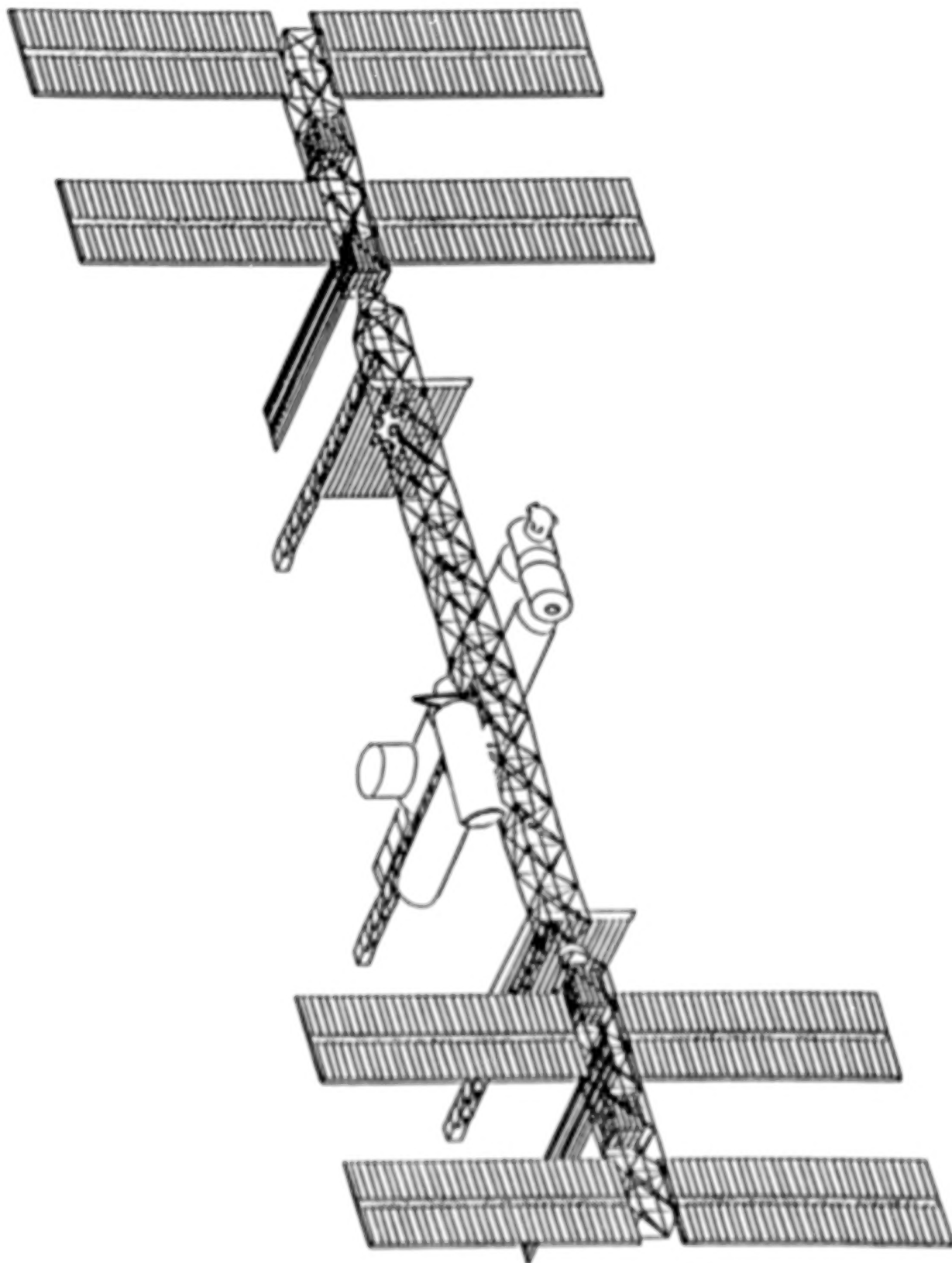
- (a) STARTING AT THE HIGHEST "LEVEL" IN THE SYSTEM AT THE LAST "BRANCH" OF THE LAST "BASE BODY" IN THIS LEVEL, IDENTIFY THE "LEAF BODY" IN THE BRANCH AND PERFORM THE "SHIFT" STEPS AS OUTLINED PREVIOUSLY.
- (b) WHEN THE ALGORITHM REACHES THE BASE BODY WE PROCEED TO THE REMAINING BRANCHES.
- (c) ADD THE CONTRIBUTIONS OF ALL BRANCHES TO THIS BASE BODY.
- (d) IDENTIFY THE NEXT BASE BODY IN THIS LEVEL AND REPEAT STEPS (a) THROUGH (d).
- (e) WHEN ALL THE BASE BODIES AT THIS LEVEL HAVE BEEN EXHAUSTED, PROCEED TO STEP (f).
- (f) SET THE CURRENT LEVEL TO THE NEXT LOWER LEVEL AND REPEAT STEPS (a) THROUGH (f). WHEN WE HAVE REACHED THE FIRST LEVEL, i.e. THE CORE BODY, WE PROCEED WITH "BACK SUBSTITUTION".



# SOLUTION ALGORITHM OVERVIEW

## (3) "BACK SUBSTITUTION"

- (a) SOLVE BODY 1 (CORE BODY) DYNAMICS TO OBTAIN ITS SCALAR ACCELERATIONS.
- (b) USING THE BACK SUBSTITUTION KINEMATICS, PROCEED TO SOLVE FOR THE SCALAR ACCELERATIONS OF THE OTHER BODIES WORKING OUTWARD FROM BODY 1.
  - $\{\ddot{y}_i^s\}, \{\ddot{\theta}_i^s\}$  IN TERMS OF  $\ddot{R}_{w,i}^s$
  - $\{\ddot{y}_i^s\}, \{\ddot{\theta}_i^s\}$  AND KNOWN
  - $\{\ddot{y}_i^s\}$  IN TERMS OF  $\{\ddot{y}_i^s\}, \{\ddot{\theta}_i^s\}$
  - $\ddot{R}_{w,i}^s, \ddot{\omega}_{w,i}^s$  , AND KNOWN.
- (4) ASSEMBLE THE STATE VECTOR DERIVATIVE FOR NUMERICAL INTEGRATION.



## ORDER 'n' BASED SOFTWARE

- 1. Operational on the NASA-JSC

ACS software test bed.

- 2. Current Version Includes

Environment Models

Sensors-Actuators

## SYMBOLIC CODE GENERATION

- 1. Algebraic simplification
- 2. Trigonometric simplification
- 3. Storage of common terms
- 4. Simplification based on particular problem definition.

i.e Generic code has a lot of overhead,  
symbolic code is specific to the problem

## PARALLEL PROCESSING

- 1. Order 'n' algorithm has inherent parallelism.
- 2. Load balancing schemes should exploit both the  
number of processors and the problem topology.
- 3. Symbolic code combined with parallel architecture  
can approach real-time performance.

**CONTROL DESIGN CHALLENGES OF  
LARGE SPACE SYSTEMS AND  
SPACECRAFT CONTROL LABORATORY EXPERIMENT  
(SCOLE)**

**JIGUAN GENE LIN**

**CONTROL RESEARCH CORPORATION  
6 CHURCHILL LANE  
LEXINGTON, MA 02173**

**CONTRACT NAS1-18185**

#### ACKNOWLEDGEMENT

This work was performed by the Control Research Corporation (CRC) under the contract NAS1-18185. The research was supported by NASA Langley Research Center (LaRC), Hampton, Virginia. The technical monitor was Dr. Suresh M. Joshi of LaRC.

The studies were conducted by the principal investigator, Dr. Jiguan Gene Lin (CRC). We wish to thank Dr. Joshi (LaRC) for his patience and assistance in the execution of this effort. We are also grateful to Mr. Larry Taylor of LaRC for his stimulating and penetrating technical discussions.

## TABLE OF CONTENTS

<u>Section</u>	<u>Page</u>
1 INTRODUCTION .....	1
2 MATHEMATICAL MODEL OF THE ORBITAL SCOPE CONFIGURATION .....	5
2.0 Outline of the Orbital Shuttle-Mast-Antenna Configuration ....	5
2.1 Flexible-Body Dynamics .....	6
2.2 Line-of-Sight Error Expression with More Bending Terms .....	7
3 VIBRATORY RESPONSES TO BANG-BANG TYPE RAPID SLEW MANEUVERS .....	11
3.1 Excitation by the Rapid Time-Minimized Bang-Pause-Bang Slew Maneuver .....	11
3.2 Excitation by Other Rapid Time-Minimized Bang-Bang Slew Slew Maneuvers .....	14
4 ACTIVE VIBRATION CONTROL VIA MODAL DASHPOTS .....	23
4.1 Direct Velocity-Output Feedback Control .....	23
4.2 Concept of Modal Dashpots .....	24
4.3 Improvements on the Design Method .....	27
5 DESIGN OF MODAL DASHPOTS FOR SCOPE .....	29
5.1 Analysis on Vibration Modes .....	29
5.2 Analysis on Modal Control Influences of Actuators .....	38
5.3 Design of Modal Dashpot MD1 .....	40
6 PERFORMANCE OF VIBRATION CONTROL DESIGNS ON SCOPE .....	44
6.1 Simulation Results of Modal Dashpot Design MD1 .....	44
6.2 Simulation Results of A Modified Version of MD1 .....	49
6.3 Comments .....	55
7 CONCLUSIONS .....	58
8 RECOMMENDATIONS .....	61
REFERENCES .....	63



## 1. INTRODUCTION

Supported by the Spacecraft Control Branch of NASA Langley Research Center under the Spacecraft Control Laboratory Experiment (SCOLE) program, the Control Research Corporation continued the investigation into the control design challenges of large space systems and Spacecraft Control Laboratory Experiment. This study concentrated on the second stage of a two-stage approach to active control of the flexible orbital configuration of SCOLE. The principal objective was to investigate if the structural vibrations excited by **time-optimal** line-of-sight pointing slew maneuvers of the **bang-bang** type could be quickly suppressed via **"modal-dashpot"** design of velocity output feedback control.

Structural vibrations in future large space systems such as space antennas, space platform, space station, or of deployed flexible payloads attached to the space Shuttle orbiter, and their interaction with on board controllers have become a major concern in the design and operation of such control systems as, say, for pointing and stabilization. The natural vibration frequencies of such systems are unconventionally low (tenths of 1 Hz in many cases) and closely spaced, many of which lie inside or nearby the bandwidth of various traditional (rigid-body) control systems. In the past few years, many approaches were proposed for designing advanced control systems that would suppress vibrations in large flexible space structures, and various in-house laboratory experiments were also conducted, each being specifically set up for demonstrating some particular design techniques of interest. In 1983, the Spacecraft Control Branch at NASA Langley Research Center initiated the **Spacecraft Control Laboratory Experiment (SCOLE)** program and the **NASA/IEEE Design Challenge** [1] to promote direct comparison and realistic test of different approaches to control design against a common open-to-public laboratory article. As shown in Fig. 1-1, the article was intended to resemble a large space antenna attached to the Space Shuttle Orbiter by a long flexible mast, similar to the proposed space flight experiments and various space-based antenna systems, and to have a truly three-dimensional complex dynamics.

As stated in Ref. [1], the primary control task of the Experiment is to **rapidly slew or change the line-of-sight (LOS)** of an antenna attached to the space Shuttle orbiter, and to **settle or damp the structural vibrations** to the degree required for precision pointing of the antenna. The objective is to minimize the time required to slew and settle, until the antenna line-of-sight remains within a specified angle.

Research on a practical two-stage approach and some associated control design challenges in the context of SCOLE had been conducted earlier by Lin [2]-[5]. His initial efforts, also supported by the SCOLE program, were concentrated on "Stage 1" while the flexible-body dynamics of the configuration with a flexible mast beam was being actively developed at the Langley Research Center.

Among the most commonly held ideas for pointing/retargeting of large flexible space systems is the following intuitively appealing and rather practical two-stage approach: (Stage 1) slew the whole structure like a rigid body in a minimum time under the limited control moments and forces first, and then

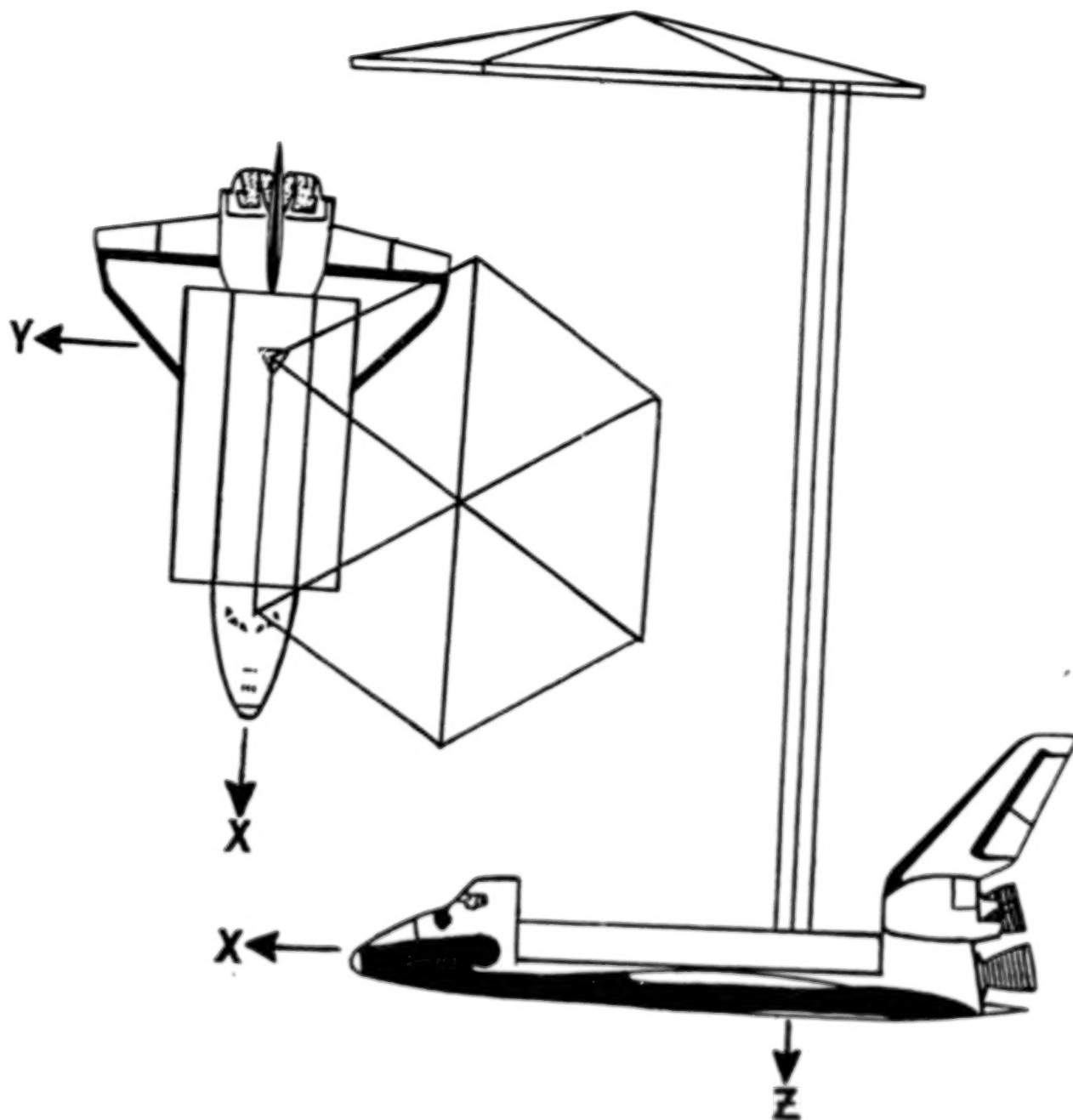


Fig. 1-1 Spacecraft Control Laboratory Experiment (SCOLE)--  
the orbital Shuttle-Mast-Antenna configuration.

(Stage 2) damp out the excited structural vibrations afterwards. Such an approach undoubtedly will be a very relevant, and realistic as well, to study with SCOPE.\*

To slew a spacecraft for a given angle in a **prespecified time**, there are many ways to command the slew actuators on board. The one that is easy to implement is a **bang-bang control**. That is, a constant force at its allowable maximum is applied in one direction half of the time and then in the opposite direction the other half. Such is the most convenient and common with reaction-jet thrusters, and most spacecraft including the space Shuttle use thrusters. As the structure considered for future space antennas and optics was becoming larger and more flexible, structural dynamicists suggested modifying the constant profile by a sine or versine function so as to smooth the switching. To explore further in their theoretical and experimental investigations, control engineers also started to apply Pontryagin's Maximum Principle of the optimal control theory [6] to develop open-loop profiles that would "minimize" excitation of the first few vibration modes.\*\* Including more than a few modes generally will make it almost impossible, even with the aid of powerful digital computers, to carry out the complicated computations necessary for applying the optimal control theory. To implement any such slew profile other than the bang-bang type will also require that the thrusters be at least "throttleable" in fine steps, which is still beyond the current state of the art.

To slew SCOPE for the desired  $20^\circ$  under the specified limits on control moments and forces in a minimum time, instead of some arbitrarily fixed time, application of the well-known time-optimal bang-bang control theory [6]-[7] was considered the most appropriate for the Stage-1 design. The theory, however, is not directly applicable to SCOPE: due to the asymmetrical configuration and the moving coordinate frame that is fixed on the Shuttle body axes, all axes are tightly coupled through **nonzero products of inertia** as well as through **different moments of inertia**. After examining the major assumptions in the theory, Lin [2]-[3] was able to develop a useful practical design technique for time-minimized single-axis bang-bang slew maneuvers. This includes the possible "**bang-pause-bang control**" when some judicious slew rate limits are imposed on the slew design.

Analytical and numerical studies were then conducted on the implicit transcendental nonlinear expression initially provided by NASA Langley Research Center for SCOPE's line-of-sight error. A designer's choice of allowable initial alignment to take advantage of the low moment of inertia in the roll, as suggested by Taylor [1], was determined directly analytically. The slew angles to achieve the desired LOS pointing were thus determined. [4]-[5]

A computer program for SCOPE's complete 3-axis rigid-body dynamics was developed and used to simulate numerically the application of various time-

---

\* The Space Shuttle, while in orbit, is under the single-axis "phase-plane" rigid-body attitude control of "Digital Auto-Pilot" (DAP). If the two-stage approach is applicable, then the current DAP can be used conveniently with various proposed flexible-structure flight experiments in space without having to make a major specific change in operation or design to suit each different experiment setup.

\*\* Usually all but 2 to 3 modes of the structure were ignored.

minimized bang-bang type attitude slew maneuvers. The numerical simulation test results indicated that the single-axis bang-bang or bang-pause-bang slew maneuvers work fairly well for pointing the LOS of SCOLE under the specified conditions. In particular, applying a maximum allowable control moment (i.e., 10,000 lb-ft) on the Shuttle and a maximum allowable control force (i.e., 800 lb) on the Reflector, plus imposing 5 deg/sec slew rate limit on the design, yields the best pointing accuracy ( $0.097^\circ$ ) with minimized slew time (3.733 sec) and least sensitivity to nonzero products of inertia. Such is a best design for LOS pointing slew maneuver for the SCOLE configuration so far as the Stage 1 is concerned.[5]

For designing vibration control systems (the Stage 2), a standard choice would be to apply the modern control and estimation theory, namely, the linear-quadratic-Gaussian (LQG) state-feedback control technique. The LQG technique has been well accepted because of its success in various other applications. **Control spillover** and **observation spillover**, however, have surfaced as major roadblocks to successful application of such a state-of-the-art state-feedback design technique to control vibrations in large flexible space structures. Current spacecraft and many other engineering systems on which the LQG technique has been very successful are of the rigid-body type that do not have as many closely spaced low-frequency vibration modes as there are in a future large flexible space system. Earlier, Balas [8] showed by an example and Herrick [9] followed by a hardware experiment that, because of control and observation spillover, even a simple flexible beam, which was initially stable in the open loop, **became unstable** when the "modern modal control" loops were closed.

On the other hand, dynamic properties of large flexible space structures can be enhanced by active augmentation of modal damping and stiffness through proper output-feedback control [10]-[24]. Lin [20]-[23] showed analytically that an appropriate output feedback control system, particularly when it is of the type of "modal dashpots" and/or "modal springs" [21], can even ensure **full-order closed-loop asymptotic stability** of a very general class of lightly damped large flexible space structures while improving their dynamic characteristics.

For Stage-2 design to damp the excited vibrations in the SCOLE configuration, one can consider using a modal-dashpot type of output feedback control system first. One may then consider using a **modal-dashpot augmented LQG** optimal state feedback control system, if the LOS stabilization performance is not enough to satisfy the specified stringent accuracy requirements.

Before proceeding to designing a vibration control system for SCOLE, many technical issues need to be addressed. For example, one needs to characterize SCOLE's vibration modes with respect to (i) the excitation by the rapid slew maneuvers, (ii) their contribution to the vibration (jittering) of SCOLE's line of sight, and (iii) the control authority of the control actuators. Which modes need to be controlled directly? Which modes only need some additional damping? Which are more likely to cause serious control spillover if not included as "modeled modes"? Those are among many technical questions one generally should look into before starting out a meaningful design for SCOLE's vibration control system.



## 2. MATHEMATICAL MODEL OF THE ORBITAL SCOLE CONFIGURATION

To assist our quantitative assessments of the vibratory impact of rapid bang-bang slew maneuvers on the flexible SCOLE configuration and the performance of proposed vibration control designs, we have developed a computer program to simulate various vibratory responses of the configuration. The computer simulation was based mainly on the modal data set D3D585 provided by Dr. Suresh M. Joshi of NASA Langley Research Center as the flexible-body dynamics, and the nonlinear LOS error expression formulated by Mr. Larry Taylor [1]. We extended a portion of the expression by including a few more terms to take a better account of the effect of bending in the mast.

### 2.0 Outline of the Orbital Shuttle-Mast-Antenna Configuration

As shown in Fig. 1-1, the configuration of the SCOLE represents a large antenna attached to the Space Shuttle Orbiter by a flexible beam as the Mast. The configuration was chosen for its similarity to proposed space flight experiments and various space antenna systems.

The dynamics of the SCOLE configuration are described [1] by a distributed-parameter beam equations with rigid bodies in the three-dimensional space, each having mass and inertia at either end. One body represents the space Shuttle Orbiter, having the mass, inertia, and dimensions typical of the real one. The other body is a large antenna reflector. The equations of motion for the complete configuration are formed by incorporating the three-dimensional rigid-body equations into the partial differential equations of beam bending and torsion. The flexible mast is treated as a standard slender beam. The boundary conditions at the ends of the beam contain the forces and moments applied to the rigid Shuttle and reflector bodies. The mast is **not attached to the mass center** of the reflector, but rather significantly away in both x and y directions. The nonlinear kinematics of the two sizable bodies and the offset attachment of the reflector couple the three otherwise uncoupled beam equations. The reader is referred to Taylor and Balakrishnan's paper [1] for the details. The rigid-body part of the mathematical model was used by Lin earlier in his studies on the LOS pointing (i.e., the Stage 1) of the configuration. The studies on vibration control reported here were based on a most recent version of the flexible-body part available; see Section 2.1 below.

The line-of-sight (LOS) error of the SCOLE configuration is a highly nonlinear implicit expression. The line of sight is defined by a ray emitted from the feed on the Shuttle which is reflected at the center of the Reflector. It is affected by the pointing error of the Shuttle, the offset attachment of the Reflector, and the misalignment due to the deflection and torsion of the Mast. The reader is again referred to Ref. [1] for the original formulation of the LOS error. An equivalent expression having a simple modification, which is more convenient than the original for both efficient numerical computations and in-depth analytical investigations, was used by Lin in his earlier rigid-body studies [3]-[5]. For the current flexible-body studies, the nonlinear LOS error expression also needs some more terms in order to have a better accounting for the bending of the mast beam; see Section 2.2 below.

## 2.1 Flexible-Body Dynamics

The bending and torsion characteristics of the SCOLE configuration were originally formulated in partial differential equations by Taylor and Balakrishnan [1]. Robertson [25] derived the corresponding equations of free motion taking into account the kinematic coupling resulted (i) from the offset attachment of the Reflector to the Mast and (ii) from the nonzero products of inertia of both the Shuttle and the Reflector. He then solved the equations in terms of trigonometric and hyperbolic functions and computed a set of natural frequencies and mode shapes. Such results are not readily useful for control studies.

To facilitate the control analysis and design for SCOLE, Joshi [26] first derived a state-space model from Robertson's results; the data set was named "BMDT3D". Later, he improved Robertson's results, and also derived another state-space model, named "D3D585". Our computer simulation program was initially based on the data set BMDT3D, which contained only the first five flexible-body vibration modes. It was then updated when Dr. Joshi furnished us with the set D3D585 later.

The set D3D585 provides modal data in the state-space (A,B,C) form. It contains only the first 10 flexible-body modes but no rigid-body modes nor any nonlinear rigid-body dynamics. This set was quite appropriate for our purpose of assessing the vibratory impact on SCOLE. We found it more efficient and convenient, however, to compute the time transition of the states using the second-order modal equations directly, because of the decoupled nature of the former, than to do so using the first-order state equations. We thus converted the furnished data back to the following standard modal form:

$$\ddot{\eta}_i + \delta_i \dot{\eta}_i + \sigma_i \eta_i = \sum_{k=1}^n \phi_i^T b_{Fk} u_k \quad i = 1, \dots, N \quad (2-1)$$

$$y_j = \sum_{i=1}^n (c_{Vj} \dot{\eta}_i + c_{Dj} \eta_i) \quad j = 1, \dots, l \quad (2-2)$$

$$\text{where} \quad \delta_i = 2\zeta_i \omega_i, \quad \sigma_i = \omega_i^2 \quad (2-3)$$

are, respectively, the damping and stiffness coefficients of the unit-mass linear oscillator representing the  $i$ th vibration mode;  $\omega_i$  and  $\phi_i$  denote the natural frequency and mode shape, respectively, of mode  $i$ ;  $\zeta_i$  denotes the inherent damping ratio of mode  $i$ , which had been assumed to be 0.3% for all flexible-body modes of SCOLE [1].  $\eta_i$  and  $\dot{\eta}_i$  denote the coordinate and velocity, respectively, of the  $i$ th mode.

The  $k$ th force (torque) input is denoted by  $u_k$ , with column vector  $b_{Fk}$  representing the corresponding actuator influences on SCOLE. The  $j$ th measurement output is denoted by  $y_j$ , with row vectors  $c_{Vj}$  and  $c_{Dj}$  representing, respectively, the velocity and displacement sensor influences.

Putting (2-1) and (2-2) into a matrix form, we get

$$\ddot{\eta} + \Delta \dot{\eta} + I\eta = \Phi^T B_F u \quad (2-4)$$

$$y = C_V \dot{\eta} + C_D \eta \quad (2-5)$$

where

$$\Delta = \text{diag} [2\zeta_i \omega_i], \quad I = \text{diag} [\omega_i^2] \quad (2-6)$$

$$\Phi = [\phi_1, \dots, \phi_n], \quad B_F = [b_{F1}, \dots, b_{Fn}] \quad (2-7)$$

$$C_V = \begin{bmatrix} C_{V1} \\ \vdots \\ C_{Vn} \end{bmatrix} \quad C_D = \begin{bmatrix} C_{D1} \\ \vdots \\ C_{Dn} \end{bmatrix}$$

$$\eta = \begin{bmatrix} \eta_1 \\ \vdots \\ \eta_n \end{bmatrix} \quad u = \begin{bmatrix} u_1 \\ \vdots \\ u_m \end{bmatrix} \quad y = \begin{bmatrix} y_1 \\ \vdots \\ y_l \end{bmatrix} \quad (2-8)$$

In accordance with Robertson's formulation, we also assume that the bending and torsion in SCOLE are referred to the coordinate system defined on its initial undeformed configuration. Thus, before any deformation, the center of mass of the Shuttle is at the origin of the coordinates; the roll, pitch, and yaw axes (i.e., body x, y, z axes) of the Shuttle, align with the x, y, z coordinate axes\* respectively; and, in particular, the straight mast beam coincides with the z coordinate axis. Note that, since the flexible mast was not treated as a cantilevered beam in Robertson's derivation, not only the mast may not be tangential to the z coordinate axis, but the center of mass of the Shuttle also may not remain at the origin, nor may the Shuttle body axes remain parallel to the coordinate axes, when a significant deformation of the mast occurs. The line of sight of the SCOLE configuration will thereby be significantly affected.

## 2.2 Line-of-Sight Error Expression with More Bending Terms

In order that the jittering of the line of sight (LOS) due to excited vibrations can be more accurately evaluated, we used almost the same nonlinear expression for the line-of-sight (LOS) error of the SCOLE configuration as originally given in Ref. [1]. Unlike the original, however, our improved version also takes into account the **x-axis dislocation of the Reflector due to bending of the mast**, and like the one Lin used earlier [4]-[5] the LOS vector  $R_{LOS}$  is not normalized. Note that the LOS error expression could be expanded in a Taylor series and a linearized version could be obtained by taking the first-order terms. A linearized version, though useful in linear-quadratic

\* Robertson's y and z axes are opposite in sign to those defined by Taylor for SCOLE. We continue to adopt Taylor's definition for consistency with Lin's earlier studies [2]-[5] on the Stage 1.

optimal control designs, is not appropriate for our current use since the excited vibrations are sufficiently large in magnitude and the second- and higher-order terms of the series expansion may not be negligible at all.

The location of the center of the Reflector, represented by  $\mathbf{R}_R$ , is defined by the location of the joint where the Reflector is attached to the Mast; see Figure 2-2. Denote by  $\mathbf{R}_J$  the location of the joint relative to the center of the Reflector, and by  $\mathbf{R}_T$  the location of the same point (also the tip of the mast) with respect to the center of the Shuttle. Then the vector  $\mathbf{R}_R$  is given by

$$\mathbf{R}_R = \mathbf{R}_T - \mathbf{T}_1^T \mathbf{T}_4 \mathbf{R}_J \quad (2-9)$$

$$\text{where } \mathbf{R}_J = \begin{bmatrix} -18.75 \\ 32.5 \\ 0 \end{bmatrix} \quad (2-10)$$

The vector  $\mathbf{R}_J$  is constant in magnitude because of the rigid reflector, but its orientation with respect to the Shuttle is affected by the deflection at the tip J. The product  $\mathbf{T}_1^T \mathbf{T}_4$  of coordinate transformations  $\mathbf{T}_1$  and  $\mathbf{T}_4$  is to take care of the angular change. As in Ref. 1,  $\mathbf{T}_1$  denotes a direction-cosine transformation from the Shuttle to the Earth (inertial) coordinates, and  $\mathbf{T}_4$  one from the Reflector to the Earth coordinates.

A reasonable approximation for the tip location is given by

$$\mathbf{R}_T = \begin{bmatrix} \text{Bend}_x \\ \text{Bend}_y \\ -\sqrt{130^2 - \text{Bend}_x^2 - \text{Bend}_y^2} \end{bmatrix} \quad (2-11)$$

$$\text{where } \text{Bend}_x = u_{xS} - u_{xR} \quad \text{Bend}_y = u_{yS} - u_{yR}$$

$u_{xS}$  and  $u_{yS}$  denote the deflections of the mast at the Shuttle end in the xz and yz planes, respectively;  $u_{xR}$  and  $u_{yR}$  are the corresponding deflections at the Reflector end.

Eqs. (2-9)-(2-11) constitute our additional modification to the LOS error expression. Note that the vector  $\mathbf{R}_R$  originally given as (18.75, -32.5, -130) in Ref. [1] corresponds to the undeformed case. To see it, assume that there

are no deflections at all. Then  $\text{Bend}_x$  and  $\text{Bend}_y$  are both zero, and  $\mathbf{T}_4$  is equal to  $\mathbf{T}_1$ . Therefore,  $\mathbf{R}_T = (0, 0, 130)$ . Consequently,  $\mathbf{R}_R = \mathbf{R}_T - \mathbf{R}_J = (18.75, -32.5, 130)$ .

In the analytical studies on the LOS error of SCOLE [4]-[5], we found it more convenient not to normalize the LOS vector  $\mathbf{R}_{LOS}$  first, although the resulting error expression is the same since division by its norm is still made later at the end. The LOS error with such a trivial modification is given by

$$e_{LOS} = \pm \sin^{-1} \left[ \frac{||\mathbf{D}_T \times \mathbf{T}_1 \mathbf{R}_{LOS}||}{||\mathbf{R}_{LOS}||} \right] \quad (2-12)$$





with the unnormalized LOS vector being defined as

$$\mathbf{R}_{LOS} = \mathbf{R}_F - \mathbf{R}_R - 2[(\mathbf{R}_R - \mathbf{R}_F) \cdot \mathbf{R}_A] \mathbf{R}_A \quad (2-13)$$

where as defined in [1],  $\mathbf{R}_F$  is the vector representing the feed location (3.75, 0, 0).  $\mathbf{R}_A$  is a unit vector in the direction of the Reflection axis in the Shuttle body coordinates, i.e.,

$$\mathbf{R}_A = \mathbf{T}_1^T \mathbf{T}_4 \begin{bmatrix} 0 \\ 0 \\ 1 \end{bmatrix}.$$

For the target direction specified in [1] as  $\mathbf{D}_T = (0, 0, 1)$ , Expression (2-12) reduces to

$$\alpha_{LOS} = \pm \sin^{-1} \left[ \sqrt{(T_{1r1} \mathbf{R}_{LOS})^2 + (T_{1r2} \mathbf{R}_{LOS})^2} / \|\mathbf{R}_{LOS}\| \right] \quad (2-14)$$

where  $T_{1r1}$  and  $T_{1r2}$  denote respectively the first and the second rows of matrix  $\mathbf{T}_1$ .

### 3. VIBRATORY RESPONSES TO BANG-BANG TYPE RAPID SLEW MANEUVERS

Several LOS pointing slew maneuvers of the bang-bang type were applied to our computer simulation of the SCOLE flexible-body dynamics. The resulting responses range from excessive to minimal, depending on the magnitude of the applied force at the Reflector. Note, however, that all these slew maneuvers were designed to provide minimized slew time under the increasingly tight limit imposed on the respective applied force.

The slew maneuver that excited the **most violent vibrations** in SCOLE was chosen for studying the control design and for generating in-depth insights into the vibration control challenges. On the other hand, the least violent one deserves further exploration in the future, since it may potentially require a smaller total time for both slew and stabilization.

In assessing the impact of structural vibrations on SCOLE, we view the slew maneuvers as **time-dependent disturbances** instead, and only the vibratory portion of the time-domain responses are of real interest. Therefore, it is reasonable that we concentrate only on the flexible-body and temporarily ignore any rigid-body dynamics in this study. This assumption is equivalent to the absence of rigid-body dynamics. It is also reasonable to assume that, before being subject to such disturbances, SCOLE was initially at rest and had no deformation nor LOS error. The former assumption is equivalent to setting to zero the initial conditions on the normal coordinates and velocities of all modes, and the latter equivalent to aligning the undeformed SCOLE configuration with the attitude  $(\theta_1, \theta_2, \theta_3)$  that corresponds to zero LOS error. Such roll-pitch-yaw Euler angles, calculated and used by Lin earlier [4]-[5], are listed below for reference:

$$\theta_1 = -14.03624347^\circ; \quad \theta_2 = -6.38707294^\circ; \quad \theta_3 = 0^\circ.$$

#### 3.1 Excitation by the Rapid Time-Minimized Bang-Pause-Bang Slew Maneuver

We first examined, through numerical simulation, the SCOLE flexible-body dynamics under the excitation of the **rapid time-minimized roll-axis bang-pause-bang (BPP)** slew maneuver that was considered a best candidate for pointing the line of sight of the SCOLE as a rigid body [4]-[5]. Among many other single-axis LOS pointing slew maneuvers of the bang-bang type previously studied, this BPP maneuver was judged to be the best compromise in terms **LOS pointing accuracy** achievable, **slew time** required, and **performance robustness** to nonzero products of inertia. It was designed to slew the SCOLE configuration about the negative roll (i.e.,  $-x$ ) axis for about  $20^\circ$  to correct the initial  $20^\circ$  LOS error specified in [1]. This slew maneuver requires that the maximum allowable moment (10,000 lb-ft) be applied to the Shuttle about the negative roll axis and simultaneously the maximum allowable force (800 lb) at the Reflector center along the negative  $y$  axis, both for only 0.867 sec.; then, after a long pause of 3.158 sec., these maximum moment and force be applied again for only 0.867 sec. but in the opposite directions (i.e., positive roll and  $y$  axes, respectively).

Such a BPP slew maneuver was applied to our computer simulation of the SCOLE flexible-body dynamics. The simulation results are summarized by the plots in Fig. 3-1a, which show that such a maneuver would cause excessive

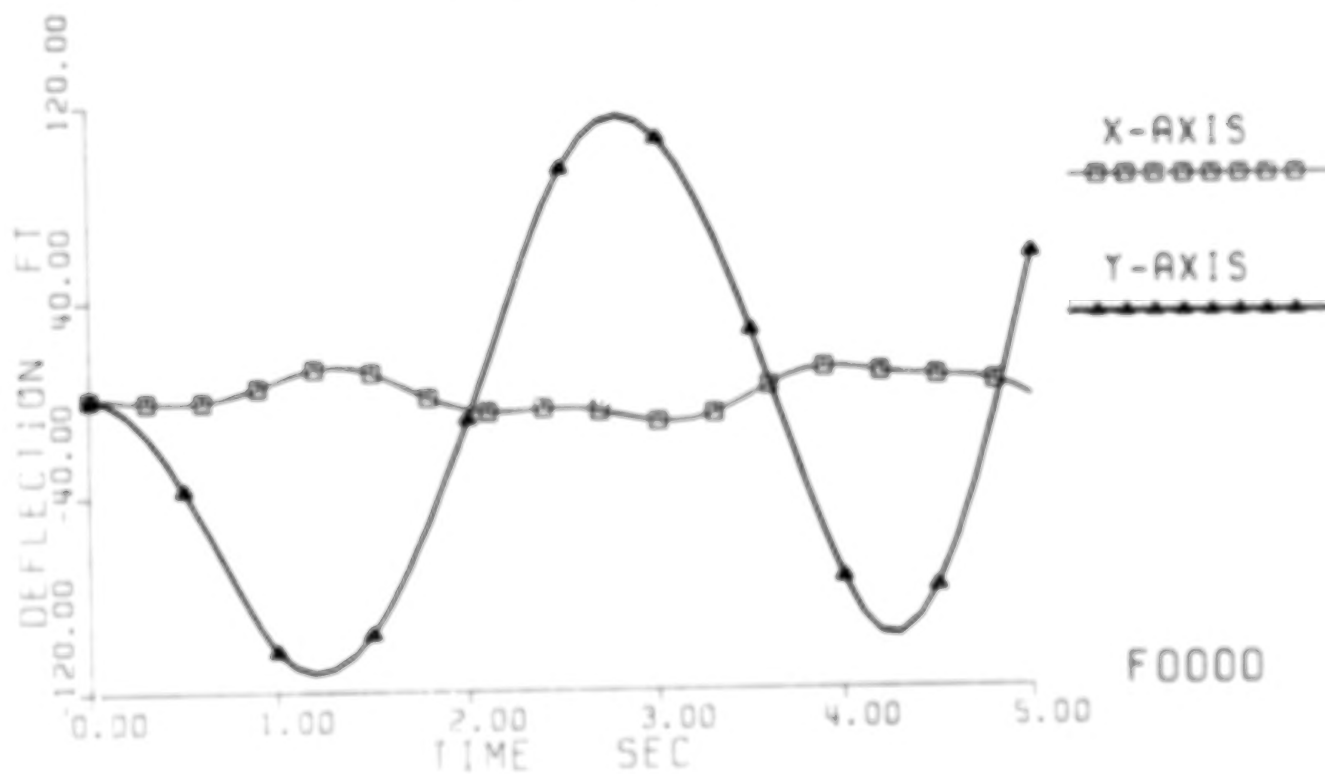
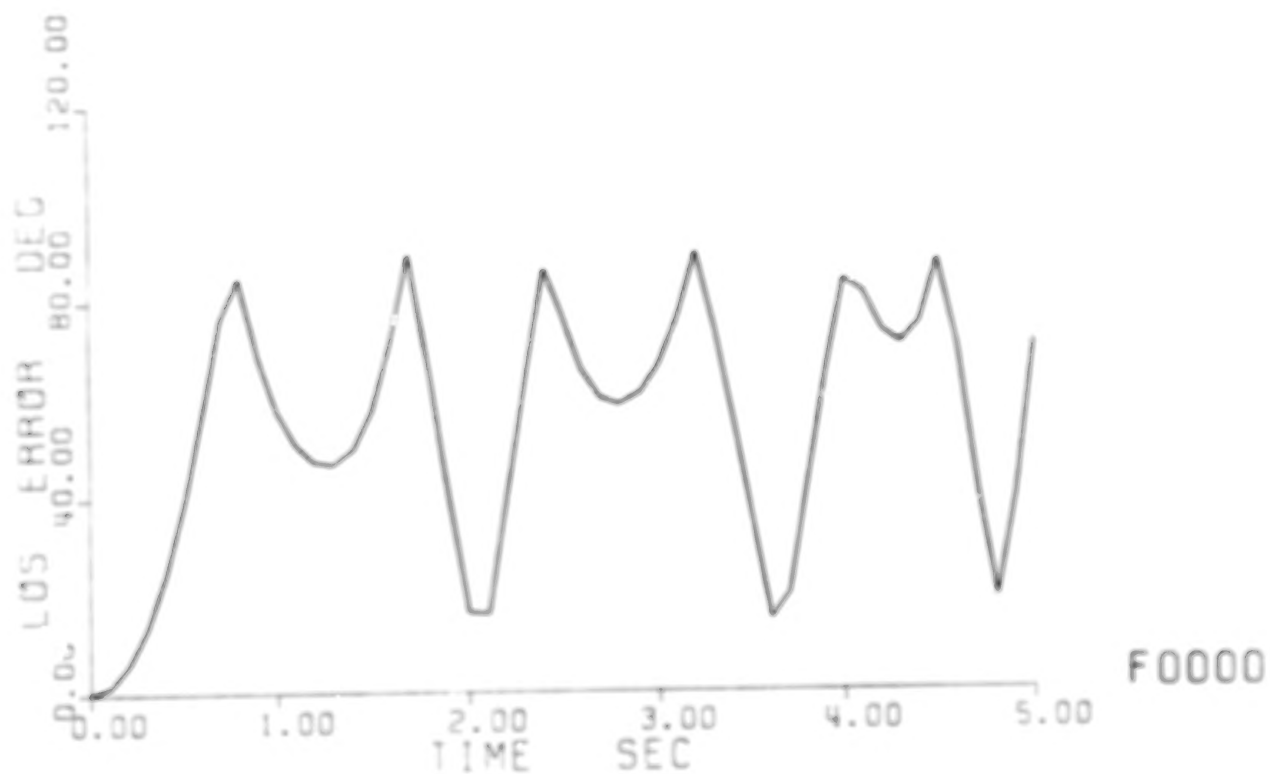


Fig. 3-1 Vibratory responses to Rapid Time-minimized Bang-Pause-Bang Slew;  
a. Line-of-sight error and Mast tip deflection.

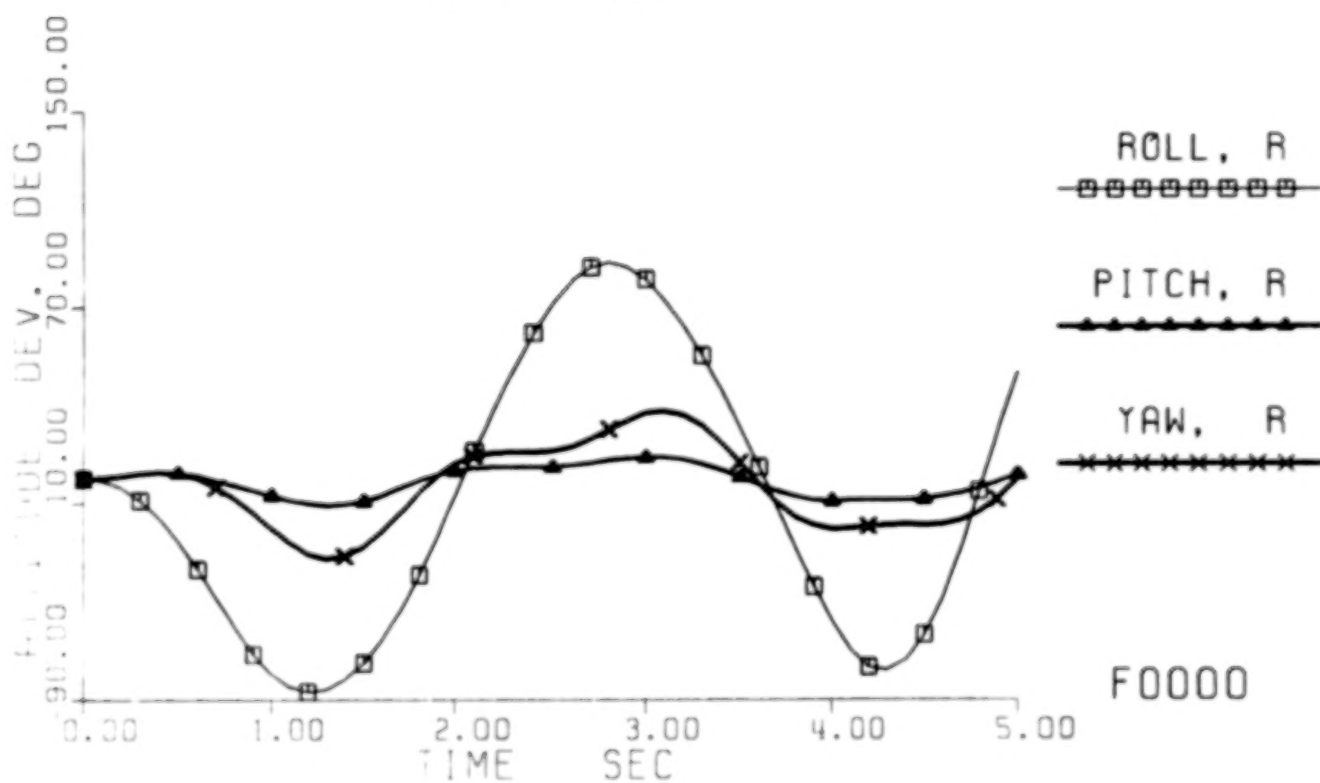
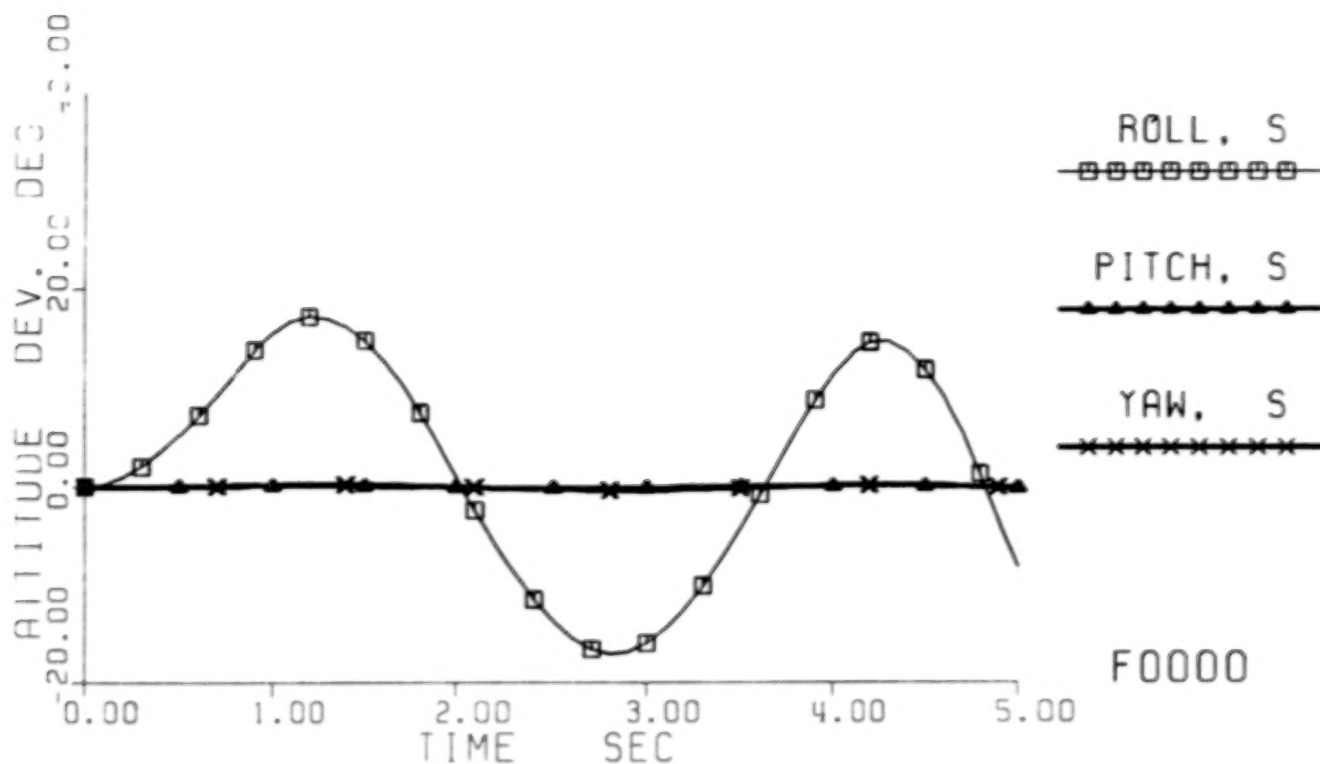


Fig. 3-1 Vibratory responses to Rapid Time-minimized Bang-Pause-Bang Slew;  
b. Attitude deviations at the Shuttle (S) and the Reflector (R) ends.

vibrations in SCOLE! Observe that: the line of sight vibrated with error between  $89.8^\circ$  (or  $133.3^\circ$  if not taking on the principal value of the arcsine in Expression (2-14)) and  $14.7^\circ$ ; the tip of the mast vibrated in the yz-plane between +114 ft and -113 ft.

Fig. 3-1b show the deviations in Euler attitude angles of the Shuttle (S) and the Reflector (R) from their "nominal" alignment of zero LOS error. These deviations correspond to the bending slopes and the torsion at the respective end of the mast. Observe that the Shuttle rolled to the right and the left between  $+17.16^\circ$  and  $-17.06^\circ$ , while the Reflector rolled to the left and right between  $-86.96^\circ$  and  $+88.35^\circ$ . There were virtually no pitch and yaw motions of the Shuttle, but the Reflector pitched between  $-10.63^\circ$  and  $8.75^\circ$  and yawed between  $-32.27^\circ$  and  $+27.97^\circ$ .

In general, some significant excitation of the vibration modes of a flexible space system, such as the orbital SCOLE configuration, should be expected when large moments and forces were used to their limits in a bang-bang manner to minimize the slew time. The appalling magnitude of the vibratory impact, however, was indeed a surprise.

Such excessive vibrations certainly post serious challenges to the Stage-2 design, i.e., the control design for suppressing such vibrations after the excitation. Can such large-magnitude vibrations be brought down to some tolerable level in about the same length of time (say, 5 sec.) as the slew maneuver? How to design such a fast effective vibration controller? We shall continue to address such design challenges in Section 4.

### 3.2 Excitation by Other Rapid Time-Minimized Bang-Bang Slew Maneuvers

Are all slew maneuvers of bang-bang type so terrible to flexible space systems? Why are the excited vibrations in SCOLE so large in magnitude? Even when one can design a powerful fast vibration controller capable of damping out such vibrations, one still cannot stop thinking of these and other puzzling questions. To investigate further, we conducted the following numerical experiments on our computer simulation of SCOLE flexible-body dynamics. All were the same as before, except that a different bang-bang slew maneuver was applied.

**3.2.1 Experiment F10 -- No force on Reflector.** First we tried to use only the 10,000 lb-ft moment on the Shuttle. The same roll-axis bang-bang slew maneuver using only such a moment for accomplishing the same  $20^\circ$  pointing task in the minimum time as was previously designed and evaluated on the rigidized configuration in [4]-[5] was tried. This maneuver requires that the maximum moment be applied first about the negative roll axis for 6.307 sec, and then switched to the opposite directions (i.e., positive roll axis) for another 6.307 sec. It was truly a **bang-bang** (BB) control.

The simulation results, as shown by plots in Fig. 3-2, clearly show that the vibratory impact was greatly reduced. The LOS error was only  $6.25^\circ$  at most, and the mast tip vibrated only between +5.06 ft and -5.18 ft.

Of course, the (minimized) slew time is much longer; it is a main reason why this maneuver has been rejected earlier [4]-[5] as a Stage 1 design for

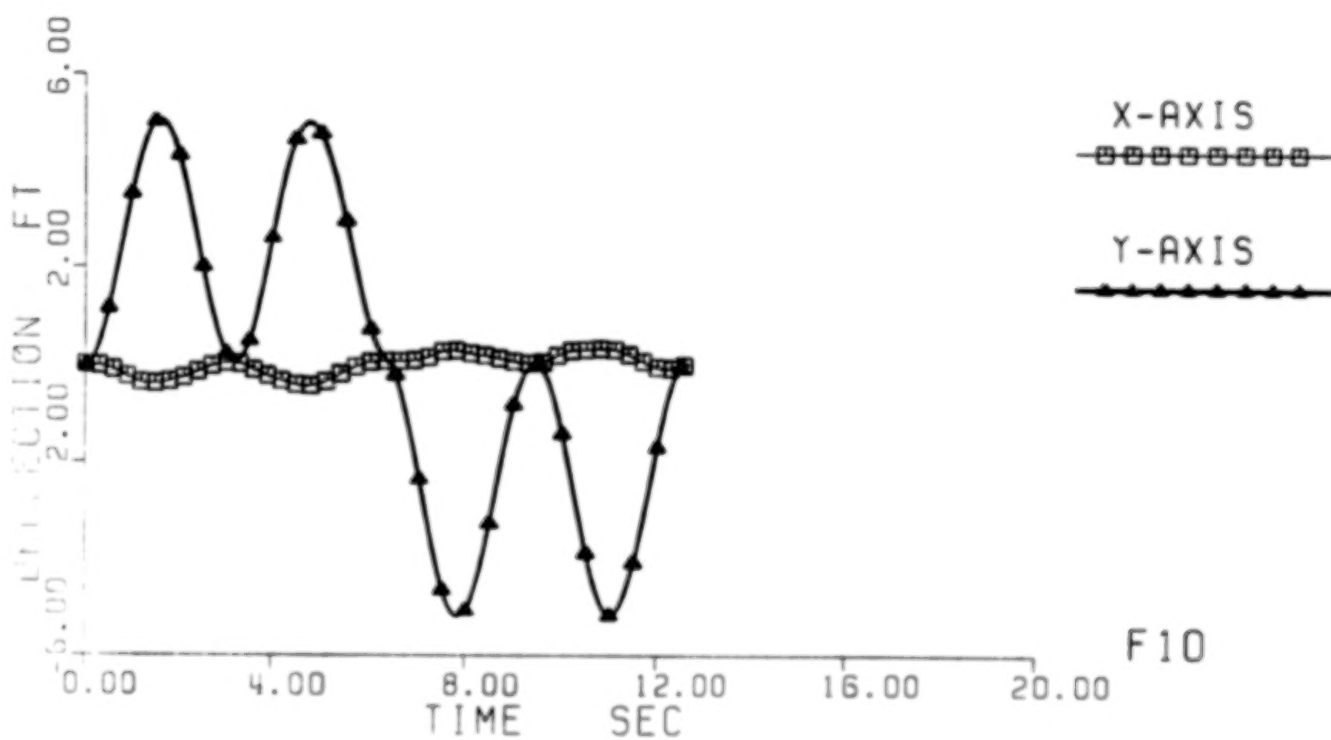
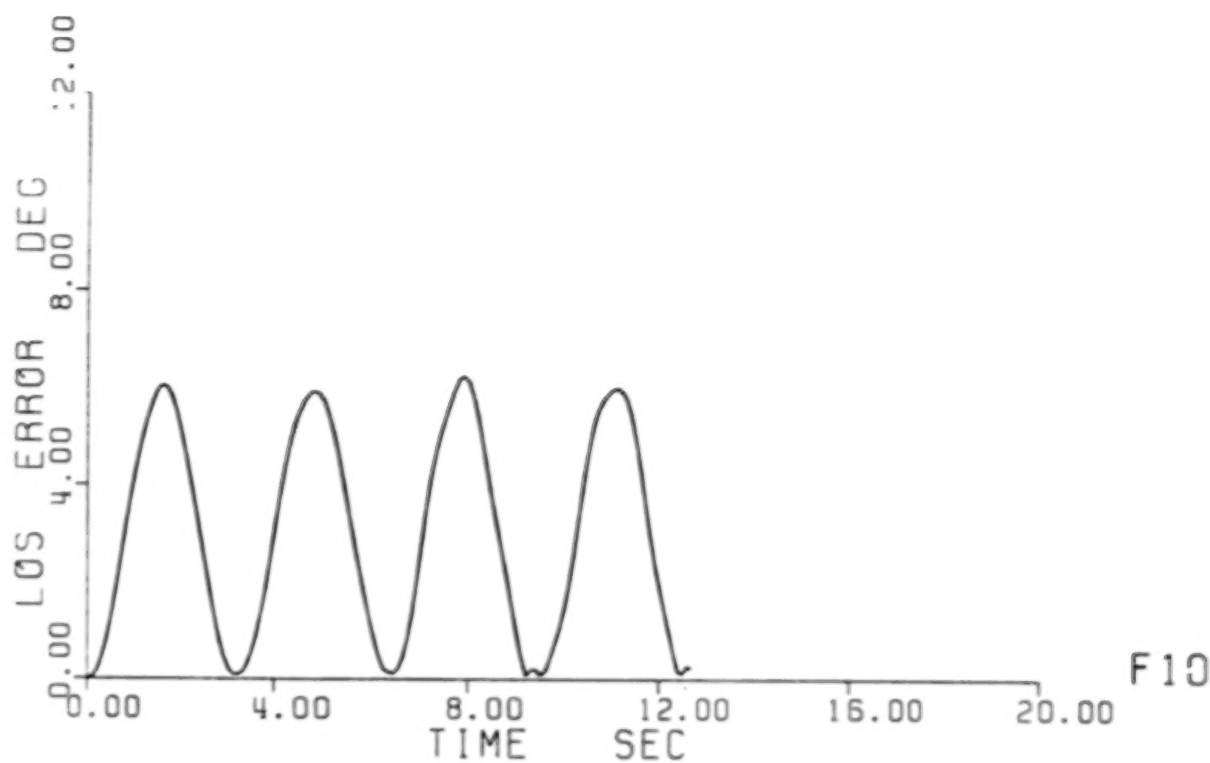


Fig. 3-2 Vibratory responses to Rapid Time-minimized Bang-Bang Slew: 0 lb;  
a. Line-of-sight error and Mast tip deflection.

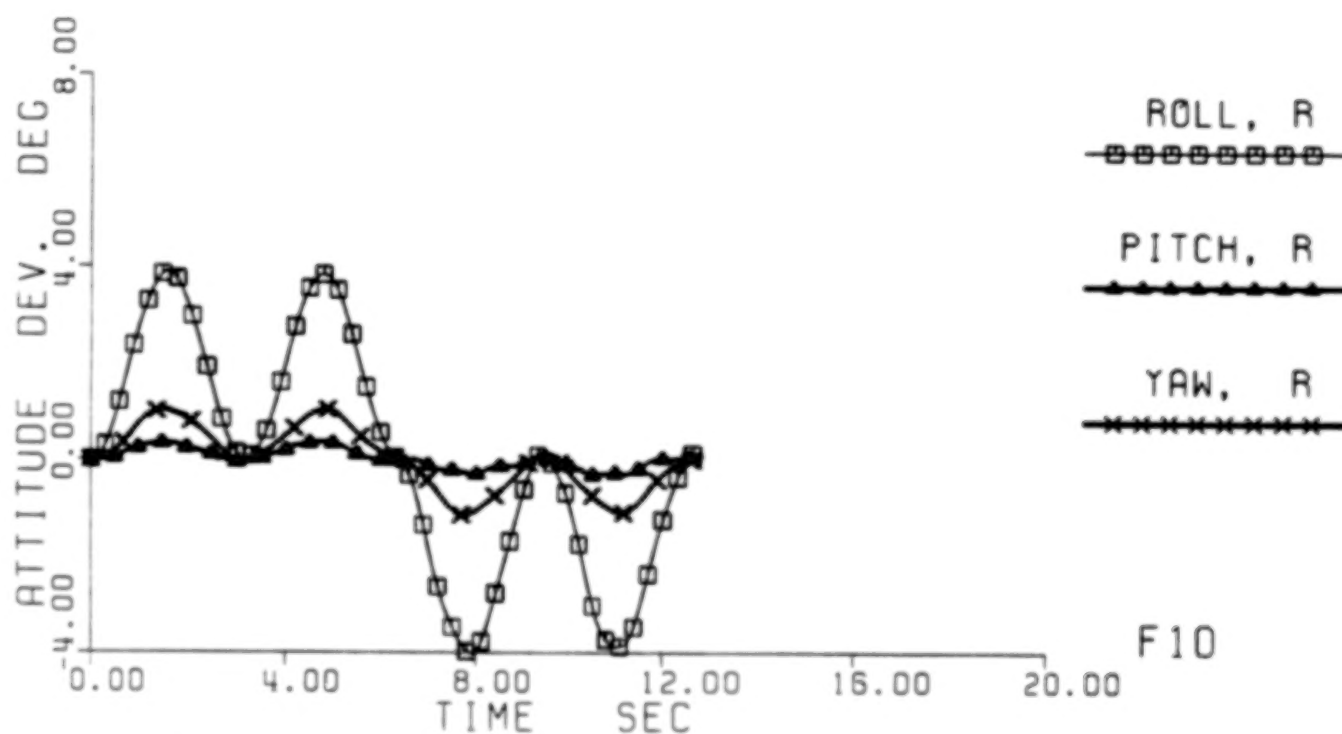
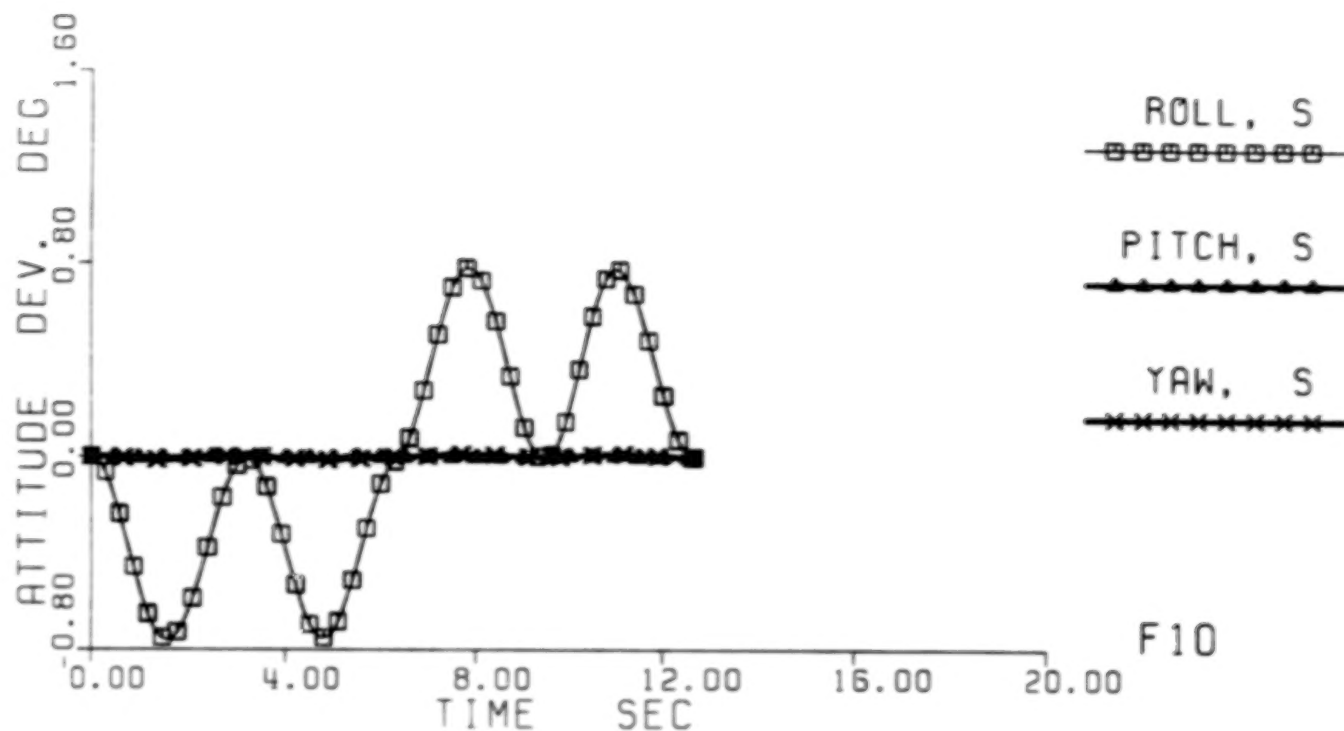


Fig. 3-2 Vibratory responses to Rapid Time-minimized Bang-Bang Slew: 0 lb;  
b. Attitude deviations at the Shuttle (S) and the Reflector (R) ends.



SCOLE. This simulation is useful only when its results are compared with the foregoing case of using additional 800 lb force on the Reflector: it serves as an opposite extreme, since no force was applied to the Reflector at all.

By a careful inspection of the time histories of the tip deflection in both cases (see Figs. 3-1b and 3-2b), we can make the following interesting observations. While the moment was being applied to the Shuttle about the negative roll axis without any force on the Reflector, the beam bent backwards and the Reflector lagged behind\*. On the contrary, the addition of the maximum force on the Reflector reversed the situation, even though the additional force had exactly the same purpose of rolling the configuration to the same side as the moment on the Shuttle! The Reflector then became leading instead of lagging.

**3.2.2 Experiment F180 -- 80 lb Force on Reflector.** The leading of the Reflector might be responsible for the huge increase in LOS error, as implied by the above observations. It is therefore reasonable that reducing the applied force might reduce the lead and hence reduce the LOS error. A second experiment was thus conducted with an 80 lb maximum force, which is only one tenth of the original allowable maximum.

A new roll-axis slew maneuver was designed, in the same way as the first BPB slew maneuver; but only 80 lb, instead of 800 lb, force was to be used in conjunction with the same 10,000 lb-ft moment to accomplish the same 20° LOS pointing in a minimized time. It turned out to be a **bang-bang** maneuver instead, since the slew rate would not reach the imposed 5 deg/sec limit. In almost the same way as in the case of 800 lb, the slew maneuver requires that both the moment and the (tighter-limited) force be applied with respect to the corresponding negative axes for 4.416 sec, and then reversed to the corresponding positive axes for another 4.416 sec, but with no pause in between.

The simulation results, as summarized by plots in Fig. 3-3, confirmed what we thought. The lead by the Reflector is now **greatly reduced**, and so are the LOS error and the mast bending, compared to the case of 800 lb (Fig. 3-1). The LOS error was only 24.7° at the highest peak of its time history; the tip deflected only between +20.59 ft and -10.83 ft; and the Reflector rolled only between +15.98° and -8.31°.

These results have clearly shown that the 800 lb force was directly responsible for the excessive vibrations and the unreasonable LOS error.

Next, compare these results with those of Experiment F10 (Fig. 3-2). A peak LOS error of 24.7° is fairly large compared to only 6.25° of Experiment F10; so is a maximum deflection of 20.59 ft compared to only 5.18 ft of F10. Does this mean that no force should be applied to the Reflector at all? No, we did not think so! Instead, we reasoned that if one could **reduce the lead** slightly further, one could further reduce both the LOS error and the tip deflection. So a third experiment with a slightly smaller force was performed.

---

\* Note that when a negative moment is applied to the Shuttle, a positive deflection indicates the lagging of both the mast tip and the Reflector.

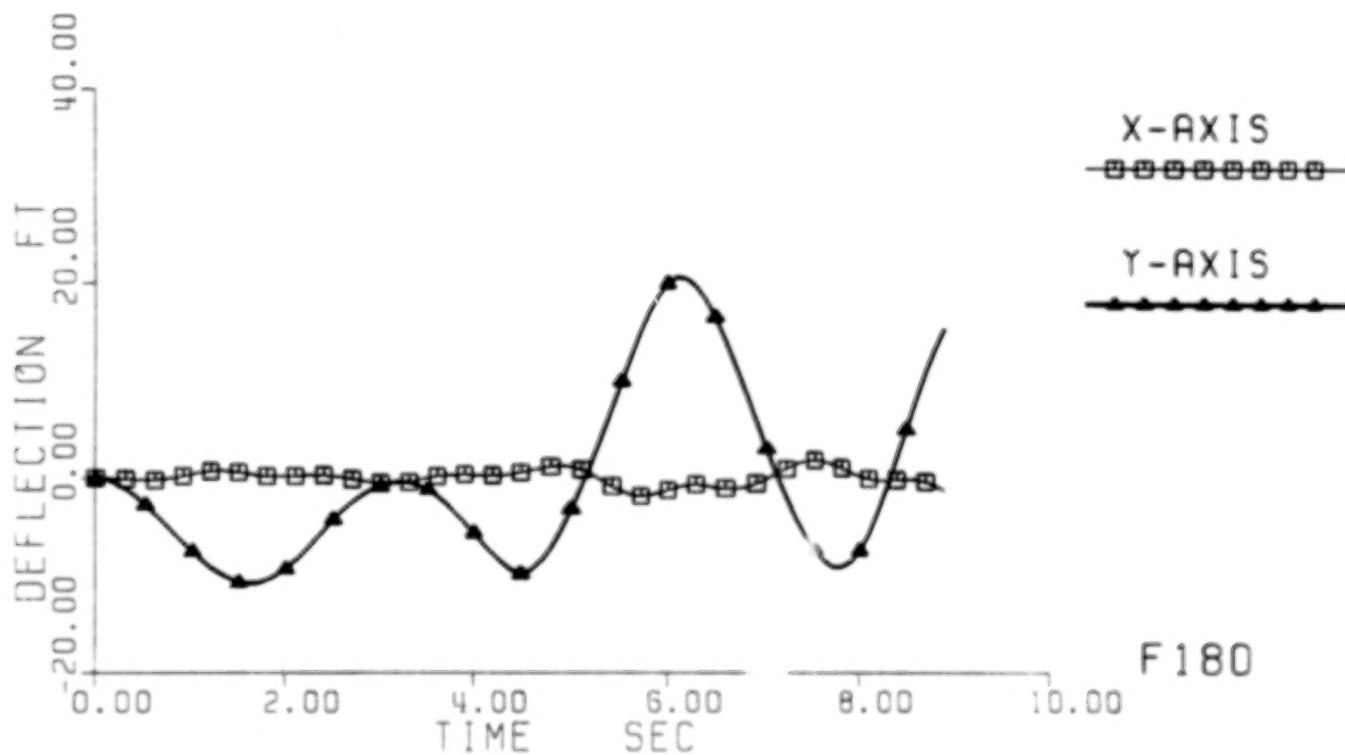
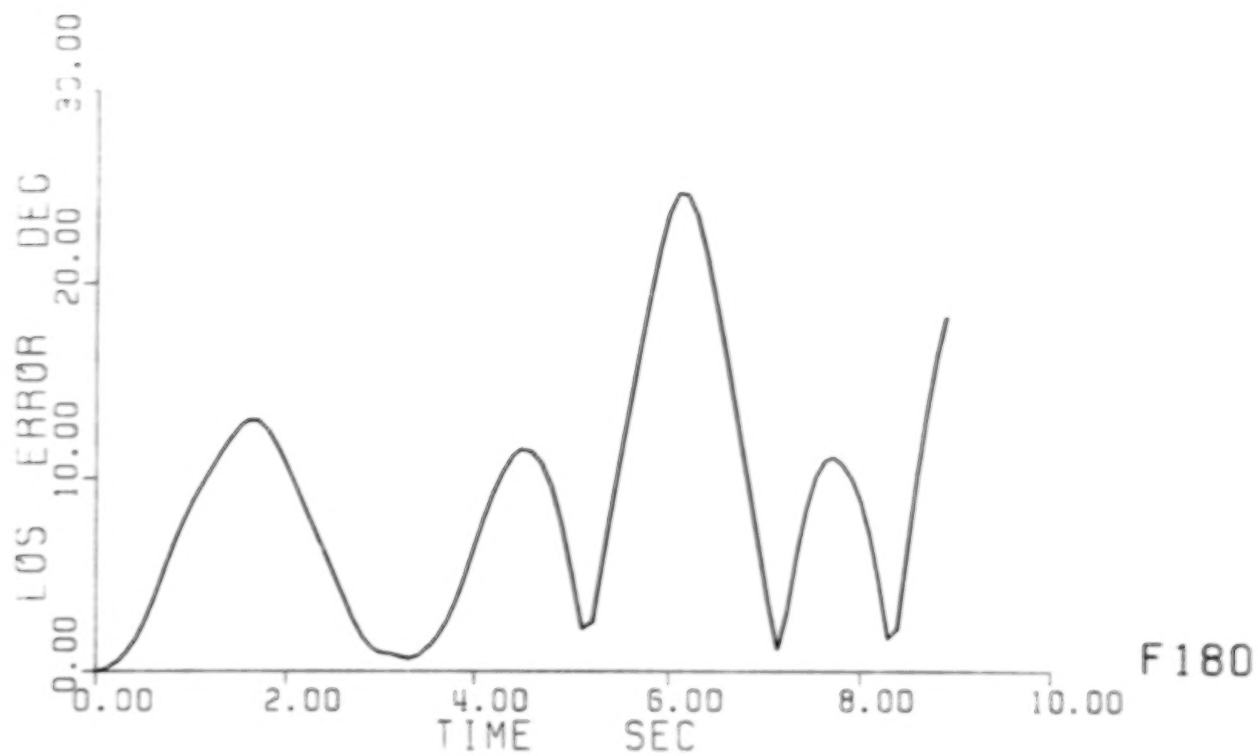


Fig. 3-3 Vibratory responses to Rapid Time-minimized Bang-Bang Slew: 80 lb;  
a. Line-of-sight error and Mast tip deflection.

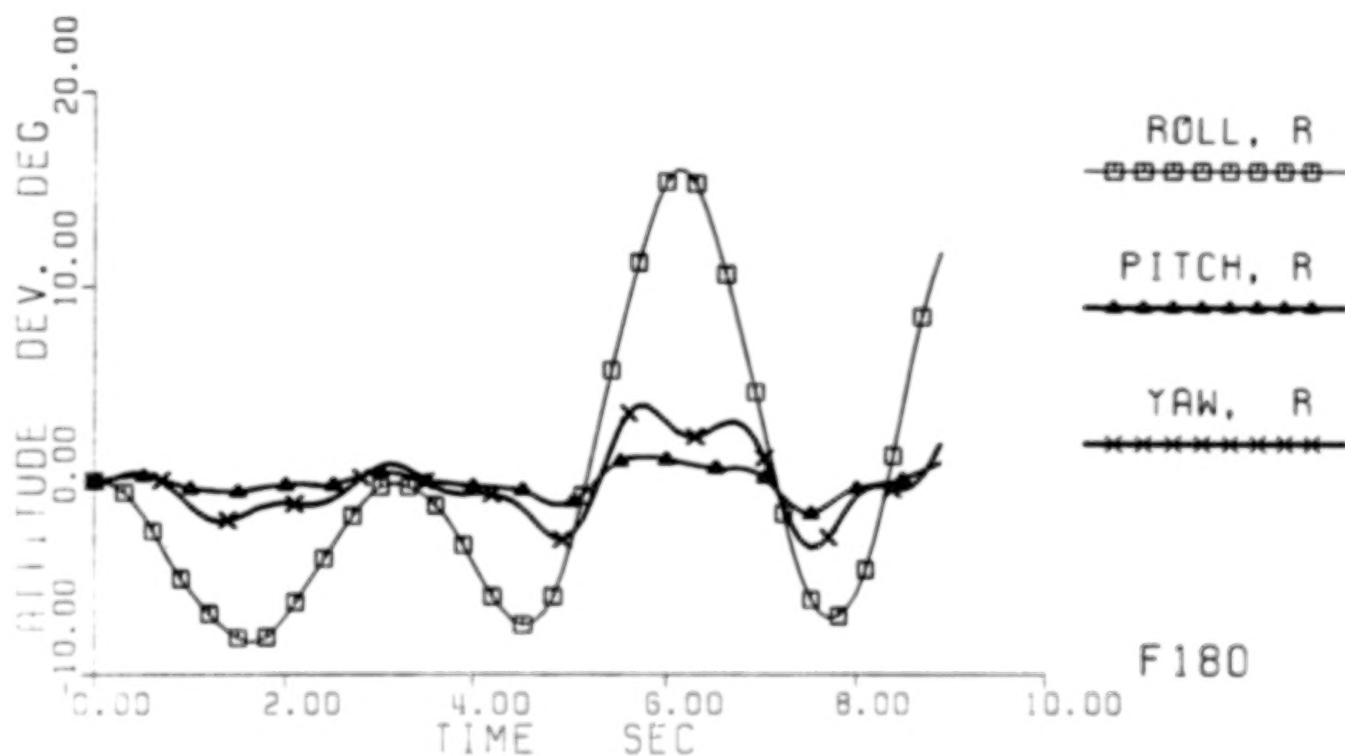
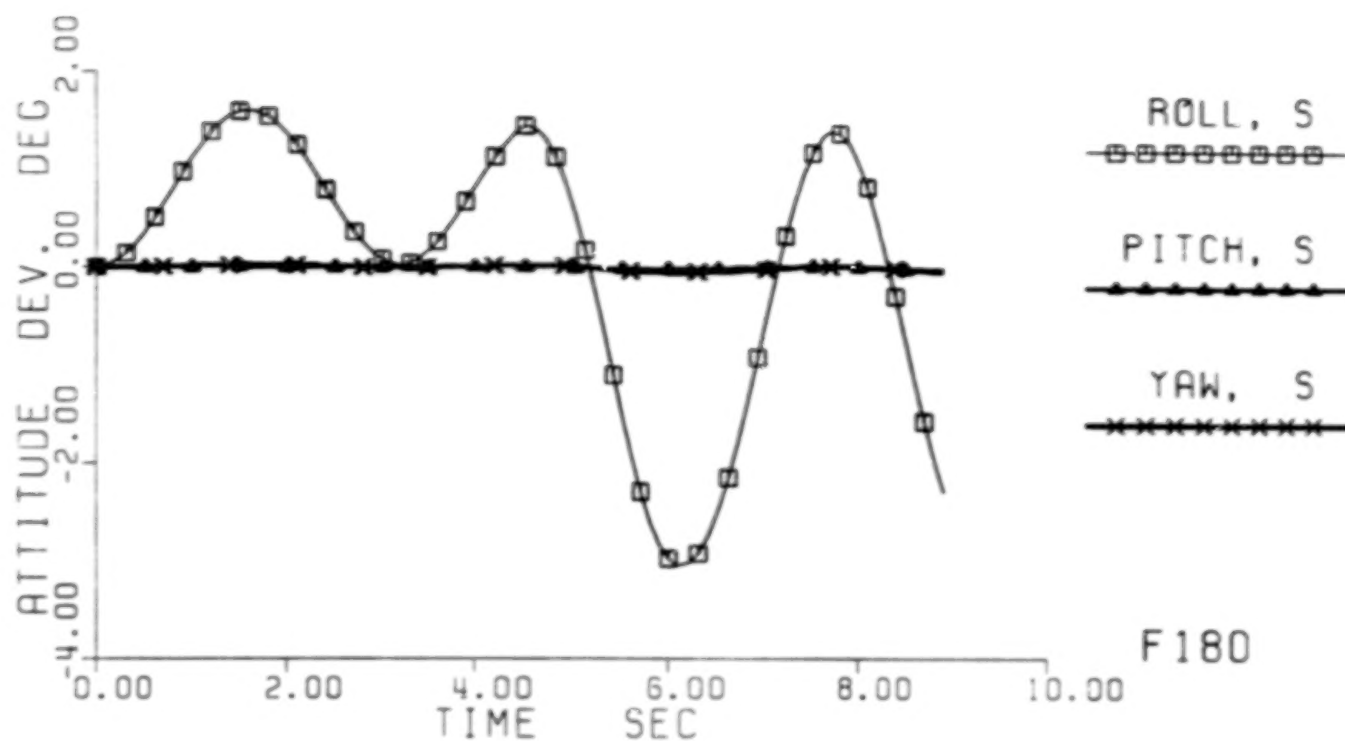


Fig. 3-3 Vibratory responses to Rapid Time-minimized Bang-Bang Slew: 80 lb;  
b. Attitude deviations at the Shuttle (S) and the Reflector (R) ends.

**3.2.3 Experiment F125 -- 25 lb Force on Reflector.** Since the Shuttle-attached SCOLE configuration was chosen because of its similarity to proposed space flight experiments [27]-[29], we thought it would also be more realistic to consider a force of about the same level as the vernier RCS thrusters on-board the Shuttle Orbiter. Since the existing vernier thrusters generate 24 to 24.5 lb thrust each [30], we simply selected 25 lb for the third experiment.

Again a new roll-axis slew maneuver was designed in the same way as before for accomplishing the same  $20^\circ$  LOS pointing in the minimum time. It certainly is a **bang-bang** maneuver, like the case with 80 lb force. This BB slew maneuver requires that both the 10,000 lb-ft moment and the 25 lb force be applied with respect to the negative roll and y axes, and then switched to the positive axes, as before, for 5.479 sec each time.

The results, as shown in Fig. 3-4 by plots, are very pleasing, indeed. The largest LOS error was less than  $0.51^\circ$ ; the tip deflected only between +0.25 and -0.3 ft; and the Reflector rolled only between  $+0.16^\circ$  and  $-0.3^\circ$ . All are **one order of magnitude smaller** than those from applying no force on the Reflector! Of course, the time required for completing the  $20^\circ$  slew of the line-of-sight is also shorter. In summary, for a BB slew maneuver of the flexible SCOLE configuration, **using a force of 25 lb on the Reflector in addition to a 10,000 lb-ft moment on the Shuttle is in all aspects superior** to using no additional force there.

The force of 25 lb is simply a rather arbitrary trial value. One could continue to search for an optimal value that would result in still smaller tip deflection, but we did not do so because we felt that our original purpose had already been served very well.

If LOS error were the only concern and time were not so important, then one should immediately stop studying the use of 800 lb force on the Reflector. On the other hand, since time is at least equally important for SCOLE, it is not clear at all that 25 lb might be preferred outright to 800 lb: the minimum time required for the same  $20^\circ$  slew is 10.959 sec for the case of 25 lb but only 4.892 sec for the case of 800 lb, that is, more than twice longer. Moreover, in both cases, some active vibration controllers are still needed to damp out the excited vibrations; and hence some additional time is required in order that the required LOS accuracy of  $0.02^\circ$  can be met.

To damp out excessive vibrations, such as excited by the BPB roll-axis maneuver using both an 800 lb force and a 10,000 lb-ft moment, can be serious challenges to the Stage-2 control design. Insight and techniques generated from dealing with such challenges certainly will be useful in designing effective vibration controllers for the case of using a smaller force, such as 25 or 80 lb.

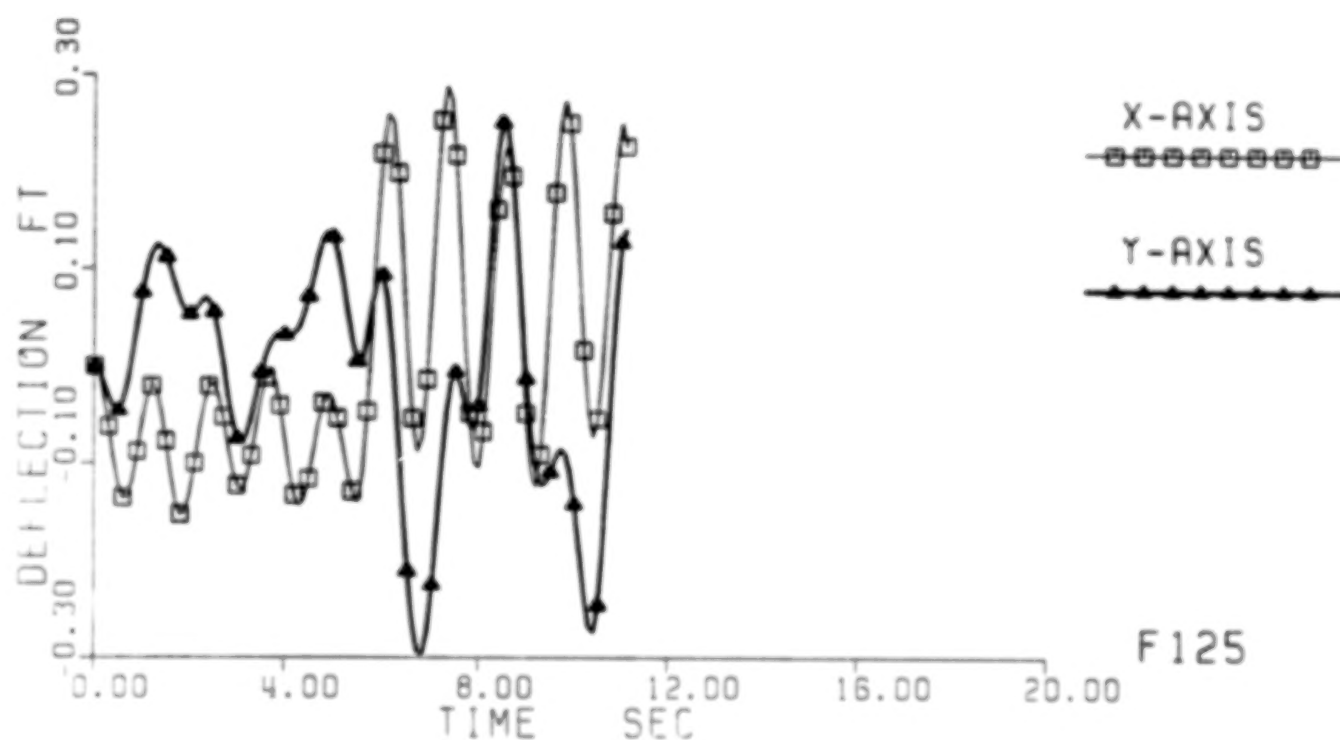
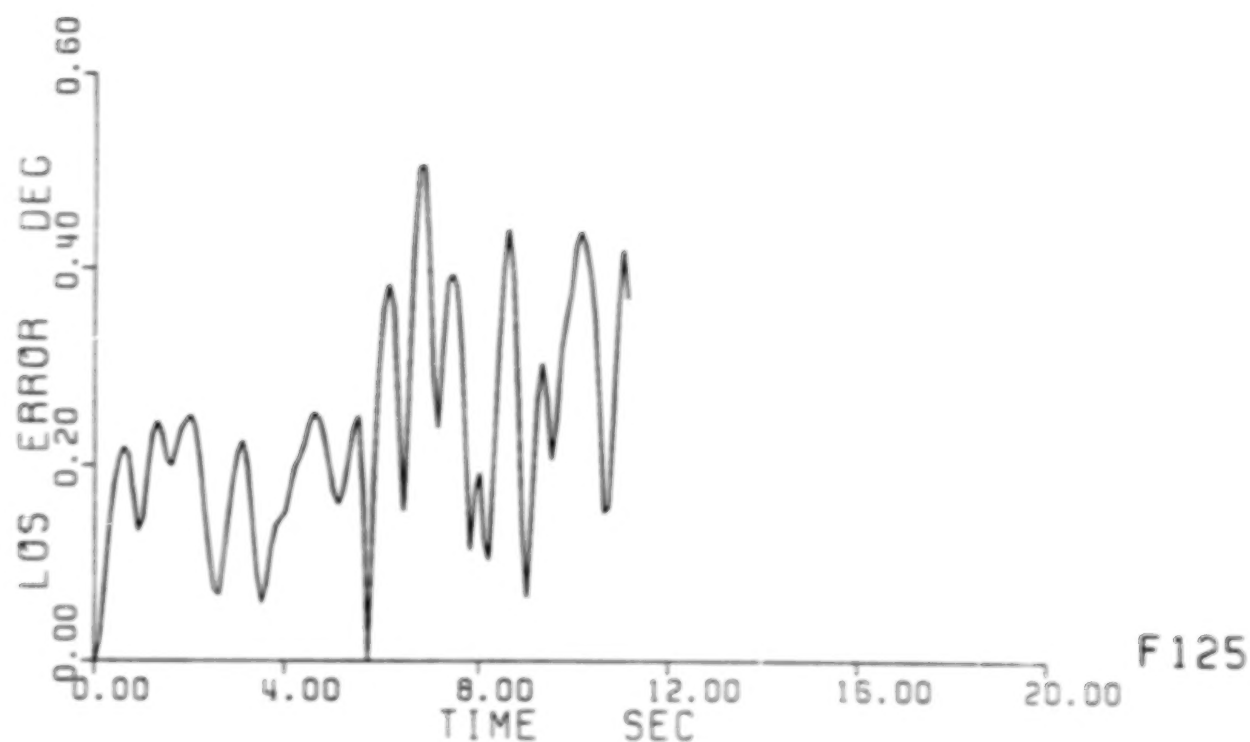


Fig. 3-4 Vibratory responses to Rapid Time-minimized Bang-Bang Slew: 25 lb;  
a. Line-of-sight error and Mast tip deflection.

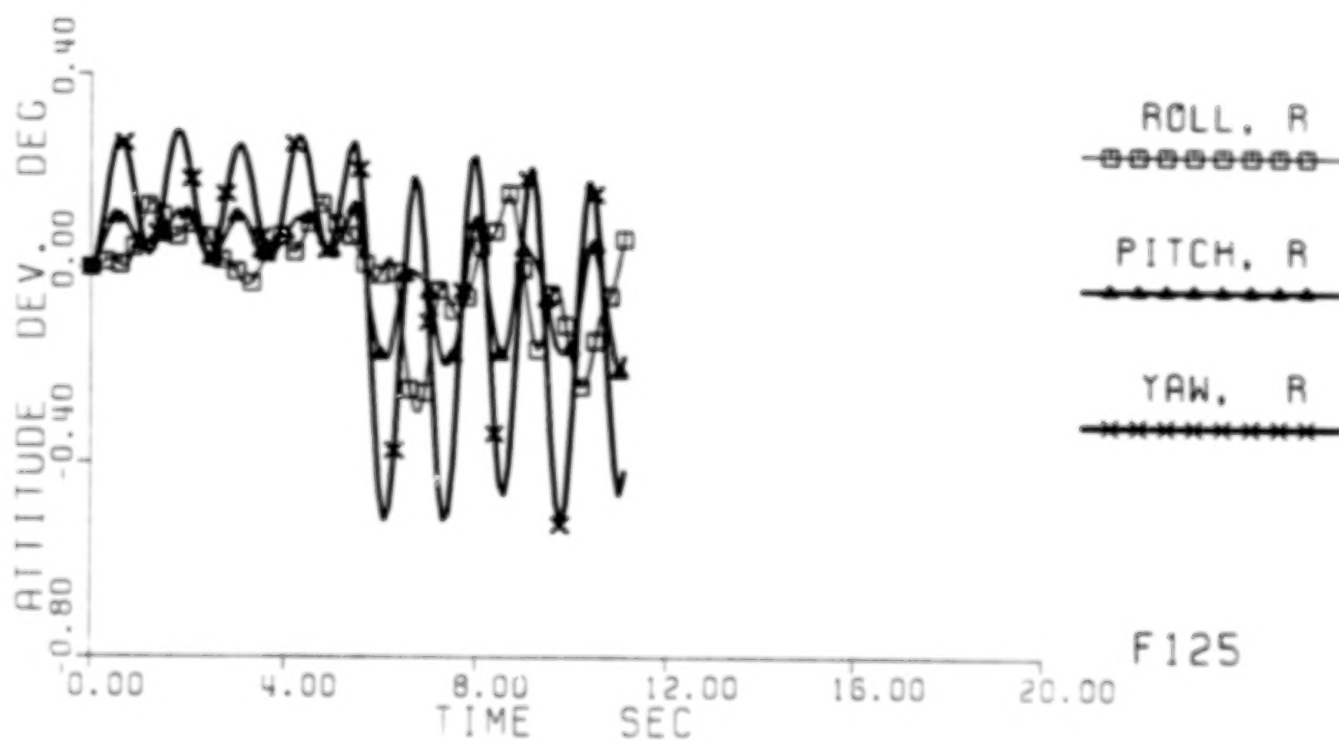
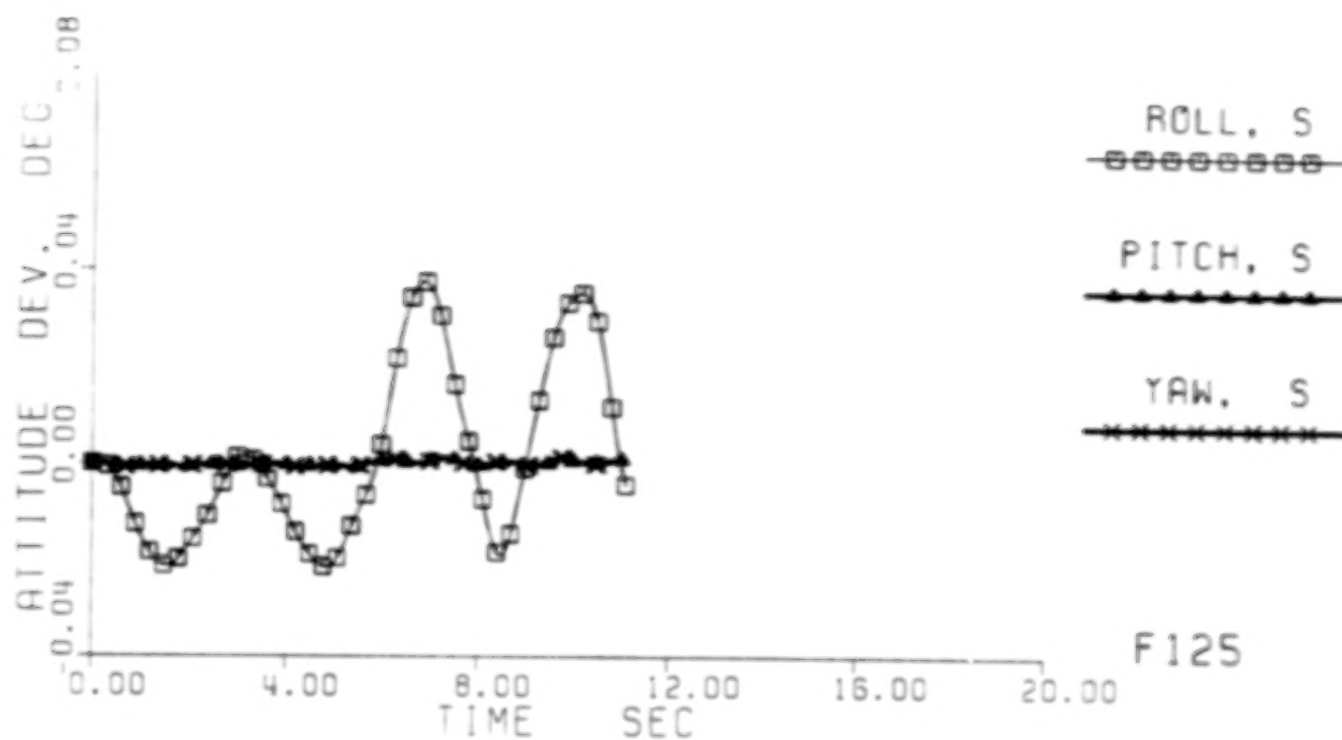


Fig. 3-4 Vibratory responses to Rapid Time-minimized Bang-Bang Slew: 25 lb;  
b. Attitude deviations at the Shuttle (S) and the Reflector (R) ends.

#### 4. ACTIVE VIBRATION CONTROL FOR SCOPE

##### 4.1 Direct Velocity-Output Feedback Control

Let  $y_V$  denote the velocity-sensor outputs. Then from the system Eqs. (2-4)-(2-5), we have

$$y_V = C_V \dot{\eta} \quad (4-1a)$$

The general form of direct velocity-output feedback control is

$$u = -G y_V \quad (4-1b)$$

where  $G$  denotes a matrix of constant feedback gains. Substituting (4-1) in (2-4) results in the following closed-loop system

$$\ddot{\eta} + (\Delta + \Phi^T B_F G C_V \Phi) \dot{\eta} + I \eta = 0 \quad (4-2)$$

The modal stiffness matrix  $I$  of SCOPE flexible-body dynamics is positive definite, since no zero-frequency rigid modes were included in dataset D3D585. By applying the classical Kelvin-Tait-Chetaev theorem, its extensions, or Liapunov's second method, one can show (see, e.g. [17]-[23]) that the closed-loop system (4-2) is:

- (i) stable (in the sense of Liapunov) if the augmented damping matrix  $(\Delta + \Phi^T B_F G C_V \Phi)$  is symmetric and nonnegative definite, and
- (ii) asymptotically stable if the augmented damping matrix is positive definite.

When the velocity sensors are, as generally assumed, co-located with the sensors, i.e.,  $C_V = B_F^T$ , the additional damping matrix  $(\Phi^T B_F G C_V \Phi)$  is always nonnegative definite<sup>\*</sup>, whether the gain matrix  $G$  is positive or merely non-negative definite. In other words, direct velocity-output feedback control at least will never destabilize the system, even when no inherent damping exists (i.e.,  $\Delta = 0$ ).

For most practical cases where there are less actuators than vibration modes and there are virtually no inherent damping (i.e.,  $\Delta$  is small and some of its diagonal elements are virtually zero), the existing theory cannot help determine whether a closed-loop system is asymptotically stable or not, though numerical results can [17].

The theory is not enough to help design the feedback gains, either. Usually designers simply restrict the gain  $G$  to be diagonal matrix, and therefore, make each co-located pair of actuator and sensor act like no more than a (passive) dashpot. Having no systematic method to help calculate the required or desirable values for the feedback gains, some designer even set the diagonal elements rather arbitrarily to some trial positive numbers. A practical ques-

\* Only in a rare special case, which is rather unrealistic to truly flexible large space systems, where there are as many independent actuators (and co-located independent sensors) as there are vibration modes and the influence matrix  $B_F$  is nonsingular, will a positive definite gain matrix  $G$  guarantee that the product  $\Phi^T B_F G C_V \Phi$  is also positive definite.



tion is: how to design the gains so as to add more damping selectively to some specific modes than others? How not to restrict the resulting design to be strictly local feedback? How to design the direct velocity-output feedback as a really multi-variable control system? A systematic design method is needed.

#### 4.2 Concept of Modal Dashpots

The diagonal form of feedback gain matrices spreads the control effort thin over all the vibration modes. One cannot design the diagonal form for adding desirable amounts of damping respectively to certain selected vibration modes. On the other hand, when one wishes to add a certain amount of damping to each mode, one might consider computing the gain matrix  $G$  as the general solution of the following  $N \times N$  matrix equation

$$\Phi^T B_F G C_V \Phi = \Delta^* \quad (4-3)$$

without restricting it to be diagonal, where  $\Delta^*$  denotes the matrix of desired additional modal damping. Expressed in terms of additional damping ratio  $\zeta_i^*$  desired of each mode, the matrix  $\Delta^*$  may take on the same simple form as Eqs. (2-6), (2-3), i.e.,

$$\Delta^* = \text{diag} \left[ \delta_i^* \right] \quad (4-4a)$$

and

$$\delta_i^* = 2\zeta_i^* \omega_i \quad i = 1, \dots, N \quad (4-4b)$$

Note that for a realistic flexible space structure there are much more vibration modes than there are locations for placing actuators or sensors (i.e.,  $N \gg l$  and  $N \gg m$ ). Thus, if one wishes to augment some indeterminate amount of active damping to all the modes, then one may try to obtain an **approximate solution** of Eq.(4-3), such as of the least squared error like the following

$$G^P = (\Phi^T B_F)^P \Delta^* (C_V \Phi)^P \quad (4-5)$$

where  $A^P$  denotes the Moore-Penrose pseudo-inverse. No conditions on the matrix  $\Phi^T B_F$  or  $C_V \Phi$  need to be satisfied, and the pseudo-inverses can be calculated numerically using the **singular value decomposition** [31]-[32].

Solutions of the form (4-5) have three major practical drawbacks. First, the number  $N$  of vibration modes in a realistic flexible structures is enormously large, making it impractical, if not impossible, to calculate the pseudo-inverses of the **extremely large** matrices  $\Phi^T B_F$  and  $C_V \Phi$ . Secondly, one still cannot really focus a specific subset of the modes, since the solution  $G^P$  is merely a least-square approximation, with **errors spread all over the modes**. Thirdly, also because of approximation errors, the resulting product

$$\Phi^T B_F G^P C_V \Phi$$

might not be symmetric, and hence stability might not be guaranteed.

In practice, one needs to concentrate on a relatively small number of important modes. In many cases, one cannot care less for those modes which are less important when one cannot even get what is required for suppressing



the more important ones. Thus, assume that some  $n$  modes ( $n < N$ ) are the most important, and a reduced-order dynamic model is formed by selecting only those  $n$  modes. Call those modes modeled modes and the rest unmodeled modes. Partition the matrices  $\eta$ ,  $\theta$ ,  $\Delta$ , and  $Z$  accordingly into the modeled (M) and the unmodeled (U) parts, i.e.,

$$\eta = \begin{bmatrix} \eta_M \\ \eta_U \end{bmatrix} \quad \theta = [\theta_M, \theta_U] \quad \Delta = \text{black-diag}[\Delta_M, \Delta_U] \quad Z = \text{black-diag}[Z_M, Z_U] \quad (4-6)$$

Then, the closed-loop equation for the reduced-order model is

$$\ddot{\eta}_M + (\Delta_M^T + \theta_M^T B_F G C_V \theta_M) \dot{\eta}_M + Z_M \eta_M = 0 \quad (4-7)$$

Now, let a reduced matrix  $\Delta_M^*$  be given that corresponds to the desired additional damping for the  $n$  modeled modes. Then the design is reduced to solving the following much smaller  $n \times n$  matrix equation, instead of the  $N \times N$  Eq. (4-3), for the gain matrix  $G$ :

$$\theta_M^T B_F G C_V \theta_M = \Delta_M^* \quad (4-8)$$

As before, a solution in the same general form as (4-5) can be obtained numerically by computing the pseudo-inverses of influence matrices  $(\theta_M^T B_F)$  and  $(C_V \theta_M)$ . It is still an approximate solution unless some rank conditions are satisfied by the influence matrices.

Of the particular interest is when the control influence matrix  $(\theta_M^T B_F)$  has the full row rank and the observation influence matrix  $(C_V \theta_M)$  has the full column rank. In other words,

$$\text{rank}(\theta_M^T B_F) = \text{row}(\theta_M^T B_F) = n \quad (4-9a)$$

$$\text{rank}(C_V \theta_M) = \text{column}(C_V \theta_M) = n \quad (4-9b)$$

Such a special case requires that  $n \leq l$  and  $n \leq m$ , i.e., the number of modeled modes do not exceed both the number of actuators and the number of sensors to be used in the feedback control. Under the full-rank conditions (4-9), the pseudo-inverses are also generalized inverses. That is,

$$\begin{aligned} (\theta_M^T B_F)^R &= (\theta_M^T B_F)^R = \text{right generalized inverse of } \theta_M^T B_F \\ &= (\theta_M^T B_F)^T \left[ (\theta_M^T B_F)(\theta_M^T B_F)^T \right]^{-1} \end{aligned} \quad (4-10)$$

$$\begin{aligned} (C_V \theta_M)^L &= (C_V \theta_M)^L = \text{left generalized inverse of } C_V \theta_M \\ &= \left[ (C_V \theta_M)^T (C_V \theta_M) \right]^{-1} (C_V \theta_M)^T \end{aligned} \quad (4-11)$$

The gain matrix  $G^*$  computed therewith solves Eq. (4-8) exactly†. The closed-form expression is given by

$$G^* = (\Phi_M^T U_F)^R \Delta_M^* (C_V \Phi_M)^L \quad (4-12)$$

Consequently, the reduced-order closed-loop system equation (4-7) thereby simplifies to

$$\ddot{\eta}_M + (\Delta_M + \Delta_M^*) \dot{\eta}_M + \Sigma_M \eta_M = 0 \quad (4-13)$$

The desired damping  $\Delta_M^*$  is thus added to the reduced-order model exactly as specified. For stability, the matrix  $\Delta_M^*$  of additional damping only needs to be nonnegative definite; it need not be diagonal.

When  $\Delta_M^*$  is chosen to be a diagonal matrix, as it is often convenient and reasonable to do in practice, the resulting velocity-output feedback control will perform like a **separate "dashpot" attached to each mode** of the reduced-order model. Specifically, let

$$\Delta_M^* = \text{diag} \left[ \delta_{Mi}^* \right] \quad (4-14)$$

Then (4-13) can be rewritten in the component form like (2-1) as follows:

$$\ddot{\eta}_{Mi} + (\delta_{Mi} + \delta_{Mi}^*) \dot{\eta}_{Mi} + \omega_{Mi}^2 \eta_{Mi} = 0 \quad (4-15)$$

where  $\eta_{Mi}$  denotes the normal coordinate of the  $i$ th modeled mode. Eq. (4-15) obviously means that the  $i$ th modeled mode, like an **independent linear oscillator**, is augmented with an additional dashpot whose damping coefficient is  $\delta_{Mi}^*$ . This is why Canavin called such a design a "decoupled controller", or "modal dashpots" [11].

The diagonal elements  $\delta_{Mi}^*$  should be nonnegative to make a practical sense. Like (4-4), it can be given in terms of damping ratios  $\zeta_{Mi}$  and natural frequencies  $\omega_{Mi}$  as

$$\delta_{Mi}^* = 2 \zeta_{Mi} \omega_{Mi} \quad (4-16)$$

---

† Given whatever values to the matrices, it is mathematically an exact solution so far as the equation (4-8) is concerned. Of course, it may not be an exact solution so far as the system (4-2) or even (4-7) is concerned, when any matrix, for example the modal matrix  $\Phi$  as usual, contains some modeling or computational errors. Small errors in  $\Phi$  may invalidate stability results of general feedback gains but not the modal-dashpot type [20]-[23].

### 4.3 Improvement on the Design Method

One can design very effective vibration controllers by the method of modal dashpots, as demonstrated by our applications to SCOLE. The interesting simple formula (4-10)-(4-12), however, **does not by itself complete the design method for an effective control of structural vibrations.** In fact, when the concept of modal dashpots was initially formulated by Canavin [10]-[12] as "decoupled controller", it was accompanied by two major technical drawbacks that almost rendered itself practically useless. Later, through various numerical evaluations and theoretical analyses, Lin and his associates [20]-[24] identified the underlying causes of these problems, and greatly enhanced the utility of this concept. In the course of applying it to the challenging SCOLE vibration control design problem, we also made some additional improvement on this design method.

A first initial technical drawback was the high-gain low-damping problem. After he applied it to a representative large space structure (of which 37 vibration modes were considered), Canavin concluded that "the decoupled controller may be of limited utility due to the high gains produced by this approach" [11]. The feedback gains were mostly in the orders of  $10^{10}$  to  $10^{12}$ , while only additional 10% of critical damping was designed for each of the 12 modes he had selected to be "controlled" (i.e., modeled) modes.

Aubrun [13] proposed the approach of low-authority control (LAC) by limiting to 10% modal damping and by using sufficiently small gains so that the amount of active damping achievable is predictable. Since then, direct velocity-output feed back control has been commonly thought to be of only low authority, low performance, and secondary importance. However, the vibration controllers of Aubrun's design should be of low authority, not because of direct velocity-output feedback, but rather because of the applicability of Jacobi's root perturbation formula on which he based his theory. **For his use of the perturbation formula to remain valid, the control authority (and specifically the feedback gains) must be sufficiently low so that the closed-loop eigenvalues and eigenvectors would be resulted from only infinitesimal perturbations, i.e., only very small increase in damping ratios.**

A second initial technical drawback of the basic design method was severe interactions between modeled and unmodeled modes. When the method was applied to another representative large space structure (i.e., ACOSS model 2 [33]), the interactions were so severe that the desired damping performance on the modeled modes was degraded very badly, although the closed-loop system remained stable [24].

The following common causes were discovered.

- (1) Some modeled modes had too small control influences ( $\Phi_M^T B_F$ ) or too small observation influences ( $C_V \Phi_M$ ). This made the generalized inverses  $(\Phi_M^T B_F)^R$  or  $(C_V \Phi_M)^L$ , and hence the resulting gain matrix, unnecessarily large. These low-influence modes should be deleted from the reduced-order model, or else some actuators or sensors should be relocated to improve their influences on these modes.
- (2) Some of the rows in matrix  $\Phi_M^T B_F$  had too small degree of independence from the others, or some columns of  $C_V \Phi_M$  had the similar situation. This also

made the generalized inverses, and the gain matrix, unnecessarily large in magnitude. Like (1) above, these modes should be excluded, or the location of some actuators or sensors be improved.

- (3) Some low-frequency unmodeled modes had too large control influences ( $\Phi_{Uj}^T B_F$ ) or observation influences ( $C_V \Phi_{Uj}$ ) compared to those of the modeled modes. This made excessive spillover. These modes should be added to the reduced-order model; otherwise, some actuators or sensors should be relocated, or their influences be properly synthesized [35]-[36].
- (3) Some of the desired additional damping coefficients ( $\delta_{M1}^*$ ) were too large for some modeled modes, even all were set equal to the same small design value (say,  $\zeta_{M1}^* \approx 0.1$ ). This made some part of the gain matrix unnecessarily large, and hence increased interactions with some unmodeled modes.

Open-loop responses of individual modeled modes should be analyzed and the need for additional damping realistically guesstimated with respect to the control/observation influences on each modeled mode. For properly designed modal dashpots, e.g., our design for SCOLE, the additional damping could be as high as 67% for some modes or as low as 3% for some others, depending on the ability of the actuators as well as on the individual open-loop responses.

We have begun to develop the concept of modal dashpots into a useful systematic design method for direct output feedback vibration control. Although the closed-form formula has reduced the design of modal dashpots to simple cranking of numbers, yet to make it really work for effective control of large excited structural vibrations in flexible space systems, such as the SCOLE configuration, many careful pre-design steps have to be taken.

The design method was initially formulated by Canavin without explicit consideration of limitations on the requirement for control forces and torques. Now, the explicit limits must be considered when applying the method to SCOLE. Also, some saturation "circuitry" must be imposed on the feedback control so that the magnitude of the forces or moments generated by the modal dashpots would automatically be limited to 800 lb and 10,000 lb-ft, respectively. Saturation may not destroy stability when actuators are co-located with sensors [37], but would somehow limit the performance of the feedback controller.

## 5. DESIGN OF MODAL DASHPOTS FOR SCOLE

The vibrations in the SCOLE configuration excited by the rapid time-minimized BPB LOS pointing slew maneuver, as reported in Section 3.1, posted three serious vibration control design challenges:

- (1) The excited vibrations were excessively and unrealistically large in magnitude: the line of sight once had an error of  $89.9^\circ$  (or beyond) and the 130-ft mast once had a tip deflection of 114 ft.
- (2) The allowable time was extremely short: it should be minimized, so only an equally short time (specifically, only 5 sec, which was approximately equal to the maneuver time) was allowed.
- (3) The available control forces and moments were limited: the 800 lb and 10,000 lb-ft limits were imposed the same way as on slew maneuvers.

In order to design effective modal dashpots for suppressing such excessively large vibrations in SCOLE in a very short time, we conducted careful pre-design analyses on the vibration modes and their influences by the actuators and sensors. The candidates for modeled modes were selected, and then divided into two groups according to the actuator influences. The design of the modal dashpots was therefore divided into two parts accordingly.

### 5.1 Analysis on Vibration Modes

Initially, two different numerical analyses of SCOLE vibration modes were made, each with a different standard measure of importance. The results were inconsistent. Then a third measure was developed and used; the results were finally fair and satisfactory.

#### 5.1.1 Measure 1: LOS Error due to Initial Modal Displacement

"LOS error contribution" is a common measure used by many structural dynamicists for determining if a vibration mode is "critical" or not, i.e., if it needs active control or not. It was used by Draper Laboratory [33]-[34], and accepted by other ACOSS\* and VCOS\*\* contractors [38]-[45] as the standard approach, in the modal analysis of both Model No. 1 (namely, the Tetrahedron) [34] and Model No. 2 [33] of representative large flexible precision space structures. The standard approach is to express the LOS error as a linear function of physical coordinates under the assumption that all the displacements are sufficiently small. When the physical coordinates are transformed into the normal coordinates of the structure, the LOS error become a linear function of the normal coordinates. The "critical modes" are then determined by comparing the modal coefficients of the LOS error.

Such a measure is not directly applicable to rapid pointing of the SCOLE configuration nor, in general, to large space structures that are subject to rapid slew or retargeting maneuvers. First, the displacements (deflections and torsions, for example) generally are large, hence the linearization of the LOS error is not valid. Thus, for SCOLE, we used the original nonlinear expression

---

\* Active Control of Space Structures, a DARPA technology program.

\*\* Vibration Control of Space Structures, sponsored by Air Force Wright Aeronautical Laboratories.



without linearization. Secondly, the LOS error is a dynamic vibratory response, instead of being simply a static displacement of the line-of-sight. Thus, instead of comparing only the LOS error coefficients, we compared the time histories of the LOS error the individual modes would separately cause if they were initially excited alone.

For this analysis, the SCOLE configuration was assumed to be initially at rest with no LOS error\*, and only one mode was excited each time because of a unit initial displacement in its normal coordinate. Specifically, for the  $i$ th time history, the initial condition was assumed to be:

$$\eta_i = 1, \text{ and } \eta_j = 0 \text{ for all } j \neq i; \quad \dot{\eta}_j = 0 \text{ for all } j.$$

For each such initial modal displacement, the time history of the resulting LOS error was calculated separately using our computer simulation program.

The results of 10 separate cases (one for each mode) are shown together by the overlapped plots in Fig. 5-1, where each curve represents a **completely separate** time history of LOS error. Listed below are the highest peak value of each time-history curve.

Mode:	1	2	3	4	5	6	7	8	9	10
Peak:	.37	.53	.54	.93	1.3	.14	.51	.002	.18	.03

The relative importance of the 10 modes is thus given in the descending order as follows.

Mode: 5, 4, 3, 2, 7, 1, 9, 6, 10, 8.

#### 5.1.2 Measure 2: Modal Response to the Rapid Pointing Maneuver

By intuition, a vibration mode is more in need of active control than others when its magnitude of excited vibration is larger. Thus, a second measure of importance for the SCOLE configuration naturally is the vibratory response of each mode to the rapid pointing maneuver. For this analysis, the configuration was assumed, as before (in Section 3.1), to be initially at rest without any LOS error or any nonzero initial conditions, and the same BPB slew maneuver was the source of excitation. The time history of the resulting modal response  $\eta_i(t)$  was calculated for each mode separately.

The results are shown by the plots in Fig. 5-2, with each curve representing an individual mode. Listed below are the highest peak value of the curves.

Mode:	1	2	3	4	5	6	7	8	9	10
Peak:	21.6	603	41.2	13.7	0.49	0.48	0.28	.058	.041	.001

Accordingly, the relative importance of the 10 modes is thus given by the following descending order:

Mode: 2, 3, 1, 4, 5, 6, 7, ...

---

\* As stated in the beginning of Section 3, we assumed that, before any of its vibration mode was subject to excitation, SCOLE was initially at rest and had no deformation nor LOS error. Specifically, the undeformed configuration was assumed to have been aligned with the attitude angles of zero LOS error. Therefore, if all the normal coordinates and velocities were zero, the LOS error would remain zero.

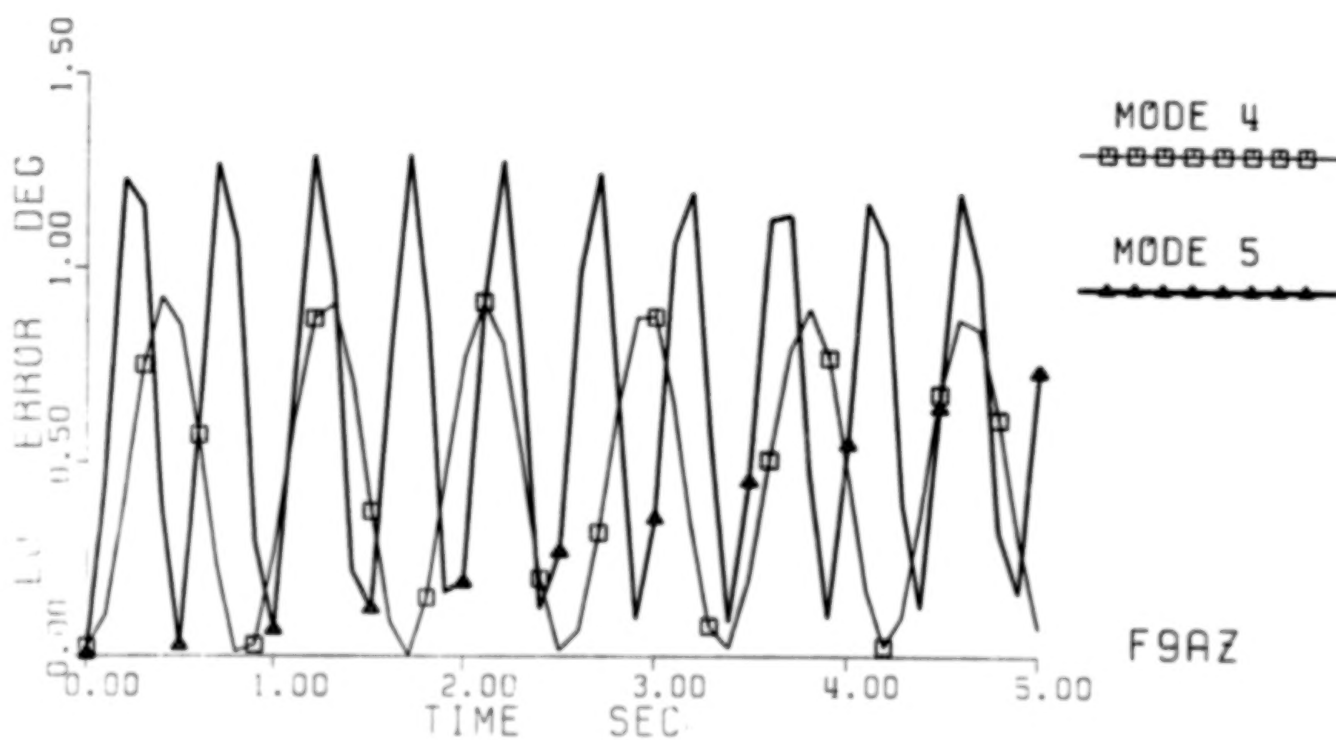
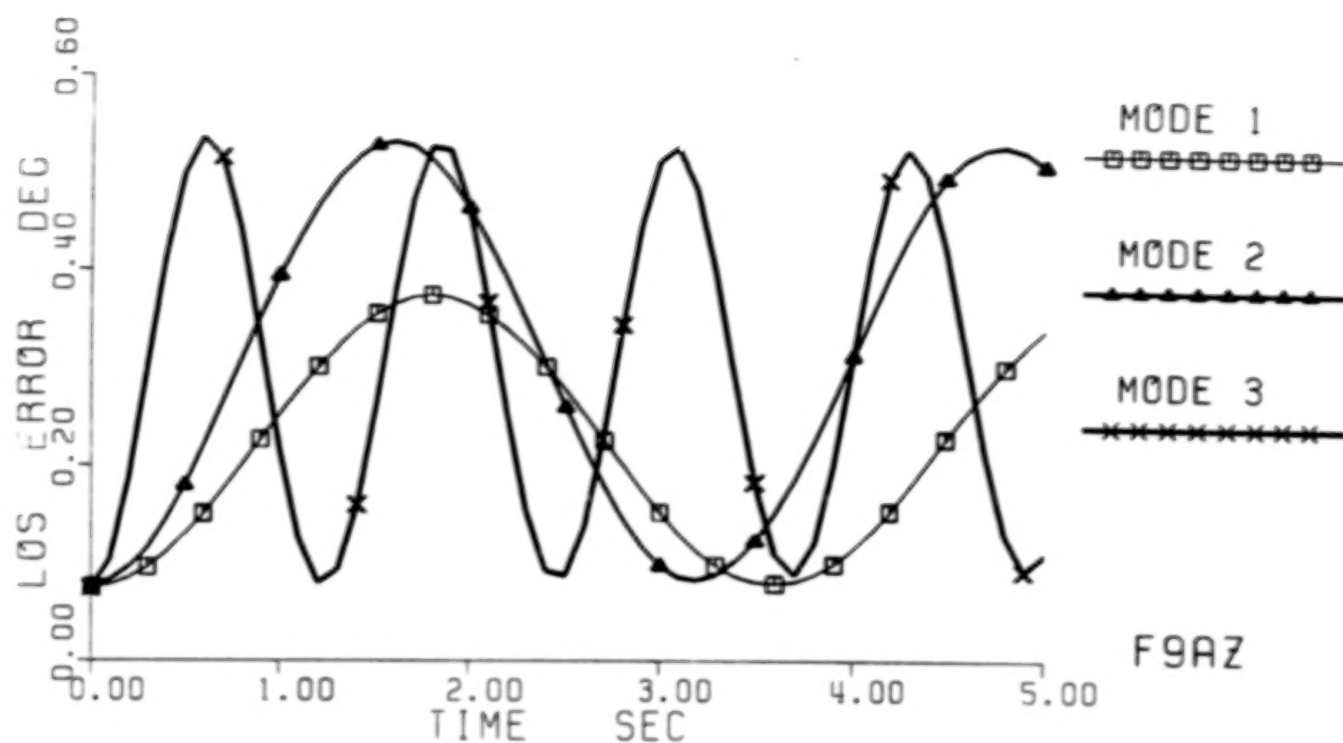


Fig. 5-1a Line-of-sight error due to unit initial modal displacement in Modes 1, 2, 3, 4, and 5, respectively. The separate time histories are plotted together for easy comparison and use with Measure 1.

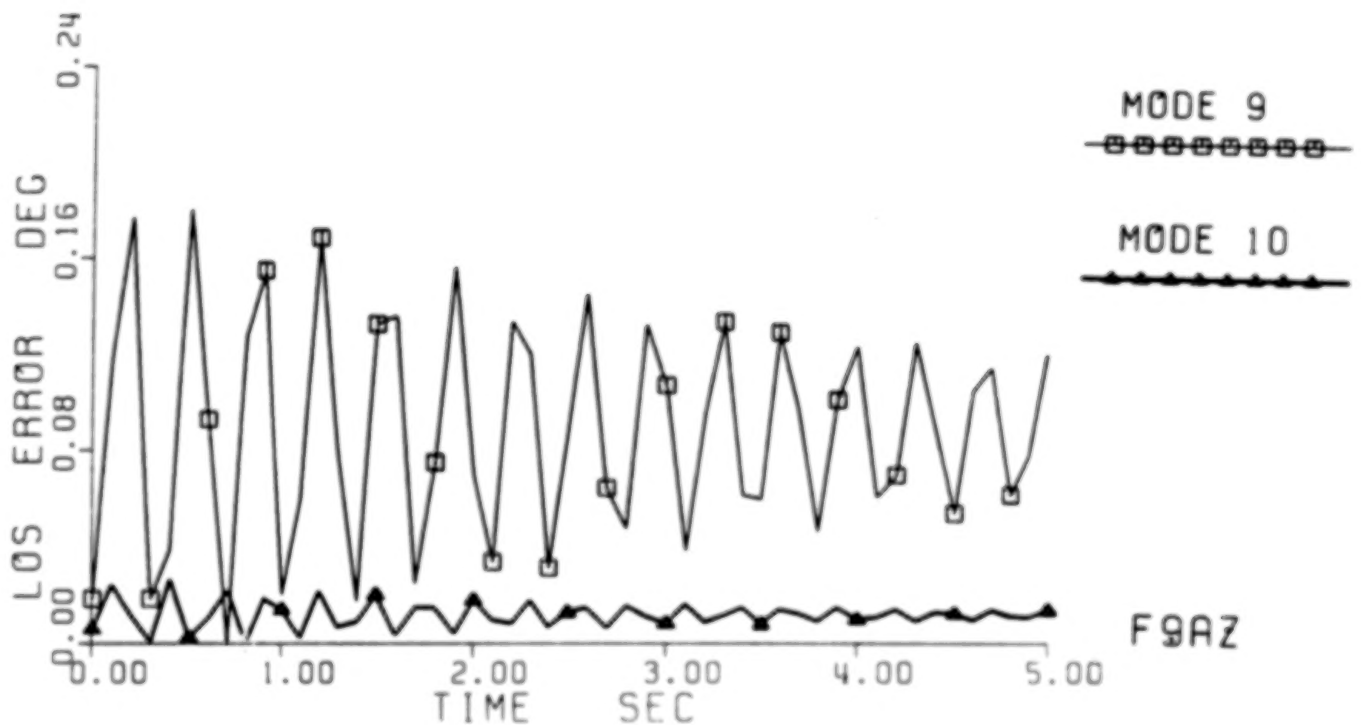
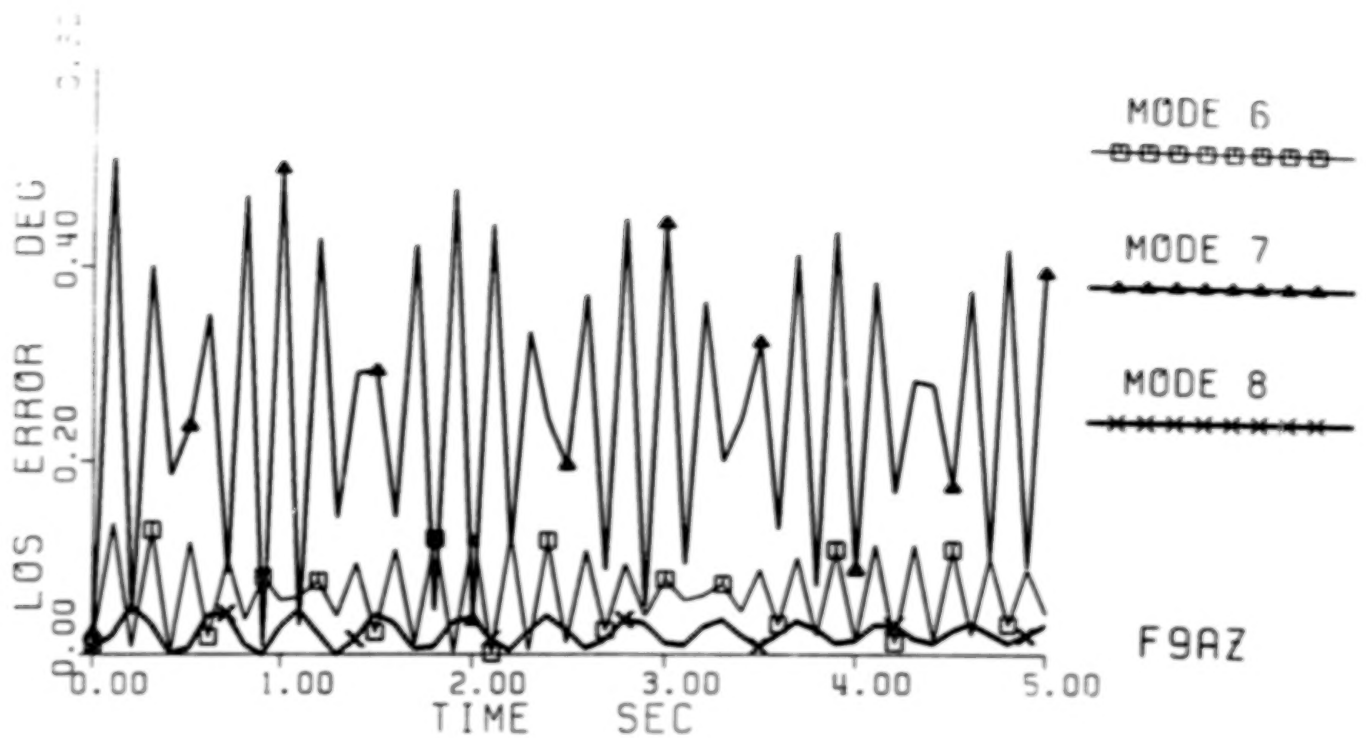


Fig. 5-1b Line-of-sight error due to an initial modal displacement in Modes 6, 7, 8, 9, and 10, respectively. The separate time histories are plotted together for easy comparison and use with Measure 1.



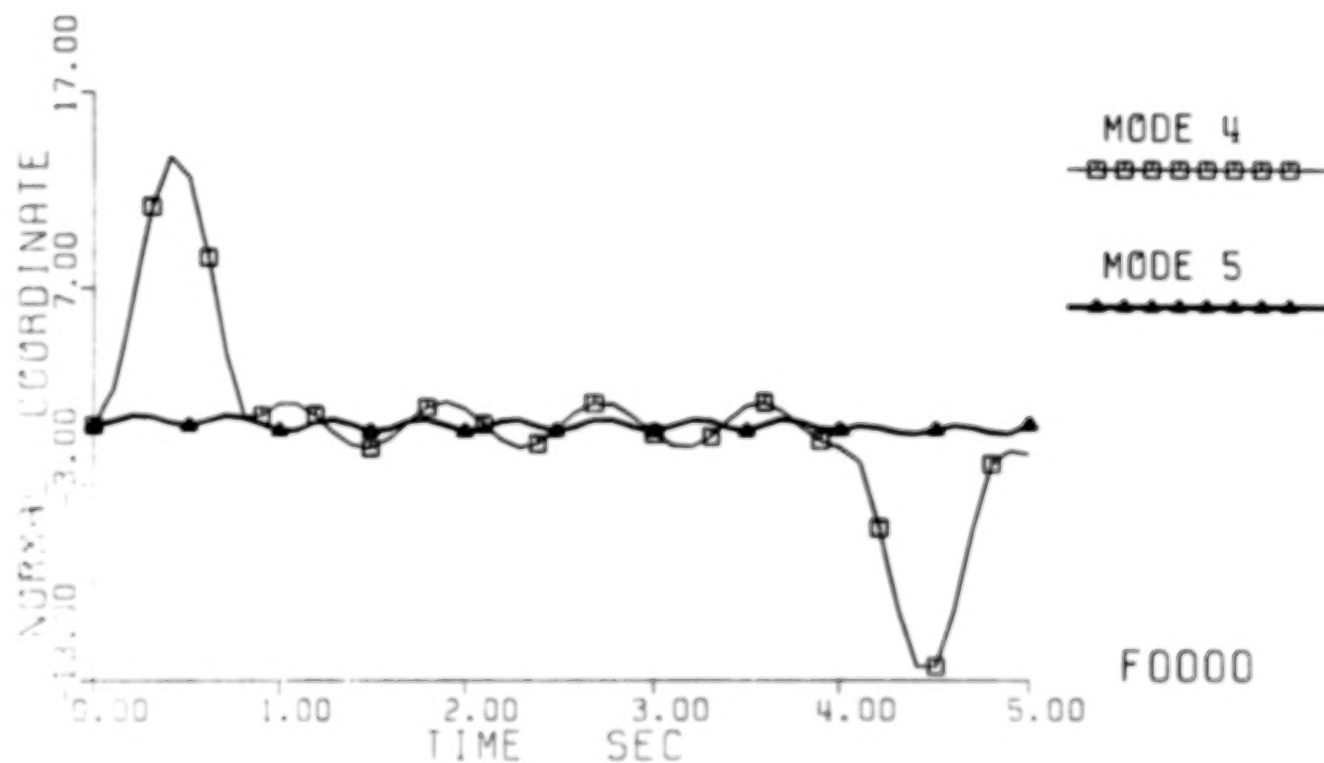
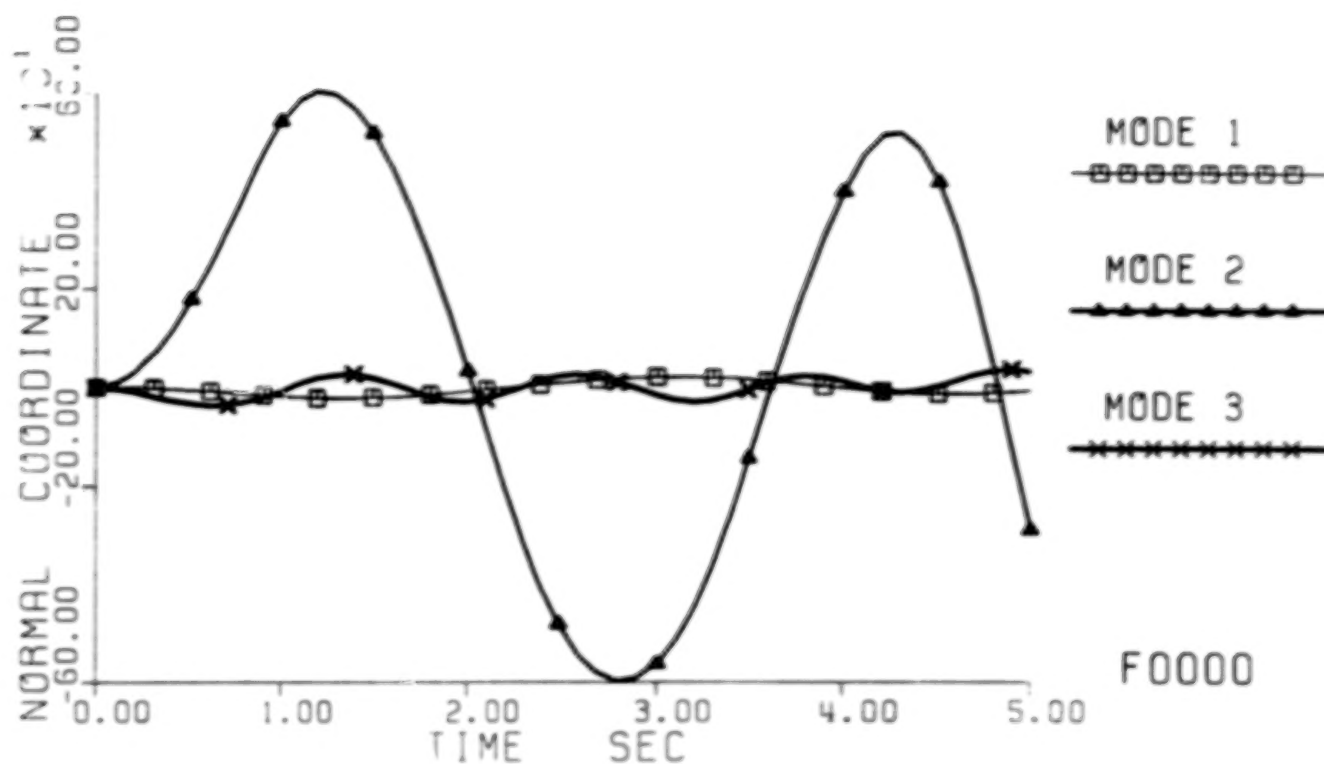


Fig. 5-2a Normal coordinates of Modes 1, 2, 3, 4, and 5, respectively. The cause of excitation was the rapid time-minimized bang-pause-bang pointing slew maneuver. These time histories are plotted together for easy comparison and use with Measure 2.

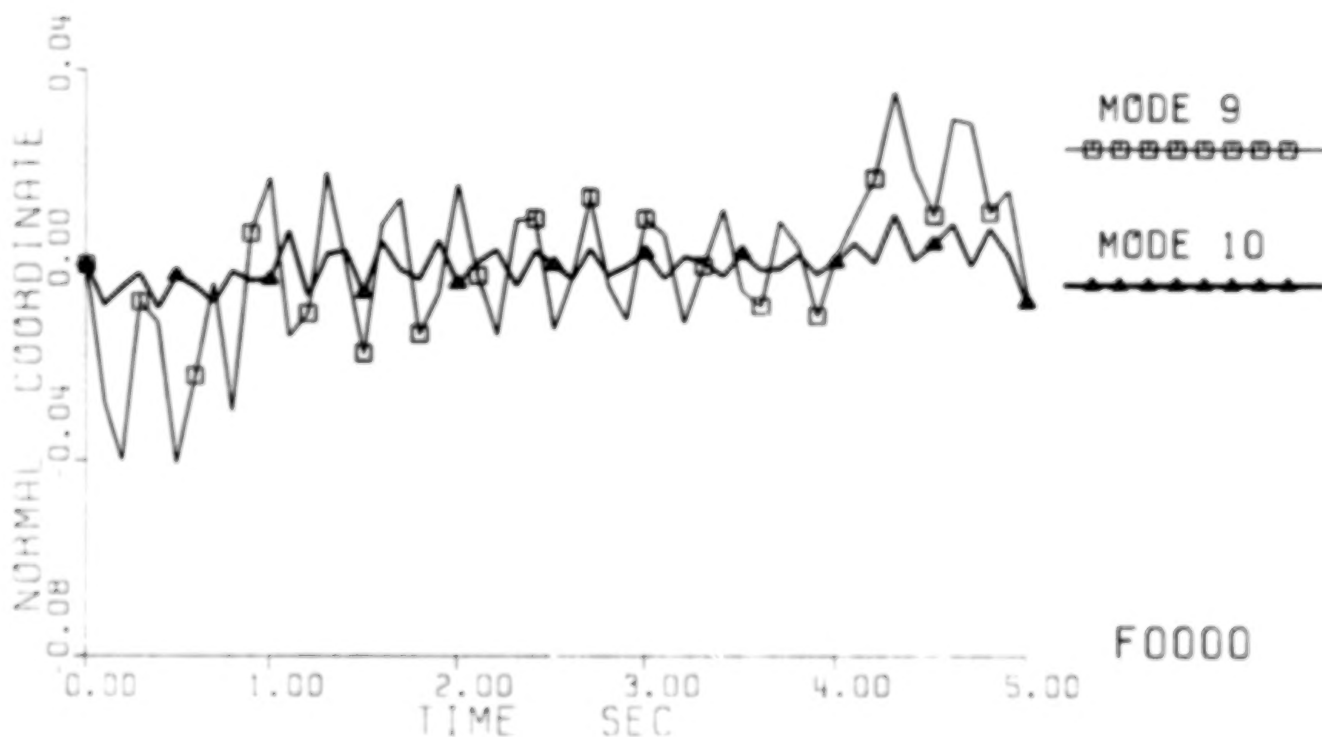
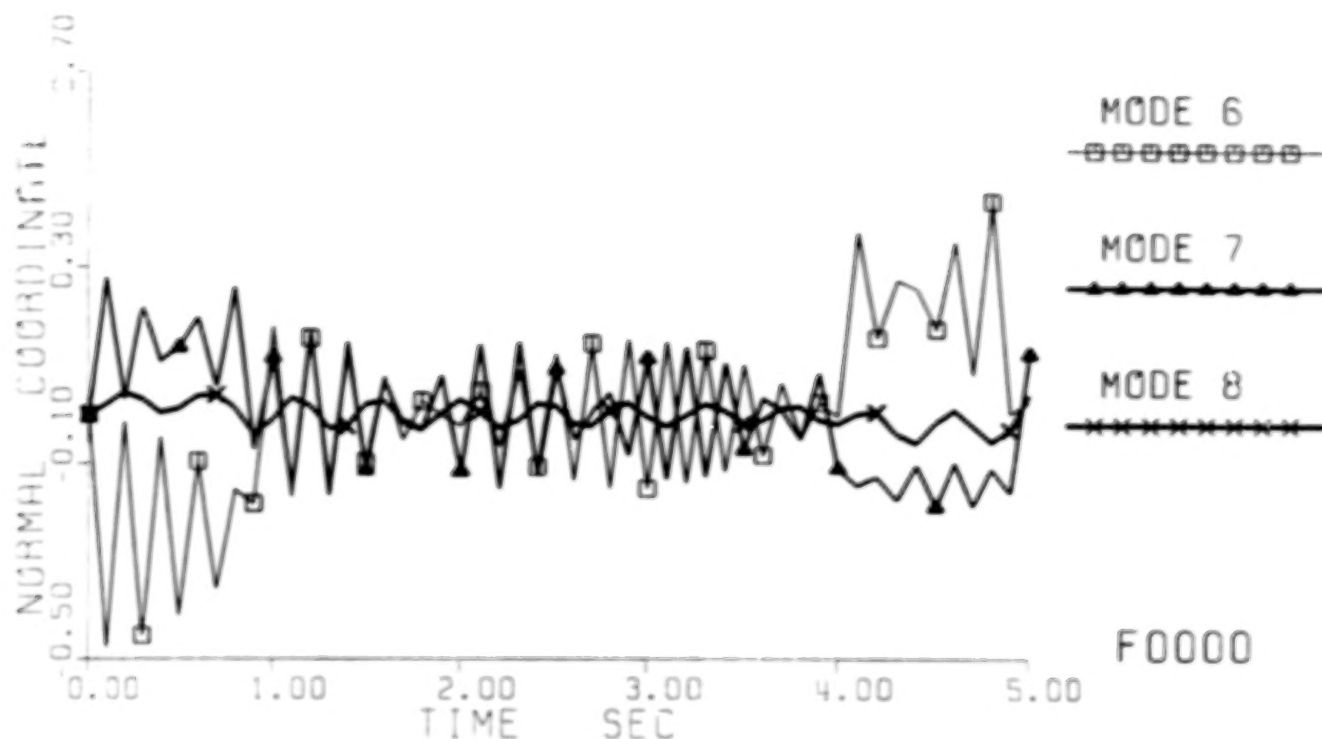


Fig. 5-2b Normal coordinates of Modes 6, 7, 8, 9, and 10, respectively. The cause of excitation was the rapid time-minimized bang-pause-bang pointing slew maneuver. These time histories are plotted together for easy comparison and use with Measure 2.

### 5.1.3 Measure 3: LOS Error Solely due to Each Mode Excited by the Maneuver

To measure by the LOS error a vibration mode could cause, or to measure by the extent to which a vibration mode could be excited, seems to be a rather reasonable technique by itself, but the resulting rankings were inconsistent and rather confusing. For example, Mode 5 is the most important one by Measure 1 but only the fifth by Measure 2. Moreover, Mode 5 could even be ignored because of its insignificant Measure-2 value (about two orders of magnitude smaller than the fourth). Similarly, Mode 1 ranks number 3 by Measure 2 but only number 6 by Measure 1. It was hard to determine rationally which modes would really need active control. A third measure was then developed.

For this analysis, the LOS error caused by a single mode alone was calculated **separately**, like for Measure 1, but the mode causing the error was excited by the very maneuver of concern, instead of initial conditions. All the initial conditions were assumed to be zero. On the other hand, the excitation of the vibration modes was exactly the same as for Measure 2, but the resulting LOS error, instead of the modal response, was taken as the measure.

This measure is a **sound rational combination of the cause (slew excitation) and the effect (LOS error) with respect to each vibration mode**. It can appropriately indicate for each mode individually the extent to which a single mode could be excited, and the degree of LOS error this mode alone could cause if it alone were so excited and, hypothetically, no other modes were present at all.

The 10 separate numerical results are shown together by the plots in Fig. 5-3. Each curve represents the LOS error caused **solely by a single mode** while the mode was being excited by the rapid slew maneuver. The table below lists the highest peak value of the each curve.

Mode:	1	2	3	4	5	6	7	8	9	10
Peak:	3.26	88.6	9.57	6.53	0.33	.036	.077	.002	.004	.0002

The relative importance of the 10 modes is thus given by the following descending order:

Mode: 2, 3, 4, 1, 5, 7, 6,...

An inspection of this ranking and the peak values will show that a significant break between the fourth- and fifth-ranked modes (i.e., modes 1 and 5, respectively). We thus selected the four top-ranked modes, i.e., modes 2, 3, 1, and 4, as the **primary candidates** for modeled modes.

Mode 5 is marginally important compared to other modes, but is the fifth in the rank and has a much higher value than the remainder. We therefore considered it to be a **secondary candidate** for modeled modes.

Mode 1 could have been ranked higher than Mode 4 if the time average were used instead. This would make no significant difference, however, since both were among the top four modes anyway, and these four had all been selected to be primary candidates for modeled modes.

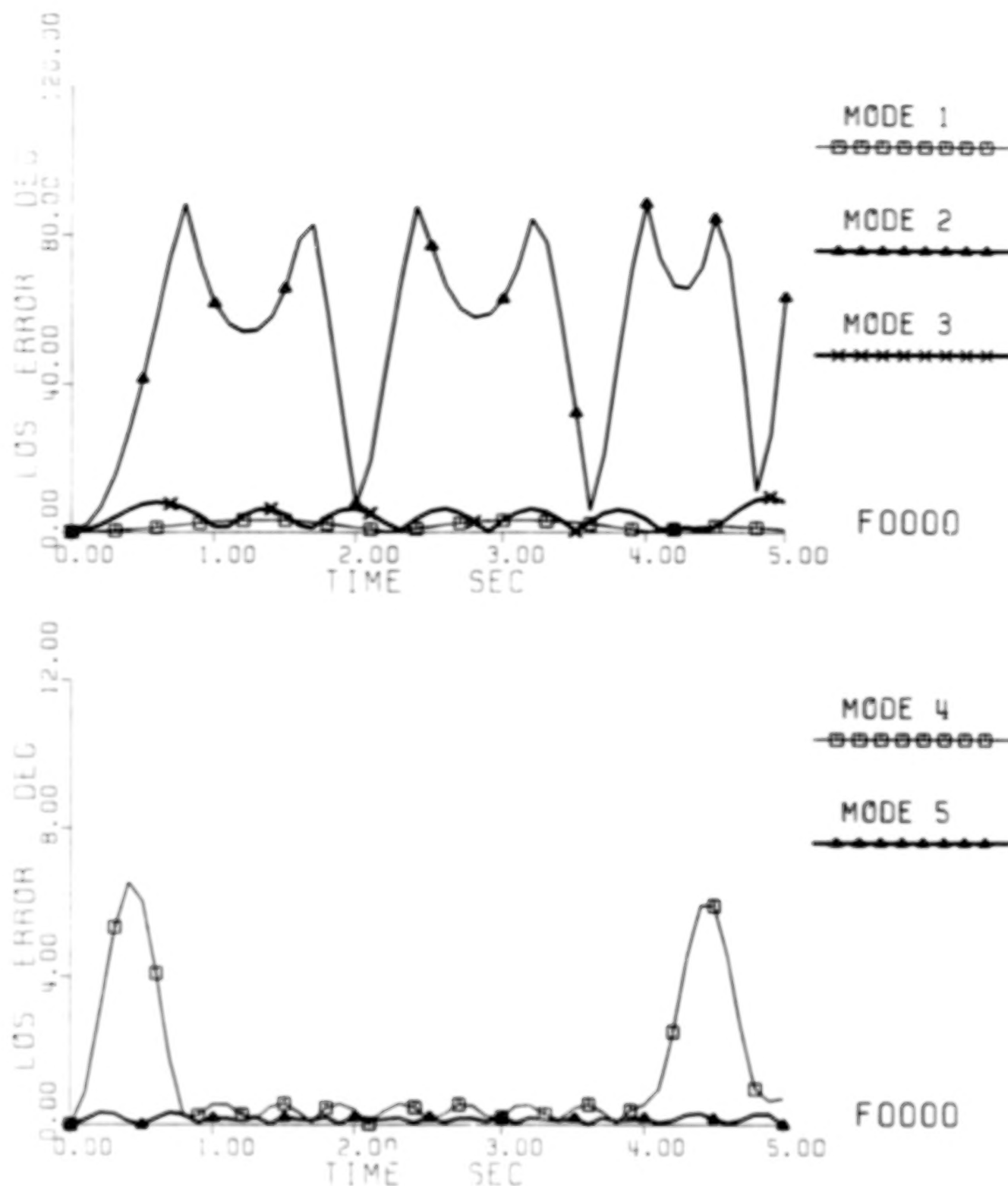


Fig. 5-3 Line-of-sight error caused by a single mode alone while the mode was being excited by the pointing maneuver. The separate time histories are plotted together for easy comparison and use with Measure 3.

a. Modes 1, 2, 3, 4, and 5.

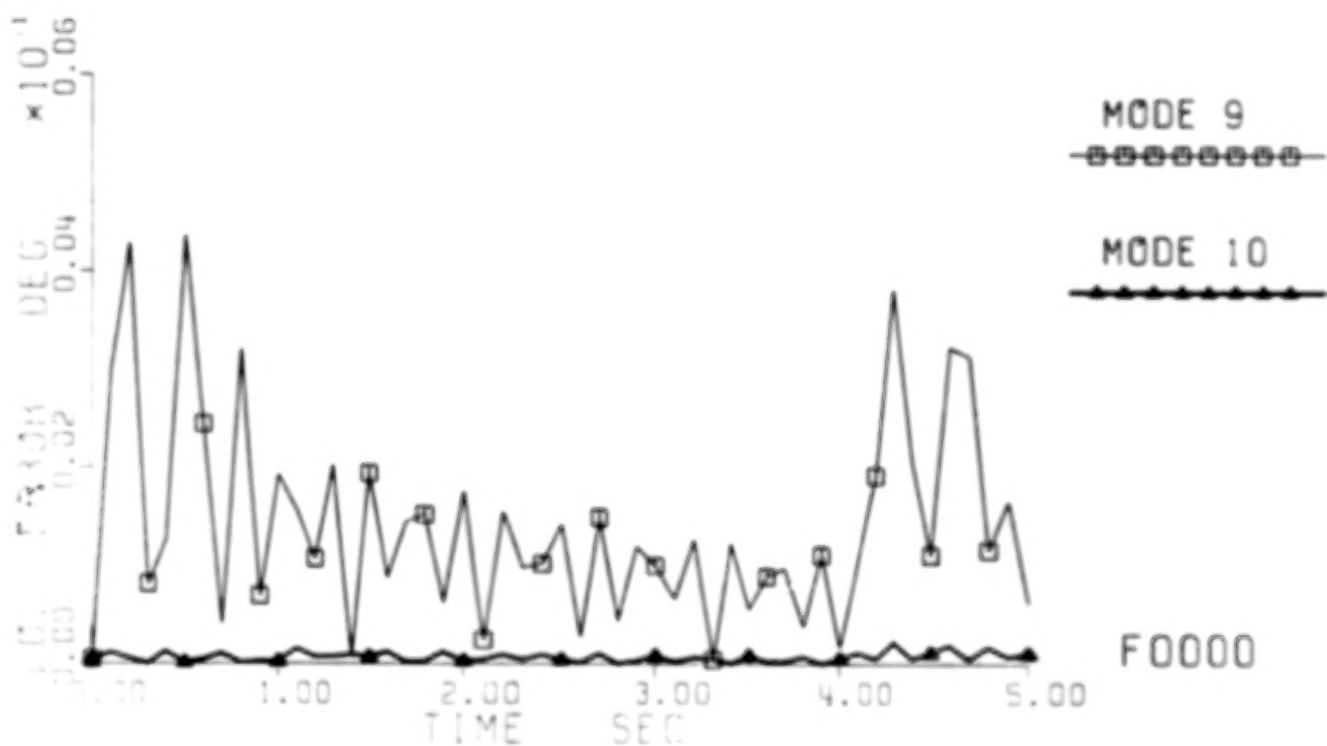
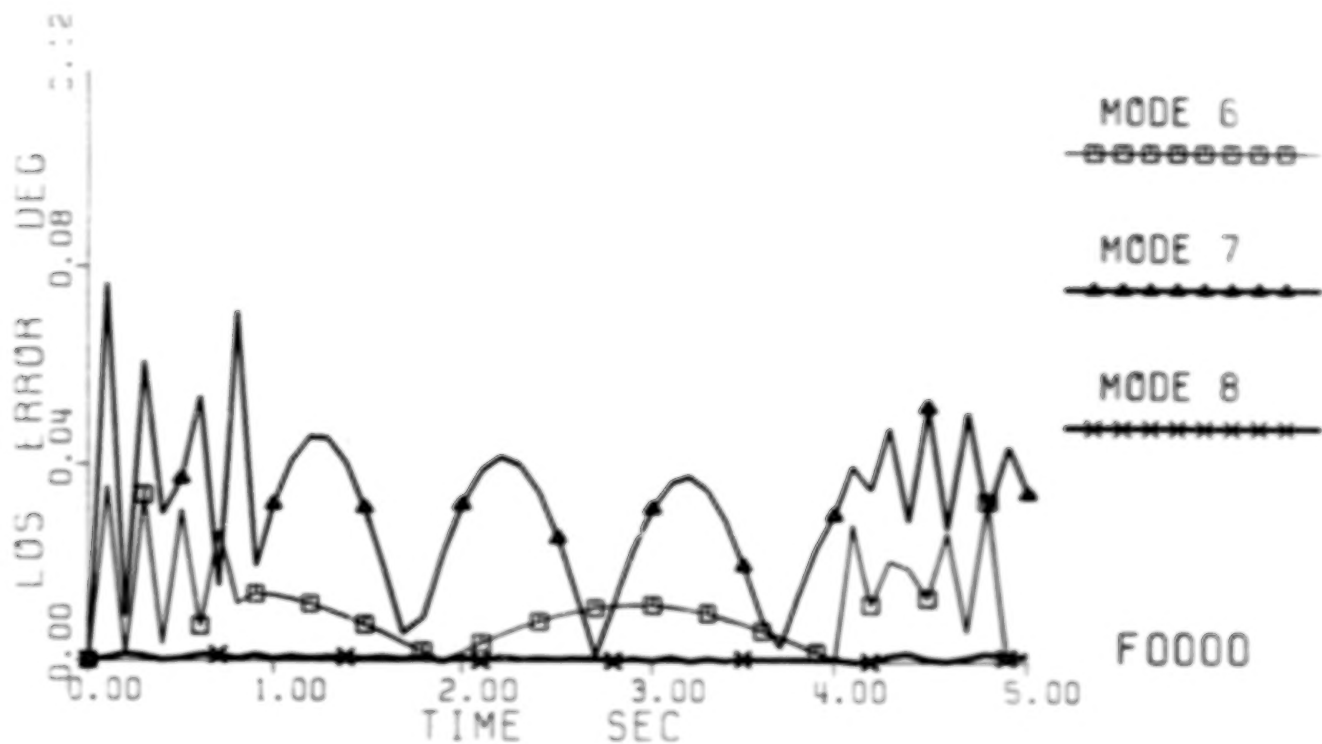


Fig. 5-3 Line-of-sight error caused by a single mode alone while the mode was being excited by the pointing maneuver. The separate time histories are plotted together for easy comparison and use with Measure 3.

b. Modes 6, 7, 8, 9, and 10.

## 5.2 Analysis on Modal Control Influences of Actuators

We recently discovered that the high-gain problem Canavin encountered in his first modal dashpot design [11] would not have existed if he had paid attention to the ill conditioning of the coefficient matrix  $\Phi_M^T B_F$  he used in his numerical example. Among the 12 "controlled modes" he selected to form his reduced-order design model, several have very little control influences from the 32 actuators he used on the structure\*. It is intuitively apparent that actuators having smaller influences on a given mode are less effective in controlling the mode, and thus require to be compensated with larger gains. Mathematically speaking, when the smallest "singular value" of the coefficient matrix  $\Phi_M^T B_F$  is one order of magnitude smaller, the largest singular value of the resulting gain matrix  $G^*$  as a solution of Eq. (4-7) generally is two orders of magnitude larger. This means that **not all his "controlled" modes should be included** in the modal-dashpot design without any discrimination against excessively small control influences by the actuators. In other words, all the available actuators need **not be lumped together to control all his "controlled" modes through one large feedback gain matrix**.

To make an effective design for the SCOLE configuration, we analyzed the control influences of the actuators first and match those modes in need of active control with the right actuators.

For evaluating and comparing their modal influences properly, we grouped the actuators according to their location on the SCOLE configuration as well as their type. As a result, the actuators\*\* were divided into the following four different groups:

- Group 1: Actuators 1 to 3, for applying moments on the Shuttle about its body x, y, and z axes, respectively;
- Group 2: Actuators 4 to 6, for applying moments on the Reflector about its body x, y, and z axes, respectively;
- Group 3: Actuators 7 and 8, for applying forces at the Reflector mass center in the x and y directions, respectively;
- Group 4: Actuators 9 to 12, for applying forces at two specific points on the Mast beam in the x and y directions, respectively.

The control influences on each mode, say mode i, from all the actuators in a specific group can be summarized by calculating their RMS (Root-Mean-Square) value

$$\sqrt{[(\Phi^T b_{F1})^2 + (\Phi^T b_{F2})^2 \dots + (\Phi^T b_{Fk})^2] / k}$$

over the group. Listed in Table 5-1 are these RMS values in the descending order.

---

\* The antenna-like structure consisted of a large dish in the forward section and a gimbaled equipment section to the aft. It had 32 member dampers (as the co-located actuators and rate sensors). Its finite-element model has 35 degrees of freedom.



Table 3-1 RMS Actuator Influences on first 10 Modes

Group 1		Group 2		Group 3		Group 4	
Mode	Act. 1 - 3	Mode	Act. 4 - 6	Mode	Act. 7 - 8	Mode	Act. 9 - 12
2	0.30019961E-02	5	0.36487188E-01	2	0.14311218E+01	2	0.10711402E+00
4	0.41220308E-03	4	0.25172627E-01	1	0.14061384E+01	1	0.10338868E+00
1	0.40146321E-03	3	0.15999462E-01	3	0.81986851E+00	3	0.10171293E+00
3	0.19184369E-03	2	0.15595800E-01	4	0.39743480E+00	4	0.69439910E-01
5	0.11186474E-03	7	0.14711439E-01	7	0.30395976E+00	9	0.68373762E-01
6	0.69881789E-04	1	0.13037169E-01	9	0.25503686E+00	8	0.67025743E-01
7	0.36829457E-04	9	0.57048416E-02	6	0.21852742E+00	5	0.63191518E-01
8	0.26261532E-04	6	0.34139471E-02	8	0.14623879E+00	10	0.46103600E-01
9	0.15072107E-04	8	0.12352261E-02	10	0.10801539E+00	6	0.39935779E-01
10	0.13497747E-04	10	0.63637015E-03	5	0.74399590E-01	7	0.32263912E-01

Table 3-2 RMS Sensor Influences on first 10 Modes

Group 1		Group 2		Group 3		Group 4	
Mode	Sen. 1 - 3	Mode	Sen. 4 - 6	Mode	Sen. 7 - 8	Mode	Sen. 9 - 12
2	0.28690067E-03	5	0.34890966E-02	2	0.13466856E+00	2	0.10711402E+00
4	0.39390128E-04	3	0.32387748E-02	1	0.12736945E+00	1	0.10338868E+00
1	0.39113598E-04	4	0.24055073E-02	3	0.12407852E+00	3	0.10171293E+00
3	0.18940789E-04	2	0.15346858E-02	4	0.38158901E-01	4	0.69439910E-01
5	0.10689848E-04	7	0.14879148E-02	7	0.36793593E-01	9	0.68373762E-01
6	0.66779044E-05	1	0.13531352E-02	9	0.30879460E-01	8	0.67025743E-01
7	0.35194691E-05	9	0.67911280E-03	6	0.20832075E-01	5	0.63191518E-01
8	0.25095521E-05	6	0.32624099E-03	8	0.14005536E-01	10	0.46103600E-01
9	0.14402938E-05	8	0.11804001E-03	10	0.10299906E-01	6	0.39935779E-01
10	0.12898448E-05	10	0.60812166E-04	5	0.90737212E-02	7	0.32263912E-01

Observe that Actuators 1 to 3 (Group 1) have an RMS value for Mode 2 that is one order of magnitude higher than all other modes, and hence are most effective in controlling Mode 2 than controlling other modes. Observe also that Mode 2 ranked the highest in RMS value with respect to Group-3 actuators 7 and 8. In addition, this RMS value is two orders of magnitude higher than that with Actuators 1 to 3. Consequently, Actuators 7 and 8 should be more effective for controlling mode 2 and require much smaller feedback gains. Note that Actuators 9 to 12 (Group 4) are less effective than Actuators 7 and 8 in controlling Mode 2.

With a similar argument, Actuators 7 and 8 are also most effective in controlling Mode 1. Therefore, Modes 1 and 2 and no more others should be selected as the "modeled modes" in the design of the modal dashpots using Actuators 7 and 8.

Since Mode 3 is a torsion mode and is more appropriate to be controlled by moments than forces. The RMS values clearly suggest that Actuators 4 to 6 (Group 3) will be more effective than Actuators 1 to 3 for controlling Mode 3. Although among the four groups, Actuators 9 to 12 did have the highest RMS values of control influences on Mode 3, we did not expect the proof-mass actu-

ators (9 to 12) to be capable of suppressing large torsional vibrations of any mode in such a very short time.

The RMS control influence on Mode 4 is larger from Actuators 4 to 6 than from Actuators 1 to 3. Consequently, both **Modes 3 and 4** should be selected as the "modeled modes" in the design of modal dashpots using **Actuators 4 to 6**.

All the four primary candidates have been selected as the "modeled modes" for the appropriate matching groups of actuators. A review of Table 5-1 will show that Mode 5, the secondary candidate, has a higher RMS value of control influences from the same Group 2 of actuators than both Modes 3 and 4. According to a previous study by Lin and Jasper [24], such a situation would result in large spillover of Mode 5, severe dynamic interactions of modeled modes with unmodeled modes, and significant degradation of damping performance if Mode 5 were not **also modeled with Modes 3 and 4** for control by **Actuators 4 to 6**.

To summarize, this analysis shows applying moments and forces at the Reflector end of the Mast beam will be more effective in controlling the excited vibrations in SCOLE (and particularly Modes 1 to 5) than at the Shuttle end or at the intermediate points of the flexible mast. Instead of lumping up all candidate modes (1 to 5) to be controlled by Actuators 4 to 8 together, the designer for modal dashpots should match these modes with their most effective or most appropriate actuators. Specifically, Modes 1 and 2 should be controlled by Actuators 7 and 8 and Modes 3 to 5 by Actuators 4 to 6.

There is no need to include more modes to each group since there are enough actuators to be distributed among all the 5 most important modes of the SCOLE flexible-body dynamics. Including more modes may not always help: it might simply increase the magnitude of the feedback gains without any real benefit, particularly when the additional modes are of significantly smaller control influences by the actuators; the increased feedback gains might instead amplify various adverse effects of control spillover and system noises.

### 5.3 Design of Modal Dashpot MD1

The modal dashpot MD1 was designed for SCOLE for quick suppression of the excessive vibrations excited by the rapid BPB LOS pointing slew maneuver. It is composed of two parts. Part 1 is for applying forces at the Reflector mass center in the two transverse directions using a feedback of linear velocities at the Reflector end of the beam. Part 2 is for applying moments also at the Reflector about the three body axes but using a feedback of angular velocities instead.

The location of these actuators are the same as specified by Taylor in Ref. 1 for the control forces and moments at the Reflector. The sensors were located where the "outputs" of Dr. Joshi's modal data set D3D585 had been calculated. Some of the control inputs ( $u_i$ ) and observation outputs ( $y_j$ ) were re-labeled for technical convenience. Sensors 1 to 8 are not really co-located with the corresponding actuators, but note that their RMS values of modal observation influences (Table 5-2) exhibit virtually the same patterns as those of modal control influences (Table 5-1).



### 5.3.1 Part 1: Linear Velocity Feedback Force Control

Two force actuators (or equivalently, a single force actuator capable of delivering separate forces in two independent axes) are assumed to be placed at the center of the Reflector. The force inputs\*  $u_7$  and  $u_8$  (in the x and y directions, respectively) are each limited to 800 lb as specified. Two linear velocity sensors (or equivalently a single velocity sensors capable of measuring the rate of linear displacements in two independent axes) are assumed to be located at the Reflector end of the mast beam. The sensor outputs\*\*  $y_{15}$  and  $y_{16}$  (in the x and y directions, respectively) represent the time rate of deflection of the Mast beam at the Reflector end relative to the Shuttle end. Note that these sensors are only **approximately co-located** with actuators: they are apart by 18.75 ft and 32.5 ft in x and y directions, respectively, whereas the beam is 130 ft long.

The design problem is thus to determine a 2x2 gain matrix  $G_{LVR}$  for the following linear velocity feedback control law

$$\begin{bmatrix} u_7 \\ u_8 \end{bmatrix} = -G_{LVR} \begin{bmatrix} y_{15} \\ y_{16} \end{bmatrix} \quad (5-1)$$

The foregoing analysis of the control influences has suggested that only Modes 1 and 2 be selected as the "modeled modes" for this part of design. Accordingly, the control and observation influence matrices  $\phi_M^T B_F$  and  $C_V \phi_M$  on the two modeled modes to be used in the modal dashpot design equation (4-8) have the following numerical values:

$$\phi_M^T B_F = \begin{bmatrix} .19875923E+01 & .62669927E-01 \\ .14599262E+00 & -.20186396E+01 \end{bmatrix} \quad (5-2a)$$

$$C_V \phi_M = \begin{bmatrix} .18012760E+00 & .21140305E-01 \\ .55188192E-04 & -.18927317E+00 \end{bmatrix} \quad (5-2b)$$

Before solving the corresponding design equation (4-8) for a specific gain matrix, we must specify the desired value for the additional damping matrix  $\Delta_M^*$ . For technical simplicity, we choose it to be diagonal, so that its diagonal elements  $\delta_{M1}^*$  and  $\delta_{M2}^*$  can be used rather directly for guiding the modal-dashpot design. Since both modes 1 and 2 substantially dominate the vibratory response of the SCOLE configuration to the BPB pointing maneuver, we wish to augment each with active damping as close to 70.7%†† of critical damping as

\* These correspond to  $u_4 = F_{rx}$  and  $u_5 = F_{ry}$ , respectively, in Dr. Joshi's notation.

\*\* These are indirectly equal to the derivatives of the deflections  $y_7 = \dot{\xi}_x$  and  $y_8 = \dot{\xi}_y$  in Dr. Joshi's notation.

† These terms represent the additional damping coefficients in the corresponding decoupled equations of motion; see Eqs. (4-14)-(4-15). In multivariable root-locus analysis, these values also represent the "rate of departure" from the open-loop poles when the feedback loops are closed.

†† 70.7% is an optimal value in the sense that the second-order system corresponding to the single mode will neither be too sluggish nor have a large overshoot.

possible. Let us attempt a theoretical 2% settling time of 3 seconds for Mode 2 in estimating the desirable additional damping coefficient  $\delta_2^*$ . The corresponding time constant is 3/4 sec; thus by definition

$$\bar{\zeta}_2 \omega_2 = 4/3$$

where  $\bar{\zeta}_2$  denotes the closed-loop damping ratio desirable of Mode 2. Substituting in the natural frequency  $\omega_2 = 1.97024$  rad/sec yields

$$\bar{\zeta}_2 = 0.6767,$$

which is acceptably close to the optimal value. Whence, the closed-loop damping coefficient desirable of Mode 2 is given by

$$\bar{\delta}_2 = 2 \bar{\zeta}_2 \omega_2 = 8/3.$$

Since an inherent damping of 0.3% has been specified in the data set "D3D585" for each mode, the desirable additional damping coefficient<sup>#</sup> desirable of Mode 2 is

$$\delta_2^* = \bar{\delta}_2 - 2 \zeta_2 \omega_2 = 8/3 - 2 \times 0.003 \times 1.97024 = 2.6548$$

Next, we choose the additional damping desirable of Mode 1 to be 60%, i.e.,  $\zeta_1^* = 0.6$ , since Mode 1 has a smaller magnitude of vibration than Mode 2.

In summary, the desired damping coefficients as in Eqs. (4-14)-(4-15) for the two modeled modes are then readily given as

$$\delta_{M1}^* = \delta_1^* = 2 \zeta_1^* \omega_1 = 2 \times 0.6 \times 1.7470 = 2.0964 \quad (5-3a)$$

$$\delta_{M2}^* = \delta_2^* = 2.6548. \quad (5-3b)$$

Now the feedback gain matrix  $G_{LVR}$  is readily obtained from solving (4-8) as

$$G_{LVR} = \begin{bmatrix} .58420630E+01 & .43392044E+00 \\ .42038249E+00 & .69796355E+01 \end{bmatrix} \quad (5-4)$$

### 5.3.2 Part 2: Angular Velocity Feedback Moment Control

Three torquers (or equivalently, a single torquer capable of delivering separate torques about three independent axes) are assumed to be located on the Reflector. The torque inputs<sup>\*</sup>  $u_4$ ,  $u_5$ , and  $u_6$  (about the x, y, and z axes, respectively) are each limited to 10,000 lb-ft as specified. Three angular velocity sensors (or equivalently a single sensor capable of measuring separately the rate of rotations about three different axes) are assumed to be located at the Reflector end. The sensor outputs<sup>\*\*</sup>  $y_{10}$ ,  $y_{11}$ , and  $y_{12}$  (about the x, y, and z axes, respectively) represent the time rate of rotations of the

# The corresponding additional damping ratio  $\zeta_2^*$  for Mode 2 is 0.6737. A few slightly modified values were also tried when the design of this part was repeated (see Section 6.2).

\* These correspond to Dr. Joshi's  $u_6 = T_{rx}$ ,  $u_7 = T_{ry}$ , and  $u_8 = T_{rz}$ , respectively.

\*\* These correspond to Dr. Joshi's  $y_{12} = \dot{\phi}_r$ ,  $y_{13} = \dot{\theta}_r$ , and  $y_{14} = \dot{\psi}_r$ , respectively.

Reflector end of the mast due to bending and torsion. Again, these sensors are **only approximately co-located** with the actuators. Note that the Reflector itself is a rigid body.

The design problem is to find a 3x3 gain matrix  $G_{AVR}$  for the following angular velocity feedback control law

$$\begin{bmatrix} u_4 \\ u_5 \\ u_6 \end{bmatrix} = -G_{AVR} \begin{bmatrix} y_{10} \\ y_{11} \\ y_{12} \end{bmatrix} \quad (5-5)$$

Similarly, as suggested by the previous analysis on control influences, we choose Modes 3, 4, and 5 to be the "modeled modes" for this part of the design. Accordingly, the specific control and observation influence matrices are given by

$$\Phi_{MB}^T = \begin{bmatrix} .10761780E-01 & -.18101653E-01 & -.18012847E-01 \\ .37541741E-01 & .22172032E-01 & .45802862E-04 \\ -.31739483E-01 & .54643290E-01 & .81303515E-03 \end{bmatrix} \quad (5-6a)$$

$$C_V \Phi_M = \begin{bmatrix} .10592386E-02 & .35194610E-02 & -.30149737E-02 \\ -.17367745E-02 & .21135667E-02 & .52175940E-02 \\ -.52450669E-02 & .13325330E-04 & .23641118E-03 \end{bmatrix} \quad (5-6b)$$

Since the vibratory responses of Modes 3, 4, and 5 are much smaller in magnitude than those of Modes 1 and 2, it is reasonable to augment them with only a relatively small amount of active damping. We chose rather arbitrarily 3% of critical damping for each. The diagonal elements of the desired additional damping matrix  $\Delta_M$  are then given as follows:

$$\delta_{M1}^* = \delta_3^* = 2 \times 0.03 \times \omega_3 = 0.3065 \quad (5-7a)$$

$$\delta_{M2}^* = \delta_4^* = 2 \times 0.03 \times \omega_4 = 0.4470 \quad (5-7b)$$

$$\delta_{M3}^* = \delta_5^* = 2 \times 0.03 \times \omega_4 = 0.7742 \quad (5-7c)$$

Substituting (5-5)-(5-7) in Eq. (4-8) and solving the resulting equation, we get the following gain matrix

$$G_{AVR} = \begin{bmatrix} .24172707E+04 & .16653096E+03 & .45158162E+03 \\ .15734103E+03 & .21781213E+04 & -.72768193E+03 \\ .13433660E+04 & -.22055215E+04 & .42951681E+04 \end{bmatrix} \quad (5-8)$$

## 6. PERFORMANCE OF VIBRATION CONTROL DESIGNS ON SCOLE

To evaluate the vibration control performance of the modal dashpot design MD1, we incorporate the two feedback laws (5-1) and (5-5) into the same SCOLE flexible-body dynamic model as was used in simulating its vibratory responses to the BPB pointing maneuver. As stated in the beginning of Section 3, the undeformed SCOLE configuration was assumed to have been aligned with the specific attitude of zero LOS error. Thus, the velocity-sensor outputs would contain only the flexible-body rates\*, just as desired for feedback control of the excited vibrations. Recall that the model is of the "full order" in the sense that it includes all the ten modes as provided in the data set D3D585. In order that the control moments and forces do not exceed their specified limits, the computer program also simulates the saturation of the actuators at their respective limits. For example, if at any time the feedback control input, say,  $u_g$  would command the actuator to exert more than 800 lb force to the Reflector, the actual force applied would be only 800 lb maximum.

The feedback control consisting of the two parts of modal dashpot MD1 is turned on **right after** the completion of the BPB pointing maneuver. Thus the terminal state of the SCOLE vibrations (i.e., the LOS error, the deflection and its rate of change, the angular displacement and its rate, modal displacements and velocities,...) at the end of the maneuver become the **initial conditions** of the feedback controlled system. The vibration control is applied for five seconds, which is about the same duration as of the pointing maneuver. We intentionally use such a rather "long" period in order to check if instability in the closed-loop system might start to develop after the excessive vibrations has been rapidly forcefully suppressed. Various versions of the modal dashpot design MD1 (each with a slightly different value for the additional damping coefficient  $\delta_i^*$ ) were evaluated. Reported below are two representative cases.

### 6.1 Simulation Results of Modal Dashpot Design MD1

The specific values of the gain matrices  $G_{LVR}$  given by (5-4) and  $G_{AVR}$  given by (5-8) were incorporated with the control laws (5-1) and (5-5) respectively in the full-order dynamic simulation. The simulation results are summarized by time-history plots in Fig. 6-1.

The history of the applied moments and forces (Fig. 6-1a) shows that the applied moment about each axis never exceeded the limit of 10,000 lb-ft, nor did the applied force in each direction exceed the limit of 800 lb. Large moments and forces were needed only during the early portion of the control period, but did not exceed the limits because of "saturation". All the applied forces and moments quickly reduced to minimum automatically because the sensed rates of vibrations rapidly became insignificant.

Fig. 6-1b shows that the LOS error was rapidly subdued to  $11.79^\circ$  from  $71.43^\circ$  where the pointing maneuver ended. Note that the initial LOS error continued to rise to  $85.29^\circ$  (or  $115.13^\circ = 180^\circ - 64.87^\circ$  if not taking the principal

---

\* If the configuration had not been so aligned, then rigid-body rate would also be present and some filtering or signal processing might be required. Alternatively, one could use relative sensors instead of inertially referenced sensors.

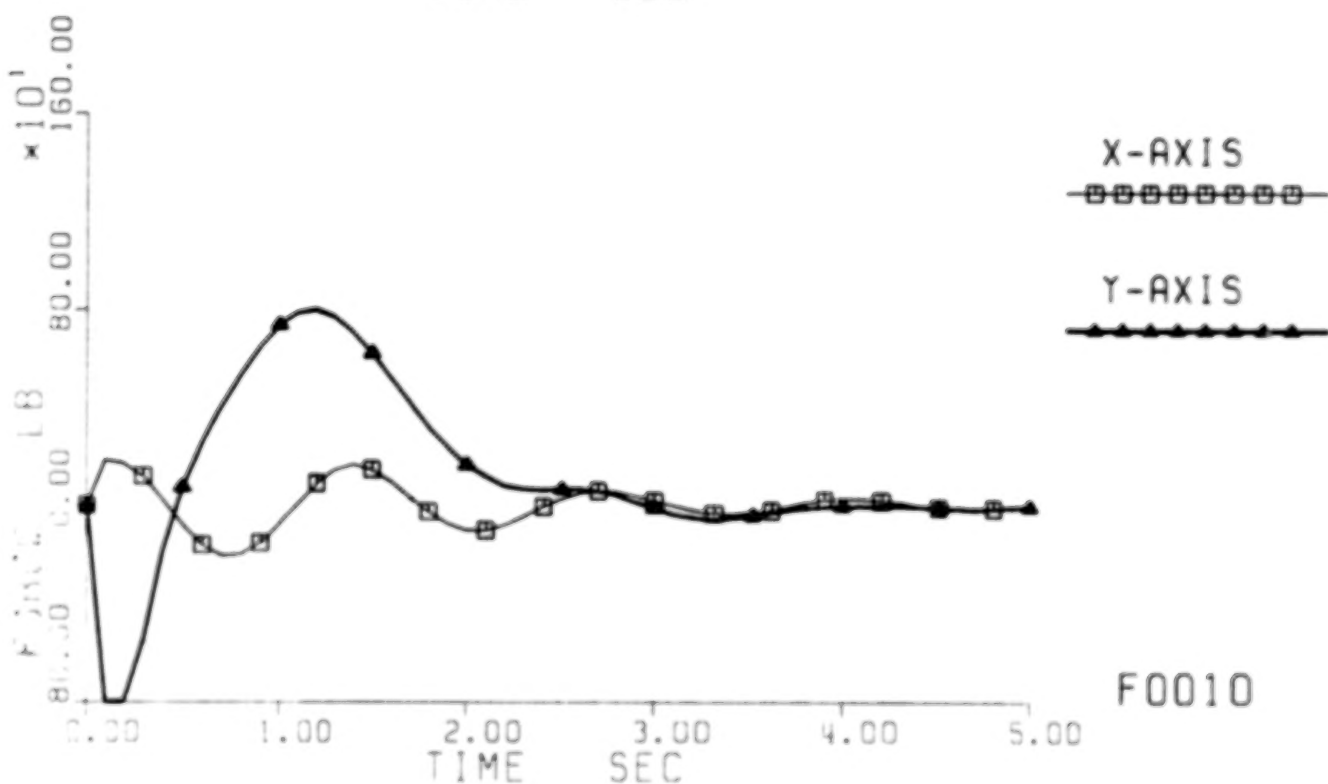
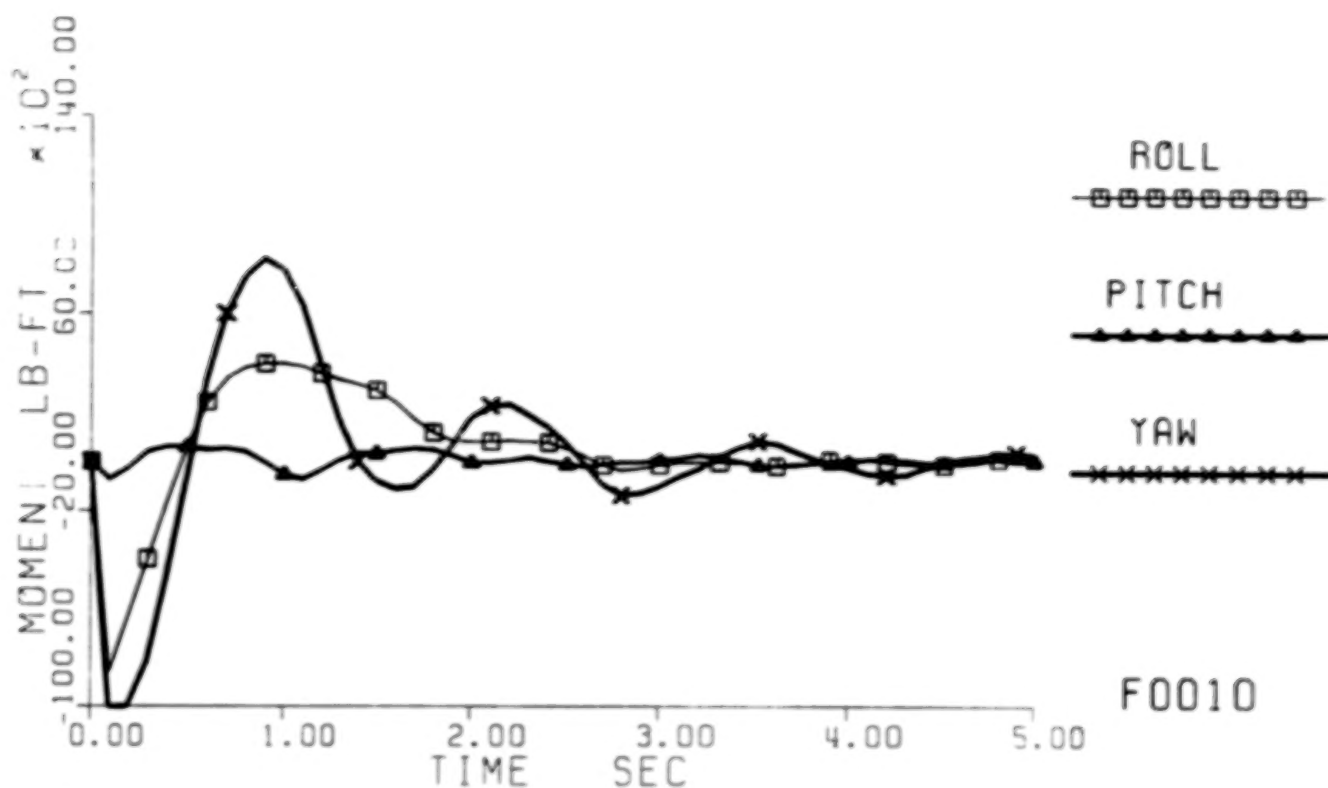


Fig. 6-1 Simulation results of vibration control design MD1;  
a. Histories of applied moments and forces at the Reflector.

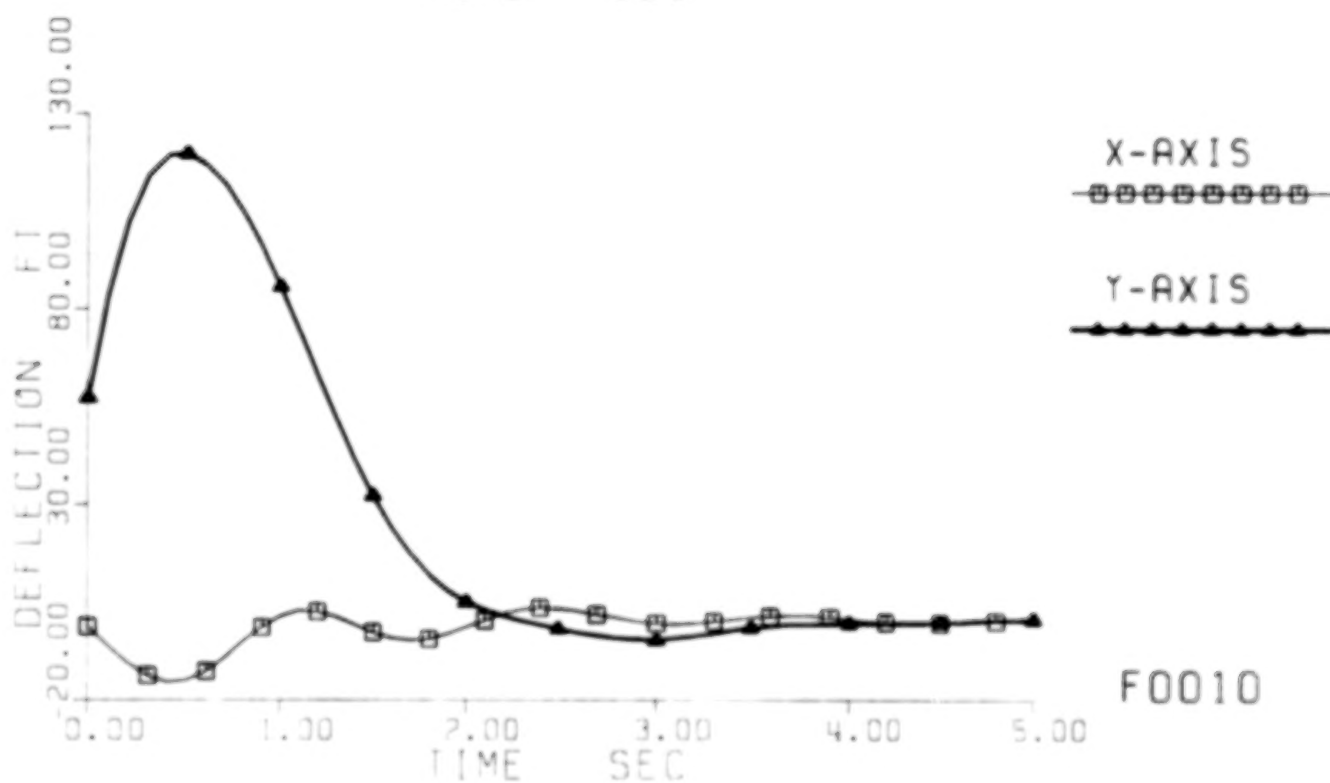
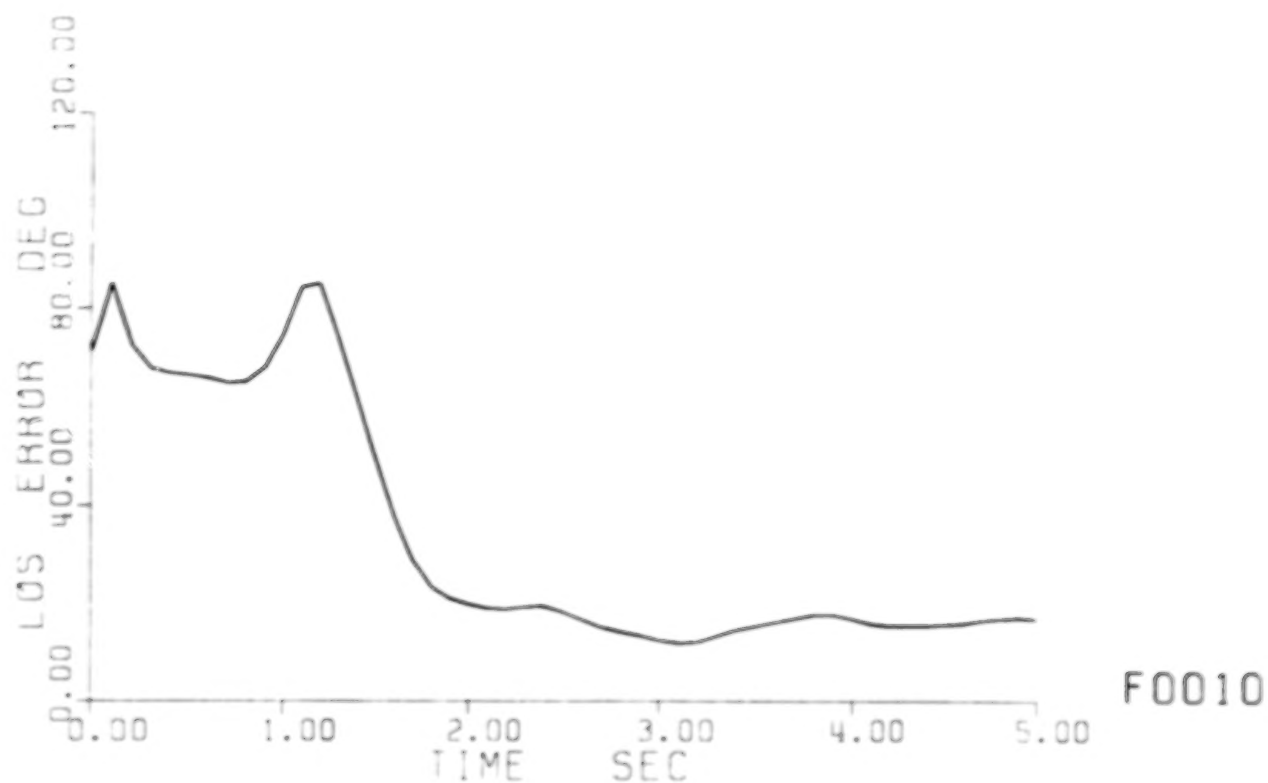


Fig. 6-1 Simulation results of vibration control design ND1;  
 b. Histories of line-of-sight error and Mast tip deflection.



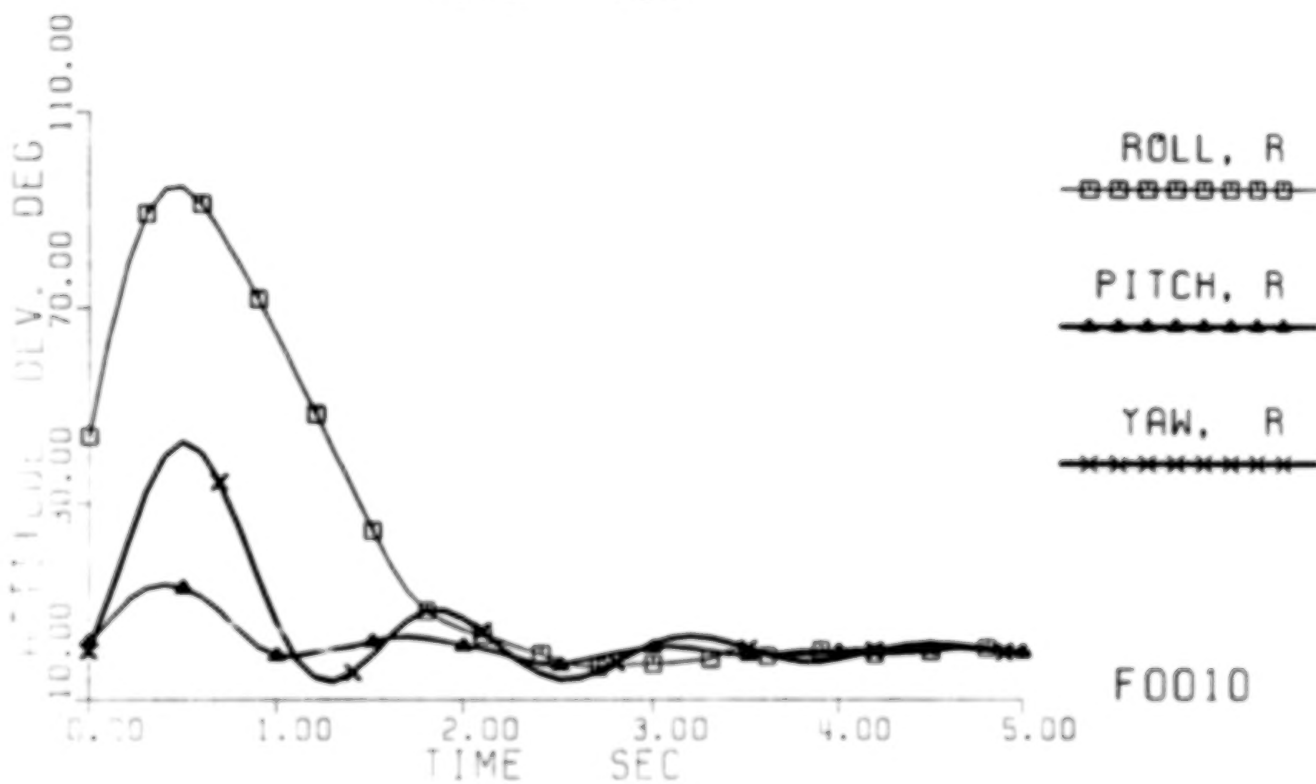
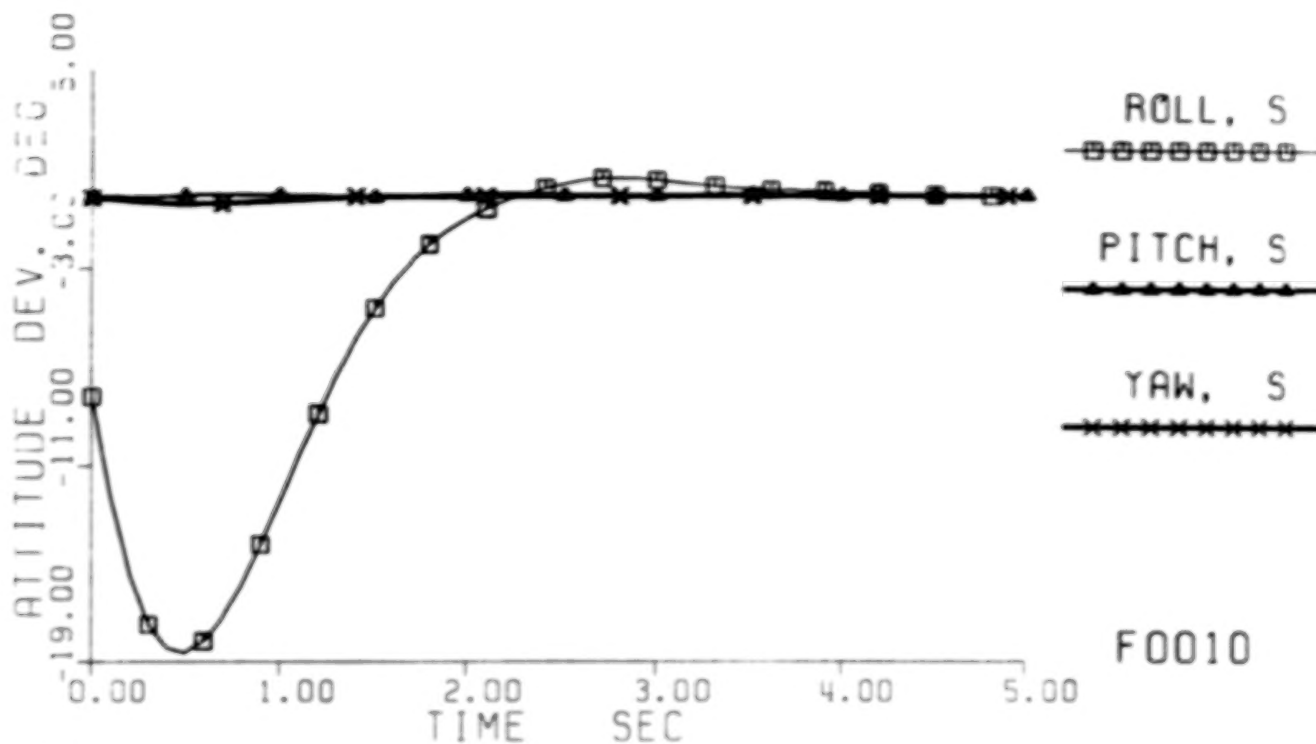


Fig. 6-1 Simulation results of vibration control design MDI;  
c. Histories of attitude deviations at Shuttle (S) and Reflector (R) ends

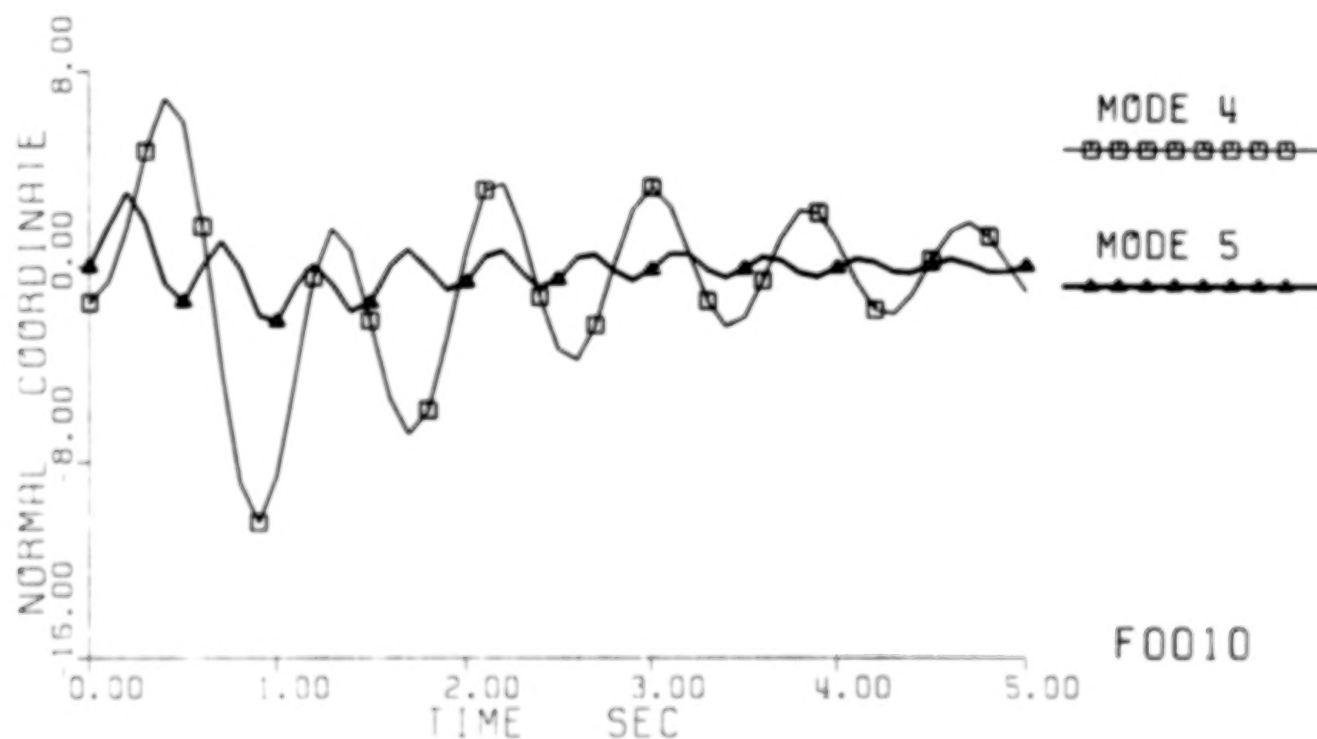
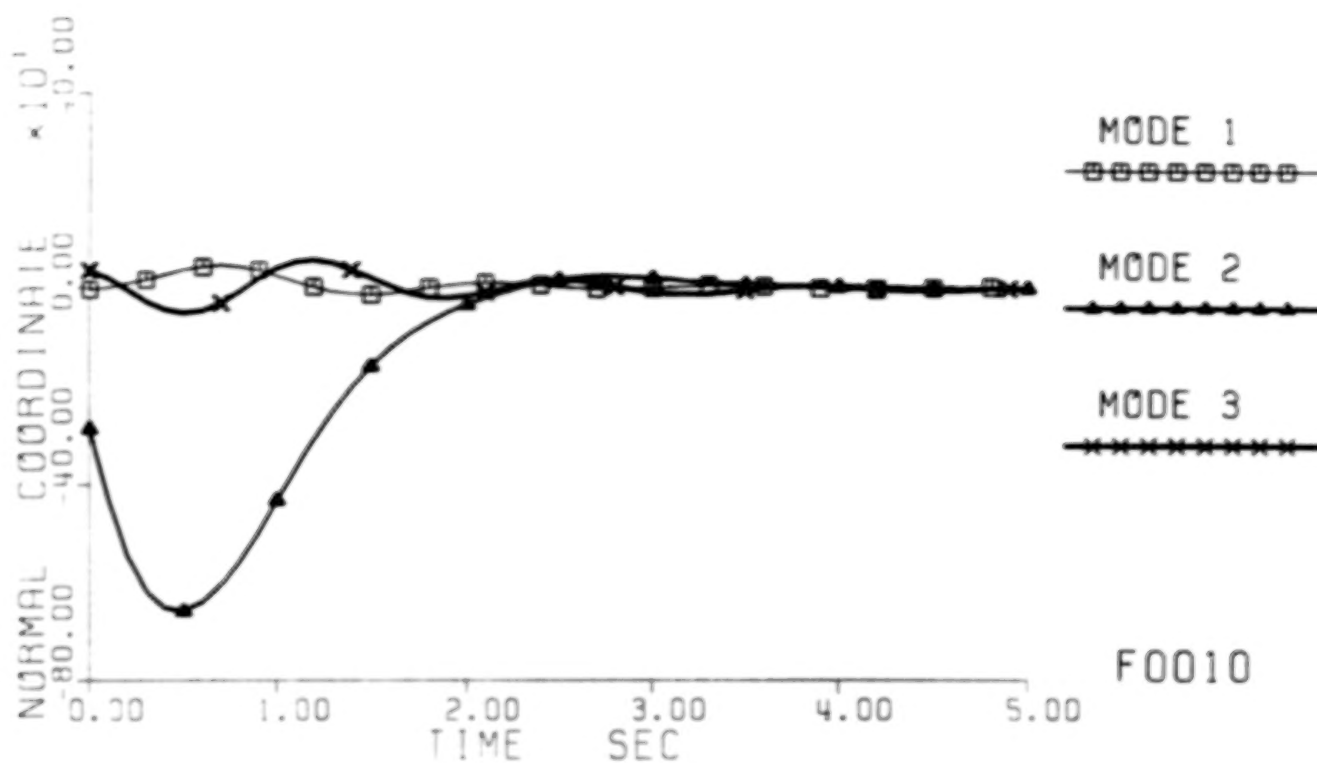


Fig. 6-1 Simulation results of vibration control design MD1;  
d. Histories of normal coordinates of the 10 modes.



value of the arcsine function) because of its large rate of change at the very instant of switching from pointing maneuver to vibration control. Nevertheless, the LOS error was suppressed down within  $18.46^\circ$  after only 2.5 sec of active vibration control and remained below  $17.54^\circ$  thereafter. Moreover, it was even reduced to  $11.79^\circ$  in 3.1 sec.

The bending of the mast beam was very rapidly suppressed to virtually null. Observe in particular that even the y-directionally deflection at the Reflector end (i.e.,  $y_{14}$ ) continued to increase to 119.7 ft (again because of the large "initial" rate of change), it was suppressed down into the band of  $\pm 5$  ft in only 2 sec, and into the band of  $\pm 0.5$  ft in 4.2 sec. It is interesting to notice that it took less than 2.9 sec\* to settle within 2.4 ft, 2% of the peak value. Recall that a 2% settling time of 3 sec for Mode 2 was used in the design.

Fig. 6-1c shows the rapid reduction of the initially large deviations in the Shuttle and Reflector attitude angles to zero in a very short time. The last peak deviation of the Reflector roll, pitch and yaw attitude angles is only  $0.460^\circ$ ,  $0.546^\circ$  and  $1.360^\circ$ , respectively.

Fig. 6-1d shows that the large-magnitude vibrations of first five modes all were rapidly suppressed to virtually zero in a very short time. Note in particular that this vibration control was **very effective** for **quick** reduction of the **excessively large magnitude** of Mode 2. Observe, on the other hand, that Mode 5, the secondary candidate, was reduced only in a moderate rate by a moderate amount, but recall that it was not really significant at first place with respect to excitation by the BPB maneuver nor its contribution to the LOS error. Mode 5 did not need much active control anyway, and hence only a very small additional damping was designed for it.

The vibrations in other modes (i.e., Modes 6 to 10) remained virtually in the same insignificant levels as before, and hence their plots are omitted. Still their magnitudes were more or less decreased with time because of some concomitant additional damping as a side benefit of spillover.\*\*

## 6.2 Simulation Results of A Modified Version of MD1A

We also tried a few other versions of the modal dashpot design MD1 by varying the additional damping coefficient  $\delta_1$ \* desired of Mode 2. Because of the saturation of the actuators at the imposed limits, it is reasonable to consider some smaller feedback gains. The following is a typical case.

---

\* The peak occurred at  $t = 0.5$  sec whereas the deflection was  $-2.24$  ft at  $t = 3.4$  sec.

\*\* In the standard LQG design, one will generally try hard to reduce spillover because it has been well known to degrade performance and even to introduce closed-loop instability. With a modal-dashpot design, **spillover can be beneficial instead**, in leaking some active damping forces to unmodeled modes. Such is particularly the case when the design is not carefully focussed. The side benefit in our design was **intentionally minimized** because we tried to maximize our effort on the most important modes and matched them with most influential control actuators to minimize the leak.

This version, let us call it MD1A, is almost the same as before, except that the additional damping ratio  $\zeta_2^*$  desired of Mode 2 was arbitrarily set equal to that of Mode 1; namely,

$$\zeta_2^* = \zeta_1^* = 0.60.$$

Therefore,

$$\delta_2^* = 2 \zeta_2^* \omega_2 = 2 \times 0.6 \times 1.97024 = 2.36429 \quad (6-1)$$

Mode 2 would then have a theoretical 2%-settling time of 3.38 sec.

Using the new value for  $\delta_2^*$  in (5-3b), and repeating Part 1 of the modal dashpot design, the following new value of the feedback gain matrix was readily obtained.

$$G_{LVR} = \begin{bmatrix} .58420557E+01 & .45784262E+00 \\ .42061494E+00 & .62209375E+01 \end{bmatrix} \quad (6-2)$$

The same simulation was then repeated with these new values. Results are summarized by the plots in Fig. 6-2. The applied moments and forces shown in Fig. 6-2a are virtually the same as before (Fig. 6-1a) with only some invisible differences. Some meaningful differences do exist in the histories of LOS error and beam deflection.

Observe that the LOS error (in Fig. 6-2b) quickly reduced to about  $9.57^\circ$  from the same initial value ( $71.43^\circ$ ). Similarly, due to large initial rate of change at the end of the pointing maneuver, the LOS error also continued to rise to  $85.61^\circ$  (or  $180^\circ - 64.81^\circ = 115.19^\circ$  if not taking the principal value of the arcsine). The large LOS error was suppressed down to the level of  $16.66^\circ$  in 1.8 sec, and remained under it thereafter. Moreover, it was reduced to  $9.57^\circ$  also 3.1 sec after the vibration control began.

The bending of the Mast was also suppressed down very rapidly. Though it continued to increase to 120.28 ft, the y-directionally deflection at the Reflector end (i.e.,  $y_{14}$ ) was suppressed down into the band of  $\pm 7.35$  ft in less than 1.8 sec., and into the band of  $\pm 0.75$  ft in 3.7 sec. It took less than 3 sec for the large deflection to settle down to the band of 2% of the peak\*, i.e.,  $\pm 2.4$  ft. Recall that 3.38 sec is the theoretical 2%-settling time used for Mode 2 in this modified design.

The histories of attitude changes (Fig. 6-2c) and modal responses (Fig. 6-2d) are again virtually the same as before (compared to Figs. 6-1c and 6-1d, respectively) with only some invisible or insignificant differences. The last peak deviation of the Reflector roll, pitch, and yaw attitude angles is only  $0.714^\circ$ ,  $0.582^\circ$ , and  $1.399^\circ$ , respectively.

---

\* The peak occurred at  $t = 0.5$  sec., whereas the deflection was only  $-1.95$  ft at  $t = 3.5$  sec.

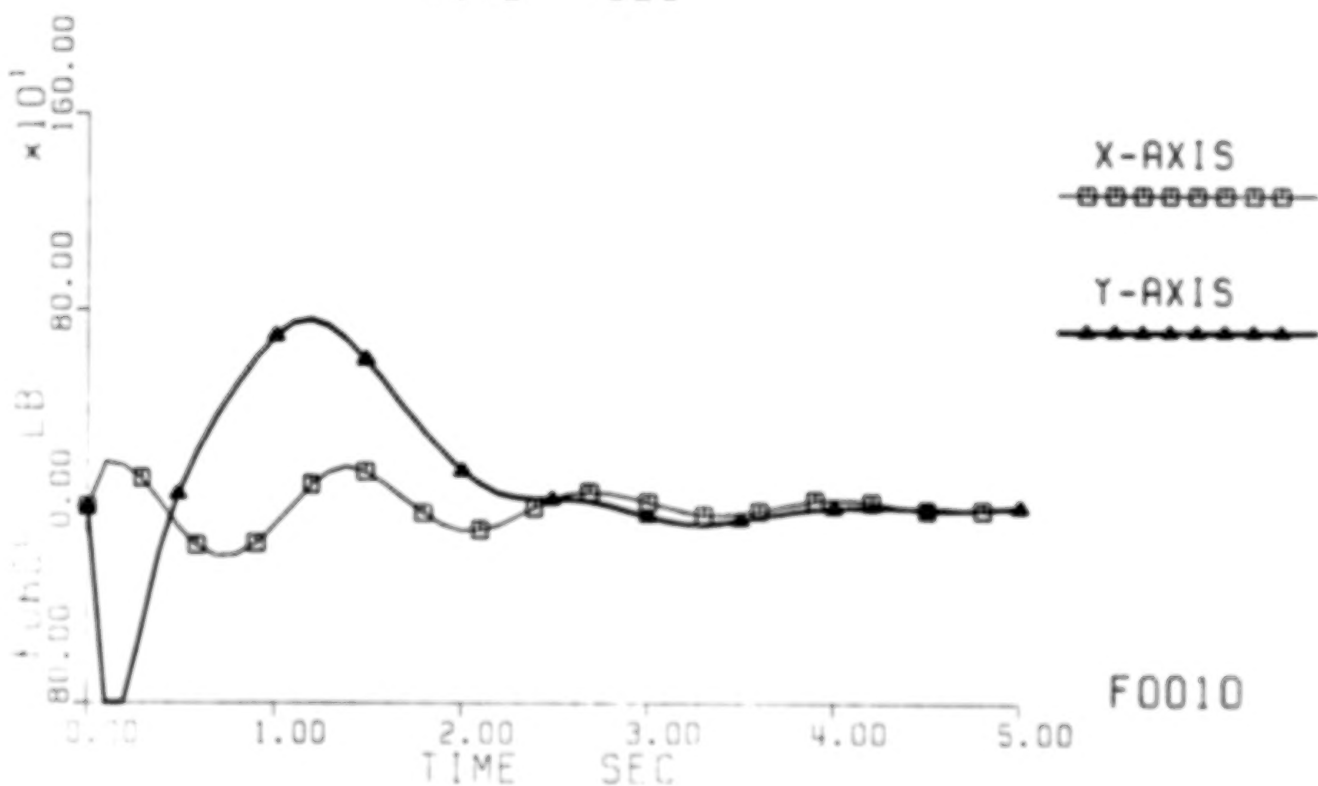
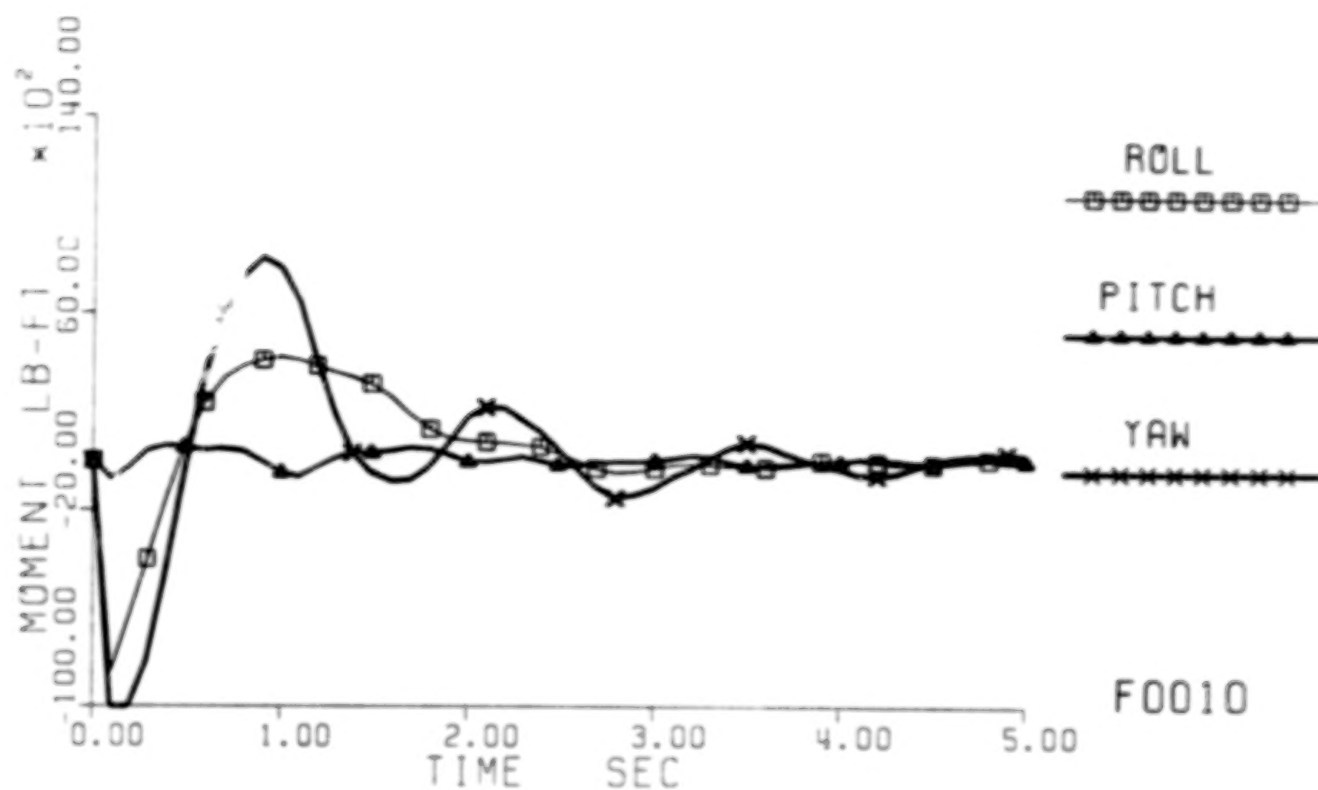


Fig. 6-2 Simulation results of vibration control design MDIA;  
a. Histories of applied moments and forces at the Reflector.

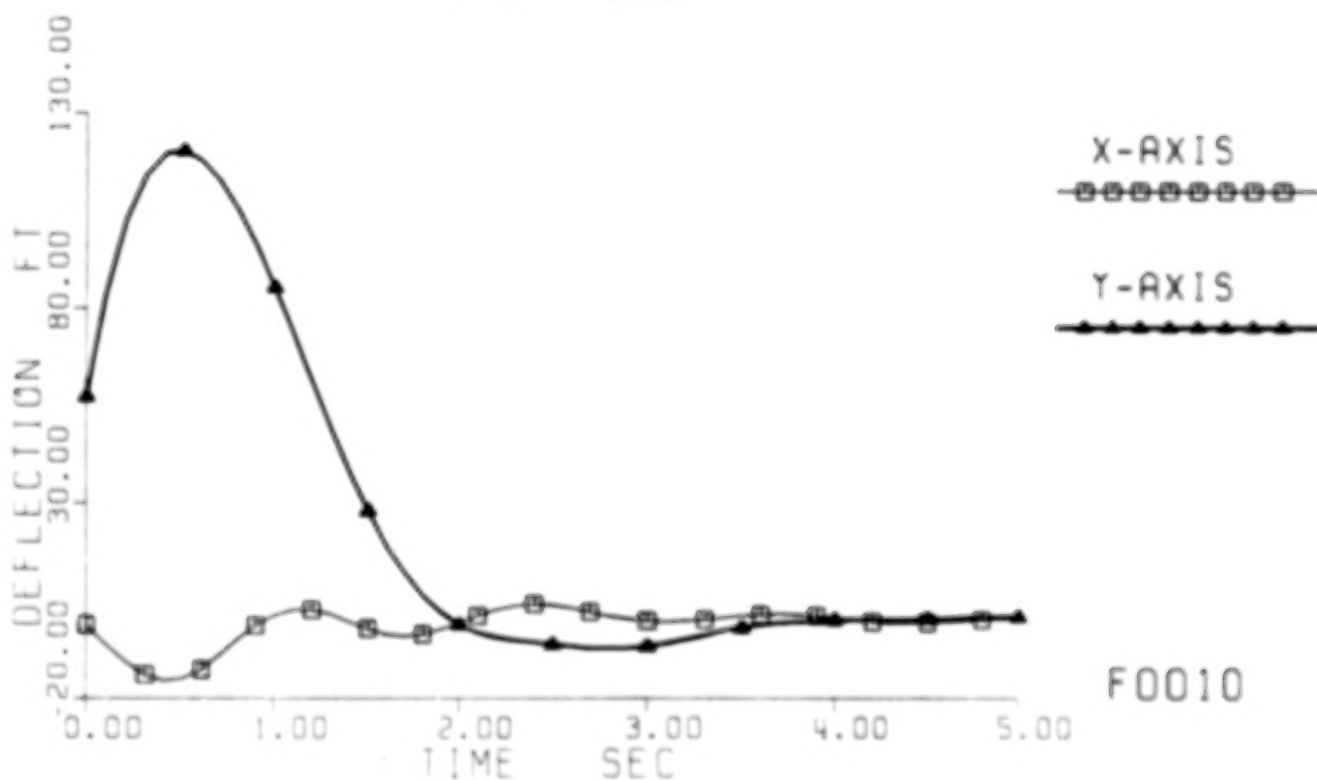
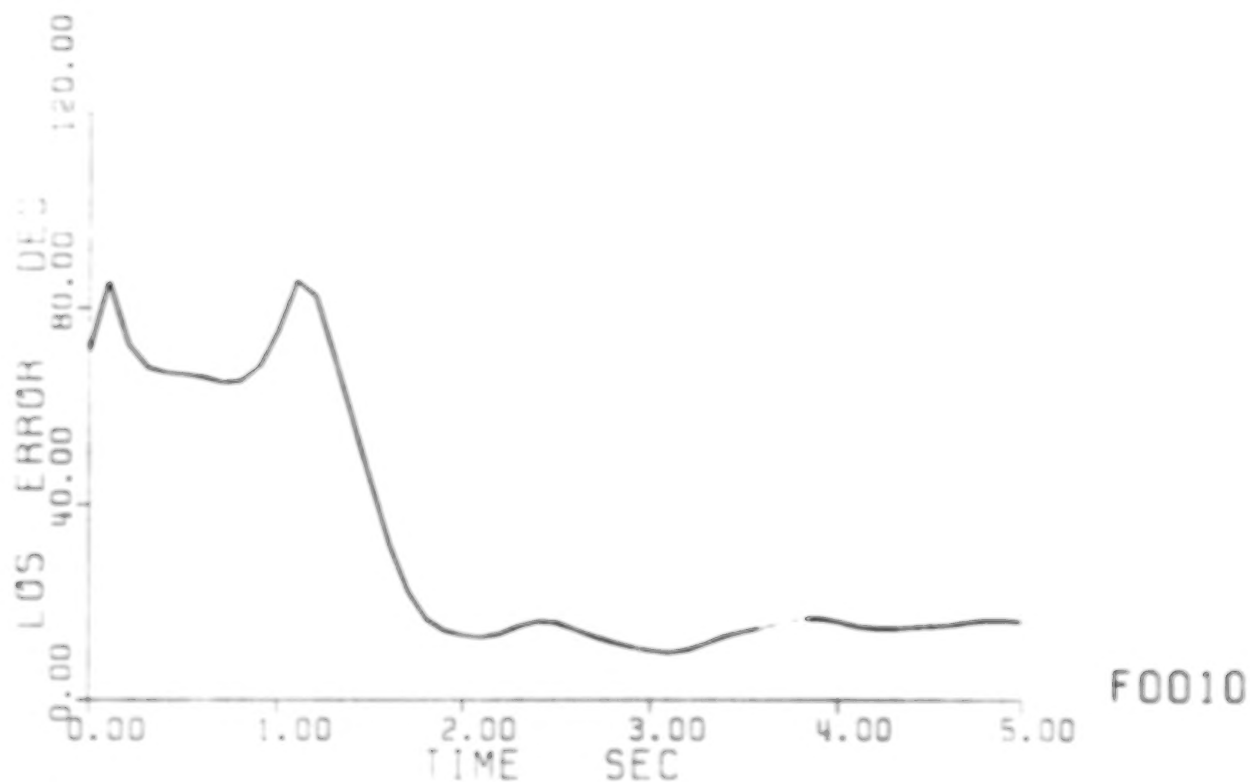


Fig. 6-2 Simulation results of vibration control design MD1A;  
 b. Histories of line-of-sight error and Mast tip deflection.

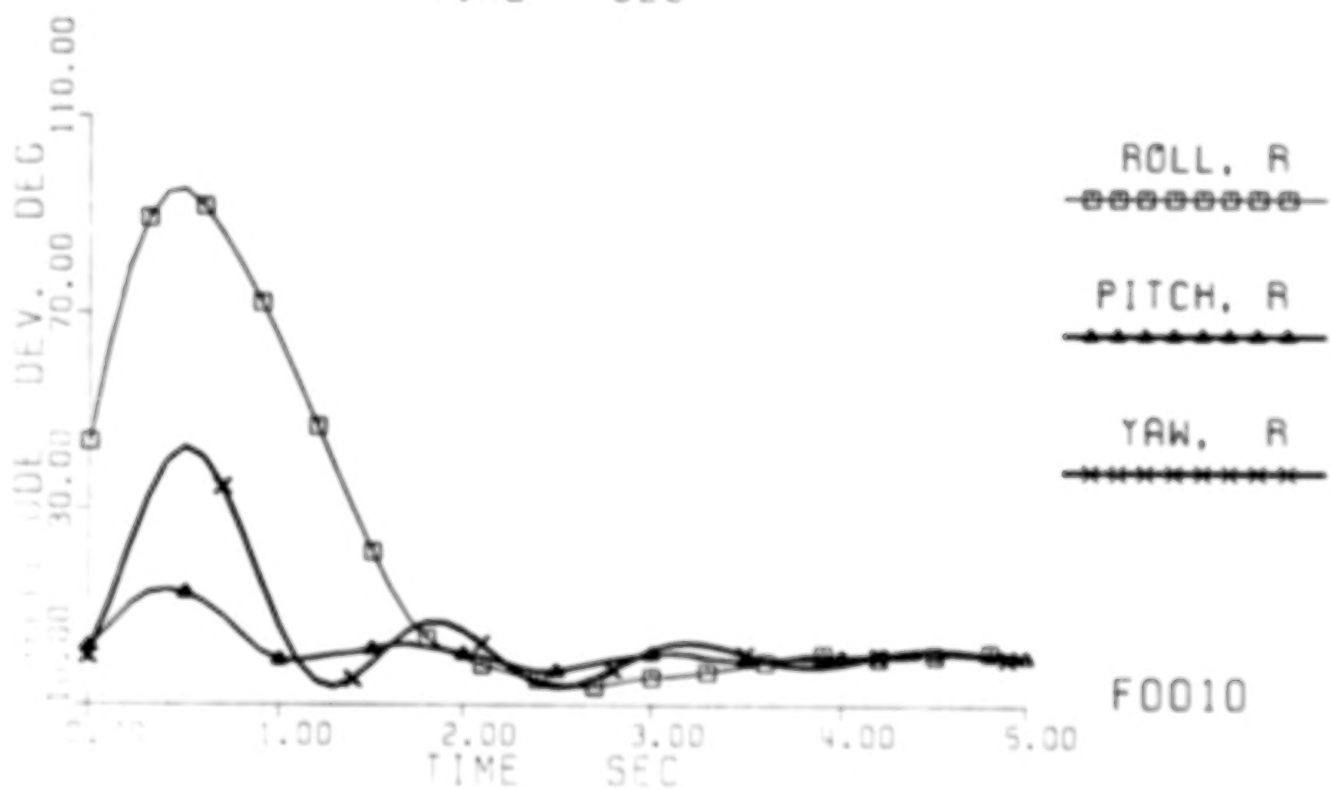
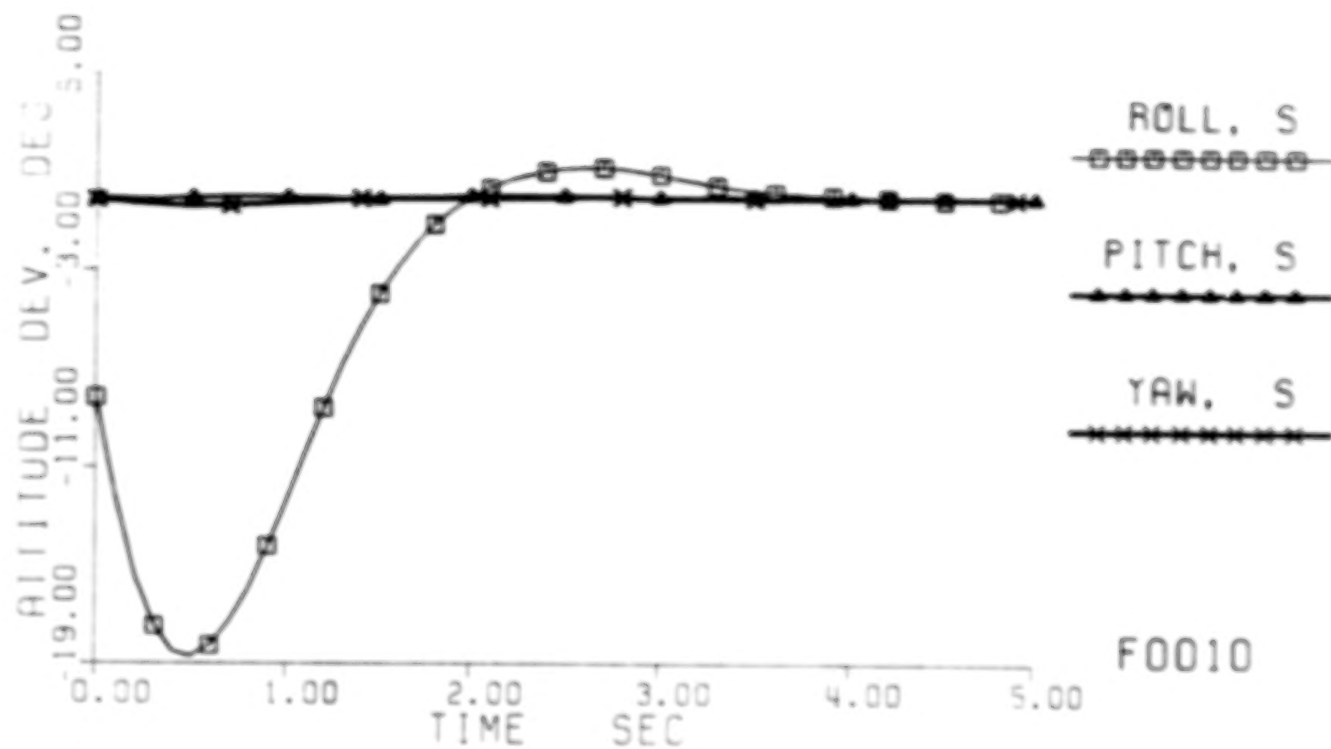


Fig. 6-2 Simulation results of vibration control design MD1A;  
c. Histories of attitude deviations at Shuttle (S) and Reflector (R) ends

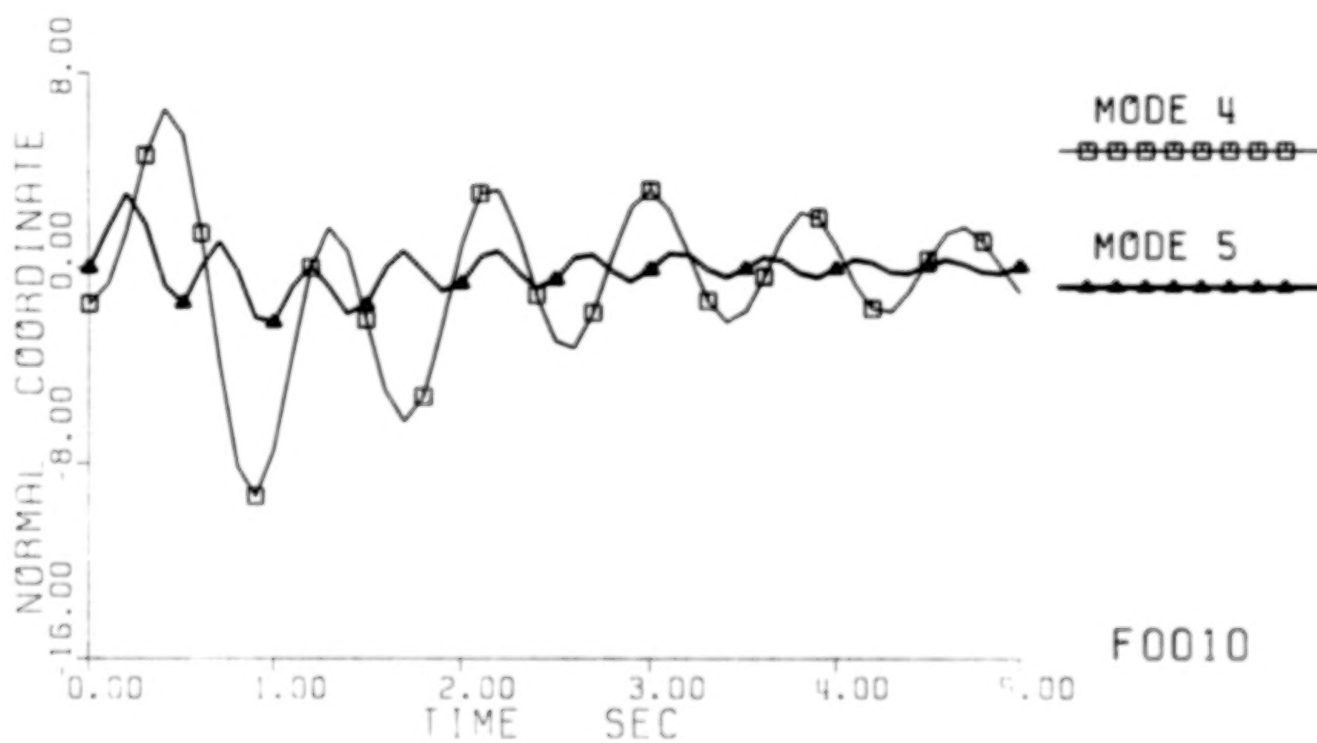
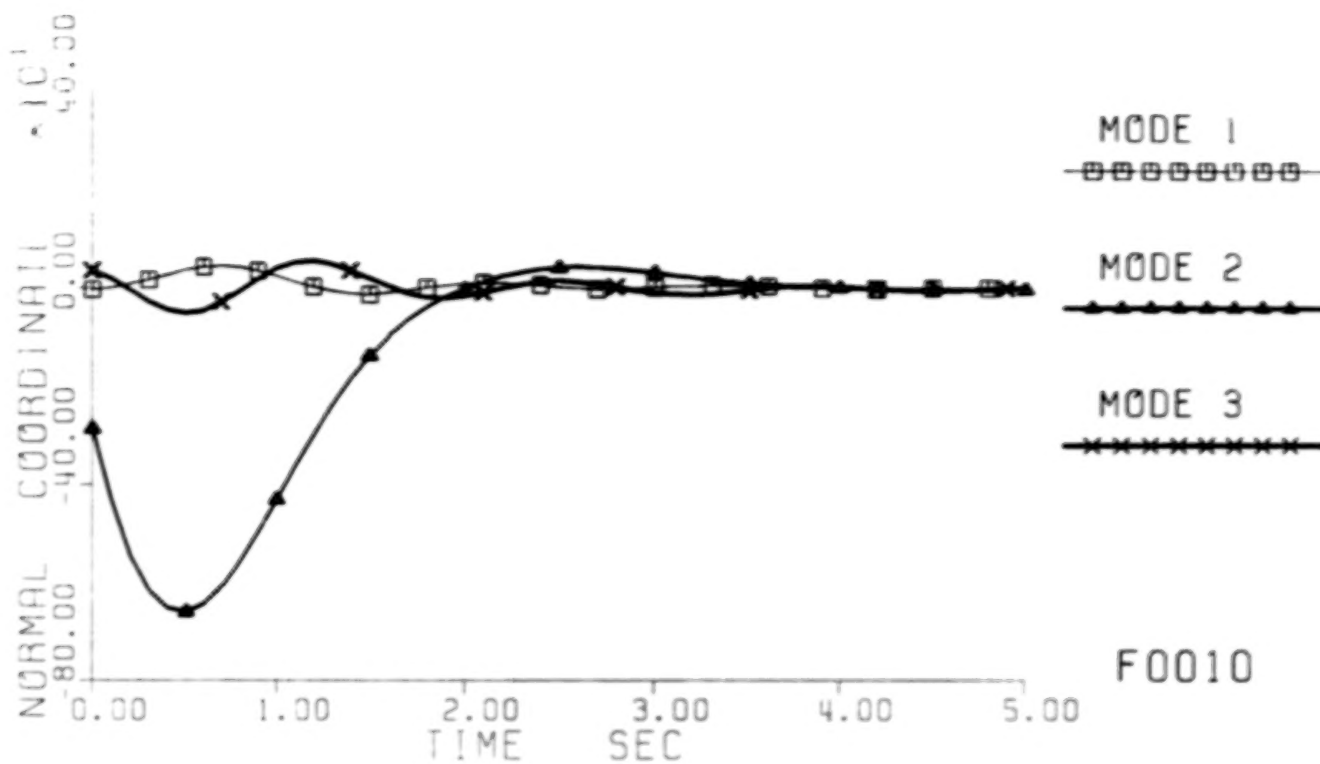


Fig. 6-2 Simulation results of vibration control design MD1A;  
d. Histories of normal coordinates of the 10 modes.

### 6.3 Comments

6.3.1 The modal dashpot designs of vibration control **met the vibration control design challenges fairly well** and are effective and fast in suppressing excessive vibrations. Excited by BPB type rapid pointing slew maneuver, the flexible mast beam deflected between +114 ft and -113 ft, but such an excessive vibration was then quickly suppressed down to less than 0.75 ft in less than 3.7 sec after a modal-dashpot vibration control was turned on. The roll vibration of the Reflector between  $-86.96^\circ$  and  $+88.35^\circ$  during the maneuver was also quickly suppressed down to less than  $0.72^\circ$ . The large LOS error of  $89.8^\circ$  (or  $133.3^\circ$  if not taking the principal value of the arcsine) was also reduced quickly to less than  $17.54^\circ$ .

6.3.2 The original version of the modal dashpot design MD1 performed slightly better than the modified version MD1A in suppressing the deflection of the Mast beam and all the attitude deviations, but not so well in reducing the LOS error. The modified version used a slightly smaller additional damping ratio for Mode 2 in the design, i.e.,

$$\zeta_2^* = 0.60 \text{ instead of } \zeta_2^* = 0.6737.$$

6.3.3 When a velocity feedback control, whether it is of the modal-dashpot type or not, is not properly designed, even feedback gains of an intermediate magnitude can cause severe interactions between modeled and unmodeled (or, equivalently, between "controlled" and "uncontrolled") modes, and hence badly degrade the desired performance of active damping augmentation [24]. The results of these two versions have shown, on the other hand, that if modal dashpots are properly designed, both the modal interactions and the performance degradation are not problems.

Thus, some of the additional damping can be as high as the optimal value 0.707 if necessary, hence can have high feedback gains, to be really effective in quick suppression of vibrations. In other words, **not all velocity output feedback vibration controllers are of low authority, low performance !**

6.3.4 Now, not having to worry about the spillover and modal interaction problems, the feedback gains of properly designed modal dashpots ideally can be as high as the designer wishes. High gains can be as desirable for flexible-body vibration control as they have traditionally been for effective control of rigid bodies.

High gains are desirable for generating comparable negative feedback to offset the vibrations. Theoretically, the higher the better. For example, the version MD1 has a higher gain (because of higher  $\zeta_1^*$ ) than the version MD1A, the deflection and attitude deviations can be continuously suppressed down to smaller values (e.g.,  $\pm 0.5$  ft vs  $\pm 0.75$  ft, in deflection;  $0.46^\circ$  vs  $0.714^\circ$  in Reflector roll angle,...).

The size of the feedback gains for a properly designed modal-dashpot vibration control is virtually limited only by the force and torque capability of the actuators. Since the vibrations were initially very large, the high gains resulted in requiring larger forces and torques than their limits. The simulated saturation thus restrict the applied force/torques to the limits. Therefore, there are no needs to be concerned with high gains as much as before, even the actuators may saturate at their force/torque limits.



6.3.5 Recall that the badly excited modes, i.e., Modes 2 and 1, were **made most strongly controllable and observable** by carefully matching them with actuators and sensors with the strongest influences. Recall also they were strongly controlled by selecting them as modeled modes in the Part 1 design of the modal dashpots and by **adding to them the highest additional damping ratios**. The results of Sections 6.1 and 6.2 show that the resulting modal-dashpot designs are **very effective for fast suppression of large vibrations**. The results also show that **spillover is minimum** and that the unmodeled modes receive some small concomitant additional damping because of spillover.

6.3.6 Unlike all other vibrations (deflections, attitude deviations and modal responses), the LOS error was not reduced to a smaller value by the version MD1 than by the version MD1A. Also, the LOS error was not continuously reduced to near zero as were all other vibrations, although the reduction from its excessively high peak was quite substantial. **Nonlinear properties** of large Euler attitude angles, and the **truncated forces and moments** from the saturated actuators (due to high feedback gains) likely are the causes. We have no clear explanations at the present time. Nevertheless, observe Figs. 3-1c, 6-1c and 6-2c that the Reflector continued to have sufficiently large pitch and yaw rotations during the initial phase of the vibration control, in addition to the main (and larger) roll rotations.

6.3.7 Figs. 6-1 and 6-2 show that after the excessive vibrations have all been suppressed down to sufficiently low levels, the **time rates of change naturally start to become much less significant**, and the modal-dashpot vibration control also starts to become less effective. Unless the feedback gains are increased thereafter, the vibrations may not continue to be reduced to the desired precision in a reasonably short time. One way to achieve the desired precision is to start to increase the modal-dashpot gains progressively after the vibrations become sufficiently small, e.g., after 2 seconds of the initial vibration control.

Another way is to **switch to some form of "modern control"** for completing the vibration suppression and precision pointing. When all the displacements and rates of change have become reasonably small, the whole dynamic system becomes legitimately linear, and the LOS error expression legitimately linearizable. The condition is **very suitable** for application of the modern optimal state-feedback control technique.

Modern control using standard Linear-Quadratic-Gaussian (LQG) optimal state regulators and optimal state estimators has traditionally performed very well in precision pointing and attitude control of rigid-body systems, even using small signals. For application to a flexible-body system, the modern control must be very carefully designed, however; otherwise the notorious spillover problems may destabilize the system instead!

6.3.8 Several major approaches to extend or adapt the LQG design techniques were proposed during the years of **ACOSS** (Active Control of Space Structures) and **VCOSS** (Vibration Control of Space Structures) programs [38]-[45], [15], [46]-[50]. Either the weighting matrices in the control performance index is modified in some ways [51]-[52], or some positivity requirement is imposed on the design [53], or some pre-design compensation of the actuator/sensor influences is made [35]-[36]. All were successful to some limited extents in addressing the major challenge of spillover problems, but are not



readily applicable to realistic large flexible space structures.

Formal applications of the robustness theory [54]-[55] were started recently [56]-[59]. The method of **loop transfer recovery (LTR)** was also applied to recover sizable gain and phase margins of LQ regulators. The modification recently proposed by Blellock and Mingori [58] appears to have made the LTR method more directly applicable to LQG controllers designed for large space structures, so far as the uncertainties in the modal frequencies of the plant are concerned. Recent results obtained by Sundararajan, Joshi, and Armstrong [59] are rather encouraging. Based on their interpretation of spillover problems as additive uncertainty [60], [55], they were able to make an innovative application of the LTR method to **overcome spillover problem** with their LQG attitude controllers designed for the Hoop/Column antenna. This approach has a great potential for practical application to realistic large flexible space structures, since it appears to be able to overcome the spillover problem of an unlimited number of unmodeled modes.

Incorporating modal dashpots into a LQG or LQG/LTR design and following a similar sequence of careful pre-design analyses certainly will greatly enhance the stability and performance of the resulting LQG/MD or LQG/LTR/MD vibration controller. The two proof-mass actuators placed on the mast beam may be used together with all the force and moment actuators on the Reflector and the Shuttle for such a low-power but high-precision control.

## 7. CONCLUSIONS

7.1 The two-stage approach is a feasible and promising one for rapid slewing and precision pointing/retargeting of large flexible space systems and, in particular, the orbital SCOLE configuration. It is capable of rapidly slewing the line-of-sight and settling the excited vibrations in a minimum time. The resulting control design, in general, will consist of the following three parts in cascade:

- Stage 1: a bang-bang type rapid slew maneuver based on the rigid-body dynamics for pointing/retargeting in a minimum time; if excessive vibrations may be excited, using smaller forces and moments should be considered.
- Stage 2, Part 1: a high-power modal-dashpot design of velocity output feedback control based on the flexible-body dynamics for fast and effective reduction of large excited vibrations to a small magnitude;
- Stage 2, Part 2: a LQG/LTR design of optimal state feedback control augmented with a broad-band low-power modal-dashpot design of velocity output feedback control, also based on flexible-body dynamics, for (i) achieving the specified pointing accuracy in a short time and (ii) maintaining the precision and closed-loop system stability. The LQG/LTR design may be incorporated or integrated with an appropriate modal-dashpot design.

7.2 Not all bang-bang (BB) type of time-minimized slew maneuvers will excite large structural vibrations. When large forces are used up to their extremes (for example, 800 lb on the Reflector) to complete the specified slew angle (20°) of the rigidized configuration in the shortest time, the excited vibrations can be excessively large in magnitude (e.g., a 114-ft peak deflection of the 130-ft Mast beam), even only moderated maneuvers of the bang-pause-bang (BPB) type is used instead. On the other hand, when properly selected small forces, e.g., 25 lb, of the kind of **vernier RCS thrusters onboard the Space Shuttle**, are used, **even BB-type maneuvers will excite very little vibrations** (e.g., 0.3 ft peak deflection of the Mast beam).

If the excited vibrations are excessive, a **"high-power" modal-dashpot design** of velocity output feedback control can be used in the first part of the Stage 2 to suppress the vibration down to a reasonable small magnitude **quickly and effectively**. If the excited vibrations are relatively small, or have already been suppressed to a small magnitude, **some modified form of linear-quadratic (LQ) optimal state feedback control augmented with a "low-power" design of modal dashpots** can be used in the Stage 2 to achieve the desired pointing precision.

7.2.1 The vibration modes of the SCOLE configuration were excessively excited when an 800-lb force was applied on the Reflector in the y direction during a BB type slew maneuver. When the best Stage-1 design, i.e., the BPB roll-axis slew having the best LOS pointing accuracy with a minimized slew time (4.89 sec) and the least sensitivity to nonzero products of inertia) was applied to the SCOLE flexible-body dynamics, the Reflector end of the mast vibrated between +114 ft and -113 ft, the Reflector rolled

between  $-86.96^\circ$  and  $+88.35^\circ$ , and the line of sight jittered between  $89.8^\circ$  (or  $133.3^\circ$  if not taking on the principal value of the sine function) and  $14.7^\circ$ .

Our carefully designed modal-dashpot type of velocity output feedback control was able to suppress the excessive vibrations quickly and effectively: the Reflector end deflection down to  $\pm 5$  ft in 2 sec, and to  $\pm 0.5$  ft in 4.2 sec; Reflector roll to  $\pm 3.48^\circ$  in 7.1 sec, and to  $\pm 0.54^\circ$  in 4.4 sec; and the LOS error down to  $11.79^\circ$  in 3.1 sec. In other words, after only about 2 to 3 seconds of applying the "high-power" modal dashpots, the vibrations were reduced to a region where some form of linear-quadratic optimal "state" feedback control (properly augmented with "low-power" modal dashpots) would be effective in further reducing the vibrations and LOS errors to the desired precision.

7.2.2 The large magnitude of the force, i.e., 800 lb, applied on the Reflector was responsible for the excessive excitation of vibrations in the SCOLE configuration. Whether bang-bang type time-optimal slew maneuvers would excite excessive vibrations or not depends on the allowable maximum magnitude of the applied forces. When the limit of the force was decreased to only one tenth (i.e., 80 lb) but the pointing slew maneuver was still performed in a similar time-optimal bang-bang manner for the same  $20^\circ$  angle, the excited vibrations were significantly decreased. The maximum LOS error was  $24.7^\circ$ , comparable to the specified initial value ( $20^\circ$ ) due to the initial misalignment of the SCOLE configuration. The maximum tip deflection (20.6 ft) of the mast beam was also quite reasonable compared to the length of the Mast (130 ft). When no additional forces were applied, however, the vibrations excited by the applied moments alone increased, instead.

We found that if the applied force on the Reflector was about 25 lb, i.e., in the range of the vernier RCS thrusters used on the Space Shuttle, the corresponding time-minimized bang-bang pointing slew maneuver would excite very little vibrations in the SCOLE configuration. The Reflector end of the mast vibrated only between  $+0.25$  ft and  $-0.30$  ft, the Reflector rolled only between  $+0.16^\circ$  and  $-0.30^\circ$ , and the LOS error was at most  $0.51^\circ$ . If the BB slew maneuver was followed immediately by some form of linear-quadratic optimal "state" feedback control (properly augmented with "low-power" modal dashpots), such small vibrations and LOS errors would be easily reduced to the desired precision.

7.2.3 During Stage 1, the BB maneuver using a 25 lb force on the Reflector required 10.96 seconds to complete the  $20^\circ$  slew while the BPB maneuver using a 800 lb force on the Reflector required only 4.89 seconds. A "high-power" modal-dashpot design of velocity output feedback control required additional 2.5 to 3 seconds to bring the excessive vibrations excited by the 800-lb maneuver down to the same order of magnitude as the vibrations excited by the 25-lb maneuver. Therefore, the total time required for both Stage 1 (slew) and Stage 2 (stabilization and precision pointing) is likely to be around 10 and 12 seconds, respectively, for the two cases.

The two stages of the 800-lb BPB maneuver will probably require the least total time, but the excessive vibrations during the maneuver are impractical and undesirable.

The 80-lb BB maneuver requires a similar high-power design of modal-dashpots for quick and effective suppression of the moderately large vibrations to the same order of magnitude as the case of 25-lb maneuver. The total time required for the two stages is likely to be also around 12 seconds or a little less.

7.3 Although modal-dashpot type of velocity output feedback control can be designed as a usual diffuse (or "broad-band") low-power (or "low-authority") control, the simulation results of our careful designs have shown that modal dashpots can also be a concentrated high-power ("high-authority") control for fast and effective suppression of large vibrations. Careful pre-design analyses made it possible to do so for SCOLE.

7.3.1 Our pre-design analysis on the vibration modes of the SCOLE configuration shows that modes 2,3,4,1,5 are the five most important modes requiring for vibration control and LOS error reduction, with mode 2 needing active control the most.

7.3.2 Our Pre-design analysis on the modal control influences of the actuators shows that: two force actuators on the Reflector in x and y directions, respectively, are most effective for controlling modes 1 and 2; three moment actuators also on the Reflector about the x, y, and z (i.e., roll, pitch, and yaw) axes, respectively, are most appropriate for controlling modes 3, 4, and 5.

7.3.3 For quick effective suppression of the excessive vibrations in the SCOLE configuration excited by the time-minimized BPB slew maneuver, it is more appropriate to design the modal dashpots into separate parts than to lumping up all the 5 most important modes to be controlled by all the five actuators together. High gains not only do not create spillover and interaction problems as usual but rather make the resulting modal dashpots truly powerful and effective for quick suppression of excessive vibrations.

7.4 In general, modal dashpots when properly and carefully designed, can add desirable amount of active damping to modeled (or "controlled") modes. Unmodeled modes can also receive some concomitant active damping, as a benefit of spillover to complement their inherent damping.

## 8. RECOMMENDATIONS

We recommend that:

1. the two-stage approach be accepted as a promising one, and included in Part Two of the Design Challenge, for validation using the hardware SCOLE laboratory facility and for comparison with other approaches, and
2. theoretical and simulation studies on the two-stage approach be continued using the mathematical models of both the orbital and the laboratory SCOLE configurations for further development of the technology.

8.1 Careful scientific studies have been successfully conducted on the two-stage approach to rapid pointing and vibration control of the flexible orbital SCOLE configuration, and the results have been very encouraging. Now that the physical SCOLE laboratory facility is operational, we recommend that the design techniques developed and the technical knowledge gained on the two-stage approach be translated to the tethered laboratory SCOLE configuration and be tested and validated by the experimental apparatus. Specifically:

- (1) Design a rapid time-minimize bang-pause-bang line-of-sight pointing slew maneuver (Stage 1), and a fast effective modal-dashpot type of vibration controller (Stage 2), using the mathematical model of the tethered configuration and the actuators and sensors actually available on the laboratory article. Test the designs on the SCOLE facility in real time.
- (2) Then, conduct a comprehensive sequence of experimental evaluations similar to Steps (a) through (e) below.

8.2 To further develop the technology associated with the promising practical two-stage approach and to gain additional technical knowledge, we recommend that studies be conducted on the use of MD-augmented LQG/LTR design of vibration control for attaining the specified LOS pointing accuracy. We also recommend that the limit on the applied force at the Reflector of the orbital SCOLE configuration be lowered by one order of magnitude from 800 lb to between 100 and 200 lb, or alternately between 20 and 30 lb, in each direction.

Specifically, we recommend that:

- (1) a series of design, simulation, study and evaluation be carried out on two representative cases,
- (2) the total time required from the beginning of the LOS pointing slew maneuver to the end of stabilization with the desired 0.02° precision be determined for each case, and
- (3) a trade-off study be conducted.



Case 1. Limit set at 150 lb\*

- (a) Use a Stage 1 design similar to the one described in Section 3.2.2 for the time-minimized pointing slew maneuver. Simulate such a BB slew maneuver on the 3-dimensional nonlinear **rigid body** dynamics of the SCOLE configuration first; evaluate the LOS accuracy, and assess the effects of nonzero products of inertia during the rapid maneuver; compare the results with BPB slew maneuver with the 800-lb limit.

Then simulate this slew maneuver on the **flexible-body** dynamics of the configuration as if it were a time-varying disturbance, and analyze the vibrations thus excited.

- (b) Design a similar high-power modal-dashpot type of velocity output feedback control (following the same design procedure as in Section 5). Such a vibration control design is to be used, as the first part of Stage 2 for suppressing the (moderately) excited vibrations quickly and effectively to some desirable low levels.
- (c) Design a "low-power" modal dashpot (MD) type of velocity output feedback control first. Augment the SCOLE configuration with the resulting modal dashpot design. Then design a LQG/LTR type of optimal state feedback control. Such a **LQG/LTR/MD control design** is to be used as the second part of Stage 2 for continuing on suppressing the vibrations quickly to the desired LOS pointing accuracy of  $0.02^\circ$ . All force and moment actuators, including the two proof-mass actuators, are to be used in both the MD and the LQG/LTR/MD designs.
- (d) Simulate the entire Stage 2 design on the SCOLE flexible-body dynamics and evaluate the vibration control performance numerically.
- (e) Integrate the Stage-1 and Stage-2 designs (for a continuous operation of both pointing slew and vibration control), simulate their application on the coupled SCOLE dynamics (i.e., flexible-body dynamics kinematically coupled with rigid-body dynamics); evaluate the **total** LOS pointing and vibration control performance and determine the **total** time required for achieving the desired precision.

Case 2. Limit set at 25 lb

Use the same Stage 1 design as described in Section 3.2.3, instead of Section 3.2.2, for the time-minimized pointing slew maneuver. Conduct all the corresponding sequence of design, simulation, and evaluation as Case 1 except step (b).

---

\* In the laboratory SCOLE configuration, the equivalent torque the thrusters on the Reflector can generate is about two times the torque producible by the CMG on the Shuttle. For the same ratio, the applied force on the Reflector of the orbital SCOLE configuration is approximately 160 lb.

## REFERENCES

- [1] L.W. Taylor, Jr., and A.V. Balakrishnan, "A Mathematical Problem and A Spacecraft Control Laboratory Experiment (SCOLE) Used to Evaluate Control Laws for Flexible Spacecraft... NASA/IEEE Design Challenge," presented at NASA/ACC Workshop on Identification and Control of Flexible Space Structures, San Diego, CA, June 4-6, 1984;  
also in Proceedings of SCOLE Workshop--1984, NASA Langley Research Center, Dec., 1984, pp. 1-27.
- [2] J.G. Lin and L.W. Taylor, Jr., "Time-Optimal Bang-Bang Slew of Rigidized SCOLE Configuration," Proceedings of Workshop on Identification and Control of Flexible Space Structures, San Diego, CA, June 1984 (JPL Publication 85-29, April 1, 1985), Vol. I, pp. 383-399.
- [3] J.G. Lin, "Rapid Single-Axis Torque-Bounded Slewing of SCOLE Configuration," paper presented at SCOLE Workshop, NASA Langley Research Center, Hampton, VA, DEC. 6-7, 1984.
- [4] J.G. Lin, "Rapid Torque-Bounded Line-of-Sight Pointing of SCOLE with a Designer's Choice of Initial Alignment," paper presented at SCOLE Workshop, NASA Langley Research Center, Hampton, VA, DEC. 6-7, 1984.
- [5] J.G. Lin, "Rapid Torque-Limited Line-of-Sight Pointing of SCOLE (Spacecraft Control Laboratory Experiment) Configuration," Paper 86-1991, AIAA Guidance, Navigation and Control Conference, Williamsburg, VA, August 1986, pp. 106-114.
- [6] L.S. Pontryagin et al, The Mathematical Theory of Optimal Processes, New York: John Wiley, 1962.
- [7] G. Leitmann, An Introduction to Optimal Control, New York: McGraw-Hill, 1966.
- [8] M.J. Balas, "Active Control of Flexible Systems," J. Optimization Theory and Applications, Vol. 25, No. 3, pp. 415-436, July 1978.
- [9] D.C. Herrick, "An Experimental Investigation of Modern Modal Control," presented at 17th Aerospace Sciences Mtg, New Orleans, AIAA Paper No. 79-0199, Jan. 1979.
- [10] J.R. Canavin, "The Control of Spacecraft Vibrations Using Multivariable Output Feedback," Paper 78-1419, AIAA/AAS Conference, Los Angeles, CA, Aug. 1978.
- [11] "Passive and Active Suppression of Vibration Response in Precision Structures -- State-of-the-Art Assessment, Volume 2: Technical Analysis," Report No. R-1138, C.S. Draper Lab., Cambridge, MA, Feb. 1978.
- [12] J.R. Canavin, "Control Technology for Large Space Structures," Paper 78-1691, presented at AIAA Conf. Large Space Platforms: Future Needs and Capabilities, Los Angeles, CA, Sept. 1978.
- [13] J.N. Aubrun, "Theory of the Control of Structures by Low-Authority Controllers," J. Guidance and Control, Vol. 3, No.3, Sept-Oct 1980, pp.444-451;  
also Paper 78-1689 presented at AIAA Conf. Large Space Platforms: Future Needs and Capabilities, Los Angeles, CA, Sept. 1978.
- [14] J.G. Lin, D.R. Hegg, Y.H. Lin, and J.E. Keat, "Output Feedback Control of Large Space Structures: An Investigation of Four Design Methods," Proc. 2nd VPI&SU/AIAA Symp. Dynamics and Control of Large Flexible Spacecraft,

June 1979, pp. 1-18.

- [15] J.G. Lin, Y.H. Lin, D.R. Hegg, T.L. Johnson, and J.E. Keat, "Actively Controlled Structures Theory-- Interim Technical Report, Volume 1: Theory of Design Methods," Report No., R-1249, C.S. Draper Laboratory, Cambridge, MA, Apr. 1979;  
also Report No. RADC-TR-79-268, Vol. I, Rome Air Force Development Center, Griffiss AFB, NY, Nov. 1979.
- [16] L.E. Elliott, D.L. Mingori, and R.P. Iwens, "Performance of Robust Output Feedback Controller for Flexible Spacecraft," Proceedings 2nd VPI&SU/AIAA Symp. Dynamics and Control of Large Flexible Spacecraft, June 1979, pp. 409-420.
- [17] S.M. Joshi and N.J. Groom, "Modal Damping Enhancement in Large Space Structures Using AMCD's," AIAA J. Guidance and Control, Vol.3, No.5, pp.477-479, Sept-Oct 1980.
- [18] S.M. Joshi, "An Asymptotically Stable Damping Enhancement Controller for Large Space Structures," paper No. AIAA-81-0455, AIAA 2nd Conf. on Large Space Platforms: "Toward Permanent Manned Occupancy in Space", San Diego, Calif., Feb. 1981.
- [19] M.J. Balas, "Direct Velocity Feedback Control of Large Space Structures," AIAA J. Guidance and Control, Vol.2, No.3, pp.252-253, May-June 1979.
- [20] J.G. Lin, "Closed-loop Asymptotic Stability and Robustness Conditions for Large-Scale Systems with Reduced-Order Controllers," Proc. 20th IEEE Conf. Decision and Control, Dec. 1981, pp. 1497-1502.
- [21] J.G. Lin, Y.H. Lin, and R.B. Preston, "Stability Augmentation for Large Space Structures by Modal Dashpots and Modal Springs," Proc. 3rd VIP&SU/AIAA Dynamics and Control of Large Flexible Spacecraft, June 1981, pp. 393-408.
- [22] J.G. Lin, "General Conditions on Reduced-Order Control for Ensuring Full-Order Closed-Loop Asymptotic Stability," Proceedings of NCKU/AAS Intl Symposium on Engineering Sciences and Mechanics, Taiwan, Taiwan, Dec. 29-31, 1981, pp. 1003-1030.
- [23] J.G. Lin, "Closed-Loop Stability and Robustness Conditions for Large Space Systems with Reduced-Order controller," Section 3 in **Active Control of Space Structures--Final Report**, Report No. R-1454, C.S. Draper Lab., Cambridge, MA, Feb. 1981;  
and in **ACOSS Six (Active Control of Space Structures)**, Final Technical Report No. RADC-TR-81-289, Rome Air Force Development Center, Griffiss AFB, NY, October 1981.
- [24] J.G. Lin and W.J. Jasper, "Interaction Problems in Active Damping Augmentation for Large Flexible Space Structures," paper presented at Symposium on Advances and Trends in Structures and Dynamics, Washington, D.C., Oct. 22-25, 1984.
- [25] D.K. Robertson, "Three-Dimensional Vibration Analysis of a Uniform Beam With Offset Inertial Masses at the Ends," NASA Technical Memo. 86393, NASA Langley Research Center, Sept. 1985.
- [26] S.M. Joshi, "A Modal Model for SCOLE Structural Dynamics," paper presented at SCOLE Workshop, NASA Langley Research Center, Dec. 6-7, 1984.
- [27] NASA Office of Aeronautics and Space Technology Notice, "Control of Flexi-



- ble Structures (COFS) Technology Program," Feb. 7, 1986; Update, April 24, 1986.
- [28] "Space Construction Experiment Definition Study (SCEDS) part II Final Report," Report No. GDC-ASP-82-004, General Dynamics Convair Div., April 1982.
  - [29] "Space Construction Experiment Definition Study (SCEDS) part I Final Report," Report No. CSDL-R-1583, C.S. Draper Lab., Aug. 1981
  - [30] J.A. Roebuck, Jr., "Shuttle Considerations for Design of Large Space Structures," NASA Contractor Report 160861, NASA Johnson Space Center, Houston, TX, Nov. 1980;  
also SSD80-0183, Rockwell International Corp; Downey, CA.
  - [31] G.H. Golub and C.F. Van Loan, Matrix Computations, Baltimore: Johns Hopkins Univ. Press, 1983.
  - [32] G.H. Golub and W. Kahan, "Calculating the singular Values and Pseudo-Inverse of a Matrix," SIAM J. Numerical Analysis, Vol. 2, pp.205-224, 1965.
  - [33] T. Henderson, "Active Control of Space Structures (ACOSS) Model 2," Technical Report No. C-5437, C.S. Draper Laboratory, Cambridge, MA, Sept. 1981.
  - [34] R.R. Strunce, D.R. Hegg, J.G. Lin, and T.C. Henderson, "Actively Controlled Structures Theory, Final Report," Report No. R-1338, Vol. 2 of 2, C.S. Draper Lab., Cambridge, MA, Dec. 1979; also, "ACOSS Four (Active Control of Space Structures) Theory Appendix," Final Technical Report RADC-TR-80-78, Vol II (of two), Rome Air Force Development Center, Griffiss AFB, NY, April 1980.
  - [35] J.G. Lin, "Three Steps to Alleviate Control and Observation Spillover Problems of Large Space Structures," Proc. 19th IEEE Decision and Control conf., Dec. 1980, pp. 438-444.
  - [36] J.G. Lin, "Reduction of Control and Observation Spillover in Vibration Control of large Space Structures," Paper No. 79-1763 presented at AIAA Guidance and Control Conf., Boulder, CO, Aug. 1979;  
also Section 2 in **Actively Controlled Structures Theory, Final Report**, Report No. R-1338, Vol. 1 of 2, C.S. Draper Lab., Cambridge, MA, Dec. 1979, and in **ACOSS Four (Active Control of Space Structures) Theory**, Final Technical Report No. RADC-TR-80-78, Vol I (of two), Rome Air Force Development Center, Griffiss AFB, NY, April 1980.
  - [37] S.M. Joshi, "Robustness Properties of Collocated Controllers for Flexible Spacecraft," J. Guidance, Control, and Dynamics, Vol. 9, No. 1, January-February 1986, pp. 85-91.
  - [38] J.R. Sesak, "ACOSS One (Active Control of Space Structures) Phase I," Report No. RADC-TR-80-79, Rome Air Development Center, Griffiss AFB, NY, Mar. 1980 (General Dynamics Convair Division: contractor).
  - [39] J. R. Sesak, "ACOSS Seven (Active Control of Space Structures) Final Technical Report," Report No. RADC-TR-81-241, Rome Air Development Center, Griffiss AFB, NY, Sept. 1981 (General Dynamics Convair Division: contractor).
  - [40] M.G. Lyons, J.N. Aubrun, G. Margulies, N.K. Gupta, et al, "ACOSS Three (Active Control of Space Structures) Phase I," Report No. RADC-TR-80-131, Rome Air Development Center, Griffiss AFB, NY, May 1980 (Lockheed Missiles & Space Company: contractor).
  - [41] J. N. Aubrun, J. A. Breakwell, N. K. Gupta, M. G. Lyons and G. Margulies,

- "ACOSS Five (Active Control of Space Structures) Phase 1A," Report No. RADC-TR-82-21, Rome Air Development Center, Griffiss AFB, NY, Mar. 1982 (Lockheed Missiles & Space Company: contractor).
- [42] J.N. Auburn, "ACOSS Twelve (Active Control of Space Structures)," Report No. RADC-TR-82-320, Rome Air Development Center, Griffiss AFB, NY, Dec. 1982 (Lockheed Missiles & Space Company: contractor)
- [43] R.P. Iwens, R.J. Benhabib, and F.C. Tung, "ACOSS Eight (Active Control of Space Structures), Phase II," Report No. RADC-TR-81-242, Rome Air Development Center, Griffiss AFB, NY, Sept. 1981 (TRW: contractor).
- [44] "Vibration Control of Space Structures VCOSS-A; High and Low Authority Implementation," AFWAL-TR-83-3074, Flight Dynamics Laboratory, Air Force Wright Aeronautical Laboratories, Wright-Patterson AFB, Ohio, July 1983 (Lockheed Missiles & Space Company: contractor).
- [45] L. Brady, G. Franco, L. Keranen, J. Kern, R. Neiswander and F. Tung, "Vibration Control of Space Structures, VCOSS B: Momentum Exchange and Truss Dampening," Report No. AFWAL-TR-83-3075, Flight Dynamics Laboratory, Air Force Wright Aeronautical Laboratories, Wright-Patterson AFB, Ohio, July 1983 (TRW Space and Technology Group: contractor).
- [46] R.R. Strunce, D.R. Hegg, J.G. Lin, and T.C. Henderson, **ACOSS Four (Active Control of Space Structures) Theory**, Final Technical Report, No. RADC-TR-89-78, Vol I, Apr. 1980 (C.S. Draper Laboratory: contractor).
- [47] R.R. Strunce, J.G. Lin, D.R. Hegg, R.K. Pearson, L.P. Govignon and T.C. Henderson, "ACOSS Six (Active Control of Space Structures) Interim Report," Report No. RADC-TR-80-377, Rome Air Development Center, Griffiss AFB, NY, Jan. 1981 (C.S. Draper Laboratory: contractor).
- [48] R.R. Strunce, J.G. Lin, D.R. Hegg, E. Fogel, J.D. Turner, R.K. Pearson, G. J. Kissel, H. M. Chun and N. H. McClamroch, "ACOSS Six (Active Control of Space Structures) Final Technical Report," Report No. RADC-TR-81-289, Rome Air Development Center, Griffiss AFB, NY, Oct. 1981 (C.S. Draper Laboratory: contractor).
- [49] J.G. Lin, G.J. Kissel, D.R. Hegg, R.K. Pearson, J.D. Turner, H.M. Chun, and E. Fogel, **ACOSS Eleven (Active Control of Space Structures)-- Interim Report, Volume II**, Report No. RADC-TR-82-131-VOL-2, May 1982 (C.S. Draper Laboratory: contractor).
- [50] R.R. Strunce, E. Fogel, D.R. Hegg, J.G. Lin, J.D. Turner, and H.M. Chun, "ACOSS-11 (Active Control of Space Structures) Volume 2 Interim Report," Report No. RADC-TR-82-295-VOL-2, Rome Air Development Center, Griffiss AFB, NY, Nov. 1982 (C.S. Draper Laboratory: contractor).
- [51] N.K. Gupta, "Frequency-Shaped Cost Functionals: Extension of Linear-Quadratic-Gaussian Design Methods," J. Guid. Contr., Vol. 3, No. 6, pp. 529-535, Nov.-Dec. 1980.
- [52] J.R. Sesak, P.W. Likins and T. Coradetti, "Flexible Spacecraft Control by Model Error Sensitivity Suppression," The J. Astronautical Sciences, Vol. 27, No.2, pp.131-156, April-June, 1979.
- [53] R.J. Benhabib, R.P. Iwens and R.L. Jackson, "Stability of Distributed Control for Large Flexible Spacecraft Structures Using Positivity Concepts," AIAA Guidance and Control Conference, Boulder, CO, Aug. 1979.
- [54] J.C. Doyle and G. Stein, "Multivariable Feedback Design Concepts for a

Classical/Modern Synthesis," IEEE Trans. on Automatic Control, Vol. AC-26, No.1, pp.4-16, Feb 1981.

- [55] N.A. Lehtomaki, N.R. Sandell, Jr., and M. Athans, "Robustness Results in Linear-Quadratic Gaussian Based Multivariable Control Designs," IEEE Trans. Automat. Contr., Vol. AC-26, No. 1, pp. 75-93, Feb. 1981.
- [56] R.L. Kosut, H. Salzwedel, and A. Emami-Naeini, "Robust Control of Flexible Spacecraft," AIAA J. Guidance, Control, and Dynamics, Vol. 6, No.2, pp. 104-111, March-April 1983.
- [57] N. Sundararajan, S.M. Joshi and E.S. Armstrong, "Robust Controller Synthesis for a Large Flexible Space Antenna," Proc. 23rd Conf. Decision Contr., 1984, pp. 202-208.
- [58] P.A. Blelloch and D.L. Mingori, "Modified LTR Robust Control for Flexible Structures," Paper 86-2051, AIAA Guidance, Navigation and Control Conference, August 1986, Williamsburg, VA, pp. 314-318.
- [59] N. Sundararajan, S.M. Joshi, E.S. Armstrong, "Attitude Control System Synthesis for the Hoop/Column Antenna Using the LQG/LTR Method," Paper 86-2139, AIAA Guidance, Navigation and Control Conference, August 1986, Williamsburg, VA, pp. 469-478.
- [60] J.B. Cruz, Jr., J.S. Freudenberg, and D.P. Looze, "A Relationship Between Sensitivity and Stability of Multivariable Feedback Systems," IEEE Trans. Automat. Contr. Vol. AC-26, No.1, pp.66-74, Feb. 1981.

## SLEW MANEUVER DYNAMICS OF SPACECRAFT CONTROL LABORATORY EXPERIMENT (SCOLE)

*Y. P. Kakad*

Dept. of Electrical Engineering  
University of North Carolina at Charlotte  
Charlotte, NC 28223

### ABSTRACT

In this article, the dynamics of slew maneuver of NASA Spacecraft Control Laboratory Experiment (SCOLE) test facility are developed in terms of an arbitrary maneuver about any given axis. The set of dynamical equations incorporate rigid-body slew maneuver and three-dimensional vibrations of the complete assembly comprising the rigid shuttle, the flexible beam, and the reflector with an offset mass. The analysis also includes kinematic nonlinearities of the entire assembly during the maneuver and the dynamics of the interaction between the rigid shuttle and the flexible appendage. The final set of dynamical equations obtained for slewing maneuvers are highly nonlinear and coupled in terms of the flexible modes and the rigid-body modes.

The equations are further simplified and evaluated numerically to include the first ten flexible modes and the SCOLE data to yield a model for designing control systems to perform slew maneuvers.

---

This work was supported by NASA Grant NAG-1-535.

## I. INTRODUCTION

The primary control objective of the Spacecraft Control Laboratory Experiment (SCOLE) is to direct the RF Line-Of-Sight (LOS) of the antenna-like configuration towards a fixed target under the conditions of minimum time and limited control authority [1]. This problem of directing the LOS of antenna-like configuration involves both the slewing maneuver of the entire assembly and the vibration suppression of the flexible antenna-like beam. The study of ordinary rigid-body slew maneuvers has received considerable attention in the literature [2,3] due to the fact that any arbitrary large-angle slew maneuver involves kinematic nonlinearities. This is further complicated in the case of SCOLE by virtue of a flexible appendage deployed from the rigid space shuttle. The dynamics of arbitrary large-angle slew maneuvers of SCOLE model are derived in this report as a set of coupled equations with the rigid-body motions including the nonlinear kinematics and the vibratory equations of the flexible appendage.

The dynamical equations of slewing maneuvers of this large flexible spacecraft are developed by writing the total kinetic and potential energy expressions for the entire system. The energy expressions are further utilized in formulating Lagrange's equations which are expressed in terms of non-generalized co-ordinates using an inertial co-ordinate system and a body-fixed co-ordinate system at the point of attachment of the flexible beam to the shuttle. The generic model used for this analysis consists of a distributed parameter beam with two end masses. The three dimensional linear vibration analysis of this free-free beam model with end masses [4] is incorporated together with rigid-slewing maneuver dynamics which are written in terms of four Euler parameters [5] and angular rotation about an arbitrary axis of rotation to yield the final set of highly nonlinear and coupled equations. In the derivation of the equations, it is assumed that the vibratory analysis is for small motions.

## 2. LIST OF SYMBOLS

$\underline{a}(z)$	Position vector of mass element on the beam from the point of attachment
$B$	Damping matrix
$C$	Inertial frame to body-fixed frame transformation
$\underline{c}$	Position vector from the point of attachment to the mass center of the beam
$D$	Mass density of the beam
$\underline{d}(z, t)$	Displacement vector of mass element in the body-fixed frame
$E$	Modulus of Elasticity
$E_o(t)$	Force applied at the orbiter mass center
$E_2(t)$	Force applied at the reflector mass center
$G_o(t)$	Moment applied about the orbiter mass center
$G_\psi$	Modulus of rigidity for the beam
$I$	Beam cross section moment of inertia
$I_x$	Beam cross section moment of inertia, roll bending
$I_y$	Beam cross section moment of inertia, pitch bending
$I_o$	Equivalent mass moment of inertia
$I_1$	Mass moment of inertia matrix of the shuttle
$I_2$	Mass moment of inertia matrix of the reflector
$J$	Mass moment of inertia matrix of the beam
$K$	Stiffness matrix
$L$	The Length of the beam
$M$	Angular velocity vector transformation
$M_\psi$	Effective moment applied at the reflector c.g.
$m$	Total mass of the flexible beam
$m_1$	Mass of the orbiter
$m_2$	Mass of the reflector



$n$	The maximum number of modes considered
$Q$	The generalized force vector
$q_i$	Generalized coordinates
$\underline{R}$	Position vector of the mass center of the orbiter in the inertial frame
$\underline{r}$	Position vector from the orbiter mass center to the point of attachment
$r_x$	x co-ordinate of the reflector mass center in the body-fixed frame
$r_y$	y co-ordinate of the reflector mass center in the body-fixed frame
$T$	Total Kinetic Energy
$U$	Total Potential Energy
$u_x(z, t)$	The beam deflection in x direction referred to the body-fixed frame
$u_y(z, t)$	The beam deflection in y direction referred to the body-fixed frame
$u_\psi(z, t)$	The torsional deflection about z axis in the body-fixed frame
$\underline{V}$	Velocity vector of the mass center of the orbiter in the body-fixed frame
$\underline{V}_o$	Velocity vector of the point of attachment in the body-fixed frame
$\rho$	Mass per unit length of the flexible beam
$\underline{\Delta}$	Vector representing the axis rotation during the slew maneuver
$\phi_{xi}$	i th Eigenfunction corresponding to $u_x$
$\phi_{yi}$	i th Eigenfunction corresponding to $u_y$
$\phi_{\psi i}$	i th Eigenfunction corresponding to $u_\psi$
$\underline{\theta}$	The attitude of the orbiter in the inertial frame
$\xi$	Slew Angle
$\underline{\omega}$	The angular velocity of the orbiter in the inertial frame

- $\Omega$       The angular velocity of the reflector in the inertial  
                 frame
- $\zeta$       Damping ratio



### 3. ANALYTICS

#### Co-ordinate Systems

The motion of SCOPE assembly when considered as a rigid body in space has six dynamic degrees of freedom: three of these define the location of the mass center, and three define the orientation (attitude) of the body. The motion of this rigid body is governed by newtonian laws of motion expressed in terms of changes in linear momentum and angular momentum. These relationships are valid only when the axes along which the motion is resolved are an inertial frame of reference [9,10]. To define the orientation of the orbiter in space, a set of orthogonal axes fixed in the body is utilized. Then the attitude of the orbiter is defined in terms of the angles  $(\theta_1, \theta_2, \theta_3)$  between the body-fixed axes and the inertial co-ordinate axes. The body-fixed frame origin is located at the point of attachment of the flexible appendage with the rigid shuttle for this analysis (Fig. 1).

The transformation from the inertial frame to the body-fixed frame is given by the matrix,  $C$  as developed in figure 2 where if  $\vec{i}, \vec{j}, \vec{k}$  represent the dexteral set of orthogonal unit vectors fixed in the body-fixed frame and  $\theta_1$  is the rotation about  $\vec{i}$ ,  $\theta_2$  is the rotation about  $\vec{j}$  and  $\theta_3$  is the rotation about  $\vec{k}$ . These rotations are carried out successively as shown in figure 1 and the matrix  $C$  is given as

$$C = \begin{bmatrix} \cos\theta_3 & \sin\theta_3 & 0 \\ -\sin\theta_3 & \cos\theta_3 & 0 \\ 0 & 0 & 1 \end{bmatrix} \begin{bmatrix} \cos\theta_2 & 0 & -\sin\theta_2 \\ 0 & 1 & 0 \\ \sin\theta_2 & 0 & \cos\theta_2 \end{bmatrix} \begin{bmatrix} 1 & 0 & 0 \\ 0 & \cos\theta_1 & \sin\theta_1 \\ 0 & -\sin\theta_1 & \cos\theta_1 \end{bmatrix} \quad (1)$$

Thus  $C^T$  is obtained as

$$C^T = \begin{bmatrix} \cos\theta_2 \cos\theta_3 & -\cos\theta_2 \sin\theta_3 & \sin\theta_2 \\ \sin\theta_1 \sin\theta_2 \cos\theta_3 + \sin\theta_3 \cos\theta_1 & -\sin\theta_1 \sin\theta_2 \sin\theta_3 + \cos\theta_3 \cos\theta_1 & -\sin\theta_1 \cos\theta_2 \\ -\cos\theta_1 \sin\theta_2 \cos\theta_3 + \sin\theta_3 \sin\theta_1 & \cos\theta_1 \sin\theta_2 \sin\theta_3 + \cos\theta_3 \sin\theta_1 & \cos\theta_1 \cos\theta_2 \end{bmatrix} \quad (2)$$

In order to completely define the attitude (orientation), it is needed to relate the rotation angles  $\theta_1$ ,  $\theta_2$ , and  $\theta_3$  to the angular velocity components ( $\omega_1$ ,  $\omega_2$ ,  $\omega_3$ ) of the orbiter. One way of obtaining the required relations is via body-three angles method [5] which was utilized in developing  $C$  matrix in equation (1) and these relations are

$$\begin{aligned}\dot{\theta}_1 &= (\omega_1 \cos \theta_3 - \omega_2 \sin \theta_3) / \cos \theta_2 \\ \dot{\theta}_2 &= (\omega_1 \sin \theta_3 + \omega_2 \cos \theta_3) \\ \dot{\theta}_3 &= (-\omega_1 \cos \theta_3 + \omega_2 \sin \theta_3) \tan \theta_2 + \omega_3\end{aligned}\quad (3)$$

Thus, the angular velocity of the orbiter can be obtained in the inertial frame by means of the following transformation

$$\underline{\omega} = M^T \underline{\dot{\theta}} \quad (4)$$

where the transformation  $M^T$  is given as

$$M^T = \begin{bmatrix} \cos \theta_2 \cos \theta_3 & \sin \theta_3 & 0 \\ -\cos \theta_2 \sin \theta_3 & \cos \theta_3 & 0 \\ \sin \theta_2 & 0 & 1 \end{bmatrix} \quad (5)$$

Although the body-three angles method is used here for obtaining the transformations  $C$  and  $M$ , there are three other methods which can be used to obtain the same transformations. A detailed discussion of all the methods is given in reference [5] and a summary of the transformations using the remaining three methods is given in the Appendix.

### Kinetic Energy

If the position vector of the mass center of the orbiter in the inertial frame (Fig. 3),  $\underline{R}$ , is given as

$$\underline{R} = \begin{bmatrix} R_X \\ R_Y \\ R_Z \end{bmatrix} \quad (6)$$

then the velocity of the mass center in the inertial frame is

$$\underline{V}^I(t) = \begin{bmatrix} \dot{R}_X \\ \dot{R}_Y \\ \dot{R}_Z \end{bmatrix} \quad (7)$$

This velocity can be transformed in the body-fixed frame as

$$\underline{V}(t) = C \begin{bmatrix} \dot{R}_X \\ \dot{R}_Y \\ \dot{R}_Z \end{bmatrix} \quad (8)$$

The velocity of the point of attachment in the body-fixed frame is

$$\underline{V}_a = \underline{V} + \underline{\omega} \times \underline{L} \quad (9)$$

where  $\underline{L}$  is the vector from orbiter mass center to the point of attachment.

Defining the position vector (Fig. 4),  $\underline{a}$ , of a mass element on the beam from the point of attachment (origin of the body-fixed frame) before deformation as

$$\underline{a} = \begin{bmatrix} 0 \\ 0 \\ z \end{bmatrix} \quad (10)$$

and the displacement vector of this mass element as

$$\underline{d}(z,t) = \begin{bmatrix} u_x(z,t) \\ u_y(z,t) \\ 0 \end{bmatrix} \quad (11)$$

the position vector after deflection is given as  $\underline{a} + \underline{d}$ . The kinetic energy in the beam [6] is

$$T_1 = (1/2) m \underline{V}_o^T \underline{V}_o + (1/2) \underline{\omega}^T [J] \underline{\omega} - m \underline{V}_o^T [\underline{c}] \underline{\omega} + (1/2) \int \underline{\dot{d}}^T \underline{\dot{d}} dm + \underline{V}_o^T \int \underline{\dot{d}} dm + \underline{\omega}^T \int \underline{\dot{d}} \underline{\dot{d}} dm + (1/2) \int \left[ \dot{u}_x \dot{u}_y \dot{u}_\psi \right] dI \begin{bmatrix} \dot{u}_x \\ \dot{u}_y \\ \dot{u}_\psi \end{bmatrix} \quad (12)$$

where the vector  $\underline{c}$  is from the point of attachment to the mass center of the beam and if it is assumed that the beam is a thin rod, then it is given as

$$\underline{c} = \begin{bmatrix} c_x \\ c_y \\ c_z \end{bmatrix} = (1/m) \int \underline{a} dm = \begin{bmatrix} 0 \\ 0 \\ -L/2 \end{bmatrix} \quad (13)$$

and using the skew symmetric form for the vector cross product for any two vectors  $\underline{c}$  and  $\underline{\omega}$  (in the same reference frame) as

$$\underline{c} \times \underline{\omega} = [\underline{\tilde{c}}] \underline{\omega}$$

$$\underline{\tilde{c}} = \begin{bmatrix} 0 & -c_z & c_y \\ c_z & 0 & -c_x \\ -c_y & c_x & 0 \end{bmatrix} \quad (14)$$

also, the moment of inertia matrix is given as

$$J = (1/3) \rho L^3 \begin{bmatrix} 1 & 0 & 0 \\ 0 & 1 & 0 \\ 0 & 0 & 0 \end{bmatrix} \quad (15)$$

where  $\rho$  is the mass per unit length of the beam. The last term in the equation (12) corresponding to torsional motion is given as

$$\begin{aligned}
& (1/2) \int \begin{vmatrix} \dot{u}_x' & \dot{u}_y' & \dot{u}_\psi' \end{vmatrix} dI \begin{vmatrix} \dot{u}_x' \\ \dot{u}_y' \\ \dot{u}_\psi' \end{vmatrix} \\
& = (1/2) \int \begin{vmatrix} \dot{u}_x' & \dot{u}_y' & \dot{u}_\psi' \end{vmatrix} \begin{vmatrix} 1/2(\rho ds)s^2 & 0 & 0 \\ 0 & 1/2(\rho ds)s^2 & 0 \\ 0 & 0 & 0 \end{vmatrix} \begin{vmatrix} \dot{u}_x' \\ \dot{u}_y' \\ \dot{u}_\psi' \end{vmatrix} . \quad (16)
\end{aligned}$$

The kinetic energy equation (12) can be simplified as

$$\begin{aligned}
T_1 = & (1/2) \rho L \underline{V}_c^T \underline{V}_c + (1/6) \rho L^3 \left( \omega_1^2 + \omega_2^2 \right) - \rho L \underline{V}_c^T \underline{\dot{C}} \underline{\omega} + \rho L \sum_{i=1}^n \dot{q}_i^2 \\
& + \underline{V}_c^T \underline{\dot{\alpha}} + \underline{\omega}^T \underline{\dot{\beta}} + (1/4) \rho \left[ \sum_{i=1}^n p_{5i} \dot{q}_i^2 + \sum_{i=1}^n p_{6i} \dot{q}_i^2 \right] \quad (17)
\end{aligned}$$

where

$$\begin{aligned}
u_x &= \sum_{i=1}^n \phi_{xi}(s) q_i(t) \\
u_y &= \sum_{i=1}^n \phi_{yi}(s) q_i(t) \\
u_x' &= \sum_{i=1}^n \phi_{xi}'(s) q_i(t) \\
u_y' &= \sum_{i=1}^n \phi_{yi}'(s) q_i(t) \\
u_\psi &= \sum_{i=1}^n \phi_{\psi i}(s) q_i(t) \\
p_{1i} &= \int_0^L \phi_{xi}(s) ds \\
p_{2i} &= \int_0^L \phi_{yi}(s) ds \\
p_{3i} &= \int_0^L s \phi_{xi}(s) ds \\
p_{4i} &= \int_0^L s \phi_{yi}(s) ds \\
p_{5i} &= \int_0^L \left[ s \phi_{xi}' \right]^2 ds \\
p_{6i} &= \int_0^L \left[ s \phi_{yi}' \right]^2 ds \quad (18)
\end{aligned}$$

and

$$\dot{\underline{\alpha}}(t) = \rho \begin{bmatrix} \sum_{i=1}^n p_{1i} \dot{q}_i \\ \sum_{i=1}^n p_{2i} \dot{q}_i \\ 0 \end{bmatrix} \quad (19)$$

$$\dot{\underline{\beta}}(t) = \rho \begin{bmatrix} \sum_{i=1}^n p_{4i} \dot{q}_i \\ \sum_{i=1}^n p_{3i} \dot{q}_i \\ 0 \end{bmatrix} \quad (20)$$

The expressions for  $p_{1i}$ ,  $p_{2i}$ ,  $p_{3i}$ ,  $p_{4i}$ ,  $p_{5i}$ , and  $p_{6i}$  are developed as follows. Note that

$$\phi_{xi}(s) = A_{xi} \sin \beta_i s + B_{xi} \cos \beta_i s + C_{xi} \sinh \beta_i s + D_{xi} \cosh \beta_i s$$

$$\text{where } \beta_i = \left( \frac{\omega_i^2 \rho}{EI} \right)^{1/4}.$$

Since for SCOLE configuration  $EI_x = EI_y$  and  $\beta_{ix} = \beta_{iy}$ ,  $EI$  and  $\beta_i$  are used for both  $\phi_{xi}(s)$  and  $\phi_{yi}(s)$ . However, this may not be true for other configurations.

$$\begin{aligned} p_{1i} &= \int_0^L \phi_{xi}(s) ds \\ p_{2i} &= \int_0^L \phi_{yi}(s) ds \\ p_{1i} &= \frac{1}{\beta_i L^2} \left[ -A_{xi} \cos \beta_i L + B_{xi} \sin \beta_i L + C_{xi} \cosh \beta_i L \right. \\ &\quad \left. + D_{xi} \sinh \beta_i L + A_{xi} - C_{xi} \right] \end{aligned} \quad (21A)$$

Defining  $\alpha_i = \beta_i L$

$$p_{1i} = \frac{1}{\alpha_i L} \left[ -A_{xi} \cos \alpha_i + B_{xi} \sin \alpha_i + C_{xi} \cosh \alpha_i + D_{xi} \sinh \alpha_i + A_{xi} - C_{xi} \right] \quad (21B)$$

similarly,

$$p_{2i} = \frac{1}{\beta_i L^2} \left[ -A_{yi} \cos \beta_i L + B_{yi} \sin \beta_i L + C_{yi} \cosh \beta_i L + D_{yi} \sinh \beta_i L + A_{yi} - C_{yi} \right] \quad (22A)$$

$$p_{2i} = \frac{1}{\alpha_i L} \left[ -A_{yi} \cos \alpha_i + B_{yi} \sin \alpha_i + C_{yi} \cosh \alpha_i + D_{yi} \sinh \alpha_i + A_{yi} - C_{yi} \right] \quad (22B)$$

$$p_{3i} = \int_0^L s \phi_{xi}(s) ds$$

$$p_{4i} = \int_0^L s \phi_{yi}(s) ds$$

and these can be given as

$$p_{3i} = A_{xi} \left[ \frac{\sin \beta_i L}{\beta_i^2} - \frac{L \cos \beta_i L}{\beta_i} \right] + B_{xi} \left[ \frac{\cos \beta_i L}{\beta_i^2} + \frac{L \sin \beta_i L}{\beta_i} - \frac{1}{\beta_i^2} \right] + C_{xi} \left[ \frac{L \cosh \beta_i L}{\beta_i} - \frac{\sinh \beta_i L}{\beta_i^2} \right] + D_{xi} \left[ \frac{L \sinh \beta_i L}{\beta_i} - \frac{\cosh \beta_i L}{\beta_i^2} + \frac{1}{\beta_i^2} \right] \quad (23A)$$

$$p_{3i} = A_{xi} \left[ \frac{L^2 \sin \alpha_i}{\alpha_i^2} - \frac{L^2 \cos \alpha_i}{\alpha_i} \right] + B_{xi} \left[ \frac{L^2 \cos \alpha_i}{\alpha_i^2} + \frac{L^2 \sin \alpha_i}{\alpha_i} - \frac{L^2}{\alpha_i^2} \right] + C_{xi} \left[ \frac{L^2 \cosh \alpha_i}{\alpha_i} - \frac{L^2 \sinh \alpha_i}{\alpha_i^2} \right] + D_{xi} \left[ \frac{L^2 \sinh \alpha_i}{\alpha_i} - \frac{L^2 \cosh \alpha_i}{\alpha_i^2} + \frac{L^2}{\alpha_i^2} \right] \quad (23B)$$

Similarly,

$$p_{4i} = A_{yi} \left[ \frac{\sin \beta_i L}{\beta_i^2} - \frac{L \cos \beta_i L}{\beta_i} \right] + B_{yi} \left[ \frac{\cos \beta_i L}{\beta_i^2} + \frac{L \sin \beta_i L}{\beta_i} - \frac{1}{\beta_i^2} \right] + C_{yi} \left[ \frac{L \cosh \beta_i L}{\beta_i} - \frac{\sinh \beta_i L}{\beta_i^2} \right] + D_{yi} \left[ \frac{L \sinh \beta_i L}{\beta_i} - \frac{\cosh \beta_i L}{\beta_i^2} + \frac{1}{\beta_i^2} \right] \quad (24A)$$

$$p_{4i} = A_{yi} \left[ \frac{L^2 \sin \alpha_i}{\alpha_i^2} - \frac{L^2 \cos \alpha_i}{\alpha_i} \right] + B_{yi} \left[ \frac{L^2 \cos \alpha_i}{\alpha_i^2} + \frac{L^2 \sin \alpha_i}{\alpha_i} - \frac{L^2}{\alpha_i^2} \right] + C_{yi} \left[ \frac{L^2 \cosh \alpha_i}{\alpha_i} - \frac{L^2 \sinh \alpha_i}{\alpha_i^2} \right] + D_{yi} \left[ \frac{L^2 \sinh \alpha_i}{\alpha_i} - \frac{L^2 \cosh \alpha_i}{\alpha_i^2} + \frac{L^2}{\alpha_i^2} \right] \quad (24B)$$

$$P_{si} = \int_0^L \left[ s \phi_{xi}(s) \right]^2 ds$$

$$P_{si} = \int_0^L \left[ s \phi_{yi}(s) \right]^2 ds$$

and these can be shown to be

$$\begin{aligned}
 P_{si} = & A_{xi}^2 \left[ \frac{\beta_i^2 L^3}{6} + \frac{1}{2} \left[ \frac{L}{2} \cos 2\beta_i L + \left( \frac{L^2 \beta_i}{2} - \frac{1}{4\beta_i} \right) \sin 2\beta_i L \right] \right] \\
 & - A_{xi} B_{xi} \left[ \frac{L}{2} \sin 2\beta_i L + \left( \frac{1}{4\beta_i} - \frac{L^2 \beta_i}{2} \right) \cos 2\beta_i L - \frac{1}{4\beta_i} \right] \\
 & + A_{xi} C_{xi} \left[ \beta_i L^2 \left( \cos \beta_i L \sinh \beta_i L + (\sin \beta_i L \cosh \beta_i L) \right) \right. \\
 & \left. - 2L \left[ \sin \beta_i L \sinh \beta_i L \right] - \frac{1}{\beta_i} \left[ (\cos \beta_i L \sinh \beta_i L) - (\sin \beta_i L \cosh \beta_i L) \right] \right] \\
 & + A_{xi} D_{xi} \left[ \beta_i L^2 \left( \cos \beta_i L \cosh \beta_i L + (\sin \beta_i L \sinh \beta_i L) \right) \right. \\
 & \left. - 2L \left[ \sin \beta_i L \cosh \beta_i L \right] - \frac{1}{\beta_i} \left[ (\cos \beta_i L \cosh \beta_i L) - (\sin \beta_i L \sinh \beta_i L) \right] + \frac{1}{\beta_i} \right] \\
 & + B_{xi}^2 \left[ \frac{\beta_i^2 L^3}{6} - \frac{1}{2} \left[ \frac{L}{2} \cos 2\beta_i L + \left( \frac{L^2 \beta_i}{2} - \frac{1}{4\beta_i} \right) \sin 2\beta_i L \right] \right] \\
 & - B_{xi} C_{xi} \left[ \beta_i L^2 \left( \sin \beta_i L \sinh \beta_i L - (\cos \beta_i L \cosh \beta_i L) \right) \right. \\
 & \left. + 2L \left[ \cos \beta_i L \sinh \beta_i L \right] - \frac{1}{\beta_i} \left[ (\cos \beta_i L \cosh \beta_i L) \right. \right. \\
 & \left. \left. + (\sin \beta_i L \sinh \beta_i L) \right] + \frac{1}{\beta_i} \right] \\
 & - B_{xi} D_{xi} \left[ \beta_i L^2 \left( \sin \beta_i L \cosh \beta_i L - (\cos \beta_i L \sinh \beta_i L) \right) \right. \\
 & \left. + 2L \left[ \cos \beta_i L \cosh \beta_i L \right] - \frac{1}{\beta_i} \left[ (\cos \beta_i L \sinh \beta_i L) \right. \right. \\
 & \left. \left. - (\sin \beta_i L \cosh \beta_i L) \right] \right] \\
 & + C_{xi}^2 \left[ \frac{1}{2} \left[ \beta_i L \cosh 2\beta_i L + \left( \frac{\beta_i L^2}{2} + \frac{1}{4\beta_i} \right) \sinh^2 \beta_i L - \frac{\beta_i^2 L^3}{3} \right] \right] \\
 & + C_{xi} D_{xi} \left[ \frac{\beta_i L^2}{2} \cos 2\beta_i L - \frac{L}{2} \sinh 2\beta_i L + \frac{1}{4\beta_i} \cosh 2\beta_i L - \frac{1}{4\beta_i} \right]
 \end{aligned}$$



$$\begin{aligned}
& + D_{xi}^2 \left[ \frac{1}{2} \left[ \beta_i L \cos 2\beta_i L + \left( \frac{\beta_i L^2}{2} + \frac{1}{4\beta_i} \right) \sinh^2 \beta_i L + \frac{\beta_i^2 L^3}{3} \right] \right] \quad (25) \\
P_{xi} = & A_{yi}^2 \left[ \frac{\beta_i^2 L^3}{6} + \frac{1}{2} \left[ \frac{L}{2} \cos 2\beta_i L + \left( \frac{L^2 \beta_i}{2} - \frac{1}{4\beta_i} \right) \sin 2\beta_i L \right] \right] \\
& - A_{yi} B_{yi} \left[ \frac{L}{2} \sin 2\beta_i L + \left( \frac{1}{4\beta_i} - \frac{L^2 \beta_i}{2} \right) \cos 2\beta_i L - \frac{1}{4\beta_i} \right] \\
& + A_{yi} C_{yi} \left[ \beta_i L^2 \left[ (\cos \beta_i L \sinh \beta_i L) + (\sin \beta_i L \cosh \beta_i L) \right] - 2L \left[ \sin \beta_i L \sinh \beta_i L \right] \right. \\
& \quad \left. - \frac{1}{\beta_i} \left[ (\cos \beta_i L \sinh \beta_i L) - (\sin \beta_i L \cosh \beta_i L) \right] \right] \\
& + A_{yi} D_{yi} \left[ \beta_i L^2 \left[ (\cos \beta_i L \cosh \beta_i L) + (\sin \beta_i L \sinh \beta_i L) \right] - 2L \left[ \sin \beta_i L \cosh \beta_i L \right] \right. \\
& \quad \left. - \frac{1}{\beta_i} \left[ (\cos \beta_i L \cosh \beta_i L) - (\sin \beta_i L \sinh \beta_i L) \right] + \frac{1}{\beta_i} \right] \\
& + B_{yi}^2 \left[ \frac{\beta_i^2 L^3}{6} - \frac{1}{2} \left[ \frac{L}{2} \cos 2\beta_i L + \left( \frac{L^2 \beta_i}{2} - \frac{1}{4\beta_i} \right) \sin 2\beta_i L \right] \right] \\
& - B_{yi} C_{yi} \left[ \beta_i L^2 \left[ (\sin \beta_i L \sinh \beta_i L) - (\cos \beta_i L \cosh \beta_i L) \right] + 2L \left[ \cos \beta_i L \sinh \beta_i L \right] \right. \\
& \quad \left. - \frac{1}{\beta_i} \left[ (\cos \beta_i L \cosh \beta_i L) + (\sin \beta_i L \sinh \beta_i L) \right] + \frac{1}{\beta_i} \right] \\
& - B_{yi} D_{yi} \left[ \beta_i L^2 \left[ (\sin \beta_i L \cosh \beta_i L) - (\cos \beta_i L \sinh \beta_i L) \right] + 2L \left[ \cos \beta_i L \cosh \beta_i L \right] \right. \\
& \quad \left. - \frac{1}{\beta_i} \left[ (\cos \beta_i L \sinh \beta_i L) - (\sin \beta_i L \cosh \beta_i L) \right] \right] \\
& C_{yi}^2 \left[ \frac{1}{2} \left[ \beta_i L \cosh 2\beta_i L + \left( \frac{\beta_i L^2}{2} + \frac{1}{4\beta_i} \right) \sinh^2 \beta_i L - \frac{\beta_i^2 L^3}{3} \right] \right] \\
& C_{yi} D_{yi} \left[ \frac{\beta_i L^2}{2} \cos 2\beta_i L - \frac{L}{2} \sinh 2\beta_i L + \frac{1}{4\beta_i} \cos 2\beta_i L - \frac{1}{4\beta_i} \right] \\
& D_{yi}^2 \left[ \frac{1}{2} \left[ \beta_i L \cos 2\beta_i L + \left( \frac{\beta_i L^2}{2} + \frac{1}{4\beta_i} \right) \sinh^2 \beta_i L + \frac{\beta_i^2 L^3}{3} \right] \right] \quad (26)
\end{aligned}$$

The equations (25) and (26) can alternatively be derived by replacing  $\beta_i = \frac{\alpha_i}{L}$ .

The kinetic energy of the reflector is

$$T_2 = (1/2) m_2 \underline{V}_o^T \underline{V}_o - m_2 \underline{V}_o^T \underline{\tilde{a}}(L) \underline{\omega} + m_2 \underline{V}_o^T \underline{\dot{d}}(L) - (1/2) m_2 \underline{\omega}^T \underline{\tilde{a}}^T(L) \underline{\tilde{a}}(L) \underline{\omega} \\ + m_2 \underline{\omega}^T \underline{\tilde{a}}(L) \underline{\dot{d}}(L) + (1/2) m_2 \underline{\dot{d}}^T(L) \underline{\dot{d}}(L) + (1/2) \underline{\Omega}^T I_2 \underline{\Omega} \quad (27)$$

where  $m_2$  is the mass of the reflector and  $I_2$  is the mass moment of inertia matrix of the reflector. The deflection vector  $\underline{d}(L)$  at the mass center of the reflector is given as

$$\underline{d}(L) = \begin{bmatrix} u_x(L) - r_y \dot{\psi}(L) \\ u_y(L) + r_x \dot{\psi}(L) \\ u_x'(L)r_x + u_y'(L)r_y \end{bmatrix} \quad (28)$$

and the position vector from the point of attachment to the reflector mass center is given by

$$\underline{a}(L) = \begin{bmatrix} r_x \\ r_y \\ -L \end{bmatrix}. \quad (29)$$

Thus,

$$\underline{\dot{d}}(L) = \begin{bmatrix} \dot{u}_x(L) - r_y \dot{\psi}(L) \\ \dot{u}_y(L) + r_x \dot{\psi}(L) \\ \dot{u}_x'(L)r_x + \dot{u}_y'(L)r_y \end{bmatrix}. \quad (30)$$

The angular velocity of the reflector in the inertial co-ordinate system  $\underline{\Omega}$  can be shown to be

$$\underline{\Omega} = \underline{\omega} + \begin{bmatrix} \dot{\psi} \\ \dot{\psi} \\ \dot{\psi} \end{bmatrix}_L. \quad (31)$$

The equation (27) can be simplified as

$$T_2 = (1/2) m_2 \underline{V}_o^T \underline{V}_o - m_2 \underline{V}_o^T \underline{\tilde{a}}(L) \underline{\omega} + m_2 \underline{V}_o^T \underline{\dot{d}}(L) + (1/2) m_2 L^2 [\omega_1^2 + \omega_2^2] \\ + m_2 \underline{\omega}^T \underline{\tilde{a}}(L) \underline{\dot{d}}(L) + (1/2) m_2 \left[ \sum_{i=1}^n \sum_{j=1}^n \phi_{xi}(L) \phi_{xj}(L) \dot{q}_i \dot{q}_j + \right.$$

$$\sum_{i=1}^n \sum_{j=1}^n \phi_{yi}(L) \phi_{yj}(L) \dot{q}_i \dot{q}_j \left| + (1/2) \dot{\underline{P}}^T I_2 \dot{\underline{P}} + (1/2) \underline{\omega}^T I_2 \underline{\omega} \right. \quad (32)$$

where

$$\begin{aligned} \dot{\underline{P}}^T &= \left[ \dot{u}_x \quad \dot{u}_y \quad \dot{u}_\psi \right]_L \\ &= \left[ \sum_{i=1}^n \phi_{xi}(L) \dot{q}_i(t) \quad \sum_{i=1}^n \phi_{yi}(L) \dot{q}_i(t) \quad \sum_{i=1}^n \phi_{\psi i}(L) \dot{q}_i(t) \right] \end{aligned} \quad (33)$$

The kinetic energy of the shuttle,  $T_0$ , is given as

$$T_0 = (1/2) m_1 \underline{V}^T \underline{V} + (1/2) \underline{\omega}^T \left[ I_1 \right] \underline{\omega} \quad (34)$$

where  $m_1$  is the mass of the shuttle and  $I_1$  is the mass moment of inertia matrix of the shuttle.

The total kinetic energy is given as

$$T = T_0 + T_1 + T_2 \quad (35)$$

This can be simplified as

$$\begin{aligned} T &= (1/2) m_0 \underline{V}^T \underline{V} + \underline{\omega}^T \left[ H \right] \underline{V} + (1/2) \underline{\omega}^T \left[ I_0 \right] \underline{\omega} + \rho L \sum_{i=1}^n \dot{q}_i^2 + \underline{V}^T \underline{\dot{\alpha}} \\ &\quad + \underline{\omega}^T \underline{\tilde{r}} \underline{\dot{\alpha}} + \underline{\omega}^T \underline{\dot{\beta}} + m_2 \underline{V}^T \underline{\dot{d}}(L) + m_2 \underline{\omega}^T \underline{\tilde{r}} \underline{\dot{d}}(L) + \\ &\quad m_2 \underline{\omega}^T \underline{\tilde{a}}(L) \underline{\dot{d}}(L) + (1/2) m_2 \left[ \sum_{i=1}^n \left( \phi_{xi}^2(L) + \phi_{yi}^2(L) \right) \dot{q}_i^2 \right] \\ &\quad + (1/2) \dot{\underline{P}}^T I_2 \dot{\underline{P}} + (1/4) \rho \left[ \sum_{i=1}^n p_{5i} \dot{q}_i^2 + \sum_{i=1}^n p_{6i} \dot{q}_i^2 \right] \end{aligned} \quad (36)$$

where

$$\begin{aligned} m_0 &= m_1 + \rho L + m_2 \\ H &= \left[ \rho L + m_2 \right] \underline{\tilde{r}} + m_2 \underline{\tilde{a}}(L) + \rho L \underline{\tilde{c}} \\ I_0 &= I_1 + (1/3) \rho L^3 \begin{bmatrix} 1 & 0 & 0 \\ 0 & 1 & 0 \\ 0 & 0 & 0 \end{bmatrix} + I_2 + J_2 - \rho L \underline{\tilde{r}} \underline{\tilde{r}} - \rho L \underline{\tilde{r}} \underline{\tilde{c}} - m_2 \underline{\tilde{r}} \underline{\tilde{r}} - m_2 \underline{\tilde{r}} \underline{\tilde{a}}(L) \end{aligned}$$

The term  $J_2$  in this equation can be shown to be:

$$J_2 = m_2 \begin{vmatrix} (r_y^2 + L^2) & -r_x r_y & r_x L \\ -r_x r_y & (r_x^2 + L^2) & r_y L \\ r_x L & r_y L & (r_x^2 + r_y^2) \end{vmatrix}.$$

The total kinetic energy expression can be further simplified as

$$T = (1/2) m_0 \underline{V}^T \underline{V} + \underline{\omega}^T \left[ H \right] \underline{V} + (1/2) \underline{\omega}^T \left[ I_0 \right] \underline{\omega} + \underline{V}^T \left[ A_1 \right] \dot{\underline{q}} + \underline{\omega}^T \left[ A_2 \right] \dot{\underline{q}} + (1/2) \dot{\underline{q}}^T \left[ A_3 \right] \dot{\underline{q}} \quad (37)$$

where

$$\begin{aligned} \left[ A_1 \right] \dot{\underline{q}} &= \dot{\underline{\alpha}} + m_2 \dot{\underline{d}}(L) \\ \left[ A_2 \right] \dot{\underline{q}} &= \tilde{r} \dot{\underline{\alpha}} + \tilde{\beta} + m_2 \tilde{r} \dot{\underline{d}}(L) + m_2 \tilde{a}(L) \dot{\underline{d}}(L) \\ \left[ A_3 \right] &= \begin{vmatrix} 0 & & \\ \rho L + m_2 + p_{5i} + p_{6i} & & \\ 0 & & 0 \end{vmatrix} + \left| \left( \phi'(L) \right)^T I_2 \left( \phi'(L) \right) \right|. \end{aligned}$$

In this equation

$$\left( \phi'(L) \right)^T = \begin{vmatrix} \phi_{1x}'(L) & 0 & 0 \\ 0 & \phi_{1y}'(L) & 0 \\ 0 & 0 & \phi_{1\psi}(L) \\ \vdots & \vdots & \vdots \\ \vdots & \vdots & \vdots \\ \phi_{ix}'(L) & 0 & 0 \\ 0 & \phi_{iy}'(L) & 0 \\ 0 & 0 & \phi_{i\psi}(L) \end{vmatrix}$$

Here  $i=2,3,\dots,n$ . The number  $n$  indicates the total number of flexible modes considered.

Equations of motion

Lagrange's equations of motion for the case of independent generalized coordinates  $q_k$  are

$$\frac{d}{dt} \frac{\partial T}{\partial \dot{q}_k} - \frac{\partial T}{\partial q_k} = Q_k - \frac{\partial U}{\partial q_k} \quad (k=1,2,\dots,n) \quad (38)$$

where,  $T = T(\underline{q}, \dot{\underline{q}})$  is the kinetic energy

$U = U(\underline{q})$  is the potential energy, and

$Q_k$  are the generalized forces arising from nonconservative sources.

The generalized co-ordinates are:

$R_X, R_Y, R_Z$  — position of orbiter mass center relative to inertial frame origin.

$\theta_1, \theta_2, \theta_3$  — roll, pitch and yaw angles of orbiter.

$q_1, q_2, \dots, q_n$  — modal deformation co-ordinates for the beam.

The previous kinetic energy expression developed in equation (37) is given in terms of nonholonomic velocities  $\underline{V}$  and  $\underline{\omega}$ , and generalized velocities  $\dot{\underline{q}}$ . Using the notation  $\bar{T}(\underline{V}, \underline{\omega}, \dot{\underline{q}})$  for this kinetic energy expression and  $T$  for kinetic energy expression in terms of generalized velocities, the equations of motion are developed. Thus, equation (37) is rewritten as

$$\begin{aligned} \bar{T} = (1/2) m_o \underline{V}^T \underline{V} + \underline{\omega}^T \left[ H \right] \underline{V} + (1/2) \underline{\omega}^T \left[ I_o \right] \underline{\omega} + \underline{V}^T \left[ A_1 \right] \dot{\underline{q}} \\ + \underline{\omega}^T \left[ A_2 \right] \dot{\underline{q}} + (1/2) \dot{\underline{q}}^T \left[ A_3 \right] \dot{\underline{q}} \end{aligned} \quad (37)$$

#### (a) Translational Equations

From the chain rule applied to equation (37) using equation (8), one gets

$$\begin{bmatrix} \frac{\partial \bar{T}}{\partial R_X} \\ \frac{\partial \bar{T}}{\partial R_Y} \\ \frac{\partial \bar{T}}{\partial R_Z} \end{bmatrix} = C^T \begin{bmatrix} \frac{\partial \bar{T}}{\partial V_1} \\ \frac{\partial \bar{T}}{\partial V_2} \\ \frac{\partial \bar{T}}{\partial V_3} \end{bmatrix} \quad (39)$$

Also, the generalized forces are  $CE(t)$  where

$$E(t) = E_o(t) + E_2(t) \quad (40)$$

$E_o(t)$  represents the force applied at the orbiter mass center and  $E_2(t)$  represents the force applied at the reflector mass center. From Lagrange's equations

$$\frac{d}{dt} \left[ \frac{\partial \bar{T}}{\partial \underline{V}} \right] + C\dot{C}^T \left[ \frac{\partial \bar{T}}{\partial \underline{V}} \right] = E(t) \quad (41)$$

and from equation (37)

$$\left[ \frac{\partial \bar{T}}{\partial \underline{V}} \right] = m_o \underline{V} - H \underline{\omega} + A_1 \dot{\underline{q}} \quad (42)$$

Substituting equation (42) in (41),

$$m_o \dot{\underline{V}} - H \dot{\underline{\omega}} + A_1 \ddot{\underline{q}} = -C\dot{C}^T (m_o \underline{V} - H \underline{\omega} + A_1 \dot{\underline{q}}) + E(t) \quad (43)$$

This can be rewritten as

$$m_o \dot{\underline{V}} - H \dot{\underline{\omega}} + A_1 \ddot{\underline{q}} = \underline{N}_1 + E(t) \quad (44)$$

where the nonlinear term  $\underline{N}_1$  is given as

$$\begin{aligned} \underline{N}_1 &= -C\dot{C}^T (m_o \underline{V} - H \underline{\omega} + A_1 \dot{\underline{q}}) \\ &= -\tilde{\underline{\omega}} (m_o \underline{V} - H \underline{\omega} + A_1 \dot{\underline{q}}) \end{aligned} \quad (45)$$

Here,  $\tilde{\underline{\omega}} = C\dot{C}^T$ .

#### (b) Rotational Equations :

From equation (4)

$$\underline{\omega} = M^T \dot{\underline{\theta}}$$

Again using the chain rule

$$\left[ \frac{\partial \bar{T}}{\partial \underline{\theta}} \right] = M \left[ \frac{\partial \bar{T}}{\partial \underline{\omega}} \right] \quad (46)$$

Also

$$\begin{bmatrix} \frac{\partial T}{\partial \theta_1} \\ \frac{\partial T}{\partial \theta_2} \\ \frac{\partial T}{\partial \theta_3} \end{bmatrix} = \begin{bmatrix} \frac{\partial V^T}{\partial \theta_1} \\ \frac{\partial V^T}{\partial \theta_2} \\ \frac{\partial V^T}{\partial \theta_3} \end{bmatrix} \left( \frac{\partial \bar{T}}{\partial V} \right) + \begin{bmatrix} \frac{\partial \omega^T}{\partial \theta_1} \\ \frac{\partial \omega^T}{\partial \theta_2} \\ \frac{\partial \omega^T}{\partial \theta_3} \end{bmatrix} \left( \frac{\partial \bar{T}}{\partial \omega} \right) . \quad (47)$$

It can be shown that

$$\frac{\partial V^T}{\partial \theta_i} = \underline{V}^T C \frac{\partial C^T}{\partial \theta_i} \dots i=1,2,3,\dots \quad (48A)$$

and

$$\frac{\partial \omega^T}{\partial \theta_i} = \underline{\omega}^T M^{-1} \frac{\partial M}{\partial \theta_i} \dots i=1,2,3,\dots \quad (48B)$$

and

$$\begin{bmatrix} \frac{\partial T}{\partial \underline{V}} \\ \frac{\partial T}{\partial \underline{\omega}} \end{bmatrix} = \begin{bmatrix} \underline{V}^T C \frac{\partial C^T}{\partial \theta_1} \\ \underline{V}^T C \frac{\partial C^T}{\partial \theta_2} \\ \underline{V}^T C \frac{\partial C^T}{\partial \theta_3} \end{bmatrix} \left( \frac{\partial \bar{T}}{\partial V} \right) + \begin{bmatrix} \underline{\omega}^T M^{-1} \frac{\partial M}{\partial \theta_1} \\ \underline{\omega}^T M^{-1} \frac{\partial M}{\partial \theta_2} \\ \underline{\omega}^T M^{-1} \frac{\partial M}{\partial \theta_3} \end{bmatrix} \left( \frac{\partial \bar{T}}{\partial \omega} \right) . \quad (49)$$

From equation (37),

$$\left( \frac{\partial \bar{T}}{\partial \underline{\omega}} \right) = H \underline{V} + I_o \underline{\omega} + A \underline{\dot{\omega}} \quad (50)$$

and as before

$$\left( \frac{\partial \bar{T}}{\partial \underline{V}} \right) = m_o \underline{V} - H \underline{\omega} + A \underline{\dot{V}} . \quad (42)$$

Using the Lagrange's equations

$$\frac{d}{dt} \left( \frac{\partial T}{\partial \dot{\underline{\theta}}} \right) - \frac{\partial T}{\partial \underline{\theta}} = M \underline{Q} \quad (51)$$

where  $\underline{Q}$  is the net moment about the mass center of the orbiter with respect to the body-fixed frame. It is given as

$$\underline{Q} = \underline{Q}_o + (\underline{r} + \underline{a}) \times \underline{F}_2 \quad (52)$$

$\underline{Q}_o$  is the external moment applied about the mass center. Equation (51) can be simplified by substituting equations (42), (49), and (50) together with the relationship developed in (46) as

$$H \dot{\underline{V}} + I_o \dot{\underline{\omega}} + A \underline{x} \ddot{\underline{x}} = \underline{Q} + \underline{N}_2 \quad (53)$$

where the nonlinear term  $\underline{N}_2$  is given as

$$\underline{N}_2 = M^{-1} \begin{bmatrix} \underline{V}^T C \frac{\partial C^T}{\partial \theta_1} \\ \underline{V}^T C \frac{\partial C^T}{\partial \theta_2} \\ \underline{V}^T C \frac{\partial C^T}{\partial \theta_3} \end{bmatrix} \left( \frac{\partial \underline{T}}{\partial \underline{V}} \right) + M^{-1} \begin{bmatrix} \underline{\omega}^T M^{-1} \frac{\partial M}{\partial \theta_1} \\ \underline{\omega}^T M^{-1} \frac{\partial M}{\partial \theta_2} \\ \underline{\omega}^T M^{-1} \frac{\partial M}{\partial \theta_3} \end{bmatrix} - \dot{M} \left( \frac{\partial \underline{T}}{\partial \underline{\omega}} \right) \quad (54)$$

### (c) Vibration Equations of the Beam

Since  $\underline{T}$  in equation (37) is given in terms of  $\dot{\underline{q}}$  which is a vector of generalized velocities,

$$\frac{\partial \underline{T}}{\partial \dot{\underline{q}}} = \frac{\partial T}{\partial \dot{\underline{q}}}$$

and

$$\left( \frac{\partial \underline{T}}{\partial \dot{\underline{q}}} \right) = A_1^T \underline{V} + A_2^T \underline{\omega} + A_3 \dot{\underline{x}} \quad (55)$$



The potential energy in the beam is given by

$$U = (1/2) \underline{q}^T K \underline{q} \quad (56)$$

where the stiffness matrix K is given as

$$K = \begin{vmatrix} & 0 & \\ & k_{ii} & \\ 0 & & \end{vmatrix} \quad (57)$$

and

$$k_{ii} = EI \beta_i^4 \left[ \int_0^L \phi_{xi}^2(s) ds + \int_0^L \phi_{yi}^2(s) ds \right] + G_\psi \beta_{\psi i}^2 \int_0^L \phi_{\psi i}^2(s) ds$$

$G_\psi$  represents the modulus of rigidity of the beam and  $\beta_{\psi i} = \left[ \frac{D \omega_i^2}{G_\psi} \right]^{\frac{1}{2}}$  where  $D$

is the mass per unit volume (mass density) of the beam. Thus,

$$\left( \frac{\partial U}{\partial \underline{q}} \right) = K \underline{q} \quad (58)$$

Using the Lagrangian Equations (38) and assuming that  $E_2 = Q$ ,

$$A_1^T \dot{\underline{Y}} + A_2^T \dot{\underline{\omega}} + A_3 \underline{\ddot{q}} = -K \underline{q} \quad (59)$$

#### (d) Slewing Equations

If it is considered to perform a slew maneuver about an arbitrary axis  $\underline{\Delta}$  and the slew angle to be  $\xi$ , then the slew maneuver can be expressed in terms of four Euler parameters. These four Euler parameters are defined as

$$\underline{\epsilon} = \begin{bmatrix} \epsilon_1 \\ \epsilon_2 \\ \epsilon_3 \end{bmatrix} = \underline{\Delta} \sin \frac{\xi}{2} \quad (60)$$

$$\epsilon_4 = \cos \frac{\xi}{2} \quad (61)$$

and their derivatives with respect to time are given as

$$\frac{d\epsilon}{dt} = \frac{1}{2} (\epsilon \dot{\omega} + \dot{\omega} \times \epsilon) \quad (62)$$

$$\frac{d\epsilon_4}{dt} = -\frac{1}{2} \dot{\omega} \times \epsilon \quad (63)$$

The four Euler parameters can be related to the angular velocity components of the rigid assembly as

$$\begin{bmatrix} \dot{\epsilon}_1 \\ \dot{\epsilon}_2 \\ \dot{\epsilon}_3 \\ \dot{\epsilon}_4 \end{bmatrix} = \begin{bmatrix} \epsilon_1 & \epsilon_4 & -\epsilon_3 & \epsilon_2 \\ \epsilon_2 & \epsilon_3 & \epsilon_4 & -\epsilon_1 \\ \epsilon_3 & -\epsilon_2 & \epsilon_1 & \epsilon_4 \\ \epsilon_4 & -\epsilon_1 & -\epsilon_2 & -\epsilon_3 \end{bmatrix} \begin{bmatrix} 0 \\ \omega_1 \\ \omega_2 \\ \omega_3 \end{bmatrix} \quad (64)$$

If a slew maneuver is considered to be purely rotational, then the translational velocity and acceleration can be shown to be negligible during the slew maneuver and only the rotational and vibration equations are required for the analysis and they are simplified by setting  $\dot{\underline{V}} \equiv \underline{0}$  in both (53) and (59) and are written as follows

$$I_o \dot{\underline{\omega}} + A_2 \underline{\ddot{q}} = \underline{Q}(t) + \underline{N}_2(\underline{\omega}) \quad (65)$$

$$A_2^T \dot{\underline{\omega}} + A_3 \underline{\ddot{q}} + K \underline{q} = \underline{Q}(t) \quad (66)$$

where,

$\underline{Q}(t)$  is the net moment applied about the mass center of the orbiter and is given by the following equations (figs. 1 & 2)

$$\underline{Q}(t) = \underline{Q}_0(t) + (\underline{r} + \underline{a}) \times \underline{E}_2 \quad (67)$$

Also,  $\underline{Q}(t)$  represents the generalized force vector which is given by the following

equation

$$Q(t) = \begin{bmatrix} \sum_{j=1}^n (Q_{jx_1}(t) + Q_{jy_1}(t)) + Q_{x_1} + Q_{y_1} + Q_{\psi_1} \\ \sum_{j=1}^n (Q_{jx_2}(t) + Q_{jy_2}(t)) + Q_{x_2} + Q_{y_2} + Q_{\psi_2} \\ \vdots \\ \sum_{j=1}^n (Q_{jx_i}(t) + Q_{jy_i}(t)) + Q_{x_i} + Q_{y_i} + Q_{\psi_i} \\ \vdots \end{bmatrix} \quad (68)$$

where, the generalized force components are given as

$$Q_{jx_i} = \int_0^L F_{jx}(z, t) \delta(z - z_j) \phi_{xi}(z) dz \quad (69)$$

$$Q_{jy_i} = \int_0^L F_{jy}(z, t) \delta(z - z_j) \phi_{yi}(z) dz \quad (70)$$

and

$$Q_{j\psi_i}(t) = 0 \quad (71)$$

Here,  $F_{jx}(z, t)$  is the  $x$  component of the concentrated force applied at location  $j$  on the flexible antenna and  $F_{jy}$  is the  $y$  component of that force.

Also,

$$\begin{aligned} Q_{x1}(t) &= F_{2x}(t) \phi_{x1}(L) \\ Q_{y1}(t) &= F_{2y}(t) \phi_{y1}(L) \\ Q_{\psi}(t) &= M_{\psi}(t) \phi_{\psi1}(L) \end{aligned} \quad (72)$$

Here,  $F_2$  is the force applied at the reflector C. G.

Thus,

$$M_{\phi}(t) = F_{2x}r_y + F_{2y}r_x + M_{2\phi} . \quad (73)$$

The location of reflector C. G. is given by coordinates  $(r_x, r_y)$  and  $M_{2\phi}$  represents the external moment applied at the reflector C. G.

Thus equations (62) - (73) completely represent the dynamics of the slew maneuver. These equations are nonlinear and coupled including both the rigid-body dynamics and the dynamics of the flexible appendage with kinematic nonlinearities. It is important to note that the nonlinear term  $N_2(\underline{u})$  is dependent on the rotational velocity and as a result determined by the slew maneuver rate. Thus the basic slew maneuver strategy has to be developed before this term can be linearized.

#### (e) Vibration Equations of the Beam with Damping

If damping is included in the derivation of vibration equations of the beam, then the damping effect can be expressed in terms of frictional forces. These are nonconservative, retarding forces and are assumed to be proportional to the generalized velocities. In deriving the vibration equations by means of Lagrange's equations, the following function is introduced

$$F_d = \frac{1}{2} \sum_{i=1}^n \sum_{j=1}^n b_{ij} \dot{q}_i \dot{q}_j . \quad (74)$$

It also has a positive definite quadratic form similar to the kinetic and potential energy expressions.

With this definition, Lagrange's equations assume the form

$$\frac{d}{dt} \frac{\partial T}{\partial \dot{q}_k} - \frac{\partial T}{\partial q_k} - \frac{\partial F_d}{\partial \dot{q}_k} = Q_k - \frac{\partial U}{\partial q_k} \quad (k=1,2,\dots,n) \quad (75)$$

Again, as before

$$\left( \frac{\partial T}{\partial \dot{\underline{q}}} \right) = A_1^T \dot{\underline{V}} + A_2^T \dot{\underline{\omega}} + A_3 \dot{\underline{q}} \quad (55)$$

and

$$\left( \frac{\partial U}{\partial \underline{q}} \right) = K \underline{q} \quad (58)$$

and it can be seen from (74) that

$$\left( \frac{\partial F_d}{\partial \dot{\underline{q}}} \right) = B \dot{\underline{q}} \quad (76)$$

where the damping matrix B is symmetrical and is given as

$$B = \begin{bmatrix} b_{11} & b_{12} & \dots & b_{1n} \\ b_{21} & b_{22} & \dots & b_{2n} \\ \vdots & \vdots & \ddots & \vdots \\ \vdots & \vdots & \ddots & \vdots \\ b_{n1} & b_{n2} & \dots & b_{nn} \end{bmatrix} \quad (77)$$

The vibration equations are given as

$$A_1^T \ddot{\underline{V}} + A_2^T \ddot{\underline{\omega}} + A_3 \ddot{\underline{q}} + B \dot{\underline{q}} = -K \underline{q} + \underline{Q}(t) \quad (78)$$

The slewing equations (65) and (66) would be modified as

$$I_2 \dot{\underline{\omega}} + A_2 \ddot{\underline{q}} = \underline{G}(t) + \underline{N}_2(\underline{\omega}, \dot{\underline{q}}) \quad (79)$$

$$A_2^T \dot{\underline{\omega}} + A_3 \ddot{\underline{q}} + B \dot{\underline{q}} = -K \underline{q} + \underline{Q}(t) \quad (80)$$

#### Nonlinear Term in the Rotational Equations

The nonlinear term  $\underline{N}_2$  in the rotational equations (65) and (79) during the slewing maneuver is simplified as

$$\underline{N}_2 = M^{-1} \begin{bmatrix} \underline{\omega}^T M^{-1} \frac{\partial M}{\partial \theta_1} \\ \underline{\omega}^T M^{-1} \frac{\partial M}{\partial \theta_2} \\ \underline{\omega}^T M^{-1} \frac{\partial M}{\partial \theta_3} \end{bmatrix} - \dot{M} \left[ I_0 \underline{\omega} + A_2 \underline{\dot{q}} \right] \quad (81)$$

where

$$\underline{\omega}^T M^{-1} \frac{\partial M}{\partial \theta_1} = \begin{bmatrix} 0 & 0 & 0 \end{bmatrix} \quad (82)$$

$$\underline{\omega}^T M^{-1} \frac{\partial M}{\partial \theta_2} = \frac{1}{\cos \theta_2} \begin{bmatrix} (-\omega_1 \sin \theta_2 \cos^2 \theta_3 + \omega_2 \sin \theta_2 \sin \theta_3 \cos \theta_3) & (\omega_1 \sin \theta_2 \sin \theta_3 \cos \theta_3) \\ -\omega_2 \sin \theta_2 \sin^2 \theta_3 & (\omega_1 \cos \theta_2 \cos \theta_3 - \omega_2 \cos \theta_2 \sin \theta_3) \end{bmatrix} \quad (83)$$

$$\underline{\omega}^T M^{-1} \frac{\partial M}{\partial \theta_3} = \frac{1}{\cos \theta_2} \begin{bmatrix} (\omega_2 \cos \theta_2) & (-\omega_1 \cos \theta_2) & 0 \end{bmatrix} . \quad (84)$$

Since the transformation matrix,  $M$ , is a function of  $\theta_2$  and  $\theta_3$ , the time derivative of  $M$  can be expressed by the chain rule as

$$\dot{M} = \frac{\partial M}{\partial \theta_2} \dot{\theta}_2 + \frac{\partial M}{\partial \theta_3} \dot{\theta}_3 \quad (85)$$

From equation (5)

$$\frac{\partial M}{\partial \theta_2} \dot{\theta}_2 = \begin{bmatrix} (-\sin \theta_2 \cos \theta_3) \dot{\theta}_2 & (\sin \theta_2 \sin \theta_3) \dot{\theta}_2 & (\cos \theta_2) \dot{\theta}_2 \\ 0 & 0 & 0 \\ 0 & 0 & 0 \end{bmatrix} \quad (86)$$

$$\frac{\partial M}{\partial \theta_3} \dot{\theta}_3 = \begin{bmatrix} (-\cos \theta_2 \sin \theta_3) \dot{\theta}_3 & (-\cos \theta_2 \cos \theta_3) \dot{\theta}_3 & 0 \\ (\cos \theta_3) \dot{\theta}_3 & (-\sin \theta_3) \dot{\theta}_3 & 0 \\ 0 & 0 & 0 \end{bmatrix} \quad (87)$$

Substituting these equations (86) and (87) in (85)

$$\dot{M} = \begin{vmatrix} (-\sin\theta_2 \cos\theta_3)\dot{\theta}_2 + (-\cos\theta_2 \sin\theta_3)\dot{\theta}_3 & (\sin\theta_2 \sin\theta_3)\dot{\theta}_2 + (-\cos\theta_2 \cos\theta_3)\dot{\theta}_3 & (\cos\theta_2)\dot{\theta}_2 \\ (\cos\theta_3)\dot{\theta}_3 & (-\sin\theta_3)\dot{\theta}_3 & 0 \\ 0 & 0 & 0 \end{vmatrix} \quad (88)$$

From equation (4), this can also be expressed as

$$\dot{M} = \frac{1}{\cos\theta_2} \begin{vmatrix} (-\sin\theta_2 \cos\theta_3)(\omega_1 \cos\theta_2 \sin\theta_3 + \omega_2 \cos\theta_2 \cos\theta_3) + (-\cos\theta_2 \sin\theta_3)(-\omega_1 \sin\theta_2 \cos\theta_3 + \omega_2 \sin\theta_2 \sin\theta_3 + \omega_3 \cos\theta_2) & (\sin\theta_2 \sin\theta_3)(\omega_1 \cos\theta_2 \sin\theta_3 + \omega_2 \cos\theta_2 \cos\theta_3) + (-\cos\theta_2 \cos\theta_3)(-\omega_1 \sin\theta_2 \cos\theta_3 + \omega_2 \sin\theta_2 \sin\theta_3 + \omega_3 \cos\theta_2) & \cos\theta_2(\omega_1 \cos\theta_2 \sin\theta_3 + \omega_2 \cos\theta_2 \cos\theta_3) \\ (\cos\theta_3)(-\omega_1 \sin\theta_2 \cos\theta_3 + \omega_2 \sin\theta_2 \sin\theta_3 + \omega_3 \cos\theta_2) & (-\sin\theta_3)(-\omega_1 \sin\theta_2 \cos\theta_3 + \omega_2 \sin\theta_2 \sin\theta_3 + \omega_3 \cos\theta_2) & 0 \\ 0 & 0 & 0 \end{vmatrix} \quad (89)$$

Also,  $M^{-1}$  is given as

$$M^{-1} = \frac{1}{\cos\theta_2} \begin{vmatrix} \cos\theta_3 & \cos\theta_2 \sin\theta_3 & -\sin\theta_2 \cos\theta_3 \\ -\sin\theta_3 & \cos\theta_2 \cos\theta_3 & \sin\theta_2 \sin\theta_3 \\ 0 & 0 & \cos\theta_2 \end{vmatrix} \quad (90)$$

Thus, the nonlinear term  $N_2$  can be rewritten as

$$N_2 = A'_3(\underline{\omega}, \underline{\theta}) \left[ I_o \underline{\omega} + A_2 \underline{\dot{q}} \right]$$

Where the term  $A'_3$  is

$$A'_3(\underline{\omega}, \underline{\theta}) = M^{-1} \begin{bmatrix} 0 \\ \underline{\omega}^T M^{-1} \frac{\partial M}{\partial \theta_2} \\ \underline{\omega}^T M^{-1} \frac{\partial M}{\partial \theta_3} \end{bmatrix} - \dot{M}$$

$$\begin{aligned} N_2 &= A'_3(\underline{\omega}, \underline{\theta}) I_o \underline{\omega} + A'_3(\underline{\omega}, \underline{\theta}) A_2 \underline{\dot{q}} \\ &= A_4(\underline{\omega}, \underline{\theta}) + A_5(\underline{\omega}, \underline{\theta}) \underline{\dot{q}} \end{aligned} \quad (91)$$

where  $A_4$  depends on the rigid-body slewing and is nonlinear in terms of  $\underline{\omega}$  and  $\underline{\theta}$ . The second term relates the coupling between the rigid-body slewing and the flexible modes. This equation can be further simplified in terms of Euler parameters by relationships developed in appendix II as

$$\underline{N}_2 = A_6(\underline{\omega}, \underline{\epsilon}) + A_7(\underline{\omega}, \underline{\epsilon}) \underline{\dot{q}} \quad (92)$$

where  $\underline{\epsilon}$  is the Euler vector comprising all four Euler parameters,

From equations (65) and (66) and by defining  $A = A_2^T I_o^{-1} A_2 + A_3$ , the following equations are obtained

$$\begin{aligned} \underline{\dot{q}} &= I_o^{-1} \left[ A_2 A^{-1} B \underline{\dot{q}} + A_2 A^{-1} K \underline{q} + \left[ A_2 A^{-1} A_2^T I_o^{-1} + I_3 \right] \underline{Q}(t) \right. \\ &\quad \left. + \left[ A_2^{-1} A_2^T I_o^{-1} + I_3 \right] \underline{N}_2(\underline{\omega}, \underline{\epsilon}) \right] \end{aligned} \quad (93)$$

$$\begin{aligned} \underline{\ddot{q}} &= A^{-1} B \underline{\ddot{q}} - A^{-1} K \underline{q} - A^{-1} A_2^T I_o^{-1} \underline{Q}(t) + A^{-1} A_2^T I_o^{-1} \\ &\quad + A^{-1} \underline{Q}(t) . \end{aligned} \quad (94)$$



It is assumed that control forces applied for vibration suppression has negligible effect on rotational maneuver of the spacecraft in developing equations (93) and (94). Also,  $I_3$  represents 3x3 identity matrix in these equations.

#### 4. NUMERICAL DATA

The analytics developed in the previous section are utilized together with the basic SCOLE data [1] and the three dimensional linear vibration analysis [4] to generate the following numerical data.

$$m_1 = 6366.46 \text{ slugs.}; \quad m_2 = 12.42 \text{ slugs.}; \quad \rho = 0.0955 \text{ slugs/ft.}; \quad L = 130 \text{ ft.}$$

$$G_\phi = 7.2E+8 \text{ lb/ft}^2; (EI)_x = (EI)_y = (EI) = 4E+7 \text{ lb-ft}^2;$$

$$\underline{L} = \begin{bmatrix} 0.036 \\ -0.036 \\ -0.379 \end{bmatrix}$$

$$\underline{c} = \begin{bmatrix} 0 \\ 0 \\ -65.0 \end{bmatrix}$$

$$I_1 = \begin{bmatrix} 905443.0 & 0.0 & 145393.0 \\ 0.0 & 6789100.0 & 0.0 \\ 145393.0 & 0.0 & 7086601.0 \end{bmatrix}$$

$$I_2 = \begin{bmatrix} 18000.0 & -7570.0 & 0.0 \\ -7570.0 & 9336.0 & 0.0 \\ 0 & 0.0 & 27407.0 \end{bmatrix}$$

The three dimensional vibration analysis is given in terms of the first ten modal frequencies and mode shapes in table 1. Here,

$$\phi_{xi}(s) = A_{xi} \sin \frac{\alpha_i s}{L} + B_{xi} \cos \frac{\alpha_i s}{L} + C_{xi} \sinh \frac{\alpha_i s}{L} + D_{xi} \cosh \frac{\alpha_i s}{L}$$

$$\phi_{yi}(s) = A_{yi} \sin \frac{\alpha_i s}{L} + B_{yi} \cos \frac{\alpha_i s}{L} + C_{yi} \sinh \frac{\alpha_i s}{L} + D_{yi} \cosh \frac{\alpha_i s}{L}$$

$$\phi_{\psi i}(s) = A_{\psi i} \sin \alpha_{\psi i} \frac{s}{L} + B_{\psi i} \cos \alpha_{\psi i} \frac{s}{L}$$

$$\alpha_i = \left( \frac{\omega_i^2 \rho L^4}{EI} \right)^{\frac{1}{4}}$$

$$\alpha_{\psi i} = \left( \frac{DL^2 \omega_i^2}{G} \right)^{\frac{1}{2}} .$$

Using these data the following matrices are obtained.

$$I_o = \begin{bmatrix} 1216640 & -1.530307 & 175667.1 \\ -31.66433 & 7082976 & -52474.84 \\ 175690 & -52503.9 & 7131493 \end{bmatrix}$$

TABLE 1

## FIRST TEN FLEXIBLE MODES OF SCOLE MODEL

THREE DIMENSIONAL MODE SHAPE CHARACTERISTICS		
MODE No.	1	2
FREQ. (HZ.)	0.27804240E+00	0.31357296E+00
$\alpha$	0.12012084E+01	0.12756518E+01
$A_x$	0.16282665E+00	0.38855291E-02
$B_x$	-0.19670286E+00	-0.14998387E-01
$C_x$	-0.16983450E+00	-0.43321018E-02
$D_x$	0.19616259E+00	0.14985820E-01
$A_y$	-0.10274618E-01	0.14219781E+00
$B_y$	0.57579133E-02	-0.22695797E+00
$C_y$	0.11810057E-01	-0.19283105E+00
$D_y$	-0.57220462E-02	0.22644561E+00
$\alpha_z$	0.19360955E-01	0.21835058E-01
$A_z$	-0.50748354E-01	0.31115282E-01
$B_z$	0.13978018E-04	-0.75992337E-05
MODE No.	3	4
FREQ. (HZ.)	0.81300189E+00	0.11856099E+01
$\alpha$	0.20540387E+01	0.24804687E+01
$A_x$	0.40868188E-01	0.80641794E-01
$B_x$	-0.61958845E-01	-0.67233377E-01
$C_x$	-0.41309992E-01	-0.80913938E-01
$D_x$	0.61880796E-01	0.67106316E-01
$A_y$	-0.22438404E-01	0.13728679E+00
$B_y$	0.36509234E-01	-0.11746932E+00
$C_y$	0.24390447E-01	-0.14085209E+00
$D_y$	-0.36464758E-01	0.11725057E+00
$\alpha_z$	0.56611842E-01	0.82557693E-01
$A_z$	0.92698901E-01	-0.16158934E-03
$B_z$	-0.87320799E-05	0.10437718E-07
MODE No.	5	6
FREQ. (HZ.)	0.20536300E+01	0.49716090E+01
$\alpha$	0.32645546E+01	0.49716090E+01
$A_x$	0.99278129E-01	0.45739784E-01
$B_x$	-0.92344553E-01	-0.46365581E-01
$C_x$	-0.99442145E-01	-0.45763106E-01
$D_x$	0.92225801E-01	0.46329676E-01
$A_y$	-0.57396019E-01	0.78612940E-01
$B_y$	0.53976008E-01	-0.79952853E-01
$C_y$	0.58114853E-01	-0.78914485E-01
$D_y$	-0.53906980E-01	0.79891039E-01
$\alpha_z$	0.14300062E+00	0.33165303E+00
$A_z$	-0.16588614E-02	-0.93394833E-05
$B_z$	0.61861804E-07	0.15017211E-09

THREE DIMENSIONAL MODE SHAPE CHARACTERISTICS		
MODE No.	7	8
FREQ. (HZ.)	0.55157833E+01	0.12281249E+02
$\alpha$	0.53501560E+01	0.79833305E+01
$A_x$	0.81311804E-01	0.44835061E-01
$B_x$	-0.82056569E-01	-0.44834914E-01
$C_x$	-0.81344923E-01	-0.44840508E-01
$D_x$	0.81997259E-01	0.44813000E-01
$A_y$	-0.47145439E-01	0.77404756E-01
$B_y$	0.47703590E-01	-0.77465629E-01
$C_y$	0.47289807E-01	-0.77475327E-01
$D_y$	-0.47669155E-01	0.77427782E-01
$\alpha_z$	0.38408110E+00	0.85518143E+00
$A_z$	-0.23855560E-02	0.15830371E-05
$B_z$	0.33122041E-07	-0.98715017E-11
MODE No.	9	10
FREQ. (HZ.)	0.12890442E+02	0.23679520E+02
$\alpha$	0.81789349E+01	0.11085347E+02
$A_x$	0.78743585E-01	0.44348498E-01
$B_x$	-0.78755259E-01	-0.44367373E-01
$C_x$	-0.78752483E-01	-0.44350511E-01
$D_x$	0.78717693E-01	0.44351763E-01
$A_y$	-0.45569244E-01	0.76707490E-01
$B_y$	0.45609474E-01	-0.76762782E-01
$C_y$	0.45607884E-01	-0.76733612E-01
$D_y$	-0.45587726E-01	0.76735779E-01
$\alpha_z$	0.89760145E+00	0.16488784E+01
$A_z$	0.94995483E-03	-0.51105957E-06
$B_z$	-0.56437766E-08	0.16528495E-11

$$A_3 = \begin{bmatrix} 0.45879E+2 & 0.36305E-1 & -0.89042E-1 & -0.14067E0 & 0.1457E0 \\ 0.36305E-1 & 0.6211E+2 & 0.11263E0 & -0.1471E0 & -0.5518E-1 \\ -0.89042E-1 & 0.11263E0 & 0.32737E+2 & -0.6392E-1 & -0.14526E0 \\ -0.14067E0 & -0.1471E0 & -0.6392E-1 & 0.2547E+3 & 0.1908E0 \\ -0.1457E0 & -0.5518E-1 & -0.14526E0 & 0.1908E0 & 0.8103E+3 \\ 0.1914E-1 & 0.19839E-1 & 0.7925E-2 & -0.4278E-1 & -0.2570E-1 \\ 0.84597E-1 & 0.3935E-2 & -0.8369E-1 & -0.76115E-1 & -0.12912E0 \\ -0.6893E-2 & -0.7165E-2 & -0.2829E-2 & 0.1543E-1 & 0.9222E-2 \\ -0.4269E-1 & 0.5969E-2 & 0.89767E-1 & 0.2859E-1 & 0.4611E-1 \\ 0.4204E-2 & 0.41227E-2 & 0.1866E-2 & -0.9067E-2 & -0.5947E-2 \end{bmatrix}$$

$$\begin{bmatrix} 0.1914E-1 & 0.84597E-1 & -0.6893E-2 & -0.4269E-1 & 0.4204E-2 \\ 0.19839E-1 & 0.3935E-2 & -0.7165E-2 & 0.5969E-2 & 0.4127E-2 \\ 0.7925E-2 & -0.8369E-1 & -0.2829E-2 & 0.89767E-1 & 0.1866E-2 \\ -0.4278E-1 & -0.76115E-1 & 0.1543E-1 & 0.2859E-1 & -0.9067E-2 \\ -0.2570E-1 & -0.12912E0 & 0.9222E-2 & 0.4611E-1 & -0.5947E-2 \\ 0.23209E+5 & 0.10383E-1 & -0.2089E-2 & -0.3955E-2 & 0.1227E-2 \\ 0.10383E-1 & 0.55561E+5 & -0.37286E-2 & -0.3859E-1 & 0.2397E-2 \\ -0.2089E-2 & -0.37286E-2 & 0.1342962E+8 & 0.1421E-2 & -0.4427E-3 \\ -0.3955E-2 & -0.3859E-1 & 0.1421E-2 & 0.2095672E+8 & -0.9108E-3 \\ 0.1227E-2 & 0.2397E-2 & -0.4427E-3 & -0.9108E-3 & 0.8662547E+10 \end{bmatrix}$$

$$A_2^T = \begin{bmatrix} -0.2133821E0 & -0.3687057E+3 & -0.7253901E-1 \\ 0.3808921E+3 & -0.3030935E+2 & -0.8427658E-1 \\ -0.1808478E+3 & -0.1318596E+3 & -0.125799E0 \\ 0.1423380E+3 & -0.1135851E+1 & -0.2367351E-1 \\ -0.2416743E+2 & 0.574383E+2 & -0.9150328E-1 \\ -0.6802273E0 & 0.3104929E2 & -0.3843062E-1 \\ 0.2784792E+2 & 0.6651585E+2 & 0.596075E-1 \\ 0.7842818E+1 & -0.1930097E+2 & -0.4363533E-2 \\ -0.2694455E+2 & -0.5544252E+2 & -0.4200623E-1 \\ -0.9225328E-1 & 0.1594045E+2 & -0.1626004E-1 \end{bmatrix}$$

The stiffness matrix  $K$  is calculated using equation (57) and the mode shape coefficients given in Table 1. This matrix is a diagonal matrix and is represented in terms of the diagonal elements as

$$K = \begin{bmatrix} k_{1,1} = 0.2820217E0 \\ k_{2,2} = 0.3574692E0 \\ k_{3,3} = 0.2412807E1 \\ k_{4,4} = 0.5285116E1 \\ k_{5,5} = 0.1588654E2 \\ k_{6,6} = 0.8573860E2 \\ k_{7,7} = 0.1146118E3 \\ k_{8,8} = 0.5686101E3 \\ k_{9,9} = 0.6254598E3 \\ k_{10,10} = 0.2114612E4 \end{bmatrix} .$$

The damping matrix  $B$  used for this analysis is a diagonal matrix and for damping ratio  $\zeta = 0.003$ , it is calculated to be

$$B = \begin{bmatrix} b_{1,1} = 0.9685964E-3 \\ b_{2,2} = 0.1088608E-2 \\ b_{3,3} = 0.2834016E-2 \\ b_{4,4} = 0.4256808E-2 \\ b_{5,5} = 0.7387177E-2 \\ b_{6,6} = 0.1719014E-1 \\ b_{7,7} = 0.1984237E-1 \\ b_{8,8} = 0.4421234E-1 \\ b_{9,9} = 0.4633434E-1 \\ b_{10,10} = 0.8527647E-1 \end{bmatrix} .$$

## 5. REFERENCES

- [1] L. W. Taylor, Jr. and A. V. Balakrishnan, "A Mathematical Problem and a Spacecraft Control Experiment (SCOLE) Used to Evaluate Control Laws for Flexible Spacecraft... NASA/IEEE Design Challenge," Proceedings of the Fourth VPI/AIAA Symposium on Dynamics and Control of Large Structures, pp 311-318, June 1983.
- [2] A. S. Debs and M. Athans, "On the Optimal Angular Velocity Control of Asymmetrical Space Vehicles," IEEE Trans. Automat. Contr., pp 80-83, Feb. 1969.
- [3] T. A. W. Dwyer, III, "The Control of Angular Momentum for Asymmetric Rigid Bodies," IEEE Trans. Automat. Contr., pp 686-688, June 1982.
- [4] D. K. Robertson, "Three-dimensional Vibration Analysis of a Uniform Beam with Offset Inertial Masses at the Ends," NASA TM-86393, September 1985.
- [5] T. R. Kane, P. W. Likins, and D. A. Levinson, Spacecraft Dynamics, New York: McGraw-Hill, 1983.
- [6] J. Storch, S. Gates and D. O'Connor, "Three Dimensional Motion of a Flexible Beam with Rigid Tip Bodies," Charles Stark Draper Laboratory Report, Interlab Memorandum, October 1985.
- [7] Y. P. Kakad, "Slew Maneuver Control of the Spacecraft Control Laboratory Experiment (SCOLE)," Proceedings of ACC Conference, pp 1039-1044 June 1986.
- [8] Y. P. Kakad, "Dynamics and Control of Slew Maneuver of Large Flexible Spacecraft," Proceedings of AIAA Guidance, Navigation and Control Conference, pp 629-634, August 1986.
- [9] B. Friedland, Control System Design - An Introduction to State-space Methods, New York: McGraw-Hill, 1986.
- [10] H. Goldstein, Classical Mechanics, Reading: Addison-Wesley, Second Edition, 1981.
- [11] M. Balas, "Feedback Control of Flexible Systems," IEEE Trans. Automat. Contr., pp 673-679, August 1978.
- [12] A. E. Bryson, Jr. and Y. C. Ho, Applied Optimal Control - Optimization, Estimation, and Control, New York: John Wiley, revised printing, 1975.
- [13] L. Meirovitch, Analytical Methods in Vibrations, New York: The Macmillan Company, 1967.
- [14] E. S. Armstrong, "ORACLS - A System for Linear-Quadratic-Gaussian Control Law Design," NASA TP-1106, 1978.

- [15] S. Joshi, "SCOLE Equations of Motion-A New Formulation," Proceedings of the 2nd Annual SCOLE Workshop, NASA TM-89048, pp. 14-25, December 1985.
- [16] Y. P. Kakad, "Dynamics of Spacecraft Control Laboratory Experiment (SCOLE) Slew Maneuvers," NASA CR-4098 October 1987.
- [17] M. G. Singh, Dynamical Hierarchical Control, New York: North-Holland Publishing Company, 1980.
- [18] J. L. Junkins, and J. D. Turner, Optimal Spacecraft Rotational Maneuvers, New York: Elsevier Science Publishers B.V., 1986.
- [19] P. L. Falb, and J. L. de Jong, Some Successive Approximation Methods in Control and Oscillation Theory, New York: Academic Press, 1969.
- [20] H. B. Keller, Numerical Methods for Two-point Boundary-Value Problems, Waltham, Massachusetts: Blaisdell Publishing Company, 1968.
- [21] R. E. Bellman, and R. E. Kalaba, Quasilinearization and Nonlinear Boundary-Value Problems, New York: American Elsevier Publishing Company, 1965.
- [22] M. G. Singh, and A. Titli, "Closed Loop Hierarchical Control for Non-linear Systems Us'ng Quasilinearization," Automatica, Vol. 11, pp 541-546, 1975.
- [23] S. M. Roberts, and J. S. Shipman, Two-point Boundary Value Problems: Shooting Methods, New York: American Elsevier Publishing Company, 1972.
- [24] M. S. Mahmoud, M. F. Hassan, and M. G. Darwish, Large-Scale Control Systems, New York: Marcel Dekker Inc., 1985.
- [25] D. Luenberger, Optimization by Vector Space Methods, New York: John Wiley, 1969.
- [26] D. E. Kirk, Optimal Control Theory - An Introduction, Englewood Cliffs, New Jersey, Prentice-Hall Inc., 1970.



# APPENDIX I

The following is a summary of transformations between inertial frame and body-fixed frame. Here,  $s_i$  and  $c_i$  ( $i=1,2,3$ ) denote  $\sin\theta_i$  and  $\cos\theta_i$  ( $i=1,2,3$ ) respectively.

## (a) Space-three Angles

$$C = \begin{bmatrix} c_2 c_3 & c_2 s_3 & -s_2 \\ s_1 s_2 c_3 - s_1 s_3 c_1 & s_1 s_2 s_3 + c_1 s_3 c_1 & s_1 c_2 \\ c_1 s_2 c_3 + s_1 s_3 c_1 & c_1 s_2 s_3 - c_1 s_3 c_1 & c_1 c_2 \end{bmatrix}$$

$$M^T = \begin{bmatrix} 1 & 0 & -s_2 \\ 0 & c_1 & s_1 c_2 \\ 0 & -s_1 & c_1 c_2 \end{bmatrix}$$

## (b) Space-two Angles

$$C = \begin{bmatrix} c_2 & s_2 s_3 & -s_2 c_3 \\ s_1 s_2 & -s_1 c_2 s_3 + c_1 c_3 & s_1 c_2 c_3 + s_1 s_3 c_1 \\ c_1 s_2 & -c_1 c_2 s_3 - c_1 s_3 & c_1 c_2 c_3 - s_1 s_3 \end{bmatrix}$$

$$M^T = \begin{bmatrix} 1 & 0 & c_2 \\ 0 & c_1 & s_1 s_2 \\ 0 & -s_1 & c_1 s_2 \end{bmatrix}$$

## (c) Body-two Angles

$$C = \begin{bmatrix} c_2 & s_1 s_2 & -c_1 s_2 \\ s_2 s_3 & -s_1 c_2 s_3 + c_1 c_3 & c_1 c_2 s_3 + c_1 s_3 c_1 \\ s_2 c_3 & -s_1 c_2 c_3 - s_1 s_3 c_1 & c_1 c_2 c_3 - s_1 s_3 \end{bmatrix}$$

$$M^T = \begin{bmatrix} c_2 & 0 & 1 \\ s_2 s_3 & c_3 & 0 \\ s_2 c_3 & -s_3 & 0 \end{bmatrix}$$

## APPENDIX II

The transformation that relates the orientation angles  $\underline{\theta}$  to Euler parameters  $\underline{\epsilon}$  is a nonlinear transformation. This transformation is developed for body-three angles representation in this appendix and similar transformations can be derived for other three representations, namely space-three angles, space-two angles, and body-two angles.

(a) For  $\sin\theta_2 \neq 1$ :

If  $-\frac{\pi}{2} < \theta_2 < \frac{\pi}{2}$ , then

$$\theta_2 = \sin^{-1} \left| 2(\epsilon_3\epsilon_1 + \epsilon_2\epsilon_4) \right|. \quad (\text{A.1})$$

If  $(\cos\theta_1\cos\theta_2) \geq 0$ , then

$$\theta_1 = \sin^{-1} \left| \frac{-2(\epsilon_2\epsilon_3 - \epsilon_1\epsilon_4)}{\cos \left[ \sin^{-1} \left| 2(\epsilon_3\epsilon_1 + \epsilon_2\epsilon_4) \right| \right]} \right|. \quad (\text{A.2})$$

If  $(\cos\theta_1\cos\theta_2) < 0$ , then

$$\theta_1 = \pi - \sin^{-1} \left| \frac{-2(\epsilon_2\epsilon_3 - \epsilon_1\epsilon_4)}{\cos \left[ \sin^{-1} \left| 2(\epsilon_3\epsilon_1 + \epsilon_2\epsilon_4) \right| \right]} \right|. \quad (\text{A.3})$$

If  $(\cos\theta_2\cos\theta_3) \geq 0$ , then

$$\theta_3 = \sin^{-1} \left| \frac{-2(\epsilon_1\epsilon_2 - \epsilon_3\epsilon_4)}{\cos \left[ \sin^{-1} \left| 2(\epsilon_3\epsilon_1 + \epsilon_2\epsilon_4) \right| \right]} \right|. \quad (\text{A.4})$$

If  $(\cos\theta_2\cos\theta_3) < 0$ , then

$$\theta_3 = \pi - \sin^{-1} \left| \frac{-2(\epsilon_1 \epsilon_2 - \epsilon_3 \epsilon_4)}{\cos \left[ \sin^{-1} \left| 2(\epsilon_3 \epsilon_1 + \epsilon_3 \epsilon_2) \right| \right]} \right|. \quad (\text{A.5})$$

(b) For  $\sin \theta_2 = \pm 1$ ,  $\theta_2$  is a constant. For  $\sin \theta_2 = 1$ ,  $\theta_2 = \frac{\pi}{2}$ . However, if  $\sin \theta_2 = -1$ , then  $\theta_2 = -\frac{\pi}{2}$ . For this case, if  $(\sin \theta_1 \sin \theta_2 \sin \theta_3 + \cos \theta_3 \cos \theta_1) \geq 0$ , then

$$\theta_1 = \sin^{-1} \left| 2(\epsilon_2 \epsilon_3 + \epsilon_1 \epsilon_4) \right|. \quad (\text{A.6})$$

If  $(\sin \theta_1 \sin \theta_2 \sin \theta_3 + \cos \theta_3 \cos \theta_1) < 0$ , then

$$\theta_1 = \pi - \sin^{-1} \left| 2(\epsilon_2 \epsilon_3 + \epsilon_1 \epsilon_4) \right|. \quad (\text{A.7})$$

For this entire case,  $\theta_3 = 0$ .

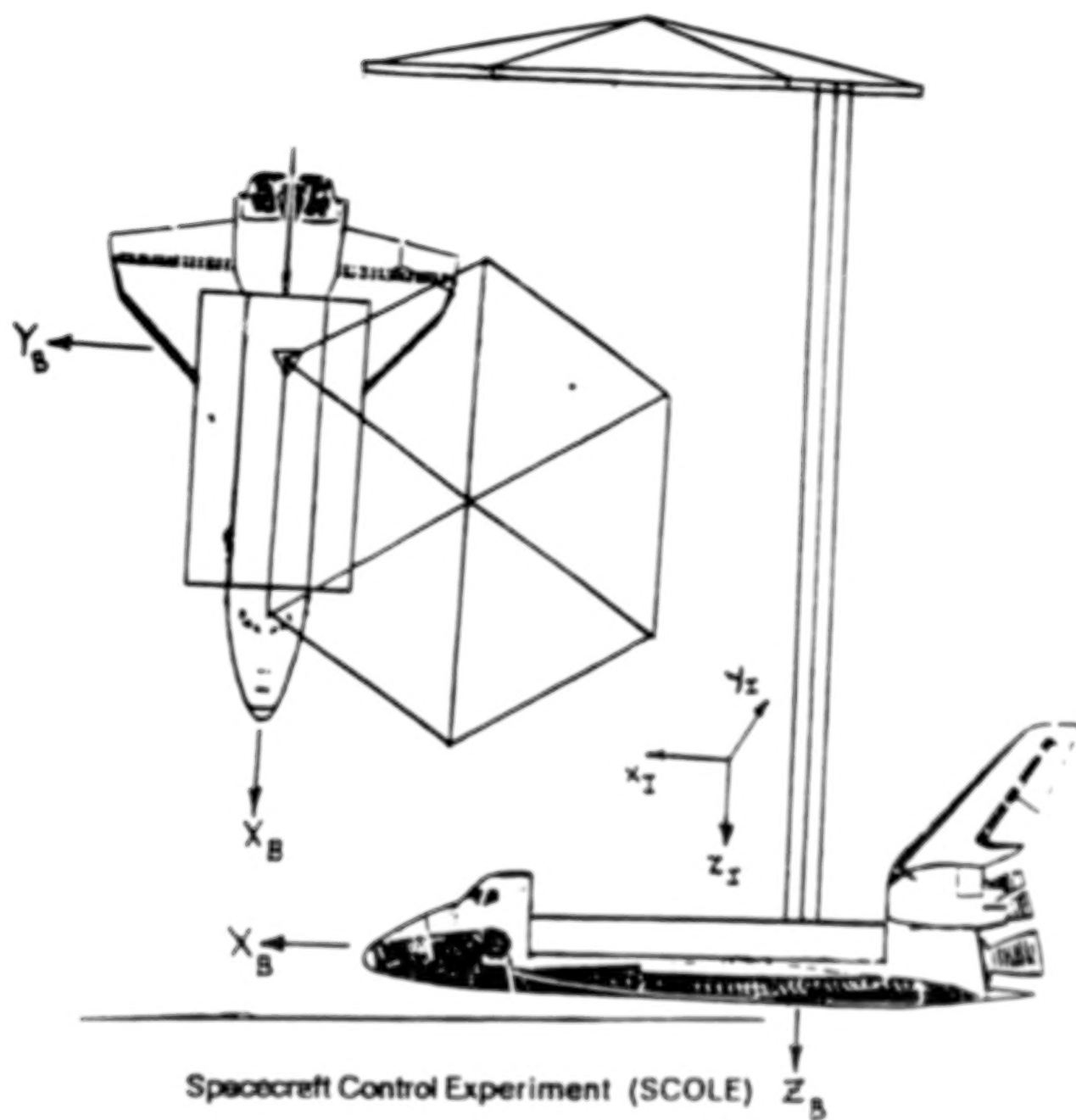
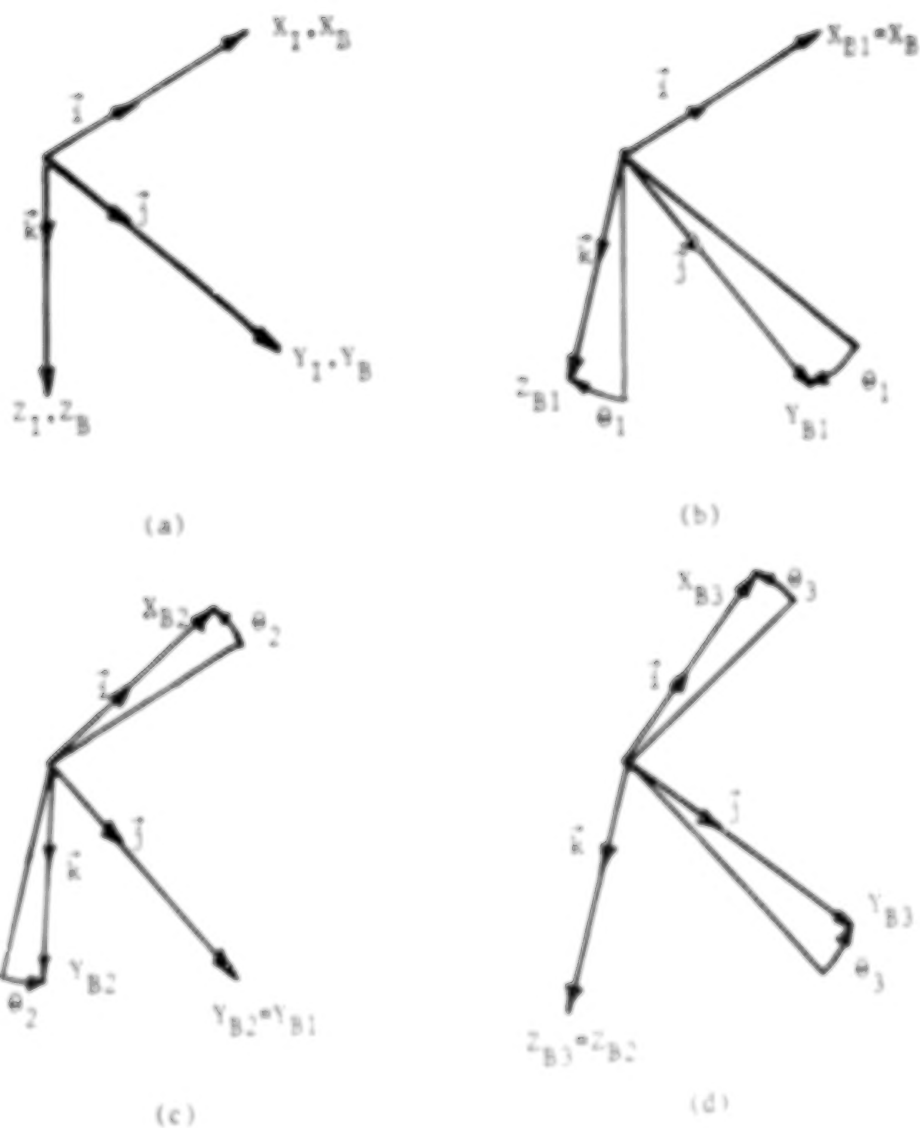


FIGURE 1



(a) Axes in reference position (b) First rotation-about x axis  
(c) Second rotation-about y axis (d) Final rotation-about z axis

FIGURE 2

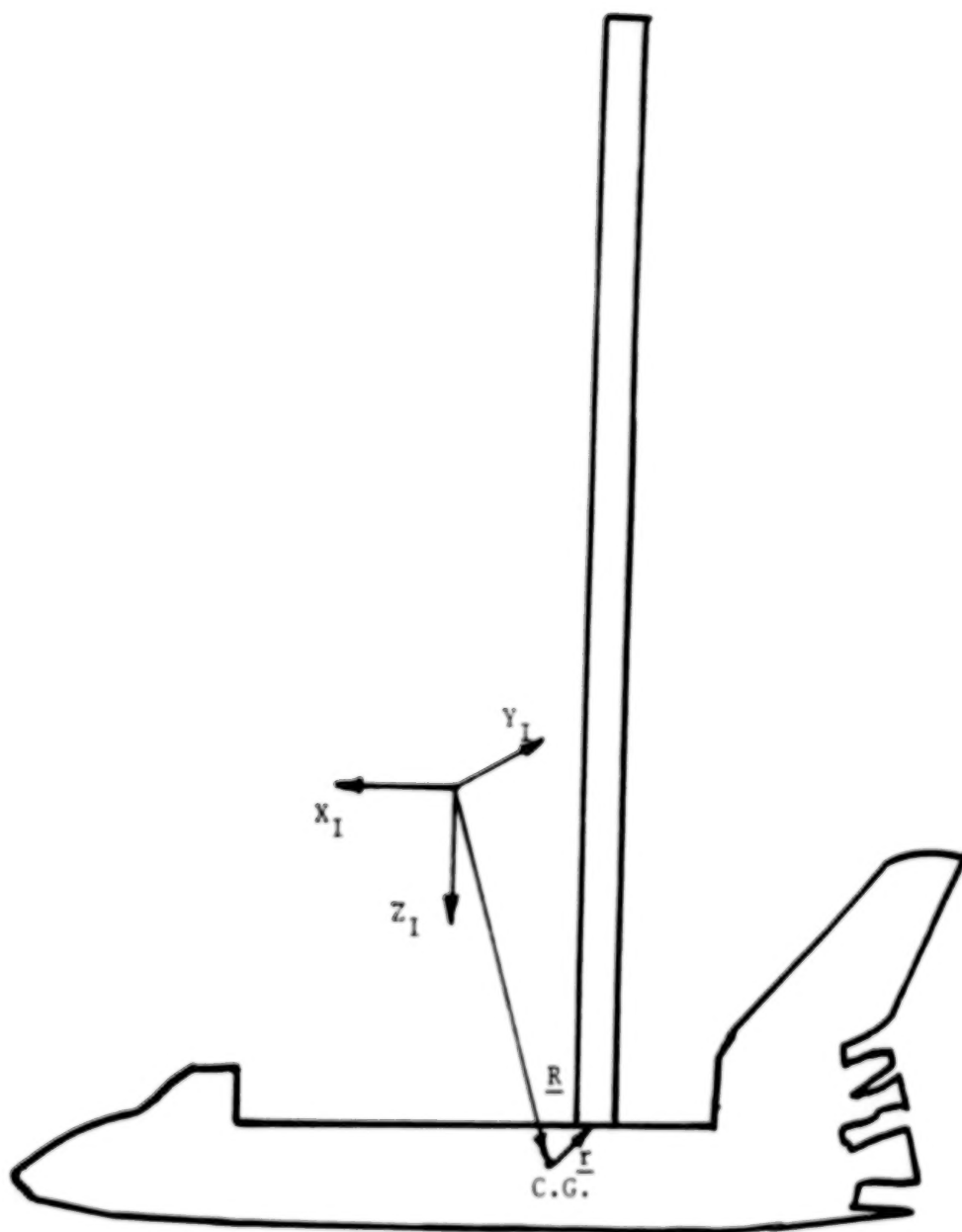


Figure 3- Position Vectors in Inertial Frame

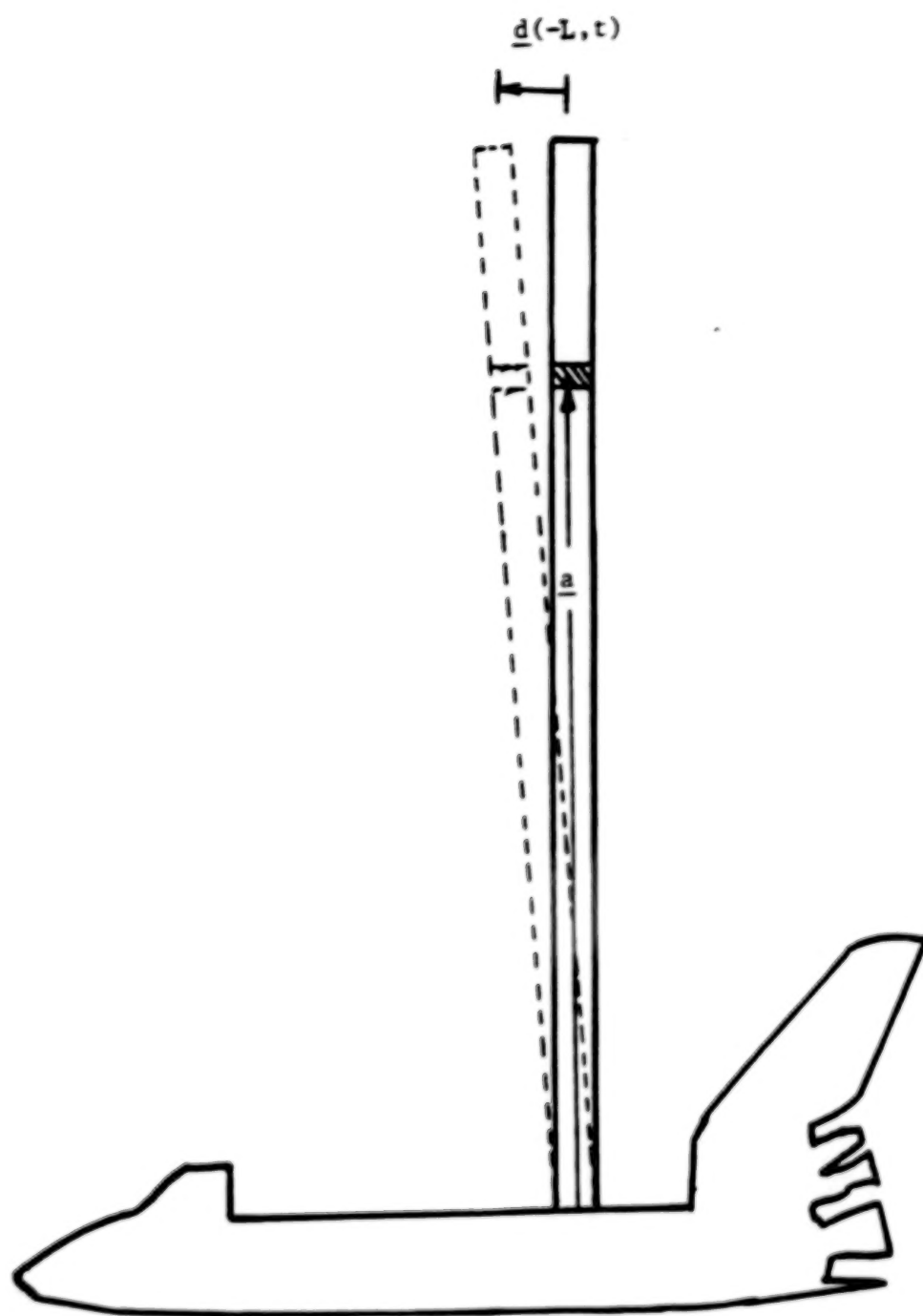


Figure 4- Vectors in Body-fixed Frame

**Optimal Planar Slewing of the Flexible Orbiting SCOLE**

**P. M. Bainum**

**Professor of Aerospace Engineering**

**Feiyue Li**

**Graduate Research Assistant**

**Department of Mechanical Engineering**

**Howard University, Washington, D.C. 20059**

**The 5th Annual SCOLE Workshop**

**Lake Arrowhead, California**

**Oct. 31- Nov. 1, 1988**



# Optimal Planar Slewing of the Flexible Orbiting SCOLE

P. M. Bainum and Feiyue Li

Department of Mechanical Engineering

Howard University, Washington, D.C. 20059

## Abstract

The nonlinear equations for the planar motion of the flexible SCOLE are derived by using Lagrange's equations. The displacements of the flexible parts are assumed small as compared with the SCOLE dimensions. The linearized version of the motion equations is obtained. The Maximum Principle is applied to the planar maneuver of the SCOLE to obtain the associated optimal control. The resulting nonlinear two-point boundary-value problem is solved by using the quasilinearization method, in which the solution of the linearized version is used as a starting solution. Some numerical results are presented to show the application of this method.

## Introduction

Pontryagin's Maximum Principle has been used for the optimal attitude maneuvers of a spacecraft in the following cases:

1) Rigid (3-D, multi-control source)

(Junkins, J.L. and Turner, J.D., 1978)

(Bainum, P.M. and Li, F., 1986-1988)

(Lin, Y.Y. and Kraige, L.G., 1987)

2) Flexible

a) Linearized Eq. (single-axis rotation, rigid-hub-2

symmetric beams; Breakwell, J.A., 1979)

b) Nonlinear Eq. (single-axis rotation, rigid-hub-4

symmetric beams, 1 control torquer;

Junkins and Turner, 1980)

c) Nonlinear Eq. (single-axis rotation, rigid-hub-4

symmetric beams, 5 control torquers;

Turner and Chun, 1984)

d) The Present Problem:

Nonlinear Eq. (single-axis rotation, Shuttle-beam-

reflector, control torquers and

control forces)

The methods used in solving the two-point boundary-value problem are:

1) For Rigid Spacecraft:

- a) Differential Correction (of unknown initial costates) and Relaxation Process (to increase the participation of the nonlinearity in the solution)  
(Junkins and Turner)
- b) Hybrid Approach (direct gradient method and the method of particular solutions) (Lin and Kraige)
- c) Quasilinearization Method (Bainum and Li)

2) For Flexible Spacecraft:

- a) Linear Eq.  
Transition Matrix Method (closed form solution of the unknown initial costates)
- b) Nonlinear Eq.  
Differential Correction and Relaxation Process  
(Junkins, Turner, and Chun)  
  
Quasilinearization Method (Bainum and Li)

## MAXIMUM PRINCIPLE

### STATE EQUATIONS

$$\dot{x} = f(x) + B(x)u, \quad x(0) = x_0, \quad x(t_f) = x_f \quad (1)$$

### PERFORMANCE INDICES

$$J_1 = (1/2) \int_0^{t_f} (x^T Q x + u^T R u) dt \quad (2)$$

$$J_2 = \int_0^{t_f} (1) dt = t_f \quad |u_i| \leq u_{ib}, \quad i=1 \dots n \quad (3)$$

### NECESSARY CONDITIONS

$$H_1 = (1/2)(x^T Q x + u^T R u) + \lambda^T (f(x) + Bu) \quad (4)$$

$$\dot{\lambda} = -(\partial H_1 / \partial x), \quad \lambda(0) \text{ unknown} \quad (5)$$

$$(\partial H_1 / \partial u) = 0, \quad Ru = -B^T \lambda \quad (6)$$

$$H_2 = 1 + \lambda^T (f(x) + Bu) \quad (7)$$

$$\dot{\lambda} = -(\partial H_2 / \partial x), \quad \lambda(0) \text{ unknown} \quad (8)$$

$$u_i = -u_{ib} \operatorname{sign}(B^T \lambda), \quad i=1 \dots n \quad (9)$$

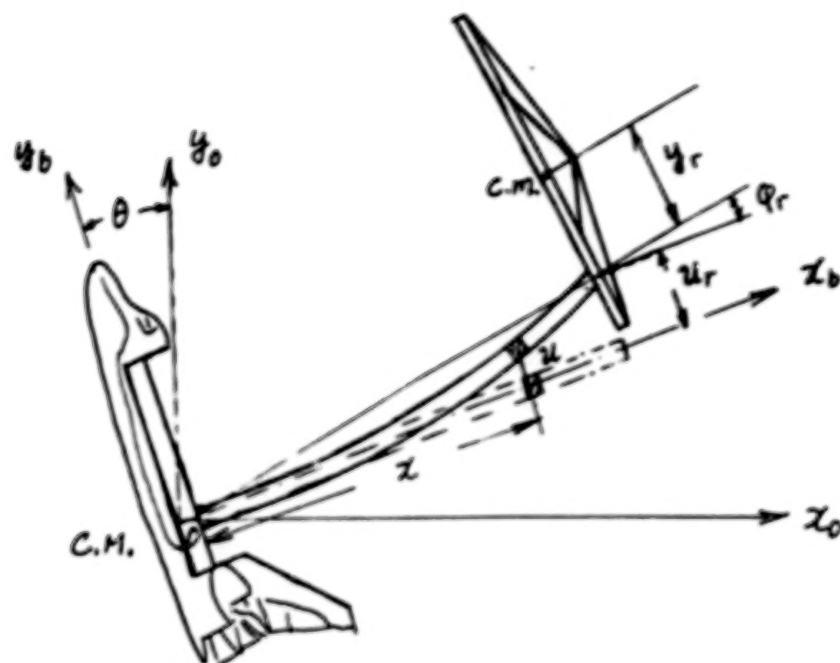
### TPBVP

$$\dot{z} = g(z), \quad z = [x, \lambda]^T = [z_1, z_2]^T \quad (10)$$

$z_1(0), z_1(t_f)$  known;

$z_2(0), z_2(t_f)$  unknown.

$z_2(0)$  to be determined.



### Kinetic Energy

$$T = T_{\text{shuttle}} + T_{\text{beam}} + T_{\text{reflector}}$$

$$T_s = \frac{1}{2} I_s \dot{\theta}^2$$

$$T_b = \frac{1}{2} \rho \int_0^L [ (u^2 + x^2) \dot{\theta}^2 + \dot{u}^2 + 2x \dot{u} \dot{\theta} ] dx$$

$$T_r = \frac{1}{2} I_r (\dot{\theta} + \dot{\phi}_r)^2 + \frac{1}{2} M_r [ (u_r^2 + L^2) \dot{\theta}^2 + 2L \dot{\theta} \dot{u}_r + \dot{u}_r^2 - 2u_r (\dot{\theta} + \dot{\phi}_r) [ (\dot{u}_r + L \dot{\theta}) \sin \phi_r - \dot{\theta} u_r \cos \phi_r ] ]$$

$I_s$  - Moment of inertia of the shuttle,

$I_r$  - Moment of inertia of the reflector,

$$u = \sum_{i=1}^n \eta_i \psi_i = \eta^T \psi, \quad \eta - \text{amplitude vector}$$

$\psi$  - mode shape function vector

# EQUATIONS OF MOTION

$$M(y_1) \ddot{y}_2 = F(y_1, y_2) + B(y_1) u, \quad y_1 = \begin{bmatrix} \theta \\ \eta \end{bmatrix}, \quad y_2 = \begin{bmatrix} \dot{\theta} \\ \dot{\eta} \end{bmatrix}$$

$u$  — control vector

$$M(y_1) =$$

$$\begin{bmatrix} I + \eta^T M_2 \eta - 2\eta^T m_0 \cos \varphi_r + 2m_y \sin \varphi_r & \text{symmetric} \\ m_2 + M_1 \eta \cos \varphi_r - m_5 \sin \varphi_r & M_3 - M_5 \sin \varphi_r \end{bmatrix}$$

$$F(y_1, y_2) =$$

$$\begin{bmatrix} -2\dot{\theta} \dot{\eta}^T (M_2 \eta + m_a \cos \varphi_r - M_1 \eta \sin \varphi_r) + \dot{\eta}^T [N_2 \cos \varphi_r + N_1 (\psi_r^T \eta) \sin \varphi_r] \dot{\eta} \\ \dot{\theta}^2 (M_2 \eta + m_a \cos \varphi_r - M_1 \eta \sin \varphi_r) - 2\dot{\theta} M_a \dot{\eta} \cos \varphi_r + (\dot{\eta}^T \psi_r') M_1^T \dot{\eta} \cos \varphi_r - K \eta \end{bmatrix}$$

$$B(y_1) =$$

$$\begin{bmatrix} 1 & x_1 \cos \varphi_1 + u_1 \sin \varphi_1 & x_2 \cos \varphi_2 + u_2 \sin \varphi_2 & x_3 \cos \varphi_3 + u_3 \sin \varphi_3 \\ 0 & \psi_1 \cos \varphi_1 & \psi_2 \cos \varphi_2 & \psi_3 \cos \varphi_3 \end{bmatrix}$$

where  $M_a, M_2, M_1, M_3, M_5, N_1, N_2, K$  — constant matrices

$m_2, m_5, m_0, m_a$  — constant vectors

$I, m_y$  — constants

## QUASILINEARIZATION ALGORITHM

### (A) LINEAR DIFFERENTIAL EQUATION:

$$\text{Nonhomogeneous: } \dot{z} = Az + B, \quad z = [z_1, z_2]^T, \quad (11)$$

$z_1(0), z_1(t_f)$  known,  $z_2(0)$  to be determined

$$\text{Homogeneous: } \dot{z} = Az \quad (12)$$

(a)  $n$  solns. of (12) + 1 particular soln. of (11)

(b)  $n + 1$  particular solns. of (11)

### (B) NONLINEAR CASE:

Linearized equation of (10):

$$\dot{z}^{(k+1)} = (\partial g / \partial z) z^{(k+1)} + h(z^{(k)}) \quad (13)$$

where

$z^{(k)}$  is the  $k^{\text{th}}$  approximate solution  
of the nonlinear equation (10),

$$z^{(k+1)} = z^{(k)} + \Delta z^{(k)}$$

$$z = [z_1, z_2]^T,$$

$z_1^{(k+1)}(0), z_1^{(k+1)}(t_f)$ , known

$z_2^{(k+1)}(0)$  to be determined

## PLANAR SLEWING OF FLEXIBLE SCOPE

### LINEARIZED EQUATION OF MOTION:

$$\begin{bmatrix} 1 & \mathbf{m}^T \\ \mathbf{m} & \mathbf{M} \end{bmatrix} \begin{bmatrix} \ddot{\theta} \\ \ddot{\eta} \end{bmatrix} + \begin{bmatrix} 0 & \mathbf{0}^T \\ \mathbf{0} & \mathbf{K} \end{bmatrix} \begin{bmatrix} \theta \\ \eta \end{bmatrix} = \begin{bmatrix} 1 & z_1 & z_2 & L \\ 0 & \phi_1 & \phi_2 & \phi_L \end{bmatrix} \begin{bmatrix} u_s \\ u_1 \\ u_2 \\ u_3 \end{bmatrix}$$

where

$\theta$  is the angle of rotation,

$\eta_{n \times 1}$  is the amplitude vector of the flexible modes,

$n$  is the number of mode used,

$I$  is the moment of inertia about the axis of rotation

$\mathbf{m}, \mathbf{M}$  are the inertia parameter vector, matrix.

$\mathbf{K}$  is the stiffness matrix,

$\phi(z)$  is the mode shape function vector,

$\phi_1 = \phi(z_1)$ ,  $z_1$  is the coordinate along  $z$  axis,

$L$  is the length of the beam,

$u_s$  is the control torque on the Shuttle,

$u_i$  are the control actuators on the beam and the reflector.



## STATE EQUATIONS

$$\dot{s} = As + Bu$$

$$s = \begin{bmatrix} s_1 \\ s_2 \end{bmatrix}, \quad s_1 = \begin{bmatrix} \theta \\ \dot{\eta} \end{bmatrix}, \quad s_2 = \begin{bmatrix} \dot{\theta} \\ \ddot{\eta} \end{bmatrix}$$

## BOUNDARY CONDITIONS FOR s

$$s(0) = \begin{bmatrix} \theta_f \\ \underline{0} \\ \underline{0} \\ \underline{0} \end{bmatrix}, \quad s(t_f) = \begin{bmatrix} 0 \\ \underline{0} \\ \underline{0} \\ \underline{0} \end{bmatrix}_{2(n+1) \times 1}$$

where  $n$  is the number of mode shapes used.

## PERFORMANCE INDEX

$$J = (1/2) \int_0^{t_f} (x^T Q x + u^T R u) dt$$

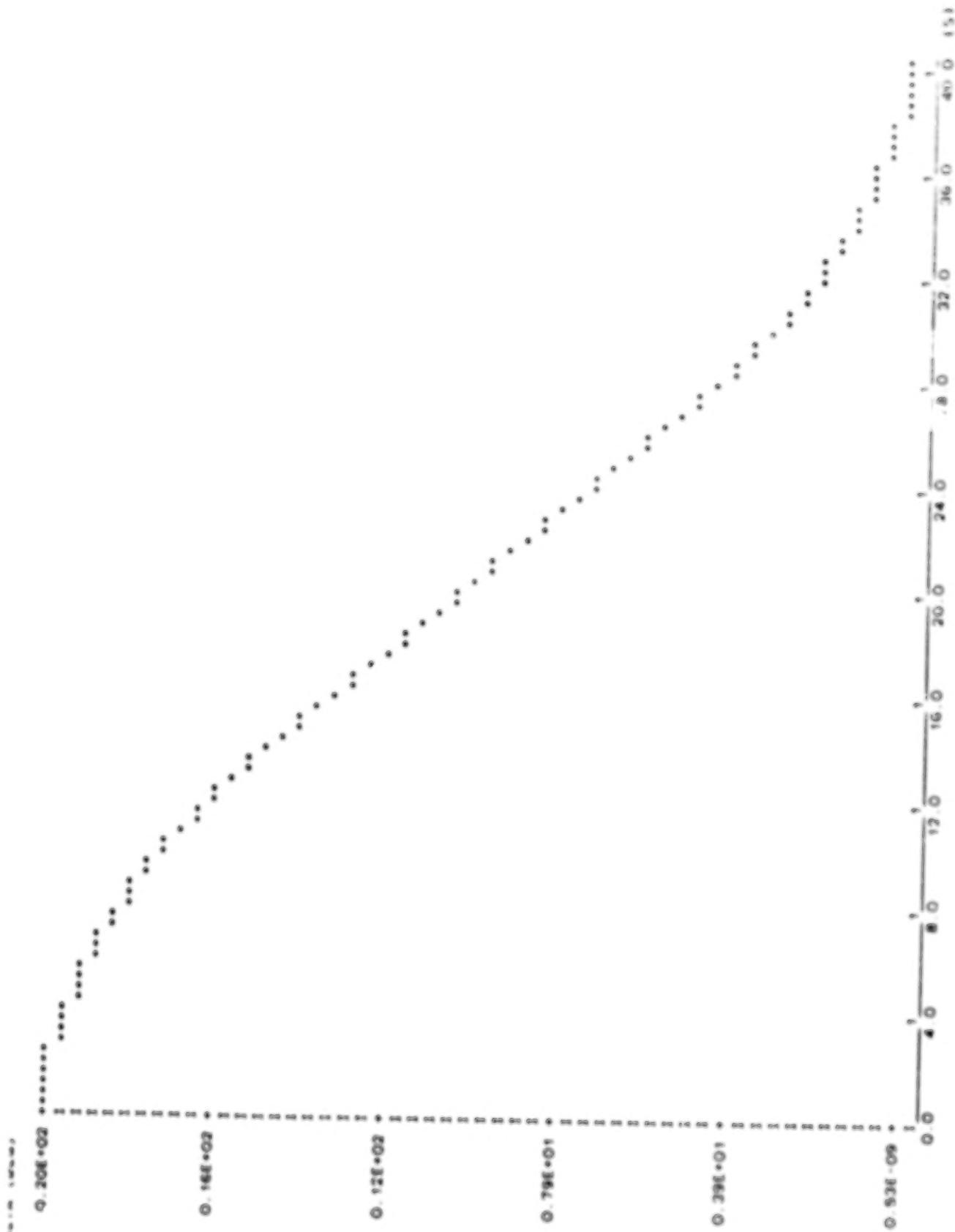
## TPBVP

$$\dot{z} = Cz, \quad z = [s, \lambda]^T = [z_1, z_2]^T$$

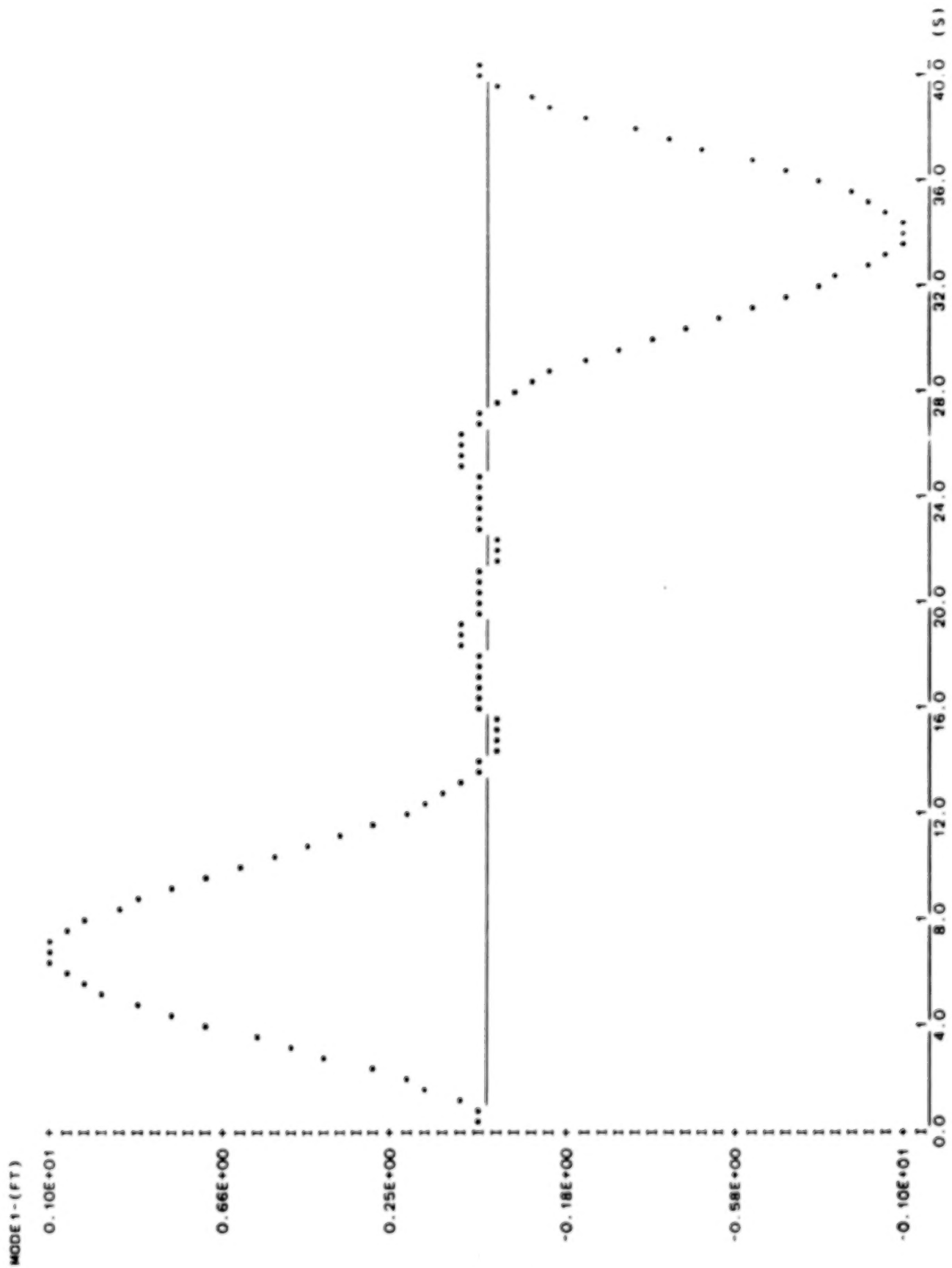
$\lambda$  is the costate vector,

$z_1(0), z_1(t_f)$  known;

$z_2(0)$  to be determined.

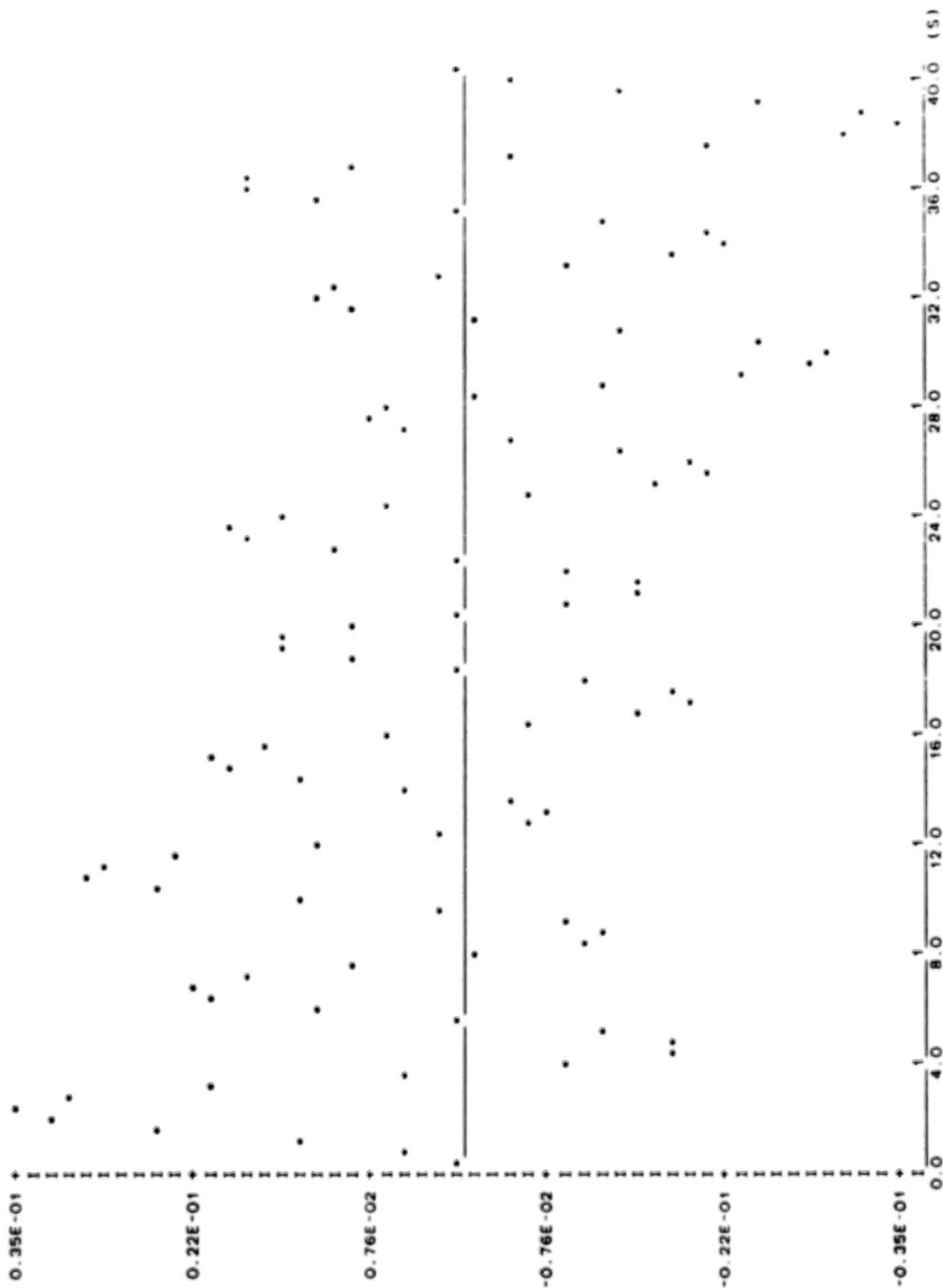


3-MODE LINEARIZED CASE: U=1 0 0 0 1, Q-DIAG 0. 0. 0. 0. 1

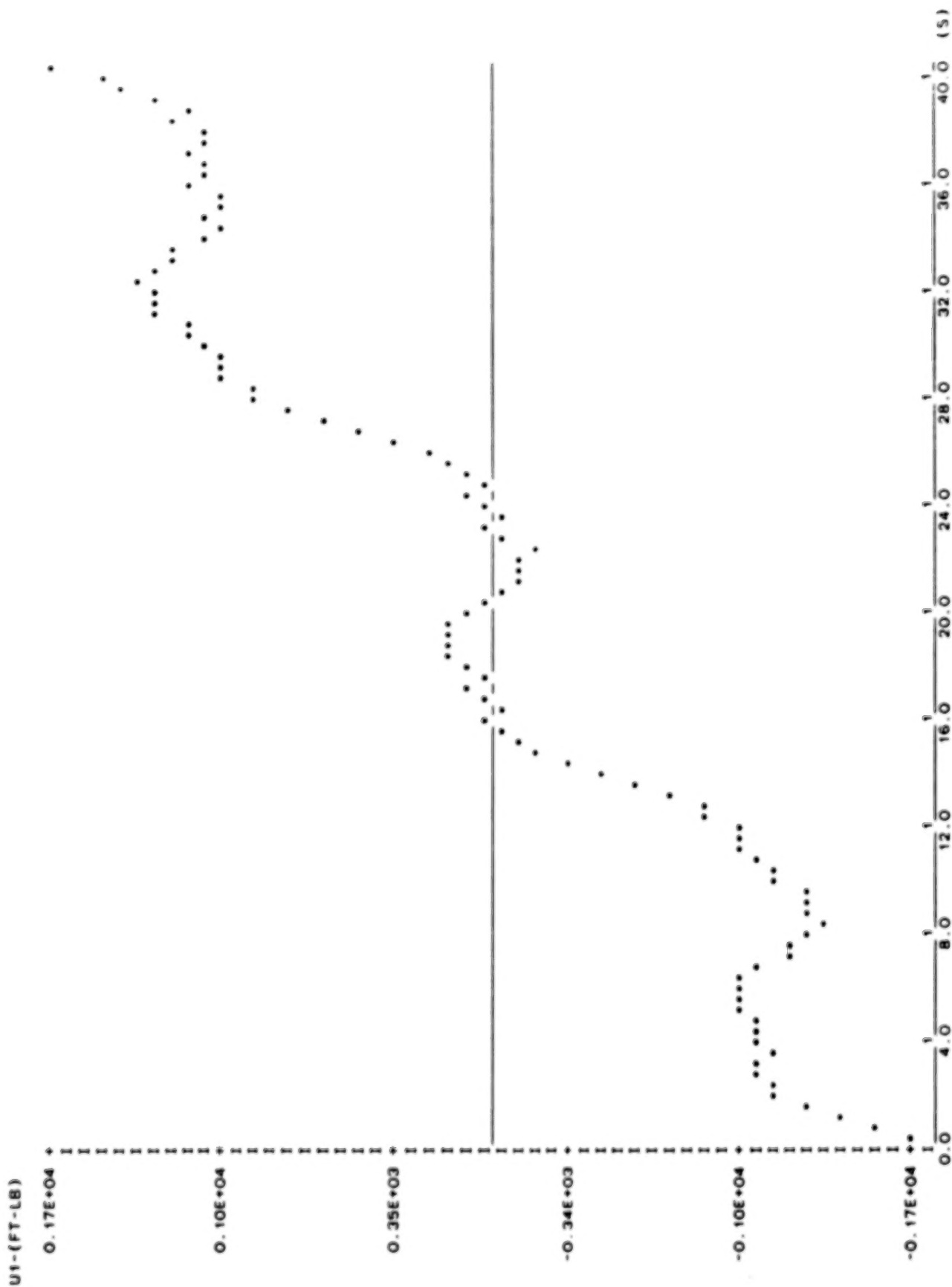


3-MODE LINEARIZED CASE: U=( 1 0 0 0 ), Q-DIAG( 0, 0, 0, 0 )

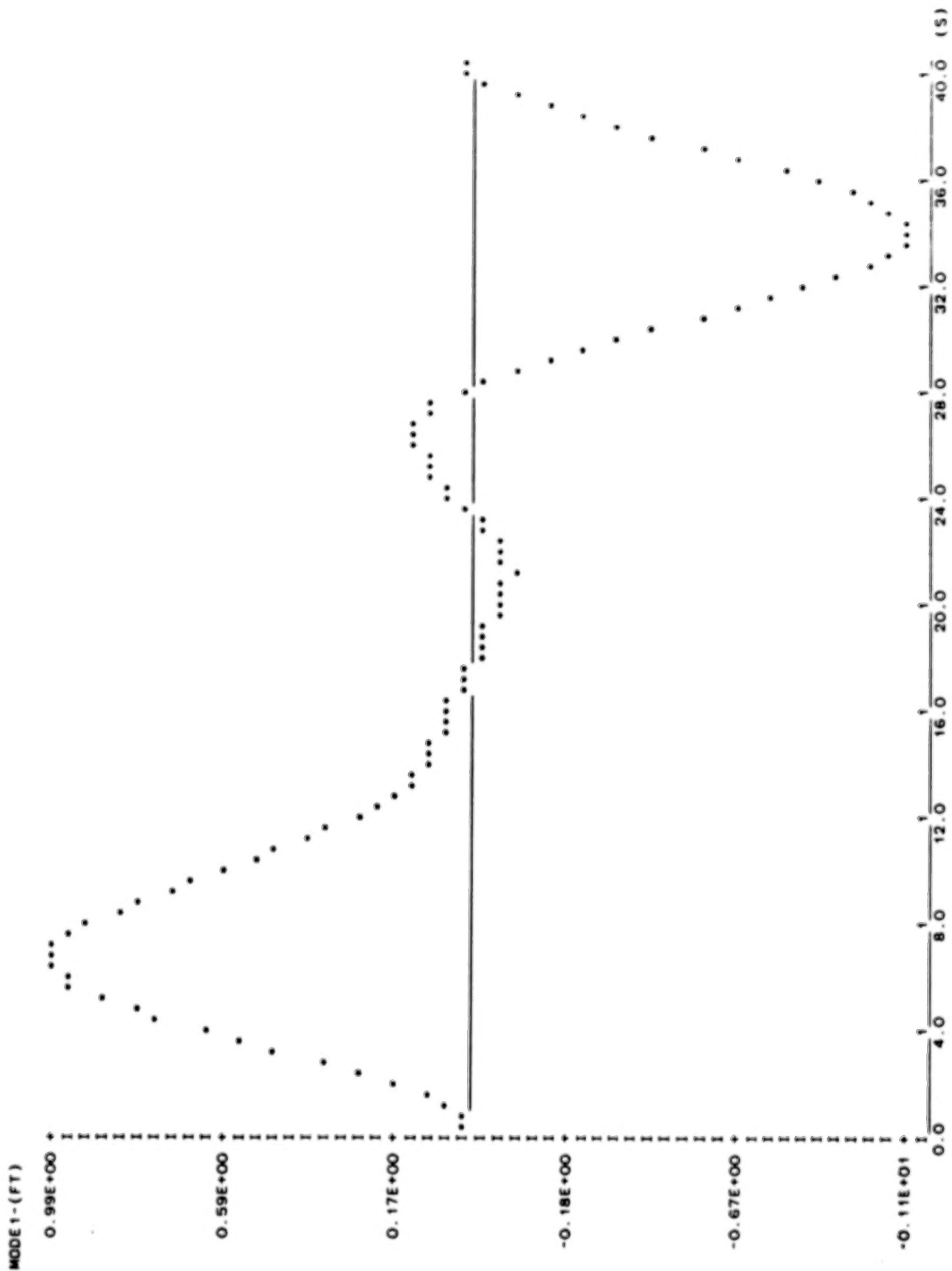
MODE2-(FT)

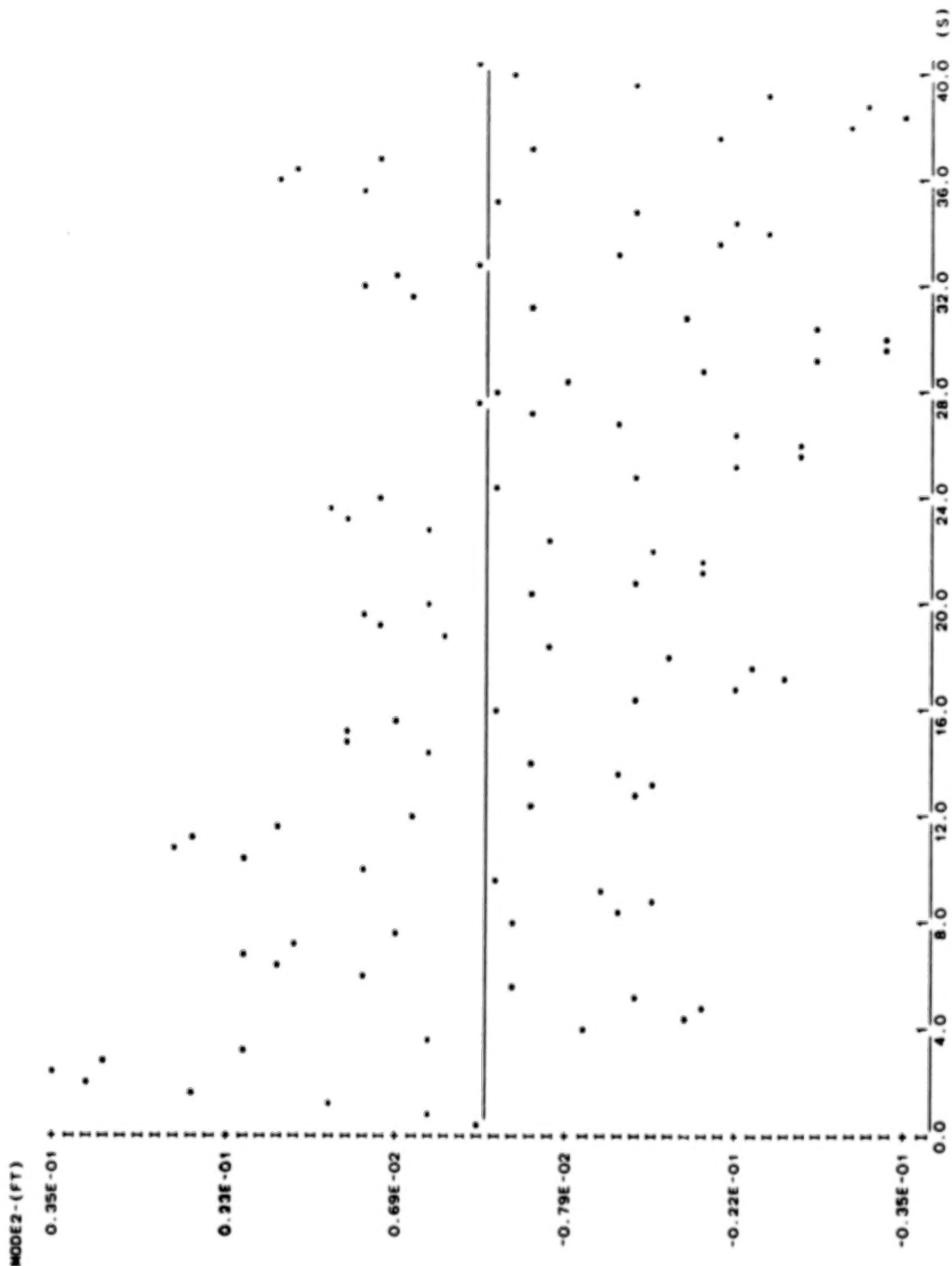


3-MODE LINEARIZED CASE: U=( 1 0 0 0 ), Q-DIAG( 0, 0, 0, 0 )



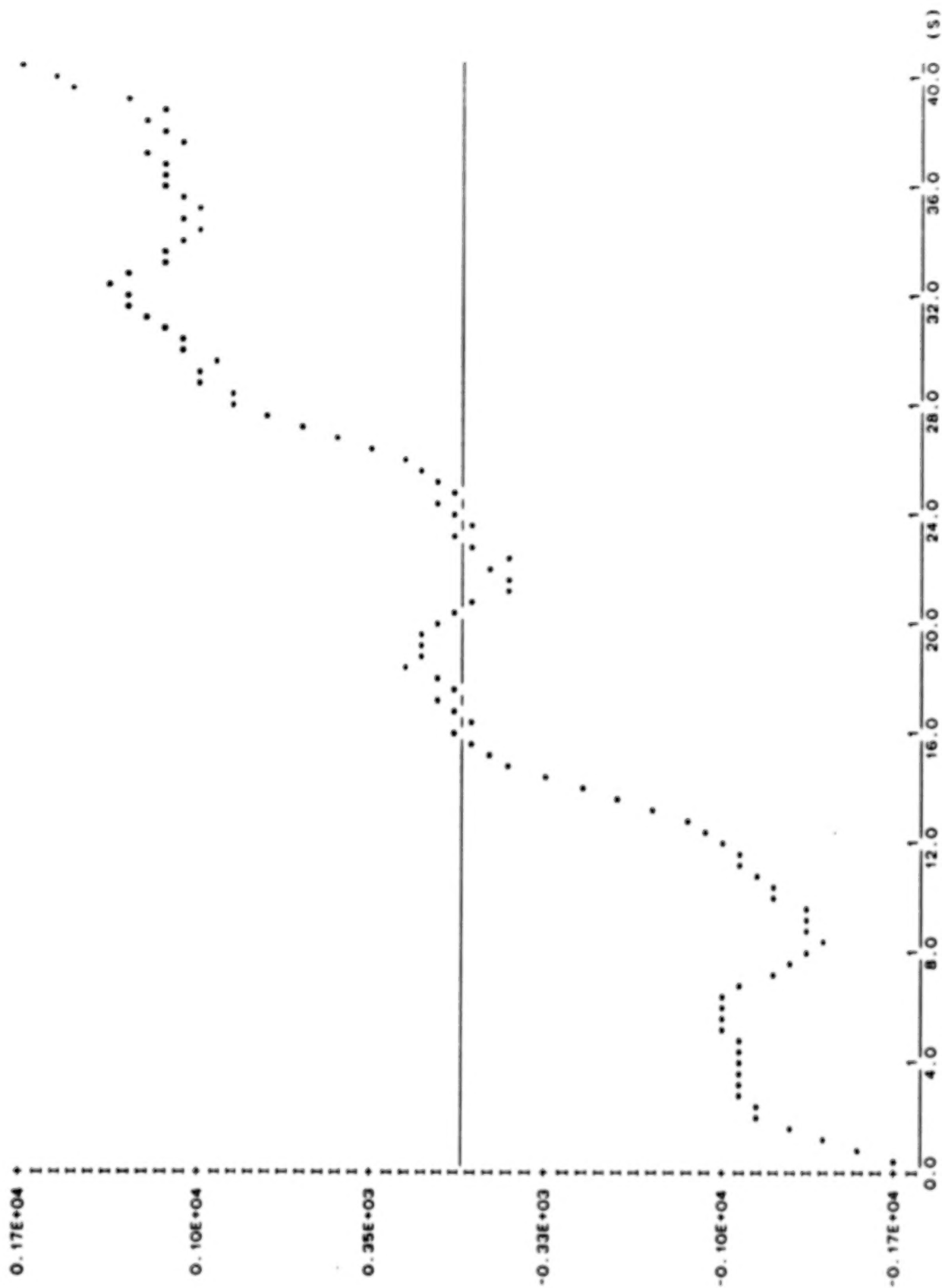
3-MODE LINEARIZED CASE: U=( 1 0 0 0 ), Q-DIAG( 0, 0, 0, 0 )





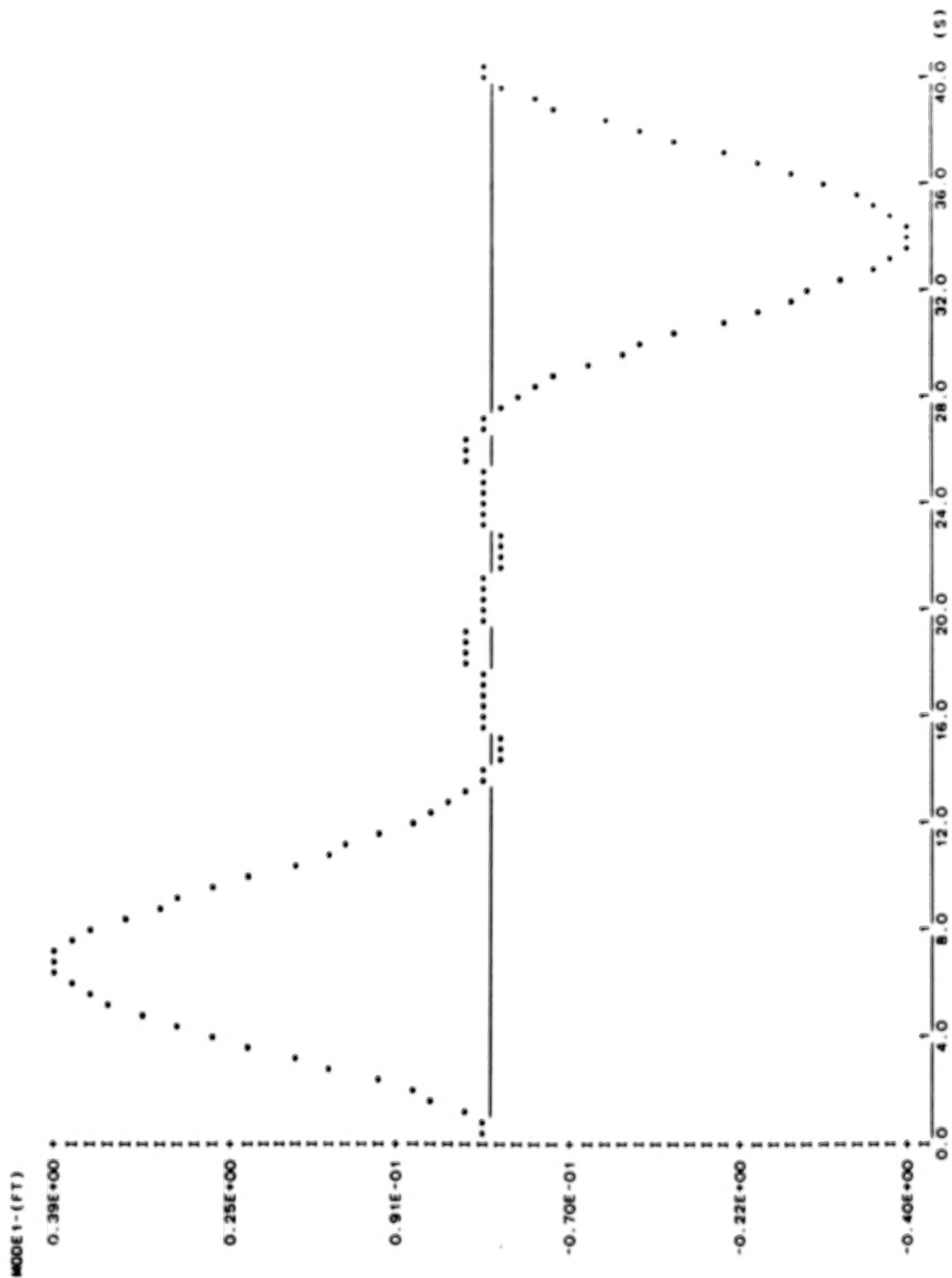
3-MODE NONLINEAR CASE: U=( 1 0 0 0 ), Q=DIAG( 0, 0, 0, 0 )

U1-(FT-LB)



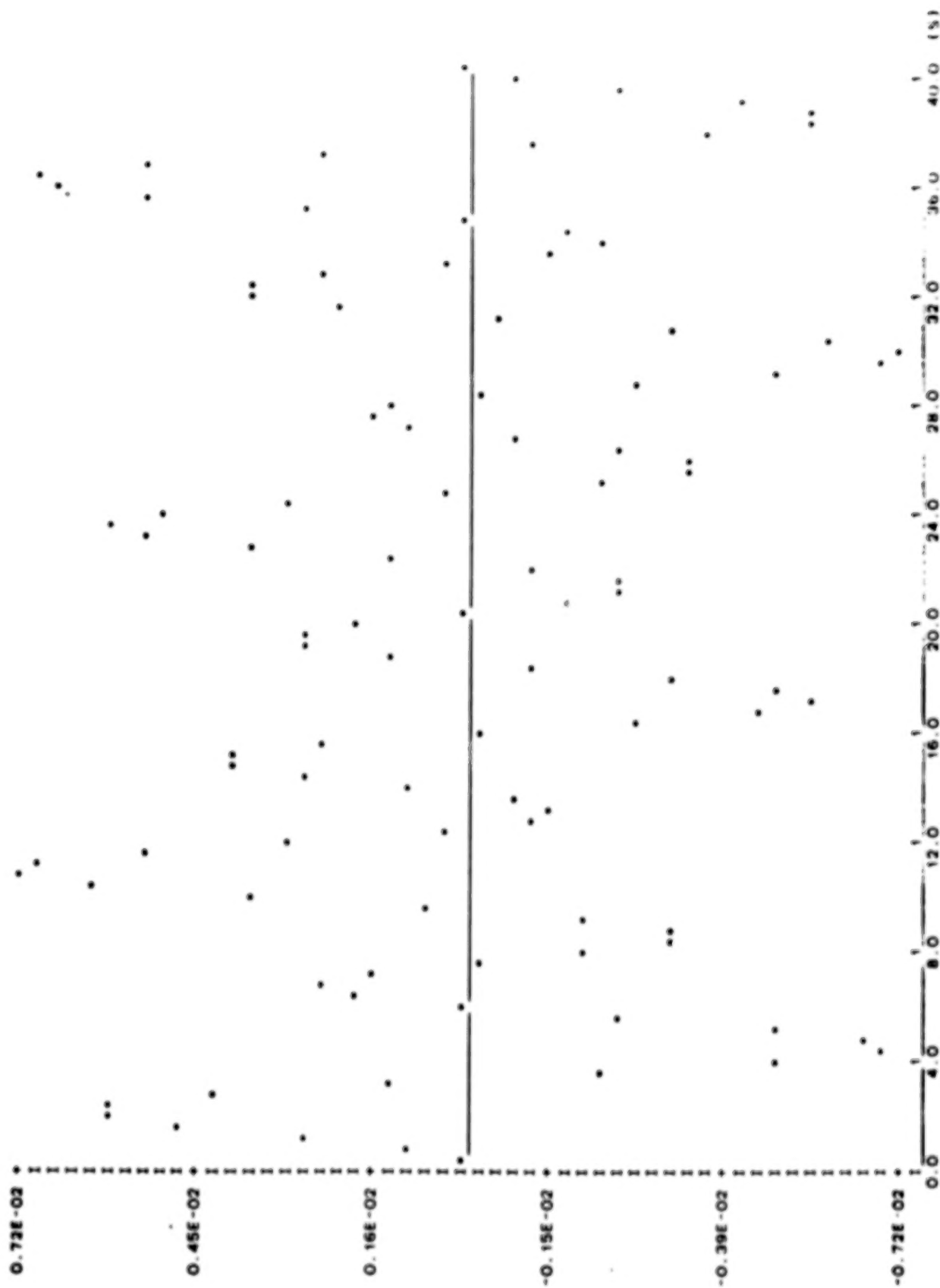
3-MODE NONLINEAR CASE: U=( 1 0 0 0 ), Q=DIAG( 0, 0, 0, 0 )



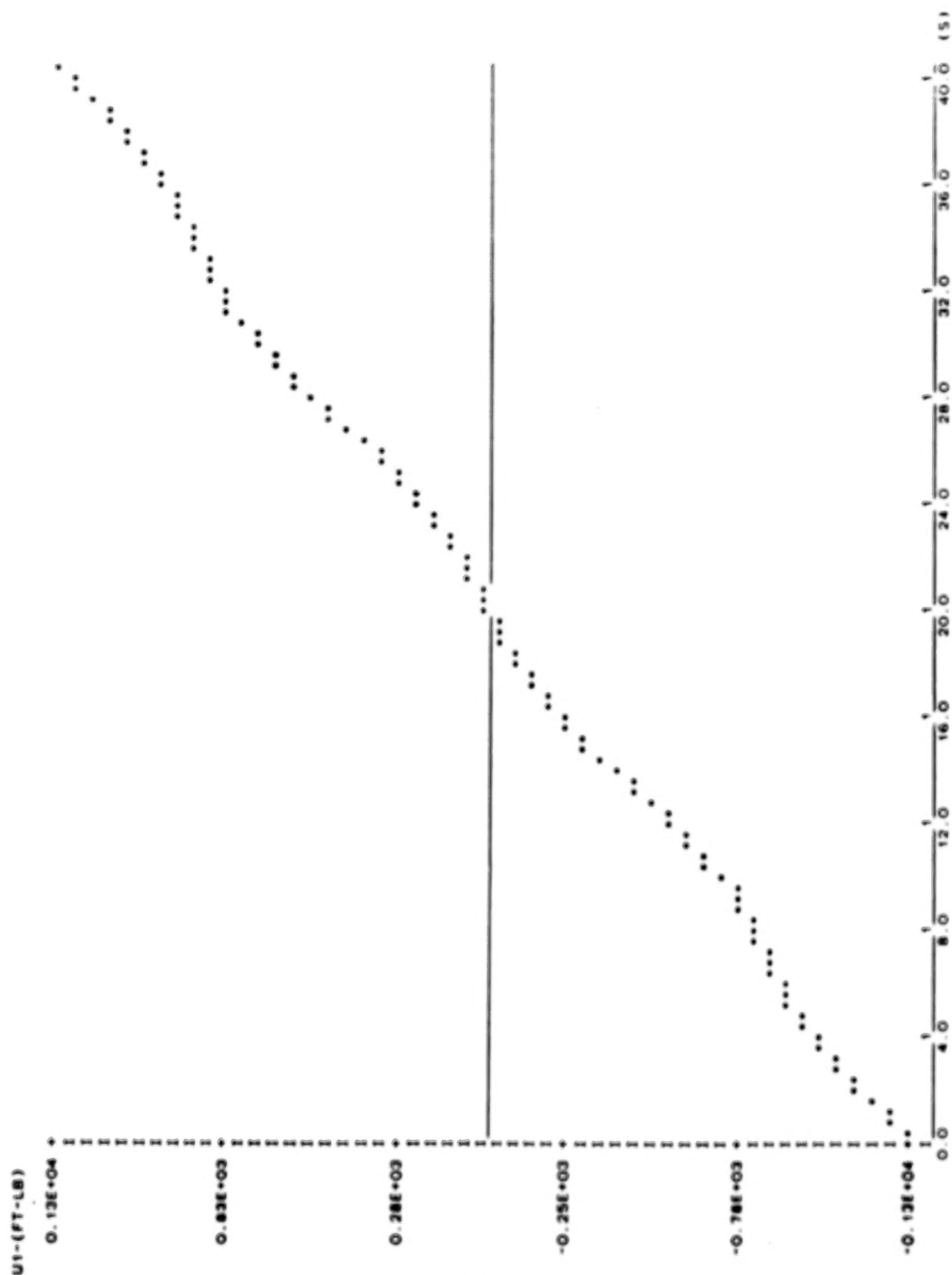


3-mode linearized CASE: U=( 1 0 0 4 ), q=diag(0, 0, 0, 0), r=diag(1.e-6, 0, 0, 1.e-1)

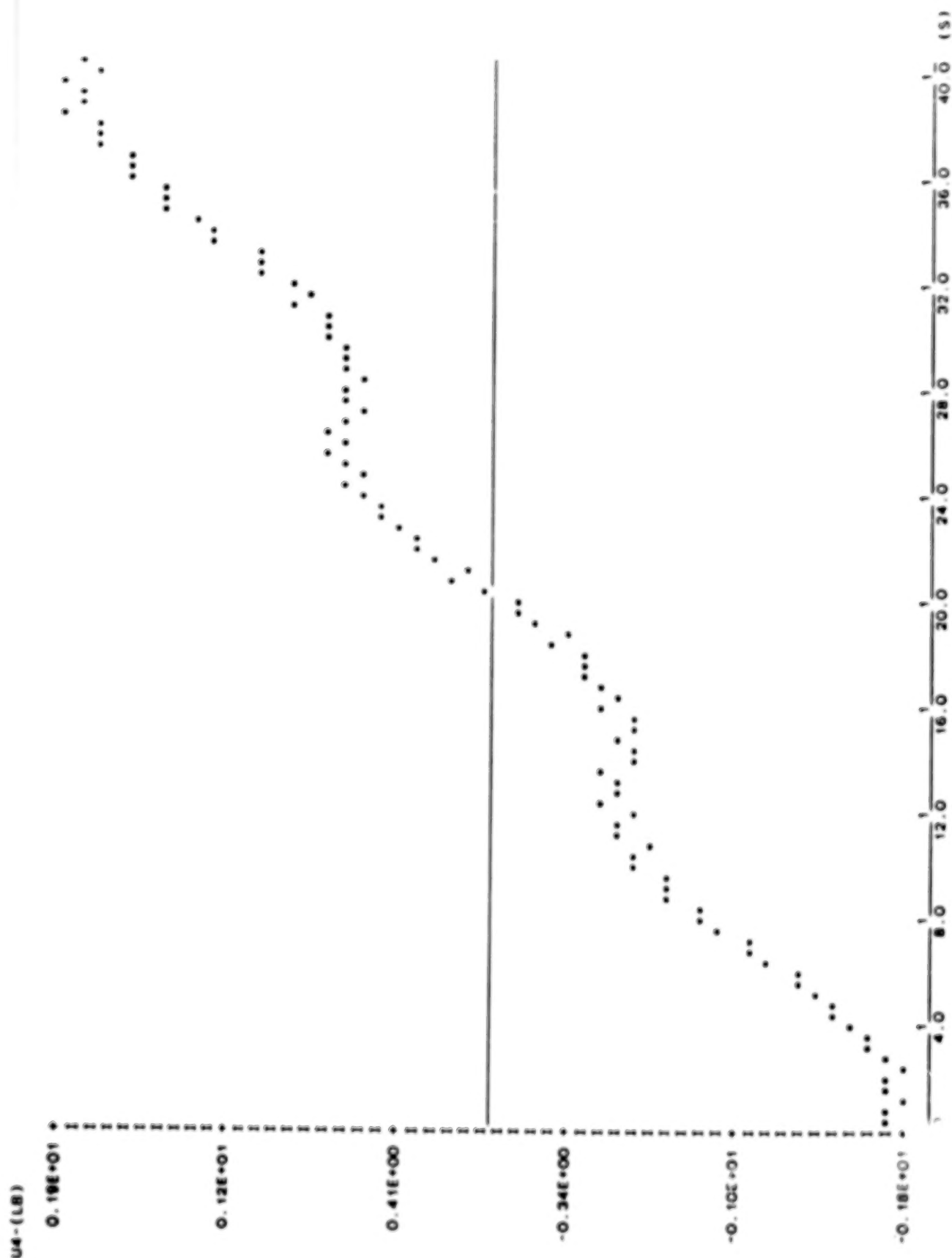
MODE2-(FT)



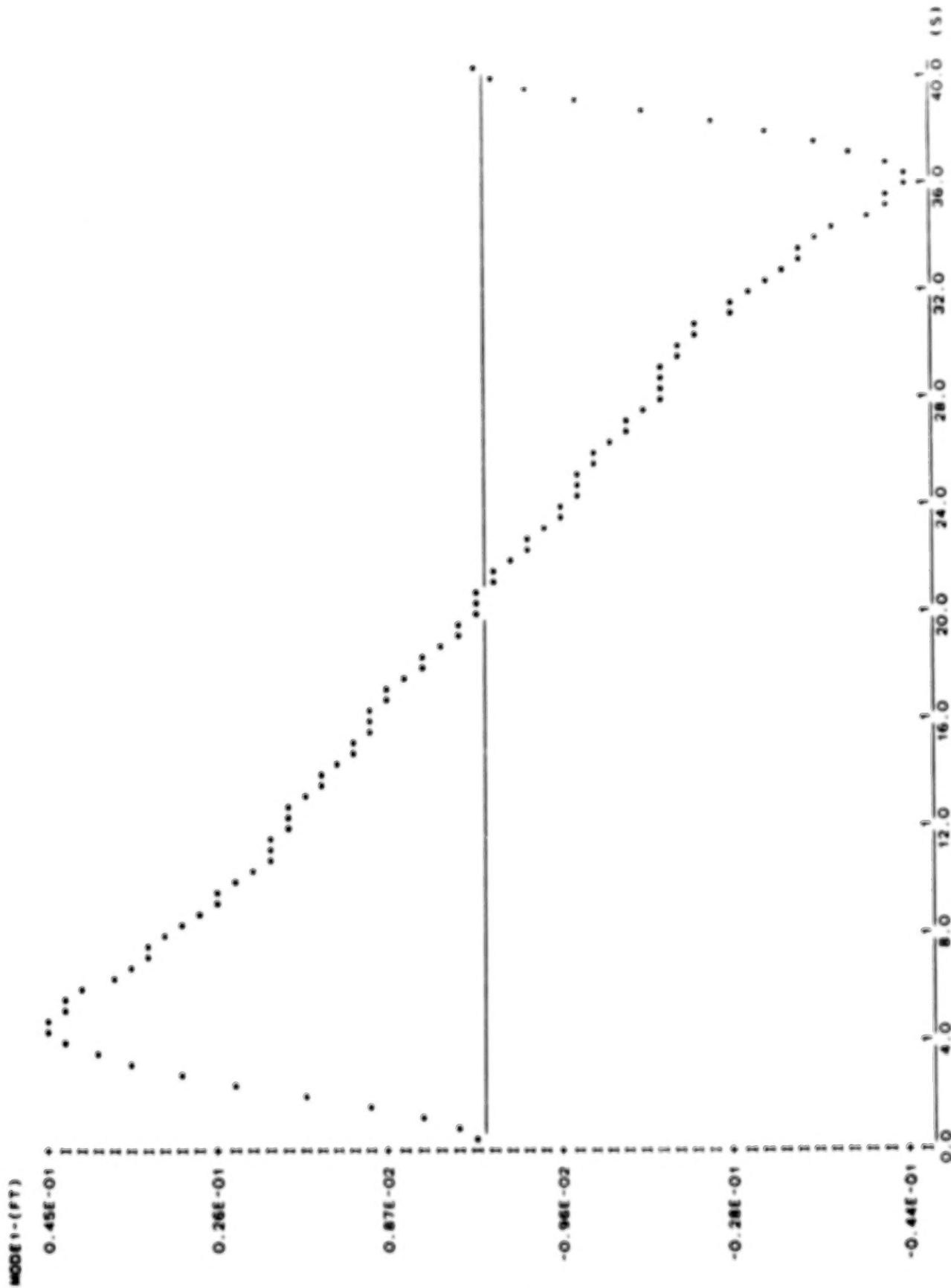
3-mode linearized CASE: U=( 1 0 0 4 ), q=diag(0, 0, 0, 0), r=diag(1.e-6, 0, 0, 1.e-1)



3-node linearized CASE: U=( 1 0 0 4 ), q=diag(0, 0, 0, 0), r=diag(1.e-6, 0, 0, 1.e-1)

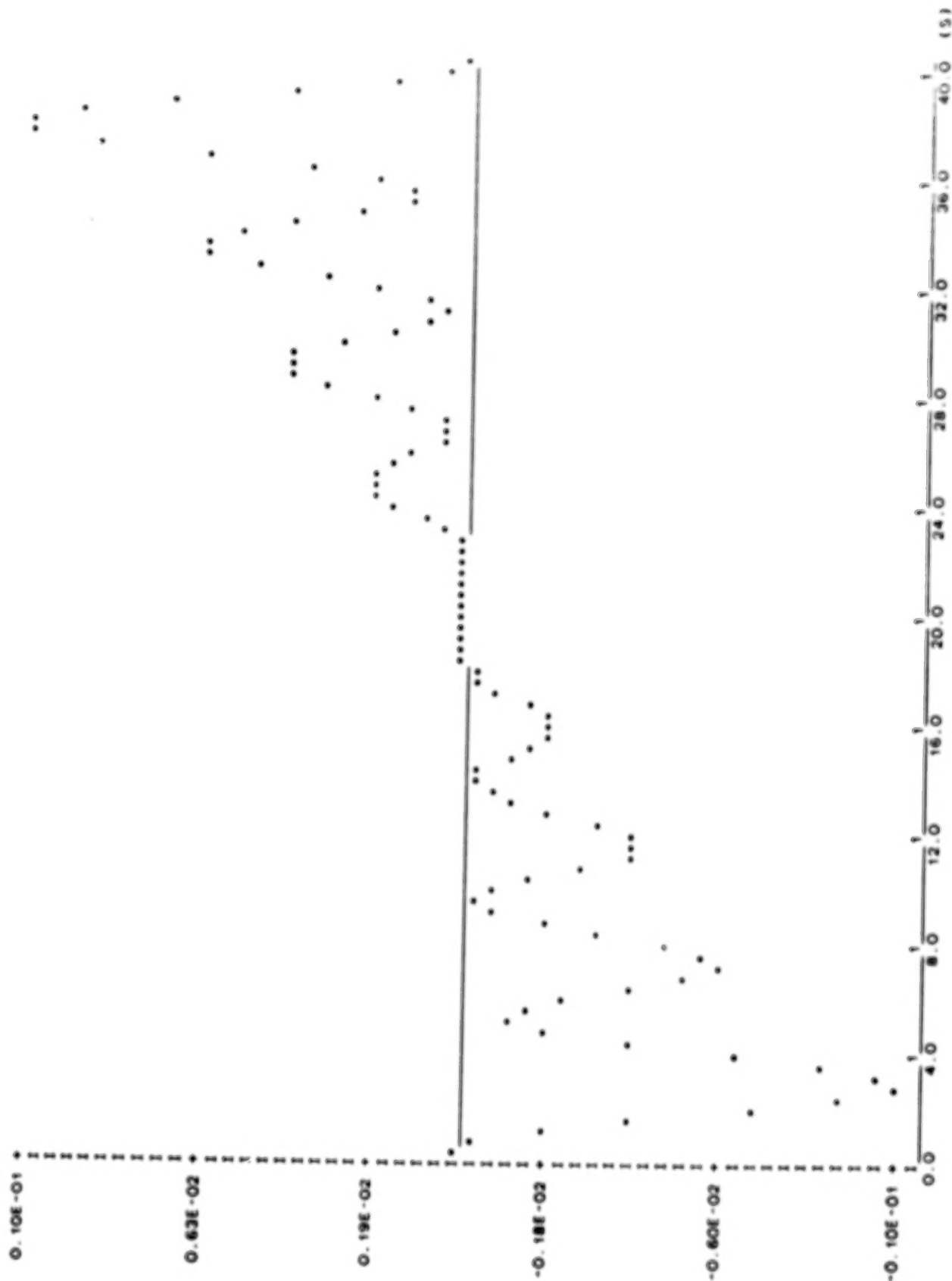


3-mode linearized CASE: U=(1 0 0 4), q=diag(0, 0, 0, 0), r=diag(1.e-6, 0, 0, 1.e-1)

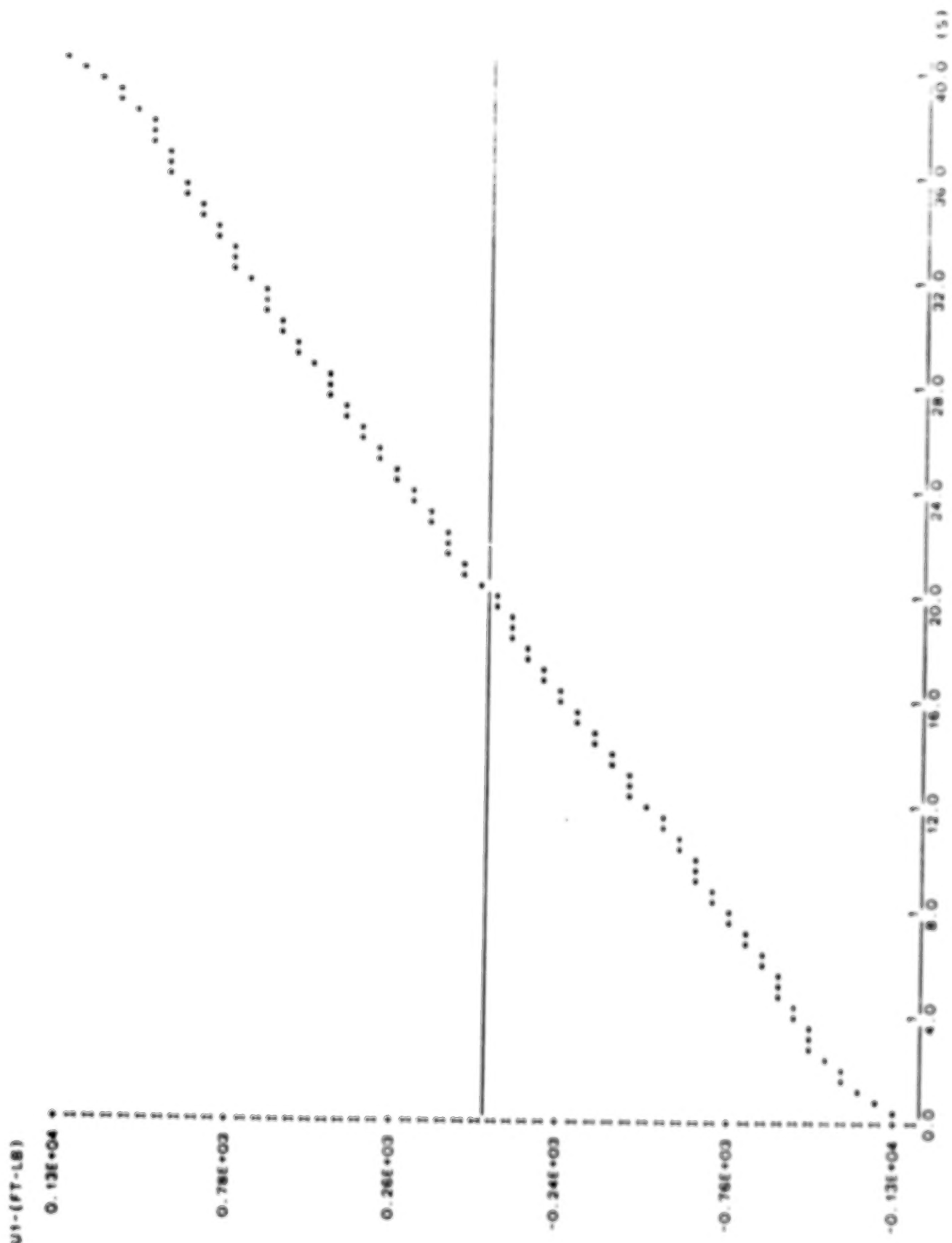


3-mode linearized case: u(1 0 0 4), q=diag(0, 10, .1, .1, .1, .1, .1), r=diag(1.e-6, 0, 0, 1.e-1)

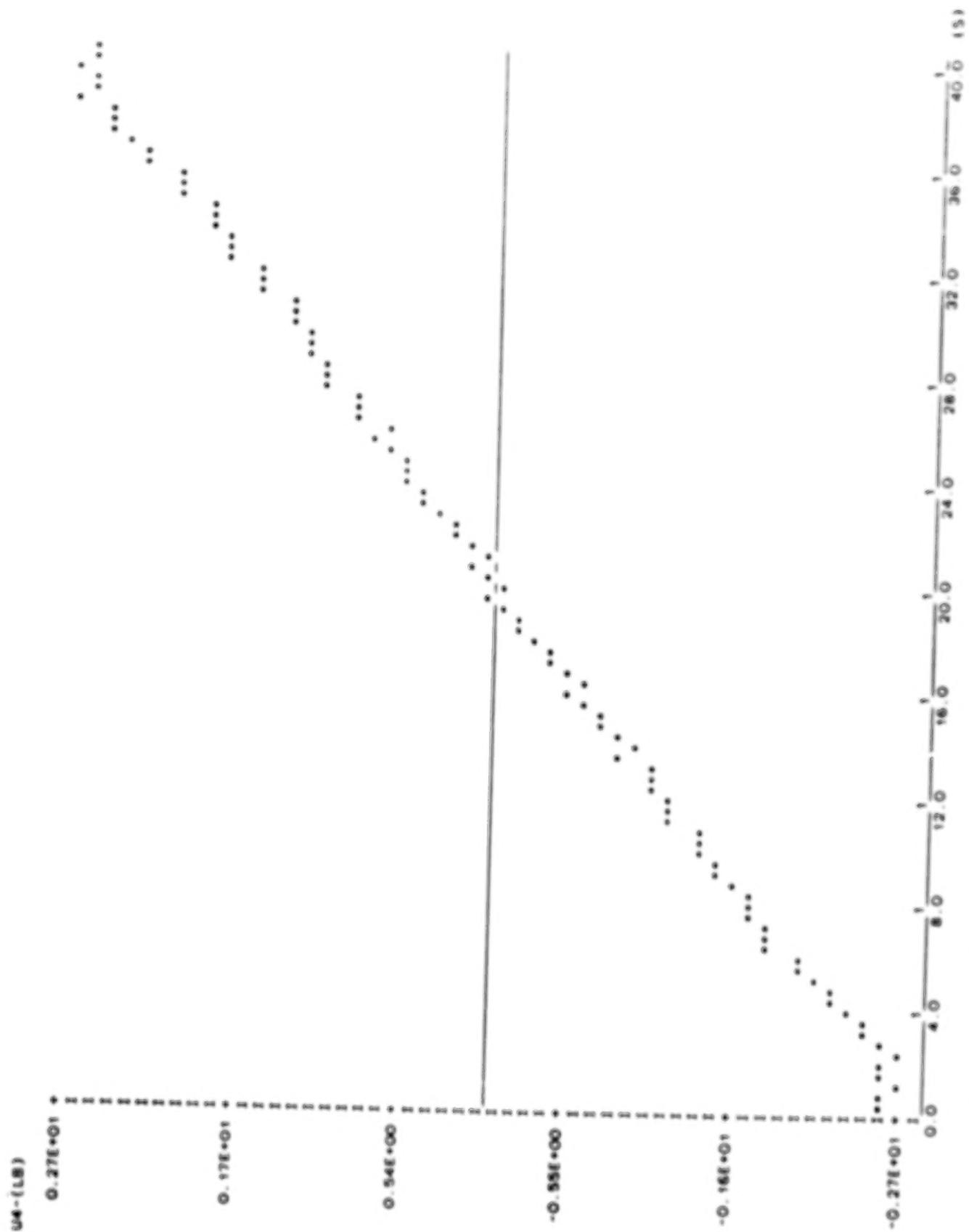
MODE2--(FY)



3-mode linearized case: u(1 0 0 4), q=diag(0, 10, .1, .1, .1, .1, .1), r=diag(1e-6, 0, 0, 1e-1)



3-mode linearized case: u(1 0 0 4), q=diag(0, 10, 1, 1, 1, 1, 1, 1), r=diag(1e-5, 0, 0, 0, 1e-1)



3-mode linearized case: u(1 0 0 4), q=diag(0, 16, 1, 1, 1, 1, 1), r=diag(1e-6, 0, 0, 1e-1)



### Concluding Remarks

- 1) For the examples given here, the solutions of the linearized equation and the nonlinear equation are close.
- 2) Use of the Maximum Principle can make the states satisfy the boundary conditions very well.
- 3) Due to the fact that the costates must be used in the method, the number of equations of the system is doubled, and more time is needed for the computation.
- 4) Further work on more complicated models (3-D) is needed.
- 5) Need to consider different cost functions and perform parametric studies.

# **EXPERIMENTAL RESULTS IN MODELING, ANALYSIS, AND CONTROL OF FLEXIBLE MULTI-BODY SYSTEMS**

5th Annual SCOLE Workshop  
October 31-November 1, 1988  
Lake Arrowhead, California

Sponsored by:  
Langley Flight Research Center, NASA  
Flight Systems Research Laboratory, UCLA

---

**M**

**A. Galip Ulsoy**

**Mechanical Engineering and Applied Mechanics  
University of Michigan, Ann Arbor, Michigan**

## MOTIVATION

- Modeling, analysis, and control of multi-body systems with flexible elements is of interest in many technologies including robotics, space structures, and high speed mechanisms.
- While the basic problem is well studied and understood, there are some important aspects requiring further research. These include full nonlinear coupling, prismatic joints, controller design, and impact.
- In all the research areas cited above, there is a need for experimental as well as analytical and numerical studies.

---

**M**

**A. Galip Ulsoy**

**Mechanical Engineering and Applied Mechanics  
University of Michigan, Ann Arbor, Michigan**

## **BACKGROUND**

### **Modeling:**

- Song and Haug 1980
- Shabana and Wehage 1983
- Ryan 1985

### **Analysis and Simulation:**

- ADAMS, DADS, TREETOPS, etc
- Sunada and Dubowsky 1983
- Wang and Wei 1987
- Wehage and Haug 1982; Khulief and Shabana 1984

### **Control:**

- Book, Maizzo-Neto and Whitney 1975
- Meckl and Seering 1983

### **Experiments:**

- Zalucky and Hardt 1982
- Cannon and Schmitz 1983

---

**M**

**A. Galip Ulsoy**

**Mechanical Engineering and Applied Mechanics  
University of Michigan, Ann Arbor, Michigan**

## RECENT RESEARCH AT MICHIGAN

- Control of a spherical coordinate robot arm with one flexible link using only the joint actuators, but with both joint and end-of-arm sensors. Modeling, analysis, and controller design. Modeling of the rigid/flexible manipulator including the non-backdrivable leadscrew transmission mechanisms. Comparison of simulation and experimental results. Evaluation of a rigid body motion controller and a rigid and flexible motion controller.
- Modeling and simulation of robots with rigid and/or flexible links and revolute and/or prismatic joints. Employs a Lagrangian formulation with kinematic constraints and a finite element discretization. Euler-Bernoulli beam theory is employed, but the axial stiffening effect is included. Experimental evaluation of the modeling approach and solution method.
- Modeling of impact in systems with flexible links. Various impact modeling methods are compared with each other and with the results of experiments for a radially rotating elastic beam. The impact models employed all provide reasonably accurate results when appropriately employed; even the momentum balance (coefficient of restitution) method which strictly speaking is not applicable to flexible systems.

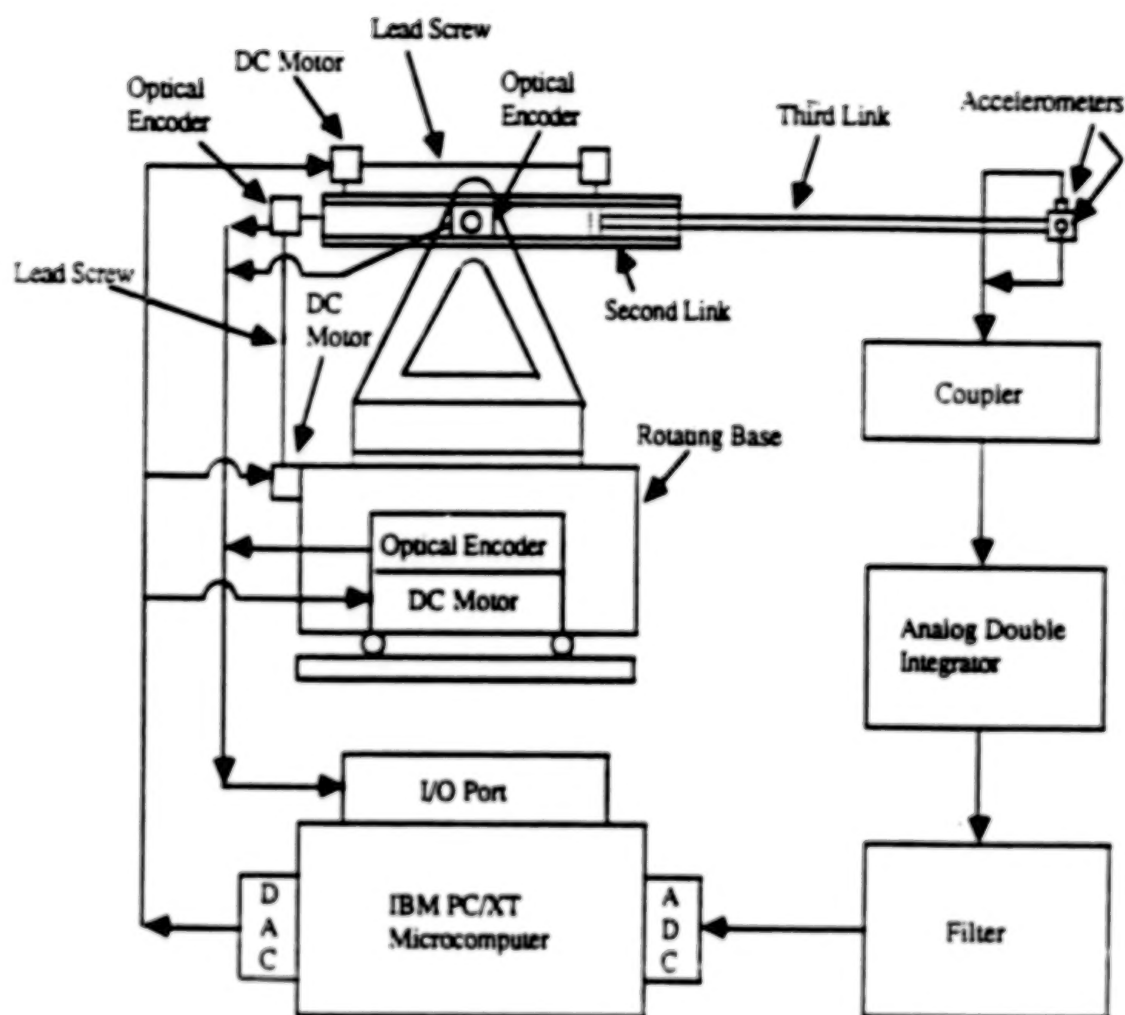
---

**M**

**A. Galip Ulsoy**

**Mechanical Engineering and Applied Mechanics  
University of Michigan, Ann Arbor, Michigan**

# FLEXIBLE MANIPULATOR CONTROL



Schematic of the experimental setup.

**M**

**A. Galip Ulsoy**

**Mechanical Engineering and Applied Mechanics  
University of Michigan, Ann Arbor, Michigan**

## **FLEXIBLE MANIPULATOR CONTROL**

- **The laboratory robot is used to compare the performance of a rigid body motion controller with that of a rigid and flexible motion controller.**
- **The rigid body motion controller uses only the joint motion measurements and joint actuators. The rigid and flexible motion controller also uses the end of arm motion measurements, but no additional actuators.**
- **The leadscrew transmission characteristics as well as observation and control spillover are considered.**
- **The numerical and experimental results show good agreement, and indicate that significant reductions in arm vibration are possible through use of the rigid and flexible motion controller.**

---

**M**

**A. Galip Ulsoy**

**Mechanical Engineering and Applied Mechanics  
University of Michigan, Ann Arbor, Michigan**

## FLEXIBLE MANIPULATOR CONTROL

Equations of motion:

$$\underline{M}(\underline{x}) \underline{\ddot{x}} + \underline{F}(\underline{x}, \underline{\dot{x}}) = \underline{F}'(\underline{I})$$

$$\underline{x}^T = [r, \theta, \phi, q_{11}, q_{12}, q_{21}, q_{22}]$$

$$\underline{I}^T = [\tau_1, \tau_2, \tau_3]$$

Linearized equations:

$$\underline{\dot{y}} = \underline{A} \underline{y} + \underline{B} \underline{u}$$

$$\underline{y}^T = [\delta \underline{x}^T \ \delta \underline{\dot{x}}^T] ; \quad \underline{u} = \delta \underline{I}$$

$$\delta \underline{x}^T = [\delta r, \delta \theta, \delta \phi, \delta q_{11}, \delta q_{21}]$$

Integral plus state feedback controller:

$$y_{11} = \int_0^t (y_1 - R_1) dt ; \quad y_{12} = \int_0^t (y_2 - R_2) dt ; \quad y_{13} = \int_0^t (y_3 - R_3) dt$$

$$\underline{u} = -\underline{K}^F \underline{y}$$

$$\underline{\dot{y}} = (\underline{A} - \underline{B}\underline{K}^F) \underline{y}$$

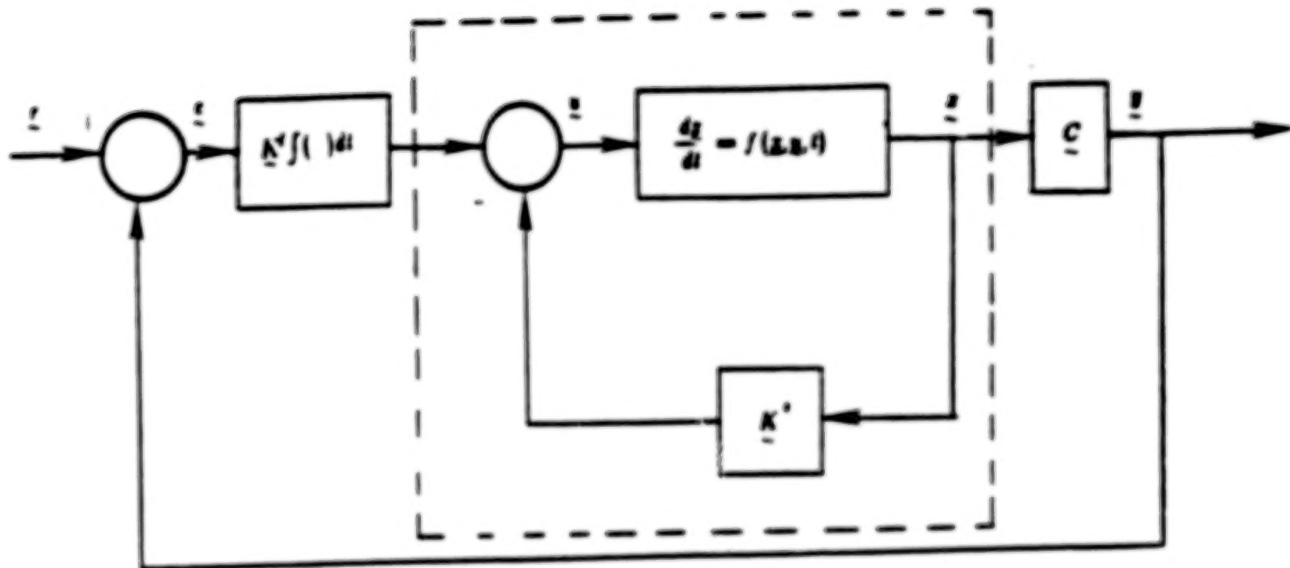
# M

A. Galip Ulsoy

Mechanical Engineering and Applied Mechanics  
University of Michigan, Ann Arbor, Michigan



## FLEXIBLE MANIPULATOR CONTROL



Block diagram of the integral plus state feedback controller.

**M**

**A. Galip Ulsoy**

Mechanical Engineering and Applied Mechanics  
University of Michigan, Ann Arbor, Michigan

## FLEXIBLE MANIPULATOR CONTROL

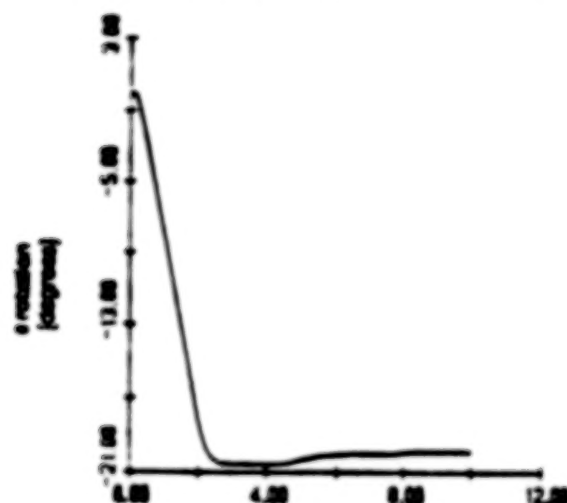
Standard Set of Physical System Parameters	VALUE
Mass of the first beam ( $m_1$ )	0.454 Kg
Mass of the second beam ( $m_2$ )	0.816 Kg
Mass of the Payload ( $m_p$ )	0.07 Kg
Cross sectional area of the second beam ( $A_2$ )	0.000151 m <sup>2</sup>
Length of the first beam ( $L_1$ )	0.233 m
Length of the second beam ( $L_2$ )	2 m
Gravitational acceleration ( $g$ )	9.81 m/sec <sup>2</sup>
Aluminum density ( $\rho$ )	2707 Kg/m <sup>3</sup>
Flexural rigidity ( $EI$ )	770.87 Pa
Reference position for $r$	1.85 m
Reference position for $\theta$	0 rad
Reference position for $\phi$	0 rad
Desired reference position for $r$	2m
Desired reference position for $\theta$	0.5 rad
Desired reference position for $\phi$	0.5 rad
Servo natural frequency for $r$ ( $\omega_{nr}$ )	4 rad/sec
Servo natural frequency for $\theta$ ( $\omega_{n\theta}$ )	4 rad/sec
Servo natural frequency for $\phi$ ( $\omega_{n\phi}$ )	8 rad/sec
Flexible motion gain, $K_{19}^F$	-0.000178
Flexible motion gain, $K_{29}^F$	-0.084
Flexible motion gain, $K_{410}^F$	1.568

# M

A. Galip Ulsoy

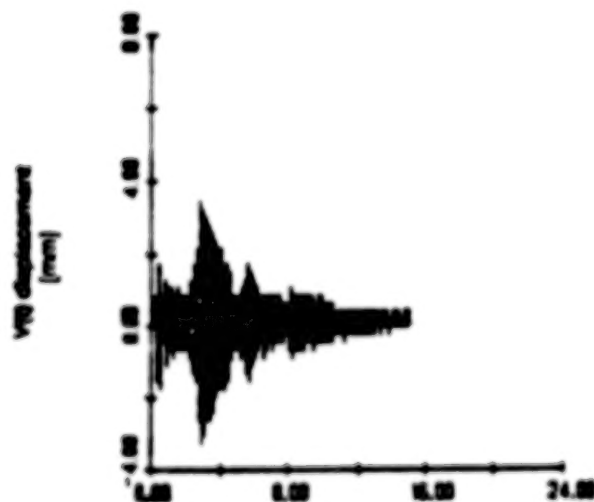
Mechanical Engineering and Applied Mechanics  
University of Michigan, Ann Arbor, Michigan

## FLEXIBLE MANIPULATOR CONTROL



Time (seconds)

$\theta$  response obtained from the rigid body controller in the experimental work.



Time (seconds)

Total vertical deflection in response to the rigid body controller in the experimental work.

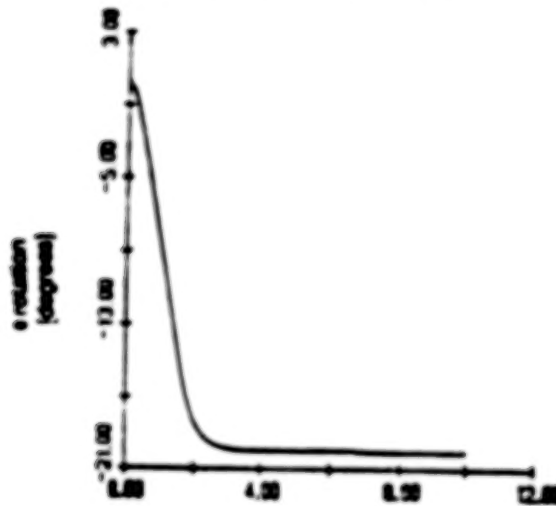
---

# M

A. Galip Ulsoy

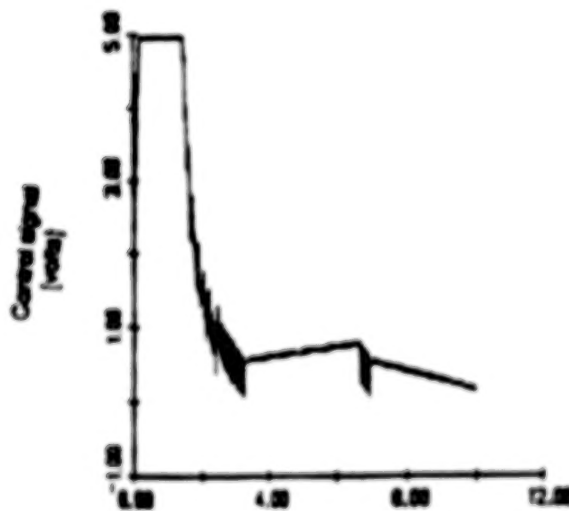
Mechanical Engineering and Applied Mechanics  
University of Michigan, Ann Arbor, Michigan

## FLEXIBLE MANIPULATOR CONTROL



Time, s seconds

$\theta$  response obtained from the rigid and flexible motion controller in the experimental work.



Time, s seconds

Control signal for the second joint obtained from the rigid and flexible motion controller in the experimental work.

---

# M

A. Galip Ulsoy

Mechanical Engineering and Applied Mechanics  
University of Michigan, Ann Arbor, Michigan

## FLEXIBLE MANIPULATOR CONTROL

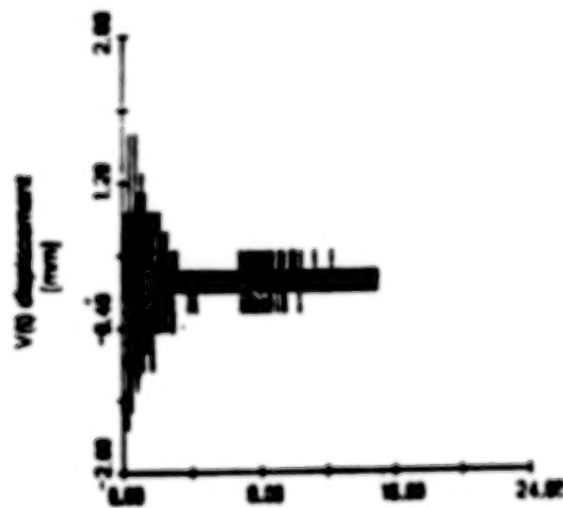


Fig. 3 Results

Total vertical deflection in response to the rigid and flexible motion controller in the experimental work.

	settling time (seconds)	maximum deflection (peak to peak)
rigid body controller	11.0	7.5mm
rigid and flexible motion controller	3.0	2.7mm

**M**

A. Galip Ulsoy

Mechanical Engineering and Applied Mechanics  
University of Michigan, Ann Arbor, Michigan

## FLEXIBLE MANIPULATOR CONTROL

### Simulation

- \* Control spillover effect can be observed, but does not cause significant deterioration.
- \* Control and observation spillover can destabilize the residual mode. However, a small amount of damping (0.0145) eliminates the problem.
- \* Settling time is reduced from 3.5 to 1.07 seconds, and maximum vibration amplitude is reduced by 50%.

### Experiment

- \* With low pass filtering and light structural damping, no detrimental spillover effects were observed.
- \* Settling time is reduced from 11 to 3 seconds, and maximum vibration amplitude is reduced by 75%.

---

**M**

A. Galip Ulsoy

Mechanical Engineering and Applied Mechanics  
University of Michigan, Ann Arbor, Michigan

## FLEXIBLE SYSTEMS WITH PRISMATIC JOINTS

- Robots with both rigid and flexible links attached with revolute and/or prismatic joints can be modeled and analyzed.
- The equations of motion are derived using Lagrange's equations. The prescribed motion, and prescribed torque/force cases can both be handled.
- Flexible elements are represented as Euler-Bernoulli beams, and the axial shortening effect is also included.
- Finite element analysis is used for the discretization of the resulting hybrid equations of motion.
- Constraints are handled using Lagrange multipliers.
- The resulting algebraic-differential equations are solved numerically using constraint stabilization methods.

---

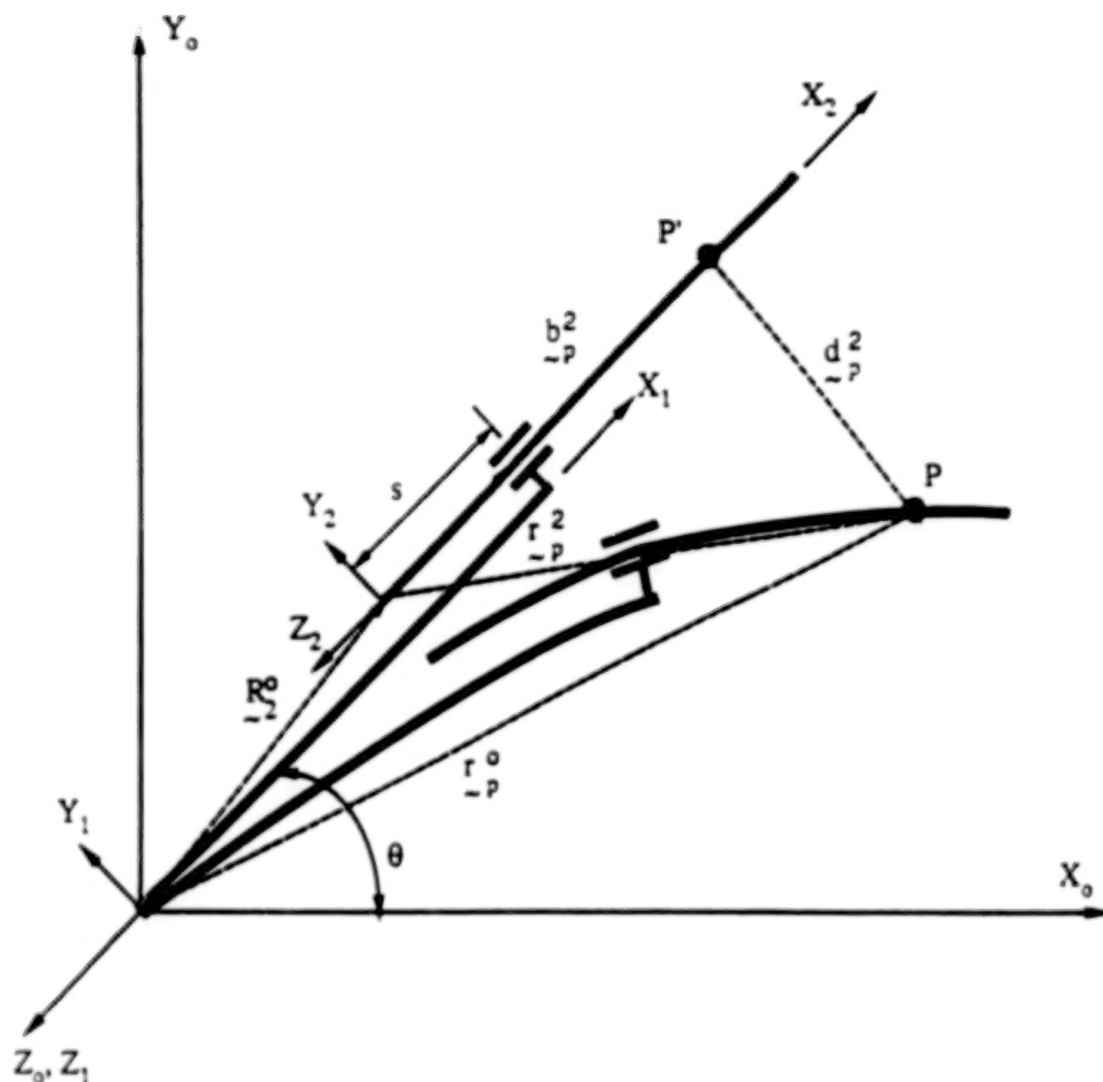
**M**

A. Galip Ulsoy

Mechanical Engineering and Applied Mechanics  
University of Michigan, Ann Arbor, Michigan

# FLEXIBLE SYSTEMS WITH PRISMATIC JOINTS

- Nominal configuration
- Actual configuration



Schematic of a two-link robot.

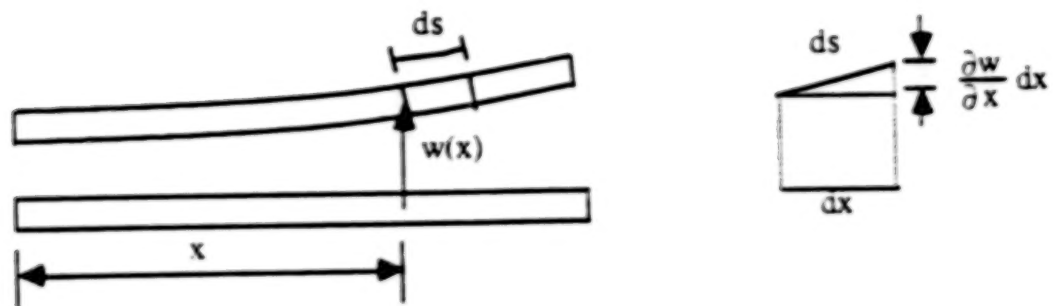
**M**

**A. Galip Ulsoy**

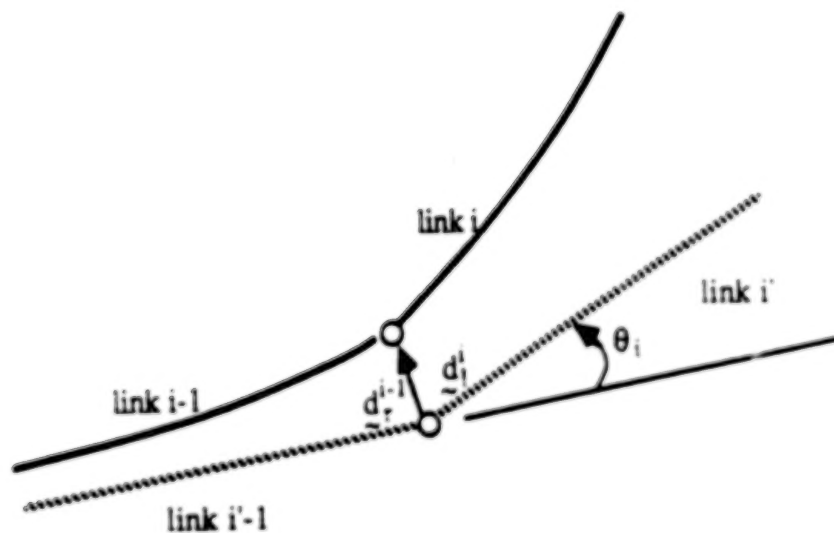
Mechanical Engineering and Applied Mechanics  
University of Michigan, Ann Arbor, Michigan



# FLEXIBLE SYSTEMS WITH PRISMATIC JOINTS



Axial shortening of a beam under plane transverse deflection.



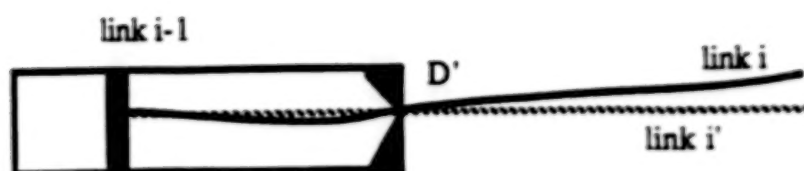
Schematic of revolute joint  $i$ .

**M**

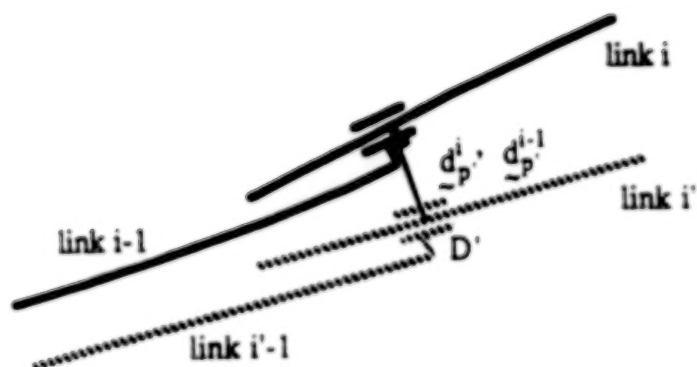
**A. Galip Ulsoy**

Mechanical Engineering and Applied Mechanics  
University of Michigan, Ann Arbor, Michigan

# FLEXIBLE SYSTEMS WITH PRISMATIC JOINTS



Schematic of prismatic joint i.



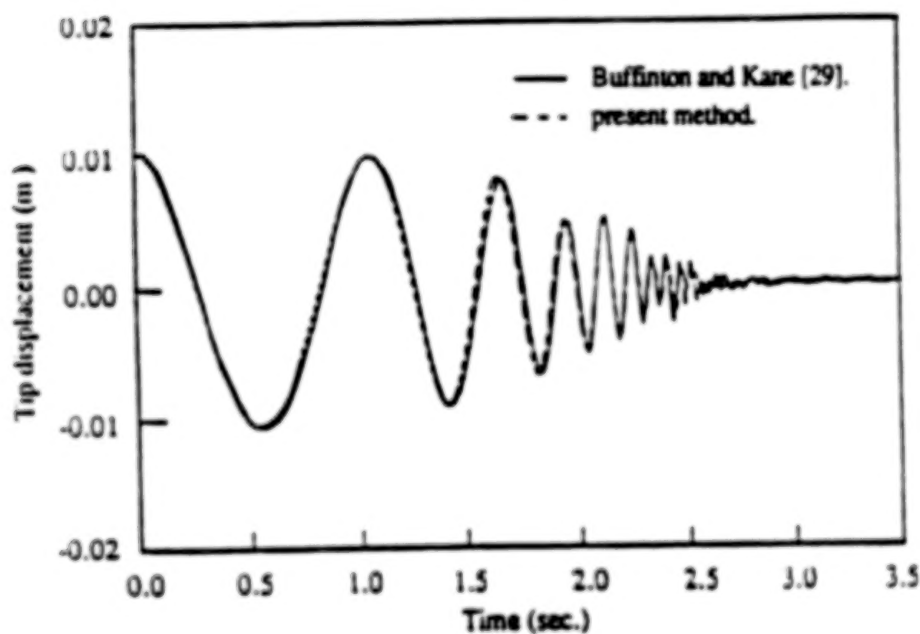
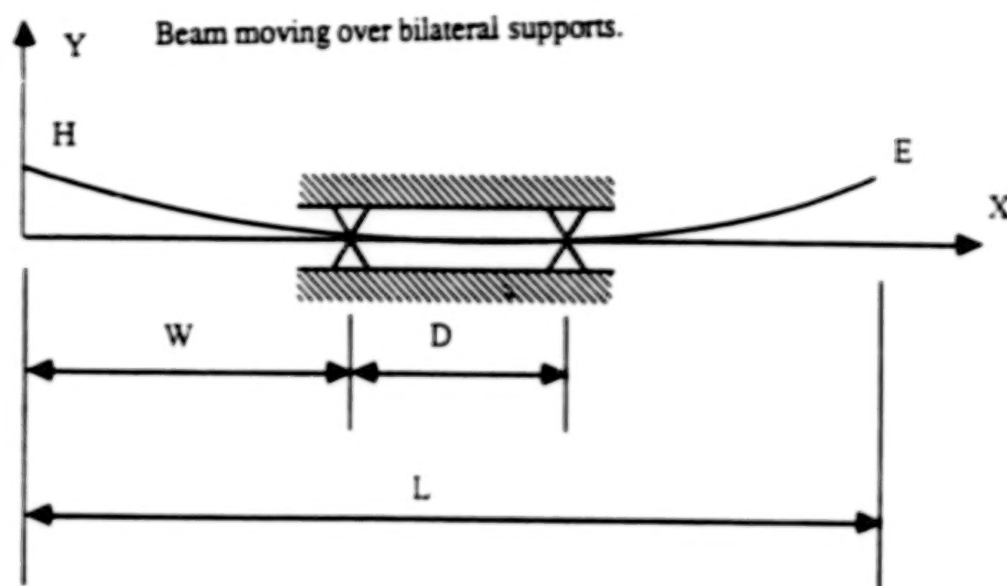
Schematic of prismatic joint i.

**M**

**A. Galip Ulsoy**

**Mechanical Engineering and Applied Mechanics  
University of Michigan, Ann Arbor, Michigan**

# FLEXIBLE SYSTEMS WITH PRISMATIC JOINTS



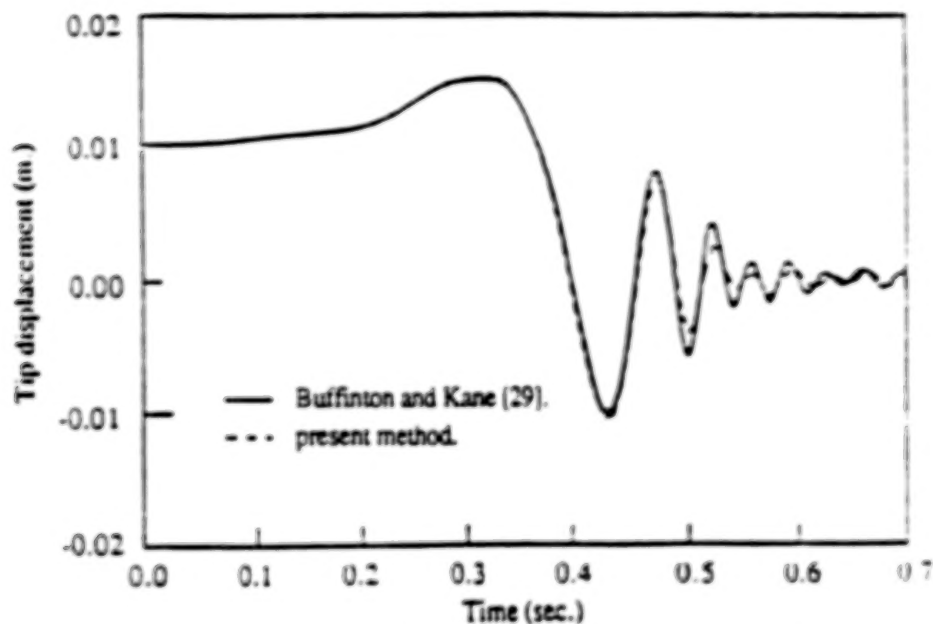
Tip displacement in "slow push" case with  
 $C_1 = 0.725$  m,  $C_2 = 0.7$  m and  $T = 3.5$  sec.

**M**

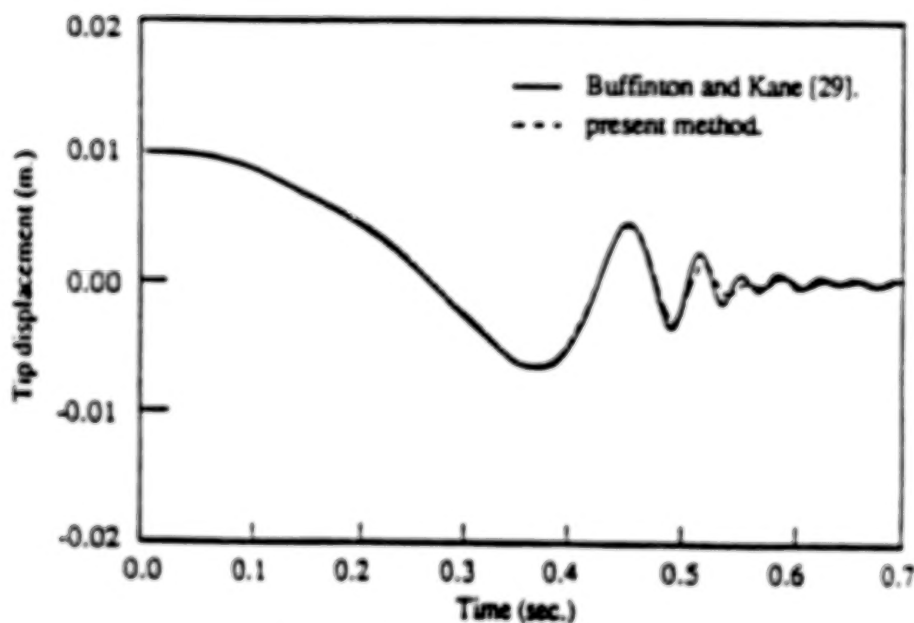
**A. Galip Ulsoy**

Mechanical Engineering and Applied Mechanics  
 University of Michigan, Ann Arbor, Michigan

## FLEXIBLE SYSTEMS WITH PRISMATIC JOINTS



Tip displacement in "fast push" case with  
 $C_1 = 0.725$  m,  $C_2 = 0.7$  m and  $T = 0.7$  sec.



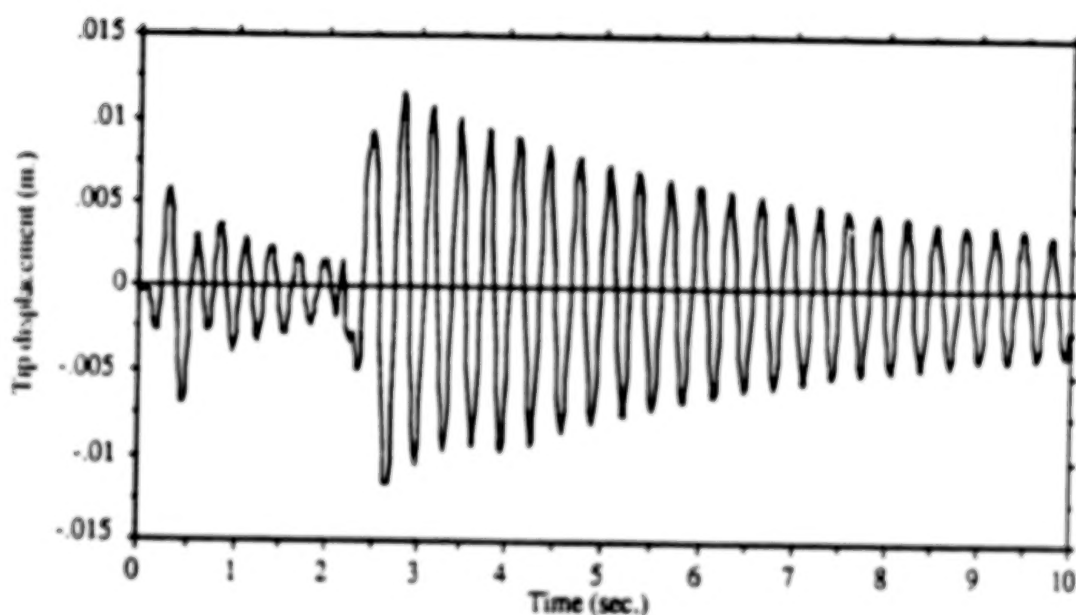
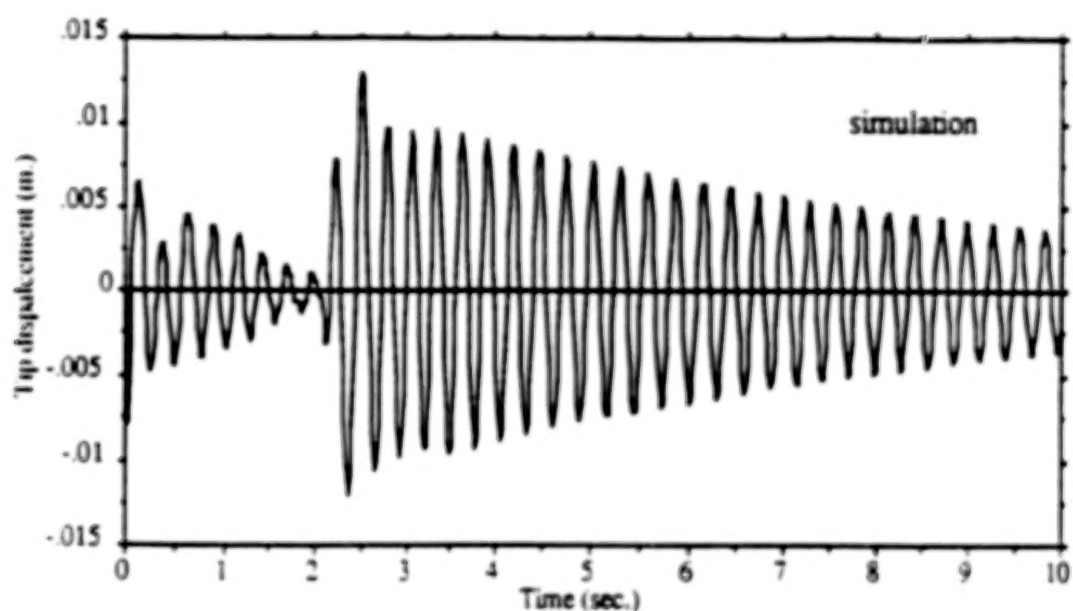
Tip displacement in "fast pull" case with  
 $C_1 = 0.025$  m,  $C_2 = -0.7$  m and  $T = 0.7$  sec.

# M

A. Galip Ulsoy

Mechanical Engineering and Applied Mechanics  
University of Michigan, Ann Arbor, Michigan

## FLEXIBLE SYSTEMS WITH PRISMATIC JOINTS



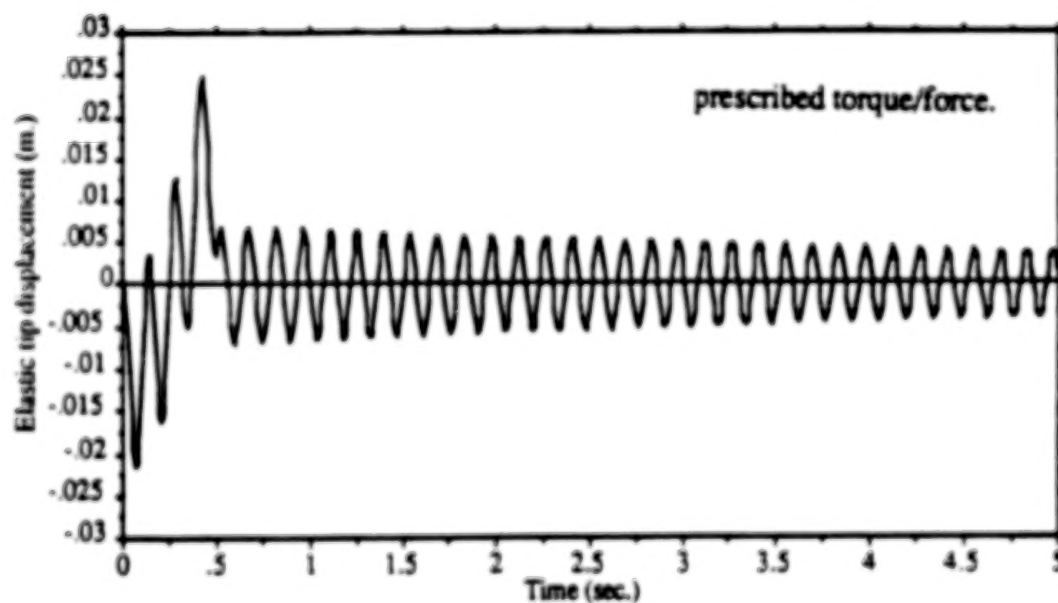
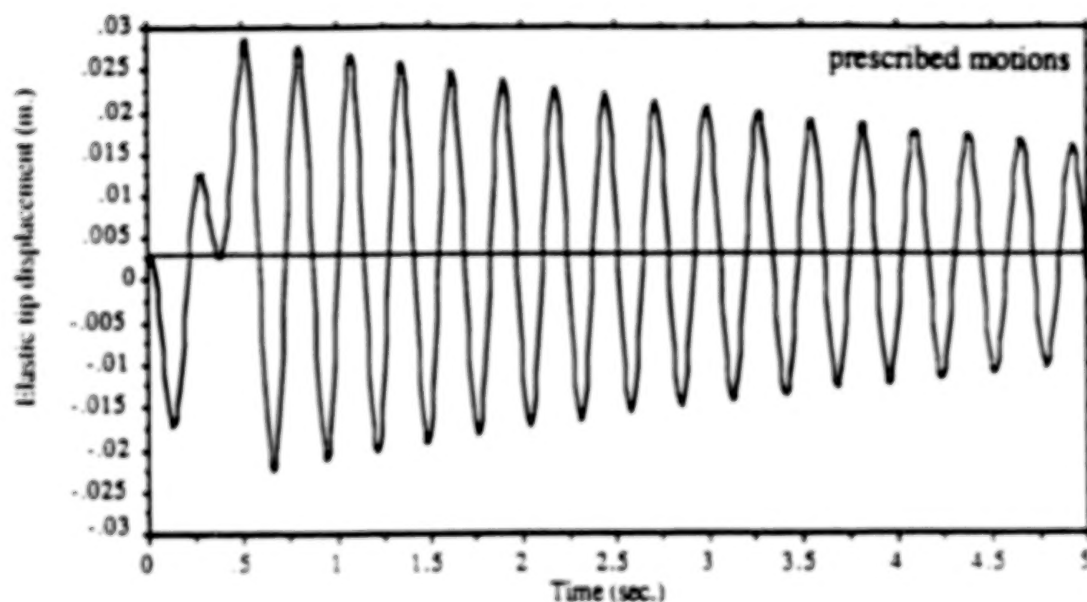
Vertical elastic tip displacement of the last link in the two-dimensional maneuver.

**M**

**A. Galip Ulsoy**

**Mechanical Engineering and Applied Mechanics  
University of Michigan, Ann Arbor, Michigan**

## FLEXIBLE SYSTEMS WITH PRISMATIC JOINTS



**M**

**A. Galip Ulsoy**

**Mechanical Engineering and Applied Mechanics  
University of Michigan, Ann Arbor, Michigan**

## **FLEXIBLE SYSTEMS WITH PRISMATIC JOINTS**

- **A general modeling procedure for robot arms consisting of rigid and flexible links connected by revolute and/or prismatic joints has been developed and experimentally validated.**
- **The significance of full coupling (effect of flexible motion on rigid body motion) has been demonstrated.**
- **The axial shortening effect is shown to be significant for high speed operation of lightweight manipulators.**

---

**M**

**A. Galip Ulsoy**

**Mechanical Engineering and Applied Mechanics  
University of Michigan, Ann Arbor, Michigan**

## **FLEXIBLE SYSTEMS WITH IMPACT**

**The effect of impact on mechanical systems**

**Impact**

- gives rise to impulsive forces

These impulsive forces in turn

- Induce high stress levels at different joints  
damage to the mechanical components of the system
- Cause higher modes of vibration to be excited  
deviation from a desired performance

---

**M**

**A. Galip Ulsoy**

**Mechanical Engineering and Applied Mechanics  
University of Michigan, Ann Arbor, Michigan**



# FLEXIBLE SYSTEMS WITH IMPACT

## Spring-Dashpot Models

Dubowsky and Freudenstein (1971) Impact pair model

Crossley and Hunt (1975) Viscous damping model

Lee and Wang (1982) Damping functions

Dubowsky and Gardner (1975) Impact beam model

- Based on a force-displacement law, and a form of damping
- Does not neglect the contact duration
- It is possible to predict the contact forces directly
- Requires the determination of stiffness and damping
- Computationally expensive

---

**M**

**A. Galip Ulsoy**

**Mechanical Engineering and Applied Mechanics  
University of Michigan, Ann Arbor, Michigan**

# **FLEXIBLE SYSTEMS WITH IMPACT**

## **Methods based on Momentum Balance (Coefficient of Restitution Model)**

Haug and Wehage (1981) For rigid body impact

Khulief and Shabana (1984) Extension to flexible bodies

- Simplest model for impact
- Computationally efficient
- It is possible to predict the contact forces directly
- Does not require determination of stiffness and damping parameters
- Neglects the period of contact
- A direct prediction of stresses and frequency content of impulse during contact is not possible
- Mathematically discontinuous

---

# **M**

**A. Galip Ulsoy**

**Mechanical Engineering and Applied Mechanics  
University of Michigan, Ann Arbor, Michigan**

## FLEXIBLE SYSTEMS WITH IMPACT

### Procedure for Momentum Balance Method:

- 1- Natural frequencies and mode shapes are determined for each flexible body in the system; analytically, experimentally, or by using a finite element approximation.
- 2- Discretized equations of motion are generated and integrated forward in time using this modal information.
- 3- Impact conditions are checked. if an impact is detected to occur, integration is stopped, and the equations of momentum balance are generated using the coefficient of restitution and solved for jump discontinuities in velocities.
- 4- The velocity vector is updated
- 5- Integration is started once again with the new initial conditions found from above.  
(It is assumed that the system configuration does not change with impact.)

---

**M**

**A. Galip Ulsoy**

**Mechanical Engineering and Applied Mechanics  
University of Michigan, Ann Arbor, Michigan**

## FLEXIBLE SYSTEMS WITH IMPACT

### Coefficient of Restitution, $e$

Newtonian Concept:

$e = f$  (material pair)

Modern Concept:

$e = f$  (severity of the impact)

for rigid bodies

severity of impact  $\equiv$  impact velocity

$e = f$  (material pair, impact vel.)

experimental data or analytical/emprical formulas

for flexible systems

the severity of impact  $= f$  (impact vel., flexibility, configuration)

No experimental data or analytical formula available  
for  $e$

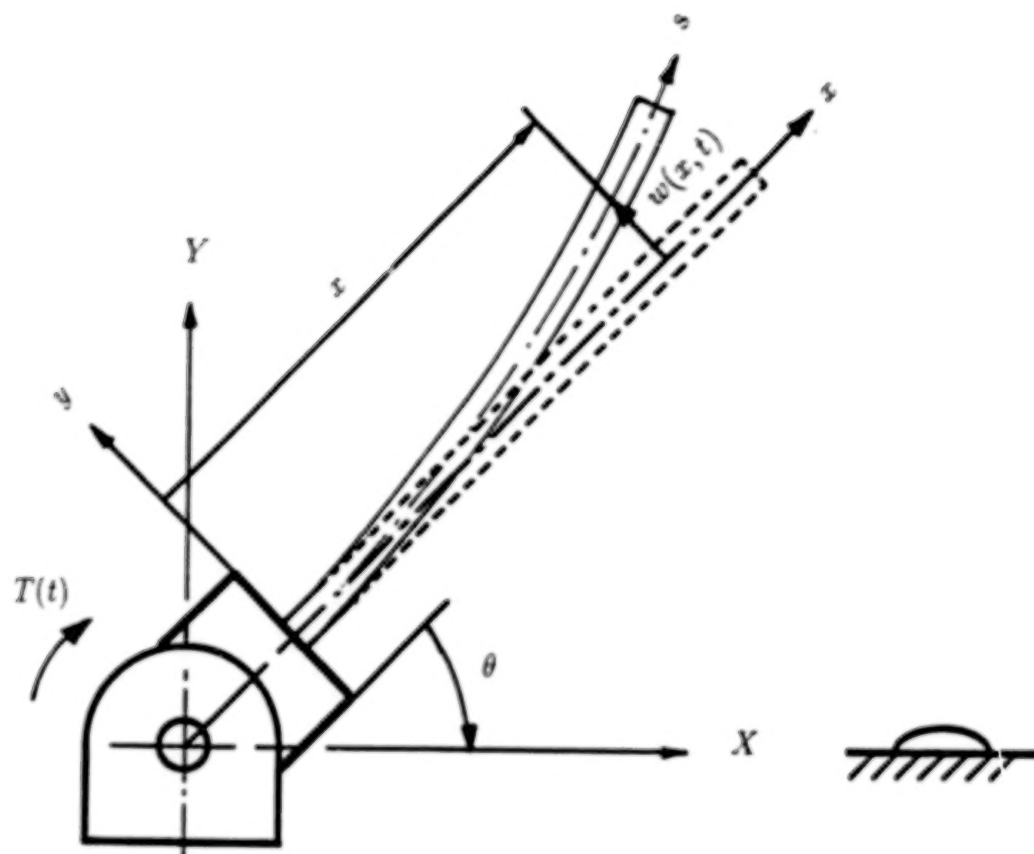
---

**M**

**A. Galip Ulsoy**

**Mechanical Engineering and Applied Mechanics  
University of Michigan, Ann Arbor, Michigan**

## FLEXIBLE SYSTEMS WITH IMPACT



---

**M**

**A. Galip Ulsoy**

**Mechanical Engineering and Applied Mechanics  
University of Michigan, Ann Arbor, Michigan**

# FLEXIBLE SYSTEMS WITH IMPACT

## Equations of Motion

- Euler-Bernoulli Beam Theory
- Hamilton's Principle
- Neglect higher order elastic terms
- Galerkin's Method

$$w(x, t) = \sum_{j=1}^N \phi(j)q(t)$$

- Neglect higher order elastic terms

$$(I_R + J)\ddot{\theta} + \sum_{j=1}^N S_j \ddot{q}_j = M(t)$$

$$S_r \ddot{\theta} + \sum_{j=1}^N [m_{rj} \ddot{q}_j + \dot{\theta}^2 q_j (c_{rj} - m_{rj}) + k_{rj} q_j] = 0$$

$$r = 1, 2, \dots, N$$

where

$I_R$  : Inertia of the Rigid Shaft

$J$  : Inertia of the Flexible Beam

---

**M**

**A. Galip Ulsoy**

**Mechanical Engineering and Applied Mechanics  
University of Michigan, Ann Arbor, Michigan**

# FLEXIBLE SYSTEMS WITH IMPACT

## Simulations

- A variable order variable time step integrator
- A velocity dependent coefficient of restitution

$e = f(v)$  (experimental data) for low velocities

$e = \alpha v^{(-1/4)}$  (analytical data) for high velocities

## Contact algorithm

based on the distance between impact point and the impact surface

- define a clearance zone
- monitor the location and the velocity of the impact point
- first penetration into the clearance zone → back up one time step and reduce the time step.
- second penetration with the smaller time step → **impact** if the velocity is toward the surface
- keep the smaller time step size as long as the impact point is within the clearance zone

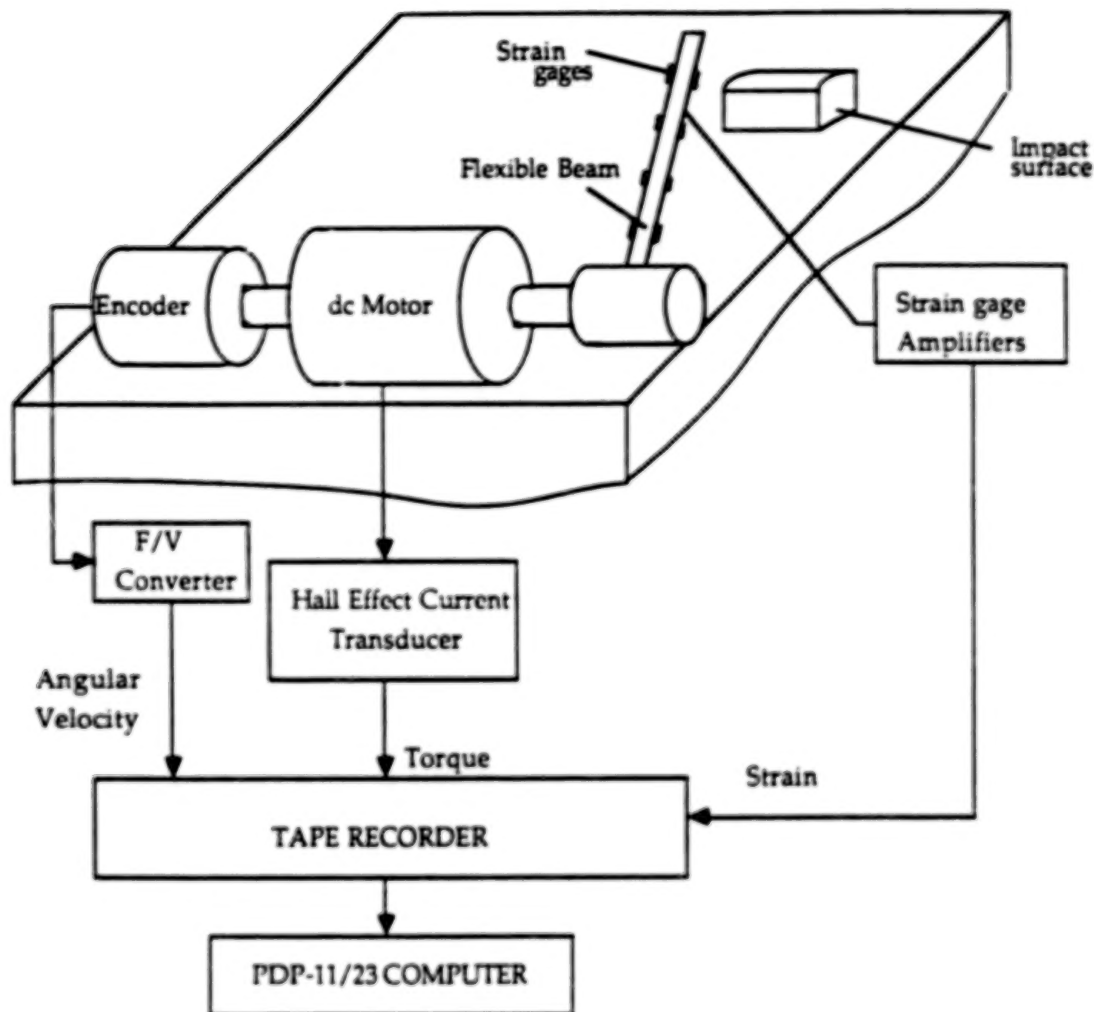
---

# M

**A. Galip Ulsoy**

**Mechanical Engineering and Applied Mechanics  
University of Michigan, Ann Arbor, Michigan**

## FLEXIBLE SYSTEMS WITH IMPACT

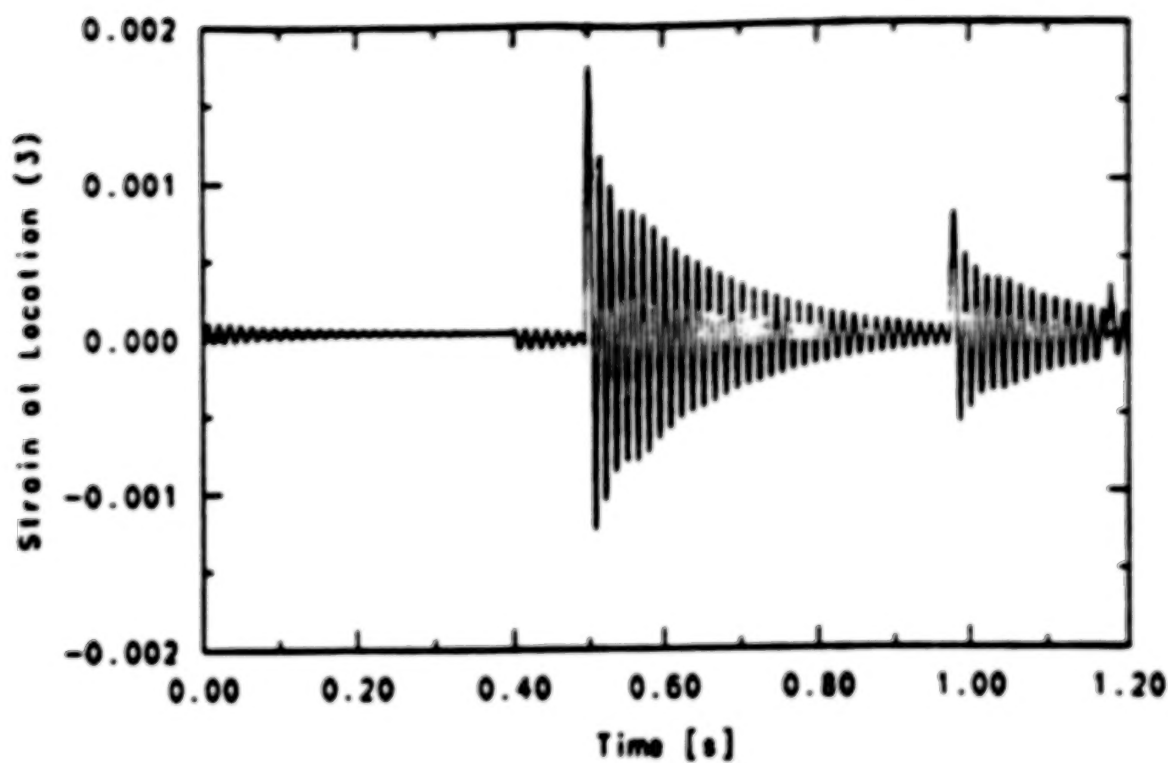


**M**

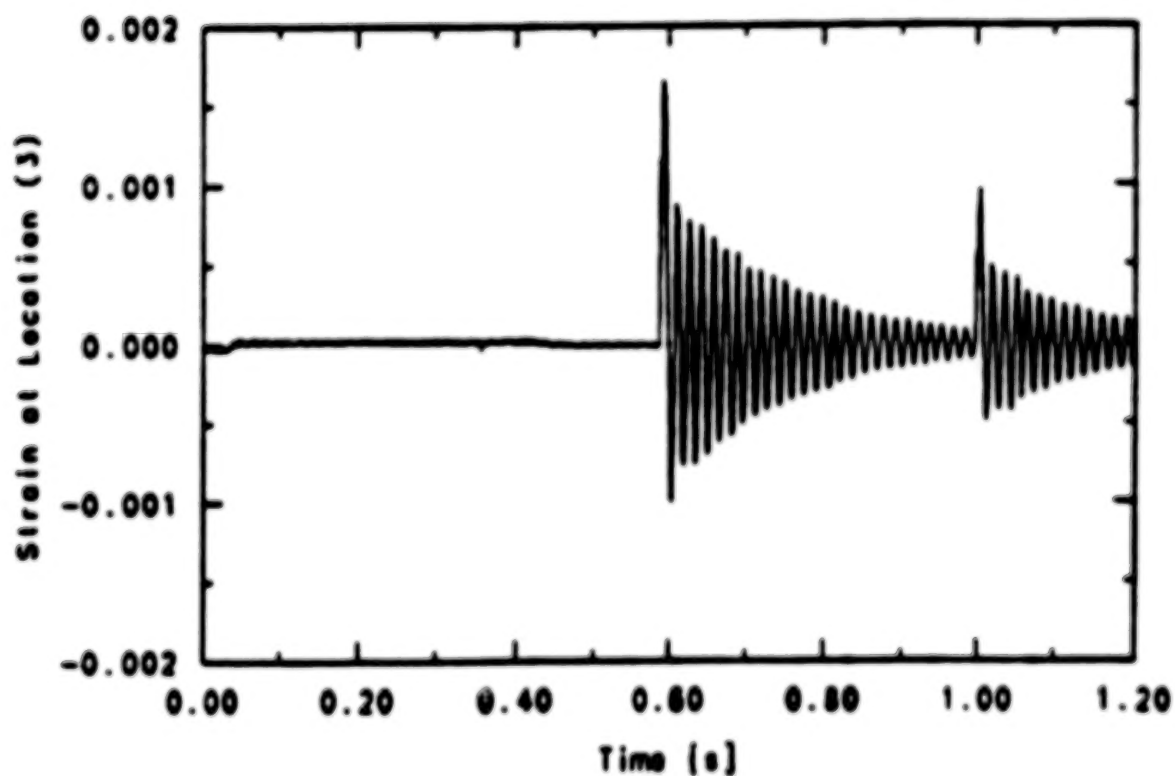
**A. Galip Ulsoy**

**Mechanical Engineering and Applied Mechanics  
University of Michigan, Ann Arbor, Michigan**

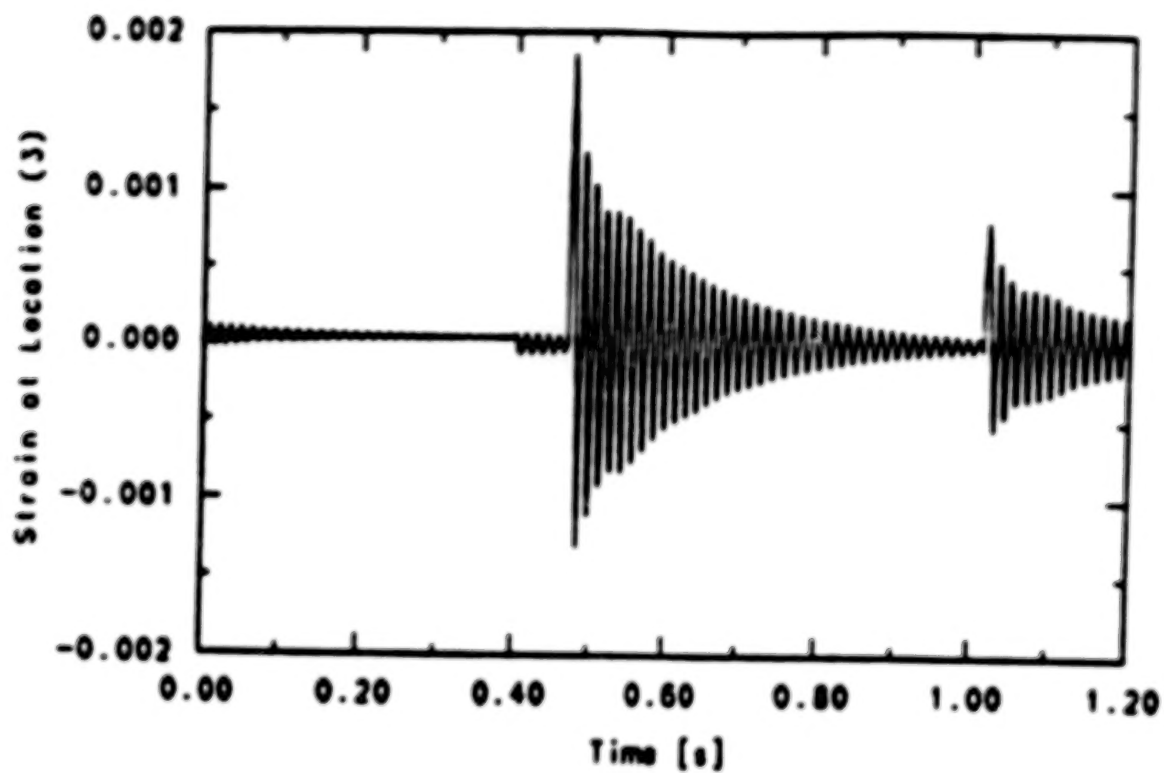




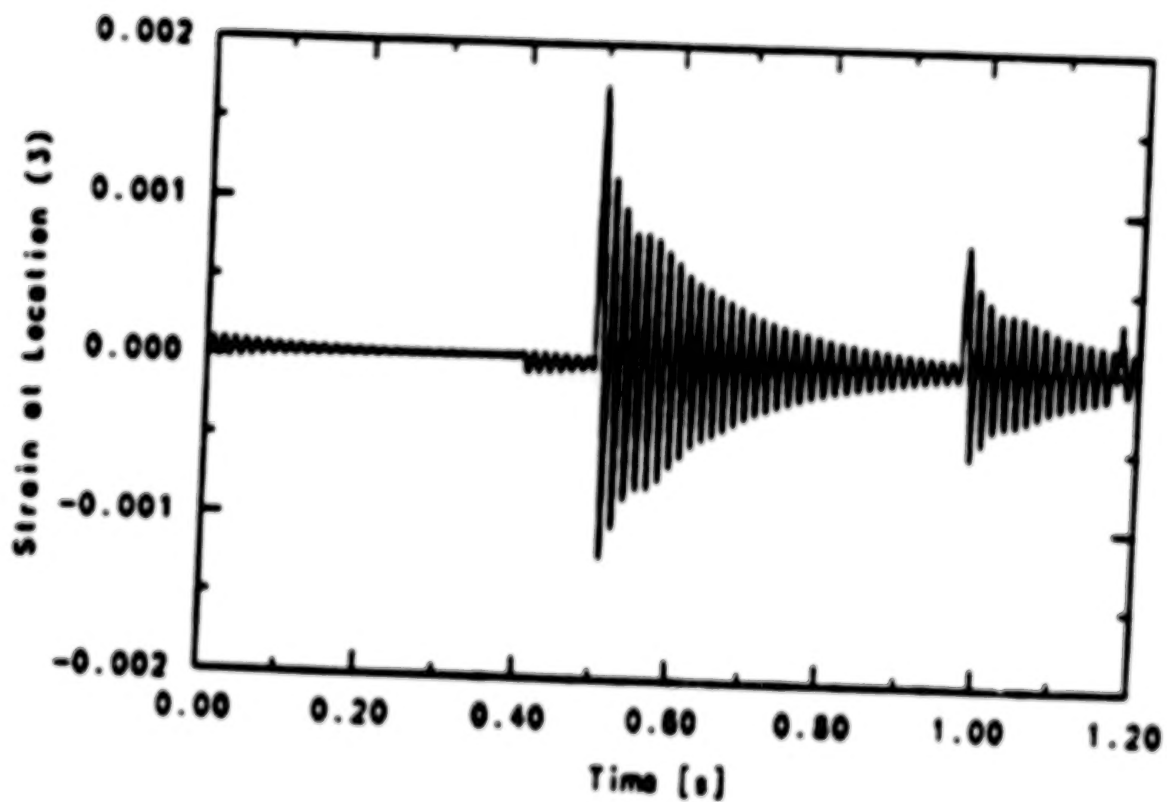
Strain history at location (3), variable  $e$



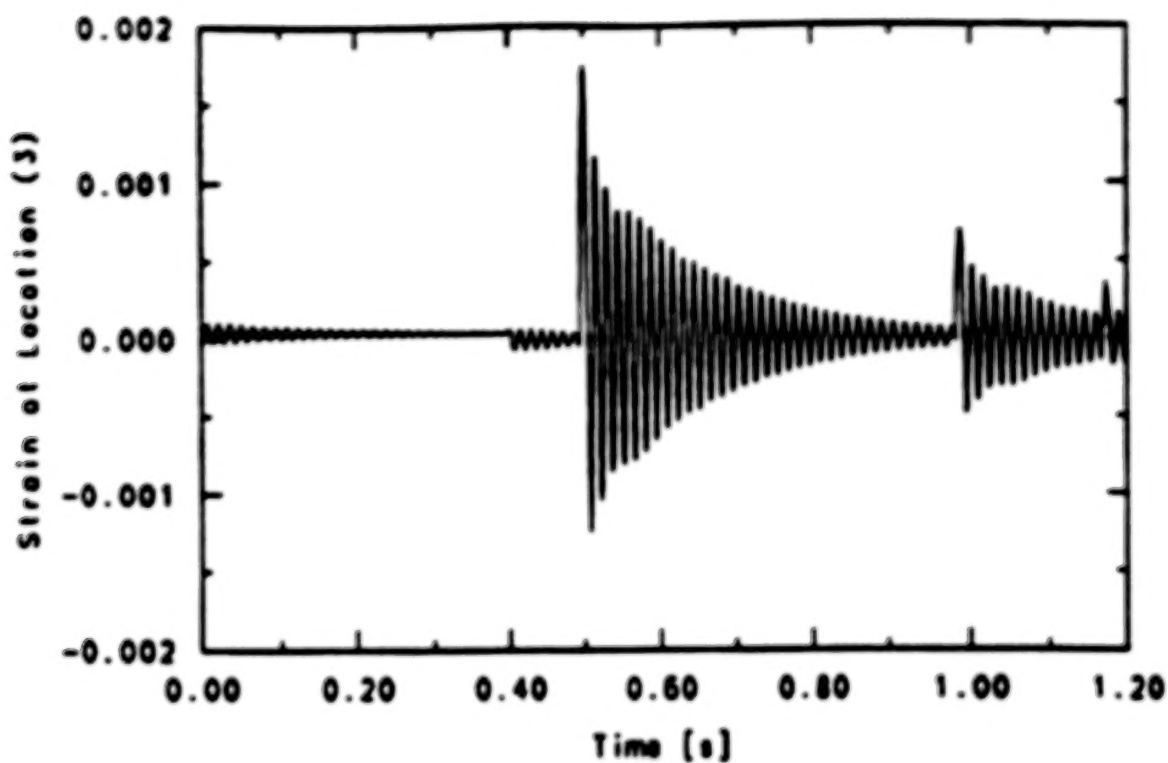
Strain history, impact on aluminum surface



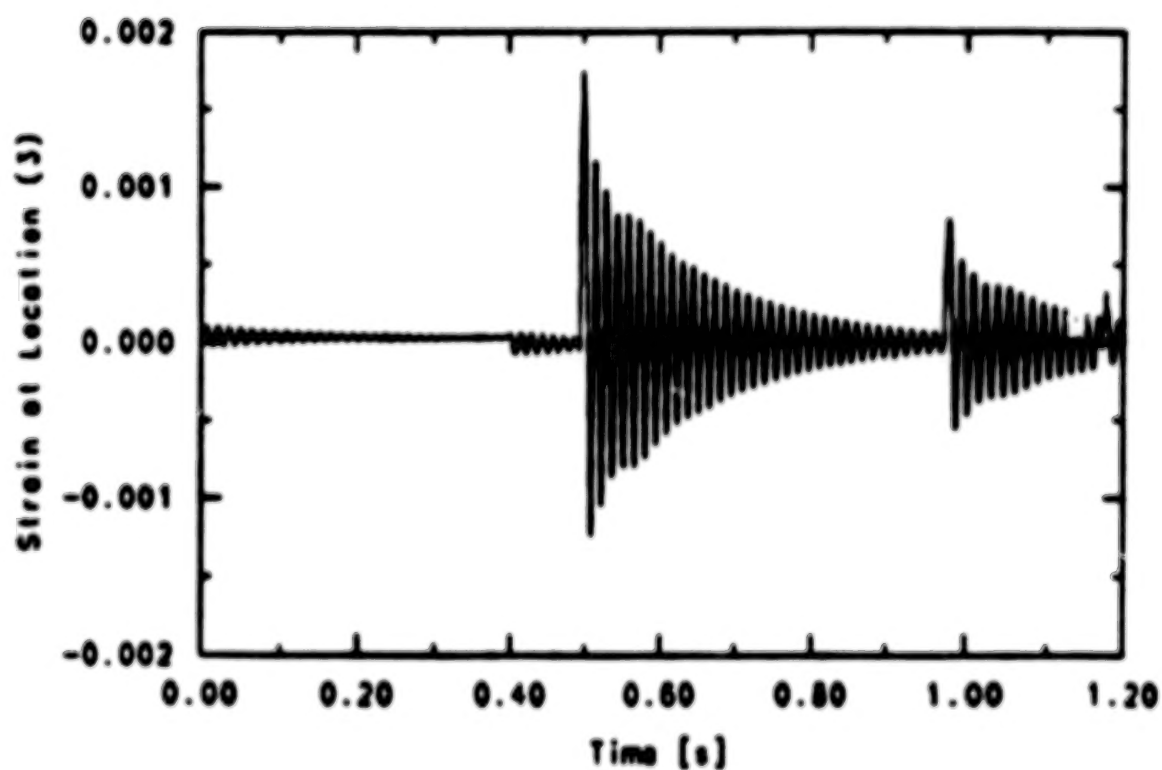
Strain history at location (3), constant  $e$



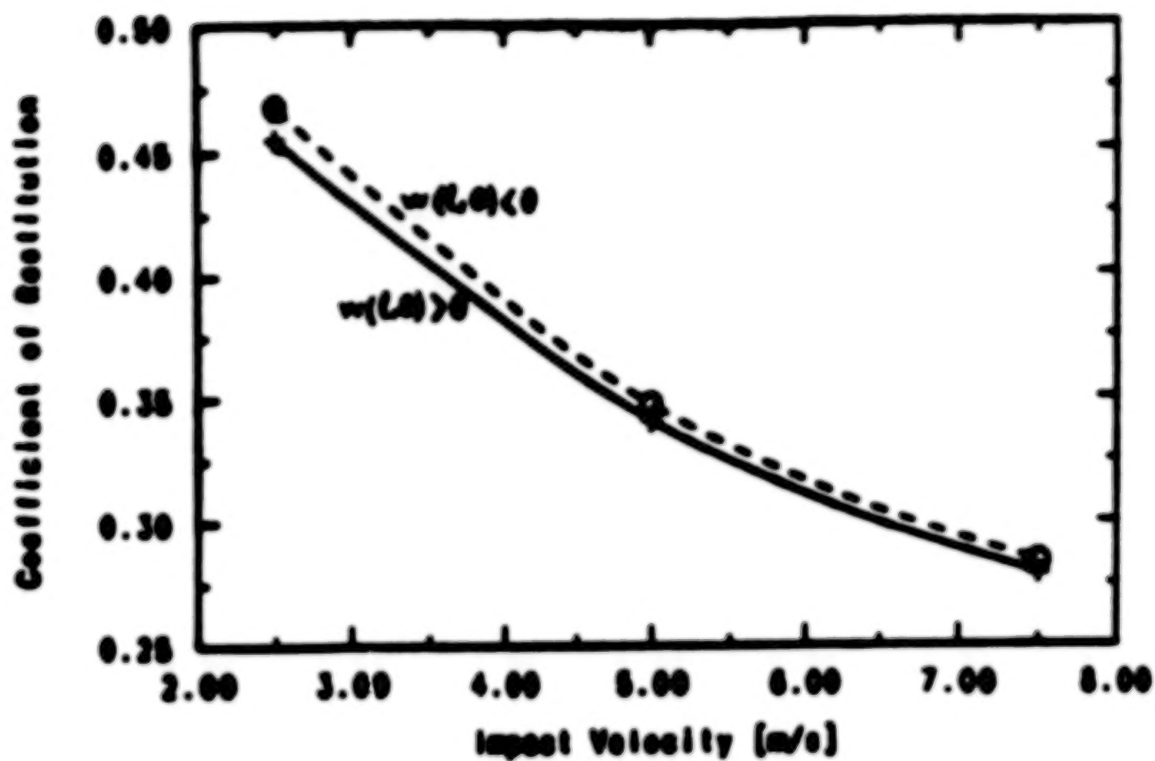
Strain history at location (3), variable  $e$



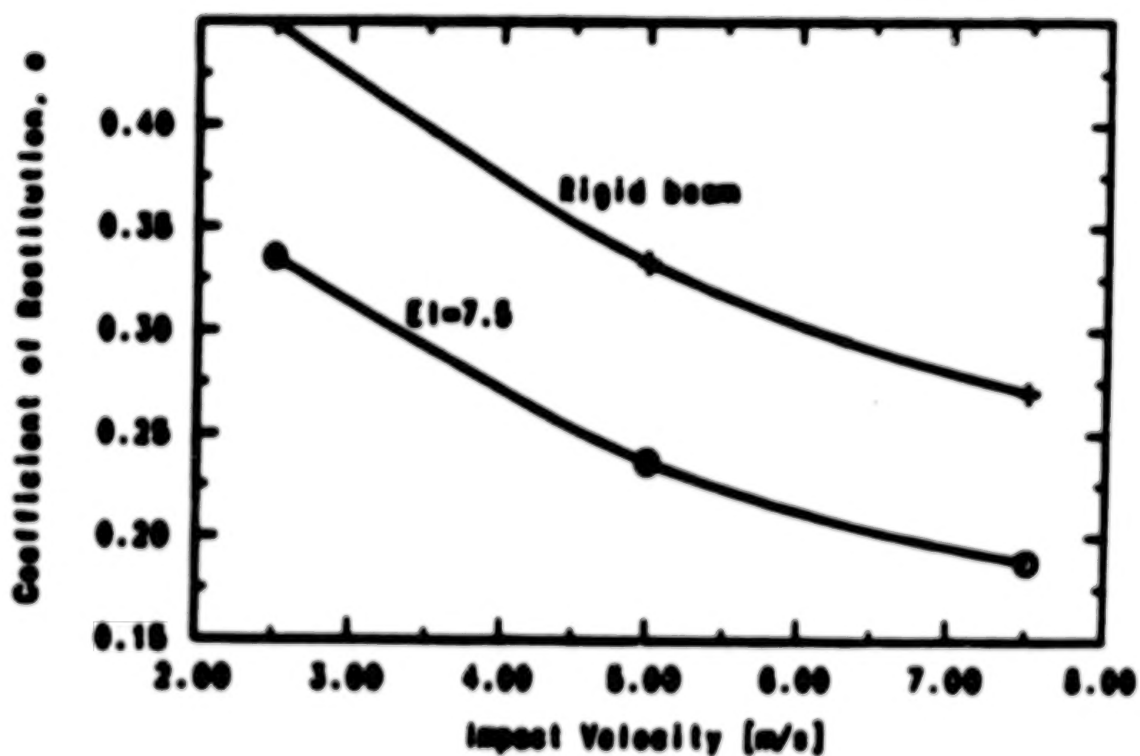
Strain history at location (3), spring-dashpot model



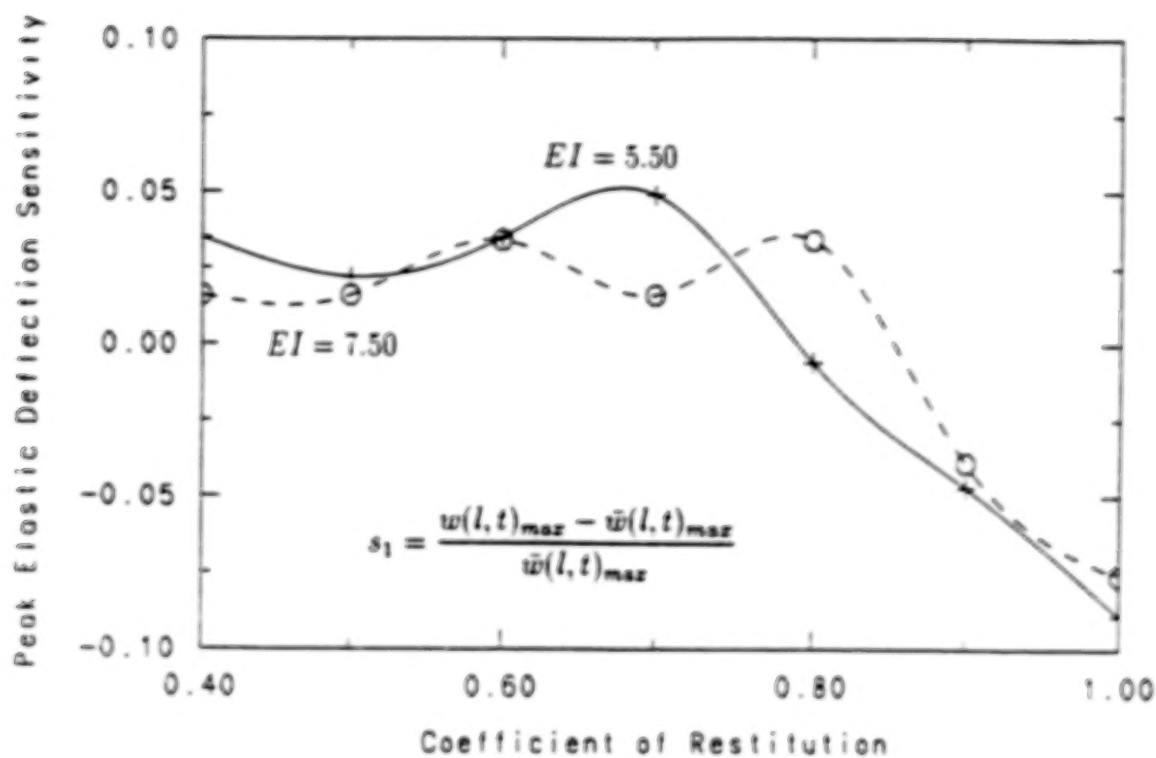
Strain history at location (3), variable  $\epsilon$



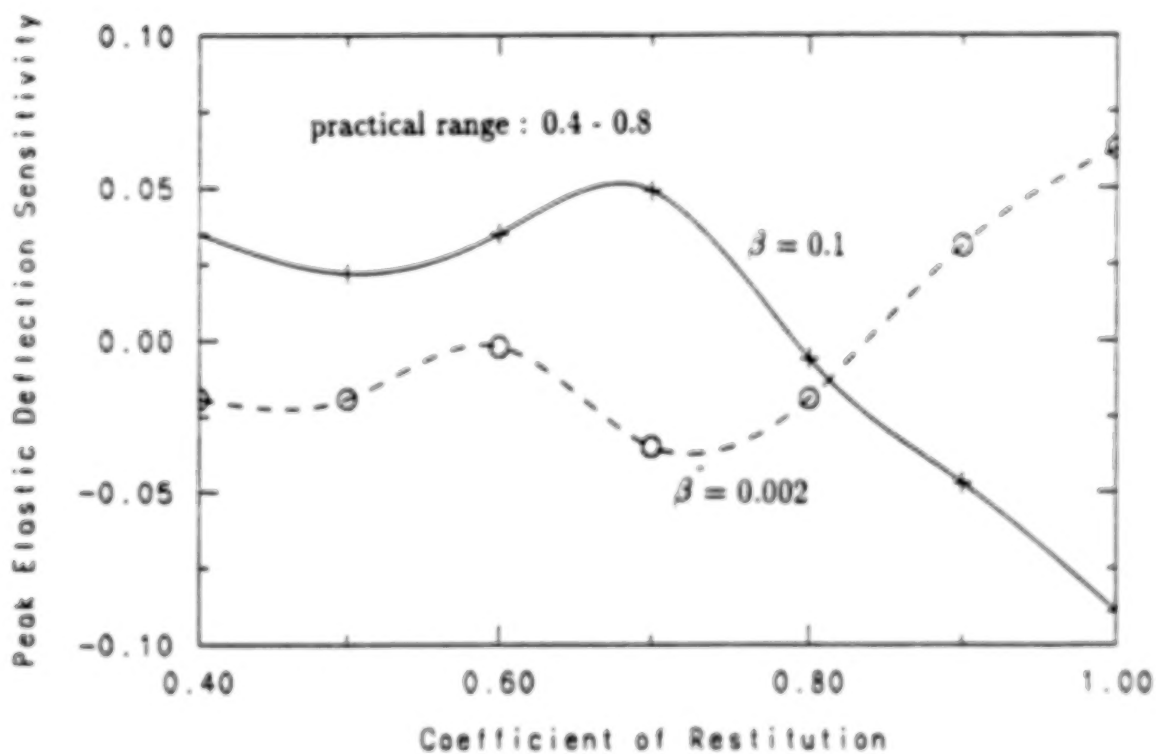
Variation of the coefficient of restitution with the configuration



Variation of the coefficient of restitution with the rigidity



Elastic peak deflection sensitivity



Elastic peak deflection sensitivity

## FLEXIBLE SYSTEMS WITH IMPACT

The momentum balance (coefficient of restitution) method has been demonstrated, through experiments on a specific system, to be capable of adequately predicting the dynamic behavior, with impact, of systems which consist of both rigid and elastic links.

It has been demonstrated experimentally that using a constant coefficient of restitution value (chosen for a particular initial impact velocity) throughout the simulation does not significantly affect the accuracy of the model, even in the presence of multiple impacts.

Sensitivity studies were used to show that the momentum balance (coefficient of restitution) model will also work reasonably well for a wide range of system parameters.

Employing high speed video techniques the existence of multiple impacts which appear to the naked eye as a single contact were demonstrated. Contact algorithms have been developed which captures these multiple impacts in the simulation.

---

**M**

**A. Galip Ulsoy**

**Mechanical Engineering and Applied Mechanics  
University of Michigan, Ann Arbor, Michigan**

## SUMMARY AND CONCLUSIONS

- This presentation has reviewed the results of some recent studies, experimental and theoretical, in the modeling, analysis, and control of flexible multi-body systems. The control of a leadscrew driven robot with a flexible link was considered. The modeling of robots with rigid and/or flexible links connected by revolute and/or prismatic joints was developed. Studies were conducted to evaluate various competing impact models for use in simulations of flexible systems.

- The major conclusions to be drawn from these studies are:

For robots with sufficient actuator bandwidth, the use of end-of-arm sensors can enable effective control of the joint motions as well as active damping of the end-of-arm vibration.

A general modeling and simulation approach for robots consisting of rigid and/or flexible elements connected by revolute and/or prismatic joints has been developed and experimentally validated.

Impact models for systems with flexible elements have various problem dependent characteristics, however, even the simplest of these can give good results in many problems of engineering interest.

---

**M**

A. Galip Ulsoy

Mechanical Engineering and Applied Mechanics  
University of Michigan, Ann Arbor, Michigan

## ACKNOWLEDGEMENTS

This presentation summarizes several different studies that were carried out by the graduate students N.G. Chalhoub, Y.C. Pan, and A. Yigit under the supervision of A.G. Ulsoy and R.A. Scott. These studies were financially supported in part by AFOSR Contract # F49620-82-C-0089, and by the U.M. Robotics Affiliates Program. The assistance of R. Giles, J. Turney, and S. Culp with the experimental work is also greatly acknowledged.

---

**M**

**A. Galip Ulsoy**

**Mechanical Engineering and Applied Mechanics  
University of Michigan, Ann Arbor, Michigan**



## REFERENCES

- "Dynamic Simulation of a Leadscrew Driven Flexible Robot Arm and Controller," N.G. Chalhoub and A.G. Ulsoy, *ASME Journal of Dynamic Systems, Measurement and Control*, Vol. 108, No. 2, June 1986, pp 119-126.
- "Control of a Flexible Robot Arm: Experimental and Theoretical Results", N.G. Chalhoub, and A.G. Ulsoy, *ASME Journal of Dynamic Systems, Measurement, and Control*, Vol. 109, No. 4, December 1987, pp 299-309.
- "Flexural Motion of a Radially Rotating Beam Attached to a Rigid Body", A. Yigit, R.A. Scott, and A.G. Ulsoy, *Journal of Sound and Vibration*, Vol. 121, No. 2, 1988, pp 201-210.
- "Dynamic Modeling of a Self-Locking Leadscrew and its Implication in Robotics," N.G. Chalhoub, and A.G. Ulsoy, *Proceedings of the American Control Conference*, Pittsburg, Pennsylvania, June 1989.
- "Dynamics of a Radially Rotating Beam with Impact, Part 1: Experimental Results," A. Yigit, A.G. Ulsoy, and R.A. Scott, *ASME Journal of Vibration, Acoustics, Stress, and Reliability in Design*, (accepted for publication).
- "Dynamics of a Radially Rotating Beam with Impact, Part 2: Numerical Results," A. Yigit, R.A. Scott, and A.G. Ulsoy, *ASME Journal of Vibration, Acoustics, Stress, and Reliability in Design*, (accepted for publication).
- "Dynamic Modeling and Simulation of Flexible Robots with Prismatic Joints," Y.C. Pan, R.A. Scott, and A.G. Ulsoy, *ASME Journal of Mechanisms, Transmissions, and Automation in Design*, (submitted for publication).
- "Experimental Model Validation for a Flexible Robot with a Prismatic Joint," Y.C. Pan, A.G. Ulsoy, and R.A. Scott, *ASME Journal of Mechanisms, Transmissions, and Automation in Design*, (submitted for publication).
- "A Comparison of Spring-Dashpot and Momentum Balance Methods for Impact in a Radially Rotating Beam," A. Yigit, R. A. Scott, and A.G. Ulsoy, *Journal of Sound and Vibration*, (submitted for publication).

---

**M**

**A. Galip Ulsoy**

**Mechanical Engineering and Applied Mechanics  
University of Michigan, Ann Arbor, Michigan**

## MINIMUM ATTAINABLE RMS ATTITUDE ERROR USING CO-LOCATED RATE SENSORS

A. V. Balakrishnan†

### Abstract

In this paper we announce a closed form analytical expression for the minimum attainable attitude error (as well as the error rate) in a flexible beam by feedback control using co-located rate sensors. For simplicity, we consider a beam clamped at one end with an offset mass (antenna) at the other end where the controls and sensors are located. Both control moment generators and force actuators are provided. The results apply to any beam-like lattice-type truss, and provide the kind of performance criteria needed under CSI — Controls-Structures-Integrated optimization.

---

† Research Supported in part under NAS1-18585 Task Assignment 49.

Paper presented at the 3rd Annual Conference on Aerospace Computational Control, Oxnard, August 1989.

## 1. Introduction

One of the challenges in the Design Challenge For Flexible Flight Structure Control System Design formulated in the inaugural paper on SCOPE [1] was to hold the antenna pointing error within  $\pm 0.02$  degrees after slewing by appropriate feedback control. In this paper we derive a closed form expression for the minimal achievable mean square pointing error using co-located rate sensors. A slightly simplified form of the SCOPE article (which eliminates rigid-body modes) is used: a cantilevered beam with an offset mass where the controls — both c.m.g.'s and force actuators — and the rate sensors are located. Our results are in terms of continuum model parameters — the uniform Bernoulli version is used. The beam dynamics are given in Section 2. The main results are in Section 3. We note that a technique for deriving equivalent Bernoulli beam parameters for various types of trusses is described by Noor and Anderson in [4]. Recently Noor and Russell [5] presented equivalent anisotropic Timoshenko beam models for beam-like lattice trusses with an arbitrary degree of modal coupling, which appear to yield excellent agreement with modal frequencies derived from finite element models. Our theory is able to handle these Timoshenko models, and moreover we can also use it for rigid-body modes, although they are not included here. Thus our results can be used for any beam-like lattice truss structure.

## 2. The Model

We consider a uniform Bernoulli beam clamped at one end with an offset mass (antenna) at the other end which also houses the sensors and actuators. See Figure 1. We allow for both force actuators and moment actuators. The sensors are rate gyros. Because of the clamping at one end, no rigid-body modes are involved and hence no attitude sensors are needed.

We allow bending in two mutually perpendicular planes containing the beam axis, as well as torsion in the plane perpendicular to the beam axis, all uncoupled. The continuum model (uniform Bernoulli beam) dynamics can then be described by the following partial differential equations (similar to those in [2, 3]). Let the beam extend along the  $z$ -axis,  $0 < s < L$ , and let  $u_\phi(s, t)$ ,  $u_\theta(s, t)$ , denote the bending displacements and  $u_\psi(s, t)$  the torsion angle about the beam axis. Let in the usual notation (cf. [1]),  $EI_\phi$ ,  $EI_\theta$  denote the flexural stiffness and  $GI_\psi$  the torsional rigidity. Let  $\rho$  denote the mass per unit area and  $A$  the cross-sectional area. Then we have:

$$\rho A \frac{\partial^2 u_\phi(s, t)}{\partial t^2} + EI_\phi \frac{\partial^4 u_\phi(s, t)}{\partial s^4} = 0, \quad 0 < s < L; \quad 0 < t$$

$$\rho A \frac{\partial^2 u_\theta(s, t)}{\partial t^2} + EI_\theta \frac{\partial^4 u_\theta(s, t)}{\partial s^4} = 0, \quad 0 < s < L; \quad 0 < t$$

$$\rho I_\psi \frac{\partial^2 u_\psi(s, t)}{\partial t^2} - GI_\psi u_\psi''(s, t) = 0, \quad 0 < s < L; \quad 0 < t$$

with the clamped boundary conditions at  $s = 0$ :

$$u_\phi(0, t) = u_\theta(0, t) = u_\psi(0, t) = 0$$

$$u_\phi'(0, t) = u_\theta'(0, t) = 0.$$

The antenna center of gravity is located at

$$(r_x, r_y, L).$$

The distance from the beam tip to antenna center of gravity is denoted by

$$|r| = \sqrt{r_x^2 + r_y^2}.$$

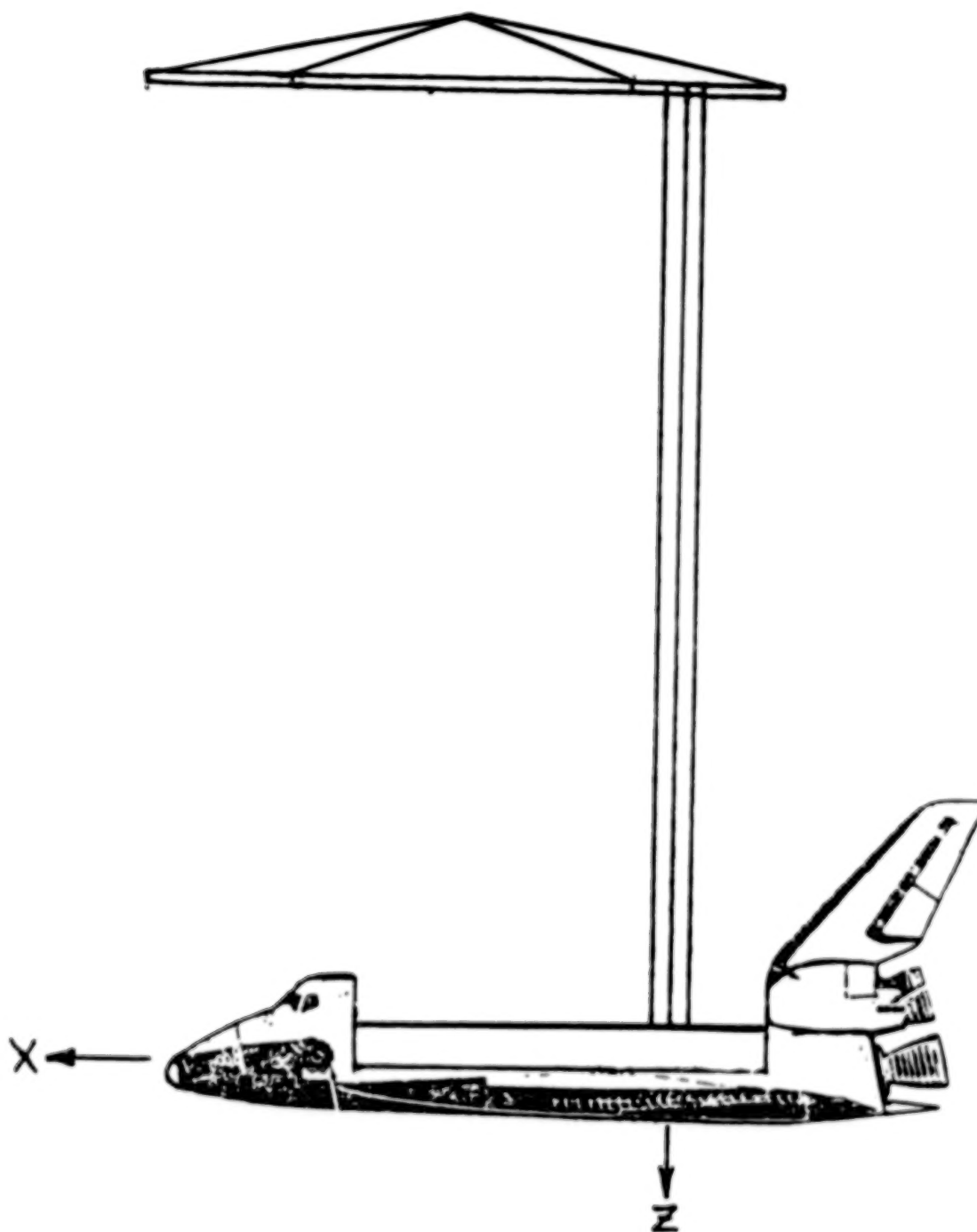


Figure 1: Shuttle/Antenna Configuration

The force balance equation at  $s = L$  yields

$$m \begin{bmatrix} 1 & 0 & r_x \\ 0 & 1 & r_y \end{bmatrix} \begin{bmatrix} \ddot{u}_\phi(L, t) \\ \ddot{u}_\theta(L, t) \\ \ddot{u}_\psi(L, t) \end{bmatrix} + \begin{bmatrix} f_1(t) \\ f_2(t) \end{bmatrix} = \begin{bmatrix} EI_\phi u_\phi'''(L, t) \\ EI_\theta u_\theta'''(L, t) \end{bmatrix}$$

where  $m$  is the antenna mass and  $f_1(\cdot)$ ,  $f_2(\cdot)$  are the applied control forces. The torque balance equations yield

$$0 = \begin{bmatrix} EI_\phi u_\phi'''(L, t) \\ EI_\theta u_\theta'''(L, t) \\ GI_\psi u_\psi'(L, t) \end{bmatrix} + \hat{I}_a \dot{\omega} + M(t) + r \otimes \begin{bmatrix} f_1(t) \\ f_2(t) \\ 0 \end{bmatrix} \\ + r \otimes \begin{bmatrix} \ddot{u}_\phi(L, t) + r_x \ddot{u}_\psi(L, t) \\ \ddot{u}_\theta(L, t) + r_y \ddot{u}_\psi(L, t) \end{bmatrix}$$

where the superdots indicate time derivatives and the primes the derivatives with respect to the spatial variable  $s$ ;  $\otimes$  denotes the vector cross-product and  $\omega$  the angular rate vector

$$\omega = \begin{bmatrix} \dot{u}_\phi'(L, t) \\ \dot{u}_\theta'(L, t) \\ \dot{u}_\psi(L, t) \end{bmatrix},$$

$\hat{I}_a$  denotes the moment of inertia of the antenna about the beam tip ( $s = L$ ) and finally,  $M(t)$  denotes the applied control moment.

It is convenient to denote by  $b(t)$  the boundary vector:

$$b(t) = \begin{bmatrix} u_\phi(L, t) \\ u_\theta(L, t) \\ u_\phi'(L, t) \\ u_\theta'(L, t) \\ u_\psi(L, t) \end{bmatrix}.$$

The boundary rate vector would thus be  $\dot{b}(t)$ . Hence our sensor model is:

$$v(t) = \dot{b}(t) + N_0(t)$$

where we assume that  $N_0(t)$  is white Gaussian noise with spectral density matrix  $d_0 I$ , where  $I$  is the identity ( $5 \times 5$ ) matrix. Similarly we assume that the control actuators are also

characterized by additive white Gaussian noise. Denoting the applied control vector by  $u(t)$ :

$$u(t) = \begin{bmatrix} u_1(L, t) \\ u_2(L, t) \\ u_3(L, t) \\ u_4(L, t) \\ u_5(L, t) \end{bmatrix}.$$

we have

$$\begin{bmatrix} f_1(t) \\ f_2(t) \\ M(t) \end{bmatrix} = u(t) + N_s(t)$$

where  $N_s(t)$  is white Gaussian with spectral density  $d_s$ . We shall also use  $M_b$  to denote the actuator mass/inertia matrix

$$M_b = \begin{bmatrix} m & 0 & 0 & 0 & mr_x \\ 0 & m & 0 & 0 & mr_y \\ 0 & 0 & & \hat{I}_a & \\ 0 & 0 & & & \\ mr_x & mr_y & & & \end{bmatrix}$$

where

$$\hat{I}_a = I_a + \begin{bmatrix} r_y^2 & -r_x r_y & 0 \\ -r_x r_y & r_x^2 & 0 \\ 0 & 0 & r_x^2 + r_y^2 \end{bmatrix}$$

where  $I_a$  is the antenna moment of inertia about its center of gravity. For any control input  $u(\cdot)$  (which must perforce be a "feedback" control, based on the sensor data  $v(\cdot)$ ) the mean square pointing error is then expressed by:

$$\lim_{T \rightarrow \infty} \frac{1}{T} \left\{ \int_0^T u_\theta(L, t)^2 dt + \int_0^T u_\phi(L, t)^2 dt + |r|^2 \int_0^T u_\psi(L, t)^2 dt \right\}$$

and the mean square pointing *rate* is given by

$$\lim_{T \rightarrow \infty} \frac{1}{T} \left\{ \int_0^T \dot{u}_\theta(L, t)^2 dt + \int_0^T \dot{u}_\phi(L, t)^2 dt + |r|^2 \int_0^T \dot{u}_\psi(L, t)^2 dt \right\}.$$

From the results in [6] it follows that the minimal attainable mean square pointing error is given by

$$aM_b^{-1}a^*$$

where

$$a = \text{row vector } (1, 1, 0, 0, |r|)$$

$$a^* = \text{transpose of } a$$

### 3. Main Results

We need some notation first. The mean square attitude response, whatever the feedback control used is defined by

$$\lim_{T \rightarrow \infty} \frac{1}{T} \left\{ \int_0^T u_\theta(t, \xi)^2 dt + \int_0^T u_\phi(t, \xi)^2 dt + |r|^2 \int_0^T u_\psi(t, \xi)^2 dt \right\}. \quad (3.1)$$

This is recognized as the mean square displacement of the center of gravity of the antenna which is then also proportional to the mean square "pointing" error — see [1] for the relationships.

Next let  $u$  denote any (vector) of control inputs — a constant "step" input:

$$u = \begin{bmatrix} u_1 \\ u_2 \\ u_3 \\ u_4 \\ u_5 \end{bmatrix}. \quad (3.1)$$

Solve the equations

$$\left. \begin{aligned} El_\theta u_\theta''(s) &= 0 \\ El_\phi u_\phi''(s) &= 0 \\ Gl_\psi u_\psi''(s) &= 0 \end{aligned} \right\} \quad 0 < s < L, \quad (3.2)$$



subject to the end conditions

$$\left. \begin{aligned} EI_{\theta} u_{\theta}'''(L) &= u_1 \\ EI_{\theta} u_{\theta}''(L) &= u_2 \\ EI_{\theta} u_{\theta}'(L) + u_3 &= 0 \\ EI_{\theta} u_{\theta}(L) + u_4 &= 0 \\ GI_{\psi} u_{\psi}'(L) + u_5 &= 0 \end{aligned} \right\} . \quad (3.3)$$

Note that the solution can be recognized as the steady-state response of the system to the step-input  $u$ , assuming that there is some damping. We only need to calculate the response to three specialized inputs:

Calculate the response to  $u_{\theta}(L)$  to the special case, Case 1, where:

$$u_1 = 1$$

$$u_i = 0, \quad 2 \leq i \leq 5.$$

Calculate the response  $u_{\theta}(L)$  to the special case, Case 2, where:

$$u_1 = 0$$

$$u_2 = 1$$

$$u_3 = u_4 = u_5 = 0.$$

Calculate the response  $u_{\psi}(L)$  to the special case, Case 3, where

$$u_1 = u_2 = u_3 = u_4 = 0$$

$$u_5 = 1.$$

Then the minimal achievable mean-square response whatever the choice of the feedback and whatever the mean-square control effort, is given by

$$\sqrt{d_1 d_0} (u_{\theta}(L)^2 + u_{\theta}(L)^2 + r^2 u_{\psi}(L)^2). \quad (3.4)$$

This is our main result. Unfortunately the derivation is beyond the scope of this report and

will be published elsewhere. To proceed further with (3.4) we calculate the solution of (3.2), (3.3) explicitly. Thus for any  $u$ , the solution is of the form

$$u_\theta(s) = a_3 s^3 + a_2 s^2, \quad 0 < s < L$$

$$u_\theta(s) = b_3 s^3 + b_2 s^2, \quad 0 < s < L$$

$$u_\psi(s) = c_1 s, \quad 0 < s < L$$

where

$$a_3 = -\frac{u_1}{6EI_\theta}$$

$$b_3 = -\frac{u_2}{6EI_\theta}$$

$$a_2 = \frac{1}{2} \left[ \frac{u_3}{EI_\theta} + \frac{u_1 L}{EI_\theta} \right]$$

$$b_2 = \frac{1}{2} \left[ \frac{u_4}{EI_\theta} + \frac{u_2 L}{EI_\theta} \right]$$

$$c_1 = \frac{u_5}{GI_\psi}$$

Thus for Case 1 we have

$$u_\theta(L)^2 = \frac{L^3}{3EI_\theta}$$

and for Case 2 we have

$$u_\theta(L)^2 = \frac{L^3}{3EI_\theta}$$

and for Case 3:

$$u_\psi(L)^2 = \frac{L}{GI_\psi}$$

Hence the mean-square attitude error

$$= \sqrt{d_s d_0} \left( \frac{L^3}{3EI_\theta} + \frac{L^3}{3EI_\theta} + \frac{|r|^2 L}{GI_\psi} \right). \quad (3.5)$$

Note the appearance of the noise parameters in (3.5) in product form.

The technique for calculating the minimal mean square attitude error in more complex models than that illustrated is the same: calculate the mean square step response (assuming

some damping) to unit step inputs.

In conclusion we suggest this result (3.5) can be the basis for combined structures-controls optimization — CSI, since the required structural parameters can be calculated for a lattice truss from the material gage and physical dimensions as in [4, 5]. We omit the details of these calculations.

## References

1. L. W. Taylor and A. V. Balakrishnan. "A Mathematical Problem and a Spacecraft Control Laboratory Experiment (SCOLE): NASA/IEEE Design Challenge." *Proceedings of the NASA SCOLE Workshop, Langley Research Center, December 1984.*
2. A. V. Balakrishnan. "A Mathematical Formulation of the SCOLE Control Problem, Part I." NASA CR 172581. May 1985.
3. A. V. Balakrishnan. "Control of Flexible Flight Structures." In: *Analyse mathématique et applications*. Paris: Gauthier-Villars, 1988.
4. A. K. Noor and C. M. Anderson. "Analysis of Beam-like Trusses." *Computer Methods in Applied Mechanics and Engineering*, Vol. 20 (1979).
5. A. K. Noor and W. C. Russell. "Anisotropic Continuum Models for Beam-like Lattice Structures." *Computer Methods in Applied Mechanics and Engineering*, Vol. 57 (1986).
6. A. V. Balakrishnan. "A Mathematical Formulation of the SCOLE Control Problem, Part II: Optimal Compensator Design." NASA CR 181720. December 1988.

## A WAVE EQUATION FORMULATION FOR THE SCOLE

Roberto Araya  
AutoMind  
Providencia 591 D.51  
Santiago Chile.

This paper review the modeling and control strategy proposed by the author [1][2] for the slewing and stabilization problem of the Space Shuttle Orbiter with a large Antenna attached to it through a long flexible mast.

The main distinguished feature of the problem treated here as compared with the standard problems studied in this area is the requirement to find optimal solutions for a nonrigid spacecraft configuration which is subject to nonlinear kinematic forces.

A distributed parameter model of the Space Shuttle/Antenna Configuration is derived from first principles of rigid body dynamics and elementary beam theory. The model is then put in the form of a compact semilinear abstract wave equation. Within this framework, the slewing and stabilization problem is then formulated as a nonlinear infinite-dimensional control problem.

A linear feedback control law is proposed to simultaneously solve the slewing and stabilization problem. This control law is a generalization of standard position-plus-rate feedback controls used for similar purposes in rigid spacecrafts and is also an extension of linear feedback controls used in stabilization theory of linear infinite dimensional systems.

## STATEMENT OF THE PROBLEM

Difficulties in controlling lightly damped Large Space Structures has motivated NASA to offer a design challenge called Spacecraft Control Laboratory Experiment (SCOLE) [5]. The aim of this "design challenge" is to evaluate control laws for flexible spacecraft.

The SCOLE configuration consists of a flexible beam with two rigid bodies at either end. One body represents the Space Shuttle orbiter, the other is the Antenna reflector.

There are two types of control : control moments and the control force. Control moments denoted by  $M_1$ ,  $M_2$  are applied to the Shuttle orbiter and the reflector, respectively. The components of these moments for each axis are limited to 10,000 ft-lb. Control force  $F$  is applied at the center of the reflector in two perpendicular directions along the plane of the reflector. The control force in a particular direction is limited to 800 lbs.

Measurements consist of the inertial attitude direction cosine matrices for the Shuttle body and the Antenna, angular velocities  $\omega_1$ ,  $\omega_2$  for the Shuttle and the reflector body respectively and accelerations measured by three axis accelerometers located on the Shuttle and the center of the reflector.

A certain ray is emitted towards the center of the reflector from the feed located on the Shuttle. The direction of reflection of this ray is called the line-of-sight. Initially the error between the line-of-sight and the target is 20 degrees and the SCOLE configuration is at rest.

The problem is to minimize the time required to slew or change the line-of-sight towards a fixed target and to settle or stabilize the induced structural vibrations of the Shuttle/Antenna configuration to

the degree required for precise pointing.

## THE EQUATIONS OF MOTION AND THE CONTROL SATRATEGY

The derivation of the equations of motion is based on basic principles of rigid body dynamics and elementary beam theory.

Under the assumption that the flexible beam is subject to only small deformations, a linear Euler/Bernoulli beam model is utilised. Nonlinearities are due only to kinematic effects caused by the large angular velocities that the whole configuration can reach in a time optimal maneuver.

Since inherent structural damping is very weak and the phenomenon is not well known, no damping is assumed in the model. Therefore energy dissipation is caused only by the control action.

Given that the main concern is spacecraft orientation, only rotational dynamics is considered.

A coupled system of hyperbolic partial differential equations and ordinary differential equations is obtained. The variables considered are the elastic deformations  $u^1$  and  $u^2$ , the torsion  $u^3$  and the longitudinal deformation  $u^4$  along the beam axis.

To obtain these equations, the angular momentum  $\mathbf{p}_0$  of the whole configuration about the center of gravity of the Shuttle and the momentum  $\mathbf{p}_1$  ( $\mathbf{p}_1$ ) and the angular momentum  $\mathbf{p}_2$  ( $\mathbf{p}_2$ ) of each element of the beam (Antenna) are computed.

After deriving the equations of motion, the following Lyapunov equation can be obtained:

$$\frac{d}{dt} [D(t) + T(t) + V(t)] = \omega \cdot (N_1 - \sum_{i=1}^3 \lambda_i D_i \otimes R_i) + \omega_a \cdot N_a + v \cdot F$$

where

$T$  is the kinetic energy,

$V$  is the potential energy

$D$  is a measure of the distance to the target orientation

$$D = \frac{1}{2} \sum_{i=1}^3 \lambda_i D_i \cdot D_i$$

$$D_i = R_i - S_i \quad i=1, \dots, 3$$

$(S_i, i=1, \dots, 3)$  is an orthonormal triplet in the inertial frame

$(R_i, i=1, \dots, 3)$  is an orthonormal triplet fixed to the Shuttle

$\omega$  angular velocity of the shuttle

$\omega_a$  is the angular velocity of the antenna

$v$  is the linear velocity of the mass center of the antenna

This equation provides a clear insight into our problem. It suggests a straightforward and implementable feedback control law: choose  $N_1, N_a$ , and  $F$  so that the right hand side in becomes strictly negative.

Thus, the problem is broken down into two parts

- i) Orientation of the whole configuration as a rigid spacecraft.

This is achieved by choosing  $N_1$  to make  $\omega \cdot (N_1 - \sum_{i=1}^3 \lambda_i D_i \otimes R_i)$  negative.

- ii) Stabilization of the induced structural deformations

Choosing  $N_a$  and  $F$  to make  $\omega_a \cdot N_a + v \cdot F$  negative

The first control strategy is well known for rigid spacecraft



stabilization and slewing. The second one, is the classical stabilization control for rigid and flexible structures.

#### THE ABSTRACT WAVE EQUATION SET UP

The equations of motion can be written as an abstract semilinear wave equation:

$$\ddot{x}(t) = Ax(t) + K_1(x(t)) + K_2(x(t)) + Bu(t)$$

$$x(0) = x_0$$

in a Hilbert space  $H$ . Here,  $A$  is an infinitesimal generator of a group with compact resolvent,  $B$  is a linear operator with finite dimensional range,  $K_1$  and  $K_2$  are nonlinear but continuous operators:

$K_1$  with finite dimensional range and representing the orientation of the configuration as a rigid spacecraft;

$K_2$  represents the nonlinear kinematics and satisfies

$$[K_2(x), x] = 0 \quad \forall x \in H.$$

More specifically,

$$H = D(A_0^{1/2}) \times D(A_0^0)$$

with the inner product

$$\left[ \begin{pmatrix} x_1 \\ x_2 \end{pmatrix}, \begin{pmatrix} y_1 \\ y_2 \end{pmatrix} \right]_H = [A_0^{1/2}x_1, A_0^{1/2}y_1] + [Mx_2, y_2],$$

where

$$D(A_0^*) = \mathbb{R}^3 \times (L_2(-L, 0))^3 \times \mathbb{R}^3$$

$$A_0 \begin{pmatrix} D_1 \\ D_2 \\ u^\theta \\ u^\dagger \\ u^z \\ u^\ddagger \\ r_1 \\ r_2 \\ r_3 \\ \varepsilon_1 \\ \varepsilon_2 \\ \varepsilon_3 \end{pmatrix} = \begin{pmatrix} \lambda_1 D_1 \\ \lambda_2 D_2 \\ EI \frac{\partial^3 u^\theta}{\partial \xi^3} \\ EI \frac{\partial^3 u^\dagger}{\partial \xi^3} \\ -EA \frac{\partial^2 u^z}{\partial \xi^2} \\ -GI \frac{\partial^2 u^\ddagger}{\partial \xi^2} \\ EI \frac{\partial^3 u^\theta}{\partial \xi^3}(-L) \\ EI \frac{\partial^3 u^\dagger}{\partial \xi^3}(-L) \\ -EA \frac{\partial u^z}{\partial \xi}(-L) \\ EI \frac{\partial^2 u^\ddagger}{\partial \xi^2}(-L) \\ -EI \frac{\partial^2 u^\theta}{\partial \xi^2}(-L) \\ -GI \frac{\partial u^\ddagger}{\partial \xi}(-L) \end{pmatrix}$$

and the domain of  $A_0$  is

$$D(A_0) = \{(D_1, D_2, u^\theta, u^\dagger, u^z, u^\ddagger, r_1, r_2, r_3, \varepsilon_1, \varepsilon_2, \varepsilon_3) \in D(A_0^*) \text{ such that}$$

$$u^\theta, u^\dagger \in H^1(-L, 0), \quad u^z, u^\ddagger \in H^1(-L, 0)$$

$$u^\theta(0) = u^\dagger(0) = u^z(0) = u^\ddagger(0) = \frac{\partial u^\theta}{\partial \xi}(0) = \frac{\partial u^\ddagger}{\partial \xi}(0) = 0$$

$$u^0(-L)=r_1, u^1(-L)=r_2, u^2(-L)=r_3,$$

$$\frac{\partial u^0}{\partial \xi}(-L)=\epsilon_2, -\frac{\partial u^1}{\partial \xi}(-L)=\epsilon_1, u^1(-L)=\epsilon_3,$$

M is the mass moment operator, defined from  $D(A_0^*)$  into itself by:

$\lambda,$	$0$	$0$	$0$	$0$	$0$
$0$	$I$	$\int_{-L}^0 p\theta(\cdot)FAd\xi$	$\int_{-L}^0 PI_{\frac{1}{2}}(\cdot)\dot{z}d\xi$	$m_1(p_1+p)\theta(\cdot)$	$I_1+m_1p_1\theta((\cdot)\theta p)$
$0$	$FA(\cdot)\theta p$	$PA$	$0$	$0$	$0$
$0$	$PI_{\frac{1}{2}}\dot{z}^*$	$0$	$PI_{\frac{1}{2}}$	$0$	$0$
$0$	$m_1(\cdot)\theta(p_1+p)$	$0$	$\theta$	$m_1$	$m_1(\cdot)\theta p$
$0$	$I_1+m_1p\theta((\cdot)\theta p_1)$	$0$	$0$	$m_1p\theta(\cdot)$	$I_1$

In this abstract set up, the norm induced by the inner product is:

$$(1/2) \|x(t)\|_E^2 = D(t) + T(t) + V(t)$$

and therefore the slewing and stabilization problem can be viewed as driving the initial state  $x_0$  towards the origin.

This compact and geometric formulation of the problem is very fruitful. It allows a detailed mathematical analysis of the evolution equation and the control strategy. This gives existence results of mild and strong solutions under suitable conditions. It gives also the correct framework to do modal analysis:

$$A_0x = \mu Mx$$

This compact formulation gives also the insight to understand the proposed control laws as a natural generalisation from a finite

dimensional to an infinite dimensional set up.

The proposed control strategy can be expressed as:

- i)  $Rx$  : a standard linear feedback control used for slewing of rigid spacecraft.
- ii)  $-B^*x$  : a standard feedback stabilization control used in infinite dimensional control theory and widely known for stabilization of flexible beams.

Both components have simple physical interpretation and can be computed directly from the sensor data.

The Lyapunov equation and the proposed control law, is expressed as:

$$\frac{d\|x(t)\|^2}{dt} = -\|u\|^2 - \|v\|^2 - \|v\|^2,$$

Thus,  $\|x(t)\|^2$  is decreasing. The original evolution equation is converted to the autonomous system:

$$\begin{aligned}\dot{x} &= Ax + Y(x) \\ x(0) &= x_0\end{aligned}$$

or, the integral equation version:

$$x(t) = e^{At}x_0 + \int_0^t e^{A(t-s)}Y(x(s))ds$$

The major result obtained with this approach is the ability to show that if the system is initially at rest and the line-of-sight error is within 20 degrees, then the linear feedback position-plus-rate control law :

$$u = -B^*x + Rx$$

or equivalently

$$M_i = -e + \sum_{j=1}^3 \lambda_j D_j R_i$$

$$M_i = -e_i$$

$$F = -v_i$$

will drive  $x(t)$  to zero as  $t$  goes to infinity. Thus, in finite time the line-of-sight will be pointed to the target up to an error  $\delta$  and simultaneously the oscillations of the flexible configuration will be settled down, in the strong sense, to the degree required to precise pointing.

To achieve this result is necessary to prove the controllability of the flexible modes. That is, when linearising and considering only flexible modes, the obtained linear model has to be controllable.

This abstract wave equation formulation is a basic framework for the complete problem analysis. It also offers a correct and compact set up to study the different control strategies. In particular, non linear feedback controls on the angular and linear velocities [3][4][6].

#### REFERENCES

- [1] Araya, R.: "Control of a Large Space Structure Using a Distributed Parameter Model" UCLA Ph.D Thesis 1986.
- [2] Araya, R.: "A Controllability-Stabilizability Result for the SCOLE" Proceedings of the NASA SCOLE Workshop, Hampton, Virginia December 6-7, 1984.
- [3] Balakrishnan, A.V.: "A Mathematical Formulation of the SCOLE Control Problem" Revised version of NASA CR-17258 July 10, 1985
- [4] Balakrishnan, A.V.: "A Mathematical Formulation of a Large Space Structure Control Problem" Proceedings of the 24th Conference on Decision and Control, December 11-13, 1985
- [5] Taylor, L.W. and A.V. Balakrishnan: "A Mathematical Problem and a Spacecraft Control Laboratory Experiment (SCOLE) Used to Evaluate Control Laws for Flexible Spacecrafts ... NASA/IEEE Design Challenge". January 1984. Revised June and December 1984.
- [6] A.V. Balakrishnan: "Some Nonlinear Damping Models in Flexible Structures". 4th Annual NASA SCOLE Workshop. November 1987.



## Report Documentation Page

1. Report No.  NASA CP-10057, Part 1	2. Government Accession No.	3. Recipient's Catalog No.
4. Title and Subtitle  5th Annual NASA Spacecraft Control Laboratory Experiment (SCOLE) Workshop		5. Report Date  December 1990
		6. Performing Organization Code
7. Author(s)  Lawrence W. Taylor, Jr. (Compiler)		8. Performing Organization Report No.
		10. Work Unit No.  506-46-11-01
9. Performing Organization Name and Address  NASA Langley Research Center Hampton, VA 23665		11. Contract or Grant No.
12. Sponsoring Agency Name and Address  National Aeronautics and Space Administration Washington, DC 20546		13. Type of Report and Period Covered  Conference Publication
		14. Sponsoring Agency Code
15. Supplementary Notes		
16. Abstract  This publication is a collection of papers presented at the Fifth Annual Spacecraft Control Laboratory Experiment (SCOLE) Workshop held at the Hilton Lodge, Lake Arrowhead, California, October 31, 1988. The papers address the modeling, systems identification, and control synthesis for the Spacecraft Control Laboratory Experiment (SCOLE) configuration.		
17. Key Words (Suggested by Author(s))  Large Flexible Spacecraft Control Structural Dynamics		18. Distribution Statement  Unclassified-Unlimited Subject Category - 18
19. Security Classif. (of this report)  Unclassified	20. Security Classif. (of this page)  Unclassified	21. No. of pages  385
		22. Price  A17

**END**

**DATE**

**FILMED**

**APR 25 1991**